REPORT DOCUMENTATION PAGE

1. Recipient's Reference	2. Originator's Reference	3. Further Reference	4. Security Classification of Document
	AGARD-CP-332	ISBN 92-835-0329-5	UNCLASSIFIED

5. Originator: Advisory Group for Aerospace Research and Development
North Atlantic Treaty Organization
7 rue Ancelle, 92200 Neuilly sur Seine, France

6. Title: PROPAGATION ASPECTS OF FREQUENCY SHARING INTERFERENCE AND SYSTEM DIVERSITY

7. Presented at: the 31st Symposium of the Electromagnetic Wave Propagation Panel held in Issy-les-Moulineaux, France, 18–22 October, 1982.

8. Author(s)/Editor(s): H.Soicher

9. Date: March 1983

10. Author's/Editor's Address: US Army Communications-Electronics Command
Center for Communications Systems
ATTN: DRSEL-COM-RN-1
Fort Monmouth, N.J. 07703 USA

11. Pages: 432

12. Distribution Statement: This document is distributed in accordance with AGARD policies and regulations, which are outlined on the Outside Back Covers of all AGARD publications.

13. Keywords/Descriptors

Frequency Spectrum Management
Frequency Sharing
Frequency Interference
Electromagnetic Wave Propagation
Propagation Phenomena
Radio Communication
Propagation Models

14. Abstract

These Proceedings include the papers and discussions presented at the AGARD Electromagnetic Wave Propagation Panel Symposium on "Propagation Aspects of Frequency Sharing, Interference and System Diversity" held in Issy-les-Moulineaux, France, in October 1982.

Increasing demands for radio service will necessitate more frequency sharing. An assessment of the possibility of additional frequency sharing included the following points: propagation effects on the practicability of frequency sharing, mechanisms responsible for and limits posed by interference from strong signals, and techniques available for the control of such interference and for the increase in channel capability.

The overview session examined frequency sharing with reference to RF propagation limitations, principles and international procedures. Other sessions dealt specifically with the subject with regard to terrestrial propagation (ionospheric modifications and ionospheric modes), terrestrial propagation (ground and tropospheric modes), EHF propagation, propagation along earth-space paths, and interference control and increase in channel capacity.

Included with the 36 papers presented are the discussions that followed the presentation of each paper.

Papers presented at the 31st Symposium of the Electromagnetic Wave Propagation Panel held in Issy-les-Moulineaux, France, 18–22 October, 1982.

LIBRARY
RESEARCH
NAVAL PC
MONTEREY, CALIFORNIA 93943

AGARD-CP-332

AGARD

ADVISORY GROUP FOR AEROSPACE RESEARCH & DEVELOPMENT

7 RUE ANCELLE 92200 NEUILLY SUR SEINE FRANCE

AGARD CONFERENCE PROCEEDINGS No. 332

Propagation Aspects of Frequency Sharing, Interference and System Diversity

NORTH ATLANTIC TREATY ORGANIZATION

DISTRIBUTION AND AVAILABILITY
ON BACK COVER

NORTH ATLANTIC TREATY ORGANIZATION

ADVISORY GROUP FOR AEROSPACE RESEARCH AND DEVELOPMENT

(ORGANISATION DU TRAITE DE L'ATLANTIQUE NORD)

AGARD Conference Proceedings No.332

PROPAGATION ASPECTS OF FREQUENCY SHARING, INTERFERENCE AND SYSTEM DIVERSITY

Edited by

H.Soicher
US Army Communications-Electronics Command
Center for Communications Systems
ATTN: DRSEL-COM-RN-1
Fort Monmouth, N.J. 07703
USA

Papers presented at the 31st Symposium of the Electromagnetic Wave Propagation Panel held in Issy-les-Moulineaux, France, 18–22 October, 1982.

THE MISSION OF AGARD

The mission of AGARD is to bring together the leading personalities of the NATO nations in the fields of science and technology relating to aerospace for the following purposes:

- Exchanging of scientific and technical information;
- Continuously stimulating advances in the aerospace sciences relevant to strengthening the common defence posture;
- Improving the co-operation among member nations in aerospace research and development;
- Providing scientific and technical advice and assistance to the North Atlantic Military Committee in the field of aerospace research and development;
- Rendering scientific and technical assistance, as requested, to other NATO bodies and to member nations in connection with research and development problems in the aerospace field;
- Providing assistance to member nations for the purpose of increasing their scientific and technical potential;
- Recommending effective ways for the member nations to use their research and development capabilities for the common benefit of the NATO community.

The highest authority within AGARD is the National Delegates Board consisting of officially appointed senior representatives from each member nation. The mission of AGARD is carried out through the Panels which are composed of experts appointed by the National Delegates, the Consultant and Exchange Programme and the Aerospace Applications Studies Programme. The results of AGARD work are reported to the member nations and the NATO Authorities through the AGARD series of publications of which this is one.

Participation in AGARD activities is by invitation only and is normally limited to citizens of the NATO nations.

The content of this publication has been reproduced
directly from material supplied by AGARD or the authors.

Published March 1983

Copyright © AGARD 1983
All Rights Reserved

ISBN 92-835-0329-5

Printed by Specialised Printing Services Limited
40 Chigwell Lane, Loughton, Essex IG10 3TZ

LIBRARY, NAVAL POSTGRADUATE SCHOOL
MONTEREY, CA 93940

THEME

Frequency spectrum management is an extremely important activity that facilitates the orderly use of the electromagnetic spectrum for many telecommunications and other purposes.

When considering the propagational aspects of frequency spectrum requirements and allocations one needs to address two questions: What frequency bands are most suitable for various services? and, How do the propagation factors affect the suitability of frequency sharing between the services? The first question refers to system performance reliability in the face of limitations posed by natural and man-made phenomena, while the second refers to frequency sharing and interference where sharing is limited by interference from unusually strong signals.

The system reliability aspect involves the choice of parameters that achieve the required service with a minimum acceptable signal for a specified percentage of time. The sharing and interference aspect involves the possibility that strong signals might be a source of interference to another system operating in the same or another cochannel service.

In this symposium the sharing and interference aspect of the problem was addressed. Increased demand for radio services has necessitated the sharing of radio frequencies between terrestrial services and space services, and between services in both categories. Further demand will call for more sharing – assuming this is technically feasible – and the possibility will depend critically on propagation factors. In assessing such possibility one has to consider the following points: propagation effects on practicability of frequency sharing between services, mechanisms responsible for, and limits posed by, interference from strong signals, and techniques available for control of such interference and for increase in channel capacity.

It was the aim of the symposium to stimulate discussion on the above points and to bring together scientists and engineers who are studying the propagation phenomena with those who design and frequency manage RF systems, so that they might understand each other's problems.

THEME DU SYMPOSIUM

Le gestion du spectre de fréquences constitue une activité extrémement importante qui facilite l'exploitation méthodique du spectre électro-magnétique pour de nombreuses télécommunications et d'autres applications.

Lors qu'on considère les impératifs et les attributions du spectre de fréquences sous l'angle de la propagation, deux questions se posent: Quelles sont les bandes de fréquence convenant le mieux aux divers services? et Dans quelle mesure les facteurs de propagation affectent-ils l'adéquation du partage de fréquence entre services? La première question porte sur la fiabilité des performances des systèmes face aux limitations imposées par les phénomènes naturels et les activités humaines, alors que la seconde porte sur le partage de fréquences et le brouillage, lorsque le partage de fréquence est limité par le brouillage que créent des signaux d'une intensité inhabituelle.

La fiabilité des systèmes implique le choix de paramètres permettant de fournir le service requis avec un signal minimum acceptable pour un pourcentage de temps spécifié. Quant au partage de fréquence et au brouillage, ils impliquent la possibilité que des signaux de forte intensité puissent constituer une source de brouillage pour un autre système fonctionnant dans le même service ou dans un autre service utilisant le même canal.

Au cours de ce symposium ont été traités les aspects du problème constitués par le partage de fréquence et le brouillage. La demande accrue dans le domaine des services radio a nécessité le partage de fréquences radio entre services terrestres et services spatiaux, d'une part, et, d'autre part, entre services appartenant à ces deux catégories. Un accroissement de la demande existant déjà conduira obligatoirement à un partage plus poussé, en supposant que cette solution soit techniquement réalisable. Cette possibilité dépendra de façon critique des facteurs de propagation, et, pour l'évaluer, il nous faut examiner les points suivants: effets de la propagation sur la practicabilité du partage de fréquence entre services, mécanismes responsables du brouillage créé par les signaux de forte intensité, limites imposées par ce brouillage, et techniques disponibles pour maîtriser ce brouillage et accroître la capacité des canaux.

Ce symposium s'est donné pour but de stimuler les débats sur les divers points mentionnés et de permettre aux scientifiques et ingénieurs étudiant les phénomènes de propagation et aux responsables de la conception et de l'exploitation des systèmes RF de se rencontrer afin de mieux comprendre leurs problèmes respectifs.

PROGRAM AND MEETING OFFICIALS

PROGRAM CHAIRMAN: Dr Haim Soicher
US Army Communications-Electronics Command
Center for Communications Systems
ATTN: DRSEL-COM-RN-1
Fort Monmouth, N.J. 07703
USA

MEMBERS

Dr H.J.Albrecht
FGAN
Königstrasse 2
D-5307 Wachtberg-Werthhoven
Germany

Mr L.Boithias
C.N.E.T.
38–40, rue du Général Leclerc
92131 Issy-les-Moulineaux
France

Dr R.K.Crane
Thayer School of Engineering
Dartmouth College
Hanover, N.H. 03753
USA

Mr M.P.M.Hall
Rutherford Appleton Laboratories
Chilton, Didcot
Oxon, OX 11 0QX
UK

Dr Ing. E.W.Lampert
Postfach 70 00 60
Siemens AG
8000 München 80
Germany

Dr W.F.Utlaut
Dir. Inst for Telecommunication Sciences
National Telecommunications & Information Administration
Dept of Commerce
Boulder, Co 80303
USA

ELECTROMAGNETIC WAVE PROPAGATION PANEL

CHAIRMAN: Dr J.S.Belrose
P.O. Box 11490
Communications Research Center
Station H,
Ottawa, K2H 8S2
Canada

DEPUTY CHAIRMAN: Dr J.H.Blythe
Marconi Research Laboratories
West Hanningfield Road
Great Baddow
Chelmsford, CM2 8HN
UK

HOST COORDINATOR

Mr L.Boithias
C.N.E.T.
38–40, rue du Général Leclerc
92131 Issy-les-Moulineaux
France

PANEL EXECUTIVE

Major T.B.Russell
AGARD/NATO
7, rue Ancelle
92200 Neuilly-sur-Seine
France

EDITOR'S COMMENTS

These proceedings represent the totality of the AGARD/EPP symposium on "Propagation Aspects of Frequency Sharing, Interference and System Diversity" held in Issy-les-Moulineaux, France, 18-22 October 1982. It is hoped that these proceedings will constitute the state-of-the-art document on this important subject.

The papers appearing in the proceedings of this symposium have been printed from copies furnished directly by the authors. For the most part, the question-and-answer comments which followed individual presentations, were written by the discussors for inclusion in these proceedings. This procedure gave the discussors the opportunity to re-phrase and possibly re-think their comments. The session summaries, which highlight the subject matter presented and discussed during the session, were prepared by the session chairmen. The editor wishes to thank them for their efforts here and for ably directing the presentation and discussion periods during the symposium.

The general discussion portion of these proceedings were summarized by the session chairman from taped transcriptions. Quite often the coherency of thought is lost in the transcription, and considerable freedom was used in the interpretation of the comments. The editor apologizes for any changes in meaning or style that may have been made in preparing a printable version of the discussions.

The success of the symposium was assured by the collective support afforded by members of the program committee whose names are given elsewhere in these proceedings.

The editor wishes to thank the EPP Chairman and Deputy Chairman for their interest and support in the preparation and execution of the symposium. Further, he wishes to acknowledge the support of the EPP Executive and his staff as well as his own organization in the preparation of these proceedings.

Haim Soicher

SESSION CHAIRMEN

SESSION I	**OVERVIEW**	
	Dr W.F.Utlaut	Dir. Inst. for Telecommunication Sciences National Telecommunications & Information Administration Dept. of Commerce, Boulder, CO 80303, USA
SESSION II -A	**TERRESTRIAL PROPAGATION (IONOSPHERIC MODIFICATION)**	
	Dr H.J.Albrecht	FGAN Königstrasse 2 D-5307 Wachtberg-Werthhoven Germany
SESSION II -B	**TERRESTRIAL PROPAGATION (IONOSPHERIC MODE)**	
	Dr H.Soicher	Fort Monmouth, USA
SESSION III -A	**TERRESTRIAL PROPAGATION (GROUND AND TROPOSPHERIC MODES)**	
	Mr L.Boithias	C.N.E.T. 38–40, rue du Général Leclerc 92131 Issy-les-Moulineaux France
SESSION III -B	**EHF PROPAGATION**	
	Dr H.J.Albrecht	FGAN Germany
SESSION IV	**PROPAGATION ALONG SPACE/EARTH PATHS**	
	Mr M.P.Hall	Rutherford Appleton Laboratories Chilton, Didcot Oxon, OX 11 OQX UK
SESSION V	**INTERFERENCE CONTROL AND INCREASE IN CHANNEL CAPACITY**	
	Dr Ing. E.Lampert	Postfach 70 00 60 Siemens AG 8000 München 80 Germany
SESSION VI	**FINAL ROUND TABLE DISCUSSION**	
	Dr R.K.Crane	Thayer School of Engineering Dartmouth College Hanover, NH 03753 USA

CONTENTS

	Page
THEME	iii
PROGRAM AND MEETING OFFICIALS	iv
EDITOR'S COMMENTS	v
SESSION CHAIRMEN	vi
	Reference
SESSION I – OVERVIEW	
CHAIRMAN'S SUMMARY	CS1-1
FUNDAMENTAL LIMITATIONS CAUSED BY RF PROPAGATION by R.K.Crane	1
SOME PROPAGATIONAL ASPECTS OF FREQUENCY ALLOCATION AND FREQUENCY SHARING by H.T.Dougherty and C.M.Rush	2
OVERVIEW OF FREQUENCY SHARING by E.J.Holliman	3
RADIO REGULATORY ASPECTS OF FREQUENCY SHARING by L.W.Barclay	4
SESSION II-A – TERRESTRIAL PROPAGATION (IONOSPHERIC MODIFICATION)	
CHAIRMAN'S SUMMARY	CS2A-1
ANOMALOUS ABSORPTION EFFECTS PRODUCED BY HIGH POWER RADIO WAVES IN THE HIGH LATITUDE IONOSPHERE by T.B.Jones, T.Robinson, P.Stubbe and H.Kopka	5
Paper 6 Cancelled	
SESSION II-B – TERRESTRIAL PROPAGATION (IONOSPHERIC MODE)	
CHAIRMAN'S SUMMARY	CS2B-1
Paper 7 Cancelled	
VHF-LONG-DISTANCE-PROPAGATION BY AURORAL BACKSCATTER by G.Lange-Hesse	8
INTERFERENCE AND SHARING AT MEDIUM FREQUENCY: SKY WAVE PROPAGATION CONSIDERATIONS by J.C.H.Wang	9
SIGNAL AND NOISE VARIABILITY IN HIGH FREQUENCY SKY-WAVE RADIO-SERVICE PLANNING by P.A.Bradley	10
ANOMALOUS PROPAGATION BEHAVIOR OF RADIO SIGNALS AT HIGH LATITUDES by R.D.Hunsucker	11
THE APPLICATION OF REAL-TIME MODEL UPDATE BY OBLIQUE IONOSPHERIC SOUNDERS TO FREQUENCY SHARING by D.R.Uffelman, L.O.Harnish and J.M.Goodman	12

Reference

THE DEVELOPMENT OF AN IONOSPHERIC MODEL THESAURUS AND USER'S GUIDE
by J.M.Goodman 13

SESSION III-A – TERRESTRIAL PROPAGATION (GROUND AND TROPOSPHERIC MODES)

CHAIRMAN'S SUMMARY CS3A-1

MEDIUM WAVE GROUND WAVE PROPAGATION MODEL – NUMERICAL AND EXPERIMENTAL RESULTS
by A.F.Fer and A.Hizal 14

A COMPUTATIONAL MODEL FOR MULTIPLE KNIFE–EDGE DIFFRACTION
by L.E.Vogler and P.M.McManamon 15

VHF/UHF PROPAGATION STUDIES ON LONG OVER THE HORIZON SALT WATER RADIO PATHS
by R.E.Grantham and W.P.Lonc 16

MODELLING ON INTERFERENCE DUE TO DUCTING AT FREQUENCIES ABOVE 1 GHz
by J.Dijk, J.Neessen and J. van Tiggelen 17

STATISTICAL STUDY OF ELEVATED DUCTS EXTENSION
by B.Strauss and J-L.Dumas 18

LA DIFFUSION MULTIPLE PAR LES HYDROMETEORES: UNE SIMULATION NUMERIQUE
par N.Spanjaard et J.Lavergnat 19

BISTATIC RADAR REFLECTIVITIES IN THE RANGE 11–30 GHz
by D.G.Charlton, A.R.Holt and B.G.Evans 20

OVERSHOOT INTERFERENCE ON MICROWAVE RADIO LINKS DUE TO THE CO-EXISTENCE OF MULTIPATH FADING AND TRANS-HORIZON PROPAGATION
by J.E.Doble 21

SESSION III-B – EHF PROPAGATION

CHAIRMAN'S SUMMARY CS3B-1

SYSTEM ASPECTS OF CLEAR AIR PROPAGATION ABOVE 40 GHz
by J.D.Hopponen and D.Theobold 22

PROPAGATION CONSTRAINTS IN THE MILLIMETRE WAVEBANDS DUE TO PRECIPITATION SCATTERING
by B.G.Evans and A.R.Holt 23

A MM-WAVE COLLISION WARNING DEVICE FOR HELICOPTERS
by B.Rambold, H.G.Wippich, M.Bischoff and W.F.X.Frank 24

SESSION IV – PROPAGATION ALONG SPACE/EARTH PATHS

CHAIRMAN'S SUMMARY CS4-1

A PREDICTOR MODEL FOR EHF COMMUNICATION SATELLITE SYSTEM AVAILABILITIES IN THE PRESENCE OF RAIN
by L.M.Schwab and A.J.Simmons 25

DIVERSITY RECEPTION OF COMSTAR 19/20 GHz SATELLITE BEACONS IN CONVECTIVE RAIN CLIMATE OF FLORIDA, 1978–1981
by D.Davidson, D.D.Tang and S.C.Bloch 26

Reference

SCINTILLATION MODELLING AND MEASUREMENT. A TOOL FOR REMOTE-SENSING SLANT PATHS
by E.Vilar and J.Haddon 27

LONG TERM CROSS-POLAR STATISTICS AT 12 AND 14 GHz ON A 30° SLANT PATH
by R.G.Howell, J.Thirlwell and D.J.Emerson 28

Paper 29 Cancelled

FADING STATISTICS OF C-BAND SATELLITE SIGNAL DURING SOLAR MAXIMUM YEARS (1978–1980)
by D.J.Fang and C.H.Liu 30

SESSION V – INTERFERENCE CONTROL AND INCREASE IN CHANNEL CAPACITY

CHAIRMAN'S SUMMARY CS5-1

NEW ASPECTS IMPROVING THE AVAILABILITY OF DIGITAL LOS-RADIO RELAY LINKS DEDUCED FROM WIDE-BAND MEASUREMENTS AT 5 AND 15 GHz
by M.Niemeyer, W.Schwarz and B.Sommer 31

OCCUPANCY MEASUREMENTS ACROSS THE ENTIRE HF SPECTRUM
by G.F.Gott, S.Dutta and N.F.Wong 32

PROPAGATION DATA FOR VHF PLANNING IN THE UK AREA
by K.A.Hughes and J.A.Lane 33

IMPLICATIONS OF PROPAGATION UNCERTAINTIES IN FREQUENCY SHARING ANALYSES
by T.M.Sullivan 34

PROPAGATION PREDICTION USAGE IN AUTOMATED FREQUENCY ASSIGNMENTS BASED ON COSITE AND REMOTE SYSTEM SPECTRUM SHARING
by S.M.Segner 35

ON COMBATING MULTIPATH EFFECTS USING SPREAD-SPECTRUM SYSTEMS
by C.P.Tou 36

A SPECTRAL EMISSION MASK FOR DIGITAL TROPOSPHERIC SCATTER TRANSMISSION
by R.K.P.Galpin 37

INTERFERENCE REJECTION BY AUXILIARY FEEDS IN CASSEGRAIN EARTH TERMINALS
by J.Arnbak, M.H.A.J.Herben and R.A.C.M. van Spaendonk 38

GAIN PATTERNS OF MICROWAVE COMMON CARRIER ANTENNAS
by A.G.Hanson and P.M.McManamon 39

SESSION VI – FINAL ROUND TABLE DISCUSSION

DISCUSSION RTD-1

APPENDIX A – LIST OF PARTICIPANTS A

SUMMARY OF SESSION I

OVERVIEW

by

Dr William F.Utlaut
Session Chairman

This introductory session focused on four main topics: fundamental limitations caused by RF propagation, propagation aspects of frequency allocation and sharing, frequency sharing principles, and the international forums and procedures in frequency sharing.

Crane summarized the lower atmospheric propagation phenomena which affect the design of radio frequency systems and how these phenomena limit the suitability of portions of the radio spectrum for specific applications, reliability of operation, and density of system occupancy in allocated bands through the possibility of interference. In the frequency range from about 1 to 300 GHz, the tropospheric processes causing signal attenuation are mainly gaseous absorption and rain-caused scatter. Gradients or irregularities in the refractive index/height profile of the lower atmosphere can cause signal angle-of-arrival fluctuations, multipath, and ducting. All of these factors can be of importance to questions of frequency suitability, system performance reliability, and potential for interference.

Dougherty discussed ground wave, atmospheric, and ionospheric influences on frequency allocation and sharing. His discussion noted a dichotomy of concern from the perspective of service fields or interference fields, noting that the grade of telecommunications service provided by a system are normally achieved by reliance upon standard modes or signal paths, whereas both the standard mode and anomalous modes must be considered when describing interference phenomena. Further, standard modes are viewed as being rather stable and predictable while anomalous modes are described with a degree of uncertainty as they are viewed as tending to be less stable and predictable either in occurrence or characteristic.

Holliman provided an overview on considerations requiring attention of spectrum managers in the process of developing frequency sharing processes and plans.

Barclay continued discussion concerning frequency sharing problems and potential. He also describes some of the aspects of frequency allocation and sharing carried out by the International Telecommunication Union and its component activities in the CCIR, IFRB, and various WARCs.

Overall, the views presented by researchers, modelers, and spectrum managers re-emphasized that the process of developing systems which will provide satisfactory performance and which of necessity must share portions of the radio spectrum is complex and highly dependent upon constraints imposed by natural phenomena of the earth's environment upon the propagation of radio waves.

FUNDAMENTAL LIMITATIONS CAUSED BY RF PROPAGATION

by

Robert K. Crane

Thayer School of Engineering
Dartmouth College
Hanover, New Hampshire 03755

Invited Paper for Presentation at
AGARD Electromagnetic Wave Propagation Panel

Fall 1982

Symposium on

Propagation Aspects of Frequency Sharing,
Interference and System Diversity
in Issy-les-Moulineaux, France

18 - 22 October 1982

ABSTRACT

Atmospheric propagation phenomena affect the design of radio frequency transmission systems. They limit the suitability of portions of the frequency band for some applications, the reliability of system operation, and the density of system occupying each allocated frequency band through the possibility of interference. The suitability, reliability and possibility of interference are considered for frequencies in the range from 1 to 300 GHz. Within this range, the tropospheric processes causing attenuation by gaseous absorption and rain scatter, angle-of-arrival fluctuation, multipath, and ducting by refractive index gradients and scattering by hydrometeors are most important to the questions of suitability, reliability, and interference.

1. INTRODUCTION

The recent World Administration Radio Conference allocated radio frequencies from 9 KHz to 275 GHz for use by radiocommunication, radiodetermination (includes radar), radio astronomy, and earth exploration satellite (includes passive remote sensing) services[1]. Within the frequency range, the ionosphere, the non-ionized regions of the atmosphere, and the surface of the earth produce significant propagation effects[2] which result in spatial and temporal variations in the amplitude, phase, frequency, group velocity and propagation direction of a radio frequency (rf) wave. The dominant propagation mechanisms for the production of variations in the wave parameters depend upon the frequency, the propagation medium, and the geometry of the propagation path.

A consideration of the fundamental limitations imposed by rf propagation effects requires focus. An examination of the effects of all possible propagation mechanisms on all possible uses of the radio frequency spectrum at all the allocated frequencies is impossible within the confines of a single lecture. Attention will be given only to propagation through the non-ionized atmosphere at frequencies ranging from 1 to 300 GHz. A range of users will be considered. In many cases, the propagation phenomenon that constrains the design of an rf system for one service provides the basis for another. For instance, attenuation produced by rain scatter will adversely affect centimeter and millimeter wave communication systems but scattering by rain at decimeter and centimeter wavelengths produces the radar echoes used to track severe storms. Rain scatter also can direct unwanted signals to the receiver of another rf system operating at the same frequency thereby producing interference. Interference ultimately limits the number of rf transmission systems that can coexist in a frequency band.

The radio spectrum is a finite resource. The same frequency band may be used for a number of services. For instance, the 92 to 95 GHz band has been allocated to the fixed (terrestrial point-to-point) radiocommunication service, the fixed-satellite (earth-to-space) radiocommunication service, the mobile (terrestrial) radiocommunication service, the radiolocation (radar) service, and the band 93.07 to 93.27 GHz was also allocated to the radio astronomy service for spectral line observations[1]. In the past, the tendency was to preserve a band for a particular service with the expectation that the assignment of frequencies within a band to stations within a geographical area could be accomplished with a minimum of interference and impact on the design of the transmission and modulation techniques used for that service. Currently, the frequency bands are being opened to use by more than one service and numerous applications are being filed for increasing the number of stations of a service in each band and geographical area.

Military radar and communication systems are often designed with the possibility of intentional interference - jamming in mind. General use systems have not been specifically designed to be interference resistant. Reliability is the primary design goal for most systems; adequate frequency assignment procedures are assumed for the

prevention of interference. The optimum use of the frequency spectrum requires a balance between reliability and interference prevention goals together with an assessment of the suitability of a frequency for a particular application. For example, radio astronomical investigations of spectral lines require observations in the near vicinity of the line center frequency whereas communication systems generally work well over a significantly broader frequency range. The allocation and assignment of frequencies to coomunication systems for use within a narrow band containing (or adjacent to) a spectral line may deny radioastronomical observation without significantly improving the performance of the communication system.

Frequency spectrum management and rf system design are constrained by propagation phenomena that affect suitability, reliability, and the possibility of interference. The limitations imposed by rf propagation must be judged in terms of these constraints. Suitability is considered in the discussion of propagation mechanisms in Section 2, reliability is considered in Section 3 and the possibility of interference in Section 4. Section 5 summarizes the limitations. The material presented in this lecture was published by the author in the journal article "Fundamental Limitations Caused by RF Propagation"[3].

2. PROPAGATION MECHANISMS

A number of atmospheric phenomena contribute to the attenuation, phase shift, and angle-of-arrival variations experienced by rf waves in the 1 to 300 GHz frequency range. An atmosphere at rest would produce no variations. It would produce attenuation by molecular gaseous absorption and a bending or propagation direction change for waves not propagating in the zenith or nadir directions by the decrease in refractive index with height. Waves propagating away from a point source in an idealized medium having no spatial variation in the refractive index would have a spherical constant phase surface (wave-front). If, in addition, the idealized medium did not produce an energy loss by gaseous absorption the radiated power per unit surface area (power flux density) would decrease as the square of the distance from the source. The inverse square law range dependence is identified with propagation in free space and is often used as the reference for evaluating the additional attenuation or power loss produced by other propagation mechanisms[4]. For propagation through the monotonically decreasing density and refractive index profile of an atmosphere at rest above the surface of the earth, the amount of ray bending depends only on the elevation angle. The change in bending that occurs as a function of elevation angle produces changes in power flux density relative to the free space values which lead to additional attenuation by focusing.

The atmosphere is not at rest but is in motion on spatial scales ranging from millimeters to thousands of kilometers. Large, synoptic (100 - 1000 km) scale motions produce slow variations in atmospheric density and water vapor concentration which cause variations in attenuation by molecular absorption and by focusing and variations in angle-of-arrival and bending. The molecules that produce absorption are in thermal equilibrium with their environment and in turn emit rf energy. The molecular emission contributes to radio noise which also affects system design.

Smaller cloud (1-10 km) and mesoscale (10-100 km) motions produce vertical lifting and the subsequent cooling of water vapor generates clouds, ice particles, snow and rain. These motions produce more rapid changes in attenuation, phase, and angle-of-arrival. In addition, the hydrometeors both absorb and scatter the rf energy. The scattering can be detected by radar as clutter which interferes with the operation of surveillance and tracking radars or as the desired signal for weather radars. The hydrometeors cause different phases and amplitudes for two orthogonal linearly polarized waves of the same frequency propagating along the same path producing depolarization and possible interference between independent communication channels utilizing the two polarizations. The scattering by hydrometeors also can couple energy from the transmitter of one system to the receiver of a second system operated at the same frequency producing interference.

Still smaller scale turbulent motions (1 mm to 1 km) can produce large gradients in refractive index which will scatter rf energy. Troposcatter communication systems utilize the scattered signals to communicate over long paths to receivers well beyond the radio horizon of the transmitter. High power, coherent radar systems are employed to measure atmospheric winds using Doppler shifted signals scattered from clear air turbulence. The small scale refractive index irregularities also produce the random, rapid amplitude, phase, and angle-of-arrival fluctuations known as scintillation. Fading caused by scintillation limits the reliability of low elevation angle communication paths through the atmosphere. At the same time, the scattering produced by turbulence can couple energy between two systems causing interference.

Internal waves (variations of atmospheric density and velocity) on the mesoscale and widespread vertical motion (subsidence) on the same scale can produce a modulation of the vertical gradients of refractive index caused by radiative cooling and earlier mixing processes which periodically can create extrememem ducting gradients and episodes of atmospheric multipath propagation. When ducting gradients occur, rf energy is trapped within a horizontal layer of limited vertical extent and can propagate over long horizontal paths with little loss[4]. Ducting is a major cause of interference between systems and can produce extended regions of ground clutter (anomalous propagation) which will affect the operation of radar systems. Atmospheric multipath propagation occurs when the strong refractive index gradients direct more than one ray from the transmitter to a receiver. The signals propagated via two or more ray paths differ in phase and

constructivity or destructively interfere with each other producing frequency selective fading which severely limits the reliability of terrestrial point-to-point (radio relay) communication systems.

2.1 Molecular Absorption

Molecular absorption in the 1-300 GHz frequency range is caused primarily by oxygen and water vapor[5]. The oxygen molecule has a permanent magnetic moment and absorption is produced by magnetic interaction with the incident field. The interaction produces a family of rotation absorption lines in the vicinity of 60 GHz and an isolated line at 119 GHz. The water vapor molecule has an electric dipole which interacts with the incident radiation to produce rotation absorption lines at 22.2, 183.3, 324 GHz and a large number of lines at still higher frequencies. The specific attenuation produced by air at standard temperature and pressure (20°C, 101.3 kiloPascal) containing water vapor with 7.5 g/m^3 density is depicted as a function of frequency in Figure 1. The figure presents a model value which includes an empirical correction to the current theoretical values[5] and all the published measurements known to the author[6]. Recent work suggests an improved revision of the empirical correction but no major changes in the relative magnetudes of the attenuation values[7].

An examination of Figure 1 reveals that some frequencies are more useful than others for communication or radar system operation. The frequency regions having high values of specific attenuation are the isolated oxygen and water vapor lines and the complex of oxygen lines. The valleys between the peaks are the window regions that are preferred for rf transmission. The absorption lines are used for passive remote sensing. The regions with high specific attenuation absorb some of the energy propagating through the region and emit equal amounts of energy to remain in thermal equilibrium. The radio noise emitted by an elemental volume of the atmosphere is proportional to the density and kinetic temperature of the molecules in that volume. A radiometer senses the integrated emission and subsequent absorption of radio noise along a path through the atmosphere. The thermal emission at frequencies near the peaks of the water vapor lines is also proprtional to the kinetic temperature and number of the water vapor molecules. Simultaneous measurements of the brightness temperature of the thermal emission at several frequencies may be processed (inverted) to remotely sense temperature and water vapor concentration.

The atmospheric pressure decreases with height, the water vapor density generally decreases with height, and the temperature generally decreases with height to the tropopause separating the lower troposphere from the higher stratosphere. The net result of the variation of temperature, pressure, and water vapor density is a reduction of specific attenuation with increasing height[8,9]. The total attenuation for a zenith path through the entire atmosphere is depicted in Figure 2. Again, the theoretical curve includes an empirical correction which summarizes a number of measurements. In this case, the model curve departs from the measurements in the window region between 200 and 300 GHz. Recent improvements in the empirical model correct the discrepency[7]. The empirical correction accounts for a major deficiency in the current theory for water vapor absorption but has little theoretical justification[10].

The thermal emission observed from above the atmosphere originates from the upper part to a depth corresponding to an attenuation of approximately 10 dB. Passive sensing systems on satellites are able to observe emission from the surface at frequencies below 50 GHz, the top of the atmosphere at the oxygen line peaks near 60 GHz and at intermediate heights for frequencies along a side of the oxygen complex of lines[11]. Remote sensing of temperature and water vapor profiles can be accomplished using both the oxygen lines and the water vapor lines.

Frequency bands near the peaks of the absorption lines may also be useful if a large number of short distance communication systems are required in a small area such as a metropolitan district because the attenuation is high for distances of more than a few kilometers reducing the possibility of interference between paths spaced by 10 or more kilometers. These frequencies are also useful for satellite-to-satellite communication over paths entirely above the atmosphere.

2.2 Refraction

The index of refraction of air is complex. The imaginary component describes the decrease in amplitude produced by molecular absorption, the real component is related to the change in phase velocity of a propagating rf wave produced by the interaction between the molecules and the wave. Refractivity is proportional to the departure of the real part of the index of refraction from unity. It is a function of the temperature, pressure, and water vapor density and it decreases with height. The decrease with height produces a bending of a ray which describes the propagation direction of a wave. The bending is primarily within a vertical plane because the dominant variation in refractivity is with height. Bending in the vertical plane produces elevation angle pointing errors.

The average elevation angle error for propagation through the entire atmosphere at a mid-latitude site is depicted in Figure 3. The model estimates were obtained from averaging a number of ray tracing calculations based upon measurements of profiles of temperature, pressure and water vapor density. The measurements were obtained from high power 1.3 GHz tracking radar observations of spheres in orbit[12]. The elevation angle errors ranged from 10 to 600 millidegrees (mdeg) depending on elevation angle. The uncertainty in the measurement of the average value of the elevation angle error is also depicted in the figure.

The elevation angle errors produced by refraction effects are nearly independent of frequency for frequencies below the 60 GHz oxygen line complex. The refractivity values display anomalous dispersion in the vicinity of each absorption line and decrease slightly as the frequency increases from one window region to the next[13]. To first order, the frequency variations may be neglected and the model values applied for any frequency in the 1 to 300 GHz range.

The elevation angle error varies as the meteorological conditions change along a propagation path. Figure 4 displays the observed variations within time period ranging from five minutes to months. The deviation about the mean values are root mean square (rms) values for several months of observation and approximate the expected day-to-day variations in elevation angle error. The deviation about the correction values are the within-a-day fluctuations observed after correction using local meteorological parameters (measured at the surface). The radar observed deviations were significantly larger than the deviations expected on the basis of ray tracing calculations. The increased uncertainty was produced by refractive index inhomogeneities that vary on time scales of less than a few hours - scales corresponding to the cloud and mesoscale spatial scales. Shorter lived fluctuations produce less uncertainty as illustrated by the beacon observations[14].

The fluctuations in elevation angle error may affect the design of radar and communication systems. Data from monostatic radars (employing a single antenna) designed to track and report the location of airborne targets or satellites can be corrected to reduce the elevation angle measurement errors to the values given in Figure 4 for deviation about correction. Further correction or improvement in metric accuracy can only be obtained by using multiple, spatially separated receiving antennas (a multistatic radar). Refraction effects provide a fundamental limitation to the position measurement accuracy achievable by a monostatic radar system. This limitation applies at all frequencies within the 1 to 300 GHz band and the selection of an optimum frequency is not affected by refraction error.

Communication systems are also affected by refraction errors when the pointing uncertainties approach the beamwidth of the transmit or receive antennas. When the errors are significant relative to a beamwidth an automatic tracking capability must be included in the design of the system.

The differential ray bending that occurs over a narrow range of elevations will produce a redistribution of radiated power that results in an attenuation by focusing. Focusing loss values are typically quite small, being less than 2 dB on average for an elevation angle of less than one degree and a path through the atmosphere[15]. Scintillation produces rapid, random variation in received signal values that generally will exceed the slowly varying focusing loss. Because differential bending causes focusing loss, this propagation effect does not depend on frequency in the 1 to 300 GHz range.

Refractivity variations produce time delay measurement errors as well as angle-of-arrival errors. Except near the absorption lines, the group velocity is identical to the phase velocity for waves propagating through the non-ionized atmosphere. The slowing of the group velocity in the regions of higher refractivity near the surface must be estimated to correct transit time measurements. The naturally occurring variations in refractivity produce velocity uncertainties which manifest themselves as timing or ranging errors. The average range error for a radar system operating through the atmosphere is displayed in Figure 5 [15]. The data plotted in this figure were obtained from ray tracing calculations and the deviations about a correction may be optimistic (compared with Figure 4 which includes both measurements and ray tracing calculations). A limitation in ranging accuracy is evident which is nearly independent of frequency. The ionosphere may also affect ranging at frequencies below about 10 GHz.

Anomalous dispersion near each absorption line peak in characterized by a change of the index of refraction with frequency. The dispersion produces both a difference between the group and phase velocities of the wave and a variation in the width of a short pulse of rf energy transmitted through the region. This dispersion limits the bandwidth of the atmosphere for the transmission of rf energy. The useful bandwidth is quite large, however, being more than 2.5 GHz for transmissions centered on the peak of a strong, isolated absorption line[16] and much wider than that value throughout the window regions of the frequency range. Ionospheric dispersion is a more important limitation to transmission bandwidth at frequencies below 10 GHz.

2.3 Scattering from Hydrometeors

Rain drops, snow flakes, ice cyrstals, hail stones, cloud droplets, and fog droplets are small dielectric scatters. Their sizes range from a few microns (cloud droplets) to a few centimeters (hail stones). For simple particle shape models such as spherical water drops for rain, their scattering properties can be readily calculated; for the more complex shapes actually assumed by water drops, their scattering properties can be approximated only after a long and tedious numerical analysis. The more complex ice and snow crystal shapes, sizes and orientations have not been adequately catalogued and only relatively crude approximations have been attempted for the description of propagation through snow and ice clouds.

For application to the estimation of attenuation effects, the simplest models are adequate[8]. Model calculations of specific attenuation are displayed in Figure 6 for

several rain rates and for two different rain drop size models often encountered in rain effect analyses. The Laws and Parsons distribution has been found to provide the best match to attenuation and radar scattering observations at frequencies below 40 GHz[17] whereas the Marshall and Palmer distribution has been found useful because it has only two parameters which can be readily used to fit or model drop size distribution observations[18]. A major difference between the two distributions is in the relative number of small drops, the difference which produces the departures between the curves evident at frequencies above 40 GHz in Figure 6. Propagation near the surface or in clouds is often accompanied by a number of small droplets which do not fall and contribute to the observed rain rate. These small droplets may shift the attenuation values between the two curves or may produce even more attenuation. The specific attenuation for liquid cloud (or fog) particles is displayed in Figure 7. Both measurements[19] and theoretical calculations are depicted in this figure. Widespread rain produced by mesoscale lifting often contain large areas with rain rates of only a few millimeters per hour (mm/h) and accompanying stratiform cloud. The liquid water in the cloud can produce a higher specific attenuation than the embedded rain at frequencies above 230 GHz (for 2 mm/h rain with a Laws and Parsons drop size distribution and cloud of 0.2 g/m^3, both at a 20°C temperature).

The departure of actual rain drop shapes from the idealized sphere produces a second order correction to the attenuation estimates but is of first order in producing polarization effects[20]. Under most atmospheric conditions, the average drop symmetry axis direction is vertical and the characteristic polarizations are vertical and horizontal. The differences between the attenuation values for the two polarization states is less than the uncertainty produced by differences between the two drop size models for frequencies above 50 GHz.

The specific attenuation values for a small volume of rain and cloud particles display a monotonic increase with frequency throughout the 1 to 300 GHz range although the rain-only curves tend to show a slight decrease with increasing frequency for frequencies above 220 GHz. Because both clouds and rain are formed in regions having high relative humidity and rain falling into regions of low relative humidity will locally increase the humidity by evaporation, a positive correlation exists between the occurrence of attenuation by rain and attenuation by water vapor. At frequencies above 310 GHz or within 10 GHz of the water vapor line at 183 GHz, the increased attenuation produced by the water vapor will often be greater than the attenuation due to rain alone (15% relative humidity change produces more attenuation than rain at a rate less than 2 mm/hr). The combination of rain, cloud size particles and increased water vapor makes the empirical observation of attenuation by rain difficult at the lower rain rates and for frequencies above 100 GHz. Simultaneous observations of rain attenuation at frequencies of 110 and 890 GHz have been reported which showed a significantly higher attenuation at the higher frequency than the currently accepted drop size model(s) could produce[21]. The discrepancy can be due to either the small particles that do not contribute to the rain rate or to additional water vapor.

Radar or communication system design must accomodate the occasional occurrence of rain, cloud, and localized changes in water vapor density. At frequencies below about 6 GHz, rain attenuation is of little consequence except for the rare cases of very high rain rates and of hail. At frequencies between 6 and 200 GHz attenuation by rain may be significant. At frequencies above 200 GHz the affects of clouds and water vapor will be most important.

Attenuation by the commonly occurring frozen particles, ice crystals and snow is of little important at frequencies less than 60 GHz. At higher frequencies, the attenuation becomes more important[17] but little has been done to model or measure the effects. Hail can be an important source of attenuation even at frequencies as low as 1 GHz[22]. Hail occurs only rarely and is generally ignored in the design of communication systems. It occurs sufficiently often, however, to be of importance to aircraft safety and as a source of agricultural loss. Radar systems have been designed specifically for the detection and observation of hail[23].

Hydrometeors scatter sufficient energy to be detected by radars operating through the 1 to 300 GHz frequency range. Because of attenuation by rain, radars used for aircraft surveillance or for weather observations are generally operated at frequencies below 6 GHz. The backscatter cross section per unit volume of a rain target reaches a maximum value between 30 and 90 GHz depending upon the rain rate and drop size distribution model as shown in Figure 8. Due to the significant reduction of the scattered signal by attenuation even within the scattering volume, rain scatter is of significance only at the lower frequencies at high rain rates or at frequencies below about 60 GHz at low rain rates[24].

Scattering by ice can be of more significance at frequencies above 10 GHz because the scattering cross section per unit volume of snow is approximately equal to the scattering cross section per unit volume of the rain which falls below the snow after the snow is melted (Figure 9, the bright band is the region of melting snow) and the snow does not contribute significantly to the attenuation of the scattered signal especially at frequencies below 60 GHz. Observations of the scattering by hydrometeors at 15 GHz over long propagation paths have shown that the dominant propagation mechanism is scattering by ice crystals (high cirrus clouds) which occur without attenuation at lower heights[25].

Scattering by hydrometeors can couple unwanted (interfering signals between rf

transmission systems operating at the same frequency. Coupling can occur whenever the scattering volume is simultaneously visible (within line-of-sight) of the transmitter and receiver antennas although significant effects occur primarily when the scattering volume is within the main lobes of both antenna patterns. Coupling between systems also occur when the transmitter and receiver antennas are within line-of-sight of each other. The received signals are larger (transmission loss is lower) in the latter case, even if coupling is via the far sidelobes of both antenna patterns, if the rain scatter coupling is via the far sidelobes of one of the antennas. Otherwise, rain scatter can dominate over line-of-sight coupling via the far sidelobes depending upon the amount of attenuation simultaneously present in the intervening rain.

Scattering by hydrometeors can also interfere with the operation of surveillance radars. The volume scattering from rain or snow can produce a distributed target that masks the desired target. A number of techniques have been employed to reduce rain clutter. One of the earliest used the polarization properties of spherical water droplets to attempt to reduce the clutter[26]. The backscattered circularly polarized wave from a spherical target is of the opposite polarization sense (orthogonal to) the transmitted wave, hence will be rejected by the receiver system if the same circular polarization sense is used for transmission and reception. In practice, the use of circular polarization did not work as well as expected. The weather signals could only be cancelled by 10 to 25 dB depending on frequency, path length into the region with rain, the intensity of rain and the phase state of the hydrometeors in the scattering volume - ice, water - or a combination of ice and water. The problem was that the hydrometeors were not spheres. The major contribution to the depolarization of the circularly polarized waves propagating through rain was produced by the differential phase shift between the two characteristic linear polarizations.

The depolarization of a wave transmitted through rain or a region of ice crystals having a high degree of symmetry axis alignment affects both radars and communication systems designed to use orthogonal polarizations in the same frequency band to double channel capacity. Depolarization produces interference between the two polarization channels. Considerable effort has been expended in recent years to understand the magnitude of the polarization effects and to provide models for their prediction[27,28]. Optimally aligned linear polarization systems show little depolarization (more than 35 dB separation between channels at a frequency of 19 GHz and an elevation angle of 39°) whereas circularly polarized systems experience the maximum interference between channels (less than 10 dB separation between channels for path attenuations in excess of 30 dB for the same frequency and elevation angle).

2.4 Scattering from Turbulence

Small scale fluctuation in refractivity produced by turbulence cause a scintillation of the parameters, amplitude, phase and angle of arrival, of an rf wave propagating through the turbulent volume. Observations of satellite beacons at low elevation angles always show the fluctuations. Figure 10 depicts the rise of a 7.3 GHz satellite beacon as observed using the large aperture tracking antenna of the Haystack Observatory[14]. The received signal level, pointing angles, and the quadrature components of the tracking error voltages are displayed. Two types of fluctuations are in evidence, the deep, rapid fading and large elevation channel quadrature error voltage variations produced by atmospheric multipath (strong scintillation) and the shallow, rapid fluctuations in signal level and the quieter quadrature error voltages of weak scintillation produced by atmospheric turbulence. The angle-of-arrival excursions are of about the same magnitude in both segments of the record, at apparent elevation angles above and below 2° although the fluctuations are more abrupt during multipath conditions.

Scintillation is a low elevation angle phenomena that occurs on long paths through the lower, more turbulence regions of the atmosphere. Radar observations of backscatter from clear air turbulence reveals that the refractivity fluctuations occur just above the surface and in thin layers at higher heights[29,30]. The thickness of the surface based region may vary from a few tens of meters to several kilometers depending upon the stability of the atmosphere close to the surface. Based on the observed lack of large variations in the magnitude of radar observed levels of clear air turbulence from one location to another, the observed scintillation at one location can be used to model the scintillation to be expected at other locations.

Figures 11 and 12 display the median values of the standard deviations of the logarithm of the received signal and of the elevation angle respectively. The reported standard deviations are for fluctuations about the average value observed within a five-minute interval. The angle-of-arrival fluctuations are non-stationary and the value of the standard deviation depends upon the observation interval (see Figure 4). The measurements were made using a large aperture antenna and suffer from aperture averaging. The effects of aperture averaging can be modeled theoretically as can the frequency dependence of the scintillation[31]. An application of the model for the prediction of amplitude scintillation shows good agreement with observations using different antenna sizes and observing frequencies as shown in Figure 13[32].

For small antennas and low elevation paths through the entire atmosphere, the standard deviation of log amplitude is proportional to the seven twelfths power of the frequency and increases by a factor 28 as the frequency increases from 1 to 300 GHz. The angle-of-arrival fluctuations are independent of frequency. Angle-of-arrival scintillation tends to be more important at the higher frequencies because, for a fixed size aperature, the angle-of-arrival fluctuations increase as a percent of the beamwidth

as the beamwidth decreases. The magnitude of the fluctuations depend upon path length and are less than the values displayed in Figures 11 and 12 at elevation angles below one degree for terrestrial paths.

The refractivity fluctuations which produce scintillation and backscatter from the clear atmosphere also produce the troposcatter fields used for long distance communication[33]. The scattering process is highly anisotropic (in contrast to scattering from hydrometeors which is nearly isotropic)[34]. The bistatic scattering cross section per unit volume is more than seven orders of magnitude larger for a scattering angle of 1° than for backscattering to a monostatic radar (scattering angle of 180°). A 150 km troposcatter path with clear horizons at a 0° elevation angle at each end has a scattering angle of 1° at mid-path. Troposcatter can contribute to interference on long, great circle paths with nearly clear horizons at each end. Empirical procedures for the estimation of troposcatter field strengths have been developed for application at frequencies below about 4 GHz[2]. For higher frequencies, semi-empirical models using turbulence intensity profiles as the basis for the calculation of signal level (as was done for scintillation) have still to be developed.

High power radar systems can be used for the observation of turbulence and for the routine observations of wind profiles by using the Doppler shift of the signals scattered from the turbulence. Radar systems useful for wind observations over a reasonable height range operate at frequencies below 1 GHz[30].

2.5 Atmospheric Multipath

The deep fading which occurred in the satellite beacon observations at elevation angles below 2° displayed in Figure 10 was caused by atmospheric multipath. Atmospheric multipath is produced by local, strong gradients in refractivity which can steer a ray sufficiently to interfere with the direct ray from the transmitter to the receiver. The strong refractivity gradients often occur in relatively thin elevated layers which are 10 to 100 m thick. The layers form in stable regions of the atmosphere and are subject to mechanical perturbations by short period buoyancy (internal) waves[35]. The internal waves produce variations in the tilt of the layers with strong gradients which affect the steering of rays and cause multipath fading on the occasions when the ray geometry and direction change place more than one ray at the receiver. The difference between the angles-of-survival at the receive antenna were small, less than 7 mdeg for the data in Figure 10. The differential time delays between the two rays were also small, less than 0.6 nanoseconds (ns) because as many as four cycles of phase addition and cancellation were observed at 7.3 GHz while little variation in signal level was evident at 0.4 GHz (on a parallel ray path propagating through the same region of high refractivity gradient displaced horizontally by less than .8 km[14]).

Atmospheric multipath also can occasionally produce significant fading on long point-to-point terrestrial links[36]. For terrestrial paths, multipath is important when the strong refracting layer is close to the height of the path endpoints. Observations show fades of more than 40 dB produced by the simultaneous occurrence of two or more ray paths. Observations made using wideband swept frequency techniques (13.5 to 15 GHz) show that the second ray path often had a signal amplitude within 10 dB of the direct and a delay of less than 0.6 ns. A third ray was often evident having an amplitude of more than 30 dB below the direct ray and a time delay of 4 or more ns[37]. Multipath fading with differential time delays ranging from less than a nanosecond to as much as 15 ns will cause within band amplitude and phase distortion effectively limiting the transmission bandwidth if no compensation is attempted. A possible solution to the within band distortion problem is the use of very wide bandwidths and the detection and separation of the signals from each ray path. Vertical antenna diversity can also be employed to mitigate multipath effects since ray path geometries generally do not occur that can simultaneously cause deep fades at two antennas spaced in the vertical.

Atmospheric multipath is important to low elevation angle propagation over long atmospheric paths at frequencies above 1 GHz. Fading is often encountered on slant paths to satellites at elevation angles below 2° because the thin layers with high refractivity gradients are frequently encountered in the lowest few kilometers of the atmosphere. Deep fading is not as common an occurrence on terrestrial paths since the high gradient layer must be closer to the surface to affect the path. Multipath fading tends to be more of a problem at frequencies below 15 GHz than above because of the practice of using shorter links at higher frequencies to combat rain effects. Multipath occurs only when the propagation geometry is correct, a situation encountered more often on longer paths.

Multipath ray paths can also be produced by reflections from the surface or large objects especially when they are near one of the antennas. Surface mutlipath generally does not produce the deep fades associated with atmospheric multipath because the power reflection coefficients of the ground or scattering objects usually are less than unity and are often less than 0.1. The antenna pattern can also be used to mitigate the effects of surface reflection as long as the antennas beamwidth is not made too small to accomodate the angle-of-arrival fluctuations to be expected at low elevation angles.

2.6 Ducting

The layers with refractivity gradients strong enough to redirect a ray incident from below toward the earth are termed ducting layers. Energy steered back to the earth by such a layer can be redicted upwards again by reflection from the surface, by changes

in the refractivity profile below the ducting layer, or by the curvature of the earth in regions with a refractivity gradient near the value expected for an atmosphere at rest (average conditions)[38]. For a horizontally homogeneous atmosphere, the energy will be trapped between the ducting layer and the surface for a surface based duct or between the ducting layer and the lower turning point for an elevated duct. In either case, the propagating wave is confined between two horizontal surfaces (spherical shells concentric with the earth) and can spread only in the horizontal resulting in a field whose power flux density decreases inversely with distance (rather than inversely with the square of the distance as expected in free space). The net result is a wave whose amplitude is increasing relative to free space producing a gain rather than a loss (attenuation).

Atmospheric ducts are not lossless and ducted fields rarely exceed a 30 dB increase above fee space on long propagation paths but are generally lower than free space (have some attenuation relative to free space). Under the appropriate synoptic scale conditions a large area of subsidence can occur which will intensify the refractive index gradients near the surface and produce ducts which can span distances of more than 1000 km[35]. Early radar observations showed relatively low loss propagation over distances of up to 1400 km. Conditions are best for long range duct propagation over warm seas in the tropics. Over land, topography interferes with the formation of long ducts near the surface and the higher elevated layers which form over the terrain are less likely to produce trapping because of the larger decreases of refractivity in the layer relative to the surface value (at station antenna height) needed to cause trapping.

Losses within a duct are caused by surface reflection, by scattering by turbulence especially within the ducting layer, by gaseous absorption and for thin ducts, by the losses associated with each propagating waveguide mode within the duct (lossy modes produce leakage from the duct). For elevated ducts with a ducting layer thickness of 10 m (duct thickness of approximately 30 m), the waveguide mode losses are small compared with the loss by gaseous absorption for frequencies above 4 GHz provided both the transmitter and receiver are embedded in the duct. Thicker ducts support propagation at lower frequencies. Under normal conditions, the antennas will not be immersed in the duct. Energy can be coupled into the duct by diffraction processes, by scattering from turbulence at small scattering angles, and by a tilting of the duct caused by short period gravity waves. A simplified model for duct propagation at frequencies above 4 GHz combines the coupling loss, a gaseous absorption loss within the duct and an inverse distance dependence. At lower frequencies, an additional waveguide mode loss must be included when the duct thickness is as thin as 30 m.

Ducts cannot be relied upon for communication but can provide an efficient means of coupling interfering signals from one rf transmission system to another. Ducting is the source of the extended ground clutter (anomalous propagation) echoes that interfere with the operation of surveillance radars[33].

3. RELIABILITY

The propagation mechanisms described in Section 2 affect the reliability of rf systems. The important effects are summarized in Table 1, itemized by the type of system. The classification is by the characteristics of the system, not the service used for allocation. For the purposes of this table, a communication system is a line-of-sight transmission system used to transmit information. A navigation system is a line-of-sight transmission system providing sufficient information (time delay) to enable position determination, a system used for time standards is a line-of-sight transmission system used for communicating timing information. All three systems suffer from the same propagation phenomena. The importance of the refractive phenomena differ from one system to the other depending upon the accuracy required in the estimation of the delay.

Systems used for radio astronomy are of two general types, radiometer and very long baseline interferometer (VLBI). Both entail line-of-sight transmission from sources outside the atmosphere but timing uncertainties are crucial to VLBI operation. These systems should be classed as line-of-sight systems in analyzing their susceptibility to imparement by propagation phenomena. The frequencies used for observation, however, are defined by the source under investigation. Observations of emission from the absorption lines of a particular interstellar molecule can only be made near the center frequencies of the lines.

Passive remote sensing systems employ radiometers for the detection of the energy emitted from the atmosphere and, for airborne sensors, from the ground. They are susceptible to the problems of line-of-sight paths but, by employing observations at a number of different frequencies, they use the relative amplitudes of the attenuated emissions to infer the structure of the atmosphere and the underlying surface.

Radar systems employed for surveillance and tracking or active remote sensing (radar) systems employed to study the atmosphere or the underlying surfaces are susceptible to the problems of line-of-sight systems for the transmission paths from the transmitter to the scatterer and from the scatterer to the receiver. In addition, turbulence and hydrometeors can produce competing (interfering) targets that can either mask the desired target or be the desired target. The extended ranges to ground clutter which occur under ducting conditions can provide interfering signals which mask the desired targets for radars used for surveillance or for remote sensing.

TABLE 1

FACTORS AFFECTING SYSTEM RELIABILITY

PROPAGATION MECHANISM	COMMUNICATION	RADAR	NAVIGATION	RADAR ASTRONOMY	TIME STANDARDS	PASSIVE REMOTE SENSING (RADIOMETER)	ACTIVE REMOTE SENSING (RADAR)
GASEOUS ABSORPTION	attenuation	attenuation	attenuation	attenuation	attenuation	phenomena sensed	attenuation
REFRACTION	angle-of arrival	pointing errors ranging errors	ranging Doppler	angle-of-arrival time delay	time delay	-	-
HYDROMETEOR SCATTER	attenuation depolarization	attenuation clutter	attenuation	attenuation	attenuation	phenomena sensed	phenomena sensed attenuation
TURBULENT SCATTER	scintillation	-	scintillation	scintillation	scintillation	-	-
MULTIPATH	fading bandwidth	fading	fading bandwidth	-	fading bandwidth	-	-
DUCTING	-	anomalous propagation	-	-	-	-	clutter

The deleterious effects produced by variations in attenuation, angle-of-arrival errors, timing errors, or extended clutter regions are not present all the time but depend on the varying meteorological conditions which affect the propagation path. System designers require probability distribution data for the magnitudes of each of the propagation effects at the frequency, location, and geometry of the propagation paths to decide if a system is feasible and to specify the parameters of the system for reliable operation. A system that was required to perform only 90 percent of the time could be designed without considering the effects of rain; systems that must provide reliable operation for all but a few minutes a year must consider the effects of rainfall. The service reliability of the system must be established before the constraints imposed by propagation effects can be assessed. Conversely, the propagation specialist is required to provide statistical information on each of the phenomena that affect system reliability.

The current state-of-the-art of supplying reliable statistical information to a system designer for application at a geographical location specified by the designer is primative. The atmospheric structures which produce the different propagation effects are known. The occurrence statistics are generally not available.

Phenomena of importance at small percentages of the year corresponding say to 5 to 10 minutes per year are produced by a limited number of rare events. Severe rain events are local in nature, spanning distances of only a few kilometers and have lifetimes measured in tens of minutes[39]. At typical cell translation velocities, a severe cell will affect a line-of-sight path for between 5 and 20 minutes. The rain attenuation exceeded for 5 to 10 minutes per year is usually produced by a single cell. Statistics on the occurrences of such cells take more than 10 years to amass at a single location to provide an estimate of the attenuation with less than a 10 percent standard error of estimate[17]. Observations sufficient to compile statistics with less than a 10 percent standard error of estimate are available at a relatively small number of locations. In the absence of such data models are required to extend valid data to other regions[40]. Even after the prediction of the expected value of attenuation for a rare event, the observed value for any one year will vary considerably about the expected value. Figure 14 illustrates the year-to-year variation of the attenuation statistics for a single path[41]. The magnitude of the variability is predictable but the value for any one year cannot be established apriori. This basic uncertainty in the values to be observed in any one year is fundamental to propagation phenomena.

Similarly, the received signal level or angle-of-arrival cannot be established apriori with uncertainties less than the rms values displayed in Figures 11 and 12 for transmission through the atmosphere. These uncertainties are fundamental to the metric accuracy of radar systems. Figure 3 displayed the rms fluctuations in angle-of-arrival observed within measurement intervals of different lengths. The variation observed about the mean value has to be accomodated if no correction system is applied. The variation

about the correction is the best that can be accomplished on the basis of meteorological data readily available at the radar site.

The attenuation by gaseous absorption also can vary along a transmission path. Figure 15 displays the variation expected for attenuation for a vertical (zenith) path through the atmosphere. Both the expected variation about the mean value and the expected variation about an attenuation estimate based on surface meteorological data are displayed. The curves are for observations anywhere on the globe; some reduction in variance can be accomplished if application is for a specific location.

Transmission systems must be designed to accomodate the maximum attenuations expected for a specified service probability. Fading caused by multipath or by rain attenuation can exceed the margin allowed by available system components and alternative schemes to the brute force procedure of increasing transmitter power, reducing receiver noise, or reducing receiver bandwidth are required. Since multipath fading is critically dependent on path geometry, antenna or path diversity can be used to reduce the margin requirements on a single path. The localized nature of severe rain invites the use of path diversity with spacings between the paths of several cell diameters. In the latter case, path diversity means the introduction of a number of independent propagation paths which can significantly increase system cost.

4. INTERFERENCE

The propagation phenomena considered in Section 3 affect the reliability of rf transmission systems when operated with no other users in the frequency band. Whenever two different users operate separate systems at the same frequency, the potential for interference exists. The propagation mechanisms contributing to interference at frequencies in the 1 to 300 GHz range are terrain diffraction, hydrometeor scatter, turbulent scatter, and ducting. Ducting has the potential of producing the highest field strengths when the conditions are right for the formation of a ducting layer at the correct geometry to provide efficient coupling. Terrain diffraction and scattering by turbulence produce the lower level fields which are present most of the time. Scattering by hydrometeors may be important at time percentages less than 1 to 5 percent of the year depending upon frequency and location. Ducting may be important for more than 50 percent of the time in some areas of the tropics.

The possibility of coupling energy from one system to another limits the number of systems that can coexist in the same frequency band. The extent of the limitation depends upon the shielding provided by the terrain in reducing coupling via ducting or troposcatter and on the susceptibility of one system to the signals produced by another. The propagation mechanisms contributing to the possibility of interference are frequency dependent. In general, the increased attenuation due to gaseous absorption which obtains at higher frequencies; frequencies above 20 GHz tend to reduce the importance of interference on long paths relative to interference at lower frequencies. At frequencies corresponding to the stronger absorption regions (Figure 1) the separations between non-interfering systems operating at the same frequency can be quite small.

The conditions which lead to the possibility of interference level fields can persist for periods ranging from tens of minutes to hours. The intense rain cells which are important contributions to scattered fields especially at frequencies suffering little attenuation by rain, frequencies below 10 GHz, last for only a few tens of minutes. The conditions producing ducting last for hours. Although interference can be a rare event, when it occurs it will last for some time.

The occurrence of high level, beyond the radiohorizon fields during a two-week period in August 1966 for a 175 km path along the New Jersey coast are depicted in Figure 16. These data were obtained at a frequency of 5 GHz during the POPSI experiment[42] one antenna pointed at an elevation of 1/2° along the great circle between the transmittter and receiver and the other pointed at an elevation angle of 2° and 3° off the great circle path in azimuth. The occurrence of ducting conditions was established from an analysis of weather radar data from a radar near the midpoint of the path. Coupling was via a sidelobe of the antenna pointed off-path. The low level fields were produced by scattering from turbulence (fields occurring roughly 50 percent of the time for the weather conditions experienced on the path). For this path which was designed to simulate the coupling between radio relay and satellite communication systems when the radio relay transmitter was pointed toward the earth station. Interference would have been produced by signals having attenuations relative to free space less than 91 dB.

5. LIMITATIONS BY PROPAGATION

Atmospheric propagation phenomena affect radio frequency propagation in the 1 to 300 GHz range. Several types of limitations have been presented. One is the suitability of different frequency bands for rf transmission. Long propagation paths are not possible at frequencies corresponding to the peaks of the absorption spectrum at 50 GHz and higher frequencies. The specific attenuation is too high to be combatted by system design. The frequency windows between the peaks are useful for transmission systems. The emission produced by the absorbing gases is, however, useful for sensing the structure of the atmosphere using the frequencies inappropriate for transmission systems. A complete passive survey of the structure of the atmosphere and the underlying terrain from a satellite requires the use of frequencies that can sense the surface through the atmosphere. Therefore, both the earth exploration service and the fixed-satellite service require frequencies with low loss.

The properties of the atmosphere vary on a wide range of spatial and temporal scales. The average properties of the larger scale motions are accessible to measurement and useful for the estimation of the magnitudes of the separate propagation phenomena. The smaller scale variations produce a component of the propagation effect that cannot be estimated in advance and cannot be compensated. The second type of limitation is the essential variability of the phenomena. Systems must be designed to operate over a wide range of atmospheric conditions and to fail during the rare events that are bound to occur. Conversely, for a given system design a measurement accuracy or transmission reliability level exists which cannot be improved.

The fundamental limitation imposed by propagation phenomena is the inadvertent coupling between systems operating in the same or different services. The chance of interference must be considered as a factor affecting the reliability of the system. Interference depends both on the atmosphere and on other systems. When the density of systems using the same frequency band is high, interference is likely. The chance of interference limits the number of users within or among the services that can operate in a geographical area within the same band.

6. REFERENCES

1. Final Acts of the World Administrative Radio Conference, Geneva, 1979, Book I of IV, Terminology, Technical Provisions, and Frequency Allocations, International Telecommunications Union, Geneva, (1979).

2. Recommendations and Reports of the CCIR, Volume V, Propagation in Non-Ionized Media, and Volume VI, Propagation in Ionized Media, International Telecommunications Union, Geneva, (1982).

3. Crane, R.K. "Fundamental Limitations Caused by RF Propagation", Proc. IEEE, 69:196-209, (1981).

4. Kerr, D.E. Propagation of Short Radio Waves, Rad. Lab. Series, Vol. 13, McGraw-Hill, (1951).

5. Waters, J.W. "Absorption and Emission by Atmospheric Gases" in Methods of Experimental Physics, Vol. 12B, Ch. 2.3 (M.L. Meeks, ed.), Academic Press, New York, (1976).

6. Crane, R.K. "Attenuation Estimates for the Millimeter Wave Windows Near 94, 140 and 220 GHz", ERT Doc. No. P-A502, Environmental Research & Technology, Inc.,Concord, MA, (1980).

7. Zammit, C.C., R.E. Hill and R.W. Barker "Atmospheric Emission and Attenuation in the Range 100 to 600 GHz Measures from a Mountain Site", Inter. Jour. Infrared and Millimeter Waves, 3:189-203, (1982).

8. Crane, R.K. "Propagation Phenomena Affecting Satellite Communication Systems Operating in the Centimeter and Millimter Wavelength Bands", Proc. IEEE, 59:173-188, (1971).

9. Liebe, H.J. and G.G. Gimmestad "Calculation of Clear Air EHF Refractivity", Radio Sci., 13:245-251, (1978).

10. Liebe, H.J. "Atmospheric EHF Window Transparencies Near 35, 90, 140 and 220 GHz", Submitted to IEEE Trans. Antennas and Propagation, (1982).

11. Staelin, D.H. "Passive Remote Sensing at Microwave Wavelengths", Proc. IEEE, 57:427-439, (1969).

12. Crane, R.K. "Analysis of Tropospheric Effects at Low Elevation Angles", RADC-TR-78-252, Rome Air Development Center, Griffiss Air Force Base, New York, (1978).

13. Liebe, H.J. and W.M. Welch "Molecular Attenuation and Phase Dispersion between 40 and 140 GHz for Path Models from Different Altitudes", OT Repot 73-10, Office of Telecommunications, U.S. Dept. of Commerce, (1973).

14. Crane, R.K. "Low Elevation Angle Measurement Limitations Imposed by the Troposphere: An Analysis of Scintillation Observations made at Haystack and Millstone", Tech. Rept. 518, MIT Lincoln Laboratory, Lexington, MA, (1976).

15. Crane, R.K. "Refraction Effects in the Neutral Atmosphere", in Methods of Experimental Physics, Vol. 12B, Ch. 2.5 (M.L. Meeks, ed.), Academic Press, New York, (1976).

16. Glutsyuk, L.I. Sharapov and I.K. Vohser "Distortion of Short Electromagnetic Pulses Propagation at the Frequencies of Atmospheric Oxygen Absorption Lines", Proc. URSI Comm. F Open Symposium, Labaule, France, Centre National d'Etudes des Telecommunications, Paris, pp. 637-642, (1977).

17. Crane, R.K. "Prediction of the Effects of Rain on Satellite Communication Systems", Proc. IEEE, 65:456-474, (1977).

18. Waldvogel, A. "Uber den No-Sprung von Tropfenspektrun", W.M., No. 68, Laboratorium fur Atmospharenphysik ETH, Zurich, (1972).

19. Basharinov, A.E. and B.G. Kutuza "Millimeter and Centimeter Radiofrequency Radiation and Absorption of Cloudy Atmospheres" in Transfer of Microwave Radiation in the Atmosphere (K.S. Shipriu, ed.), Trudy No. 222, Mari Geophysical Observatory (USSR), trans. by Israel Program for Scientific Translations, Jerusalem, (1970).

20. Fedi, F. "Attenuation due to Rain on a Terrestrial Path", Alta Frequenza, 48:61E-78E, (1979).

21. Llewllyn-Jones, D.T. and A.M. Zavody "Rainfall Attenuation at 110 and 890 GHz", Electr. Letters,7:320-322, (1971).

22. Herman, B.M. and L.J. Battan "Calculations of the Total Attenuation and Angular Scatter of Ice Spheres", Proc. 9th Weather Radar Conf., Amer. Meteorl. Soc., Boston, pp. 259-265, (1961).

23. Eccles, P.J. and D. Atlas "A Dual Wavelength Radar Hail Detector", Tech., Rept. 14, Laboratory for Atmospheric Probing, Univ. of Chicago, Chicago, (1970).

24. Crane, R.K. "Bistatic Scatter from Rain", IEEE Trans. Antennas and Propagat., AP-22:312-320, (1974).

25. Olsen, R.L. and W.H.W. Lammers "Bistatic Radar Measurements of Ice-Cloud Reflectivities in the Upper Troposphere", Electr. Letters, 14, 7, (1978).

26. Nathanson, R.E. Radar Design Principles, McGraw-Hill, (1969).

27. Cox, D.C. "Depolarization of Radio Waves by Atmospheric Hydrometeors in Earth-Space Paths: A Review", Radio Sci. 16:781-812, (1981).

28. Olsen, R.L. "Cross Polarization during Precipitation on Terrestrial Units: A Review", Radio Sci. 16:761-779, (1981).

29. Crane, R.K. "Radar Measurements of Wind at Kwajalein", Radio Sci., 15:383-394, (1980).

30. Crane, R.K. "A Review of Radar Observations of Turbulence in the Lower Stratosphere", Radio Sci., 15:177-193, (1980).

31. Tatarski, V.I. Wave Propagation in a Turbulent Atmosphere, Nanka, Moskow [Englished Trans. The Effects of the Turbulent Atmosphere on Wave Propagation, NTIS, Springfield, Virg., (1971)].

32. Crane, R.K. and D.W. Blood "Handbook for the Estimation of Microwave Propagation Effects - Link Calculations for Earth-Space Paths (Path Loss and Noise Estimation)", Tech. Rept. No. 1, ERT Doc. No. P-7376-TR1, Environmental Research & Technology, Inc., Concord, MA, (1979).

33. Crane, R.K. "A Review of Transhorizon Propagation Phenomena", Radio Sci., 16:649-669, (1981).

34. Crane, R.K. "Analysis of Data from the Avon-to-Westford Experiment", Tech. Rept. 498, MIT Lincoln Laboratory, Lexington, MA, (1973).

35. Gossard, E.E. "Clear Weather Meteorological Effects on Propagation at Frequencies Above 1 GHz", Radio Sci. 16:589-608, (1981).

36. Stephansen, E.T. "Clear-Air Propagation on Line-of-Sight Radio Paths - A Review", Radio Sci. 16:609-629, (1981).

37. Sandberg, J. "Multipath Parameters and Multipath Propagation Related to PSK Modulation", Report LD-34 (2 Parts), Electromagnetics Institute, Technical University of Denmark, Lyngby, (1978).

38. Dougherty, H.T. and B.A. Hart "Recent Progress in Duct Propagation Predictions", IEEE Trans. Antennas and Propagat., AP-27:542-548, (1979).

39. Crane, R.K. "Automatic Cell Detection and Tracking", IEEE Trans. Geoscience Electro., GE-17:250-262, (1979).

40. Crane, R.K. "Prediction of Attenuation by Rain", IEEE Trans. Comm. COM-28:1717-1733, (1980).

41. Ippolito, L.J. "Radio Propagation for Space Communication Systems", Proc. IEEE, 69:697-727, (1981).

42. Carey, R.B. and G.S. Kalagian "Detailed Analysis of Precipitation Data, FCC/USAF POPSI Project", No. R-7003, Research Division, Federal Communications Commission, (1970).

43. Crane, R.K. and H.J. Burke "The Evaluation of Models for Atmospheric Attenuation and Backscatter Characteristic Estimation at 95 GHz", ERT Doc. No. P-3606, Environmental Research & Technology, Inc., Concord, MA, (1978).

44. Crane, R.K. "Evaluation of Uncertainties in the Estimation of Hydrometeor Mass Concentrations Using Spandar Data and Aircraft Measurements", Sci. Report No. 1, Environmental Research & Technology, Inc., (1978).

45. Baxter, R.A. and D.B. Hodge "Spectral Characteristics of Earth-Space Paths at 2 and 30 GHz", Tech. Rept. 784299-7, Ohio State University, ESL, (1978).

46. Hodge, D.M. Theobold and R.C. Taylor "ATS-6 Millimeter Wavelength Propagation Experiment", Report 3863-3, Ohio State University, ESL, (1976).

7. LIST OF ILLUSTRATIONS

Figure	Title
1	Specific attenuation by atmospheric gases at a pressure of one atmosphere, 20°C temperature and 7.5 g/m^3 water vapor density (6).
2	Zenith attenuation through the atmosphere at mid-latitudes for surface conditions of 20°C temperature and 7.5 g/m^3 water vapor density (6).
3	Elevation angle errors observed at mid-latitude (12).
4	Variations in elevation angle observed at mid-latitude (12).
5	Range error and variations in range error calculated for a mid-latitude location (15).
6	Specific attenuation for rain calculated for two model drop size distributions (43).
7	Specific attenuation for fog and cloud particles with 0.1 g/m^3 liquid water content (6).
8	Backscatter cross section per unit volume for two model drop size distributions (43).
9	Reflectivity profile from Wallops Island, VA, December 15, 1976, obtained at a range of 75 km (44).
10	Satellite beacon observations during the rise of one of the IDCSP satellites (14).
11	Standard deviation of the fluctuations in received power within a five-minute interval observed at a mid-latitude site using a large aperture antenna (14).
12	Standard deviation of the fluctuation in elevation angle within a five-minute interval observed at a mid-latitude site (14).
13	Signal variance normalized by the average power observed at three frequencies (45, 46) compared with model predictions (32).
14	Attenuation statistics for three separate years of observations at 11.7 GHz near Washington, D.C. (41) compared with model prediction (32).
15	Variations in zenith attenuation (32).
16	Received signal level statistics for a 175 km transhorizon path along the New Jersey shore (33, 42).

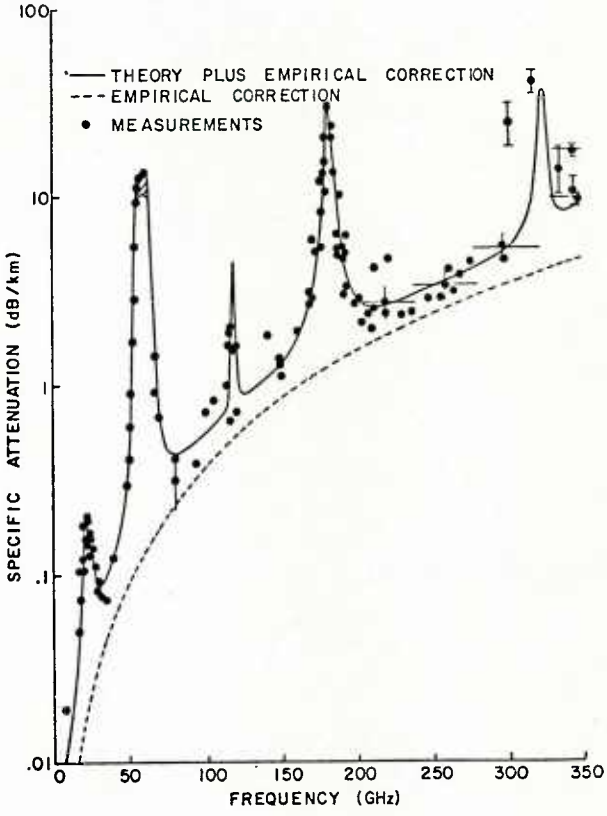

FIGURE 1.

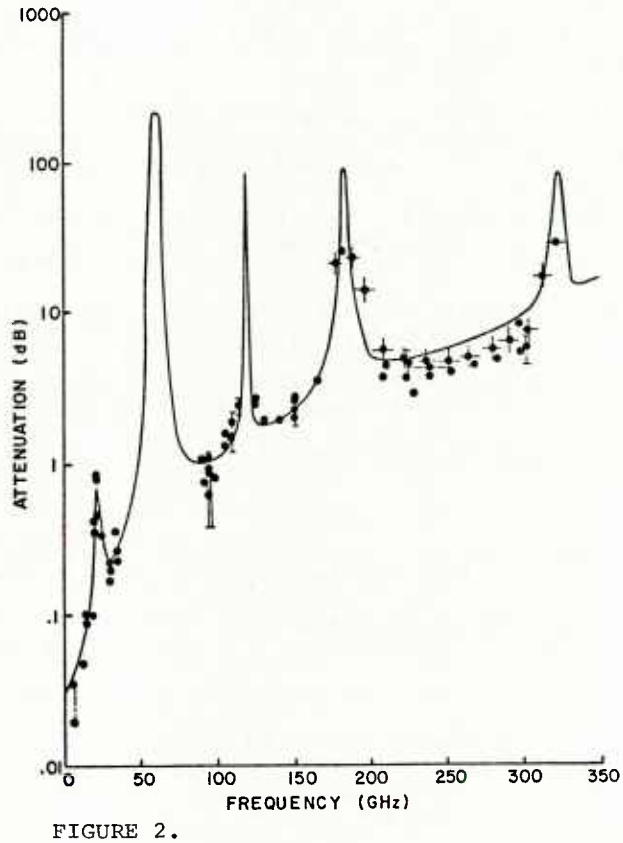

FIGURE 2.

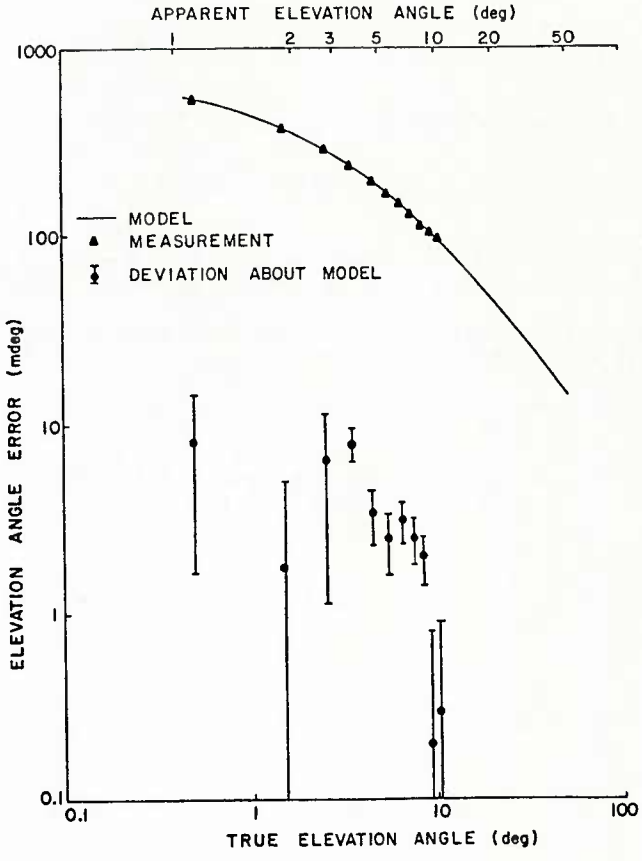

FIGURE 3.

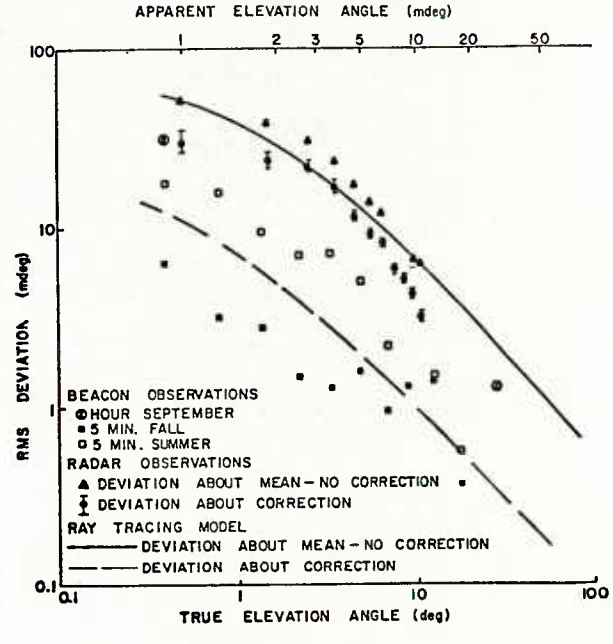

FIGURE 4.

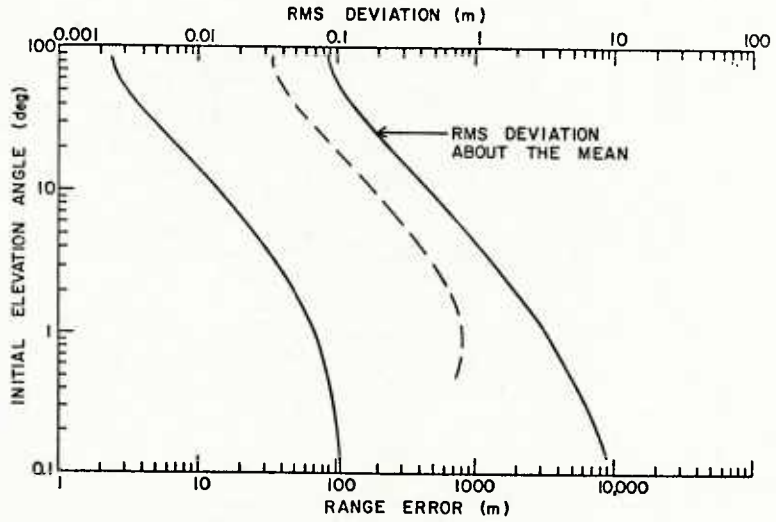

FIGURE 5.

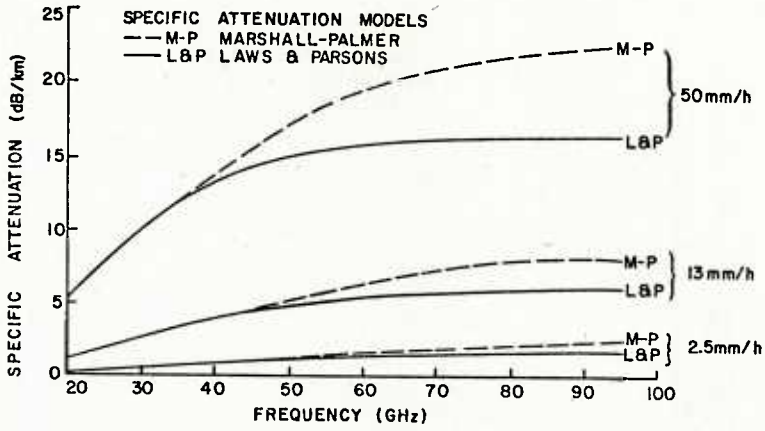

FIGURE 6.

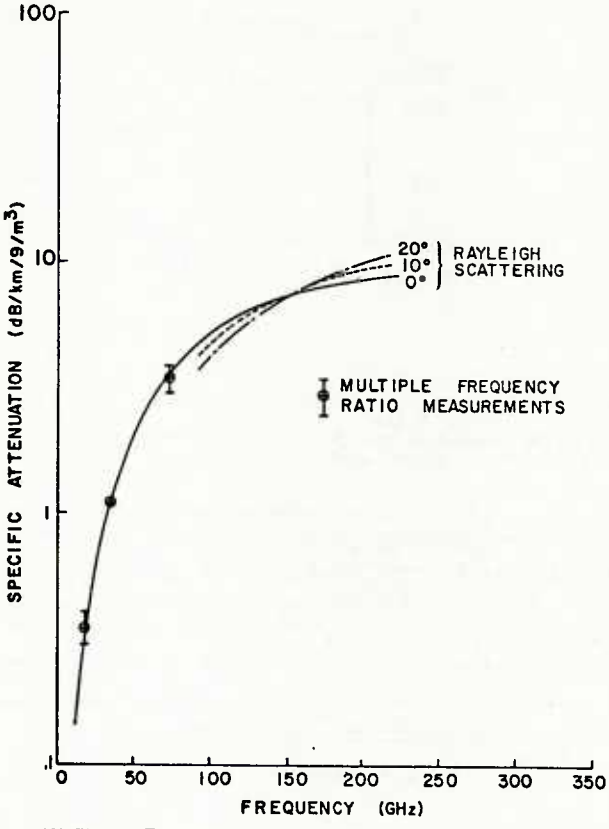

FIGURE 7.

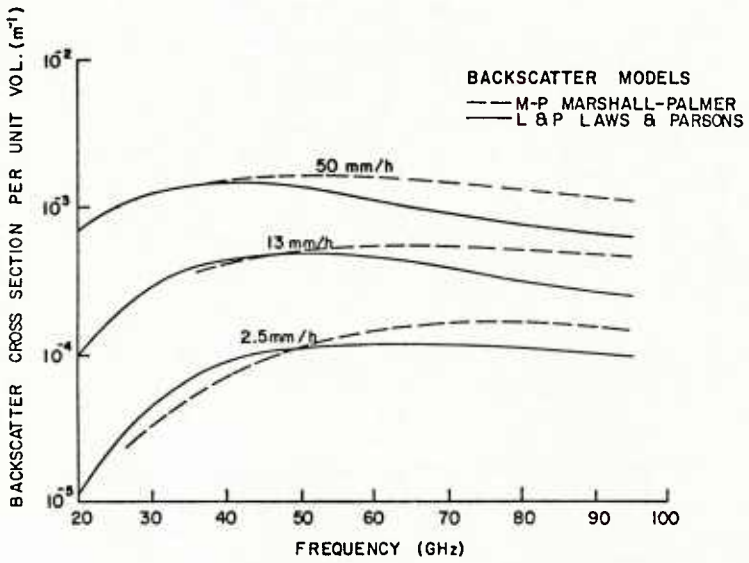

FIGURE 8.

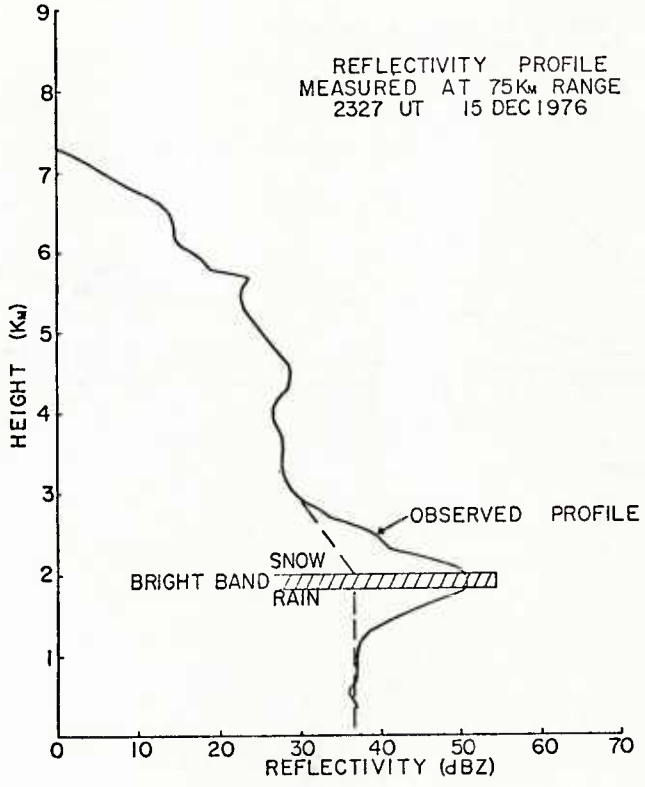

FIGURE 9.

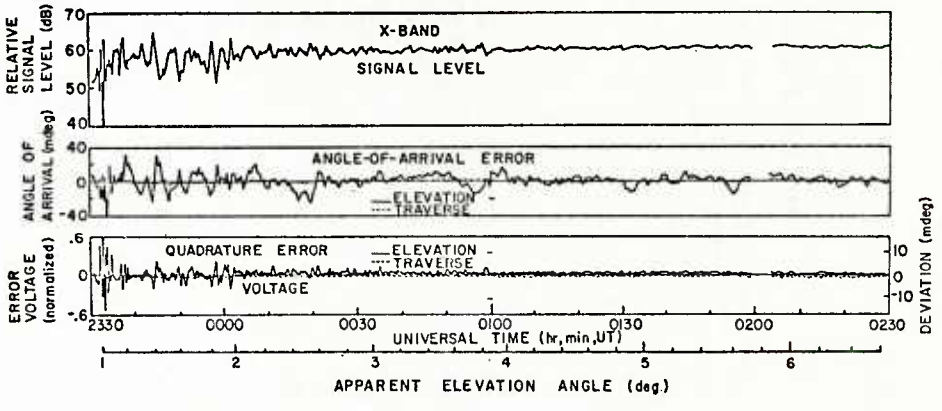

FIGURE 10.

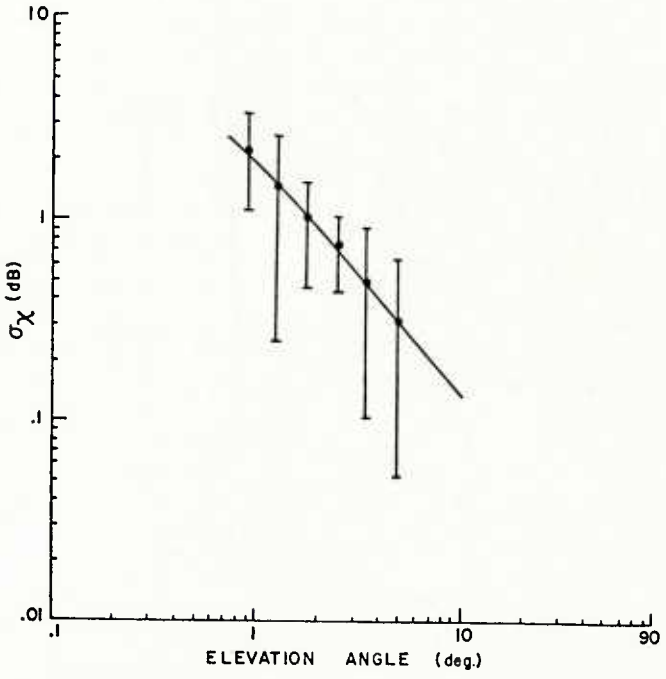

FIGURE 11.

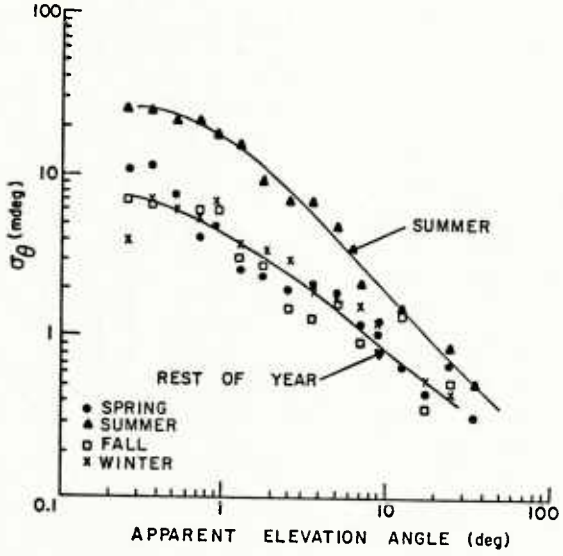

FIGURE 12.

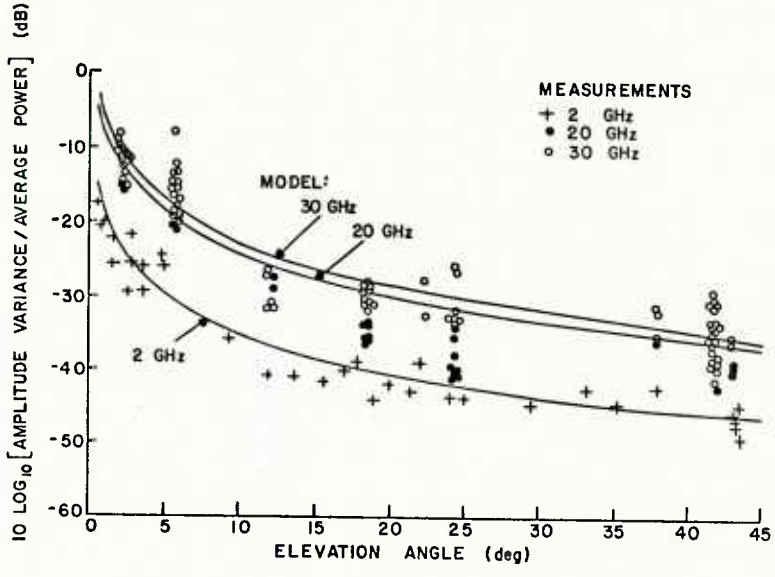

FIGURE 13.

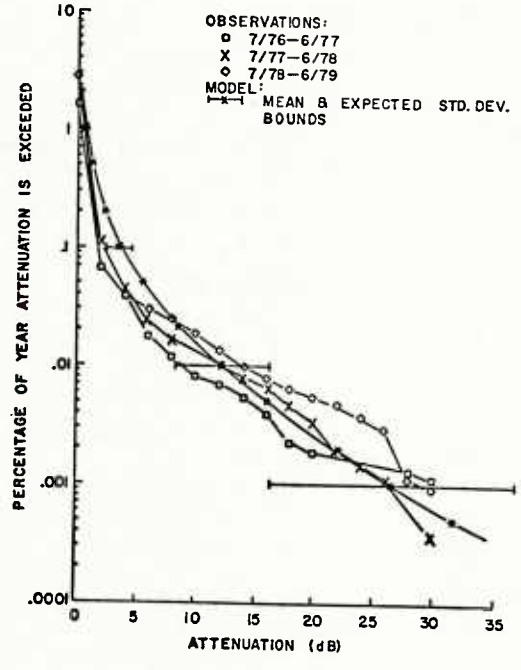

FIGURE 14.

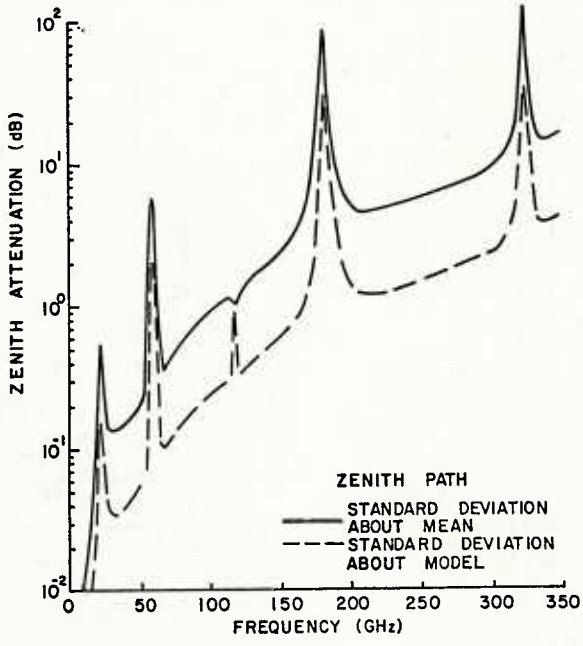

FIGURE 15.

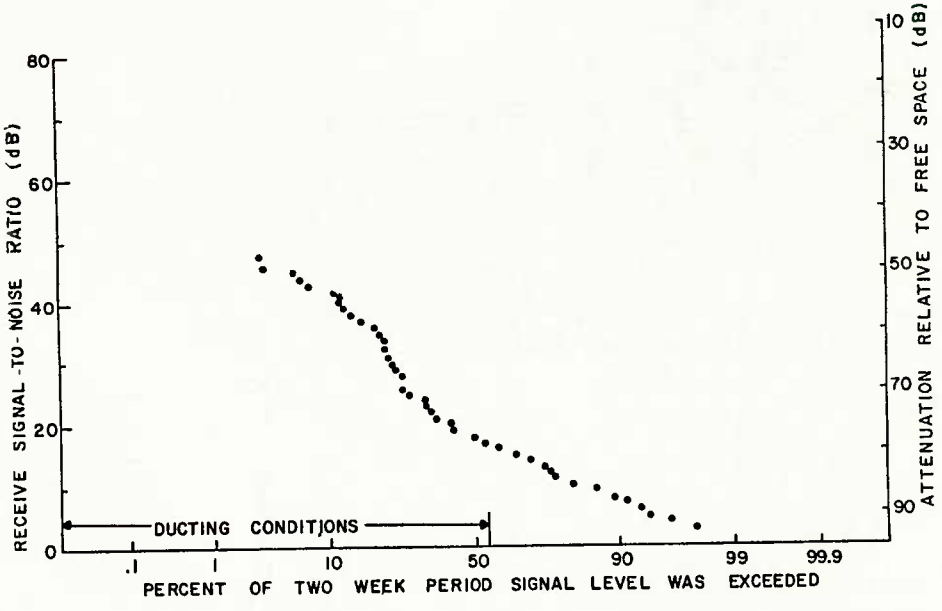

FIGURE 16.

DISCUSSION

J.Aarons, US

There are ionospheric fading problems in the equatorial region within ±20° of the magnetic equator. There are serious fades at L Band (1.4—1.6 GHz) which should be brought to the attention of the group.

Author's Reply

Yes – I have concentrated only on the effects of the troposphere but the ionosphere can affect propagation through induced scintillations and dispersion at frequencies up to perhaps 8 GHz.

R.Howell, UK

Dr Crane, you mentioned the effect of electrical fields on high altitude ice crystals and snow. Have you observed any abrupt changes in radar reflectivity during thunderstorms which can be attributed to rapid changes in electric field?

Author's Reply

I have not but Hendry and McCormick of the National Research Council, Ottawa, Canada have observed rapid changes in the orientation of ice particles which they attribute to rapid changes in the electric field.

E.Vilar, UK

You have shown in Figure 14 an example of cumulative distribution of attenuation A due to (mainly) precipitation. This kind of statistics is now widely used and carry the "rubber stamp" of the location. However, I cannot help to think that surely what matters is a joint statistics of A and duration τ; that is, determine the joint probability that having exceeded A(dB), that attenuation may or may not be exceeded for a specified duration τ. Could you please comment on the requirement of a joint statistics p(A, τ) and in your opinion how to attempt to tackle this problem which is likely to be more relevant to civil telecommunications than to defense?

Author's Reply

I agree that the distribution of outage duration for a given level of attenuation should be of importance to a system designer. Only a few organizations have made the effort to measure the outage time distribution (COMSAT for instance) suggesting that the problem is not as important as some of us think it should be.

SOME PROPAGATIONAL ASPECTS OF FREQUENCY ALLOCATION AND FREQUENCY SHARING

by
H. T. Dougherty
International Vice-Chairman
CCIR Study Group 5
and
Charles M. Rush
Acting Chief, Applied Electromagnetic Science Division
Institute for Telecommunication Sciences
National Telecommunications and Information Administration
U.S. Department of Commerce
Boulder, Colorado 80303
United States of America

SUMMARY

The propagation phenomena of importance to the allocation and sharing of frequency bands are briefly summarized. Those aspects most significant for the various frequency bands are highlighted, illustrated, and referenced. Systems normally achieve their required grade of telecommunications service (service fields) by reliance upon standard modes of electromagnetic propagation. However, both standard modes (so-called) and anomalous modes of propagation must be considered when describing interference phenomena (interference fields). Further, these standard modes are described for any specific service as tending to be stable (relatively) and predictable. The anomalous modes, however, are described as involving some degree of uncertainty; they tend to be less stable and less predictable either in their occurrence or propagational characteristics. This dichotomy, standard/anomalous, can involve different selections across the spectrum and with various services. Hence, for interference fields, the categorization is described herein as essentially by geometry. That is, interference situations are terrestrial, earth-to-space, or space-to-space propagational situations.

1. INTRODUCTION

The telecommunications system planners need answers to the following questions:

(a) What frequency bands are most suitable, from the aspect of radio propagation, for various services?

(b) How do propagation factors affect the practicability of frequency sharing between services?

The necessary propagation data to answer these questions can be assembled under two headings. The first heading, RELIABILITY, addresses question (a) above, where system performance is limited by natural phenomena (terrain, the ionized or gaseous atmosphere, noise, etc.), and the propagation modes of interest are those effective for high percentages of the time (90 percent, 99 percent, and 99.9 percent or 99.99 percent for high reliability services). The second heading, FREQUENCY SHARING AND INTERFERENCE, addresses question (b), where sharing is limited by interference from unusually strong signals. These strong signals are associated with modes of propagation effective for small percentages of the time (10 percent, 1 percent, 0.1 percent, or 0.01 percent of the time). These concepts are illustrated in Figure 1. We note, for example, that the systems design engineer is concerned with the choice of parameters that achieve the required service. This implies a minimum acceptable signal that is achieved for at least some specified percentage of the time; a minimum level expected for 99 percent of the time is illustrated (at S for "Service") in Figure 1. On the other hand, the spectrum manager is concerned more with the unusually strong signals that might be a source of interference to another system (operating in the same service or that of another co-channel service). This is also illustrated in Figure 1 at a 1 percent level (at I for "Interference").

This introduction has defined the dichotomy of concern (service and interference) when radio wave propagation is applied to system planning. Section 2. identifies the propagation phenomena of importance to the allocation and sharing of frequency bands. Section 3. deals with the propagational aspects of frequency allocation (service reliability) for terrestrial and for space services. Section 4. deals with the propagation factors relating to the possibilities of frequency sharing.

2. PROPAGATION PHENOMENA

This section briefly identifies the variety of radio-wave propagation phenomena of importance to the allocation and sharing of frequency bands. Expressions or curves for their quantitative evaluation are contained in the referenced CCIR texts.

2.1 Ground Wave and Diffraction

Two closely related modes of propagation, ground wave and diffraction, are of interest over most of the allocated radio spectrum (10 kHz to 300 GHz). They are illustrated in Figure 2. At VLF (3 to 30 kHz), transmitted signals, guided by the earth's surface travel efficiently to large distances. At increasing frequencies, the LF (30 to 300 kHz), MF (300 to 3000 kHz), and HF (3 to 30 MHz) ground

waves are restricted more closely to the surface of the earth as they propagate with increasing losses to decreasing maximum ranges beyond the horizon. At VHF (30 to 300 MHz) and higher frequencies, the ground wave is severely attenuated, and the most efficient terrestrial mode is via direct radio line-of-sight (LOS) paths that are relatively remote (in terms of wavelength) from the surface. In Figure 2, note the VHF terminals at 0 and 50 km, with LOS segments from 0 to 25 km and from 35 to 50 km. From 25 to 35 km, the VHF signal travels by ground wave between the horizons of the two terminals.

2.2 Ionospheric Propagation

From approximately 60 to 400 km above the earth's surface, the ionized atmosphere (ionosphere) is arrayed in regions of generally increasing electron density that may reflect radio waves at frequencies sometimes up to 100 MHz. Figure 3 illustrates how reflection occurs at higher and higher elevation, for higher and higher transmission frequencies, until the waves penetrate the ionosphere. This reflecting condition permits a variety of sky-wave modes sufficiently stable to provide reliable service fields, as illustrated by the solid-line ray paths in Figure 4.

At VLF the ionosphere can support propagation of radio signals to very large distances (thousands of km) with little attenuation (2–4 dB/megameter). In the LF range, radio signals do not propagate to as long a distance, particularly during the daytime. Marked differences in signal strengths are observed between day and night because of the enhanced daytime absorption by the lower ionosphere. The stability of VLF/LF signals tends to be greater during the daytime than at night, however. Radio signals at MF are heavily absorbed by the ionosphere during the daytime, and any ionospherically reflected signal is so weak compared to the ground wave that it is generally of little consequence to the performance of radio systems. Propagation of MF waves by reflection from the ionosphere is important during the nighttime hours and can provide coverage out to thousands of miles. At HF, the ionospherically reflected sky wave provides the basis for long-distance radio communication and surveillance systems during both daytime and nighttime. In addition to the normal modes of propagation associated with ionospheric reflection, propagation modes can result that are nonstandard or anomalous. Scatter of radio waves from meteor trails, sporadic-E layers, or irregularities in the electron density at upper ionospheric heights are possible. Further, the structure of the ionosphere can give rise to substantial off-the-great-circle propagation and to trapping of radio energy between ionosphere layers (ducting) over great distances.

2.3 Transionospheric Propagation

At VHF and above, a radio signal transmitted along an earth-space path normally penetrates the ionosphere. However the signal is affected by irregularities in the electron density as well as by the path-integrated electron density. The effects generally decrease with increasing frequency and increasing elevation angle.

Scintillations are produced as the radio signal propagates through electron density irregularities and occur as variations in the amplitude, phase, polarization, and direction-of-arrival of the radio signal. These scintillations may represent practical limitations to space communication systems. They have been observed at frequencies up to 7 GHz, primarily as a nighttime phenomenon which tends to maximize near the geomagnetic equator and at high latitudes.

Radio signals at VHF and higher frequencies tend to suffer little absorption as they pass through the ionosphere, except perhaps during severe magnetic disturbances. However such signals are slowed down and refracted by an amount that depends upon the path-integrated electron density. The path-integrated electron density can affect the accuracy of satellite navigation systems, cause signal-frequency shifts, introduce dispersion of signals, and can cause rotation of the plane of polarization.

2.4 Tropospheric Propagation

Above about 30 MHz, the dominant modes of propagation sufficiently stable for service fields depend very much upon the path geometry. Figure 5 illustrates three categories of these as solid-line ray paths. The first is line-of-sight ("space-wave") propagation, either on paths directed toward airborne and space terminals or on paths between terrestrial stations, but remote (in terms of wavelength) from most of the intervening terrain. The second is diffraction propagation on slightly transhorizon paths, with ground wave propagation only between horizons. The third is tropospheric forward scatter (troposcatter) on longer transhorizon paths.

Infrequent atmospheric conditions permit the occurrence of anomalous modes of tropospheric propagation. Some of these are illustrated by the dashed-line ray paths of Figure 5; they are generally insufficiently stable (persistent and predictable) to provide tropospheric service fields, but could cause severe interference to other co-channel services. For example, ducts (by the guiding of radio waves) and rainfall (by the scattering of radio waves) can provide relatively strong signals to well beyond the horizon.

2.5 Absorption and Attenuation by the Gaseous Atmosphere

Figure 6 shows the specific attenuations (dB/km) expected for terrestrial paths due to various constituents of the atmosphere at sea level. The total attenuation (in decibels)

would be proportional to the actual radio-wave path length through the ubiquitous gaseous atmosphere and through the occasional fog or rain. Note the transmission windows (of low attenuation) in Figure 6 that occur in the absence of rain and fog or clouds.

2.6 Hydrometeoric Effects at SHF (3 to 30 GHz) and EHF (30 to 300 GHz)

Hydrometeors (commonly clouds, occasionally rain, and more rarely snow or hail), particularly rain and wet snow or wet hail, strongly attenuate (by absorption and scattering) radio waves above about 10 GHz. This effect increases with frequency to a plateau at about 100 GHz and with increasing rainfall rate, as illustrated in Figure 6. The attenuation can be determined for specific frequencies, rainfall rates, geographical location, slant-path elevation angles, and percent of hours of the year by the methods given in the CCIR documents identified under REFERENCES.

Because of the nonsphericity and possible orientations of raindrops and ice crystals (in clouds aloft and in icy fog), their effect is to depolarize radio waves (reduce the co-polarized component and produce a cross-polarized component). Depolarization by rainfall is related to the strong attenuation by rainfall. The depolarization by ice crystals occurs despite the absence of strong attenuation, so that at EHF (30 to 300 GHz) the attenuation (primarily by rainfall) and depolarization (primarily by ice crystals) are no longer simply related.

2.7 Other Phenomena

At VHF (30 to 300 MHz) and UHF (300 to 3000 MHz) and under the influence of atmospheric refraction, the reflection of radio waves by terrain and man-made structures produces received signals that arrive by two or more paths. At SHF and EHF, there may be multiple paths through the atmosphere due to stratification. These all constitute multipath, which produces time-distributed fading on terrestrial and low-angle slant paths.

At SHF, but particularly at EHF, atmospheric turbulence produces tropospheric scintillation much as the structure of the ionosphere causes an ionospheric scintillation on signals traversing the ionosphere at VHF, UHF, or lower SHF.

The radio noise emitted by all matter is a source of information in radio astronomy and remote sensing. However, noise is also a limiting condition for service fields, particularly in the presence of localized sources. Their added contribution (atmospheric noise due to lightning, galactic, and other extraterrestrial sources; the sun; and man-made noise) tend to decrease with frequency from the VLF to the middle or upper UHF range. Thereafter atmospheric noise increases rapidly with frequency through the SHF (due to absorption and reradiation by our gaseous atmosphere, clouds, and rain) to a maximum external noise temperature of 290°K.

3.0 RELIABILITY

The CCIR Reports and Recommendations describe manual and computer methods for the quantitative determination of field strength over the allocated range of radio frequencies for various services and geometries.

For VLF, LF, and MF (3 to 300 kHz), the ground-wave mode of propagation is highly stable, providing reliable coverage to several hundred kilometers (see Figure 2). There are systematic variations in the hourly median field strengths (i.e., for annual, seasonal, and diurnal distributions) as well as short-term (within-the-hour) Rayleigh-distributed fades (3 to 30 fades/hour). In the nighttime, the maximum service range may be limited by self interference via sky-wave transmission.

For HF (3 to 30 MHz), signals are provided by the stable sky wave, up to the maximum-usable-frequency (MUF). This MUF varies appreciably with geographical position, time, and the desired path length. See the solid-line paths of Figure 4. The HF signals exhibit amplitude fluctuations with periods of less than a second up to a few minutes. Further, ionospheric disturbances lasting hours to days can modify the sky-wave propagation paths and their resultant field strengths. Reflection from associated ionospheric irregularities also permit self-interference via off-the-great-circle sky-wave modes.

Above 30 MHz, the modes of propagation are: line-of-sight (LOS) for short paths, diffraction for the shorter transhorizon paths, and troposcatter for the longer transhorizon paths. These are all highly stable modes, providing field strengths that exhibit only long-term (annual, seasonal, and diurnal) variations. See the solid-line paths of Figure 5. Terrain reflections are normally avoided for point-to-point services by site selection, although they may be unavoidable for mobile services. Terrain reflections and atmospheric layering constitute multipath propagation whose effects (self-interference or fading) vary rapidly in the changing refractivity structure of the atmosphere. Multipath fading is usually remedied by diversity techniques.

There are other fading mechanisms, all associated with atmospheric conditions. Atmospheric layering and ducting can isolate one service terminal from another, causing severe attenuation that is avoidable only by repositioning the terminal's antennas. At SHF, hydrometeors, particularly rainfall and wet snow or hail, can severely attenuate and depolarize radio waves. For terrestrial services, route diversity (the use of alternate circuits) serves as a remedy. For earth-space services, site diversity (separated earth stations) serves as a remedy. At EHF, the gaseous atmosphere (water vapor, oxygen, etc.)

severely attenuates radio waves, effectively isolating space stations from terrestrial stations and limiting the feasible range for terrestrial systems.

4.0 FREQUENCY SHARING

The increased demand for radio services that has already required the sharing of frequencies, often between services in the same band, continues. Now the possibilities for further sharing depend, perhaps critically, upon propagation factors. The previous section (Section 3.0) touched upon the role of propagation in achieving service reliability. The next step is to determine under what conditions, if at all, it may be feasible for two or more services to share a particular band. In general, therefore, one must evaluate the interference potential between services in the terrestrial category, between services in the space category, or between terrestrial and space services (see Figure 7, for example).

For the propagational aspect of the interference problem, it is convenient to consider the potential interference paths between pairs of stations (one station from each of two services):

(a) Both of which are on or near the earth's surface; e.g., either of which is a terrestrial station (of either of the broadcasting, fixed, or mobile services) or an earth station (of either of the fixed- or mobile-satellite services and the space research services). This pair determines a potential terrestrial interference path.

(b) Both of which are space stations; e.g., either of which is a satellite (of either the broadcasting- or fixed-satellite services) or a space probe (of the space research service). This pair determines a potential space-space interference path.

(c) One of which is on or near the earth's surface, as in (a) above, and the other of which is a space station, as in (b) above. This pair constitutes a potential earth-space interference path.

For each of these interference paths, more than one mode of propagation is usually possible, but their relative importance and difficulty of evaluation vary somewhat with frequency. Therefore, for each type of interference path, we treat interference here over three frequency ranges: 30 to 30000 kHz, 30 MHz to 40 GHz, and above 40 GHz.

4.1 Terrestrial Interference Paths

For potential interference between two stations on or near the surface, actual interference normally would be avoided by the choices of antenna orientation and directivity, as well as the geographical separation of the stations, based upon the standard modes of propagation that determine service reliability (Section 3.0). However, generally there are also nonstandard (anomalous) modes of propagation available. These modes are often more efficient than the standard mode (recall point I in Figure 1), propagating beyond the normal coverage area. However, these anomalous modes are not sufficiently stable (reliable) to provide service fields, except perhaps in very special applications. The occurrence of these anomalous modes generally depends upon unusual conditions in the propagation media.

To illustrate some general principles of sharing, we note the hypothetical case of sharing at HF between an intercontinental, high-power, broadcast transmitter and medium-distance, fixed services:

(a) Whenever the fixed-services terminals are within the intended reception area of the broadcast service and are operating co-channel, severe interference is very likely.

(b) If the tendency is for the fixed and broadcast services to operate at optimum frequencies, these frequencies will usually be in different bands, resulting in the feasibility of sharing frequencies.

(c) As the fixed-service terminals move away from the intended broadcast reception area, the sharing feasibility becomes greater. This is due to the fact that at greater distances there are greater losses and the time overlap when both services would operate at the same frequency decreases, because there is an increased likelihood that different frequencies will be used for optimum performance on the different circuits.

4.1.1 Frequencies from 30 to 30000 kHz

At VLF, LF, and MF, the normal service coverage is provided by the highly stable ground-wave propagation, as in Figure 2. However, at VLF, whistler-mode propagation can provide signals to the opposite hemisphere. In addition, at LF and MF, although the ionosphere is only partially reflecting, the reflection coefficients are much higher at night and can support propagation to longer ranges. Special antenna designs may alleviate such effects.

At HF, the normal service coverage is via ionospheric reflection, the sky-wave mode of propagation. The interference mode is provided by the ground wave or intermittent

scattering from sporadic-E layers, ionospheric irregularities, and meteor trails, as well as the less common, but highly efficient, guided or ducted modes along ionospheric layers (see Figure 4).

At LF and MF, the propagation of deeply modulated, strong waves through the ionosphere can cause a cross-modulation and thereby interfere with another wave passing through the same portion of the ionosphere. By a different phenomenon, high transmitter powers and strongly directive antennas can impart sufficient energy at MF and HF to artifically modify the ionosphere, generating local irregularities which can scatter interference signals.

4.1.2 Frequencies from 30 MHz to 40 GHz

In this frequency range, service coverage is provided by line-of-sight (LOS) for short paths, by diffraction over intermediate paths, and by forward scatter (troposcatter) over long paths. From about 30 to 150 MHz, the dominant interservice interference mode is due to scattering from ionospheric irregularities, sporadic-E layers, and meteor trails to distances that can readily exceed 1000 km. From about 30 to 1000 MHz and for small percentages of the time (1 percent or less), strong interference fields occur in association with surface and/or elevated tropospheric ducts (see Figure 5).

Over the range from 1 to 40 GHz, transhorizon interference fields occur by four modes:

(1) by diffraction over short paths for 1 to 20 percent of the time;

(2) by tropospheric forward scatter (troposcatter), which dominates at greater distances than (1) but not for much less than 1 percent of the time;

(3) by hydrometeor (rain, snow, hail, ice clouds) forward-, side-, or back-scattering from antenna main- or side-lobe intersections on or off the great circle path for 1.0 percent, 0.1 percent, 0.01 percent, or 0.001 percent of the time; and

(4) by tropospheric ducting for 1.0 percent, 0.1 percent, 0.01 percent, or 0.001 percent of the time and (depending upon climatic zone) whether the path is over land or over water (temperate or tropic), and for the maximum distances over which the ducts can extend.

4.1.3 Frequencies above 40 GHz

Because of the marked increase in absorption by the gaseous and hydrometeoric atmospheric consitutents in the range from 40 GHz to $3 \cdot (10)^5$ GHz (see Figure 6), interference problems are somewhat eased. Although the LOS path provides the most likely potential interference path, the possibility of significant transhorizon interference paths should be considered, particularly in the gaseous absorption windows.

Rain scatter is expected to continue as a significant mechanism for interference, but primarily in a back-scatter mode, and scattering by ice clouds is expected to become more important as well as more common at these frquencies. Because of absorption and scattering from layer irregularities (no longer small relative to wavelength), ducting is expected to play a less significant role.

4.2 Space-to-Space Interference Paths

On a space-to-space path, interference can arise between satellites whose (main- or side-lobe) antenna beams are directed towards earth stations and other satellites. Generally these interference paths are beyond the earth's atmosphere so that free-space propagation would apply over the entire spectrum. However atmospheric ducting may provide an efficient interference path between two satellites normally isolated by the intervening limb of the earth.

4.3 Earth-to-Space Interference Paths

Because of ionospheric and atmospheric absorption, interference on earth-to-space paths is unlikely outside the approximate frequency range of 30 MHz to 40 GHz. The most efficient interference path between a space station and an earth or terrestrial station is the direct free-space path. For frequencies above about 6 GHz and small percentages of the time (<1 percent), there is the indirect free-space path via hydrometeor scattering. For slightly transhorizon paths, tropospheric ducting may provide approximately free-space interference paths for small percentages of the time (<1 percent).

5.0 REFERENCES

C.C.I.R. (1982), Recommendations and Reports of the CCIR, 1982, XV Plenary Assembly, Geneva, 1982, Volume V, Propagation in Non-ionized Media.

C.C.I.R. (1982), Recommendations and Reports of the CCIR, 1982, XV Plenary Assembly, Geneva, 1982, Volume VI, Propagation in Ionized Media.

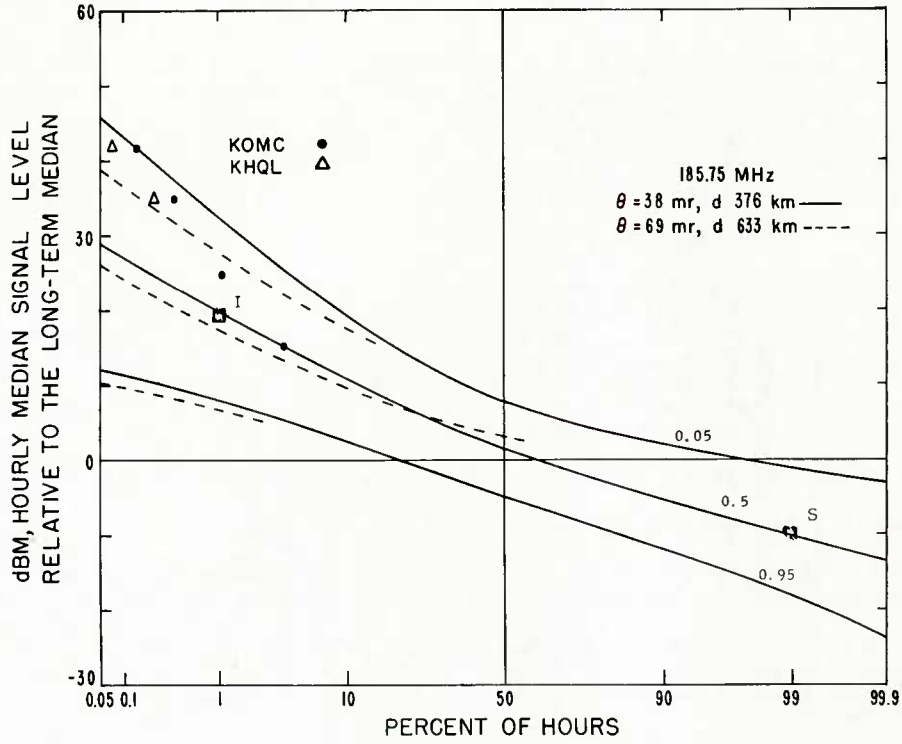

Figure 1. Predicted troposcatter field median distribution (0.5) in decibels above a long-term median (dBM) and the fiducial limit curves (0.05, 0.95) between which the signal distributions would lie for 90 percent of all systems with the same path parameter values. The point S marks the level required to provide the system performance for 99 percent of all hours. The point I marks the median level exceeded for 1 percent of all hours and which has a potential for interference with other services.

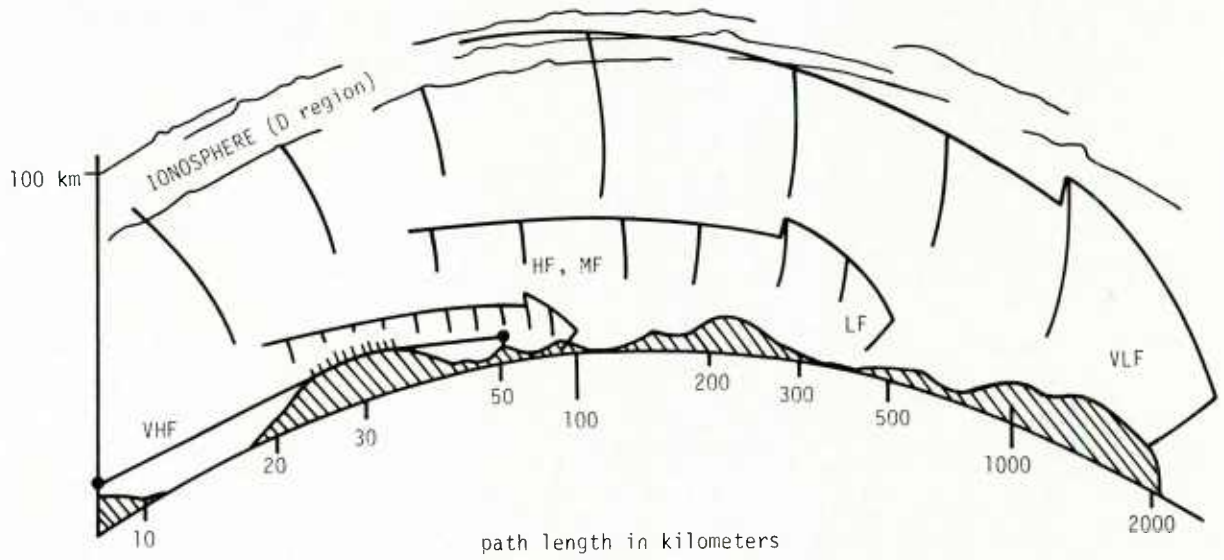

Figure 2. Diffraction over terrestrial transhorizon paths. At HF and lower frequencies, this mode of propagation consists of the ground wave for which the attenuation increases sharply with frequency. At VHF and higher frequencies, both the "space" and ground waves are involved (sequentially). The ground wave contributes to the propagation here only between the horizons of the circuit's terminals.

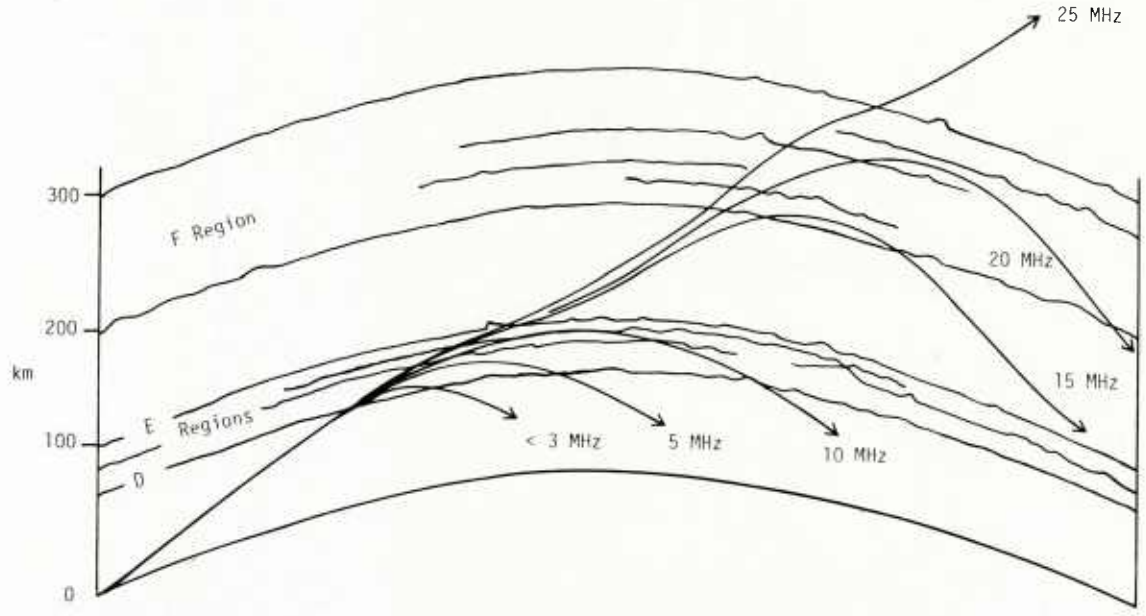

Figure 3. Ionospheric refraction and reflection vary with frequency. Sky-wave propagation is the usual mode of long-distance propagation at HF (3 to 30 MHz). At lower frequencies, D-region absorption is important, and the reflected signal weakens with decreasing frequency. As the frequency of an HF signal is increased, it can penetrate to higher portions of the ionosphere before reflection occurs. Beyond a maximum frequency, the electron density gradient is insufficient for reflection, and the signal penetrates the ionosphere.

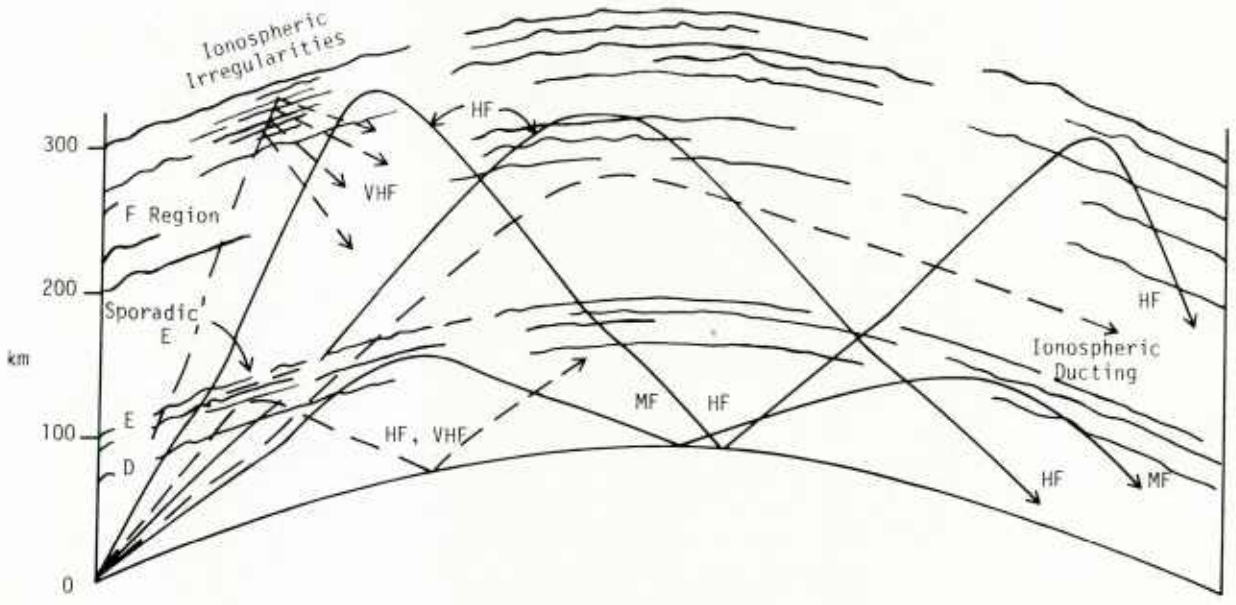

Figure 4. Some ionospheric sky-wave modes of propagation. The solid lines are stable modes suitable for service fields. The dashed-line paths may provide service fields, but are mainly of interest for their potential for causing interference.

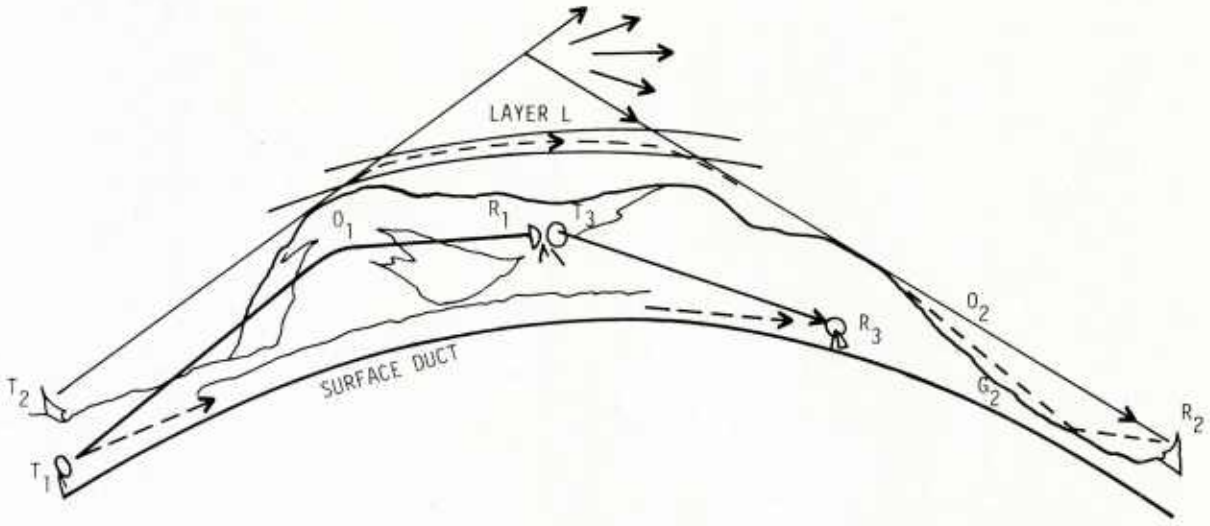

Figure 5. Tropospheric modes of propagation. The solid-line paths are the stable modes suitable for service fields. The dashed-line paths are not sufficiently stable (reliable and predictable) for service fields except perhaps in very special applications. T_1 O_1 R_1 (diffraction); T_2 R_2 (troposcatter); T_3 R_3 (LOS); T_1 R_3 (surface ducting); T_2 L R_2 (via elevated layer); O_2 G_2 R_2 (via ground reflection).

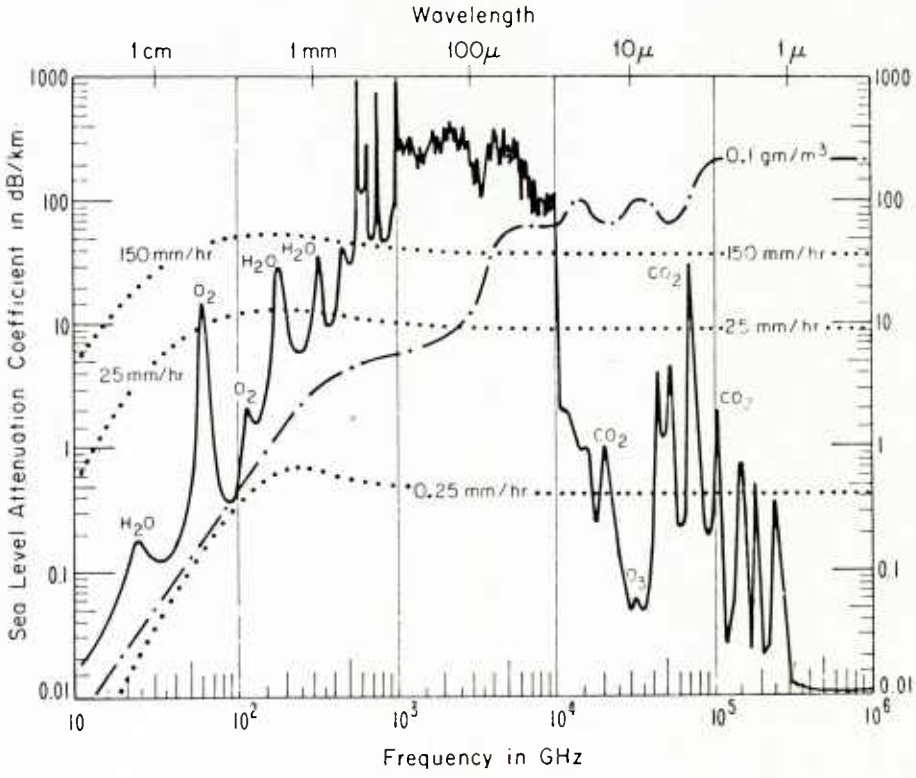

Figure 6. Attenuation due to gaseous constituents and precipitation for propagation within the atmosphere. The rainfall effects are indicated for rain rates of 0.25, 25, and 150 mm/hr. The dash-dot curve is that for clouds or fog.

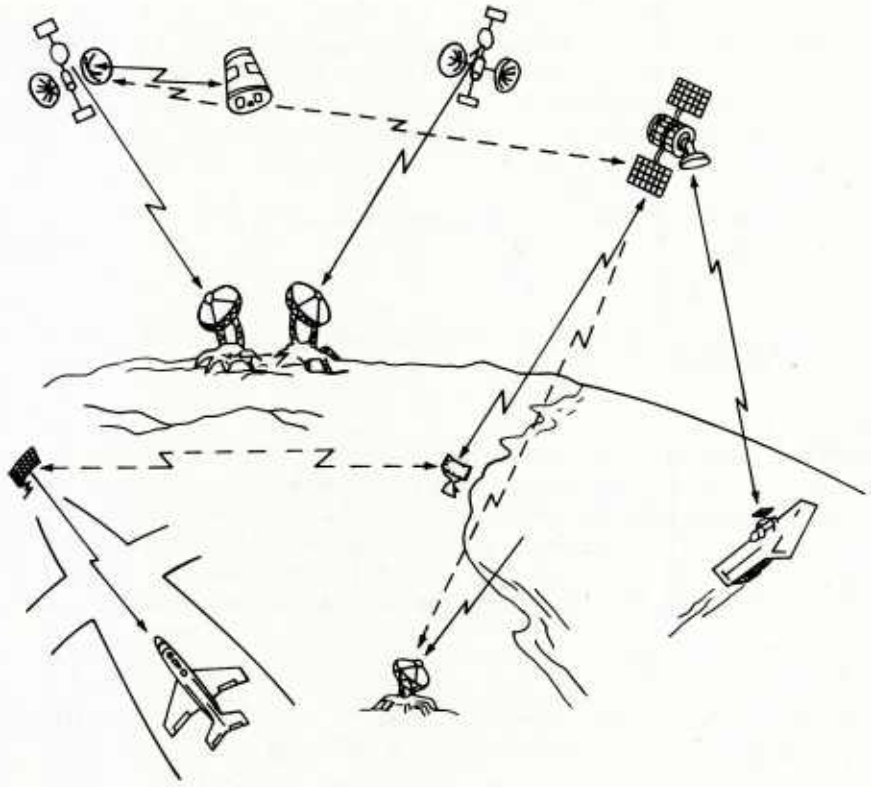

Figure 7. Some terrestrial and space services (solid-line service signals) with potential interservice interference (dashed-line) paths.

DISCUSSION

J.S.Belrose, Ca

There are problems with the authors' text since it is not in accord with the usual description of ground and sky-waves. While it is true that the ground wave is a guided wave, (see Section 2.1 and Figure 2), it is guided by only the lower boundary of the "earth-ionosphere wave guide", viz. by the earth's surface; although diffraction by the lower atmosphere plays a significant role particularly at the greater distances. Propagation to great distances is by way of skywave, and there are two methods or models that are used to describe the mechanism of propagation: (1) the waveguide mode; and (2) the wave hop method. Since VLF waves propagate to around the world distances with little attenuation (2–3 dB/megametre) whatever method one employs to interpret propagation, the upper boundary, the ionosphere, must be a good reflector. As frequency increases above VLF (> 30 kHz) the ionospheric reflection coefficient decreases rapidly with increase in frequency, reaching minimum values in the frequency range 100–500 kHz (equivalent vertical incidence frequency*). The reflection coefficient is particularly small during summer at midday in solar maximum years.

During nighttime, the decrease of this strong daytime absorption, which is particularly large in the frequency range for which absorption is greatest, permits regular skywave propagation at all frequencies below MF. This is contrary to what is said in Section 2.2 paragraph 2. Long distance nighttime skywave propagation at MF is also significant; field strengths are particularly strong during magnetically quiet intervals on winter nights.

Author's Reply

Yes, we shall endeavour to modify the text to avoid this difficulty.

H.Soicher, US

What are the propagation effects of atmospheric particulates, other than rain/snow (e.g. dust)? Are they unique? Are they modelable?

Author's Reply

I have seen such modelling for generalised particles (spheres of contrasting dielectric constant immersed in the homogeneous medium) with adjustments for irregular shape or multiple layering, but they are much less advanced than the more fully developed (albeit still evolving) modelling for raindrops and particularly for rainstorms. I've heard of undocumented observations of the effects of duststorms at microwave frequencies; they report effects ranging from negligible to severe. Severe attenuations have been attributed to dust storms intruding into very moist air (mud storms?). Clearly, frequency dependence is crucial. Documented studies are needed.

R.K.Crane, US

On dust storms – Is the attenuation produced by the bulk scattering by dust particles or by the refracture index gradients associated with the meteorological processes driving the dust storms?

Author's Reply

I assume both play a role, their relative significance determined by other factors (moisture sources, etc.). You raise a question well worth systematic study.

L.W.Barclay, UK

One of the features of the autumn in the UK is the burning of straw stubble on the fields after harvest. At the RAL observatory at Chilbolton, observations have been made of the back-scatter from such smoke clouds. The intensity of the returns can only be explained by assuming that water condenses on the particles in the cloud.

J.T.Ong, UK

Dr Dougherty's division of propagation under two separate headings, viz. (1) reliability and (2) interference, may be implying no relationship between the two. Could Dr Dougherty comment on the correlation between these two "mechanisms"?

Our experience in the Gulf indicate that microwave line-of-sight links (approximately 20 km) fade regularly at night in summer. At the same time, tropospheric scatter/diffraction links duct giving rise to very high signal levels. Has such high correlations between these two mechanisms been reported elsewhere? (I understand the paper by J.Doble addresses this problem.)

Author's Reply

The separate headings imply a contrast in signal levels, occurrences, and (often) in propagation mechanisms. Generally, the variations in service and interference signal levels tend to be uncorrelated. However, some supportive

---

* fcosi – where i equals angle of incidence on the ionosphere.

atmospheric conditions (stratification, rainstorms, etc.) may occur sufficiently widespread that the service fields and the interference fields are strongly correlated – positively or negatively (depending upon the interference and service propagation path geometries). Examples have been more widely observed than reported, but reports are always needed and welcomed, since such documentation is much more persuasive than assertions.

L.Boithias, Fr

Il me semble que dans cet exposé le terme "mode de propagation" devrait être plutôt remplacé par "mécanisme de propagation". Un mode de propagation est seulement une solution particulière d'un mécanism de propagation. Par exemple dans le mécanisme de propagation guidée il y a plusieurs modes de guidage.

Author's Reply

Yes, thank you; I agree. Not only is your distinction between the two correct, it is also important. We identify the propagation mechanisms with specific atmosphere or terrain conditions that are physically recognisable by adequate sensors (our eyes, refractometers, etc.). Of course, for some propagation phenomena the mathematical solutions or modes are also relatable to physically observable conditions (angle of launch or arrival, etc.); however, there are also phenomena for which (mode/physical-measure) relationships have not as yet been achieved.

OVERVIEW OF FREQUENCY SHARING

EARL J. HOLLIMAN
Army Spectrum Manager
Department of the Army
Washington, D.C. 20310

1. FREQUENCY SHARING CONCEPTS

1.1 Introduction

Frequency engineering is the process of sharing spectrum space among many requirements in a manner which attempts to control potential operational interference. In most cases, the point that operational degradation occurs can be identified by technical parameters. All frequencies are shared. In the case of the United States Army, the communication requirements exceed all possible spectrum space by approximately 8 times. The individual user of the radio spectrum would like to be unconcerned with sharing. However, this is not practicable for two reasons. First, the user must share his frequency with noise which is intrinsically involved with his system's design and environment. It influences his own design approaches and establishes limiting conditions of performance for the proposed operation. Secondly, the sharing environment forces him to recognize the presence of other users. In the assignment process, sharing is considered in one or more variations of four concepts.

1.2 Spectral (or frequency) Variations

Spectral variations are the most widely recognized spectrum sharing technique. For example, if 64 kHz of spectrum space is available in a band and each user requires 8 kHz for his voice transmission, then the first 8 requirements in a local area may be satisfied by assigning a different frequency to each user. Spectral sharing is governed by the transmitted bandwidth, the selectivity of receivers, the power distribution in the signal and the spectrum space available for assignment. Spectral approaches to frequency sharing are usually applied together with other approaches to increase the total possible assignments. These include several assignment techniques such as channel-splits, interstitial, and off-sets to increase the number of possible sharing assignments. With present filter network technology, spectral boundaries are limited more by the bandwidth essential to proper operation than by filter technology. However, sharing by spectral relationships alone is inadequate to meet spectrum requirements.

1.3 Spatial Variations

a. Decreases in signal strength as a function of radio path distance and dispersion permit frequency reuse. This technical phenomena may be defined by radio propagation and antenna scientists with considerable accuracy. By maintaining adequate physical separation, additional assignments may be made through spatial differences. The objective in this approach is to apply path loss so as to control relative signal strengths. The criteria which determines those levels involves a number of complex relationships including local noise, respective radio system designs, and the performance demand of the users since the user now decides what interference level is harmful. Spatial variations for terrestrial system frequency sharing assume four forms. These are geographical distance, antenna characteristics, terrain shielding and radio propagation. For space systems, additional forms include orbital separation of satellites. Antenna nulls may be arranged to reduce interference either at transmitter sites or at receivers and thereby permit additional sharing.

b. Geographical assignment patterns have existed since World War II where frequency lists were prepared for specified zones. This concept is receiving renewed interest in the grid or cellular system. This concept, however, uses small grids with very reduced transmission ranges and with an automated frequency assignment responsive to the location of the caller. The cellular concept has two forms. Either the mobile terminal is automatically switched to the cell frequency as it enters the cell, or the mobile may have one frequency and the cell shifts frequency to respond to the mobile's frequency. An approach to a geographical pattern but on a larger scale is illustrated by Enroute Air Traffic Control. Each air sector operates on a specific frequency, and the aircraft pilot shifts frequencies on entering each sector. Spatial and spectral sharing are the most common of present sharing techniques.

1.4 Chronological Variations

Chronological variations using time or queuing are among the earliest frequency sharing techniques. However, today's concepts have advanced far beyond the early uses of day or night scheduling. The availability of precise timing sources now permits time division multiple access schemes to divide each second of frequency use among several users. Data flow is stored awaiting the station's turn in the timing sequence, and as each assigned time slot occurs, the station transmits information. Adaptive approaches to time slots exist where the time for transmission is increased for the user with larger amounts of traffic. In such systems, preplanned interruptions to traffic flow are programmed to poll all users for any higher precedence messages and reassign time slots. For non-communications systems such as used for radio navigation, several systems operate without interference on the same frequency by dividing each second into

a million parts and assigning frequency use in absolute time domains. Time division systems which are adaptive to traffic loads require a central control, and correction for radio path distances or motion velocity. However, these techniques are within contemporary technology.

1.5 Orthogonal Variations

a. A mathematical term meaning mutually non-interactive - orthogonal - has been applied to one approach to radio frequency sharing. Although the cancellation of potential interference effects is less effective because of the fluctuations in the radio path, the term illustrates a sharing approach. Its most common forms to date have been in polarization differences through antenna selection and in application of the laws of probability that interfering signals will not be present on the same frequency at the same instant. Differences in polarization provide additional sharing of frequencies, but are less effective when reflected or refracted radio paths vary the polarization from the intended optimum. Some limited applications of sharing are enhanced by modulation differences between systems competing for the same frequency. An illustration of probability application is demand access systems serving a number of low duty cycle users. In a manner governed by Poisson's Laws of Chance, frequencies assigned to a low duty cycle group of users may be searched for an available (free) channel. For intermittent users, this approach achieves a high degree of utilization of frequency channels. The system fails in performance by excessive waiting time, however, if saturated with users with longer holding times.

b. Much attention has been given to orthogonal approaches in the last decade, and a number of advanced concepts emphasize their potential value into future solutions of spectrum utilization. These studies are so dynamic that several terms are applied. Their potential value in meeting increased congestion of the radio spectrum is so significant that they are discussed separately.

2. QUASI ORTHOGONAL CONCEPTS

2.1 General

If one starts with an interfering environment, it is possible to exploit several approaches designed to enhance successful communications. Although a number of different terms are applied, these advanced concepts are generally categorized in three forms. These are bandwidth expansion, signal processing to recognize a desired pattern, probability of success schemes, or hybrids of these three. These approaches greatly improve utilization of each frequency and increase the sharing of identical spectrum space by many users.

2.2 Bandwidth Expansion

This technique follows from Shannon's early work and analytical investigations published over the last decade. This approach results in greatly expanding the information bandwidth, such as a thousand times, to create a widely dispersed radio signal achieved in a coded manner. Although the information is now so widely distributed as to appear similiar to noise, the information transfer is precisely determined by settings in the code generators. Detection at the receiving terminal is accomplished only with synchronization of identical codes, and any received energy which does not correlate is vastly reduced at the receiver output. These approaches are also recognized as pseudo-noise spread spectrum or direct sequence spread spectrum. Where spread spectrum techniques are utilized only to overcome interference, codes may be greatly simplified. Simplified forms of bandwidth expansion are utilized to offer advantages in overcoming interference, and can greatly reduce the impacts in frequency sharing. However, there are some limits to the number of sharing users through bandwidth expansion alone.

2.3 Frequency Hopping

a. The orthogonality of frequency hopping systems results from coding in both the time and frequency domain. The concept is related to bandwidth expansion schemes but, by using a transmission duty cycle less than unity on any frequency in the hop set, it exploits the probability of success in an environment of many users. For a given error rate not to be exceeded, the number of frequencies in the hop set must be increased as active users are increased. Typical requirement of the number of frequencies required as a minimum hop set to achieve a reasonable success probability is approximately 200 pre-set frequencies. Although the pattern is pseudo-random in appearance, a precisely controlled pattern common to the transmitter and receiver exists. By assigning different users different codes, many users may share the same frequencies. However, the frequencies available for hopping must be high if low error rates are essential. The utilization factor of spectrum space involved is increased by frequency hopping systems.

b. Whereas many users with frequency hopping systems may share a set of frequencies, the conventional user (i.e., non-hopping) is affected by the dwell time of the hoppers on "his" frequency. The extent of this interference depends upon a number of factors depending upon the non-hopping transmission system employed. From a frequency assignment approach, operating instructions must be included with the assignments to designate the patterns among users. The usual frequency hopping system is assigned specific frequencies for the hop set. Where a band of frequencies is swept rather than discrete frequencies, a related system identified as pulsed FM is employed. All effects

of sharing between conventional (non-hopping) and frequency hopping have not been fully examined for all system approaches.

2.4 Pattern Recognition

In an interfering environment of signals, it is possible to recognize a particular pattern using signal processing. This frequency sharing technique is useful for serving many stations where short transmissions are involved. It is illustrated by a very large number of transmitters on the same frequency which are self-triggering to repeat short messages on a random basis in respect to all transmitters. However, although the entire group of transmitters have random selected time intervals for self-triggering, the short term timing of a particular unit is fairly precise. The time interval between each transmission and the total reporting period is established by analytical techniques to ensure at least one interference-free report. Each transmitter in random sends its identity and message. For example, 100 sensor transmitters may be distributed along a road to detect movement. Since each transmitter is self-triggering on a periodic basis, no complex timing control is needed. If each sensor were received on a separate frequency, it would require 100 frequencies and receivers. In this approach, one receiver on one frequency is used with a signal processor to recognize individual patterns and reproduce the information. A similar application received publicity in monitoring wild animals fitted with radio transmitters on collars.

3. CONCLUSIONS

3.1 Operational commanders and doctrinal planners must assume greater roles in validating requirements and the reviewing of efficient spectrum utilization.

3.2 A close relationship between the spectrum manager, the operational planner and the equipment developer must be established if the impacts of spectrum congestion are to be controlled.

3.3 Equipment developers must continually endeavor to design equipment which is efficient of spectrum space to meet operational requirements.

3.4 Enhanced methods of radio propagation analysis and prediction must continue to be developed and provided to the spectrum management system including analyses of conventional and orthogonal compatibilities.

3.5 The frequency management process must be supported by automation aids to evaluate feasible sharing conditions which can be related to performance standards.

DISCUSSION

D.Scholz, Ge

To what extent and under what prerequisites are the conceptual approaches of frequency sharing applicable to HF-radio operations. The question is put in the light of a recent over-occupancy of more than 500% in the 2–8 MHz range of military users only.

Author's Reply

The four basic variations used in frequency assignment by which frequencies may be shared apply throughout the radio spectrum. Of course, some forms, such as a true spread spectrum approach, are constrained in the 2–8 MHz range by the laws of physics. However, the spatial variations useful in the 2–8 MHz band are accurate to the extent that skywave coverage is determined. Otherwise, the four sharing techniques apply to all frequencies in the spectrum.

RADIO REGULATORY ASPECTS OF FREQUENCY SHARING

L W Barclay
Home Office
Directorate of Radio Technology
Waterloo Bridge House
Waterloo Road
London SE1 8UA

1. INTRODUCTION

The requirement for communications, civil and military, analogue and digital, continues to expand and advances in technology have facilitated the expansion. Although much of the demand for data transmission in connection with information technology may be met by the provision of cable and optical-fibre links, the pressure for expansion of radio communications continues. This paper discusses some of the regulatory aspects of the use of the radio frequency spectrum and highlights one or two of the problems associated with frequency re-use.

2. WORLD ADMINISTRATIVE RADIO CONFERENCES

Radio communication is not confined by national boundaries. The international character of radio planning was recognised many years ago and the administrations of the member countries of the International Telecommunications Union have, at a series of conferences, agreed a set of Radio Regulations which specify frequency bands for particular radio services and also provide for the control of radio spectrum usage.

It should be noted that it is the administration, the government, of each country which has the right and the authority to regulate and control the use of radio in that country. Thus in making an International agreement each country needs to have some assurance that its neighbours will all honour that agreement and will apply all the rules. A remarkable decision made at the World Administrative Radio Conference (WARC) in 1947 was to the effect that

> "each Sovereign State undertakes to submit evidence of its use of each frequency and proposed use of a frequency to an independent body, the International Frequency Registration Board (IFRB), whose responsibility includes among its essential duties
>
> a) scrutinising these submissions (i.e frequency assignment notices) for conformity of the declared use with the Radio Regulations.
>
> b) the examination with respect to the probability of causing harmful interference to existing recorded assignments and the adoption and promulgation of Findings, and
>
> c) recording of such use in the Master International Frequency Register."

Thus, with some exceptions where the use and interference potential of a signal is wholly within one country, all have agreed to surrender some autonomy because of the mutual benefits of control of interference.

The IFRB continues to work as an important arm of the ITU.

The most recent general WARC was held in Geneva in 1979. This meeting considered the whole of the spectrum between 9 kHz and 400 GHz and allocated frequency bands up to 275 GHz to services. It also dealt with methods by which the expected interference should be determined, designation of emissions, power limits etc, as well as with the continued maintenance of the master frequency lists.

This major conference dealt only with general matters but it cleared the way for a further series of WARCs throughout the 1980s which deal with frequency assignment plans for particular services.

The terms used at such administrative conferences have specific definitions.

2.1 Frequency Usage

An allocation refers to a given frequency band, and bands are allocated to one or more radio services. Thus the band 9 - 14 kHz, for example, is allocated worldwide for radionavigation.

An assignment of a radio frequency or channel is the authorisation given by an administration for a radio station at a specified location and under specified conditions. Thus in the UK, for example, the frequency of 60 kHz is assigned to the station MSF located at Rugby. WARCs may prepare assignment plans taking into account locations and transmitter characteristics when considering mutual interference but it remains the prerogative of the appropriate administration to decide whether a particular assignment shall be made.

There is a third definition for a category of frequency designation and this is a frequency allotment. This is where a WARC allots frequency channels to be used in particular countries or areas without specifying the precise location. This has been done for example, for the coast radio stations operating at HF in the maritime mobile bands. It seems likely that allotment plans, with their less precise specifications of transmitter locations and the corresponding more general assessment of interference, would only be used at HF where distance is a less critical parameter than at higher frequencies.

2.2 Services

The ITU have another series of definitions dealing with categories of use. An activity involving the transmission, emission and/or reception of radio waves for a specific telecommunications purpose is called a radiocommunication service. There are definitions covering probably all of the uses of radiocommunication service between specified fixed points and, in the same way, the mobile services, the land mobile service, the standard frequency service, etc, are self explanatory. It should be noted that these definitions refer to terrestrial services. When a satellite is involved it is stated, thus the fixed satellite service refers to a service between earth stations at specified fixed points when one or more satellites are used en route. There are also services for navigation, position fixing and radar: the radiodetermination and radiolocation services. Some services may employ reception only, for example passive sensors operating in the earth exploration satellite service and also the radio astronomy service.

Thus the ITU concerns itself with the type of radiocommunication and not with the particular user or with the information transmitted. For example, broadcasting may be commercial or for public service; mobile communication may be for emergency, military or business purposes. The decision on the application and on the allocation to different users of frequency bands within the agreed ITU framework is made by each administration.

2.3 Regions

The ITU has divided the world into 3 geographical regions, see Fig. 1. Essentially these are:

Region 1. Europe, Africa and the USSR
2. The Americas
3. Asia and Australasia

Because of geographical separation there is scope for Regional differences in radio spectrum usage, particularly in Region 2, and this has been taken into account by the ITU. Some WARCs relate to a particular Region whereas others are worldwide.

Fig. 1 also shows the tropical zone. Due to the nature of the environment and the high levels of atmospheric noise, there are special provisions for ionospheric broadcasting at the bottom end of the HF band in this zone.

3. ALLOCATED FREQUENCY BANDS

The Table of frequency allocations in the Radio Regulations was agreed at the 1979 WARC. In some cases allocations are worldwide. Such cases would be where propagation occurs over long distances, such as at VLF and HF; where there is a worldwide need for the same type of communications, such as in the aeronautical mobile service; or in other cases where worldwide conformity could be agreed. As a generalisation it is easier to find worldwide agreement where the existing uses have already been constrained at previous conferences or where the demand is less intense, such as at millimetre wavelengths. It is at VHF and UHF where the pressure on spectrum space is greatest and where terrestrial propagation ranges are comparatively short, that differences between the regions are most pronounced; Fig. 2 shows the regional differences for the band between 174 and 235 MHz.

In each allocated frequency band there may be a system of priority of use and here another definition is needed. A service which has the greatest right to use a band is a primary service and is denonted by capital letters in the allocation table. A permitted service, denoted by capital letters but with diagonal lines at each end of the word, has equal rights with a primary service except when a frequency assignment plan is being prepared. Then the primary service has prior choice of frequencies. A secondary service, denoted by lower case letters in the table, can operate in the band but must not cause harmful interference to primary services which are already operating or which are assigned later, and cannot claim protection from interference caused by primary services. Perhaps it should be stressed here that the ITU and the WARCs are concerned with international compatibility; within a country provision might be made for sub-bands or in some other way to regulate the use by primary and secondary services in an orderly manner.

The differing needs of various administrations is highlighted by the use of footnotes to the frequency allocation table. For example footnote 621, which is referred to against the 174 - 223 MHz band in region 1, states that in a number of countries in Western Europe, together with the Yemen, this band is also allocated to the land mobile service on a permitted basis, provided that interference from the land mobile service is not caused outside those countries. There are many footnotes through the tables which give national and regional differences which were found to be acceptable at the WARC.

As an indication of the extent to which frequency sharing is increasing and of the pressure there is on the spectrum. Fig. 3 is an extract from the 1959 WARC frequency allocation table for the band from 10.55 - 13.25 GHz, That band was not properly within the state-of-the-art at that time and there are liberal worldwide allocations with only one footnote relating to the radio astronomy service in various sub-bands. Twenty years later, Fig. 4, the same piece of spectrum is much more intensively allocated, particularly to satellite services and there are many regional differences. There are also 2½ pages of footnotes associated with these entries.

4. ASSIGNMENT PLANS

The allocation of frequency bands to services makes a general provision, but each administration requires an orderly and efficient way of assigning specific frequencies within each band. Some bands are organised according to a channelling plan and then a specialised WARC or RARC is likely to be the forum at which assignments are agreed. Examples of this are the Region 1 conference to plan the FM broadcasting band at around 100 MHz; that conference has just completed its preliminary session and meets again in 1984. There is also a mobile service conference in 1983, a worldwide conference in 1984 and 1986 for the HF broadcast bands, a conference for the geostationary orbit in 1985 and 1987 and a Region 2 conference for the top 100 kHz of the MF broadcast band in 1986.

In cases where there is no internationally agreed channel plan, such as is often the case in the fixed service bands, the assessment of compatibility is made on an individual basis by the IFRB and by the administrations concerned.

Whether as a technical standard at an administrative radio conference as a basis for a bilateral agreement between administrations, a set of agreed planning standards is essential. Included in such standards will be items such as the required protection ratio for the service, the quality of the service in terms of time availability and occurrence of interference (taking account of location variability where appropriate), propagation characteristics including polarisation changes, noise levels, antenna performance, transmitter and receiver performance including spurious emission levels. Definitive statements are required for each item and, particularly for the propagation characteristics the prediction uncertainties and the confidence limits must be minimised and quantified.

For some services interference levels expected for, say, 10% of the time is required and this information may not be too difficult to compile. For some fixed services however interference which causes outages for 0.1% or even 0.01% is important and this implies a great deal of difficulty in establishing reliable propagation data.

The propagation information used in international negotiation is based on CCIR Recommendations. The IFRB standards use these Recommendations where they exist and where they are practical for the IFRB workload. A WARC has complete autonomy to approve whatever standards it chooses but it is likely to take full account of the studies undertaken by the CCIR.

Many frequency bands are shared between terrestrial and satellite services and this is a topic of great concern because of the great interference potential. Side lobes from the antennas of satellite earth station may cause interference to or receive interference from the side lobes of terrestrial radio-relay links and there may also be direct interference paths between the satellite and terrestrial systems. A co-ordination procedure has been agreed, in Appendix 28 of the Radio Regulations, which sets bounds for the locations of co-channel terrestrial and space systems. A central part of the procedure is a propagation calculation, derived from the studies of Study Group 5 of CCIR.

Appendix 28 deals mainly with fixed services and even though both terrestrial and satellite services are involved the performance requirements are well understood. In other cases the services are different, as the service standards are not well known and certainly not yet agreed between administrations. For example, the band from 406.1 to 410 MHz is allocated worldwide to three primary services: the fixed, mobile and radio astronomy services. The only way the passive radio astronomy service could share a band with active services is by very careful planning. However, there is so far no definition of the mutual planning standards to be adopted and it may be that the important parameters have not yet been completely identified.

The band 406.1 to 410 MHz, like a number of other bands which are shared by several services, is subject to the provisions of Article 14 of the Radio Regulations. The effect of this Article is to ensure that possible interference is considered by the particular administrations concerned on a case-by-case basis. It sets out a procedure for the notification of the proposed use of a frequency assignment, for the lodging of objections and for subsequent bilateral negotiation.

5. CONCLUSIONS

Frequency sharing is inevitable due to the increasing demands for communication and the Radio Regulations approved at the World Administrative Radio Conference in 1979 provides an administrative framework within which sharing can be planned. However, planning requires definition and agreement on the various relevant technical parameters. In particular, definitive propagation information is required for which the uncertainty statistics are minimised.

6. ACKNOWLEDGEMENT

This paper is published with the permission of the Director of Radio Technology, Home Office.

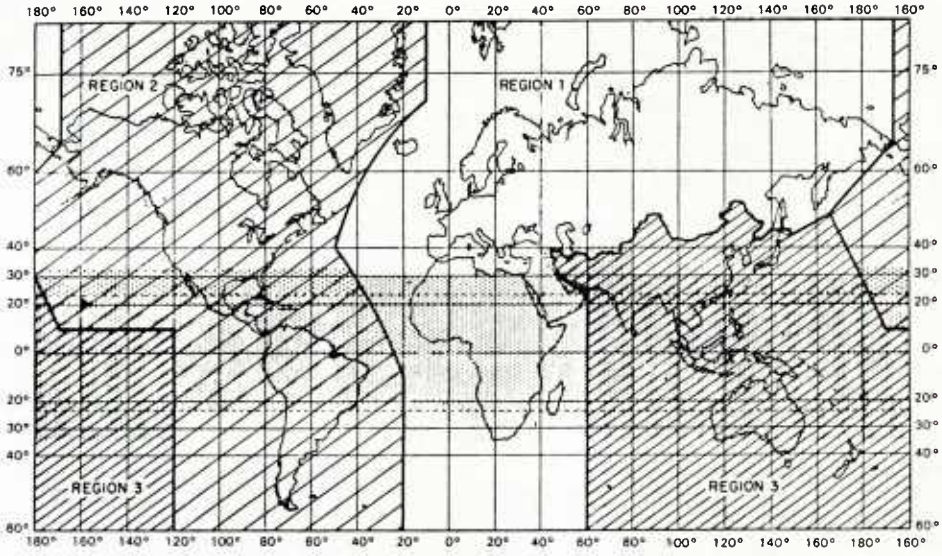

Fig. 1. The three ITU Regions of the World together with the tropical zone.

MHz
174 — 235

Allocation to Services		
Region 1	Region 2	Region 3
174 — 223 BROADCASTING 621 623 628 629	**174 — 216** BROADCASTING Fixed Mobile 620	**174 — 223** FIXED MOBILE BROADCASTING 619 624 625 626 630
	216 — 220 FIXED MARITIME MOBILE Radiolocation 627	
	220 — 225 AMATEUR FIXED MOBILE Radiolocation 627	
223 — 230 BROADCASTING Fixed Mobile 622 628 629 631 632 633 634 635		**223 — 230** FIXED MOBILE BROADCASTING AERONAUTICAL RADIONAVIGATION Radiolocation 636 637
	225 — 235 FIXED MOBILE	
230 — 235 FIXED MOBILE 629 632 633 634 635 638 639		**230 — 235** FIXED MOBILE AERONAUTICAL RADIONAVIGATION 637

Fig. 2. Frequency allocations, 174 - 235 MHz

Gc/s
10·5 — 13·25

Allocation to Services		
Region 1	Region 2	Region 3
10·55 — 10·7	FIXED MOBILE *Radiolocation* 405	
10·7 — 11·7	FIXED MOBILE	
11·7 — 12·7	FIXED MOBILE except aeronautical mobile BROADCASTING	
12·7 — 13·25	FIXED MOBILE	

Fig. 3. Frequency allocations in 1959 10.55-13.25 GHz

GHz
10.55 — 11.7

Allocation to Services		
Region 1	Region 2	Region 3
10.55 — 10.6	FIXED MOBILE except aeronautical mobile Radiolocation	
10.6 — 10.68	EARTH EXPLORATION-SATELLITE (passive) FIXED MOBILE except aeronautical mobile RADIO ASTRONOMY SPACE RESEARCH (passive) Radiolocation 831 832	
10.68 — 10.7	EARTH EXPLORATION-SATELLITE (passive) RADIO ASTRONOMY SPACE RESEARCH (passive) 833 834	
10.7 — 11.7 FIXED FIXED-SATELLITE (space-to-Earth) (Earth-to-space) 835 MOBILE except aeronautical mobile	10.7 — 11.7 FIXED FIXED-SATELLITE (space-to-Earth) MOBILE except aeronautical mobile	

GHz
11.7 — 13.25

Allocation to Services		
Region 1	Region 2	Region 3
11.7 — 12.5 FIXED BROADCASTING BROADCASTING-SATELLITE Mobile except aeronautical mobile 838 840	11.7 — 12.1 FIXED 837 FIXED-SATELLITE (space-to-Earth) Mobile except aeronautical mobile 836 839 840 12.1 — 12.3 FIXED 837 FIXED-SATELLITE (space-to-Earth) MOBILE except aeronautical mobile BROADCASTING BROADCASTING-SATELLITE 839 840 841 842 843 844 12.3 — 12.7 FIXED MOBILE except aeronautical mobile BROADCASTING BROADCASTING-SATELLITE 839 840 843 844 846 12.7 — 12.75 FIXED FIXED-SATELLITE (Earth-to-space) MOBILE except aeronautical mobile 840	11.7 — 12.2 FIXED MOBILE except aeronautical mobile BROADCASTING BROADCASTING-SATELLITE 838 840 12.2 — 12.5 FIXED MOBILE except aeronautical mobile BROADCASTING 838 840 845 12.5 — 12.75 FIXED FIXED-SATELLITE (space-to-Earth) MOBILE except aeronautical mobile BROADCASTING-SATELLITE 847 840
12.5 — 12.75 FIXED-SATELLITE (space-to-Earth) (Earth-to-space) 840 848 849 850		
12.75 — 13.25	FIXED FIXED-SATELLITE (Earth-to-space) MOBILE Space Research (deep space) (space-to-Earth)	

Fig. 4. Frequency allocations in 1979 10.55 - 13.25 GHz

DISCUSSION

J.Arnbak, Ne

Mr Barclay was stating that the international Radio Regulations do not refer to the actual users of a radio communication service (because these will be authorised by application of national procedures). I wonder whether this statement is true without exceptions. For example, the fixed satellite service may be used for point-to-multipoint unilateral links *provided* that these are *not* intended for reception by the general public. This is the widely used commercial TV-distribution method adopted in North America at 4 GHz, and recently also by a UK company via the Orbital Test Satellite. Another example is that of the broadcasting-satellite service allocation at 2.6 GHz, which is only allowed for community reception, *not* for individual reception, by the general public. What is the purpose of those specific international user restrictions in the Radio Regulations?

Author's Reply

The band 3.4–4.2 GHz has a primary allocation to the fixed satellite service. A point to multi-point system comprises a number of fixed links and thus, from a regulatory viewpoint, the service is appropriate. As I indicated in my talk the use of a service, (the information that is conveyed), is not considered in the allocation process. Thus, the broadcast modulation on a fixed service transmission is in order. In the band 2.5–2.69 GHz, allocated to the broadcasting satellite service, there is a flux level limitation similar to that for the fixed satellite service. Thus, large earth station antenna gains would be required for reception. There was an agreement at the WARC that broadcasting use would be limited to community reception and this seems to be a pragmatic decision in view of the limitations. Note that the broadcasting service can only use this band subject to the procedures of Article 14.

R.S.Sandell, UK

I fully endorse Mr Barclay's comments regarding the importance of prediction accuracy. CCIR Rec. 370 has been an important basis for 20 years, but it is now widely known that there are more accurate techniques available employing computers. The drawback is that they require detailed terrain data banks. What is Mr Barclay's opinion regarding the likelihood of international application of such systems?

Author's Reply

Detailed computer-based prediction methods using path profiles derived from numerical terrain-height mapping are becoming more readily available and are suitable for point-to-point applications. Recommendation 370-4 of the CCIR is intended for broadcasting; for area coverage purposes. In such circumstances a number of point to point predictions would have to be made in order to obtain a representation of the area coverage. Although this method is likely to be more accurate, the complexity and the lack of world-wide terrain-height maps are likely to preclude the approach for international planning. However, Recommendation 370-4 is capable of improvement, particularly in respect of the terrain roughness parameter and the location variability concept. The CCIR have recently set up Interim Working Party 5/5, under the chairmanship of M.Berthod, to consider these matters.

SUMMARY OF SESSION II-A

TERRESTRIAL PROPAGATION (IONOSPHERIC MODIFICATION)

by

Dr H.J.Albrecht
Session Chairman

Fundamentally based on first experiments conducted by the United States more than a decade ago, ionospheric modification has become an interesting variety of influencing a propagation medium by anthropogenic action. In the meantime, some considerable progress has been made in some areas; AGARD-EPP symposia have dealt with this subject in the past. The area of ionospheric modification is very relevant to the general topic of propagation aspects of frequency sharing, interference, and system diversity.

Since 1979, a new ionospheric heating facility has been operated by the Max-Planck Institute for Aeronomy (Lindau, FRG) at Ramfjordmoen near Tromsø, Norway. A series of investigations has been carried out within a joint project with the University of Leicester, UK. In a paper on anomalous absorption effects produced by high-power radio waves in the high-latitude ionosphere, **T.B.Jones, T.Robinson, P.Stubbe,** and **H.Kopka** reported on new results obtained.

The experiments performed seem to confirm the prediction that anomalous absorption is more pronounced at high latitudes. In addition, the following effects were indicated:

- anomalous absorption depends in a somewhat complicated way on pump power and ionospheric variability
- there may be an apparent "super self-absorption" of the pump wave
- a kind of hysteresis effect may be associated with the generation of field-aligned irregularities
- cross-modulation effects have been observed in the F-region.

The discussion following the presentation of the paper concerned the ionospheric disturbances reported and generally supplemented the information contained in the paper; also addressed were reproducibility and installation characteristics.

In summary, the session dealt with the state of the art reached with the ionospheric modification experiments at Tromsø and indicated areas deserving future attention.

ANOMALOUS ABSORPTION EFFECTS PRODUCED BY HIGH POWER RADIO WAVES IN THE HIGH LATITUDE IONOSPHERE

T.B. Jones and T. Robinson
Department of Physics
University of Leicester
Leicester LE1 7RH, U.K.

P. Stubbe and H. Kopka
Max-Planck-Institut fur Aeronomie
3411 Katlenburg-Lindau 3, W. Germany

SUMMARY

High power HF radio waves can produce plasma instabilities in the ionosphere which induce major changes in the propagation characteristics of other HF signals propagating through the disturbed region. Experiments to investigate some of these disturbance effects have been undertaken using the Max Planck Institut fur Aeronomie, Lindau heating facility at Tromso, Norway. Particular attention is given to the anomalous absorption effects discovered and to the induced phase changes observed in the diagnostic signals. The observations are interpreted in terms of the plasma instabilities generated and are of interest in assessing the performance of HF communication systems when disturbances of this nature are produced in the ionosphere.

1. INTRODUCTION

The generation of small scale field aligned irregularities (FAI) within the reflection region of high power radio was discovered during ionospheric modification experiments at Platteville, Colorado (Fialev, 1974; Minkoff, 1974). The FAI, which were detected by radar backscatter techniques, were produced only when the high power EM wave (pump) was in O-mode. It has therefore been suggested that the excitation of Langmuir waves at the upper hybrid frequency plays a part in the generation mechanism of FAI (Vaskov and Gurevich, 1975; Grach et al 1977; Das and Fejer, 1979).

In an earlier experiment at Platteville, Cohen and Whitehead (1970) observed that during O-mode heating a low power O-mode diagnostic radio wave passing through the heated ionospheric plasma suffered strong anomalous absorption when its frequency was within a few hundred kilohertz of the pump frequency. Graham and Fejer (1976) suggested that mode conversion of the EM diagnostic to Langmuir waves due to the presence of FAI generated by the high power pump, was responsible for anomalous absorption. The link between FAI and anomalous absorption is thus well established both experimentally and theoretically.

Theory suggests that anomalous absorption should be stronger the smaller the angle between the EM wave and the earth's magnetic field. Thus anomalous absorption effects are expected to be stronger at high latitudes. This prediction has recently been confirmed during an experimental campaign carried out jointly by Leicester University and the Max Planck Institut (MPI) fur Aeronomie using the new MPI ionospheric modification facility at Ramfjordmoen near Tromso, Norway (Jones et al 1982a). In addition, a number of other important new results were obtained during the campaign. These results include the discovery of several completely new effects such as

(a) a complicated dependence of anomalous absorption on pump power and which is affected by ionospheric variability,

(b) the phenomenon of super self-absorption of the pump wave,

(c) a hysteresis effect associated with the generation of FAI,

(d) an F-region cross modulation effect.

In the following sections of this paper these results will be described and their relationship to an overall understanding of the FAI generation mechanisms will be briefly discussed.

2. ANOMALOUS ABSORPTION - DEPENDENCE ON PUMP POWER

During an experiment on 12 October 1980 the heater was operated on 3.515 MHz, O mode, 2 minon - 2 min off. The effective radiated power (ERP) was changed from one on period to the next as ERP = p.160 MW, p = 1, ½, ¼, ⅛. At the same time the signal strength of a low power (30W) 3.778 MHz diagnostic wave which was reflected from the ionosphere just above the heated volume was measured. Fig. 1 illustrates the diagnostic amplitude as a function of time.

In fig. 1(a) the fading rate during off periods is low indicating a fairly quiet ionosphere. During the four on cycles, the anomalous absorption of the diagnostic exhibits very little dependence on ERP. During subsequent on-off cycles (figs 1b,c) the fading rate increased and the anomalous absorption decreases overall but exhibits an increasing power dependence. It is clear that the background motion of the ionosphere

plays an important role in the generation mechanism of FAI which cause anomalous absorption. In a quiet ionosphere the FAI amplitude saturates at a low pump threshold and is insensitive to pump amplitude above the threshold. In a variable ionosphere the FAI amplitude does not necessarily saturate even at the highest pump power employed and is very sensitive to ERP. Stubbe et al (1981a) have extended the FAI generation theory of Das and Fejer (1979) to explain this result.

3. ANOMALOUS PLASMA HEATING - LATITUDINAL DEPENDENCE

During the experiment outlined in the previous section, the phase of the 3.778 MHz diagnostic was measured relative to a standard oscillator at the receiver site. Diagnostic phase is sensitive to changes in ionospheric refractive index which occur when the temperature of the electron plasma increases. In the lower F region this causes a decrease in the ion-electron recombination rate which increases the ambient electron density. In fig. 2 graphs relating phase changes to ERP and anomalous absorption have been plotted. They indicate that the phase changes and consequently the plasma heating are far more sensitive to anomalous absorption than ERP. Thus, it appears that at high latitudes ionospheric heating is dominated by anomalous absorption due to the strong excitation of field aligned irregularities (Jones et al, 1982a). At mid and low latitudes on the other hand, experiments indicate that anomalous absorption and direct ohmic heating are roughly of equal importance.

4. 'SUPER' SELF-ABSORPTION OF HIGH POWER RADIO WAVES

During an experiment on 10 September 1981 the amplitude of the ionospherically reflected pump wave was measured as the transmitted pump ERP was increased uniformly from 0 to 260 MW (full power) over a period of 6 min. Subsequently the ERP was decreased uniformly from 260 MW down to 0 MW. Fig. 3 is a graph of reflected pump amplitude against time during this experiment. It clearly illustrates the essentially non linear nature of the reflectivity of high power radio waves. Moreover, a striking new effect is exhibited when ERP is increased above about 40% of full power. While ERP is increasing from 0 to 40% full power the reflected pump power increases with increasing ERP as expected even though its amplitude is diminished by self-absorption due to the generation of FAI. However, when ERP is increased beyond 40% full power, the reflected pump power starts to decrease; hence, 'Super' self-absorption. 'Super' self-absorption has been explained by Kopka et al (1982) in terms of a power dependent absorption coefficient for high power EM waves.

Another new phenomenon which is also clearly illustrated in fig. 3 is a hysteresis effect, i.e. the anomalous absorption of the pump has different values depending on whether the ERP is increasing or decreasing. Using the data in fig. 3 a hysteresis curve for absorption coefficient against ERP is plotted in fig. 4. The existence of a hysteresis effect in the anomalous absorption coefficient is evidence for a two stage FAI generation mechanism the second stage of which has a FAI amplitude dependent threshold (Stubbe et al, 1982b; Jones et al, 1982b).

5. F-REGION CROSS-MODULATION

Because the electron collision frequency in the ionospheric plasma is temperature dependent, an amplitude modulated pump wave will superimpose a modulation on the collision controlled absorption coefficient of radio waves passing through the heated region. This results in a cross modulation effect. This effect is normally strong only in the D region where EM wave heating can cause large electron temperature changes (Gurevich, 1978). In the F region, only very small temperature changes can be achieved and so the effect described is expected to be unobservable there. However, during a recent experimental campaign spectral analysis of a diagnostic wave passing through a portion of the F region subjected to modulated heating by a high power (260 MW) pump did exhibit a cross modulation effect (fig. 5). It is thought that this occurred because of the modulation of FAI amplitudes by the pump (Stubbe et al, 1982b). Detailed measurements of cross modulation depth as a function of modulation frequency may well provide an extremely efficient technique for determining the time constants of the instabilities which cause FAI.

6. OTHER HEATING EFFECTS

The effects described above are associated with the absorption of HF waves in the heated volume of the ionosphere. There are, in addition, other disturbances induced by the heater which influence HF propagation. For example, the heated volume can reflect and scatter HF waves thus providing an additional "reflecting" region embedded in the ambient ionosphere. The magnitude of the effects depends on the heater frequency, power and the geometry of the HF reflection path.

Recently strong HF emissions have been detected at frequencies close to the pump frequency (Thidé et al, 1982). These are produced by various parametric plasma instabilities induced by the interaction of the pump and low amplitude natural plasma fluctuations. The magnitude and frequency range of these radiations are therefore somewhat variable and depend on the ambient ionospheric conditions.

These heater induced features will clearly affect the performance of any HF system operating through, or close to, the heated volume.

7. CONCLUSIONS

The modification of the ionosphere by high power radio waves produces marked disturbances on HF signals propagating through the heated volume. Many of these disturbances are associated with the creation of striations and the anomalous absorption that these structures produce. Reflection, scatter and emission of radio energy can also occur which further complicates the characteristics of HF propagation in the vicinity of the heated region.

Further research is necessary before the full extent of ionospheric modification on HF propagation can be quantitatively assessed.

REFERENCES

Cohen, R and J.D. Whitehead (1970), J. Geophys. Res., 75, 6439

Das, A.C. and J.A. Fejer (1979), J. Geophys. Res., 84, 6701

Fialer, P.A. (1974), Radio Sci., 9, 923

Grach, S.M., A.N. Karashtin, N.A. Mityakov, V.O. Rapoport and V.Yu. Trakhtengarts (1977), Radio Phys. Quantum Electron. Eng. Trans., 20, 1254

Graham, K.N. and J.A. Fejer (1976), Radio Sci., 11, 1057

Gurevich, A.V., Nonlinear phenomena in the ionosphere, Springer-Verlag, New York, 1978

Jones, T.B., T. Robinson, H. Kopka and P. Stubbe, (1982a), J. Geophys. Res., 87, 1557

Jones, T.B., T.Robinson, P. Stubbe and H. Kopka (1982b), 'A hysteresis effect in the generation of field aligned irregularities by a high power radio wave' - submitted to Radio Sci.

Kopka, H., P. Stubbe, T.B. Jones and T. Robinson (1982), Nature, 295, 680

Minkoff, J. (1974), Radio Sci., 9, 997

Stubbe, P., H. Kopka, T.B. Jones and T. Robinson, (1982a), J. Geophys. Res., 87, 1551

Stubbe, P. et al (1982b), Ionospheric modification experiments in Northern Scandinavia - submitted to J. Atmos. Terr. Phys.

Thidé, B., H. Kopka and P. Stubbe (1982), Observations of stimulated scattering of a strong HF radio wave in the ionosphere - submitted to Phys. Rev. Lett.

FIGURE CAPTIONS

Fig. 1: Diagnostic amplitude as a function of time during heating with 3.515 MHz, 0-mode pump, 2 min on - 2 min off.

Fig. 2: Graphs showing the relation between induced phase change and anomalous absorption of the diagnostic and ERP of the pump.

Fig. 3: Reflected pump amplitude as a function of time as pump ERP was changed uniformly from 0-260 MW-0.

Fig. 4: Hysteresis curve for pump self-absorption.

Fig. 5: Gross modulation side bands induced in diagnostic wave during heating with modulated pump wave.

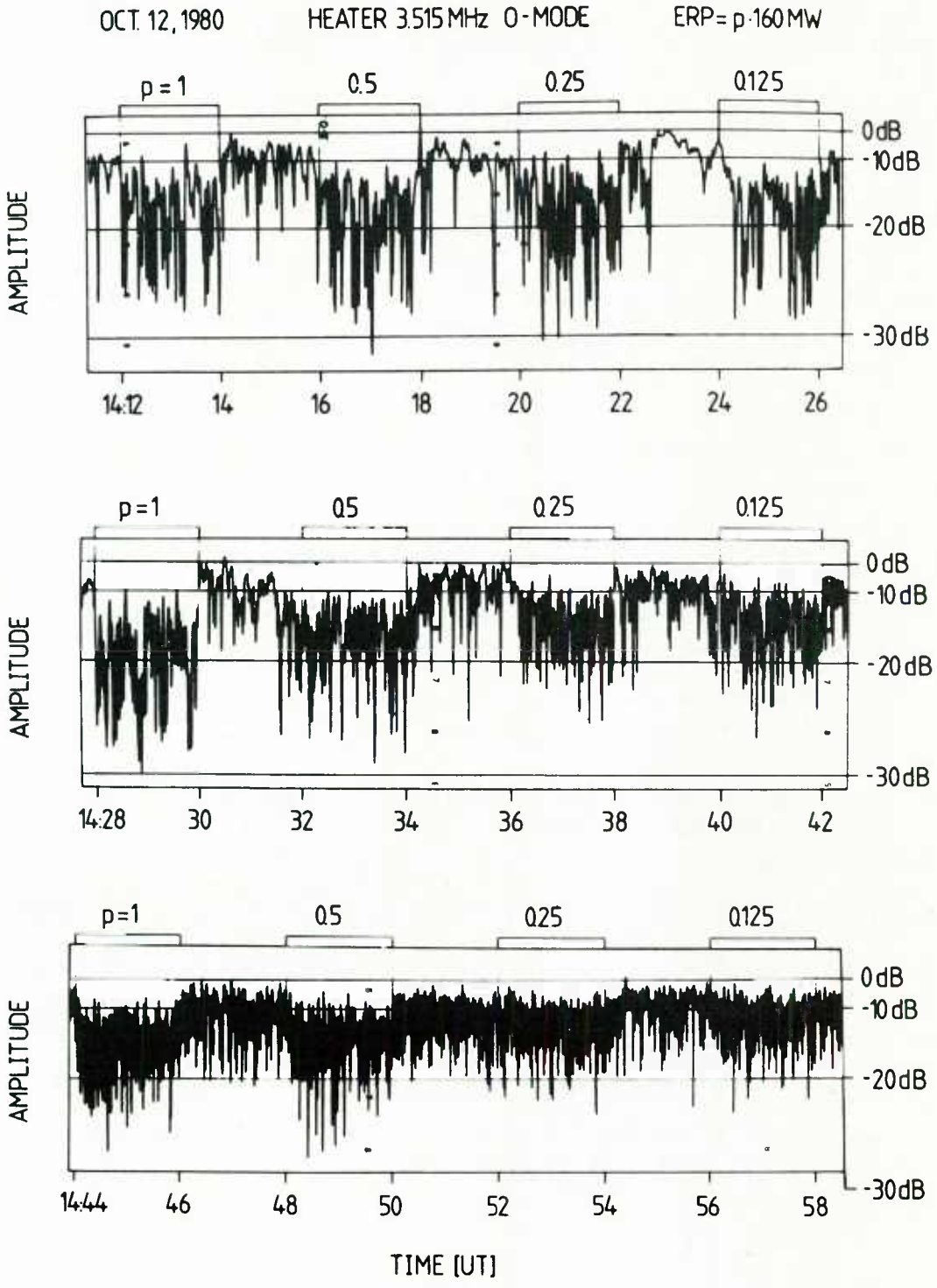
OCT. 12, 1980
HEATER 3.515 MHz O-MODE
ERP = p·160 MW
p = 1
0.5
0.25
0.125
0 dB
-10 dB
-20 dB
-30 dB
AMPLITUDE
14:12
14
16
18
20
22
24
26
p=1
0.5
0.25
0.125
0 dB
-10 dB
-20 dB
-30 dB
AMPLITUDE
14:28
30
32
34
36
38
40
42
p=1
0.5
0.25
0.125
0 dB
-10 dB
-20 dB
-30 dB
AMPLITUDE
14:44
46
48
50
52
54
56
58
TIME [UT]

Figure 1

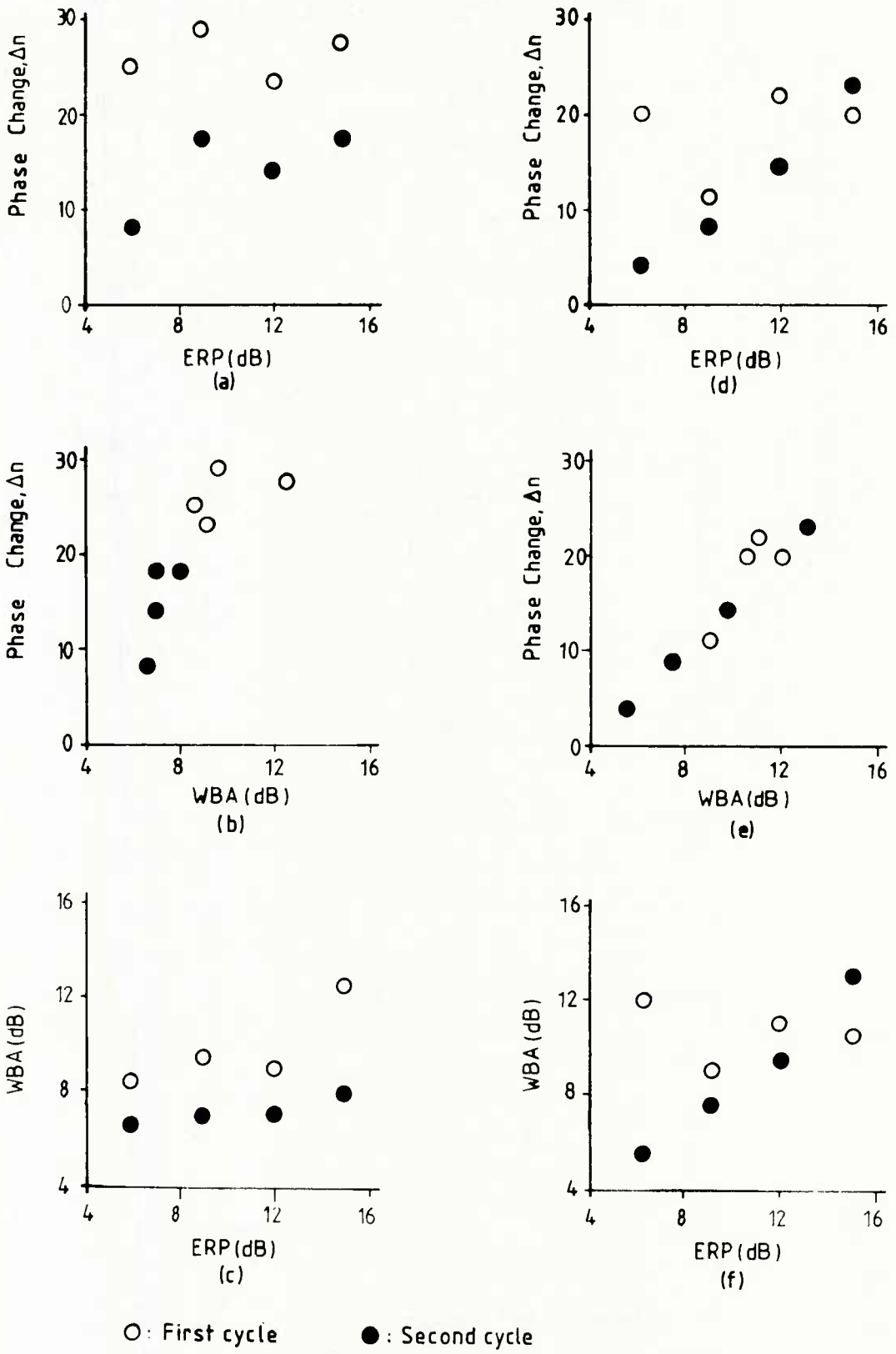
Phase Change, Δn
30
20
10
0
4
8
12
16
ERP(dB)
(a)
Phase Change, Δn
30
20
10
0
4
8
12
16
ERP(dB)
(d)
Phase Change, Δn
30
20
10
0
4
8
12
16
WBA(dB)
(b)
Phase Change, Δn
30
20
10
0
4
8
12
16
WBA(dB)
(e)
WBA(dB)
16
12
8
4
4
8
12
16
ERP(dB)
(c)
WBA(dB)
16
12
8
4
4
8
12
16
ERP(dB)
(f)
○: First cycle
●: Second cycle

Figure 2

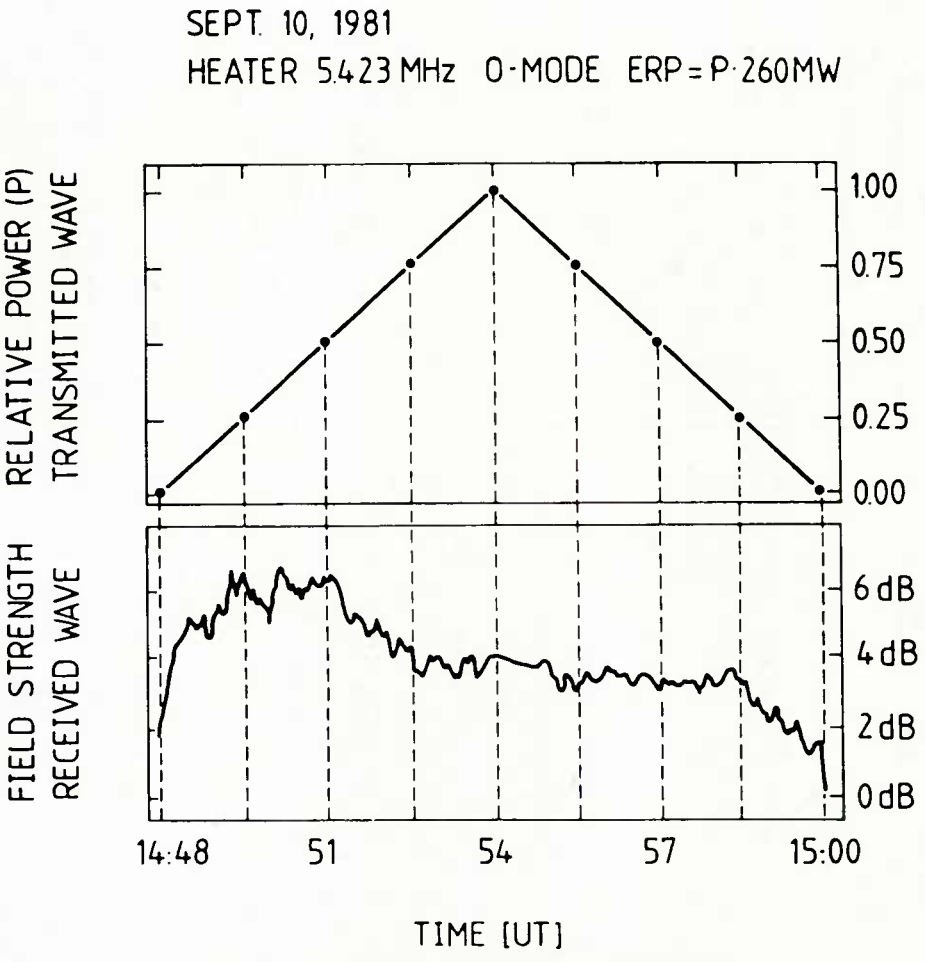

Figure 3

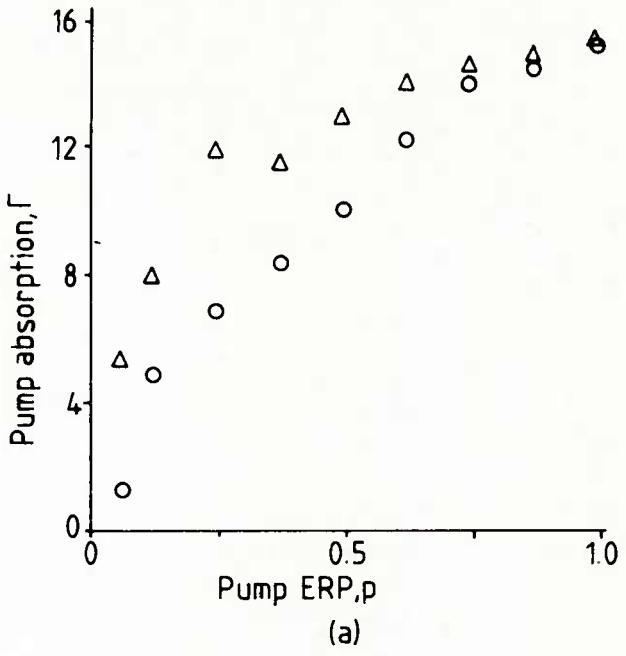

Figure 4

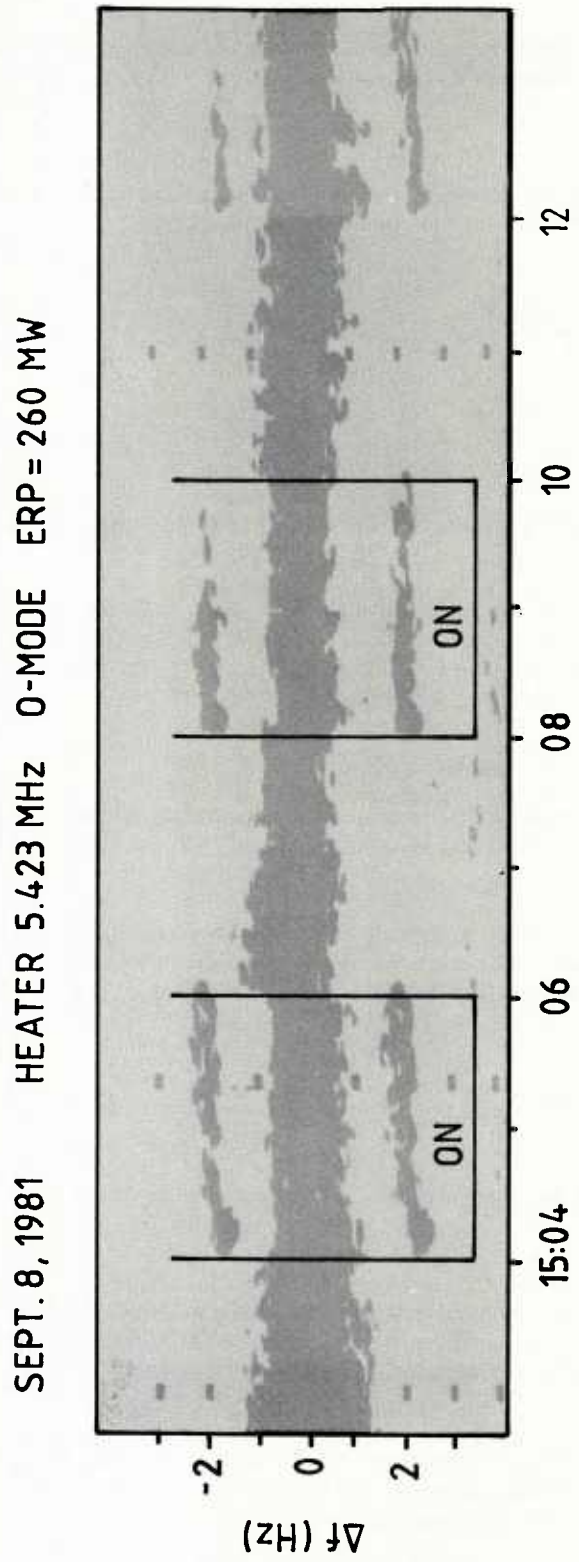
SEPT. 8, 1981 HEATER 5.423 MHz O-MODE ERP = 260 MW
ON
ON
15:04
06
08
10
12
TIME (UT)
-2
0
2
Δf (Hz)

Figure 5

DISCUSSION

E.J.Holliman, US

Although your study was in regard to radio propagation observation, did you observe any visible light being generated in the ionosphere?

Author's Reply

In the Boulder experiments, we know that such simulated emissions did occur. However, in the experiments at Tromso it has not yet been observed although there are indications that weak emissions might occur.

K.D.Becker, Ge

Can you say something on the physical model and the theoretical background of your investigations (experiments)? Is there anything concerning this subject in the literature?

Author's Reply

The plasma physics of these heating effects is somewhat complicated. I would refer to the following papers:

(1) Jones et al., Jour. Geophys. Res. 87, 1557, 1982.
(2) Stubbe et al., Jour. Geophys. Res. 87, 1551, 1982.
(3) Kopka et al., Nature, 295, 680, 1982.

D.Davidson, US

What limit is there on the upper frequency of the heating wave? What would happen if f_{htr} went up into VHF?

Author's Reply

In the experiments reported, the highest frequency on which heating was undertaken was 5.423 MHz. There is no possibility to use frequency greater than about 10 MHz. For VHF waves the effect would be very small since the frequency would be very much greater than the F region critical frequency. As far as I am aware, no heating effects have so far been observed with very high power VHF transmitters.

K.A.Hughes, UK

Whilst the impact of artificially generated irregularities on existing communications is fairly obvious, what, in ılity, reality, is the impact of the increased absorption on existing systems? Is the effect not very local?

Author's Reply

The absorption effects are limited to waves passing through the disturbed region and are therefore localised. However, the presence of a scattering volume in the ionosphere could provide additional propagation paths and so produce modal interference. There is also the possibility of simulated emissions producing interference.

P.A.Bradley, UK

Have you attempted to monitor effects of high power heating at the conjugate point?

Author's Reply

No. However, it would be expected that some conjugate effects would be produced.

H.J.Albrecht, Ge

In view of the fact that the experiments reported have been repeated a sufficient number of times to prove that effects can be reproduced, have such additional experiments been done at different times of a day and has a diurnal variation been noticed in occurrence and/or intensity?

Author's Reply

These experiments have now been repeated many times with the same results. The critical factors in these observations is the state of the background ambient ionosphere. The effects produced will depend on whether the ionosphere is quiet or disturbed when heating takes place.

H.Soicher, US

Are the heating effects instantaneous? at turn on? at turn off?

Author's Reply

The time constants for the F region effects reported in this presentation are about 20 sec in both cases.

J.M.Goodman, US

How did you determine whether the various frames in the figure referred to in the previous question were disturbed or undisturbed?

Author's Reply

By examining the fading rate of the diagnostic wave when the heater was off, we assume that a slow fading rate (1 fade every few minutes) indicates an undisturbed ionosphere whereas fast fading (several fades per minute) indicates that the ionosphere is disturbed. Ionograms were also used to establish the state of the ambient ionosphere.

SUMMARY OF SESSION II-B

TERRESTRIAL PROPAGATION (IONOSPHERIC MODE)

by

Dr H.Soicher
Session Chairman

This session comprised of five papers and focused on the following topics: high latitude ionospheric effects, MF skywave interference and frequency sharing, ionospheric modelling and real-time updates of models for prediction purposes.

Lange-Hesse discussed aspects of bistatic auroral backscatter VHF propagation for communication purposes and their important potential for interference. Since auroral backscatter is possible over long distances, careful frequency assignments are necessary in order to avoid interference between widely-separated circuits. The physics of the backscatter phenomena is discussed, as are its daily variations, and frequency of occurrence as a function of geomagnetic activity, latitude, time-of-day, season and sunspot cycle.

Wang discussed MF skywave field strength data. Whereas stress has been placed on the prediction of yearly median values of nighttime field strength, potential interference from daytime MF skywave necessitates future studies of short term variabilities. Effects of magnetic storms on MF field strength have indicated that absorption increases with frequency.

Bradley reported on the procedures existing under the auspices of the International Telecommunications Union for allocating frequency blocks to radio services and for the assignment of specific frequencies to individual radio operators. The compatibility analysis undertaken by the International Frequency Registration Board at HF to test harmful interference is described. Such analysis takes into account the important factors of signal and noise variability.

Hunsucker pointed out the anomalous propagation behavior unique to the high-latitude region. The effects mentioned were across the radio spectrum and included propagation modes along ground, tropospheric, ionospheric, and trans-ionospheric paths. Specifically, some new results include the measurement of ground constant of tundra/permafrost, MF skywave signals appear to be limited to almost north-south paths with lower signal strengths than had been expected, and precipitation depolarization of satellite down link signal at 4 GHz.

In the last two papers of the session **Goodman** examined the scheme by which a computer model of the HF channel may be used to anticipate channel characteristics in a short term prediction mode, as well as reported on an EPP sponsored effort to compile existing ionospheric models. In the former, the proposed scheme would permit automated frequency management by anticipating frequency availability and thereby allowing sharing of frequencies between several users. Model parameters are updated by a real-time oblique sounding at a control circuit. In the latter, a survey of physical and empirical models which are or will be employed to evaluate the operation of military radio systems, is presented.

VHF-Long-Distance-Propagation by Auroral Backscatter

by

Günther Lange-Hesse
Max-Planck-Institut für Aeronomie, D-3411 Katlenburg.Lindau 3, Postfach 20, WEST GERMANY

SUMMARY:
Extended investigations of VHF auroral backscatter communications had been carried out in Europe in the years from 1958 to 1969 using the results of the observations of beacon transmitters and of an extended network of amateur radio stations covering big parts of Europe.

The frequency of occurrence of this kind of propagation as a function of geomagnetic activity and latitude, time of day, season and sunspot cycle is shown by several diagrams. The physical reasons for this backscatter phenomenon and especially for the typical daily variation in the frequency of occurrence are discused.

Propersals are made for special arrangements to suppress this kind of propagation in case of frequency sharing.

1. INTRODUCTION

The fact that aurora influences radio wave propagation was known before World War II. Reflections of radio waves from ionization associated with aurora ——called: radio aurora*) —— were first investigated in 1938 by HARANG and STOFFREGEN at Tromsö/Northern Norway (1940) in the lower VHF range. At the same time amateurradio operators in North America had discovered that VHF radio wave propagation via auroral ionization was possible (TILTON, 1944; MOORE, 1951). In the years after World War II radio aurora has been studied by a number of researchers at different parts of the world. Most investigetions of this phenomenon have been made by means of radar, i.e. with transmitter and receiver at the same place. Several review papers of the results of these radar auroral experiments have been published by numerous authers e.g. LITTLE et al. (1956), LANGE-HESSE (1957), BIRFELD (1960), PETERSON (1960), BAGARYATSKY (1960),BOOKER (1960), CHAMBERLEIN (1960), HULTQVIST et al. (1964),and LEADARBRAND (1965a).

2. ASPECT SENSITIVITY CONTROL BY THE GEOMAGNETIC FIELD

The reduction of VHF radar echoes from aurora has shown that these echoes can only be obtained from a very restricted strip of sky corresponding to the region where the line of sight from the radar location to the aurora intersects the local geomagnetic field lines at right angles. Figure 1 shows the geometry of the VHF auroral backscatter problem. On the condition that perpendicularity is necessary, auroral displays at points A and B in Figure 1 use to give backscatter-echoes at the radar site, but not at the points C and D. Perfect 90^0 intersection, however, is not required, because of the finite length of the auroral scatters. Depending upon the frequency, peak power and sensitivity of the radar, echoes can be obtained at intersection angles that differ from 90^0 by as much as 5^0 to 10^0. The deviation of the intersection angle from 90^0 is called the "off-perpendicular angle".

3. WAVELENGTH DEPENDENCE

The wavelength dependence of the auroral echoes is well pronounced. The echo power decreases strongly with increasing frequency. Wavelength dependence together with aspect sensitivity have been measured by a number of workers, e.g. PRESNELL et al. (1959), BLEVIS et al. (1963), FLOOD (1960), STONE et al. (1959). The results obtained by LEADABRAND (1962) and LEADABRAND et al. (1965b) with elaborate auroral equipment located at Fraserburgh, Scotland, however, could be interpreted most easily, primarily because of the narrow beam involved. The radar was specifically designed for this purpose having identical beamwidths(1.2^0)at 400 and 800 MHz. Thus the identical volume of aurora was illuminated simultaneously at both frequencies. Wave length dependence observations carried out with this equipment resulted in a power law depencence of λ^7 and aspect sensitivity observations in an energy decrease of 10 db/per degree off-perndicular.

4. GEOMETRY FOR BISTATIC AURORAL BACKSCATTER COMMUNICATION

As well as by radar studies, radio aurora have also bee studied by investigating oblique ——or bistatic—— auroral reflections, i.e. with transmitter and receiver at different places. Fig. 2 shows a representation of the geometry of the propagation path in the vertical direction in the case of bistatic auroral backscatter communication between the points S_0 and S_1. The z-axis of a three-dimensional xyz-coordinate system in Fig.2 is tangential to the geomagnetic line of force at the point of the backscattering centre or irregularity. The xy-plane is perpendicular to the geomagnetic line of force; k_0 and k_1 are the vectors of the wave normal of incident and backscattered wave, resp.; Ω_0 and Ω_1 are the "propagation angles" = the angles between the direction of radio wave propagation and the magnetic line of force; ε_0 and ε_1 are the angles between k_0 and k_1, resp. and the xy-plane. Optimum conditions are given for the possibility of VHF aurora backscatter propagation, if the relation $\cos \Omega_0 + \cos \Omega_1 = 0$ is fulfilled at the point of the backscattering centre. This means that the vectors k_0 and k_1 describe the same angle with the xy-plane, in this case is $\varepsilon_0 = \varepsilon_1$ and the vector$(k_0 - k_1)$ is perpendicular to

*) In this paper the following expressions are mostly used as synonyms without alluding to different physical mechanisms: radio aurora, auroral echoes, auroral backscatter, and auroral reflections.

the xy-plane. Optimum conditions of that kind will be referred to as"ideal backscatter conditions".

If the angles ε_0, ε_1 or Ω_0, Ω_1 deviate from the ideal backscatter conditions by only a few degrees (similar to the radar off-perpendicular backscatter case) bistatic backscatter propagation in principle is possible according to the theory. The backscattered power, however, descreases very rapidly with increasing angle deviation from the ideal conditions. One therefore needs very strong transmitters and antennas with high gain, in order to establish communication, if the angles mentioned before deviate by only a few degrees from the ideal backscatter conditions especially in the UHF and higher VHF range. For particulars see the curves in the papers EGELAND (1962) pp. 198 to 201, and CZECHOWSKY (1966) Figure 14 and A 11.

5. THEORY FOR GENERATION OF THE BACKSCATTERING CENTERS

According to the theory the backscattering of VHF radio waves by aurora not only is controlled be the visual aurora but on a larger scale by the polar electrojet (PEJ). This is an extended current system at a height of about 100-110 km in polar regions which has its highest current density along the main auroral regions (Fig. 8, left). The PEJ and the visual aurora are caused by the precipitation of solar particle radiation. The magnetic field of the current system give rise to pertubations of the geomagnetic field on the ground which are called "geomagnetic activity". Higher geomagnetic activity is called "geomagnetic storm". About 20 years ago BUNEMAN (1963) and FARLEY (1963) pointed out independently that in an ionospheric current system like e.g. the equatorial electrojet (EEJ)* plasma instabilities of a "two-stream" type can occur so that acoustic plasma waves are generated. The plasma instability appears when the relative drift velocity between the ions and electrons in the electrojet (EJ) exceeds a certain critical speed which is close to the thermal velocity of the ions.It is said that the electrojet at this phase has exceeded the threshold.Acoustic plasma waves then are generated in shape of longitudinal density waves, which propagate along the electrojet transverse to the geomagnetic lines of force. The periodical density oscillations caused by the plasma waves (which represent a special fine structure of the EJ) are the field aligned centers (field aligned to the geomagnetic lines of force) which give rise to the backscattering of VHF radio waves. BOWLES et al. (1963) and COHEN and BOWLES (1963) have shown that the VHF waves backscattering centers in the EEJ are caused by acoustic plasma waves. In the same publication the authors pointed out that the VHF waves backscattering centers in the PEJ obviously are caused by the same mechanism.

Backscatter echoes from irregularities caused by plasma waves are called "Typ I Echoes". In 1969 BALSLEY (1969) described a second type of backscatter echoes called "Type II Echoes". They occur mainly at times and in regions of lower current density in the electrojet and show the characteristics of the "gradientdrift-theory" developed by SIMON (1963) and HOH (1963).

6. COMPUTATION OF THE LOCATION OF THE BACKSCATTERING CENTERS IN CASE OF OF BISTATIC AURORAL BACKSCATTER PROPAGATION

On the map of Europe in Figure 3 the solid curves at the left represent the location where the line of sight from London in different directions intersects the geomagnetic lines of force at constant angles at the height of 110 km. This is about the mean observed height of the backscattering centers (see e.g. UNWIN 1958, UNWIN 1959, BARBER et al, 1962, LEADABRAND et al, 1965b). In Figure 3 the curves are shown for an angle of intersection of 88^0, 90^0 and 92^0. The curves were computed with the help of an electronic computer using magnetic dip angle and declination from the ground (description of the method see MILLMAN, 1959 and EGELAND, 1962). The calculation of the curves was restricted to elevation angles E_0, E_1 (Figure 2) greater than or equal to zero for the line of sight to 110 km height. The dotted curves to the right in Figure 3 show the same as the solid curves to the left but referred to Wolszyn (Poland). It can be seen in the Figure that the curves intersect each other. For the two locations, London and Wolszyn, the ideal backscatter condition $\cos \Omega_0 + \cos \Omega_1 = 0$ or $\varepsilon_0 = \varepsilon_1$ (Figure 2) is fulfilled along the dashed line in Figure 3 for elevation angles E_0, E_1 of the wave-normal with the ground greater than or equal to zero. As one can see in Figure 3 the dashed line connects the point of intersection of a) the 88^0 - London curve with the 92^0 - Wolszyn curve, b) the 92^0 -London curve with the 88^0 - Wolszyn curve, and c) the 90^0 -London and Wolszyn curves.

The locations where the ideal backscatter conditions (as shown in Fig. 3) are fulfilled at 110 km height are shown in Fig. 4 for the two points Oslo and Aberdeen. If auroral backscatter communication occurs between these two points irregularities must be generated in the PEJ at one point along the solid curve in the figure.

The backscattered power also depends on the angle θ between the two wave normale k_0, k_1, of the incident and backscattered wave (Figure 4). θ can vary between $\theta = 180^0$ (radar case, the two points fit together, Fig. 1) and small values of θ (forward-scatter case). The backscattered power varies in these extreme cases according to the theory in a ratio of about one to two.

7. MAXIMUM DISTANCE FOR BISTATIC AURORAL BACKSCATTER COMMUNICATIONS

The three curves shown in Figure 5 represent the computed maximum distances which can be contacted by VHF bistatic auroral backscatter communications from Hamburg (dotted curve), Stockholm (dashed curve), and Oslo (solid curve). The curves are computed using the observed magnetic dip angle and the declination from the ground and are valid for a height of the backscattering centers of 110 km above the ground. For the computation of

---

* This is a current system in the upper atmosphere at a height of about 100 km similar to the PEJ but concentrated along the geomagnetic equator

the curves only those directions of propagation of the backscattered wave are taken into consideration which fulfil the ideal backscatter condition. That means $\cos \Omega_0 + \cos \Omega_1 = 0$ or $\varepsilon_0 = \varepsilon_1$ (Figure 2). According to theoretical estimations mentioned before (CZECHOWSKY, 1966) the ideal backscatter condition must be fulfilled for communications with low power transmitters (e.g. the power used by radio amateurs is only of the order of 50 to 100 watts) in order to have sufficient signal strength at the receiving point.

In a supplement to Figure 5 the curves show in Figure 6 represent the computed maximum-distance-curves for Munich for the two heights of the backscattering centres of 110 and 200 km. The dots in Figure 6 represent stations which could be contacted from Munich via VHF auroral backscatter communication on 144 MHz. A few of these stations were contacted from Munich more than once. If these recurring contacts are taken into consideration by corresponding (statistical) weights, only 5% of the total number of contacts were carried out with stations located outside the maximum-distance-curve for 110 km height, but 30% of the contacts were carried out with stations located outside the 200 km curve (dotted curve in Figure 9). It follows from the results presented in Figure 6 that the computed maximum distances for a height of the backscattering centres at 110 km coincide to a first approximation with the observations.

8. PROBABLE REASONS FOR MAXIMUM DISTANCE VARIATIONS

All of the propagation angles, backscatter and maximum-distance-curves shown in the figure of this paper are computed using the assumption of an undisturbed geomagnetic field or for the "static situation". It is well known that during stronger geomagnetic activity called "geomagnetic storms" the geomagnetic lines of force can change their orientation in space, that means that the dip angle J deviates from its normal value (STRØMER, 1926). In connection with a variation ΔJ of the dip angle the ideal backscatter condition may be fulfilled for propagation paths which do not normally fulfil this condition under geomagnetic undisturbed conditions. The propagation path for the communication Munich-Aberdeen deviates from the ideal backscatter condition by 1.3^0. For this special case it is computed, that a ΔJ of 1^0 will result in the exact fulfilment of the ideal backscatter condition (Figure 2), (CZECHOWSKY, 1966; LANGE-HESSE et al. 1966). The auroral backscatter communications from Munich to stations beyond the 110 km maximum distance-curve in Figure 6 were carried out during times of stronger geomagnetic storms which have caused dip angle variation of 1^0 or more (CZECHOWSKY, 1966; LANGE-HESSE et al. 1966). Dip angle variations in connection with geomagnetic storms therefore can cause deviations from the meximum-distance-curves up to 300 km and more. These deviations are larger than those caused by radio meteorological influences CZECHOWSKY, 1966; LANGE-HESSE et al. 1966). The dip angle variations therefore provide an explanation of the observed communications beyond the computed maximum distances (Figure 6).

9. TIME VARIATIONS OF BISTATIC BACKSCATTER COMMUNICATIONS

9.1) Diurnal Variations

As already mentioned in connection with Fig. 6 investigations of VHF bistatic auroral reflections have made by means of a geographically extended net for amateur radio stations. Observation of this kind were first carried out in North America during the years before the IGY (MOORE, 1951, DYCE, 1955, GERSON, 1955a, b). During the IGY and later years some observations were carried out in Europe especially in the U.K. (e.g. STONE, 1960, 1965, SMITH-ROSE, 1960 NEWTON, 1965) and Germany (LANGE-HESSE, 1962, 1963a, b, 1964A, b, 1967, LANGE-HESSE et al. 1965, 1966). The amateur observations later on had been supported and supplemented by observations of a net of VHF beacon transmitters and receiving stations shown in Fig. 7. (LANGE-HESSE, 1969, and CZECHOWSKY et al. 1970, 1971).

The three right diagrams in Fig. 8 show the average diurnal time variation of the frequency of occurrence of VHF auroral backscatter communications on the beacon line from Borlänge (SM4MPI) to Kjeller (see Fig. 7, solid line backscatter curve). The numbers in the stepped curves signify the total number of backscatter registrations (100 percent) made during the specified observed period. Fig. 9 shows the average diurnal variation of the frequency of occurence of VHF auroral backscatter communications according to amateur observations in Germany in $48^0 \leq \Phi \leq 55^0$ geomagnetic latitudes, that means in lower latitudes compared to those in Fig. 8, right.

According to the diagrams in Fig.8 right, auroral communications are less frequent during daytime hours especially in the time from 08.00 to 15.00 MET. The reason is that according to Fig. 8 left, visual auroras*) are most frequent at this daytime at higher latitudes, 75^0 to 80^0 geomagnetic latitude, that means 6 to 11 latitude degrees north of the backscatter curve for the line Borlänge - Kjeller (Fig. 7).

During nighttime hours the auroral oval and the polar electrojet (PEJ) moves more to lower latitudes and is extended about between 63^0 and 71^0 geomagnetic latitude (Fig. 8, left), that means that both intersect fully the backscatter curve for the line Borlänge - Kjeller (Fig. 7, solid backscatter curve). This is a first explanation for the much more frequent occurrence of backscatter communication during the hours from 15.00 to 06.00 MET. The PEJ flows in a first approximation parallel to the auroral oval and in the afternoon and evening hours from west zu east. The magnetic pertubation field of this current on the ground therefore has northern direction. Since the horizontal component of the geomagnetic field on the ground on the northern hemisphere points to the north too, the geomagnetic variations show an increase of H during aurora in the after noon and evening hours (Fig. 10, H-Komp.). During midnight and morning hours the PEJ

---

*) and simultaneously backscattering centers generated in the polar electrojet current (PEJ) which coincide in space to a first approximation with the auroral oval.

flows in a first approximation from east to west parallel to the auroral oval. The magnetic pertubation field of the current in this case points to the south on the ground and the geomagnetic variations therefore show a decrease of H during these hours (Fig. 10, H-Komp.).

In the transition period from eastward to westward flowing PEJ before midhight the current strength is low and more frequent below the treshold (see section 5), therefore less backscattering centers are generated in the PEJ during these hours. This is the reason for the pronounced occurrence minima in the diagrams of Fig. 8 right and Fig.9 in the time two to three hours before midnight.

9.2) Correlation between Signal Strength Variation and Geomagnetic Variations

Fig. 10 shows VHF auroral backscatter recordings from the beacon station Borlänge, SM4MPI, at three different stations compared with the geomagnetic variations from the scandinavian observatories Lovö, Lycksele, Abisko and Tromsö. The backscatter curve for the line Borlänge - Lycksele is located over Tromsö (Fig. 7, dash-dotted curve). The geomagnetic variation of the horizontal-component (H-Komp) from the Tromsö-Observatory in Fig. 10 ——which are caused by the PEJ over Tromsö—— shows a remarkable correlation in shape with the signal strength variation on the line Borlänge - Lycksele. This is a typical characteristic of signal strength variations of auroral bakcscatter communications and the variations of the corresponding geomagnetic horizontal component.

Due to the reversial of the direction of the current in the PEJ in the hours before midnight ——as mentioned in section 9.1)—— the amplitude of the geomagnetic variation of the horizontal component (H-Komp) from Tromsö (Tr) and Abisko (Ab) in Fig. 10 between 20.00 and 21.00 UT (about 21.00 and 22.00 local time) is nearly zero and no backscatter signal occur on the lines in Fig.10 since the PEJ is at this time below the treshold (see section 5) so that no backscattering centers can be generated.This characteristic could already be seen in the average diurnal variations of Fig.8,right and Fig.9.

9.3) Influence of Geomagnetic Activity and Geomagnetic latitude

The results shown in Fig. 10 exhibit the controle of the geomagnetic variations on the occurrence and signal strength of auroral backscatter communication. Geomagnetic variations are also called "geomagnetic activity" A measure of the planetary geomagnetic activity degree is the Kp-index with the scale from Kp = 0 to Kp = 9. Kp = 0 is geomagnetic undisturbed, Kp = 9: strongest disturbance.

Fig. 11 shows the influence of the Kp-index on the frequency of occurrence of VHF bistatic auroral backscatter communication in different latitudes. The net of observing amateur stations in Central Europe and Scandinavia was divided into five Zones A, B, C, D, E (Fig. 11, right) according to the geomagnetic dip angle I of the observing stations. Zone A is the most southern one with dip angles I ranging from 63-66^0. It covers the region of northern France, southern Germany, Austria, and Czechoslowakia. Zone E is the most northern one with dip angles ranging from 72-74^0. It covers the region from southern Finland via southern Norway to the region north of Scotland.

The left part of Figure 11 shows the influence of the Kp-index on the probability of occurrence of VHF bistatic auroral backscatter communications for communications from station in zone B (dark zone in the figure) to stations in zones, A, B, C, D, and E. The upper diagram in Figure 11, left. shows the Kp influence on the communication frequency from stations in zone B to E (the most northern one) and the lowest diagram A the Kp influence on the communication frequency from stations in zone B to A (the most southern one). The highest occurrence frequency of auroral communication has been made to 100% in every diagram of Figure 11. In the upper diagram E the highest frequency of 100% (which occurs at Kp = 7) corresponds to 141 auroral contacts. In the lower diagram A the highest frequency of 100% (which occurs at Kp = 9) corresponds to 101 auroral communications. 100% does not mean in these cases that auroral communication is possible during 24 hr of the day, but only the highest probability of occurrence. This type of standardization makes it easier to compare the different diagrams in Figure 11.

According to the upper diagram E in Figure 11, the highest communication probability occurs at Kp = 7.At Kp = 4 and 5, auroral contacts are possible with about 30% of the maximum occurrence frequency. During geomagnetic quiet conditions, Kp = 0-2, no communications are pissible. The maximum frequency of aurora communications shifts from Kp = 7 in diagram E to higher Kp values as one moves to the more southern zones D. C. B. and A. The highest frequency of auroral communications from zone B to A (the most southern one) occurs at Kp = 9. Auroral communications between station within zone B and from stations in zone B to stations in zone A are nearly impossible during Kp = 6 and 7, contrary to contacts from stations in zone B to station in zone E, which are possible with maximal probability during these two Kp degrees. The results shown in Figure 11 can be interpreted as a shift of the backscattering centers to southern latitudes with increasing Kp degree similar to the southward movement of visual auroral displays.

9.4) Seasonal and Sunspot Circle Influence

The seasonal influence on VHF auroral backscatter communication is shown in Fig.12. Two pronounced maxima occur in spring and autumn. The reason is that the average geomagnetic activity degree shows maxima during the equinox. This leads to higher occurrence frequency of auroral communications. Finally the seasonal variation in Fig.12 has a close similarity with the monthly frequency distribution for visual aurora in subauroral region given by MEINEL et al. (1954).

Kp-index values of 8 and 9 are most frequent in years near sunspot maximum.In years near sunspot minimum they occur very seldom. In middle latitudes ($\Phi \leq 55^0$) VHF auroral backscatter communications therefore mainly occur in sunspot maximum years. During sunspot minimum conditions this kind auf communication is very rare (see also the results in Fig. 11).

10) Conclusions

Bistatic auroral backscatter propagation is potentially useful for communication purposes, but is of even more importance because of the interference it may cause in communication circuits with frequency sharing. Since the aurora is capable of backscattering over long distances, care must be taken in the assignement of operating frequencies to avoid interference between transmitters even though they are widely separated in the conventional sense. This is of great importance in the VHF range where a transmitter power of the order of 100 watts and low gain directional antennas are sufficient to obtain auroral backscattered long distance communications up to 1000 km and more. This fact is well proved by the extended observations of radio amateurs, who use the backscatter feature of the aurora in order to carry out bistatic auroral backscatter communications between two stations in the 144 and 50 MHz amateur band (a somprehensive list of bistatic auroral backscatter communications carried out by radio amateurs in the 144 MHz-band in Middle Europe from 1957 to 1962 is published by LANGE-HESSE, 1963 b). The possibility of interference by auroral backscatter in the UHF range between transmitters with powers of the order of 100 - 1000 watts and widely separated in the conventional sense is very low. As mentioned in section 4 the backscattered power decreases strongly with increasing frequency with a power law dependence of λ^7. Therefore, one can neglect in a first approximation the auroral backscatter in this frequency range for low power transmitters. UHF military radars, however, having high transmitter power and high antenna gain can be expected to show auroral echoes on their screens even at locations far from the auroral zone. In these cases targets will need to be detected among these auroral "clutter" echoes.

References

Bagaryatsky, B.A.: 1960, "Some results of radar studies of polar aurora", Spectral Electro-Photometrical and Radar Researches of Aurora and Airglow, No. 2-3, Pub. House of Acad. of Science of USSR, Moscow, pp 7-14.

Balsley, B.V.: 1969, "Some characteristic of non-two-stream irregularities in the equatorial electrojet", J.Geophys. Res. 74, 2333.

Barber, D., et al.: 1962, "Some observations of meteors and aurorae at 300 and 500 Mc/s using a large radio telescope. II. Observations of the aurora borealis", J. Atm. Terr. Phys. 24, 599-609.

Birfeld, J.G.: 1960, "Radar observations of Polar aurorae", Bull (izvestia) Acad. Sci. USSR, Geophys. Ser., No. 12, 1248-57.

Blevis, B.C. et al.: 1963, "The occurrence and characteristics of radar aurora echoes at 488 and 944 Mc/s", Can. J. Phys. 41, 1359-1380.

Booker, H.G.: 1960, "Radar studies of the aurora", in Physics of the Upper Atmosphere, ed J.A. Ratcliffe, New York: Academic, 355-375.

Bowles, K.L., Balsley, B.B. and Cohen, R.: 1963, "Field aligned E-region irregularities identified with acoustic plasma waves", J.Geophys. Res. 68, 2485-2501.

Buneman, O.: 1963, "Excitation of field aligned sound waves by electron streams", Phys. Rev. Letters, 10, 285-287.

Chamberlain, J.W.: 1960, "Physics of the Aurora and Airglow", New York: Academic.

Cohen, R. and Bowles, K.: 1963, "The association of plane-wave electron-density irregularities with the equatorial electrojet", J. Geophys. Res. 68, 2503-2525.

Czechowsky, P.: 1966, "Analyse von Rückstreubeobachtungen ultrakurzer Wellen an Polarlichtern——Steuerung durch die Richtung der erdmagnetischen Feldlinien und Zusammenhänge mit der geographischen Lage der rückstreuenden sichtbaren Polarlichter und der Mophologie der begleitenden erdmagnetischen Störungen", Diplom-Arbeit (Master's Thesis) University of Göttingen (Germany).

Czechowsky, P. and Lange-Hesse, G.: 1970, "Substorm Influences on VHF Continuous Wave Auroral Backscatter", in Intercorrelated Satelite Observations Related to Solar Events", (ed. by V.Manno and D.E. Page), D. Reidel Publishing Company, Dordrecht-Holland, pp. 405-412.

Czechowsky, P. and Lange-Hesse, G.: 1971, "Optical and Radio Observations of the Aurora", in THE RADIATING ATMOSPHERE (ed. by B.M. McCormac) D. Reidel Publishing Company, Dordrecht-Holland, pp. 314-326.

Dyce, R.: 1955, "More about VHF auroral propagation", QST 39 (Jan. 1955), 11-15.

Egeland, A.: 1962, "Studies of auroral reflections in the VHF band, II. Comparison of experimental results with theoretical models", Arkiv för Geofysik, 4, 7, 171-209.

Farley, D.T., Jr.: 1963, "A plasma instability resulting in field aligned irregularities in the ionosphere", J. Geophys. Res. 68, 6083-6097.

Flood, W.A.: 1960, "Simultaneous VHF auroral backscatter measurements", J.Geophys. Res. 2261-2268.

Gerson, N.C.: 1955a, "Diurnal variation in auroral activity",Proc.Phys.Soc. 68,408-414.

Gerson, N.C.: 1955b, "Radio observations of the aurora",J.Atm.Terr.Phys. 6, 263-267.

Harang, L. and Stoffregen. W.: 1940, "Echoversuche auf Ultrakurzwellen", Hochfrequenz und Elektroakustik 55, 105-108 and Nature 142, 832-833.

Hoch, F.C.: 1963, "Instability of penning-type discharges", Phys.,Fluids 6, 1184.

Hultqvist, B. and Egeland, A.: 1964, "Radio Aurora", Space Science Review, 3, 27-78.

Lange-Hesse, G.: 1957, "Rückstrahlung kurzer und ultrakurzer Wellen an Polarlichtern", Archiv d. elektr. Übertragung (AEÜ) 11, 253-261, 283-288.

Lange-Hesse, G.: 1962, "VHF-long-distance-propagation in Middle Europe by auroral backscatter", Arch. d. elektr. Übertr. (AEÜ), 16, 251-261.

Lange-Hesse, G.: 1963a,"Seasonal influences on VHF-auroral-backscatter in Middle Europe", Z. Geophys. 29, 35-44.

Lange-Hesse, G.: 1963b, "German Aurora Observations 1957-1962, Part A: Aurora Observations by Means of VHF Radio Waves, Part B: Observations of Visual Aurora", Abhandlungen der Akademie der Wissenschaften in Göttingen, math.-phys.Klasse, Beiträge zum Internationalen Geophysikalischen Jahr, Heft 10, published by Verlag Vandenhoek and Ruprecht, Göttingen (Germany).

Lange-Hesse, G.: 1964a, "VHF-long-distance-propagation in middle latitudes by auroral-backscatter — Influence of the geomagnetic activity-degree on the communication frequency as a function of magnetic dip of the observing stations", Arch.d. elektr. Übertr. (AEÜ) 18, 430-438.

Lange-Hesse, G.: 1964b, "VHF-bistatic-auroral communications as a function of geomagnetic activity and magnetic latitude", in Arctic Communications, AGARDograph 78, ed. B.Landmark, Oxford: Pergamon Press, 253-262.

Lange-Hesse, G.: 1967, "Radio Aurora, Part I. Observations, Part II. Comparison of the observation with a theoretical model", in AURORA and AIRGLOW, ed. B. McCormac, Reinhold Publishing Corp, New York, N.Y.

Lange-Hesse, G.: 1969, "Radio Observations of the Aurora by Continious Wave Transmission", in ATMOSPHERIC EMISSIONS (ed. by B.M. McCormac and A. Omholt), Von Nostrand Reinhold Company, New York-London, pp 201-212.

Lange-Hesse, G.: 1972, "Current Experimental Results from a VHF-CW-Auroral Backscatter Network in Scandinavia", in AGARD Conference Proceedings No.97 on "Radar Propagation in the Arctic", pp. 7-1 to 7-16.

Lange-Hesse, G. and Czechowsky, P.: 1965, "VHF bistatic auroral backscatter communications and the relation to the location of the visual aurora displays", Arch.d.elektr. Übertr. (AEÜ) 19, 511-514.

Lange-Hesse, G. and Czechowsky, P.: 1966,"VHF bistatic auroral backscatter communications, Comparison of the observations with the theory", Arch. d. elektr. Übertr.(AEÜ) 20, 365-375.

Leadabrand, R.L.: 1962, "Radio studies of the aurora", J. Phys. Soc. Japan 17, (Supp.A-1), 218-222.

Leadabrand, R.L.: 1965a, "Electromagnetic measurement of aurora", in Auroral Phenomen, ed. M. Walt, Stanford: Univ. Press, London: Oxford Univ. Press 99-129.

Leadabrand, R.L., Schlobohm, J.C., and Baron, M.J.: 1965b, "Simultaneous very high frequency and ultra high frequency observations of the aurora at Fraserburg, Scottland", J.Geophys. Res. 70, 4235-4284.

Little, G.C., Rayton, W.M., and Roof, R.B.: 1956, "Review of ionospheric effects at VHF and UHF", Proc. IRE 44, 992.

Meinel, A.B., Negaard, B.J., and Chamberlain, B.J.: 1954, J. Geophys. Res.59,407-413.

Millman, G.H.: 1959, "The geometry of the earth's magnetic field at ionospheric heights", J.Geophys. Res. 64, 717-726.

Moore, R.K.: 1951, "A VHF propagation phenomena associated with aurora", J.Geophys.Res. 56, 97-106; and "Aurora and magnetic storms", QST 35, 15 (June 1951);and QST 23, 78 (May 1939), author unknown.

Newton, C.: 1966, "The Society's IGY aurora programme - part I and II", RSGB Bulletin (Journal of the Radio Society of Great Britain) 42, 289-294, 785-790.

Peterson, A.M.: 1960, "The aurora and radio wave propagation", The Radio Noise Spectrum, ed. Donald H. Menzel, Cambridge, Mass: Havard Univ. Press, pp 7-42.

Pressnell, R.I. et al.: 1959, "VHF and UHF radar observations of the aurora at College, Alaska", J. Geophys. Res. 64, 1179-1190.

Simon, A.: 1963, "Instability of a partially ionized plasma in crossed electric and magnetic fields", Phys. Fluids 6, 382.

Smith-Rose, R.L.: 1960, "Some radio aspects of the IGY", RSGB-Bulletin (Journal of the Radio Society of Great Britain) 35, 392-394.

Stone, G.M.C.: 1960, "Amateur radio participating in the IGY", RSGB-Bulletin (Journal of the Radio Society of Great Britain) 35, 395-397.

Stone, G.M.C.: 1965, "The Radio Society of Great Britain and IQSY", Interradio. The International Radio Journal, ITU Centenary Edition, Geneva 20, 24-27.

Stone, M.L., Ingalls, R.P., Dugan, C.H., and Rainville, L.P.: 1959, "Simultaneous auroral observations at two ultra-high frequencies", paper presented at URSI meeting, Washington, D.C.

Strömer, C.: 1926, "Résultat des measures photogrammétrique des aurores boréales observées dans la norwège méridionale de 1911 á 1922", Geofysiske Publikasjoner 4, Nr. 7, Oslo, 1926.

Tilton, E.P.: 1944, "On the very highs", QST 28, 41-43 and 86.

Unwin, R.S.: 1958, "The geometry of auroral ionization", J. Geophys. Res. 63, 501-506.

Unwin, R.S.: 1959, "Studies of the upper atmosphere from Invercargill, New Zealand: Part I - Characteristics of auroral radar echoes at 55 Mc/s", Ann. de Géophys. 15, 377-394.

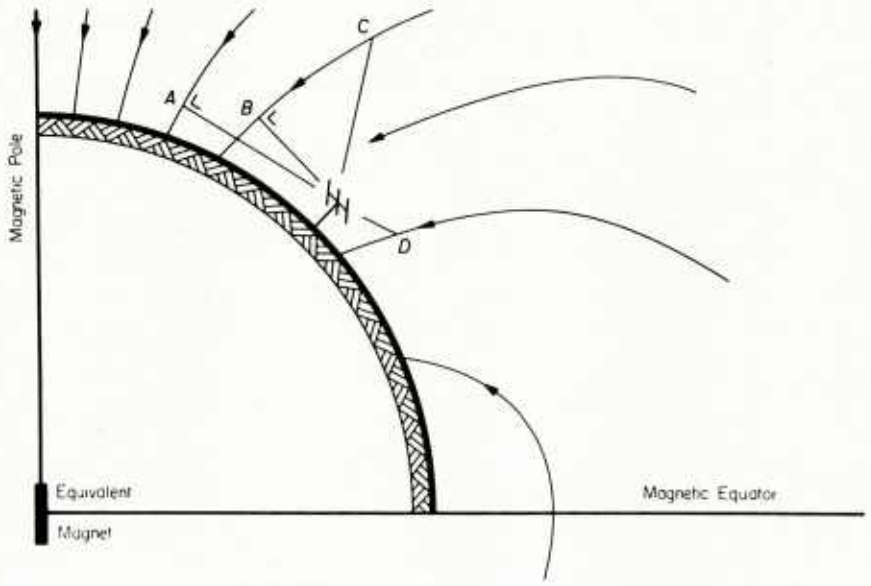

Fig. 1 VHF radio wave auroral backscatters are only possible when the direction of radio-wave-propagation and the direction of the lines of force of the earth's magnetic field are perpendicular at the reflection point. Under this assumption auroral displays at points A and B use to give backscatter-echoes, but not displays at points C and D.

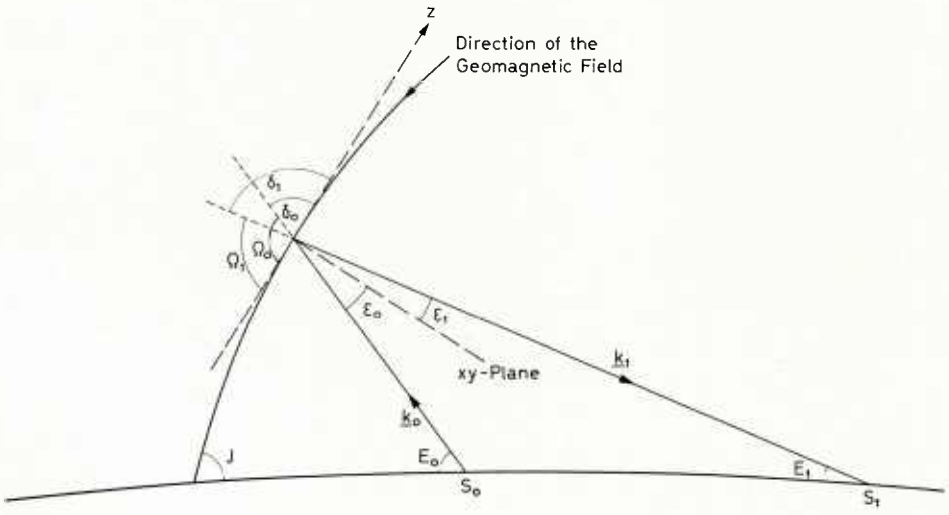

Fig. 2 Cross-sectional view of the earth with the geometry of the propagation path in the vertical direction for VHF bistatic auroral backscatter propagation between the two points S_0 and S_1

k_0, k_1 vector of the wave normal of the incident and backscattered wave, resp.,

ε_0, ε_1 angle between k_0 and k_1, resp. and the xy-plane

J magnetic dip angle,

Ω_0, Ω_1 propagation angle = angle between the direction of radio wave propagation and the magnetic lines of force,

E_0, E_1 elevation angle above the horizontal.

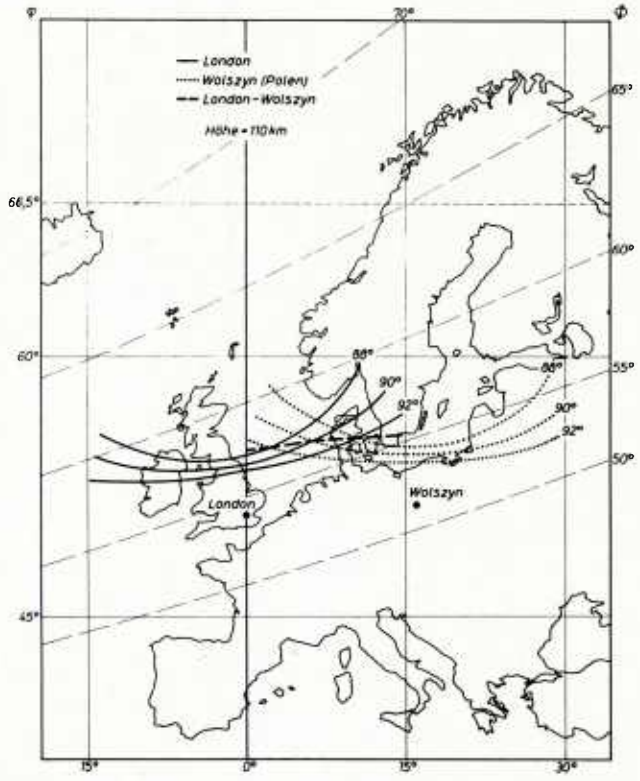

Fig. 3
Curves of constant intersection angle between the direction of radiowave-propagation and the magnetic lines of force at the 110 km height level for the two points London (——) and Wolszyn (Poland) (.....). The dashed line represents the location at the 110 km height level where the "ideal backscatter conditions" $\cos \Omega_o + \cos \Omega_1 = 0$, or $\varepsilon_1 = \varepsilon_2$ (Figure 2) are fulfilled for bistatic auroral backscatter communications from London to Wolszyn, φ = geographic latitude, Φ = geomagnetic latitude. After Lange-Hesse et al. (1965).

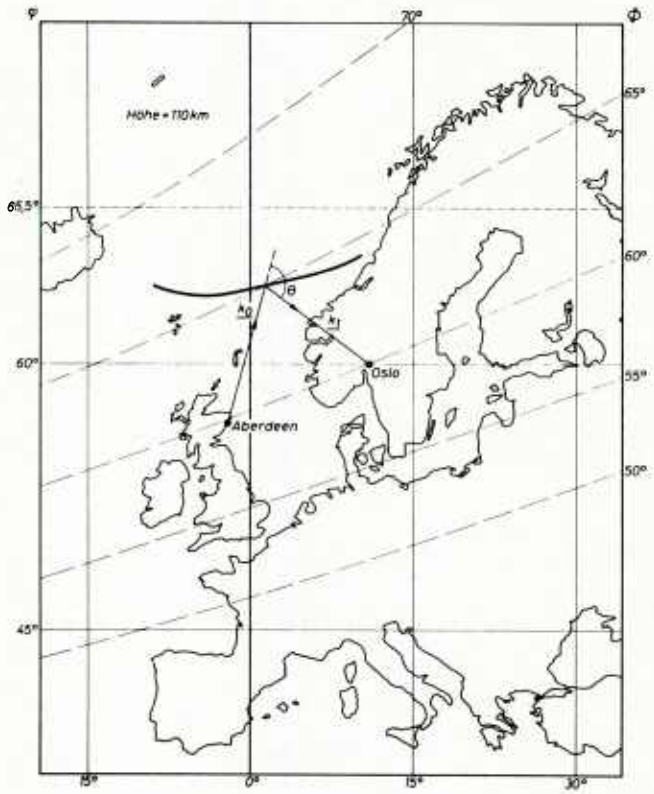

Fig. 4
Geometry in the horizontal direction for VHF bistatic auroral backscatter communications between the two points Aberdeen and Oslo. The solid curve at about $\Phi \approx 65^0$ (called "backscatter curve") represents the location at the 110 km height level where the ideal backscatter conditions (Figure 3) are fulfilled, this means where aurora (and simultaneously aurora ionization) must be located in case of the occurrence of aurora backscatter communication between Aberdeen and Oslo, θ = angle between the wave normals of the incident and backscattered wave, φ = geographic latitude, Φ = geomagnetic latitude. After Lange-Hesse et al. (1965).

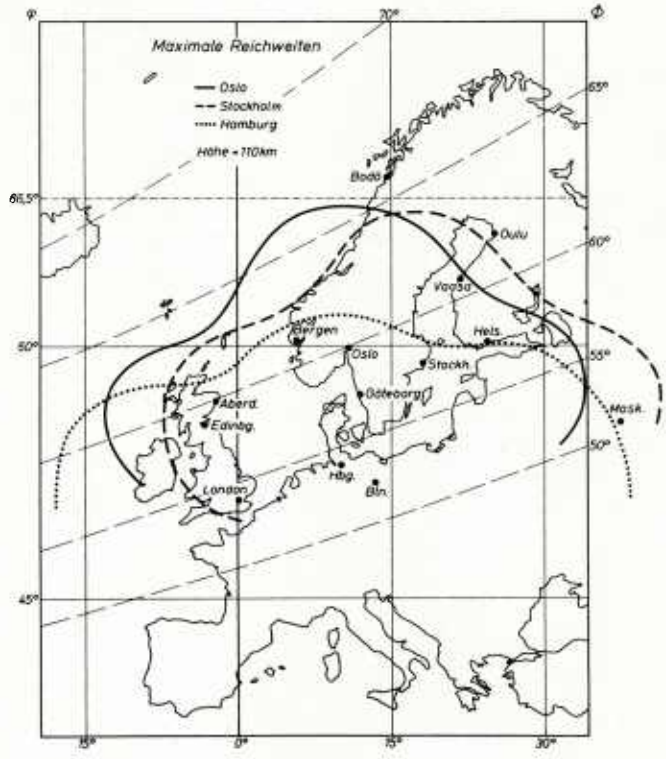

Fig. 5
Computed maximum-distance-curves for VHF bistatic auroral backscatter communications from Oslo (———), Stockholm (— — —) and Hamburg (.....). Adopted height above the ground of the backscattering centres h = 110 km. Φ = geomagnetic latitude φ = geographic latitude. After Lange-Hesse et al. (1966).

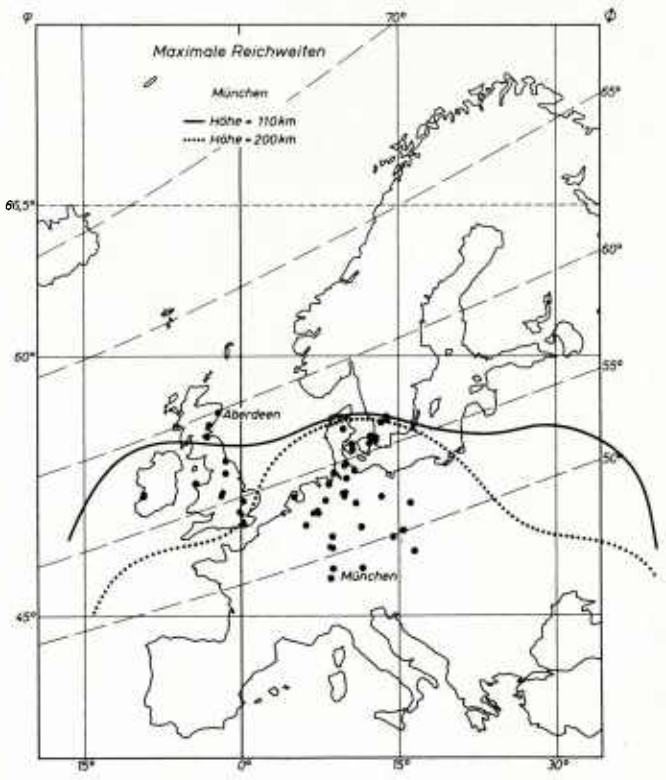

Fig. 6
Simular curves as in Figure 5 but computed for Munich for the two adopted heights h = 110 km (———) and h = 200 km (.....) of the backscattering centres. The dots represent stations which could be contacted from Munich via VHF auroral backscatter communications. Φ, φ see text Figure 5. After Lange-Hesse et al. (1966).

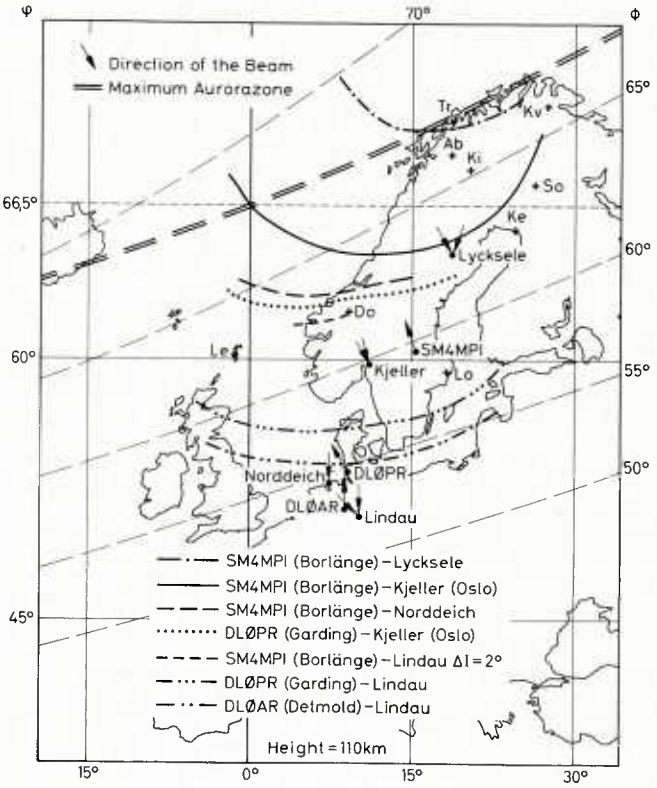

Fig. 7
Map of Europe with the location of backscatter curves (Fig.4) for VHF bistatic auroral backscatter communication between the pairs of stations specified in the figure. Height level = 110 km. The location of the VHF-beacon transmitters are:

a) SM4MPI near Borlänge, Sweden, frequency: 145.960 MHz

b) DLØPR, Garding, Schleswig-Holstein, frequency: 145.971 MHz

c) DLØAR, Bielstein, Teutoburger Wald, frequency: 29.0 MHz

The arrow at the stations indicates the direction of the antenna beam (half-power width $\pm 30^0$).
After Czechowsky and Lange-Hesse (1970).

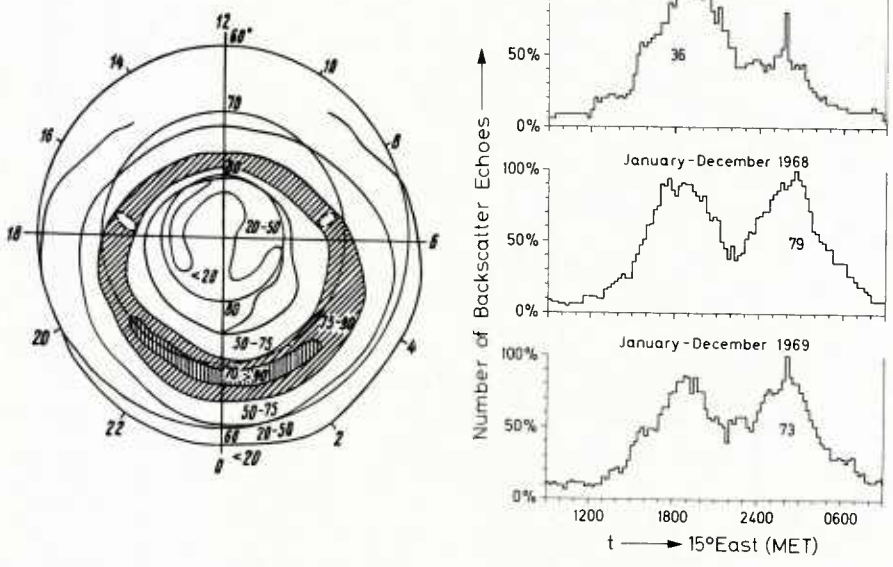

Fig. 8 Right: Average diurnal variation of the frequency of occurrence of VHF auroral backscatter communications on the beacon line from Borlänge (SM4MPI) to Kjeller (see Fig. 7, solid line backscatter curve). The numbers in the stepped curves signify the total number of backscatter registrations (100 per cent) made during the specified observed period. Left: Map of the auroral oval. It shows the regions where visual auroras are most frequent. This oval coincide in space to a first approximation with the polar electrojet current in which the backscattering centers are generated. The circles are parallels of geomagnetic latitude.

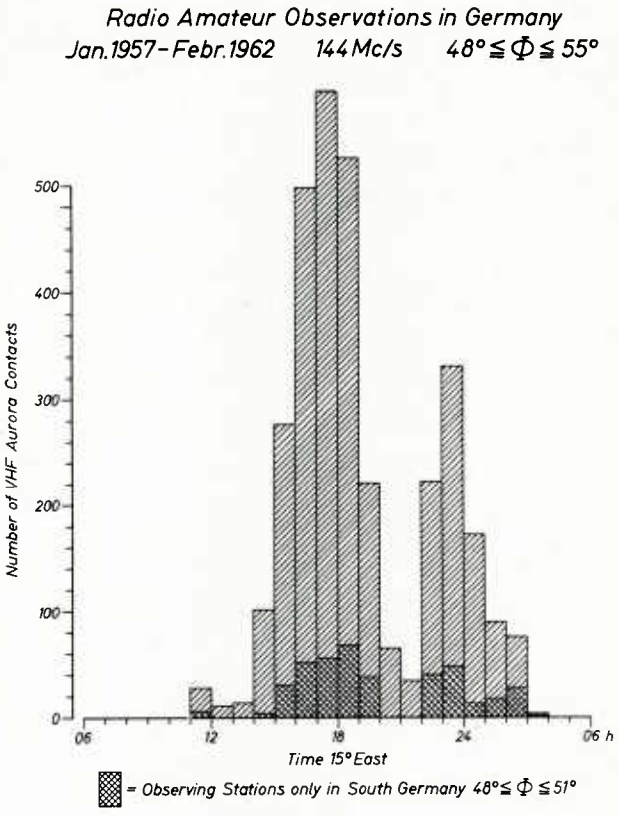

Fig. 9
Average diurnal variation of the frequency of occurrence of VHF auroral backscatter communications according to radio amateur observations in $48^0 \leq \phi \leq 55^0$ geomagnetic latitude. After Lange-Hesse (1963a).

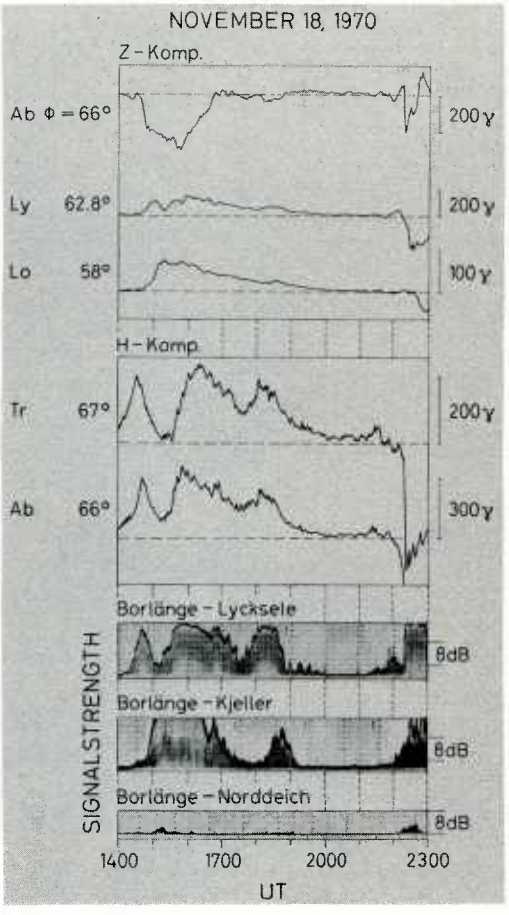

Fig. 10
VHF auroral backscatter recordings from the beacon station Borlänge, SM4MPI, at three different stations (see Fig. 7) compared with the magnetograms from the H- and Z-component from the scandinavian observatories Tromsö (Tr), Abisko (Ab), Lycksele (Ly) and Lovö (Lo), see Fig. 7. After Lange-Hesse (1972).

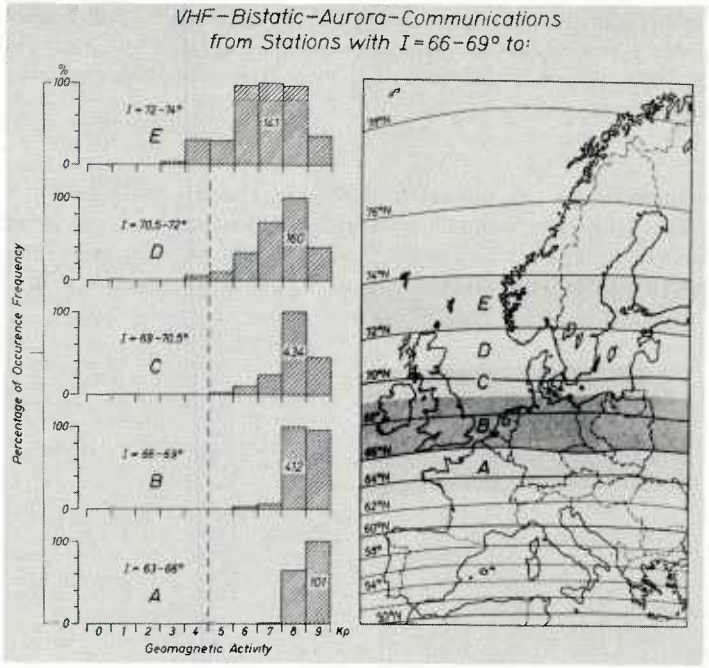

Fig. 11
Influence of planetary geomagnetic activity Kp on the frequency of occurrence of VHF bistatic auroral backscatter communications for communications from stations in zone B (dark zone in the Figure, dip angle I = 66-69^0) to stations in zones A, B, C, D, and E, according to amateur observations on 144-146 Mc/sec from 1957 to the beginning of 1963; after Lange-Hesse (1964a).The number in the 100% column of each diagram (A-E) gives the number of auroral communication which corresponds to 100%.

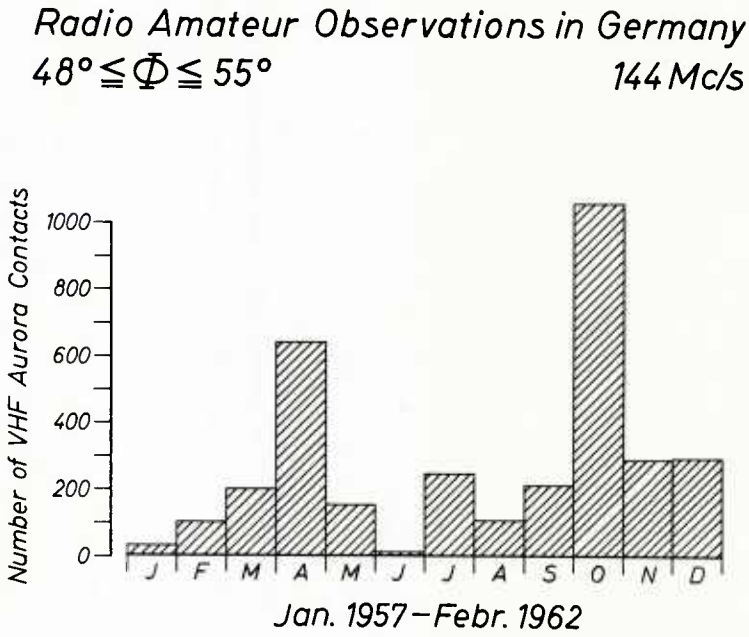

Fig. 12
Seasonal influence on VHF auroral backscatter communication. Same observational data as in Figure 9. After Lange-Hesse (1963a).

DISCUSSION

D.J.Fang, US

Have you determined the aspect-sensitivity angle (the angle between your propagation direction vs local magnetic field line in aurora) for your measurement? Does it have any effect? I would think if an angle of 90°, i.e., propagation perpendicular to the magnetic field, existed in oval, you would get maximum scattering and hence greatly enhance VHF communications. Would you care to comment?

Author's Reply

We have not determined the aspect-sensitivity angle. In the case of bi-static auroral backscatter communication, the propagation angles Ω_0 and Ω_1 (Fig.2) are a little bit greater than 90° and a little smaller than 90°, respectively. The sum of the cosines of Ω_0 and Ω_1 is zero in this case according to the theory: $\cos \Omega_0 \pm \cos \Omega_1 = 0$. This is the ideal backscatter condition. Only in exceptional cases both Ω_0 and Ω_1 can be 90° simultaneously (Fig.3).

INTERFERENCE AND SHARING AT MEDIUM FREQUENCY:

SKYWAVE PROPAGATION CONSIDERATIONS

John C. H. Wang
Federal Communications Commission
Washington, D.C. 20554 U.S.A.

SUMMARY

A considerable amount of work dealing with nighttime skywave propagation has been done; however, some areas remain to be explored. For example, short-term variation of field strengths has been overlooked. Daytime propagation is far from being quantitatively understood. Also, it is not quite possible to determine interfering signal levels which may be present for a small percentage of time with high accuracy. During sunspot cycles 18 and 19, the Federal Communications Commission conducted an extensive field-strength measurement program in the midlatitude areas of North America. These and other data are revisited with a new emphasis, namely, interference and sharing. This paper discusses, among other things, determination of field strengths exceeded for different percentages of time (1 to 99%), diurnal variation of field strengths, favorable conditions for daytime skywave propagation, effect of magnetic storms, frequency dependence as observed at daytime and nighttime.

1. INTRODUCTION

A considerable amount of work as been done in the field of medium-frequency (MF) skywave propagation. Stress has usually been placed on the prediction of yearly median values of nighttime field strength. The objectives of frequency management and conference planning have necessitated this emphasis. For these purposes, accuracy is often sacrificed for simplicity. As the demand for frequency increases, however, and as the number of high-power stations rises, the severity of interference is steadily increasing. Improved accuracy is needed and simplicity may become something we can no longer afford.

The 1979 World Administrative Radio Conference allocated the band of 1605-1705 kHz for broadcasting in Region 2 (the Americas), while fixed services elsewhere will continue to use this band. Thus, the stage is set for a different kind of interference: interregional interservice interference. A planning conference for Region 2 has been scheduled for 1986. This calls for urgent study of MF skywave propagation with emphasis on interference.

The purpose of this paper is to present some of the progress that has been made which may eventually be used in improving the accuracy of predicting skywave field strengths. A brief review of existing prediction methods is also given.

2. A REVIEW OF EXISTING PREDICTION METHODS

2.1 The FCC Curves

Two sets of MF skywave field-strength curves are contained in Part 73 of the FCC Rules and Regulations (FCC, 1980). The first set is based on short-term measurements taken in the spring of 1935. They are applicable to clear-channel broadcasting stations in the United States.

In 1939 an extensive measurement program was initiated by the FCC. Four receiving sites and 18 different transmitters were selected. Altogether, 26 propagation paths were involved. The measurements were continued for a full sunspot cycle, and results were released in 1971 (Damelin, 1971). Soon after this program was initiated, it became apparent that the skywave field strengths were functions of many factors, such as latitude, frequency, and sunspot number, etc. Consequently, the 1944 data were used to develop a second set of curves. The second set of curves differs from the first set in one respect: it gives some weight to the effects of geographic latitude. This set of curves was adopted by the Commission primarily for calculating field strengths exceeded for 10% of the time by domestic non-clear-channel broadcasting stations.

The FCC (clear-channel) curves have been regarded as a conservative and safe method when applied to the continental U.S. These curves, however, have a tendency to overpredict field-strength levels when applied to the northern part of the U.S. This is more pronounced during a period of high solar activity. The primary asset of the FCC curves is that they are easy to use. On the other hand, these curves provide no treatment of the effects of latitude, frequency, sunspot number, etc. Furthermore, when the great-circle distance of a path is greater than about 4,300 km, the FCC curves cannot be used.

2.2 The Cairo Curves

Under the auspices of the International Broadcasting Union (UIR) and the International Radio Consultative Committee (CCIR), some short-term measurements between North and South America, between North America and Europe, etc., were carried out by several administrations in the late 1930s. A working group under the leadership of Dr. B. van der Pol (Holland) was established to study the results. This working group developed two separate curves: one for propagation paths distant from the earth's magnetic poles (i.e., low-latitude paths) and one for propagation paths which pass near the earth's magnetic poles (i.e., high-latitude paths). The former is better known as the Cairo north-south curve

because it was derived from measurements made on transequatorial paths; the latter is better known as the Cairo east-west curve because it was derived from measurements made across the Atlantic. These curves were officially adopted by the CCIR at the 1938 meeting held in Cairo; hence, they are collectively called the Cairo curves (Knight, 1977).

The Cairo curves did not gain much recognition until 1975, when the LF/MF Conference adopted the Cairo north-south curve (hereafter called the Cairo curve) for official use in Asia. Field-strength measurements conducted by the Asian-Pacific Broadcasting Union (ABU) and Japan indicate that the Cairo curve is preferable for that part of the world. This is not unexpected, since the Cairo curve was derived from measurements on paths between North and South America with an average midpoint geomagnetic latitude of about 14°N.

The midpoint of an arbitrary Tokyo-Singapore path is about 10°N. Thus, the Cairo curve, in a way, represents the average propagation condition of Asia. It has also been reported (PoKempner, 1980) that, for very long paths, the Cairo curve, in general, predicts the highest field strengths.

When converted to the same conditions (power and reference hour), the two Cairo curves and the FCC curve are very similar for distances up to about 1,400 km. At 3,000 km, the low-latitude curve is about 8 dB greater than the high-latitude curve. At 5,000 km, the low-latitude curve is about 18 dB greater than the high-latitude curve. The FCC 50% curve is near the average of the two Cairo curves.

2.3 The CCIR Method

Recognizing the needs for a simple field-strength prediction method for worldwide application, the CCIR a few years ago established an ad hoc working group known as the Interim Working Party (IWP) 6/4. In 1974, under the leadership of Dr. P. Knight (UK), IWP 6/4 adopted the USSR method with modifications (e.g., UK sea-gain term). The method is recommended by the CCIR for "provisional use" (CCIR, 1982a). The 1975 LF/MF Conference adopted this method for official use in Region 1 and part of Region 3 (with modifications; ITU, 1976).

When compared with measured data from the U.S. and the southwestern part of Canada, the CCIR method shows better overall results than the FCC curves. However, qualitatively, certain limitations became apparent. Briefly stated, they are:

a. The method has a tendency to underestimate field-strength levels in low-latitude areas (e.g., Texas-to-Nebraska paths) and to overestimate in high-latitude areas (e.g., Saskatchewan-to-Oregon paths). This is perhaps an indication that its treatment of latitude is insufficient.

b. Measurements taken in North America suggest that when other factors are equal, the field strength of a higher-frequency path tends to be stronger. The frequency-dependence term of the CCIR formula is of the opposite sense.

c. The sunspot-dependence term of the CCIR formula is a simple function of sunspot number and distance. This approach may be sufficient for areas distant from the earth's magnetic poles. However, it seems to be an oversimplification for areas approaching the poles and an unnecessary overemphasis for low-latitude areas. The author has reported previously that the sunspot-dependence term is a function of geomagnetic latitude and frequency in addition to sunspot number and distance (Wang, 1977).

2.3.1 Modifications for Applications in Region 2

In preparation for the 1980 Regional Administrative Broadcasting Conference (Region 2), IWP 6/4 of the CCIR held a special meeting in Geneva (October 1979). A set of modifications to the CCIR method was adopted (CCIR, 1982b). These modifications, which were derived from a paper by Wang (1979), are believed to simplify the CCIR method while improving its accuracy when applied to Region 2. The proposed modifications include:

a. In calculating MF skywave field strengths in Region 2 by the method recommended by the CCIR, 1000 kHz should be used regardless of frequency.

b. The basic loss factor called "k" has been modified in such a way that the absorption in the high-latitude areas will be increased and that in the low-latitude areas will be decreased without affecting the prediction in the average-latitude areas.

c. For planning purposes, the sunspot number is assumed to be zero.

2.4 The EBU Method

The European Broadcasting Union (EBU) initiated a measurement program in 1952. Recordings were made over about 50 propagation paths in different parts of Europe. Measurements ended in 1960. Empirical relationships were derived for the effects of solar activity, magnetic field, frequency, and antenna gain as a function of path length (Ebert, 1962). It is to be noted that the empirical EBU formulas indicate decreasing field strength with increasing frequency. The CCIR method has replaced this method for official use in the EBU areas.

2.5 The Official Method for ITU Region 2

The first session of the Regional Administrative Broadcasting Conference for Region 2 (Buenos Aires, March 1980) considered all the available methods and decided that (ITU, 1980):

a. The metric version of the FCC curve, normalized to a characteristic field strength of 100 mV/m at 1 km, is to be used for paths up to 4,250 km in length.

b. For paths greater than 4,250 km in length, the Cairo north-south curve, converted to 100 mV/m at 1 km and "lowered" by 5.4 dB, is to be used. This lowering allows the Cairo and the FCC curves to intersect with each other smoothly at 4,250 km.

c. The polarization coupling loss factor from the CCIR method was also adopted.

d. For calculating interregional interference, the midpoint of the great-circle path is determined first. The official method for the region in which the midpoint falls shall be used. Because different regions use different reference hours, the CCIR diurnal loss-factor curve was also included in the official method for Region 2.

2.6 Other Methods

A number of other methods have been developed and reported. See papers by Barghausen (1966), Knight (1973), Norton (1959), and Wang (1977).

3. AREAS WHERE MORE WORK IS NEEDED

A number of authors have analyzed the aforementioned prediction methods and compared calculated results by using these methods with measured data collected in different parts of the world (Barghausen, 1966; Crombie, 1979; PoKempner, 1980; Wang, 1977, 1979). A compilation of their research indicates that the following are some areas where more work is needed.

3.1 Effects of Latitude

The FCC curve (and, hence, the official method for Region 2), is independent of latitude. In the later non-clear-channel FCC curve, some weight was given to the effects of geographical latitude but not of geomagnetic latitude. In this respect, the CCIR method, which is a function of, among other things, geomagnetic latitude, has made a step in the right direction.

In recognizing the need for more data from the high-latitude and low-latitude propagation paths, the FCC is currently collecting data at Cabo Rojo, Puerto Rico (in cooperation with ITS), and at Fairbanks, Alaska (in cooperation with the Geophysical Institute, University of Alaska).

3.2 Daytime MF Skywave Propagation

It is widely recognized that there is a lack of detailed data on daytime and transition-hour ionospheric propagation at MF. Interference from distant stations during daytime, particularly in winter months, has been observed from time to time.

3.3 Frequency Dependence: A North American Anomaly?

Theoretically speaking, the higher the frequency, the deeper the wave penetrates into the E layer of the ionosphere. This results in greater absorption and lower field strengths. The European data (taken at midnight) and the CCIR and EBU methods duly reflect this theory. Measurements in the United States (taken at two hours after sunset), however, repeatedly show that when other factors are equal, the field strength of the higher frequency tends to be stronger. One theory has been offered that at two to three hours after sunset, the D layer may still be present in some parts of the world. Thus, it may be very useful to reexamine the U.S. recordings and to reanalyze data for periods later than two hours after sunset, when the D layer has completely disappeared.

3.4 Short-Term Variation of Field Strength

It is generally believed that the upper decile value of field strength, on the average, is about 8 dB greater than the annual median value. Under certain conditions, values considerably different from 8 dB have been observed. A better comprehension of these conditions is desirable.

3.5 Effects of Magnetic Activity

It is well known that the 12-month smoothed sunspot number may not be the best possible index for the study of ionospheric propagation. Possible correlation between field strengths and other indices should be studied.

4. RESULTS OF STUDY

The bulk of the data used for this study is made up of the 26 propagation paths mentioned previously in Section 2.1. When measurements were originally made, around-the-clock

recordings were attempted. In most cases, nighttime recordings were highly successful. Not surprisingly, however, adequate daytime data were collected in only a few cases. Only recordings corresponding to two hours after sunset at the midpoint of a path were statistically processed and published (Damelin, 1971). Recordings for other hours have not been fully reduced. For the present study, selected key portions of these recordings have been revisited. From the FCC files some additional measurements over several other paths have also been recalled and studied. The more recent data collected by the Mexican government (Fernandez & Wang, 1981) have also been used. In the subsequent sections, the following symbols and abbreviations are used:

F(P)	Measured field strength exceeded for P% of the time, dB above 1 microvolt per meter, dB(μV/m).
R	Sunspot number.
SR - x	x hours before sunrise at the midpoint of a path.
SS + y	y hours after sunset at the midpoint of a path.
$\Delta(P) = F(P) - F(50)$, dB	
ϕ	Dipole geomagnetic latitude of the midpoint of a path, degrees.

4.1 Daytime Skywave Propagation

It is extremely difficult to collect skywave field strengths during the day because field strengths are very low. This is compounded by the fact that groundwave signals, under certain conditions, may be high enough to mask skywave reception. Nevertheless, the FCC did manage to collect a considerable amount of daytime skywave data, representing different levels of solar activity. Before analyzing daytime data, some preliminary tests were performed to make sure that the data collected were actually skywave. Groundwave field strengths were calculated, using the latest ground conductivity information available. If the groundwave field strength of a particular path was within one order of magnitude of the median value of measured data, measurements for that path were then discarded for this study. Daily readings were carefully examined. If day-to-day fluctuations were observed and the fluctuations somewhat followed the change of geomagnetic indices, the data were considered skywave. Furthermore, frequency lists for the corresponding periods were carefully examined. It was ascertained that no co-channel or adjacent-channel daytime station was located anywhere near the receiving site involved. These stringent tests were necessary to make sure that the data were reliable. Measurements of eight paths have successfully passed these tests. Some borderline cases are left for future work. Table 1 summarizes measurement results for the years of sunspot minimum and maximum together with nighttime results for comparison.

An analysis of the FCC daytime skywave data shows that:

4.1.1 Day-to-day fluctuation of midday field strengths is more pronounced with signals in the upper end of the band than that in the lower end of the band. For example, field strengths of WCKY (1530 kHz) vary by as much as two orders of magnitude. Signals of WLW (700 kHz), however, do not change very much. (See also Section 4.3, Effects of Magnetic Activity.)

4.1.2 The distribution of daytime field strengths displays appreciable skewness. It is usually skewed to the left (i.e., median values are closer to the lower-decile values than to the upper-decile values). It is to be noted that the distribution of nighttime field strengths, as observed in the United States, is more often than not skewed to the right (i.e., median values are closer to the upper-decile values than to the lower-decile values). Figure 1 is a typical case.

4.1.3 Daytime skywave field strengths vary with solar activity in a similar manner as that of nighttime. For example, consider the case of WCKY (1530 kHz, Cincinnati, Ohio) to Atlanta. Noontime field strength changed from 12.2 dB above 1 microvolt per meter in 1944 (R = 9.6) to 4.4 dB above 1 microvolt per meter in 1948 (R = 136.3), yielding a decrease of 7.8 dB. The corresponding decrease in nighttime field strengths was 6.5 dB.

4.1.4 The seasonal variation of the median values of daytime field strengths is very apparent. Field strengths are strongest in the winter months.

4.1.5 Measurements made in Germany and Japan (CCIR, 1982c) show that the annual median value of skywave field strength at noon is about 45 dB lower than the corresponding value at midnight. The U.S. measurements, in general, corroborate with this reasonably well. If one considers the winter season alone, however, the picture can be quite different. In the high-latitude areas where nighttime winter anomaly is pronounced (Hagg, 1981), the difference can be drastically smaller. For example, during the period of November 1, 1941, to January 31, 1942, signals of WLW (700 kHz, Cincinnati, Ohio) were detected in Portland, Oregon (path length = 3,192 km, midpoint geomagnetic latitude = 53.2°N), regularly around noon with a median value of 6 dB above 1 microvolt per meter. The corresponding nighttime (6 hours after sunset) field-strength value was only 17.3 dB above 1 microvolt per meter. The difference was only about 11 dB. Admittedly, this is an extreme case and will not be repeated very often. The typical difference between nighttime and daytime field strengths for the winter months, as observed in the U.S., is usually between 25 and 30 dB.

4.2 Diurnal Variation of Field Strengths

Skywave field strengths vary from hour to hour. The change is more rapid during transition periods. The CCIR, based on data collected in Australia and Europe, developed a single diurnal loss-factor curve which shows the average variation (see Figure 2).

In the United States, FCC engineers started analyzing diurnal variation of skywave field strengths many years ago, based on data collected by the FCC from North American paths in 1944, a year of low solar activity. Among other things, it was reported (FCC, 1947) that during transition hours, field strength is highly frequency dependent. The work, however, was not finalized, due primarily to the lack of any urgent need at that time. Recently, this study has been reactivated. Selected key portions of the more recent and more extensive FCC data bank have been studied. The 1947 work has been verified and, in some respects, improved. Nighttime frequency dependence is very slight. For example, during a year of low solar activity, signals of a 1530 kHz station are typically 3 dB stronger than those of a 700 kHz station while other factors coincide. As shown in Figures 3 and 4, however, at sunrise or sunset, signals of the higher-frequency station are usually about 15 dB stronger than those of the lower-frequency station. This phenomenon has been observed in a large number of cases throughout the entire solar activity cycle. Accordingly, two families of curves, one for the sunset period and another for the sunrise period, have been developed (FCC, 1982). These curves are now being reviewed by interested parties in the United States. They may become part of the Rules and Regulations of the FCC. The proposed FCC diurnal variation curves for 500 and 1600 kHz are plotted together with the CCIR curve in Figure 5. It should be mentioned that in Figure 5 all curves are normalized to two hours after sunset, the official reference hour in Region 2. For the most part, the CCIR curve is very similar to the proposed 1 MHz curve for the U.S., and may be considered as a simplified approach. For the section near sunrise, however, the difference between the CCIR and the proposed FCC curves becomes more noticeable.

According to the nighttime section of the CCIR diurnal loss-factor curve, field strength at six hours after sunset is about 2.5 dB stronger than that at two hours after sunset. A study of the U.S. data for these hours reveals that:

a. This section of the CCIR curve is most accurate for short (i.e., on hop) paths. For example, the difference in field strengths between six hours after sunset and two hours after sunset for a Texas-to-Nebraska path (WOAI, 1200 kHz, 1,297 km) was about 1 dB for 1944 and 2.5 dB for 1947. The corresponding difference for a Saskatchewan-to-Oregon path (CBK, 540 kHz, 1,439 km) was 3.1 dB for 1944 and 3.8 dB for 1947.

b. For multihop paths, particularly long east-west paths where the differences in longitudes between reflection points are substantive, the difference in field strengths between the aforementioned hours can be considerably larger; differences of 5 dB have been observed.

4.3 Effects of Magnetic Activity

It has been suggested that yearly median values of skywave field strength may be more closely related to magnetic activity than to the mean sunspot number (Barghausen & Lillie, 1965; Hagg, 1981). FCC data reveal that the nighttime field-strength minimum did not always occur in a year of maximum sunspot number; in at least three cases the field-strength minimum occurred one year after sunspot maximum. It has also been suggested that, in general, only the presence of large spots near the center of the sun coincides with magnetic disturbances (Chapman, 1951). Preliminary data collected by FCC/ITS in Puerto Rico (Washburn et al., 1982) and by the FCC and the University of Alaska in Alaska (Hunsucker, 1981) suggest that there might exist some correlation between the day-to-day variation of skywave field strengths and geomagnetic activity. These warrant the study of the effects of magnetic activity on MF skywave field strengths.

While the FCC was collecting skywave data, a number of large magnetic storms struck the world, driving the magnetic index, Ap, well into three-digit numbers. Field-strength records during these storms have been carefully studied. It is concluded that:

4.3.1 The effects of magnetic storms have a frequency variation. The inverse-square law, however, does not appear to hold. The storm-enhanced absorption, particularly during the first few days immediately after the onset of a storm, increases with increasing frequency. This suggests that at MF, storm-related absorption is deviative in nature (Davies, 1965) and takes place in the lower portions of the D layer (50 to 70 km). Consider Figure 6, which shows the effects of the storm of July 8, 1958, when Ap reached 200. Two stations in Cincinnati, Ohio, were being monitored in Atlanta, Georgia. The signal of WCKY, 1530 kHz, decreased by 12 dB from the five-day prestorm average condition in the evening of July 8. On the other hand, the signal of WLW, 700 kHz, decreased only by about 3 dB. The poststorm effects lasted for more than 10 days. On the average, the higher-frequency signal suffered a decrease of about 10.6 dB, while the lower-frequency signal suffered only 3.3 dB. The next example shows more contrast. On March 19, 1950, Ap reached 84. The field strengths of two stations in Minneapolis, Minnesota, were being recorded in Grand Island, Nebraska. During the next four days, the signal of KSTP, 1500 kHz, decreased by 32.7 dB on the average, while the signal of WCCO, 820 kHz, dropped by 19.8 dB (see Figure 7). Numerous examples similar to these two are available.

4.3.2 Unlike VLF and LF, where the immediate and poststorm effects are most pronounced during twilight periods and are virtually nonexistent at noon (Belrose & Thomas, 1968),

at MF the effects have no diurnal variation to speak of. At noon, skywave field strengths are so weak that a mild storm would usually bury the signal under atmospheric noise. Therefore, the effects should be viewed from a different angle. It has been found that strong midday skywave signals are repeatedly received on days when magnetic index Ap is low, say below 10. For example, as discussed previously in Section 4.1, signals of WLW were received regularly in Portland in the winter of 1941-42. The signal reached an audible level on December 31 when Ap was only 5. Figure 8 illustrates the lack of any pronounced diurnal variation. The case under study is CBK (540 kHz, Watrous, Saskatchewan, Canada) to Portland, Oregon (1,429 km, midpoint geomagnetic latitude = 56.2°N). The storm occurred on December 16, 1944; Ap jumped to 83 from a previous value of 8.

4.3.3 The effects of magnetic storms in the low-latitude areas are very mild, if any. For example, the storm of March 29, 1979 (Ap = 68), caused only a mild dent in two propagation paths in Mexico. The field strength of an east-west path suffered about 6 dB, while that of a north-south path dropped by 4 dB. The effects in the high-latitude areas are known to be far more striking. On November 11, 1981, Ak (College, Alaska) reached 67, while Ap was only 31. Skywave measurements being conducted by the University of Alaska were totally interrupted (Hunsucker, 1981). It is to be noted that the recovery time in the low-latitude areas is usually very short, typically two to four days. In the high-latitude areas, the effects may last for more than 15 days.

4.4 Field Strengths Exceeded for Different Percentages of Time

For simplicity, define $\Delta(P)$ = field strengths exceeded for P% of the nights of a year relative to the yearly median value (dB). It has been observed that for a year of low solar activity, $\Delta(1)$ varies between about 9.5 dB in the low-latitude areas to about 15 dB in the high-latitude areas; and that $\Delta(10)$ varies between less than 6 dB in Mexico (Fernandez & Wang, 1981) to more than 10 dB in the northern United States (Wang, 1978). For a year of high solar activity, Δ's are appreciably greater. In other words, when a high median value is expected, Δ's tend to be small. As an approximation, the following formulas are suggested for a year of low solar activity:

$$\Delta(1) = 0.275\ |\phi| - 1.5 \quad \text{(dB)} \tag{1}$$

$$\Delta(10) = 0.2\ |\phi| - 2 \quad \text{(db)} \tag{2}$$

where ϕ = midpoint geomagnetic latitude in degrees. See also Table 2. If $|\phi| > 60°$, equations (1) and (2) are evaluated for $\phi = 60°$. If $|\phi| < 40°$, equations (1) and (2) are evaluated for $\phi = 40°$. Furthermore, equations (1) and (2) and Table 2 apply to nighttime field strengths only. For daytime field strengths, the upper-percentile and upper-decile values are usually 2 to 3 dB larger. More work is needed.

4.5 Frequency Dependence

The extensive amount of MF skywave field-strength data collected at different hours of the night in different parts of North America during different levels of solar activity convincingly indicates that the median value of field strength increases with increasing frequency. This is true on a monthly basis as well as on a yearly basis. Figures 3 and 4 are two of the many available examples. The only possible exception to this observation is when large magnetic storms occur frequently (see Section 4.3).

In preparation for the 1950 North American Regional Broadcasting Conference, the government of Canada conducted a very productive skywave recording program in 1947. Measurements of six propagation paths were carried out. Part of the objective was to find the effect of frequency. Two of the six paths were from Minneapolis, Minnesota (WCCO, 830 kHz, and KSTP, 1500 kHz), to Churchill, Manitoba. It was reported that "the overall ratio for the recording period for a low-frequency to high-frequency propagation gives a factor of 0.457:1" (Mather, 1948).

5. CONCLUSION AND FUTURE WORK

Some skywave field-strength data have been studied. Since daytime skywave is invariably considered as the source of interference, yearly median values may not be the best indicator. The concept of worst month or worst season should be explored. More work is needed.

Field-strength records immediately following certain large magnetic storms have also been studied. It has been found that storm-related absorption increases with increasing frequency.

6. REFERENCES

BARGHAUSEN, A. F., 1966, "Medium-frequency skywave propagation in middle and low latitudes," IEEE Trans., BC-12, 1-14.

BARGHAUSEN, A. F., and D. A. LILLIE, 1965, "Some evidence of the influence of long-term magnetic activity on medium-frequency skywave propagation," IEEE Proc., 53, 2115-2116.

BELROSE, J. S., and L. THOMAS, 1968, "Ionization changes in the middle-latitude D-region associated with geomagnetic storms," J. Atmosph. Terr. Phys., 30, 1397-1413.

CCIR, 1982, "Prediction of sky-wave field strength between 150 and 1600 kHz," Recommendation 435-4, International Telecommunication Union, Geneva. (a)

CCIR, 1982, "Methods for predicting sky-wave field strengths between 150 kHz and 1600 kHz," Report 571-2, International Telecommunication Union, Geneva. (b)

CCIR, 1982, "Analysis of sky-wave propagation measurements for the frequency range 150 to 1600 kHz," Report 431-3, International Telecommunication Union, Geneva. (c)

CHAPMAN, S., 1951, The Earth's Magnetism, 2nd ed., Wiley, New York.

CROMBIE, D. D., 1979, "Comparison of measured and predicted signal strengths of nighttime medium-frequency signals in the U.S.A.," IEEE Trans., BC-25, 86-89.

DAMELIN, J., 1971, "Long-term skywave field-strength measurements in the 550-1600 kHz band," FCC Report No. R-7103.

DAVIES, K., 1965, Ionospheric Radio Propagation, U.S. Government Printing Office, Washington, D.C.

EBERT, W., 1962, "Ionospheric propagation on long and medium waves," EBU Review, Part A, 71-73.

FCC, 1947, "Daytime skywave at broadcast frequencies," Engineering Department Report 9075.

FCC, 1980, Rules and Regulations, Part 73, U.S. Government Printing Office, Washington, D.C.

FCC, 1982, Notice of Inquiry and Notice of Proposed Rule Making, BC Docket No. 82-538.

FERNANDEZ, M., and J. C. H. WANG, 1981, "Un Analisis de los datos de las mediciones de intensidad de campo de la onda reflejada efectuadas en Mexico," Teledato, 18, 22-23.

HAGG, E. L., 1981, "Reduction in MF skywave field strength at night due to magnetic-storm and winter-anomaly-related absorption," AGARD Conference Proceeding No. 305, paper 29.

HUNSUCKER, R. D., 1981, private communication.

ITU, 1976, Final Acts of the Regional Administrative LF/MF Broadcasting Conference (Regions 1 and 3), Geneva.

ITU, 1980, Report of the First Session of the Regional Administrative MF Broadcasting Conference (Region 2, March 10-28, Buenos Aires), Geneva.

KNIGHT, P., 1973, "MF propagation: A wave-hop method for ionospheric field-strength predictions," BBC Engineering, 100, 22-34.

KNIGHT, P., 1977, "MF propagation: The origin of the Cairo curves," BBC Report RD 1977/42.

MATHER, G. R., 1948, "Report on skywave recording," Department of Transport, Radio Division (Canada) Report No. 496.

NORTON, K.A., 1959, "Transmission loss in radio propagation:II," NBS Technical Note No. 12.

POKEMPNER, M., 1980, "Comparison of available methods for predicting medium-frequency sky-wave field strengths," NTIA Report No. 80-42.

WANG, J. C. H., 1977, "Prediction of medium-frequency skywave field strength in North America," IEEE Trans., BC-23, 43-49.

WANG, J. C. H., 1978, "Medium-frequency skywave field strengths exceeded for different percentages of time," FCC Technical Memorandum No. 8.

WANG, J. C. H., 1979, "Medium-frequency skywave propagation in Region 2," IEEE Trans., BC-25, 79-85; 155.

WASHBURN, J. S., C. M. RUSH, and F. G. STEWART, 1982, "Development of techniques to assess interference to the MF broadcasting services," NTIA Report 82-90.

Table 1

Measured Skywave Field Strengths in dB(1μV/m)

kHz	Call	Transmitter Location	Receiving Site	km	ϕ deg N	Daytime F(10)	Daytime F(50)	Nighttime (SS + 2) F(10)	Nighttime (SS + 2) F(50)	Year
1530	WCKY	Cincinnati Ohio	Atlanta Georgia	593	47.6	23.8 15.6	12.2 4.4	70.0 67.0	66.0 59.5	1944 1948
1530	WCKY	Cincinnati Ohio	Baltimore Maryland	676	50.7	19.6 15.6	8.2 8.3	65.2 61.7	60.0 50.3	1944 1947
700	WLW	Cincinnati Ohio	Grand Is. Nebraska	1,184	50.8	17.4 18.8	8.2 0.2	56.7 50.4	47.0 35.5	1944 1947
1160	KSL	Salt Lake City, Utah	Grand Is. Nebraska	1,150	50.0	20.0 17.3	13.2 -2.5	63.7 62.6	59.0 54.3	1944 1947
1200	WOAI	San Antonio Texas	Grand Is. Nebraska	1,279	45.1	14.0 10.5	8.6 -9.1	58.7 59.1	56.2 54.7	1944 1947
700	WLW	Cincinnati Ohio	Portland Oregon	3,192	53.2	4.5 Noise	Noise Noise	28.3 16.5	16.7 1.0	1944 1947
820	WFAA	Dallas Texas	Portland Oregon	2,614	48.4	3.7 2.2	Noise Noise	40.0 31.5	31.3 18.4	1944 1947
830	WCCO	Minneapolis Minnesota	Portland Oregon	2,280	54.5	5.7 0.8	2.6 Noise	37.7 15.5	27.5 5.5	1944 1947

Table 2

Variation of Δ(P) with Respect to Latitude and Sunspot Number (all figures in dB)

P	Sunspot Number	$\phi < 49°$	$49° < \phi < 51.9°$	$51.9° < \phi$	Average
1	Minimum	9.5	12.4	14.9	11.2
	Maximum	14.7	17.1	21.3	16.7
	Full cycle	12.3	15.2	19.9	15.2
10	Minimum	6.3	8.1	10.3	8.0
	Maximum	9.7	10.9	13.8	11.2
	Full cycle	8.2	9.8	13.2	9.9
30	Minimum	2.8	3.9	5.3	3.9
	Maximum	4.8	4.7	6.2	5.1
	Full cycle	3.9	4.5	5.9	4.6
70	Minimum	-3.5	-4.8	-6.8	-4.9
	Maximum	-4.7	-5.3	-6.4	-6.3
	Full cycle	-4.8	-5.5	-6.8	-5.5
90	Minimum	-11.4	-13.4	-19.4	-14.1
	Maximum	-12.5	-13.3	-14.3	-13.2
	Full cycle	-12.1	-14.5	-15.8	-13.8
99	Minimum	-20.9	-25.8	-30.6	-24.9
	Maximum	-22.8	-23.2	-22.9	-22.9
	Full cycle	-22.3	-25.5	-26.5	-24.4

For detailed information about these propagation paths, see paper by Wang (1977). See Section 4 for meanings of symbols.

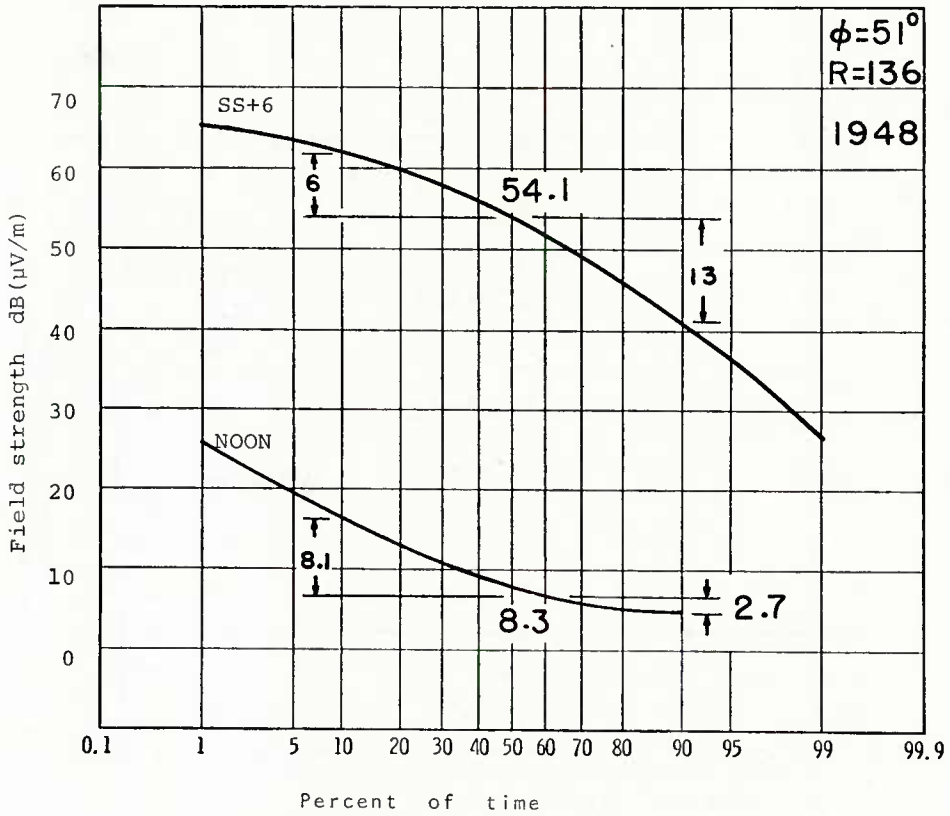

FIGURE 1 Skywave field strengths of WCKY, 1530 kHz, 50 kW, Cincinnati, Ohio; received at Baltimore, Maryland

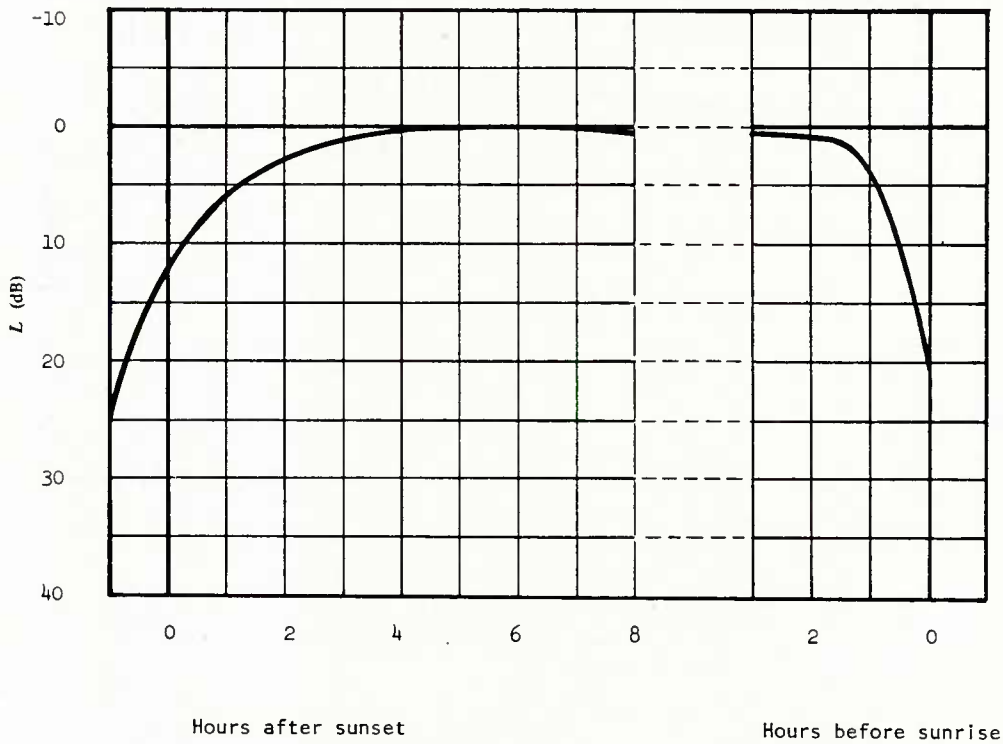

FIGURE 2: CCIR diurnal loss factor curve (reproduced from ITU, 1976)

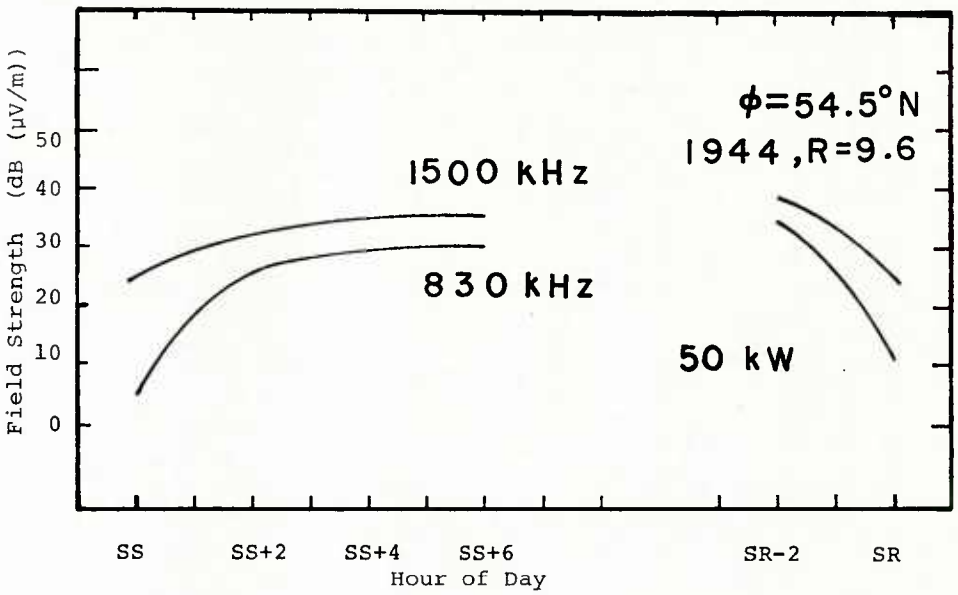

FIGURE 3 A comparison of skywave field strengths of two different frequencies for different hours, Minneapolis, Minnesota to Portland, Oregon

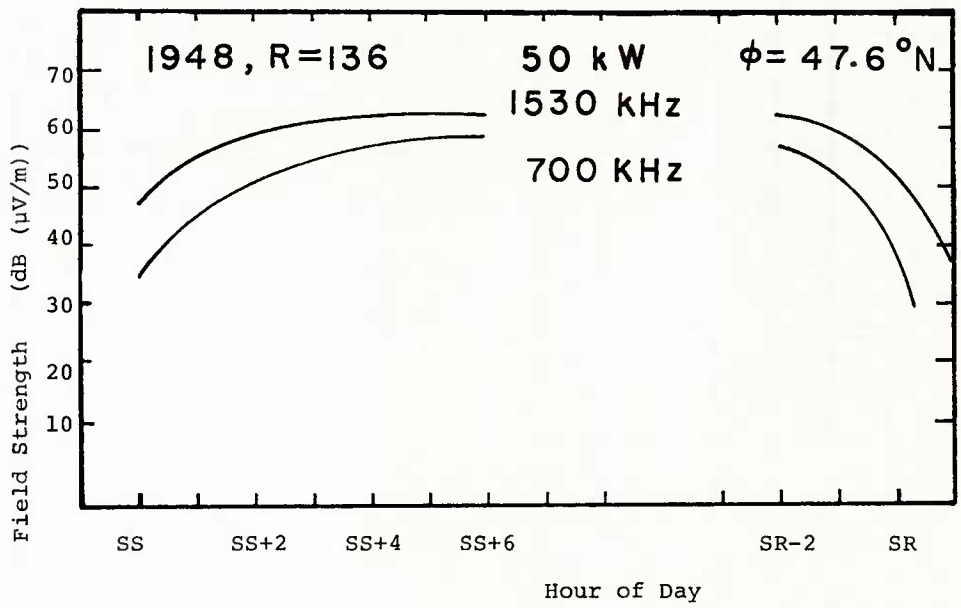

FIGURE 4 A comparison of skywave field strengths of two different frequencies for different hours, Cincinnati, Ohio to Atlanta, Georgia

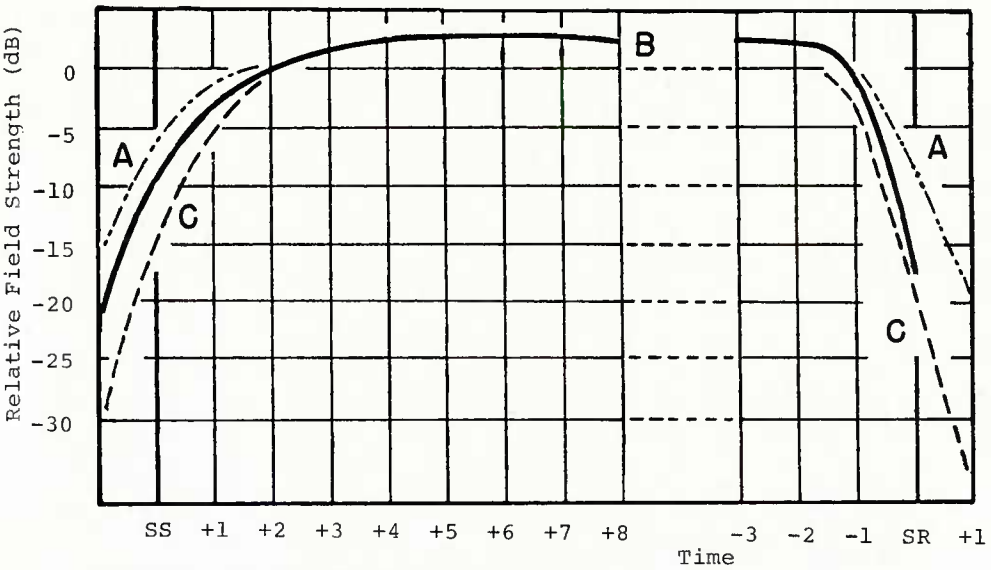

FIGURE 5 Diurnal variation curves
A Proposed FCC curve for 1600 kHz
B CCIR curve
C Proposed FCC curve for 500 kHz

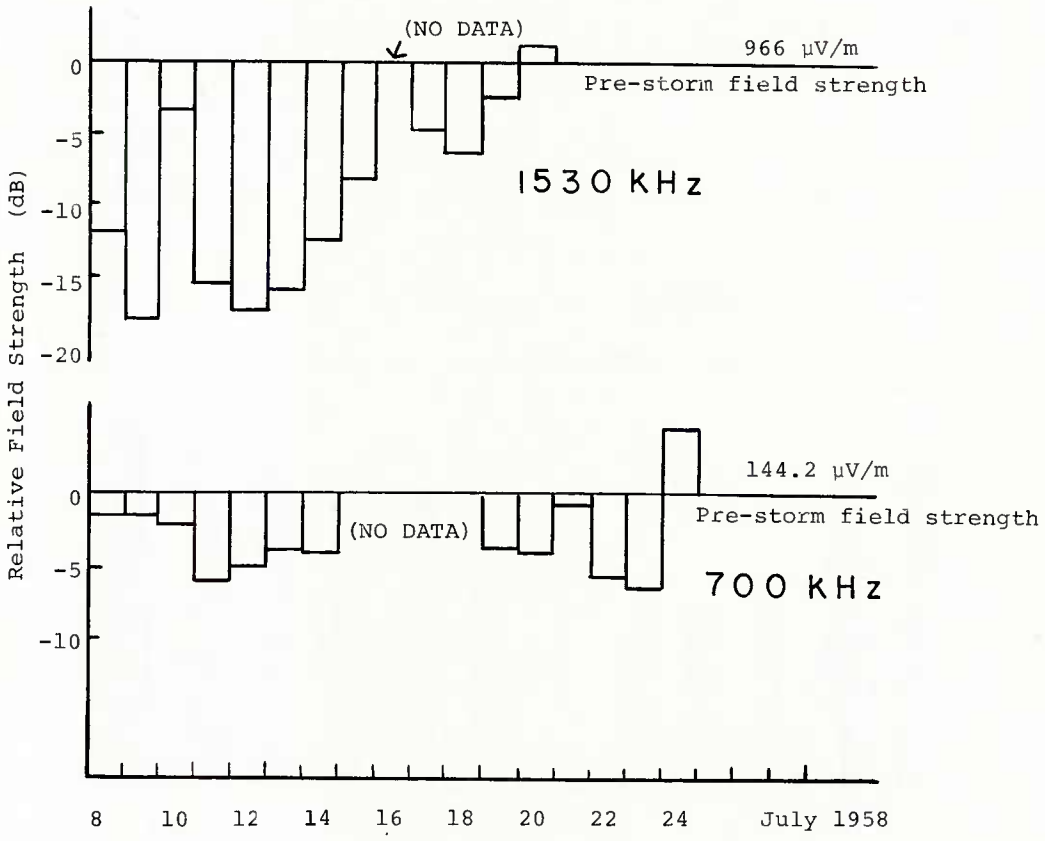

FIGURE. 6 Effects of the magnetic storm of July 8, 1958 (Ap = 200) on two paths from Cincinnati, Ohio to Atlanta, Georgia (600 km., ϕ = 47.6 deg.N, data for the hour SS+2 are given)

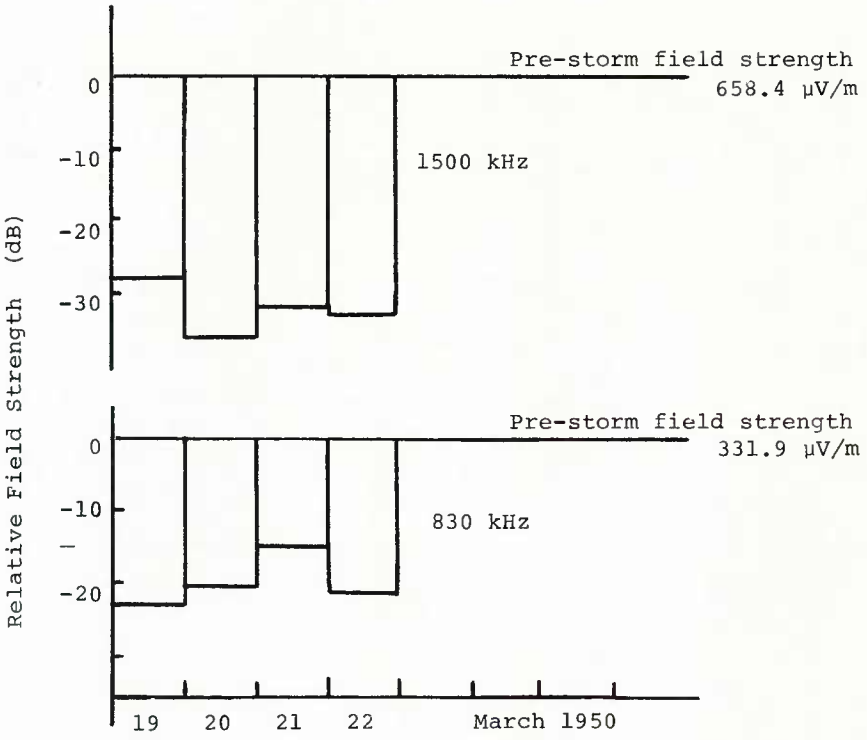

FIGURE 7 Effects of the magnetic storm of March 19, 1950 (Ap = 84) on two paths from Minneapolis, Minnesota to Portland, Oregon (2300 km, ϕ = 54.5 deg. N, data for the hour SS+2 are givin)

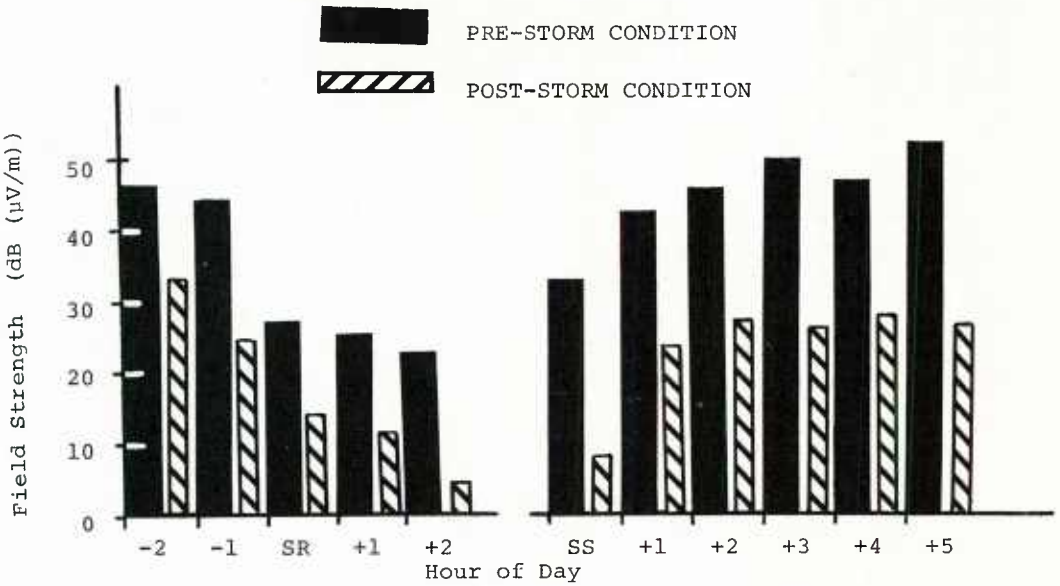

FIGURE 8 A comparison of pre-storm and post-storm skywave field strengths at different hours; Waltrous, Saskatchewan to Portland, Oregon; 540 kHz, 1439 km. ϕ = 56.2 degrees N.; Storm occured on Dec. 16, 1944, Ap = 83

DISCUSSION

J.Hortenbach, Ge

What is the difference in field strength between the daytime skywave and the ground wave, and how do you distinguish between both modes?

Author's Reply

Ground wave field strengths of the few paths where noon-hour measurements were made, were calculated and compared to measured data. Only when ground wave field strengths of a given path was sufficiently low (see Section 4.1), measured data were then considered to be skywaves. For example, noon-hour field strengths of CBK, as measured at Portland, were fairly constant, varying between one and two dB above one microvolt per meter with a slight peak occurring in August. Obviously, this was a ground wave considering the fact that conductivity in south-western part of Canada is about 40 mmho/metre!

H.Soicher, US

Has the MF field strength been determined as a function of time after the onset of magnetic storms?

Author's Reply

As far as I know, this has not been determined. To study this, original strip charts will have to be recalled from the US National Archives. We will do the best we can. Hopefully, I will be able to answer this question in the future.

J.S.Belrose, Ca

The absorption changes that affect MF nighttime propagation following some geomagnetic storms is an effect that maximises 1–3 days after the storm and lasts for 1–10 days. It is thought to be due to ionisation in the lower ionosphere caused by a regular "drizzel" of energetic electrons into the upper atmosphere during the period of build up or return to normal of the electron population in the radiation belts following the storm. This effect is particularly clear in North America due to south Atlantic anomaly in the Earth's magnetic field; that results in low mirror heights for trapped electrons. It is believed that this "drizzel" of energetic electrons into the lower ionosphere may occur at all times, only the magnitude of the effect is variable (ref. the Round Table Discussion in AGARD CP No.305).

G.H.Hagn, US

The gyrofrequency at ionospheric heights occurs in the MF band used for broadcasting. Have you looked for any relative increase in absorption (i.e., decrease in field strength) for broadcast stations operating on frequencies near the gyrofrequency?

Author's Reply

No. I have not studied this. Existing FCC data bank does not seem to be sufficient for this purpose. We will certainly keep your suggestion in mind when we make plans for our future work.

SIGNAL AND NOISE VARIABILITY IN HIGH FREQUENCY SKY-WAVE RADIO-SERVICE PLANNING

by

P A Bradley
Rutherford Appleton Laboratory, Chilton, Didcot, Oxon, UK

SUMMARY

Procedures existing under the auspices of the International Telecommunication Union for allocating frequency blocks to radio services and for the assignment of specific frequencies to individual radio operators are explained. The compatibility analysis undertaken by the International Frequency Registration Board at high frequencies to test for harmful interference is described and the technical standards used in this analysis are discussed. Work in progress within the International Radio Consultative Committee in preparation for a forthcoming World Administrative Radio Conference on High Frequency Broadcasting concerned with improved standards for field-strength estimation, fading, protection ratio and minimum usable field strength is reviewed.

1. INTRODUCTION - RADIO SERVICE PLANNING

Use of the radio spectrum is governed by the provisions of the Radio Regulations of the International Telecommunication Union (ITU) and Administrations signatory to the International Telecommunication Convention, Malaga-Torremolinos, 1973; Nairobi, 1982 - virtually all countries of the world - undertake to ensure that national legislation concerning radio usage is at least in accordance with these regulations. The Radio Regulations are amended from time to time by Administrative Conferences and the last general revision took place in 1979.

Article 1 of the Radio Regulations categorises radio usage into a number of services. For example, the fixed service is a radiocommunication service between specified fixed points, the aeronautical mobile service applies to transmissions between aircraft or between aircraft and the ground, and the maritime mobile service applies similarly between ship stations or between ship and coast stations. The broadcasting service (sound or television) is a radiocommunication service with transmissions intended for direct reception by the general public. The world is divided into three geographical regions ((1) Europe, Africa and N Asia, (2) the Americas and (3) S Asia and Australasia) together with a Tropical Zone (Article 8) and the spectrum is split into frequency blocks allocated for use either singly or on a shared basis by the various services. Some differences arise for the separate regions and the Tropical Zone with in each case the objective being an optimum compromise between the individual circuit requirements. However, it is evident that propagation considerations play an important role in determining these service allocations.

The high frequency (3-30 MHz) part of the spectrum is occupied mainly by the fixed service (approximately 35% of the band), the land and maritime mobile services (35%), sound broadcasting (15%) and aeronautical mobile service (5%). The remaining 10% of spectrum is used by the amateur service, the standard frequency and space-research services. There are separate provisions for each of these services. Whereas allotment plans exist for the aeronautical mobile service (Articles 28 and 29) with frequencies being determined on the basis of aircraft geographical location and for coast radio telephone stations operating in the maritime mobile service (Article 25), for the other services frequencies are assigned individually to each transmitter either for the period of operation required, or in the case of broadcasting (Article 17) on a seasonal basis.

The International Telecommunication Convention calls for the setting up of an International Frequency Registration Board (IFRB) with secretariat based in Geneva. The terms of reference of the Board are given in Article 10 of the Radio Regulations. These include in particular the administering and publishing from time to time of lists of transmitters registered for use, together with various technical details relating to location, intended recipient, type of service and modulation characteristics, frequency, transmitter power, antenna main lobe direction and beamwidth, and hours of operation.

The IFRB receives submissions from ITU member Administrations relating to proposed transmissions and undertakes technical examinations to assess whether favourable or unfavourable findings should be issued. It checks to see firstly whether the proposed transmissions are in accordance with the provisions of the Radio Regulations and secondly whether they are deemed to be compatible with other co-channel and adjacent channel transmissions. For the fixed service (Article 12) priority is given to existing (earlier notified) transmissions and the proposed new transmission shall not cause harmful interference to the established service at times when otherwise it would be satisfactory. For the broadcast service each seasonal schedule is determined separately and in principle all submissions published in a tentative schedule have equal status. There is no right to the use of the same frequencies in different seasons, although in practice informal procedures exist involving much international goodwill whereby individual organisations tend to maintain the same frequencies to operational advantage, albeit that sometimes these are used to different service areas with changes in propagation conditions throughout the seasons and solar cycle. Incompatibilities noted in a tentative broadcasting schedule are resolved by bilateral negotiations between the affected Administrations and in due course a definitive schedule is published.

Administrations usually carry out their own technical assessments to ensure a satisfactory service in the absence of interference before making submissions to the IFRB, although the IFRB will undertake such assessments on behalf of an Administration and offer suggestions relating to desired transmission characteristics, if specifically requested. The IFRB is mainly concerned though with performing compatibility investigations. The requirements of the broadcast community are clearly most critical since large numbers of such investigations are required each season; for the fixed and other services the load of calculation is more uniformly distributed.

Within the broadcast bands there is currently no Plan and attempts by successive conferences to agree a Plan have failed. In its latest endeavours the ITU is holding a further conference devoted entirely to HF sound broadcast planning in 1984/85 and the International Radio Consultative Committee (CCIR), which is the internationally represented technical committee of the ITU, is undertaking studies concerning parameters to be recommended to that conference. At present there are no standards on channel centre frequencies, bandwidths, maximum transmitter powers or number of frequencies radiating the same programme material to the same service area. If all transmitters used powers appropriate to their service areas and similar bandwidths (preferably with single-sideband modulation) and if channel centre frequencies were integer multiples of the bandwidth, these would be steps in the right direction. However, in the free-for-all with escalating transmitter powers over the last decade, with typically 5 transmitters on each frequency and an increasing number of third-world potential users, the means to effect a rationalised distribution of the finite spectrum without service degradation is far from clear. The need is certainly for adoption of optimum technical standards consistent with available IFRB resources,

This paper discusses aspects of the technical standards used at present by the IFRB and describes recent work with particular reference to signal and noise amplitude variability which may lead to improvements in these standards.

2. COMPATIBILITY ASSESSMENT

The detailed procedure to be applied for compatibility assessment following the forthcoming high frequency broadcasting conference is a matter for that conference to determine and at the present time several countries are giving consideration to different proposals. The elements of the procedure to be adopted will though be similar to those currently employed within the fixed and other services and will involve separate assessments for each of a number of selected reception locations within the coverage area for different seasons and solar epochs. Consider the case of a wanted transmission from transmitter T_W to receiver R_W as indicated in Fig 1 when other co-channel or adjacent transmissions may be proposed between transmitter T_I and receiver R_I. Then the separate stages of the compatibility assessment are :

(i) determination of the common hours of operation. In the case of broadcast transmissions the intended times of operation should be notified for each 15-minute period but in practice they are often quoted as the full 24 hours. The seasonal median basic maximum usable frequency (MUF) for the path $T_I \rightarrow R_I$ is determined for each UT integer hour of the common hours and T_I is deemed to be operable and potentially capable of causing harmful interference for those hours where the MUF is not more than 15% below the carrier frequency (ionospheric support limitation) and also in the case of carrier frequencies below 18 MHz the MUF does not exceed the carrier frequency by more than 70% (ionospheric absorption limitation).

(ii) determination of when the wanted transmitter provides an acceptable service in the absence of the potential interferer. The MUF over the path $T_W \rightarrow R_W$ is estimated in like fashion and for those hours that the carrier frequency is supported the seasonal median sky-wave field strength at the receiver is determined. Comparison is then made with a reference level known as the minimum usable field strength determined in the case of broadcasting on the basis of subjective tests.

(iii) determination of the strength of the interferer and comparison with the wanted signal. MUF over the path $T_I \rightarrow R_W$ is calculated for those hours that T_I is deemed to be operable and for that fraction of hours that propagation over the interference path is judged to occur, the strength of the interfering signal at R_W is assessed. Reference is then made to an agreed protection ratio, which is a measure of the amount by which the wanted signal needs to exceed the unwanted signal.

Hence the analysis involves the determination of MUF over three paths, fields strengths over two, and reference to minimum usable field strength and protection ratio standards.

The frequency assignment of all transmissions within an HF broadcasting seasonal schedule involves hundreds of thousands of compatibility assessments such as that described and it cannot be emphasised too strongly that available ITU computing resources rather than accuracy considerations dictate the sophistication that can be introduced into the technical standards used to estimate the above parameters. Approximately 100 ms of computing time is available for each such compatibility assessment.

IFRB technical standards encompassing provisions of the Radio Regulations and the recommendations of the CCIR are published from time to time. Standard M is concerned with the determination of MUF, A1 with protection ratio and A2 with minimum usable field strength. The standard describing the method of sky-wave field-strength determination has not been published but its details are readily available. An important element is the allowance for antenna gain, particularly in so far as the interference path often involves off-axis radiation. Reference antenna patterns exist in technical standard A4. Discussion of these standards and of work in progress aimed at improving them is presented in the following sections.

3. BASIC MAXIMUM USABLE FREQUENCY

The CCIR has developed a reference set of ionospheric characteristics (Report 340) which includes monthly median values of basic maximum usable frequency with reflection from regular layers for vertical incidence and for propagation to a range of 4000 km. These exist in the form of numerical maps as functions of latitude, longitude and universal time for each month and for reference low and high solar epochs. Technical standard M involves interpolation within tabular quantised values of the numbers given from these maps at the path midpoint for distances up to 4000 km and the application of the well-known two-control-point procedure for greater distances assuming great-circle propagation. E-region ionisation is also included in the standard and can be important on some short paths in the daytime. Data are used for particular months representative of the different seasons.

Work continues within the CCIR to improve the determination of basic MUF. Lockwood (1983) from ray-tracing analyses has developed an improved MUF factor algorithm. However there are unlikely to be proposals to the broadcasting conference to change fundamentally the existing method of MUF evaluation.

4. MONTHLY MEDIAN RMS SKY-WAVE FIELD STRENGTH

The method of monthly median field-strength estimation employed by the IFRB is based on adaptations of a procedure developed some 35 years ago at the then Central Radio Propagation Laboratory, USA (NBS, 1948). For unit radiation a reference night-time field is evaluated as a function of distance, and then additional allowances are included for ionospheric absorption (but not that caused by particles incident in the auroral regions) as a function of geographic latitude, time-of-day, season, solar epoch and frequency. For interference path calculations, particular interest centres on the night-time values since this is when the signals are strongest. Night-time fields are given typically as some 5-10 dB below the free-space field for propagation to the same distance.

In view of the extreme importance of the field-strength element in the compatibility analysis the CCIR has established a working party to review available procedures and to make recommendations for the preferred approach. The subject of field-strength estimation is being pursued actively in many countries and besides examining the current IFRB method, the CCIR working party has looked at 15 other methods including the first and second CCIR interim computer-based methods adopted in 1970 and 1978 respectively (CCIR Report 252-2; Supplement to CCIR Report 252-2). These CCIR methods are reference procedures encompassing more detail than could be incorporated into a compatibility analysis but they have proved particularly useful pointers to simplified ways of proceeding. Studies have been undertaken of the technical elements of the different methods and comparisons made with a data bank of measured signal strengths. At the time of writing, the working party has not yet completed its investigations but its provisional findings have been published (CCIR Report 894). It is proposing a new method which is an adaptation of the CCIR interim methods for distances up to 7000 km and an empirical approach based on procedures developed by the Deutsche Bundespost (Damboldt, 1976) for greater distances.

Figure 2 shows the maximum value at any hour of the day of the monthly median rms sky-wave field strength for 1 kW isotropic radiation given as a function of frequency and distance by the current version of this composite method. The curves have been derived from median results for a range of paths in different parts of the world in different seasons and solar epochs; there is remarkably little variation of the field strength with these location and time parameters. Night-time fields are typically 10 dB less than those yielded by the IFRB method. Some detailed changes may well be introduced to the method before submission to the conference affecting the values it yields and for planning purposes the curves of fig 2 need supplementation to allow for diurnal variations. Nonetheless the end result of the method appears to hold promise of being amenable to representation in a very simple computer code.

The lack of variation with path parameters is perhaps surprising, particularly in view of the known changes of absorption and MUF with location, season and solar epoch. It comes partly from the way in which contributions from different modes sum, but more especially from the inclusion of an above-the-MUF loss allowance giving a gradual reduction of field as the monthly median basic MUF is exceeded, rather than an artificial abrupt cut-off at a frequency estimated as being exceeded half the days.

The subject of above-the-MUF loss has been discussed in detail by Bradley et al (1982). It is shown that in order to estimate the median field over all days of the month as opposed to the median for a sample restricted to that fraction of days Q with refractive mode support, an additional 'availability' loss

$$L_m = -10 \log_{10} Q \quad , \quad \text{dB} \qquad (1)$$

must be applied. Figure 3 shows L_m for wave frequency f as a function of $\frac{f}{MUF}$ in the case of a Gaussian day-to-day distribution of MUF with decile deviations of 15%. Values for other MUF distributions and other decile deviations give significant locational and time variations but the curve quoted may be regarded as representative of mean conditions. Limited observational data collected by Wheeler (1966) on 11 nights over a single N American path are consistent with

$$L_m = 130\left(\frac{f}{MUF} - 1\right)^2 \quad , \quad \text{dB} \qquad (2)$$

These results are to be interpreted as incorporating both the availability loss and an allowance for the effects of scattering. Figure 3 shows this is equivalent to enhancing the effective MUF, leading to less above-the-MUF loss than when availability alone is considered. The field-strength curves of fig 2 are based on use of eqn (2). Increases in basic MUF leading to less above-the-MUF loss tend to occur under conditions when the absorption also is greater. Hence the two terms are compensatory, reducing field-strength variations with location, season and solar epoch. The necessity to include an above-the-MUF loss allowance in the field-strength prediction element of the compatibility analysis is now widely accepted. Whether this obviates the need for a separate preliminary test to ensure that the wave frequency lies within an empirically determined band of frequencies around the predicted monthly median basic MUF as discussed in section 2 is likely to depend on the amount of calculation involved in evaluation of the adopted field-strength procedure.

5. SIGNAL FADING

Signals which propagate via the ionosphere are known to fluctuate in intensity. There are both short-term variations over the period of an hour for which the field-strength estimates are to be regarded as mean values and there are other changes from day-to-day. Present procedures allow for these variations in a compatibility assessment by the introduction of suitable factors to the protection ratio and minimum usable field strength standards. Before considering in sections 6 and 7 respectively how this is accomplished it is relevant to review first what is known regarding the amplitude characteristics of fading.

5.1 Short-term variability

Short-term signal variability arises from changes in ionisation but there are several separate effects that occur under different conditions. Most important amongst these are :

(i) changes in ionospheric absorption with time;

(ii) defocusing, focusing and temporary disappearance of signal due to MUF failure;

(iii) multipath interference between separate modes, between the high and low-angle rays, or between the ordinary and extraordinary waves;

(iv) rotation of the axes of the polarisation ellipses, and

(v) existence of a scatter mode signal component.

Measured data have usually been fitted to idealised statistical distributions but unfortunately with very variable results depending on the measurement conditions and sampling periods adopted. For analysis intervals of 3-7 minutes distribution functions at HF close to the Rayleigh distribution seem to predominate, but over periods of 30-60 minutes the distribution seems to be better described as log-normal. Measured values of fading range, taken between the signal levels exceeded for 10 and 90% of the time, tend to be around 15 dB, except that at high signal levels the range is lower and more consistent with the Nakagami-Rice type of distribution appropriate to the existence of a strong constant term arising from specular reflection. Some differences in short-term fading on tropical paths are possible, particularly since it is known that for these flutter fading with rapid fluctuations and deep nulls is a common evening equinox phenomenon. When selective fading arises, fading depth is likely to be a function of receiver bandwidth.

Table 1 compares the upper and lower decile deviations of field strength from the median value (Δ_u and Δ_ℓ respectively) for the three mentioned types of distribution. Values for the log-normal distribution are given in terms of the standard deviation σ and those for the Nakagami-Rice distribution are quoted for selected ratios of the rms random to steady components.

Table 1 Decile deviations for idealised signal-amplitude distributions

	Δ_ℓ (dB)	Δ_u (dB)
Rayleigh	8.2	5.2
Log normal	1.28 σ	1.28 σ
Nakagami-Rice		
rms random / steady = 0.5	4.5	3
1	7.5	4.5
2	8	5

5.2 Day-to-day variability

Sources of day-to-day variability of signal strength include :

(i) changes in D and E-region ionisation giving modified absorption;

(ii) changes in F-region ionisation affecting the basic MUF and leading to different propagation modes and varying above-the-MUF loss, and

(iii) changes in ionisation affecting raypath elevation angles, thereby yielding variations in antenna gain, absorption, spatial attenuation, polarisation-coupling loss and ground-reflection loss.

An analysis by Liu and Bradley (1982) based on data for sample propagation paths leads to the conclusion that, although cause (iii) can be significant in individual situations, its effect is generally small in comparison with the other two phenomena.

The Supplement to CCIR Report 252-2 gives tables of Δ_ℓ and of Δ_u as a function of season, midpath local time and midpath geomagnetic latitude. Values are quoted separately for path ranges of less than or more than 2500 km and are grouped into 5° latitude bands and 4-hour time periods. Figures are taken from analyses of field-strength measurements carried out at the Institute for Telecommunication Sciences, USA. Statistical tests (Liu and Bradley, 1982) suggest that variations between the table entries are significant, but not large except in the auroral regions where day-to-day signal variability increases appreciably. The medians of these CCIR values are as given in Table 2.

Table 2 Median Δ_ℓ and Δ_u from the Supplement to CCIR Report 252-2 for paths with range D (km)

	D < 2500	D > 2500
Δ_ℓ (dB)	14.8	12.4
Δ_u (dB)	7.4	6.5

It is now recognised that day-to-day variability depends critically on the ratio of wave frequency to basic MUF and as a compromise between several proposals CCIR Report 894 suggests the use of single relationships for Δ_u and Δ_ℓ independent of geographical location and time but dependent on MUF as illustrated in fig 4. These are intended to be consistent with the combined median values given in Table 2 for frequencies not near the basic MUF. For comparison, values for a single mode given from a theoretical analysis described by Bradley and Lockwood (1982) in terms of known day-to-day distributions of basic MUF and absorption are also shown. Results are quoted for a representative sample case where the basic MUF follows a chi-square distribution with ratio of upper decile to median of 1.20 and lower decile to median of 0.83 and where the absorption varies according to that same law with ratio of upper decile to median (in decibels) of 1.34 and lower decile to median of 0.60. Also shown are the Δ_u and Δ_ℓ estimated by allowing only for basic MUF variability and applying the median, upper and lower decile MUF to eqn (1) to yield the corresponding median and decile above-the-MUF losses.

The approach in terms of MUF variability alone matches the full calculations for the larger frequencies. With f < 0.8 MUF it seems likely that in practice higher-order modes with comparable median field strengths will be effective and so the use of fixed allowances for Δ_u and Δ_ℓ is probably justified. These theoretical results suggest however that the decile deviations quoted in Report 894 are too large for f > 1.2 MUF. This finding is consistent with analyses of measured field-strengths for the Oslo-Norddeich and New York-Norddeich paths (Liu and Bradley, 1982). Data collected at several frequencies between June 1980 and May 1981 have been compared with path basic MUF values derived from predictions leading to the results of Fig 5. For the shorter path there is a reduction of day-to-day variability for f > 1.2 MUF possibly associated with a switch to a scatter propagation mode at the higher frequencies.

6. PROTECTION RATIO

Radio frequency protection ratio for sound broadcasting is defined (CCIR Recommendation 447) as the ratio of the radio frequency wanted to interfering signal that enables, under specified conditions, the audio frequency protection ratio to be obtained at the output of the receiver. The audio frequency protection ratio is the agreed minimum value of audio frequency signal to interference ratio considered necessary to achieve a subjectively defined reception quality. The audio frequency protection ratio is based on listener tests and figures taken are typically those corresponding to 90% of the sample of listeners. The rf protection ratio varies as a function of frequency separation betwen the wanted and interfering signals and also depends on the types of modulation and receiver selectivity. Studies in different countries suggest that HF co-channel protection ratios should lie in the range 27-42 dB under steady signal conditions. A second CCIR working party addressing the question of planning standards for the high frequency broadcasting conference has proposed (CCIR, 1981) use of the rf protection-ratio curves given in Fig 6 in the case of stable wanted and interfering signals when both have either high or limited compression. These curves correspond to a co-channel protection ratio of 27 dB in agreement with CCIR Report 794 and protection ratios at other frequencies consistent with CCIR Recommendation 560 giving higher values for frequency separations up to 5 kHz. By comparison the present IFRB technical standard is based on a co-channel protection ratio of 17 dB falling to 14 dB for a frequency separation of 5 kHz.

To all the above figures must be applied fading allowances to take account of the within an hour and day-to-day variability of both the wanted and interfering signals. Not only is it necessary to specify variability distributions but also particular percentile values of these distributions must be adopted as applying to planning. CCIR Recommendation 411 proposes a short-term fading allowance of 10 dB to ensure that the steady state ratio is attained for 90% of any given hour. The long-term fading allowance for day-to-day variability to ensure that the steady state ratio is achieved for 90% of the days of the month in 90% of the cases is given as 13 dB. The rms sum of these two allowances in decibels (16 dB) is taken as the overall variability allowance to ensure that the steady state ratio is attained for 90% of the total time. It is hard though to reconcile this general approach with the discussion of section 5 in that the day-to-day variability depends so critically on the ratio of wave frequency to basic MUF. Serious consideration needs to be given to whether decile rather than median field-strength values should be predicted in the first place.

IFRB protection ratio standard A1 published in 1968 encompasses allowances for log-normal or Rayleigh distribution short-term fading depending on conditions, with a fading correction of 4-15 dB. To this is added in quadrature an allowance of 7 dB for day-to-day variability to give the protection ratio attained for 90% of the time.

The spectrum has finite capacity and studies are in progress within the IFRB to attempt to quantify this. At present it does not seem possible to indicate how nearly the capacity has been met in the case of HF broadcasting, but the continued 'illegal' use of out-of-band frequencies, despite the extra portion of spectrum allocated to broadcasting in 1979, shows that the current position is unsatisfactory. A more rationalised approach to the assignment of frequencies would improve the situation but it may still prove necessary to reduce protection ratio standards from values based on listener satisfaction tests in order to accommodate all requirements. Even if such a political decision is taken, the compatibility analysis still has merit in identifying the worst cases of harmful interference.

7. MINIMUM USABLE FIELD STRENGTH

Minimum usable field strength is defined in CCIR Recommendation 499 as that field necessary to permit a desired reception quality under specified receiving conditions in the presence of natural and man-made noise but in the absence of interference from other transmitters. Reference information on atmospheric noise intensities is contained in CCIR Report 322. This is based on past measurements taken with a global network of standardised receivers. No systematic trends were detected throughout a solar cycle and global maps of seasonal median values of mean noise power at a frequency of 1 MHz are presented for different four-hour time blocks and for each of the four seasons. An example showing one of these so-called 'noise-grade' maps for 12-16 h local time in summer is given in Fig 7. The mean noise power at other frequencies is derived with the aid of a corresponding set of frequency conversion curves parametric in terms of 1 MHz noise grade (Fig 8). Atmospheric noise is impulsive in nature with an

amplitude structure that varies with conditions, particularly with frequency and receiver bandwidth. The structure is given in terms of a reference set of amplitude probability distributions parametric in rms noise field strength and in V_d, the ratio of rms to average field strength. The rms noise field strength is directly related to the mean noise power and V_d is given separately for each seasonal time block as a function of frequency for a receiver bandwidth of 200 Hz. Other data indicate how V_d changes with receiver bandwidth. Hence for any reception conditions the seasonal median atmospheric noise intensity may be specified. Day-to-day variability is described by the decile deviations of the mean noise power from the seasonal median values again given separately for each frequency and time block. Variations within an hour are ignored.

Man-made noise may be estimated from four reference curves taken from CCIR Report 258 (Fig 9) showing the dependence on frequency of the mean power for business, residential, rural and quiet rural receiving sites. CCIR Report 258 also gives the upper and lower decile deviations of the noise power within an hour from the quoted median values, together with estimates of the standard deviations of the locational variability. There are currently no CCIR reference data on the amplitude structure of man-made noise but measurements suggest (e.g. Spaulding et al, 1971) that at HF man-made noise is more impulsive than atmospheric noise.

IFRB technical standard A2, adopted in 1968, consists of geographically quantised values of 1 MHz noise grade for the different seasons and time periods taken from CCIR Report 322, together with a set of minimum usable field strengths in the case of high frequency broadcasting parametric in frequency, time-of-day and noise grade (Fig 10). The factors inherent in these relationships are as follows :

(i) mean allowances are applied for the frequency variation of atmospheric noise power independent of season;

(ii) the required rf input signal/noise ratio for stable propagation conditions is 49 dB in a 1 kHz bandwidth corresponding to 90% listener satisfaction;

(iii) mean allowances are applied for the day-to-day variability of the noise power and of the signals independent of season. These are taken as the quadrature sum of the atmospheric noise decile deviation (from CCIR Report 322) and a factor ranging from 6 dB at 5 MHz through 5 dB at 10 MHz to 3 dB at 20 MHz for the signals;

(iv) no allowance is included for within an hour variability of the noise or signals;

(v) satisfactory reception is achieved for 90% of the time, and

(vi) a lower limiting minimum usable field strength of 31 dB > 1 μV/m is taken, approximately consistent with estimated mean galactic noise intensities and man-made noise power for a quiet rural site.

The CCIR working party examining this standard have in their provisional conclusions endorsed the general approach adopted by the IFRB (CCIR, 1981). However they recommend a number of changes of detail relating to the atmospheric noise grade geographical quantisation and the rf input signal/noise ratio for stable conditions. Tests with a reference receiver suggest use of a figure of 46 dB corresponding to an audio frequency signal/noise ratio of 30 dB for 90% listener satisfaction. They also are proposing use of man-made noise powers appropriate to residential areas and inclusion of new allowances for both short term and long term signal and noise variability yet to be agreed.

With the need to allow for the dependence of signal day-to-day variability on the ratio of wave frequency to the basic MUF as discussed in section 5.2 and also to incorporate locational variability corrections in the case of man-made noise, it is difficult to see how this can be achieved conveniently. Of additional and perhaps greater concern is that studio tests leading to reference figures of rf input signal/noise ratio based on Gaussian noise are inappropriate. As stated previously, atmospheric and man-made noise are considerably more impulsive depending on frequency and bandwidth. Figure 11 shows that for typical HF broadcasting conditions the threshold field giving 10% occupancy for atmospheric noise is 23 dB less than that of Gaussian noise. This suggests that current minimum usable field strengths may be appreciably too large over much of the HF band. At frequencies around 20 MHz atmospheric noise becomes more nearly Gaussian in structure, but man-made noise remains impulsive so the same applies but to a lesser extent.

8. RELIABILITY

The foregoing approach to compatibility analysis involves estimation of monthly median field strength and application of fixed factors independent of location and season for day-to-day and within an hour variability in calculating protection ratio and minimum usable field strength. Many approximations are introduced and the assumption made that decile variability allowances may be summed in quadrature. It is therefore tempting to speculate whether some alternative procedure might be preferable.

One such approach would be in terms of the parameter reliability. CCIR Report 892 currently defines the circuit reliability as the probability that a required signal/noise ratio is achieved for a given circuit in the presence of natural and man-made noise and overall circuit reliability (versus noise and interference) as a similar parameter when account is taken additionally of interference. Figure 12 shows the dependence of circuit reliability on required signal/noise ratio assuming a Gaussian variation of mode signal/noise ratio with 10 dB decile deviations in the case of a single propagation mode and when a second mode, completely correlated in occurrence ($\rho = 1$) but uncorrelated in amplitude with mean field strength half that of the first mode, is also present. The existence of two modes leads to increased reliability. However, it seems likely that in practice with two modes, signal dispersion due to multipath and Doppler frequency changes would degrade system performance for the lower required signal/noise ratios to a greater extent; this would be in the manner indicated and suggests a possible need to extend the reliability definitions to encompass dispersion.

It might also be desirable to extend the definitions to include the case of broadcasting coverage. In the present IFRB compatibility assessment applied to HF broadcasting, calculations are made for 660 specified transmitter locations and for propagation to given reception points within 75 so-called CIRAF coverage zones throughout the world. The CIRAF zones are of unequal size and varying numbers of reception points up to a maximum of 9 but typically 5 are taken within each zone. An empirical rule is applied relating the maximum number of points giving an incompatibility to the number sampled before the service as a whole is deemed to be incompatible. For example, with 9 reception points not more than 6 may give an incompatibility; with 5 points not more than 4, and with 3 or less points none. With an extended reliability concept incorporating coverage, the temporal and locational variabilities might perhaps with advantage be incorporated into a single figure of merit.

9. CONCLUSIONS

Signal and noise variability are shown to be important factors in determining the compatibility of high-frequency radio transmissions. Present procedures employed by the IFRB matched to available ITU computing resources are seen to involve several elements that can be challenged, and suggestions for changes are offered. Extreme caution should however be exercised in introducing uncontrolled amendments to a procedure that demonstrably works to the satisfaction of most Administrations, albeit that it is not necessarily optimum.

Acknowledgements

Grateful acknowledgement is made to Mr C Glinz and Dr S Tsukada of the IFRB Secretariat and to Messrs J K Edwards and I Davey of the BBC External Services for useful discussions.

References

BRADLEY, P A, LIU, R Y, LOCKWOOD, M and DICK, M I, 1982, "Above-the-MUF loss", CCIR Interim Working Party 6/1, Document 209, 27 August 1982

BRADLEY, P A and LOCKWOOD, M, 1982, "Simplified estimation of HF sky-wave signal mode reliability", in 'HF communication systems and techniques', IEE Conference Publication 206, 60-63

CCIR Recommendation 411-2, 1982, "Fading allowances in HF broadcasting"

CCIR Recommendation 447-2, 1982, "Signal-to-interference ratios in sound broadcasting"

CCIR Recommendation 499-2, 1982, "Definitions of specific field strengths and coverage area in LF, MF, HF and VHF sound broadcasting"

CCIR Recommendation 560-1, 1982, "Radio frequency protection ratios in LF, MF and HF broadcasting"

CCIR Report 252-2, 1970, "CCIR interim method for estimating sky-wave field strength and transmission loss at frequencies between the approximate limits of 2 and 30 MHz"

CCIR Supplement to Report 252-2, 1978, "Second CCIR computer-based interim method for estimating sky-wave field strength and transmission loss at frequencies between 2 and 30 MHz"

CCIR Report 258-4, 1982, "Man-made radio noise"

CCIR Report 322-2, 1982, "World distribution and characteristics of atmospheric radio noise"

CCIR Report 340-4, 1982, "CCIR atlas of ionospheric characteristics"

CCIR Report 794-1, 1982, "Protection ratios in LF, MF and HF broadcasting"

CCIR Report 892, 1982, "Computation of reliability for HF radio systems"

CCIR Report 894, 1982, "Propagation prediction methods for high frequency broadcasting"

CCIR, 1981, "Report by Interim Working Party 10/5 to Study Group 10", Document 10/216 (Rev 3), 1 October 1981

DAMBOLDT, T, 1976, "A comparison between the Deutsche Bundespost ionospheric HF radio propagation predictions and measured field strengths", in 'Radio systems and the ionosphere', AGARD Conference Proceedings CP-173, 12-1 to 12-18

LIU, R Y and BRADLEY, P A, 1982, "Day-to-day variability of HF sky-wave signal intensity", CCIR Interim Working Party 6/1, Document 214, 22 September 1982

LOCKWOOD, M, 1983, "A simple M-factor algorithm for improved estimation of the basic maximum usable frequency of radio waves reflected from the ionospheric F region", submitted to Proceedings IEE (F)

NBS, 1948, "Ionospheric radio propagation", National Bureau of Standards Circular 462, US Govt Printing Office, Washington 20402

SPAULDING, A D, AHLBECK, W H and ESPELAND, L R, 1971, "Urban residential man-made radio analysis and predictions", OT Telecommunications Research and Engineering Report 14, US Govt Printing Office, Washington 20402

WHEELER, J L, 1966, "Transmission loss for ionospheric propagation above the standard MUF", Radio Science, 1(11), 1303-1308

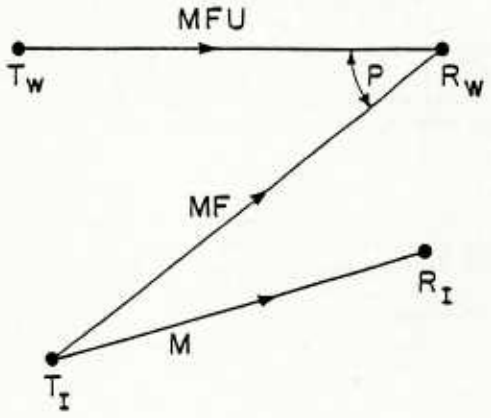

Fig 1 Elements of an IFRB compatibility analysis (M = MUF; F = field strength; U = minimum usable field strength; P = protection ratio)

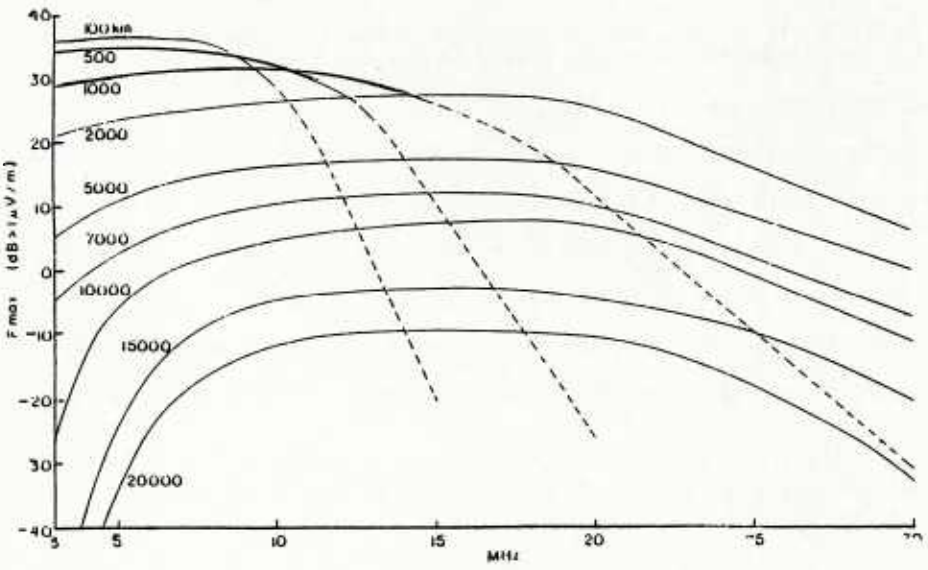

Fig 2 Maximum field strength at any hour F_{max} for 1 kW isotropic radiation given from the current prediction procedure of a CCIR working party

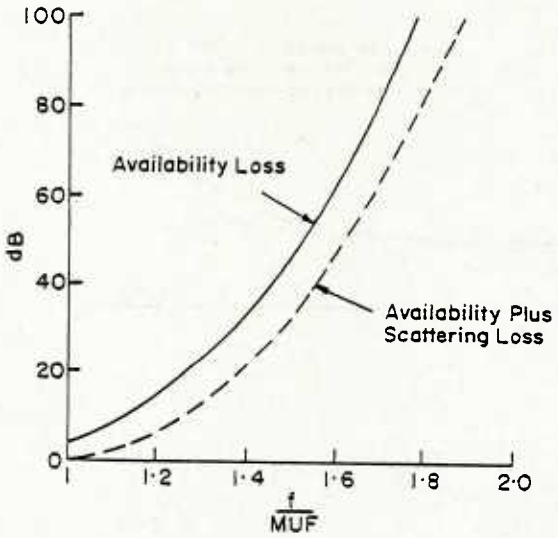

Fig 3 Above-the-MUF loss given by eqns (1) and (2) taking account of availability loss and availability plus scattering loss respectively

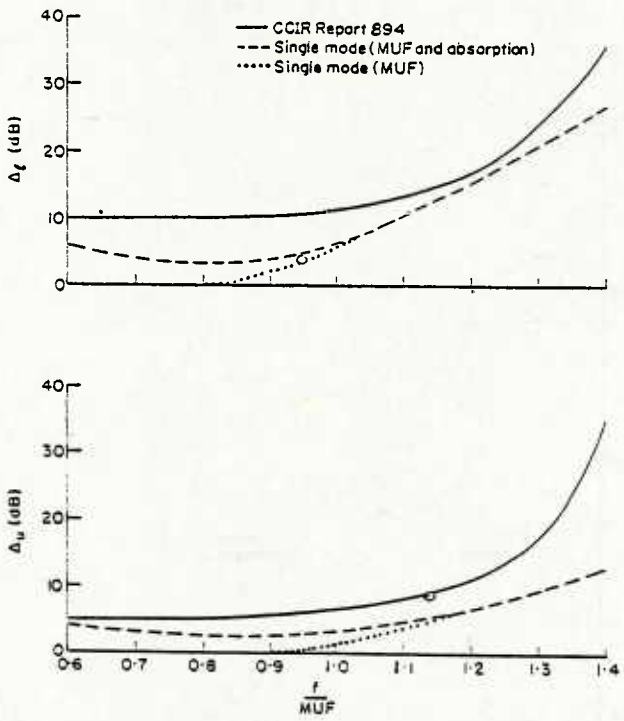

Fig 4 Lower (Δ_l) and upper (Δ_u) field strength decile deviations proposed for adoption in CCIR Report 894 and as given by theory for a single mode taking account of MUF and absorption variability

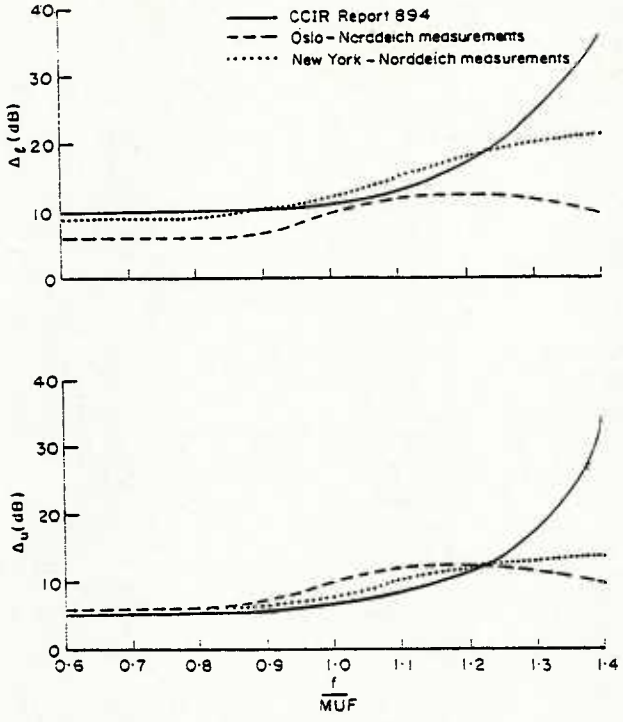

Fig 5 Lower (Δ_ℓ) and upper (Δ_u) field strength decile deviations proposed for adoption in CCIR Report 894 and as given from measurements over short (Oslo) and long (New York) paths

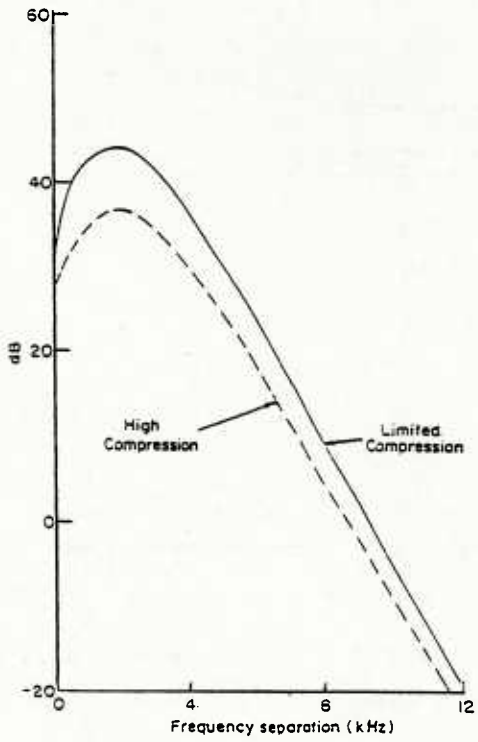

Fig 6 RF protection ratio for HF broadcasting under conditions of high and limited compression with stable wanted and interfering signals, as proposed provisionally by a CCIR working party

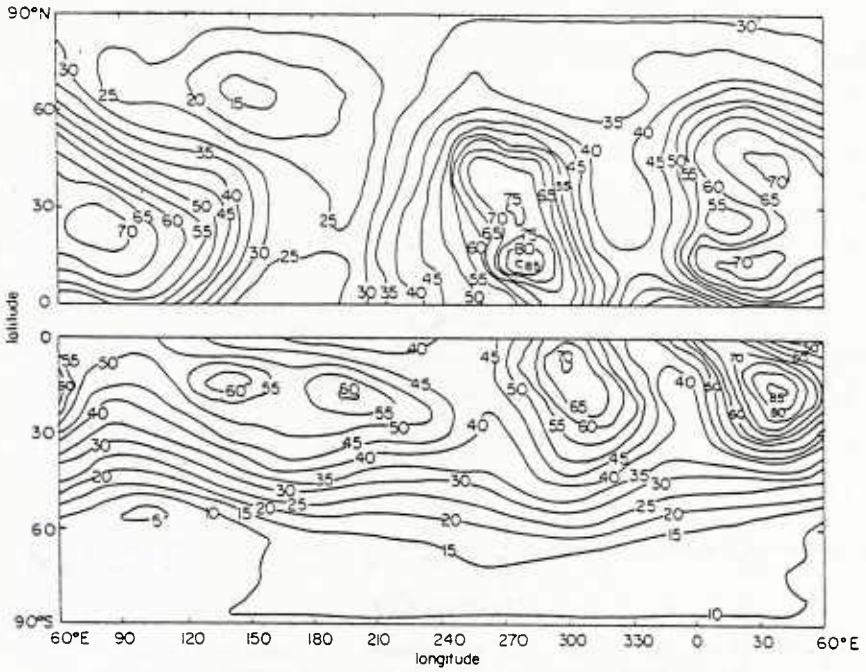

Fig 7 F_{am}, expected atmospheric noise mean power at 1 MHz in summer at 12-16 h local time, dB above $KT_o b$ where T_o is the reference temperature of 288K (from CCIR Report 322)

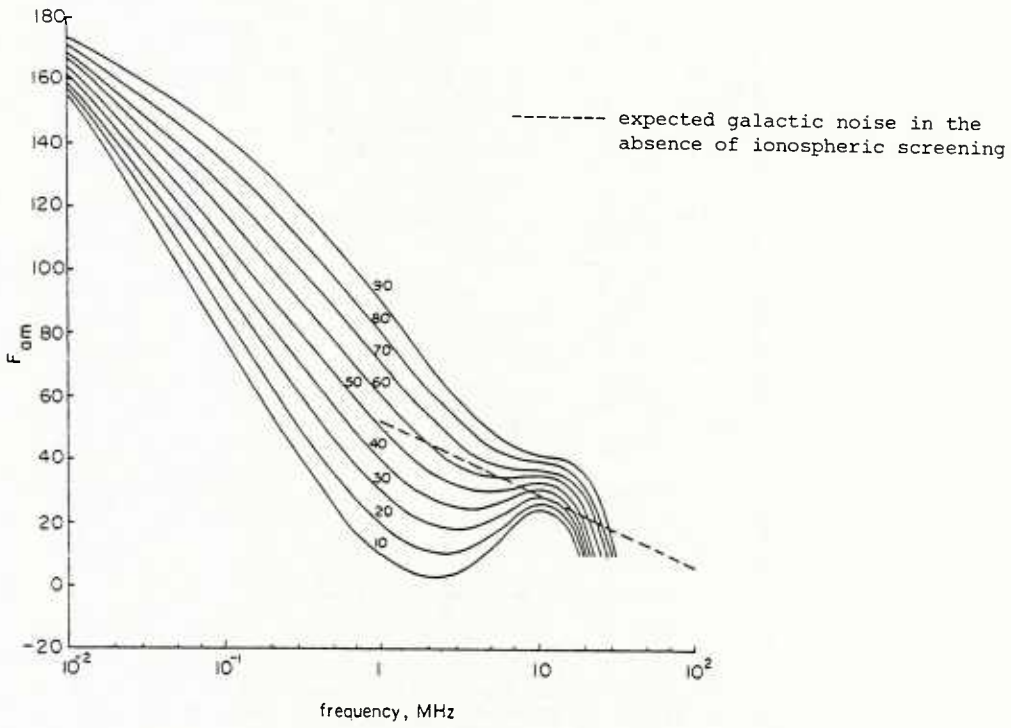

Fig 8 Expected variation of atmospheric noise mean power with frequency in summer at 12-16 h local time for different values of 1 MHz noise grade (from CCIR Report 322)

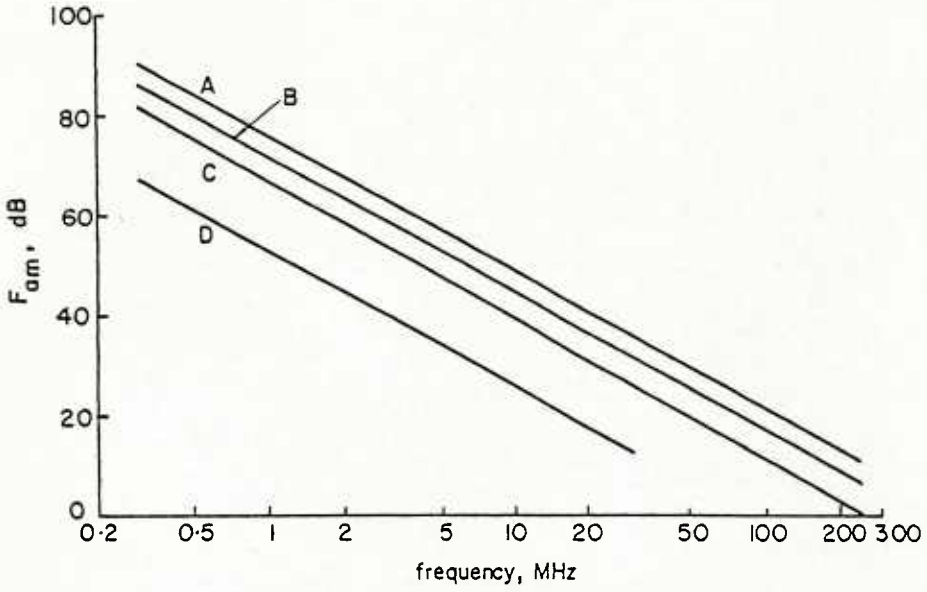

Fig 9 Mean values of man-made noise power at receiver for a short vertical lossless grounded monopole antenna situated in different areas (from CCIR Report 258)

A = business
B = residential
C = rural
D = quiet rural

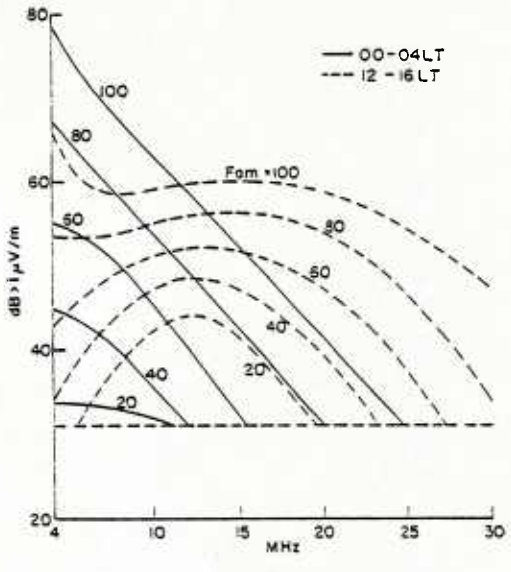

Fig 10 IFRB minimum usable field strength standard for HF broadcasting at 00-04 and 12-16 LT. Curves are parametric in 1 MHz noise grade

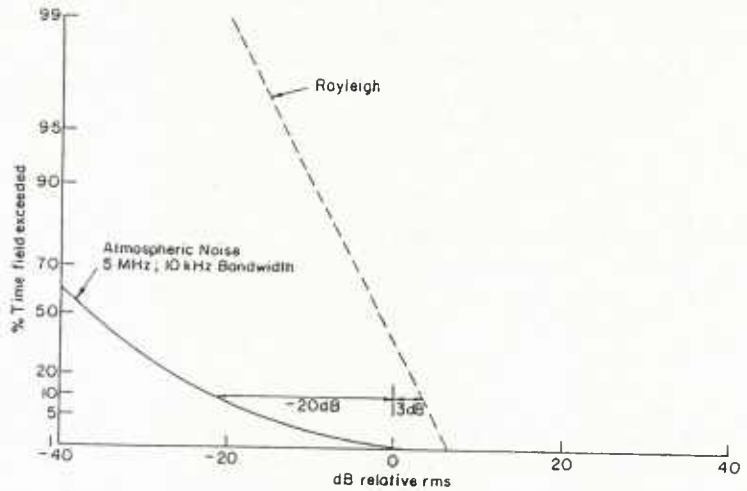

Fig 11 Probability distributions for Rayleigh and atmospheric noise

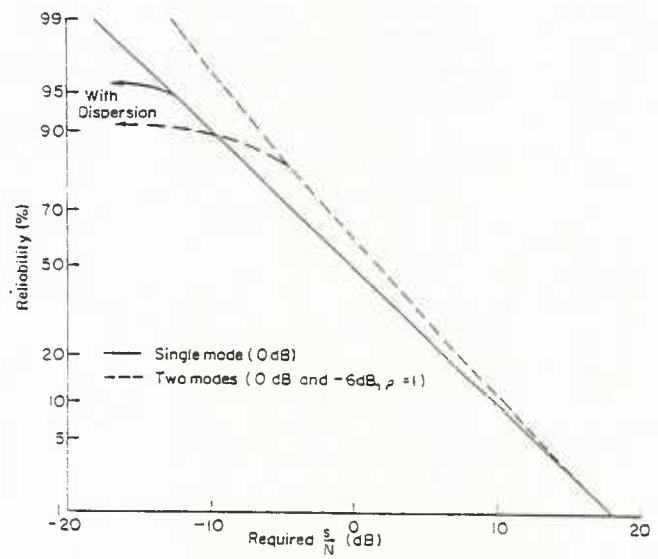

Fig 12 Circuit reliability for one and two mode signals

DISCUSSION

G.H.Hagn, US

You mention trying to predict deciles rather than medians. One would like to know the distribution. While deciles and medians have been commonly measured and reported in the literature, it is known that other quantiles permit a more accurate reproduction of a sample distribution. For example, if only 3 quantiles can be used, it is better to use the median, and the 5 percent and 95 percent points. This general area has been reviewed recently by Mr David B.Sailors, NOSC, San Diego. The conclusion is that it is better to measure and predict the median and these other quantiles than the median and the deciles – if only 3 quantiles can be used.

Author's Reply

Thank you for this information but suggestion is to predict decile values of field strength instead of median values, not as well as the medians. Deciles are chosen because these are the percentile values that the user community has decided it wants as a criterion of acceptability.

G.H.Hagn, US

Regarding your point on the distribution of man-made noise parameters, the information available is limited as you say. Empirical Models for the distribution of RMS levels of man-made noise for business, residential and rural areas have been developed by G.H.Hagn and D.B.Sailors, and these model results are now in CCIR Report 258.
Dr D.Middleton has developed models for the amplitude probability distribution (APD) of the noise envelope, and these APDs are relative to the RMS level. It remains to determine the Middleton Model parameters for man-made noise (except for the few examples in the literature) so that the model can be used to predict error rates for practical communication systems which must operate in the presence of man-made noise. It has been proposed by Hagn to determine if generic Middleton Model parameters exist for the CCIR environmental categories of business, residential and rural. As of now, this work remains to be done.

T.B.Jones, UK

Were the signal strength data you presented based on experimental observation or on modelling results?

Author's Reply

The curves of Figure 2 are derived from the medians of values for a range of sample paths at different latitudes in different seasonal and solar epochs. They have been computed by the code LIL252.81.03 produced by CCIR Interim Working Party 6/12. The method of prediction is based on (i) a simplification of the procedures of CCIR Reports 252-2 and Supplement to 252-2 for ranges up to 7000 km and (ii) the procedure of the FTZ, Darmstadt (Damboldt, 1976) for greater distances. The former has been developed mainly from physical concepts, the latter from an empirical fit to past measured data.

ANOMALOUS PROPAGATION BEHAVIOR OF RADIO SIGNALS AT HIGH LATITUDES

Robert Hunsucker[1]

Geophysical Institute
University of Alaska
Fairbanks, Alaska 99701

ABSTRACT

Signals in the 3-30 MHz (HF) band propagated through polar and auroral ionospheric regions sometimes undergo some unique and profound changes. The channel capacity, intelligibility and reliability of these signals are affected by multipath distortion, backscatter, non-great-circle propagation and other high latitude anomalies. *Signals propagated in the VLF, LF, MF, VHF/UHF and microwave portions of the radio spectrum also undergo some very deleterious effects.*

Specifically, *some* of the *newer results* obtained include:

A. *Ground Constant Measurements of Tundra/Permafrost* — $\sigma = 0.025-0.098$ mhos/m and $\epsilon = 33-788$ from open-wire-measurements made in Fairbanks in August 1982 from 500 to 12,000 KHz.

B. *MF Skywave Signals*.— In 550 to 1700 KHz band seem to be limited to almost north-south paths with much lower signal strengths than had been suspected.

C. *Precipitation Depolarization of Satellite Downlink Signal* — At 4 GHz, a "worst case" at a look angle of 11.5° showed 20 dB of depolarization due to a rain rate of 140 mm/hr.

I. INTRODUCTION

If a radio communicator were to methodically search for a region on this planet where it would be the most difficult to communicate by radio (including interference effects) he would find Alaska high on that list! This would be true over *most* of the radio spectrum (ELF, VLF, LF, MF, HF, VHF and UHF). There are even *some* propagation problems in the *microwave* bands.

The salient reasons for these propagation problems are:

High Geographic Latitude

The severe *climatic* conditions include:

- a large daily and seasonal *temperature variation* (expansion/contraction of antenna terminations, coax. connectors, etc. (Figure 1)
- *extremes* of temperature — down to -63°C (Figure 2)
- high *winds*
- *ice* accumulation
- *snow* — (blowing produces precipitation static)
  — accumulating — increases difficulty in access to installations for servicing and maintenance
- *surface and elevated temperature inversions* — these are some of the steepest inversions recorded in the world and can cause anomalous refractivity which sometimes affects propagation at UHF through microwaves.

Usually, high latitude locations for communication sites also have increased costs because of their remoteness from "temperature" latitude commercial supply centers. The auroral latitudes define that region of the ionosphere where the largest number of anomalies abound (large and small-scale irregularities in the E and F regions, enhanced absorption in the D-region, enhanced F1 layer effects, etc.). The polar ionosphere (~70°—90° Geomagnetic latitude) also displays considerably more anomalous behavior than the mid-latitude behavior. The effect of the polar and auroral latitudes on radio signals in the *HF (3-30 MHz)* portion of the spectrum are described in considerable detail by Landmark [1964], Hunsucker [1967], Lied [1967], Folkestad [1968], Hunsucker and Bates [1969] Frihagen [1962], Bates and Hunsucker [1974] and Hunsucker [1979a].

[1] Presently on sabbatical leave at Bell Laboratories, Murray Hill, NJ.

Rugged Terrain

The variability of the terrain in Alaska is striking! One can go from sea water to freshwater glacier to precipitous mountain to alpine tundra in a horizontal traverse at D≃100 Km. The altitude range within Alaska is 6194 m from sea level to the top of Mt. Mckinley compared to 4504 m from "Death Valley" to the highest point (Mt. Whitney) in the contiguous U.S. The conductivity and permittivity of these surfaces varies by several orders of magnitude and, of course, affects radio propagation in the VLF, LF, MF and HF bands. Quantitative values for the preceding parameters will be given later in this paper.

Logistics

Compared to a midlatitude (temperate) communications site, high latitude sites have significantly higher installation and maintenance costs and decreased accessibility. Alaska has a population of ~400,000 dispersed non-uniformly over an area of 565,000 miles^2 (1,446,400 km^2). There are two cities of over 50,000 population and ~300 villages and settlements. No railroads exist from Alaska to the contiguous U.S. the one highway is at times marginal and there are only a handful of ice-free ports for sea transportation. These reduced transportation routes and large distances from the communications equipment suppliers, of course, conspire to greatly increase the cost of installing and maintaining communication facilities. The hostile radio propagation conditions which are found in Alaska apply to many other countries and territories on the planet earth poleward of approximately the 60th parallel of geographic latitude (Figures 3, 4 and 5).

II. SOME CHARACTERISTICS OF THE ALASKAN PROPAGATION ENVIRONMENT

Terrain

As a typical example of the terrian of Alaska (and some other regions poleward of 65°) consider first the idealized sketch in Figure 6 which shows a typical north-south transect from the Gulf of Alaska to the Arctic ocean. The vertical scale is of course greatly exaggerated in order to portray the operative meteorological phenomena. The salient point is the tremendous *variation* in ground characteristics and terrain structure in this path. If one were trying to communicate from a ship in the Gulf of Alaska to an oil rig on the Beaufort sea ice it is rather obvious that it would not be possible in the LF-MF (ground-wave) part of the spectrum and obviously not the VHF/UHF→μwaves line-of-sight (LOS) mode. HF skywave modes are one possibility but the ionospheric "reflection" point(s) lie in the auroral zone — which as we might suspect introduces deleterious effects. The best solution is to use earth/satellite communication, which will be discussed later.

Ground Electrical Properties

As may be seen in Table 1, the conductivity can vary by as much as six orders of magnitude and ϵ can vary from ~1.0 to 80. CCIR curves also illustrate very well the variation in *field strength* between high conductivity (σ = 4 mhos/m, ϵ = 80/sea water and low conductivity (σ = 0.001 mhos/m, ϵ = 4/"poor earth").

A very thorough investigation of the electrical properties of the earth's surface in the interior regions of Alaska has been reported by *Hoekstra [1975]*. This research team used an airborne system to record the wave tilt and/or surface impedance of radio ground waves in the VLF/LF/MF bands. The aim of the study was to construct an electrical conductivity map of Alaska for use in planning radio navigational aids. Results of this investigation indicated that the mapping of all of Alaska would be extremely difficult because: a) ground conductivity in permafrost areas is very heterogeneous, so that it is not directly apparent how to assign an effective conductivity value to a path of practical length (D≈100 km), and b) the geological and permafrost conditions vary so much in Alaska, that measurements at a location are representative of *small areas* only, and c) there are also very significant seasonal variations.

Examples of the spatial variations encountered in interior Alaska and similar northern regions is illustrated in Figure 7 [Hoekstra, 1975].

Troposphere

Radio waves propagating on tropospheric paths are, of course, affected by water vapor, rain, snow, sleet, ice crystals, etc. Radio refractivity is usually expressed (CCIR, for example) as:

$$N = (n-1)\times 10^6$$

where

$$N = (77.6/T^\circ)\ (p+4810\ e/T)$$

n = refractive index of air

T = absolute temperature (°K)

e = water–vapor pressure

p = atmospheric pressure (mb)

The sea-level value of radio refractivity is given by

$$N_o = N_s \exp\{0.1057h\}$$

where

N_2 = measured values at earth surface meteorological observatory

h = altitude in kilometers

Deviations of refractive index are expressed by

$$\Delta N = N_1 - N_s$$

where N_1 = value of N at h = 1 km above ground. CCIR Publication 233 shows global contour plots of yearly and monthly mean minimum values of N_o. The sharpest gradients shown in these contours occur at equatorial and temperate latitudes. The regions poleward of 60° latitude do not show the sharp gradients, but this is due in part to a paucity of meteorological observations in these regions, and partly due to lower atmospheric water vapor content, in general, in the polar regions.

The polar regions, however, are significantly different from the equatorial and temperate regions in that they probably have steeper surface temperature inversions over larger areas than at lower latitudes. These temperature inversions at times influence radio propagation conditions significantly by the large gradients and ducts which they produce. As an example, the Fairbanks, Alaska wintertime surface inversions are considered to be the steepest in the world — up to three times steeper than the Los Angeles inversions. As one example, the Geophysical Institute operates a 2 GHz telemetry link from the University of Alaska campus to Eielson Air Force Base (D=41 km). The line-of-sight path traverses the area where the Fairbanks inversions are strongest, such as those shown in Figure 8. To account for losses caused by deviating the signal path (Fresnel zone loss), we had to increase the system gain by 6dB. This gave an adequate margin for year -round reliable and adequate $(\frac{S}{N})$ at the receiver.

Another tropospheric effect on radio propagation, especially at high frequencies is precipitation. In Alaska water precipitates as snow, ice crystals ("diamond dust") — observed under cloudless skies), rain, sleet and occasionally hail. Signal attenuation of a radio signal traversing precipitation region can be caused by absorption and/or scattering of the rf energy and by depolarization of the incident wave. In satellite communication, frequency "reuse" may be obtained by using the same antenna structure to propagate two radio signals which are oppositely polarized to each other.

Recently, the Geophysical Institute conducted an investigation of the effects of rain depolarization on a 4 GHz satellite downlink signal received at Sitka, Alaska from INTELSAT IV-A geostationary satellite, [Merritt et al., 1981] Sitka was chose because of the low look angle (11.5°) and high annual rainfall (2286 mm).

A "worst case" rain depolarization of the signal of *20dB** was observed during the period that maximum precipitation occurred in the path of the satellite signal. If design changes were made in the system, crosstalk between the Right-hand-circular-polarization and Left-hand-circular-polarization channels would certainly be objectionable at Sitka during periods of heavy rain.

Ionospheric Effects

The high-latitude ionosphere mainly affects signal propagation in the *VLF through HF bands,* though under certain conditions anomalous VHF and UHF propagation effects have been observed. The actual high latitude ionospheric anomalies which produce the effects on signals propagated in these regions of the spectrum are:

Ionospheric D-Region:	Auroral oval absorption and Polar-cap absorption
Ionospheric E-Region:	Auroral sporadic-E ionization and irregularity structure (Figures 10 and 11).

* ≃35dB isolation is considered to be adequate between two polarization modes in the satellite service.

Ionospheric Lower F-Region: Peak electron-densities in the F1-layer can be as high or higher than peak F2 layer values during summer low-sunspot number periods.

Ionospheric Upper F-Region:
(a) Large sheets of field-aligned ionization
(b) Small-scale irregularities ("spread-F")
(c) Low densities in the "trough" (Figure 12)

Noise

In general, high latitudes are at least qualitatively in a much more favorable situation than lower latitudes in respect to radio noise interference. Even *galactic radio noise* (~18–250 MHz) (with the exception of Cassiope ia A and Cygnus-A) is somewhat reduced at the lower frequency end by enhanced D-region absorption. *Man-made radio noise* originates mostly in the highly industrialized temperate latitude regions and must be propagated by ionospheric reflections to distant regions at the earth (the nearest industrial center to Fairbanks is the Vanouver-Seattle area ~2000 Km away. Similarly, most of the atmospheric noise in the world is generated by electrical storms in such places as the Caribbean, East Indies, equatorial Africa, etc. , quite far removed from the "northern regions." .

The marked decrease in *atmospheric radio noise* at latitudes greater than 60° for a summer afternoon is graphically portrayed in CCIR Report 322 as well as the behavior of *man-made and galactic radio noise.*

III. SOME SOLUTIONS TO HIGH-LATITUDE PROPAGATION PROBLEMS

From a study of the material in Sections II and III it is qualitatively obvious that "going up" in frequency tends to ameliorate most of the effects of the disturbed ionosphere and using the communications satellite method would also avoid most of the problems introduced by the rugged terrain. This was recognized in the late 1960's and experiments using the ATS-1 geostationary satellite at VHF were started at the Geophysical Institute in 1968, expanding to a "biomedical network" of *25* earth stations in 1971. This system utilized commercially available narrow band FM 100 watt transceivers (designed for taxicabs) and homemade 8-turn helical antennas. The experiments proved so successful that the state of Alaska decided in 1975 to proceed with plans to provide at least reliable voice communication to every Alaskan permanent community with a population of 25 or more. At the present time these are 125 small earth stations (using 4.5 meter dishes) in operation throughout Alaska, each representing an investment of about $100,000. The RCA SATCOM satellites F1 and F2 incorporate 24 wide band transponder channels in the 4/6 GHz band. Each of the 24 channels can accommodate a standard color TV signal with an audio subcarrier, or more than 900 FDM voice circuits on a single carrier. Transmission of TV programming to the "bush" via satellite began in January 1977 and an "electronic mail" system using a DEC PDP-1170 message switching computer in Juneau is linked to 51 microcomputers and terminals in school district offices statewide. The main problems arising in implementation of the Alaska satellite "Bush Communication Network" have been "look angles" as low as ~5° on the north coast, and the general unreliability of some village electrical power supplies. [Browne, 1979, Merritt, R. P., 1979, Walp, 1982]. Figure 13 shows the deployment of the Alaska "Bush" satellite communication system.

Some of the methods and techniques found useful in ameliorating "high-latitude propagation pathologies" are:

VLF — Use "VLF-augmented OMEGA" navigation system. Use real-time phase-correction scheme (Argo, 1975) to correct locational errors induced by solar proton events.

LF — Utilize the large expanses of low-conductivity earth surface (see Table 1) for long "Beverage" antennas. US Signal Corps used long beverage antennas for transpolar communication during World War II in Alaska.

MF — For good *ground wave* coverage, utilize the *best ground* screen available.

Skywave — Make frequency assignments of high-latitude MF stations using *realistic skywave data* for the interfering MF midlatitude stations. See Figures 14 and 15 for typical signal strength comparison.

— Use as high power as is permissible and economically feasible to help overcome D-region absorption effects.

HF — Utilize *propagation prediction programs* which include the main high-latitude ionosphere features [Hunsucker, 1980, Rush, et al., 1982] for best results.

— Use modern single sideband (SSB) systems for voice communication with maximum legal and economically feasible output power.

— Pay careful attention to *antenna* design and:

- siting to minimize objectional terrian features
- azimuthal coverage to minimize off-path effects
- take off angle, for best coverage considering the dominant propagation mode.

— Try to obtain enough frequencies (2-14 MHz) and utilize frequency management indicated by prevalent or predicted ionospheric conditions.

— Use a scheme of real-time-updated HF propagation predictions like "PROPHET" [Argo, Rothmuller, 1979].

Recognize that at times, it is possible to "relay" around a very disturbed area, i.e., Fairbanks → Chicago → Sondestrom instead of Fairbanks → Sondrestrom, ...

Rember that sometimes a groundscreen may be needed in the antenna Fresnel region to ensure proper beam-forming stability with yearly variations of σ and ϵ.

VHF/UHF— If high reliability is a requirement, use adequate power and space *diversity* systems.

— Take care in antenna tower mounting to avoid misaligning antenna main lobes due to "frost heaving" of tower, etc. (possible signal loss or QRM).

— Allow adequate "engineering overdesign" on towers to cope with extreme environmental conditions.

— Allow adequate Fresnel clearance between LOS beam and obstacles (σ and ϵ of obstacles changes markedly seasonly).

Microwaves

Terrestrial line-of-sight — same as above (even more so!)

sometimes passive reflectors are very practical (in mountainous terrain).

Satellite Communication

Entire Site, Antenna, transmitter/receiver, power supply system should be engineered for the extreme environmental conditions which may be encountered

When employing frequency reuse by polarization discrimination, allow sufficient $(\frac{S}{N})$ margin to account for precipitation depolarization in some areas of the north.

Acknowledgements

I owe many insights and ideas to extended discussions over the years with several Geophysical Institute staff members. Special thanks go to Professors; Glenn Stanley, Robert Merritt, R. Parthasarathy, Leif Owren, H. F. Bates, T. R. Roberts and to members of our engineering and technical staff; Brett Delana, John Peterson, Mel Holmgen, Eldon Thompson, Kay Driscoll, Rudy Domke, and Al Weber.

Patricia Brooks has been mainly responsible for collecting, editing, collating and producing this report. The final production of this report was done by Bell Laboratories, Murray Hill personnel.

The work described herein has been sponsored by: The National Science Foundation (Aeronomy Program), INTELSAT Corp., NOAA (E.R.L. and WDC(-A) Boulder, Colo., USAF (Cambridge Res. Labs,) Air Weather Service, the Federal Communications Commission and the state of Alaska

Special thanks are due to Drs. Steve Struharik of INTELSAT and Dickson Fang of COMSAT for analysis of the Sitka data.

Table 1: Summary of the primary ground characteristics which influence the propagation of radio waves for some of the surface types found in Alaska.

TABLE 1

Type of Surface	Conductivity, σ in mhos (or Siemens) per meter	Permittivity (ϵ)
Coastal dry sand	0.002	10.0
Flat, wet coastal	0.01 to 0.02	4.0 to 30.0
Rocky land (steep hills)	0.002	10.0 to 15.0
Highly moist soil	0.005 to 0.02	30.0
Marshy	0.1	30.0
Hills (to ~ 1000 m)	0.001	5.0
Freshwater	0.001	80.0 to 81.0
Sea water	3.0 to 5.0	80.0 to 81.0
Sea ice	0.001	4.0
Polar ice (free)	0.000025	3.0
Polar ice (cap)	0.0001	1.0
Arctic Land	0.0005 to 0.001	23-34 for silts ~12 for dry sand
*Tundra underlain with permafrost		
(a) surface	~0.018 to 0.036	~25-42
(b) two feet below surface	~0.025 to 0.098	~33-788

* Aquired in August 1982 by the Open-wire-Line (OWL) technique from 500 KHz to 12,000 KHz by G. Hagn of SRI International.

REFERENCES

Albee, P. R. and H. F. Bates [1965], VLF Observations at College Alaska, of Various D-region Disturbance Phenomena, Planet. Space Sci. *13*, 175-206.

Arcone, Steven A. and Allan T. Delaney [1982], Dielectric Properties of Thawed Active Layers Overlying Permafrost Using Radar at UHF, Radio Sci. *17*, 618-626.

Argo, P. E. (1975), Modeling OMEGA PCA Phase Changes, NELC Technical Report. Naval Electronic lab Center, San Diego, California.

Baron, M. J. [1974], Electron Densities Within Aurora and Other Aurora-E Region Characteristics, Radio Sci., *9*, 341-348.

Bates, H. F. [1959], The Height of Irregularities in the Arctic Ionosphere, JGR, *64*, 1257-1264.

Bates, H. F. [1966], On Using Direct Backscatter to Predict Communication, Proc. IEEE *54*, 1457-1458.

Bates, H. F. and P. R. Albee [1966], On the Strong Influence of the F1 layer on Medium to High Latitude HF Propagation, Sci. Rept. UAG-R175, Geophys. Inst. Univ. of Alaska Alaska-College, Alaska.

Bates, H. F., A. E. Belon and R. D. Hunsucker (1973), Aurora and the Poleward Edge of the Main Ionospheric Trough, JGR, *78*, 648-658.

Bates, H. F. and R. D. Hunsucker [1974], Quiet and Disturbed Electron Density Profiles in the Auroral Zone Ionosphere, Radio Sci., *9*, 455-467.

Bates, H. F. and T. N. Davis [1976], Effects of High Latitude Geophysical Events in the Aeronautical Radio Frequency Bands Rep. No. FAA-RD-75-198, Geophysical Institute Report.

Besprozvannaya, A. S., A. V. Shirochkov and T. I. Shchuka, [1979], On the Approach to Forecasting Polar Ionospheric Conditions, ISTP Proc., Vol. 1, 528-542.

Thrane, E. V. (Chairman) et al., [1979], D-Region Predictions, ISTP Proc. Vol. II pp. 582-584.

Browne, Stuart P. (1979), The Alaska Bush Communications Network, Telecommunications, Oct. 1979, 61-64.

CCIR [1963a], *World Distribution and Characteristics of Atmospheric Radio Noise*, CCIR Report No. 322, Published by International Telecommunications Union, Geneva 1964.

CCIR Report 233b [1963], Influence of the Atmosphere on Wave Propagation, pp. 76-120, International Telecommunications Union, Geneva.

Chesnut, W. G., J. C. Hodges and R. L. Leadabrand [1968], *Auroral Backscatter Wavelength Dependence*, Final Rep. for RADC, *SRI Project 5535*, 31-32.

Dougherty, H. T. [1981], Electromagnetic Wave Trajectories at VHF and Higher Frequencies, NITIA — Report CR-81-14, US Dept. of Commerce [Ducting Theory — pp. 31-50] Boulder, CO.

Frihagen, Jon [1972] (Editor), *Radar Propagation in the Arctic*, AGARD-CP-97.

Frihagen, [1972] pp. 10 to III-2 ISTP Proc., Vol. I.

Folkestad, Kristen (Editor) [1968], *Ionospheric Radio Communications*, Plenum Press, New York, NY.

Greifinger, Carl and Phyllis Greifinger, [1978] On the Ionospheric Parameters which Governs High Latitude ELF Propagation in the Earth — Ionosphere Waveguide, Report DNA 4685T, R and D Association Box 9695 Marina DelRay, CA 90291.

Hagn, George, [1982] Draft Interim Letter Report on SRI Project 4729.

Hoekstra, Pieter [1975], Electrical Ground Impedance Measurements in Alaskan Permafrost Regions, US Dept. of Transp. FAA Rep. No. FAA-RD-75-25.

Hunsucker, Robert D. [1967], H. F. Propagation at High Latitudes, QST Magazine, *LI* pp. 16-19 and 132.

Hunsucker, R. D. and H. F. Bates [1969], Survey of Polar and Auroral Region Effects on HF Propagation, Radio Sci., *4*, 347-365.

Hunsucker, Robert D. [1974], Simultaneous Riometer and Incoherent Scatter Radar Observations of the Auroral D-Region, Radio Sci., *9*, 335-340.

Hunsucker, Robert D. [1975], Chatanika Radar Investigation of High Latitude E-Region Ionization Structure and Dynamics, Radio, Sci., *10*, 277-288.

Hunsucker, R. (Chairman) et al. [1979], "High Latitude E & F-Region Ionospheric Predictions", pp. 513-527, ISTP Proc., Vol. I, Boulder, Colo.

Hunsucker, Robert D. [1979], Morphology and Phenomenology of the High-Latitude E & F-Regions, pp. 543-561, ISTP, Vol. I.

Hunsucker, Robert D. [1980], E and F Region predictions for Communication Purposes at High Latitudes, in *Exploration of the Polar Upper Atmosphere*, Deehr, C. S. and T. A. Holtet (Editors), NATO Advanced Study Institute Series, Series, C., D. Reidel Publ. Co. Dordrecht, Holland.

Hunsucker, Robert D., 1982, Atmosphere Gravity Waves Generated in the High-Latitude Ionosphere: A Review, Rev. of Geophys. Space Phys., *20*, 293-315.

ITT *Reference Data for Radio Engineers*, Howard Sams and Co. New York, 6th Edition — 1981.

JTAC [1964], *Radio Spectrum Utilization*, A Program for the Administration of the Radio Spectrum, Joint Technical Advisory Committee IEEE, Inc.

Kelly, Michael, James F. Vickery, C. W. Carlson and R. Torbert [1982], On the Origin and Spatial Extent of High-Latitude F-Region Irregularities, JGR, *87*, 4469-4475.

Landmark, B (Editor) [1964], *Arctic Communications,* AGARDO-GRAPH 78, Pergamon Press — MacMillan Co., NY.

Lied, Finn (Editor) [1968], High Frequency Radio Communications — with Emphasis on Polar Problems, AGARDOGRAPH 104, Technivision — Maidenhead, England.

Larsen, T. R., E. R. Swanson and E. Thrane [1978], Factors Affecting OMEGA Accuracy, NDRE Rep. No. 71, Norwegian Defense Research Establishment, Oslo.

Lomax, John B. [1972], Frequency Distortion in Auroral HF Propagation, in *Radar Propagation in the Arctic*, Edited by Jon Frihagen, AGARD CP-97, 22.

Mendillo, Michael and C. C. Chacko (1977), The Base Level Ionospheric Trough, JGR, *82*, 5129-5132.

Merritt, R. P. (1979), Alaskan Telecommunication Systems, Presented at the Pacific Telecommunications Conference, Honolulu, Hawaii.

Merritt, R. P., T. D. Roberts and R. D. Hunsucker [1981], Precipitation Depolarization of Satellite Signals in Sitka, Alaska, The Northern Engineer, A Publication of the Geophysical Institute, Univ. of Alaska, Fairbanks, *13*, 24-27.

Muldrew, D. B. (1965), F-Layer Ionization Troughs Deduced from Alouette Data, JGR, *70*, 2635-50.

Pagliarulo, Robert P., John P. Turtle, John E. Rasmussen and Wayne Klemeti, [1978], VLF/LF Reflectivity of the Polar Ionosphere, Jan. 1 — Apr. 22, 1978, Report RADC-TR-78-186, Rome Air Development Center, Grifiss AFB, New York 13941.

Petrie, L. E. and E. E. Stevens [1965], An F1-Layer MUF Prediction System for Northern Latitudes, IEEE Trans. Antenna Propagation, *13*, 542-546.

PoKempner, Margo [1980], Comparison of Available Methods for Predicting Medium Frequency Sky-wave Field Strengths, NTIA-Report-80-42/NTIA/ITS — Boulder, Colo. 80303.

Rasmussen, Ronald D., T. Neil Davis, Howard F. Bates, Glenn M. Stanley [1975], Effects on High Latitude Geophysical Events on VHF Aeronautical Navigation Aids, Final Report, Task A — Rep. No. FAA-RD-75-136, Geophys. Inst., Univ. of Alaska, Fairbanks.

Rino, C. L. and R. C. Livingston and S. J. Matthews [1978], Evidence for Sheet-Like Auroral Ionospheric Irregularities, Geophys. Res. Letters, *5*, 1039.

Rodger, A. S. and M. Pinnock [1980], The Variability and Predictability of the Main Ionospheric Trough, ISTP Proc., Vol. 1, 463-464.

Rush, C. M., R. K. Rosich, C. B. Brooks, D. L. Leise, M. Pokempner [1982], A Simplified Model of the High Latitude Ionosphere for Telecommunications Applications, NTIA Rep. 82-94, pp. 13-15, Boulder, Colo.

Saveskie, Peter N. [1980], *Radio Propagation Handbook*, TAB Books, Inc.-Blue Ridge Summit, PA.

Thrane, E. V. (Chairman) et al. [1979], "D-Region Predictions" pp. 582-583, in Solar — Terrestrial Predictions Proceedings (Editor R. F. Donnelly), Vol. II, Working Group Reports and Reviews, Gov. Printing Office, Washington, D.C. 20402.

Tolstoy, A. and T. J. Rosenberg [1982], The influence of Localized Precipitation-Induced D-region Ionization Enhancements on Subionospheric VLF Propagation, Geophys. Res. Let. *9*, 563-566.

Tsunoda, R. T. and J. F. Vickrey [1982], Evidence of East-West Structure in Large-Scale F-Region Plasma Enhancement in the Auroral Zone, Presented at the URSI International Symposium, Radio Probing of the High Latitude Ionosphere and Atmosphere, New Techniques and New Results, Geophys. Inst./Univ. of Alaska, Fairbanks, Alaska, Aug. 9-13, 1982.

Vickrey, James F. and Michael C. Kelly [1982], The Effects of a Conducting E-Layer on Classical F-Region Cross-field Plasma Diffusion, Jour. Geophys. Res., 87, 4461-4468.

Vickrey, J. F. C. L. Rino and T. A. Potemra [1980] Chatanika/TRIAD observations of unstable enhancements in the auroal F-region, Geophysic. Res. Letters, *7*, 789.

Vondrak, R. R. and M. J. Baron [1976], Radar Measurements of the Latitudinal Variation of Auroral Ionization, Radio Sci., *11*, 939-946.

Walp, Robert [1982], A Case Study of Alaskan Telecommunications, presented at the Pacific Telecommunications Conference, Honolulu, Hawaii.

Wang, John. C. [1977], Prediction of Medium-Frequency Skywave Field Strength in North America, IEEE Transactions Broadcasting, 43-49.

Washburn, J. S., C. M. Rush and F. G. Stewart [1982], Development of Techniques to Assess Interference to the MF Broadcasting Services, NTIA Rep. 82-90, Boulder, Colo.

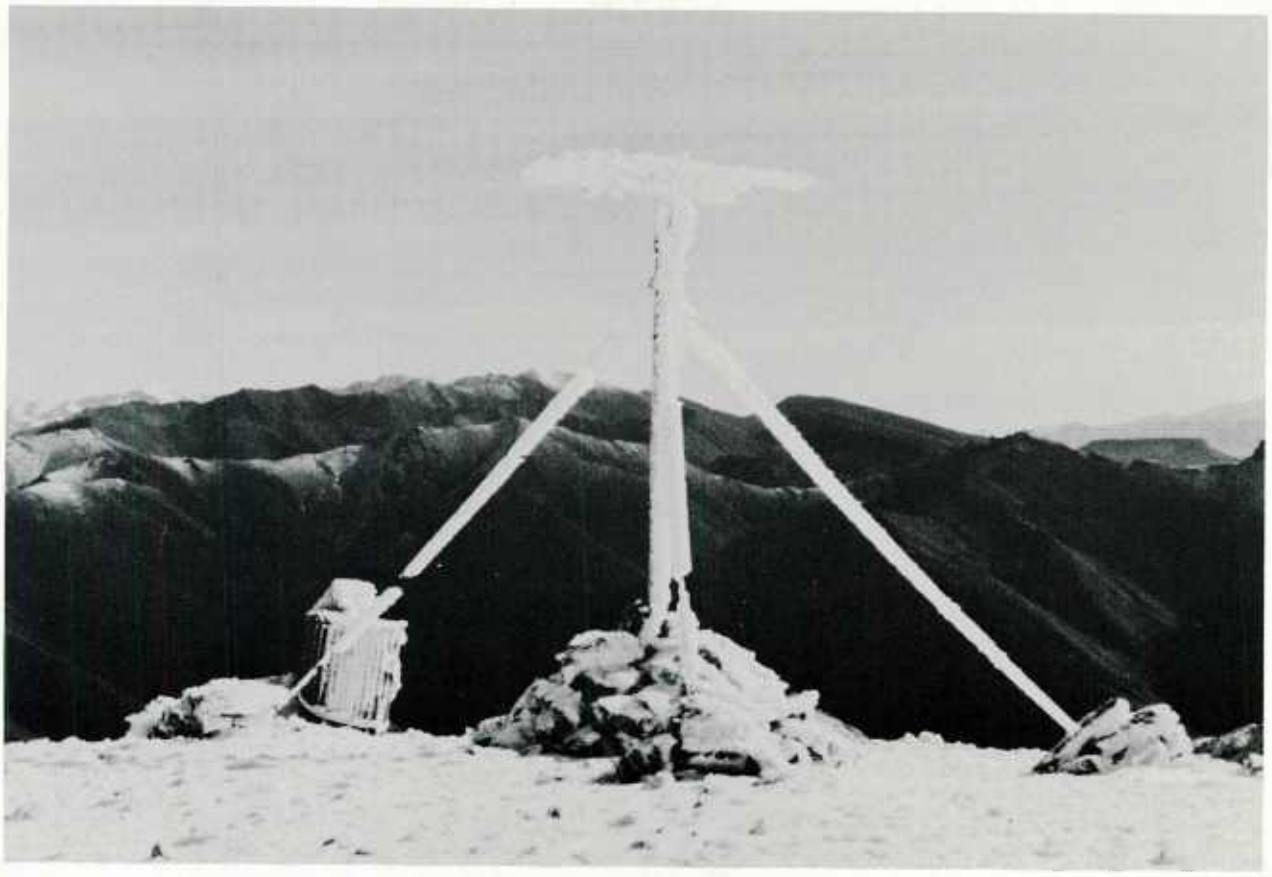

Fig.1 Illustration of the large daily or seasonal temperature variation in interior Alaska

Fig.2 Photo of Fairbanks winter inversion

RELATIVE SIZE OF ALASKA AND THE UNITED STATES

Fig.3 Map of Alaska superimposed on the continental US

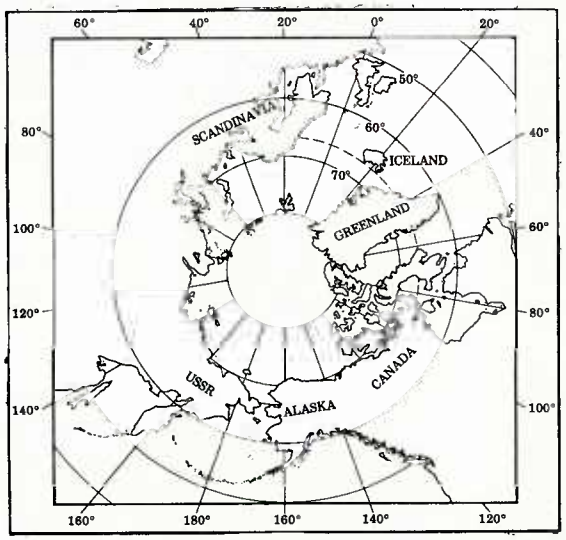

Fig.4 Polar projection map of regions north of 60°N geographic latitude

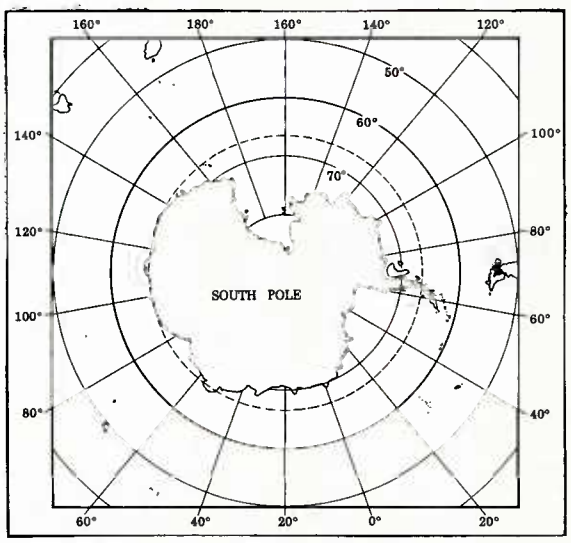

Fig.5 Polar projection map of regions south of 60°S geographic latitude

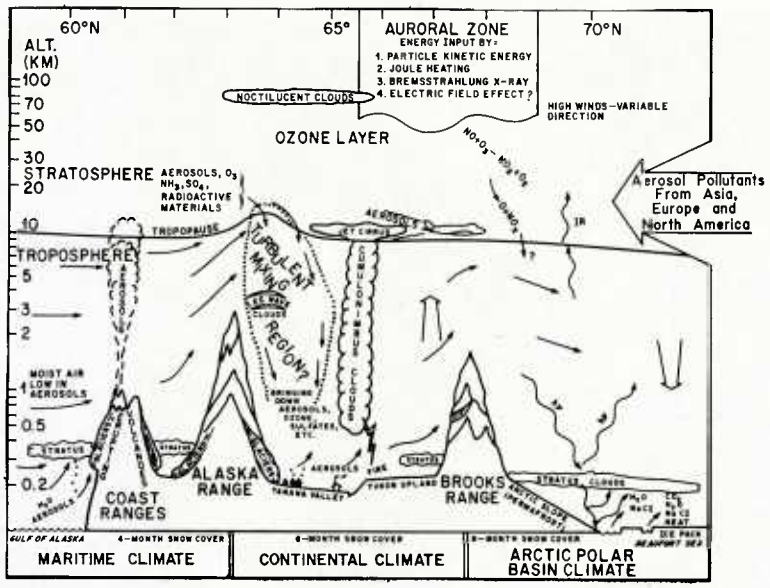

Fig.6 Anchorage-to-Prudhoe Bay meridional cross-section

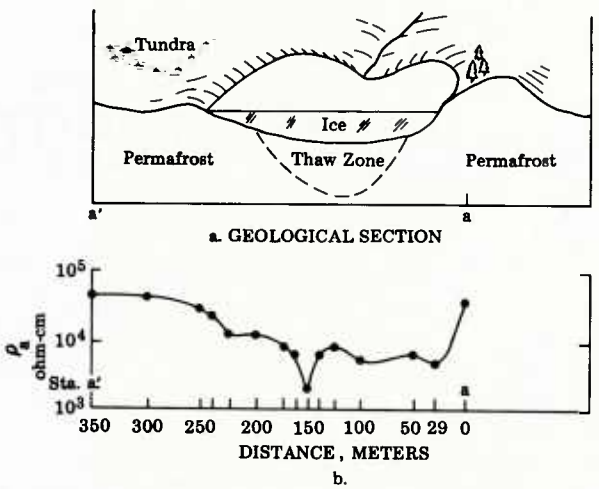

Fig.7 Idealized section and associated resistance across a lake in permafrost terrain

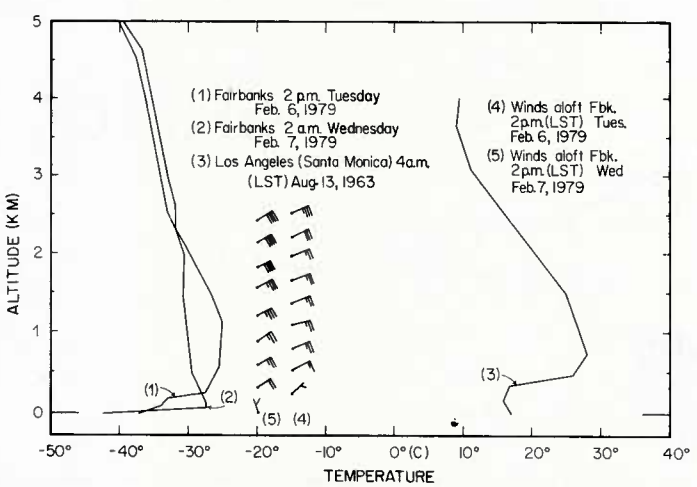

Fig.8 Radiosonde profiles of Alaska's interior region troposphere

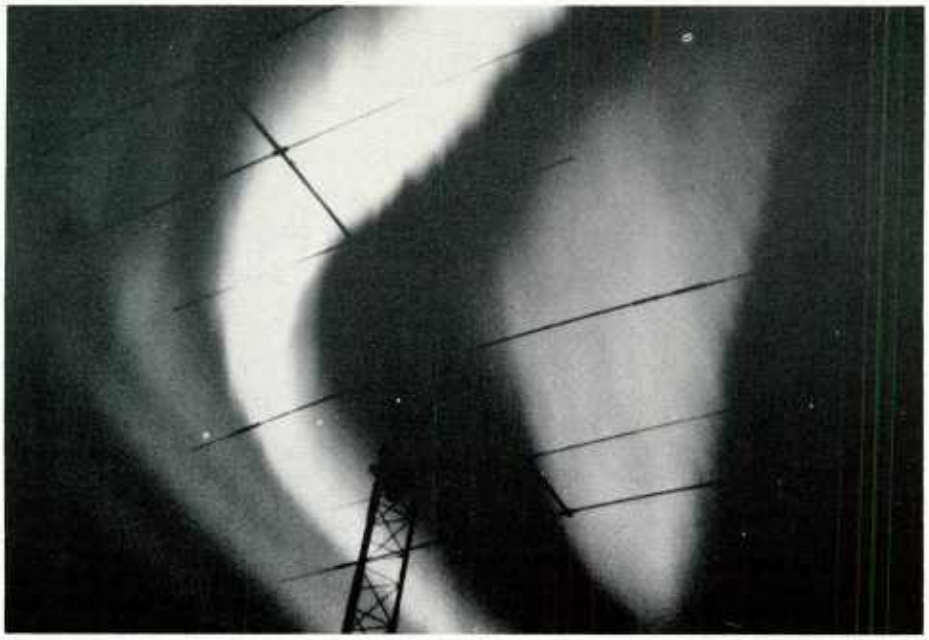

Fig.9 Aurora Borealis with communications antenna in foreground

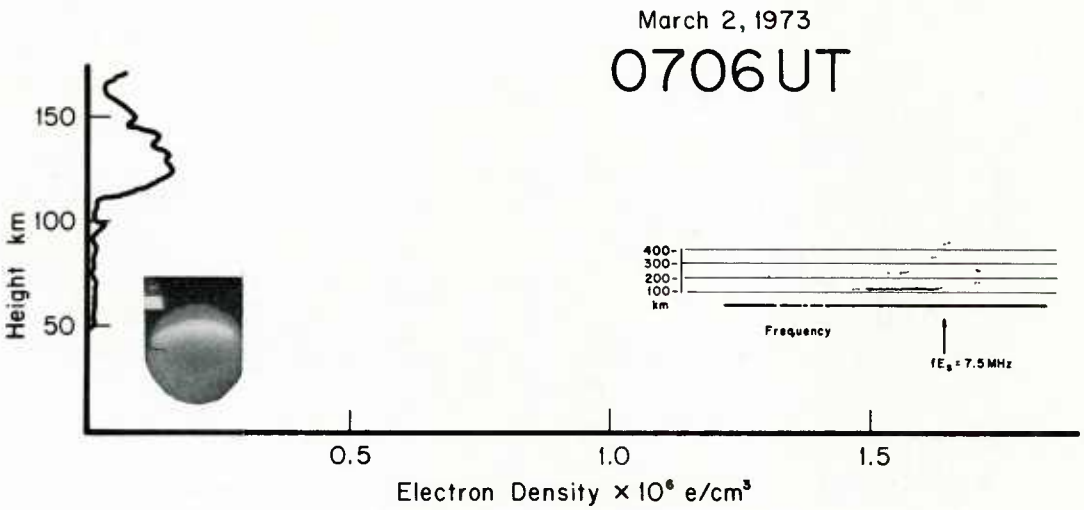

Fig.10 All-sky camera and other simultaneous data for aurora north of site

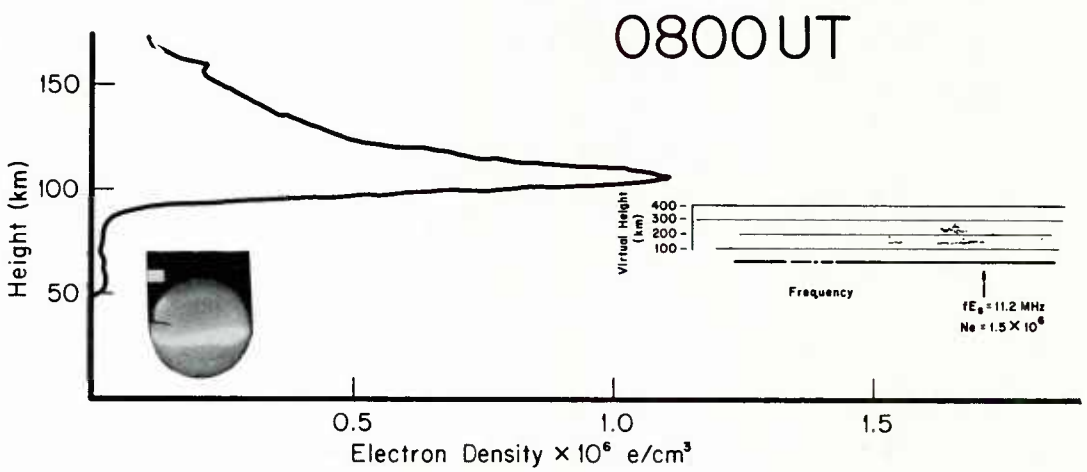

Fig.11 All-sky camera and other simultaneous data for aurora overhead

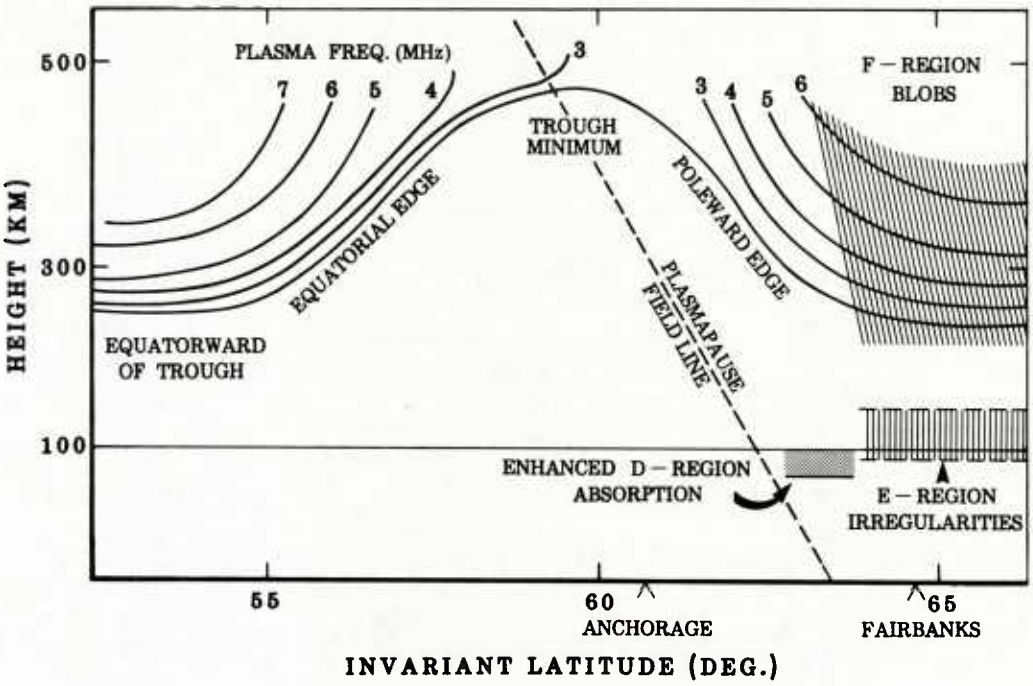

Fig.12 Idealized sketch of salient ionospheric features which influence MF/HF skywave propagation on a north/south path

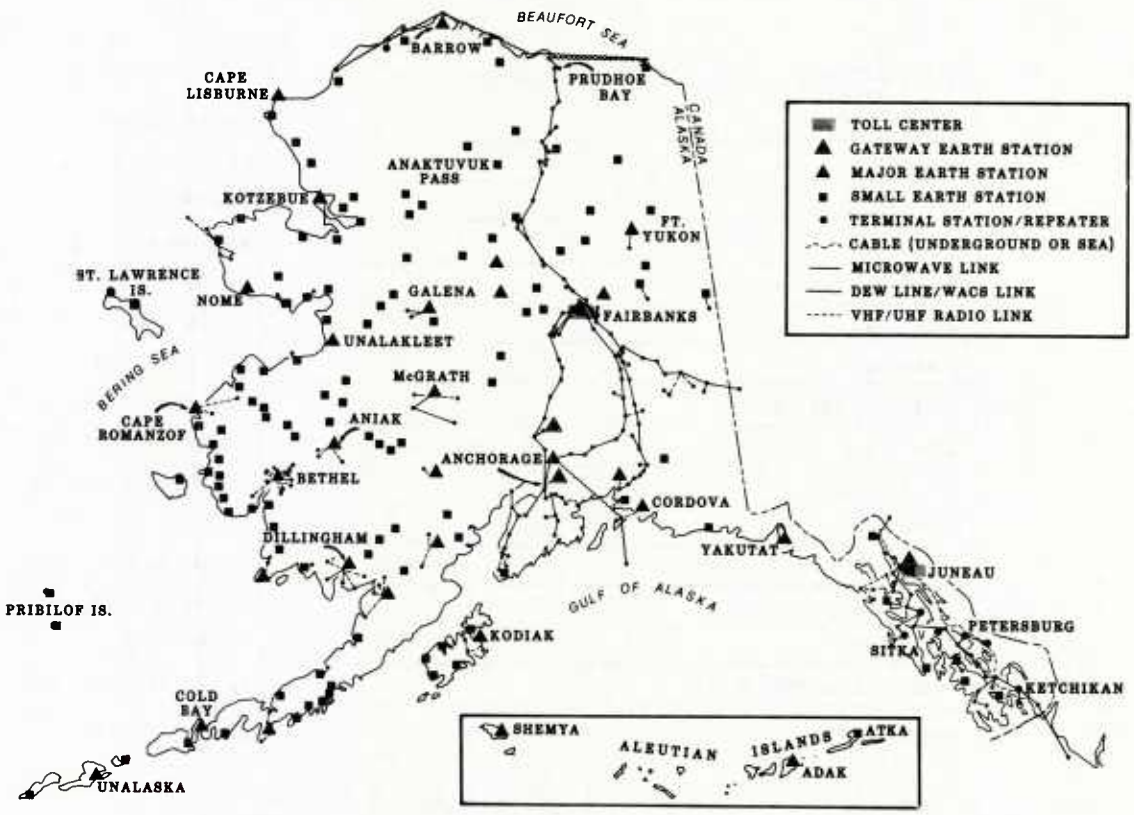

Fig.13 Map of "Alaska Bush Satellite Communication System"

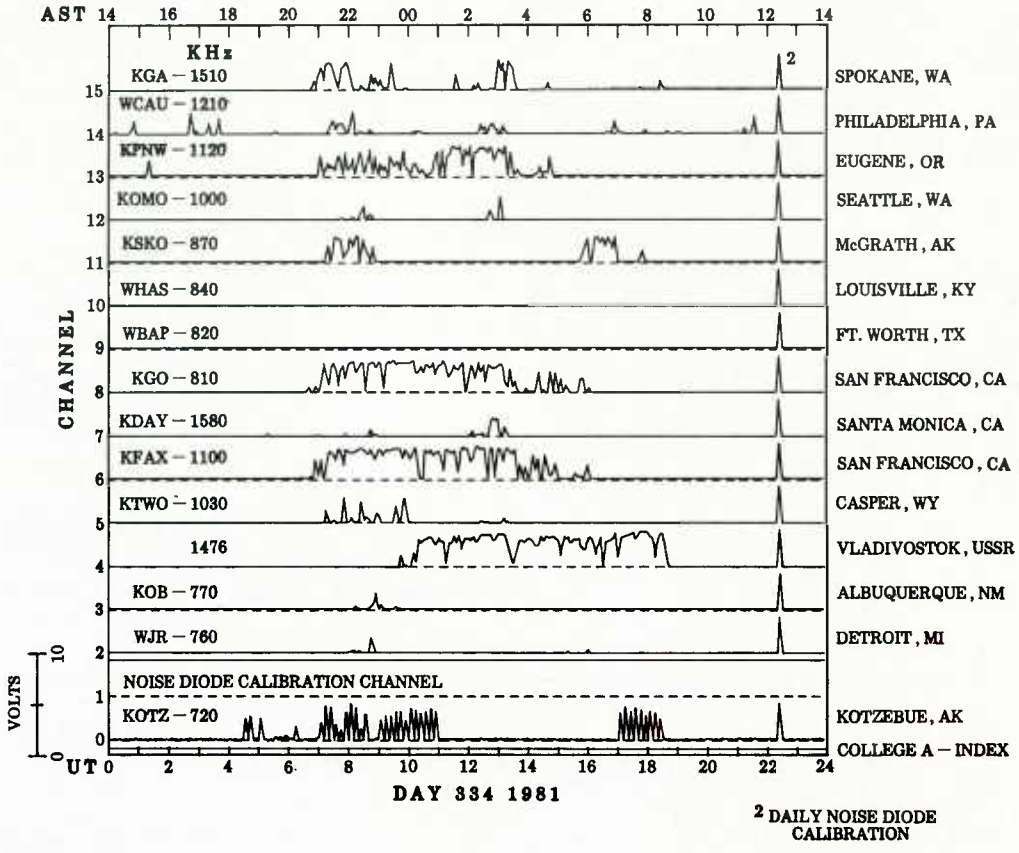

Fig.14 MF Skywave signal strength plots (good propagation)

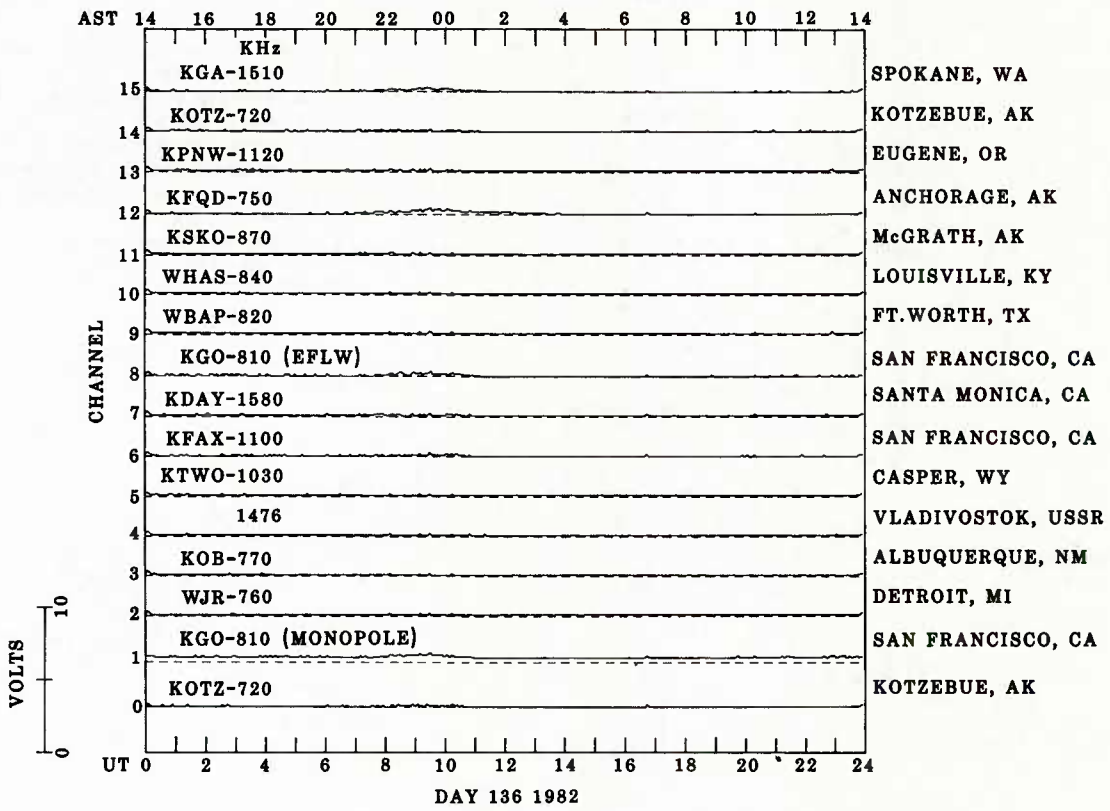

Fig.15 MF Skywave signal strength plots (poor propagation)

DISCUSSION

H.J.Albrecht, Ge

With regard to Figure 6, is there sufficient proof for the presence of aerosol pollutants from Europe in Alaska's stratosphere?

Author's Reply

University of Washington Scientists made many high-altitude instrumental balloon flights from the Naval Research Lab-Point Barrow, Alaska, during 1978–80 and reported aerosol samples from the upper polar atmosphere having traces of by-products of certain manufacturing effluents peculiar to Europe.

THE APPLICATION OF REAL-TIME MODEL UPDATE BY OBLIQUE IONOSPHERIC SOUNDERS TO FREQUENCY SHARING

Donald R. Uffelman
Lawrence O. Harnish
John M. Goodman

Ionospheric Effects Branch
E.O. Hulburt Center for Space Research
Naval Research Laboratory
Washington, D.C. 20375

ABSTRACT

Frequency management systems for the high frequencies (HF) currently in use by the US Department of Defense (DoD) rely heavily on manual selection of frequencies which have been allocated on a circuit by circuit basis. There is no capability to anticipate frequency changes (QSY's) in advance in a manner such that a frequency being released by one user can be utilized effectively and immediately by a second user. NRL has been examining a scheme by which a small computer model of the MUF of the HF channel (MINIMUF 3.5) can be made to perform very accurately to anticipate channel characteristics in a short term prediction mode. It is proposed that this model be utilized to provide automated frequency management which would allow one to anticipate frequency availability and thereby allow sharing of frequencies between several users. Utilizing data obtained from an oblique sounder net on the East Coast of the United States, this paper demonstrates the manner in which this might be accomplished.

1.0 INTRODUCTION

1.1 Objective

The objective of this paper is to demonstrate the applicability of a coupled system of oblique ionospheric sounders and a computer model of the maximum usable frequency of the HF channel to the general problem of the management of frequencies in the high frequency (HF) band.

1.2 Rationale

The technique discussed herein draws upon the strengths of information derived from both the direct measurement of a specific skywave transmission link by an oblique ionospheric sounder and the estimation of skywave propagation conditions as provided by a predictive model. The strength of the oblique ionospheric sounder is that over the particular link measured, this instrument can provide the user with specific and precise information about channel properties including the mode structure, the relative strength of the modes; and the characteristic frequencies of the link, such as the maximum observed frequency (MOF), the band of optimum transmission frequencies (FOT band), and the lowest observed frequency (LOF). These data, when coupled with channel occupancy information obtained at the receiver site, can provide the type of information which will allow one to initiate communications in the HF band which is extremely reliable. The weakness of the oblique sounder, however, is that it provides no information about circuits which are far from the circuit measured, nor does it provide information about the future state of the particular circuit measured. These two weaknesses of the oblique sounder are strong points of predictive algorithms. Predictive algorithms provide some insight as to the general circuit characteristics over a large area as well as information as to the future tendencies of the channel. The predictive algorithm's weak point, however, is that it provides imprecise information over the specific links which may be measured precisely by oblique sounders. This fact is quite understandable since predictive algorithms are based on mean values of large sets of measurements corresponding to the HF channel. Hence, one should always expect the oblique sounder to provide more precise information over a measured link in real time than the predictive algorithm.

Realizing that the oblique sounder's strength is the predictive algorithm's weakness and the predictive algorithm's strength is the oblique sounder's weakness, NRL (Code 4180) embarked on a program several years ago to couple these systems in a manner which would emphasize the strengths of each and minimize the weaknesses. Initial results from this work indicate that this idea is reasonable and, in fact, a very worthwhile prospect to pursue which may dramatically impact existing high frequency resource management systems. In fact, a highly accurate computer based propagation assessment and forecast module is believed to be the cornerstone of a new generation of automated HF resource management systems. This concept has applications to HF asset management in general including the selection of frequencies, antennas, and power levels; and includes HF problems in the areas of communications, networking, jamming, HF-DF, signal security, and anti-jamming. Benefits accruing from employing this technique include reduced required equipment assets, manpower, and training levels; and increased HF circuit reliability, message throughput, threat assessment capability, and the capability to manage HF intercept resources.

A generalized system employing a highly accurate HF propagation assessment and forecast module is visualized in figure 1. This generalized automated system would use information from various sensors as an input to a channel model. For this repoft, the oblique sounder is the input, however. Taking into account the various assets of both friends and adversaries operating in the area and the particular job required, supporting software based on a priority scheme would interact with the propagation assessment and forecast module to provide an optimum selection of resources for the particular job to be done. This system could be further improved by employing automatic selection of resources and message routing. As a side note, the NATO Cross Fox program draws heavily upon the idea of automatic resource selection and we believe it could be greatly aided by an accurate channel model. This report, however, will only discuss the application of this concept to the problem optimizing the use of frequency assets which are employed by various users.

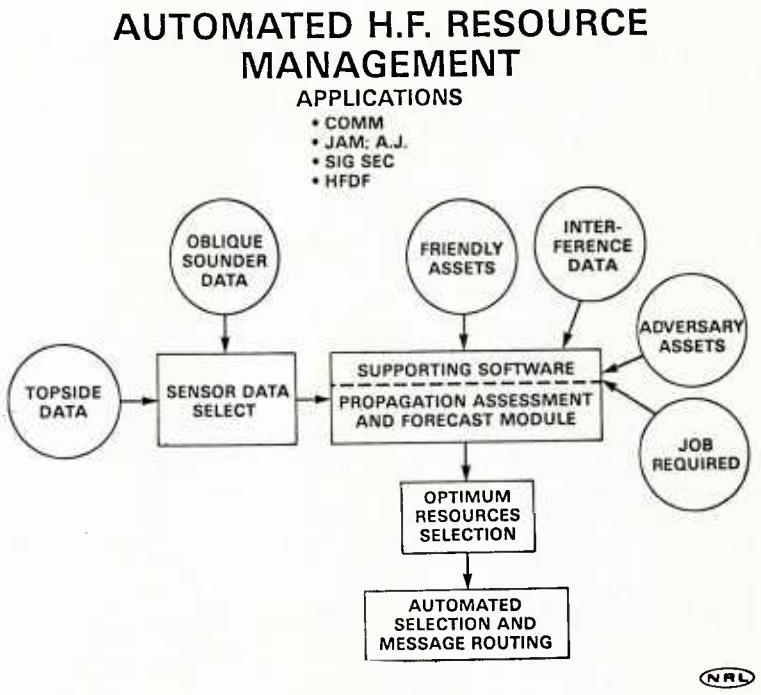

Figure 1: A generalized automated HF Resource Management System

1.3 Diurnal Variation of the Channel

Figure 2 is a representative diurnal frequency variation of the MUF and FOT over a typical day. The Naval Ocean Systems Center (NOSC) algorithm called MINIMUF 3.5 was used to derive the MOF over this representative link and the FOT was obtained by calculating .85 of the computed maximum observed frequency. Against this, a set of sample frequencies are plotted by attempting to stay close to the FOT. Note that with 5 different frequencies the diurnal variation of the channel is reasonably well matched to the FOT. If the number of frequencies available are at a premium however, one can communicate most of the day (assuming no co-channel interference) using the two frequencies which are denoted as the post-midnight frequency and the daytime frequency. With this latter scenario, HF communications would be expected to deteriorate for two periods during the day of several hours each at the post-sunrise and the pre-sunset times. If one has at his disposal accurate channel evaluation information as well as targets at a number of different ranges, the five frequency scenario could be used very effectively by several targets sharing the frequencies. However, if all the assets are at approximately the same range and the same sun-time, the ability to share these frequencies will be greatly degraded.

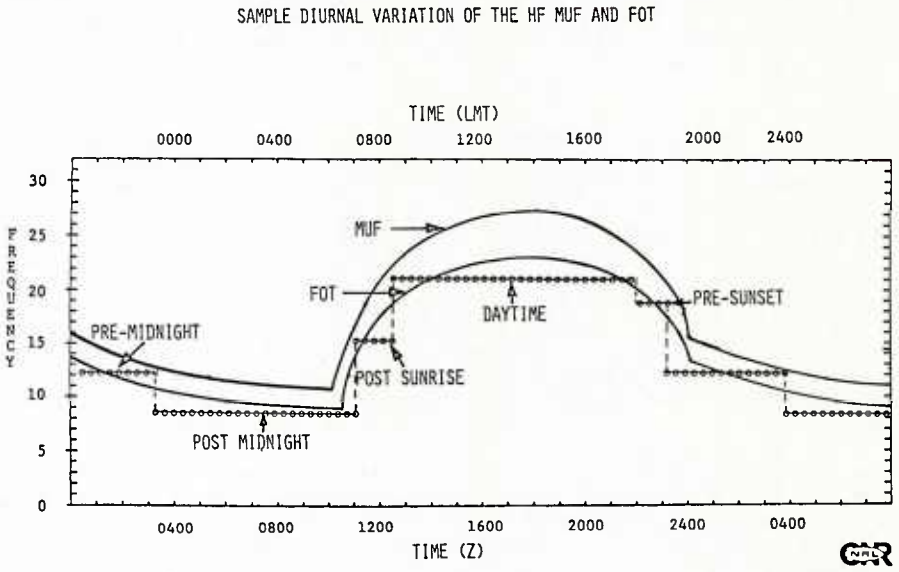

Figure 2: Example diurnal variability of the MUF and FOT for a typical day showing a frequency assignment strategy.

2.0 BACKGROUND

Several years ago NRL Code 4180 embarked on a program to establish validity limits of schemes to update currently available HF channel models using presently available as well as future envisioned data sources. This program is currently couched in the Branch's HF Propagation Assessment Program. Components of the program encompass existing models and various sources of data for the HF skywave channel. The existing models being examined include but will not be limited to MINIMUF 3.5 (incorporated in the NOSC PROPHET system) and IONCAP. The instrumentation being examined as sources of update are oblique incidence sounders (channel evaluators), topside ionospheric sounders, and vertical incidence sounders. The validity limits to be established for this concept are temporal perishability, spatial perishability, geographical dependence, and seasonal dependence.

The oblique sounder data for the model update discussed in this paper are obtained from the BR Communications Inc. AN/TRQ-35 tactical frequency management system (TFMS). These data are typically obtained during military exercises and are in the form of polaroid photographs which are subsequently scaled for maximum observed frequency (MOF)*, band of optimum transmission frequencies (FOT band)+, and lowest observed frequency (LOF)**. The AN/TRQ-35 TFMS equipment utilized to obtain these data are shown in figure 3. The upper left hand corner shows the chirp sounder transmitter and its companion receiver is in the lower center portion of the figure. The upper right hand corner of the figure shows the spectrum monitor which is an auxiliary piece of equipment used to measure channel occupancy in order to minimize the selection of frequencies where interferring signals would degrade the received signal-to-noise ratio. Each unit weighs several hundred pounds and is rack mountable when removed from its shipping case.

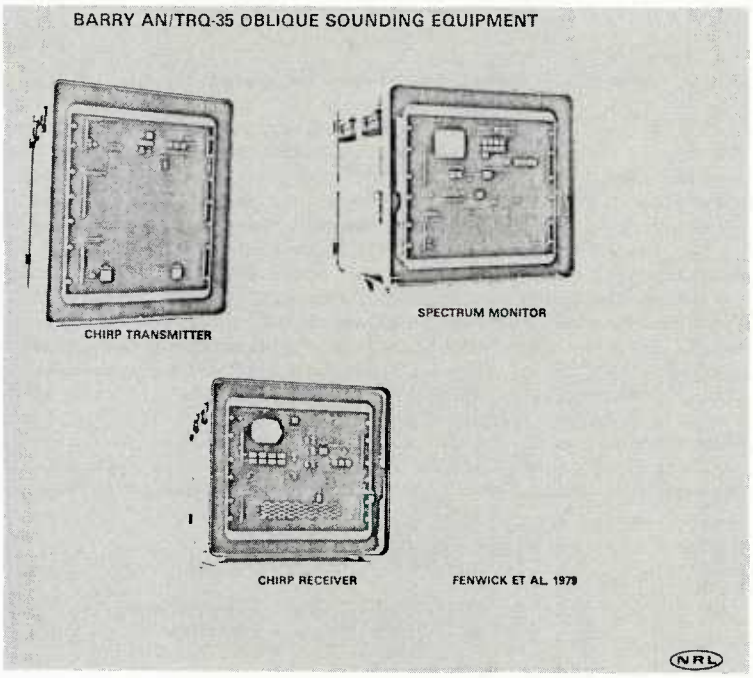

Figure 3: The B.R. Communication AN/TRQ-35 tactical frequency management system.

The computer model (MINIMUF 3.5) utilized in this report is encompassed in the Naval Ocean Systems Center PROPHET System. Figure 4 shows the programmable calculator (Tektronix 4052) based system on which the model update and frequency selection is envisioned to be implemented. The particular configuration of the PROPHET system shown in figure 4 is the Army PROPHET Evaluation System (APES) for which a version exists allowing the model to be updated every three hours. This system is used by the Army to employ "propagation tactics" in communication scenarios. At this time however, frequency management drawing upon frequency sharing capabilities is not included in APES.

---

* The MOF is defined as the highest F-region frequency over which transmission is observed on an oblique incidence ionogram.

\+ The FOT Band is the highest band of frequencies exhibiting high signal strength and no multipath.

** The LOF is the lowest frequency over which transmission is observed on the ionogram.

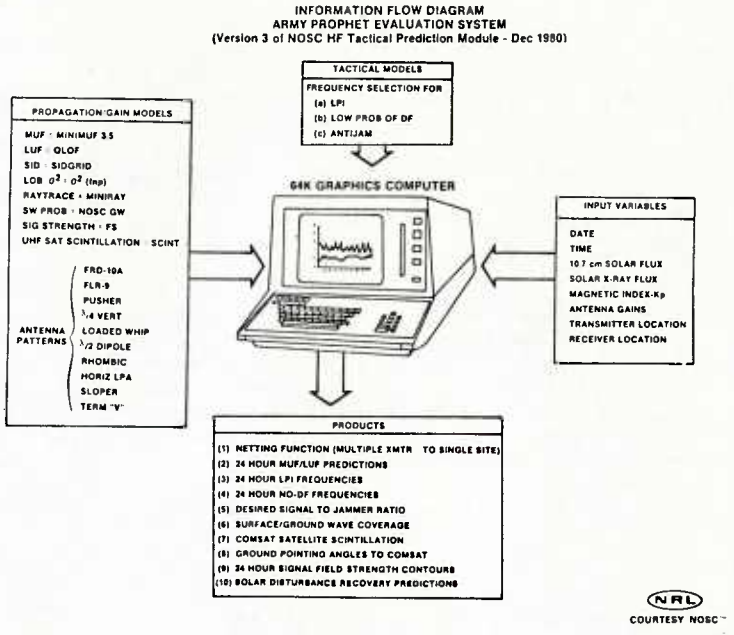

Figure 4: The NOSC PROPHET System as configured for the US Army.

Figure 5 is a drawing which illustrates the approach NRL employs to perform model update in support of frequency management. The top illustration in the figure indicates that the actual diurnal variation of the HF channel over a given link has a characteristic pattern. The model prediction has a pattern somewhat similar, but quite often a bias is present. The update process is embodied in the middle portion of the figure. A measurement of the maximum observed frequency is obtained from an oblique sounding of a known circuit. The model is forced to fit over that circuit for the specific time of the measurement. This is accomplished by varying the driving parameter for the model which in this case is the 10.7 cm flux. After fitting the model at this one point, it is then computed for the full 24 hour period and under testing conditions compared to the measured MOF's for the rest of the day. The comparison is done by calculating the rms error which is the indicator of the goodness of fit. In tactical scenarios, the parameter which was derived from the model update procedure is then used to compute other unknown paths. For testing purposes, the "unknown" paths are typically other sounder circuits in the network. The diurnal variation of the maximum observed frequency is scaled from those sounder networks, the updated algorithm is run for those circuits, and an rms error comparison is made. The model update is deemed successful if the rms error of the experimental paths (unknown paths in tactical situations) are significantly lower than that yielded by employing the unupdated model.

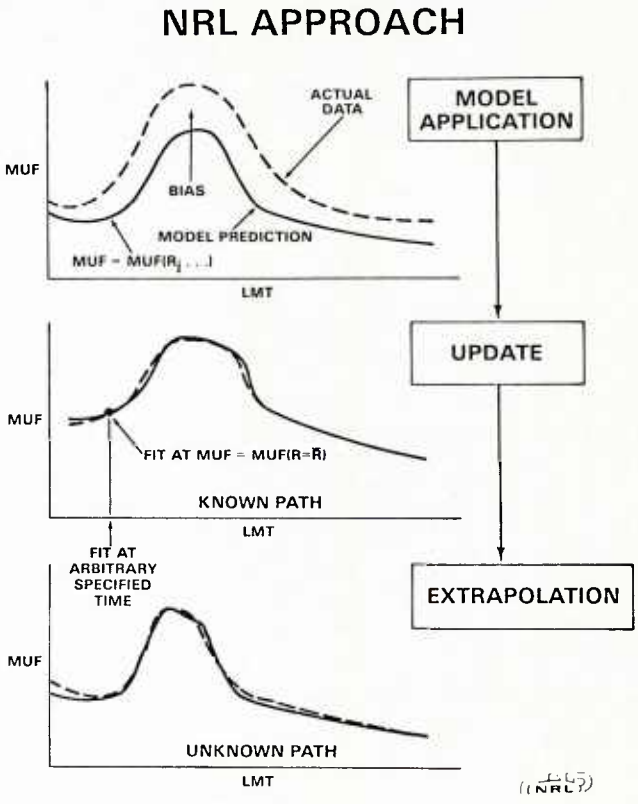

Figure 5: The NRL approach to model update.

With this basis, therefore, an attempt is made to show that the model update technique might be successfully employed to manage frequencies such that one frequency may be shared by a number of different assets at different times of the day. Further, by using this concept one obtains a capability to anticipate frequency changes yielding a significant increase in circuit reliability and message throughput. Finally, it is emphasized that this anticipation feature allows one to manage frequencies in a shared mode.

3.0 DISCUSSION

The data drawn upon for the purpose of this report was obtained during an HF communications test which occurred between 10 and 22 November, 1981. For the purposes of this test, oblique sounder transmitters were located at Robins AFB, South Carolina; Isabela, Puerto Rico and on-board a ship operating in the Atlantic. The receiver was located at the Naval Communications Station in Norfolk, Va. Figure 6 is a gnomonic projection (great circle) of the siting configuration.

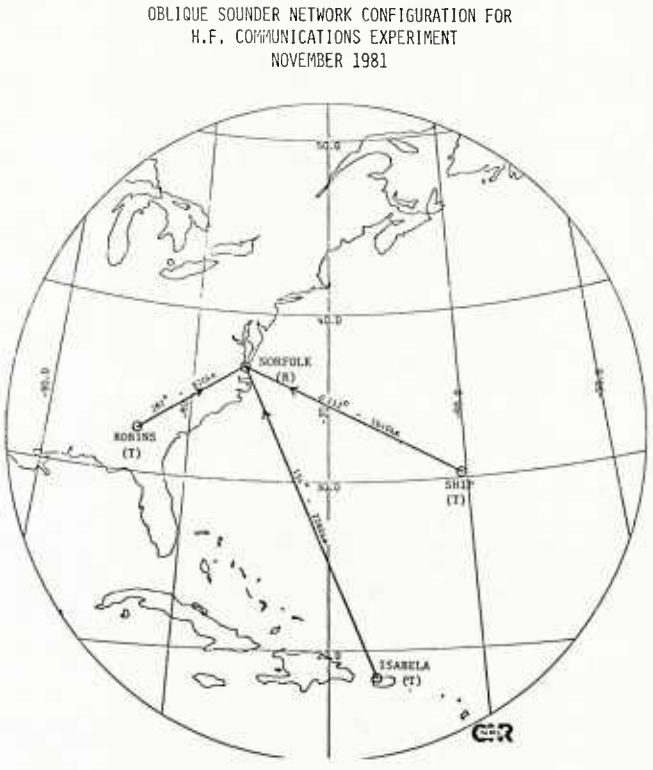

Figure 6: Great circle map of the H.F. test site configuration

For the duration of this period NRL technicians photographed output from the oblique sounder receiver when transmitters were on the air. Isabela and Robins operated continuously and the ship sounder transmitter was operated intermittantly. Data was returned to NRL and scaled for the MOF, LOF and the band of optimum frequency (FOT band) as previously defined. November 15 and 16 were selected for this report since the data set from the three transmitters is almost complete. The measured and subsequently scaled MOF, LOF, and FOT bands for these dates are plotted in figure 7. Also shown in the figure by the horizontal dark lines are a number of simulated frequency assignments which were selected from the maritime and mobile bands. The values of these frequencies are indicated along the right margin and will be used to demonstrate a capability to share frequencies among the three different sites. In no way however, are these meant to be actual frequencies used.

Since the FOT bands are areas of high signal strength and no multipath, frequencies assigned in these bands are the most desirable. Hence, the FOT bands were used to graphically select the frequency assignments along with a priority structure where the ship was given the highest priority, Isabela the next, and Robins the lowest priority. Several items should be noted. First, it is quite simple to select frequencies which are in the FOT band a large percentage of the time for the highest and second priority circuits. For the lowest priority circuit, frequencies are available near the FOT band for a smaller but still significant portion of the day. In addition, a stepped frequency assignment scheme is required in order to stay close to the FOT bands, particularly during transition times. One can imagine that if anticipatory information were available to determine the magnitude and direction of the channel variation, a new frequency could be selected in real-time in advance of the actual frequency change (QSY) and contact could be maintained during these transition times. Because of the anticipating property of the model update concept therefore, one would be able to use the existing frequency in order to communicate the selection of a new frequency such that during times of fairly rapid change, contact is continuous. The third point to note is that for two of the paths, the ship and Isabela, the distance is great enough that frequencies approach and even exceed the 30 MHz limit of the sounder during a large part of the day-time hours. In this case the FOT band which was selected may not be the true band of optimum transmission frequencies, since that true band most likely lies above 30 MHz and closer to the MOF. Hence, if frequency assets and sounding information were available above 30 MHz, it may be possible to select lower loss and less cluttered frequencies during the day for these long paths. Therefore the 25.2 MHz frequency for Isabela and the ship which matches the scaled

FOT bands may not be truly representative of the best frequency available to the user. Finally note that seven (7) frequencies service the three links and have the capability to provide high quality

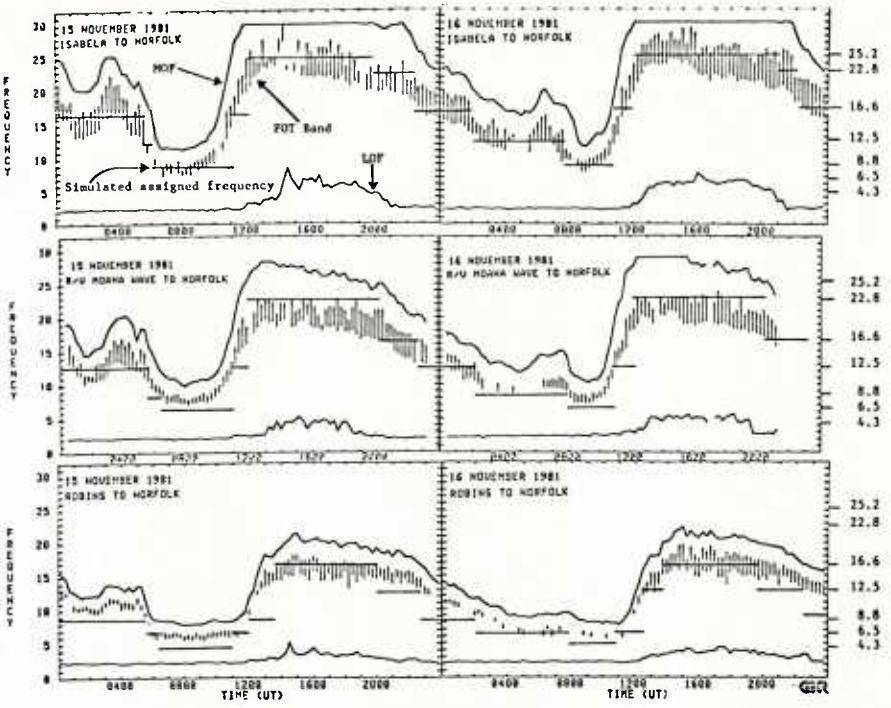

Figure 7: Measured MOF, LOF, and FOT bands for 15 and 16 November 1981.

communications for a large percentage of the day. With current frequency assignment systems these three circuits may have used up as many as 30 frequencies. Hence one might envision a large saving in frequency assets due to frequency sharing based on the ability to monitor and anticipate variations in the channel. We will use this constructed frequency assignment strategy against an updated model of the MOF and calculated FOT to demonstrate that a shared frequency assignment scheme based on the model update procedure would closely approach the idealized simulated frequency assignment pattern shown in figure 7.

3.1 The Updated Versus Unupdated Model

The updated model is the basis of the proposed frequency sharing scheme. Therefore prior to embarking on a demonstraton of the viability of updated models as applied to frequency sharing schemes, we will demonstrate the improvement obtained by applying an update derived from an oblique sounder circuit to a model of the maximum observed frequency. To illustrate this, figure 8 is provided. This figure shows the difference between the unupdated model calculation of the maximum observed frequency and the measured maximum observed frequency. The top section in figure 8 indicates the difference between the two numbers when the five day average 10.7 cm flux is used to drive the model. Note that on 15 November the rms error is 5.42 MHz and on 16 November the rms error is 4.62 MHz. The middle portion of the figure illustrates the difference between the measured and modelled numbers when the daily 10.7 cm flux is used to drive the model calculation. In this instance, the daily 10.7 cm flux provided a larger rms error on both days than did the five day average 10.7 cm flux. The daily 10.7 error flux yielded rms errors approaching 6 MHz. The bottom portion of the figure indicates the best possible fit of the MINIMUF model to the observed MUF for a once per day update. This is obtained by running the model against the measured MOF until a minimum rms error is reached for the total day. The resulting 10.7 cm "pseudo-flux" is then used to drive the computation of the MOF. The bottom portion of the figure demonstrates therefore, that with this particular model, the very best one can expect from an update for the circuit between the ship and Norfolk for 15 November is 3.88 MHz rms and 2.58 MHz rms on 16 November. Hence, any model update scheme employed is considered to be doing very well with MINIMUF when the model to observed MOF error computation approaches the minimum possible for that model. It should be noted that the rms errors can be significantly reduced if one allows the fit to occur in segments which are less than 24 hours in length. During disturbed periods of time or for other applications this in fact is done. However, this technique is not shown in this report and will be reported later.

For this report an update was performed by using a measurement of maximum observed frequency at 1300Z (0800 LMT) on each day over the Robins to Norfolk circuit. This is shortly after sunrise and this update time is selected based on prior experience with this technique. The resulting 10.7 cm flux, now designated the pseudo-flux, is then used to drive the model for the remainder to the day as well as for other circuits. In the instances shown herein, the 1300Z update drives the model in a hindcasting mode as well as forecasting for that day. This was done since our data are in 24 hour blocks internal to which the update is most usually performed. However, there is no reason why the technique cannot be extended so the update can be performed entirely in a forecasting mode for the following 24 hours of data.

Figure 9 shows the result of employing the update obtained at 1300Z from the circuit between Robins and Norfolk. The Robins to Norfolk circuit was used as the control path since at no time did that circuit

MOF exceed the 30 MHz upper limit which is inherent to the sounder.

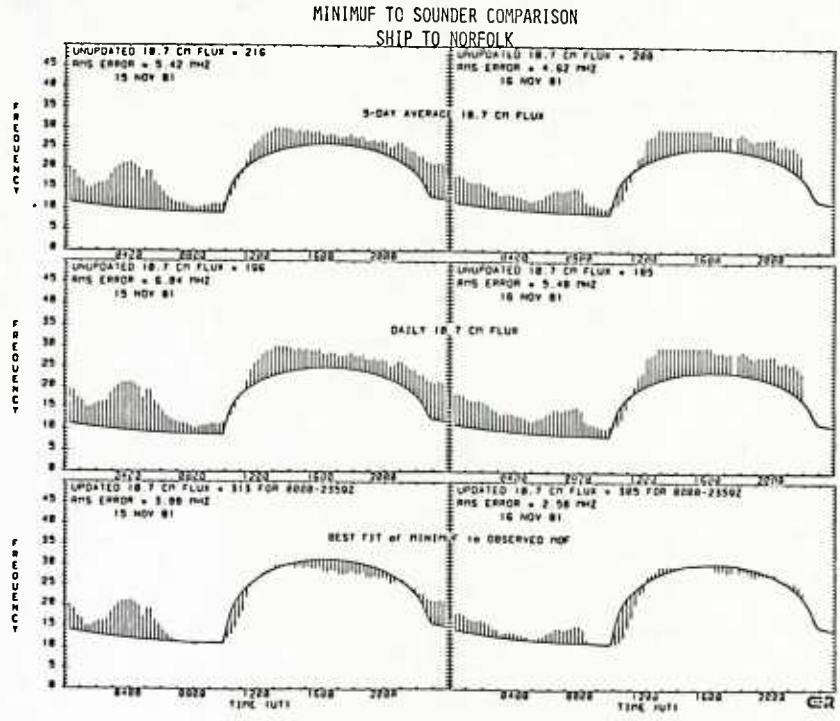

Figure 8: A comparison of the unupdated model with the MOF for data obtained on 15 and 16 November 1981

The control path update is shown as the bottom part of figure 9. The pseudo-flux as derived from the control path for each day is next used to drive the model calculation for the other paths which are designated as experimental paths. Figure 9 shows graphically the comparison between the MOF as derived from the model and the measured MOF as obtained from the sounder for these experimental paths. Vertical lines indicate the difference between the two numbers. Also indicated in the figure are the rms errors due to each calculated MOF. It should be noted that when the oblique sounder MOF yields a frequency at 30 MHz the rms error calculation is not performed for that segment since, as is obvious in the top portion of figure 9, there is no information as to the actual MOF over the path. Naturally, the rms error calculation in this case would be erroneous. This is done for both updated and unupdated cases. For example, the data obtained between 1200Z and approximately 2200Z on 15 November over the Isabela to Norfolk circuit is not factored into the rms error calculation even though the graph indicates a large difference between the two numbers. Note however, that the true error is probably quite small since the trend of the data during transition is to agree with the MINIMUF computation. Figure 9 demonstrates that the simple MINIMUF model yields a very good fit in the update mode over the various circuits.

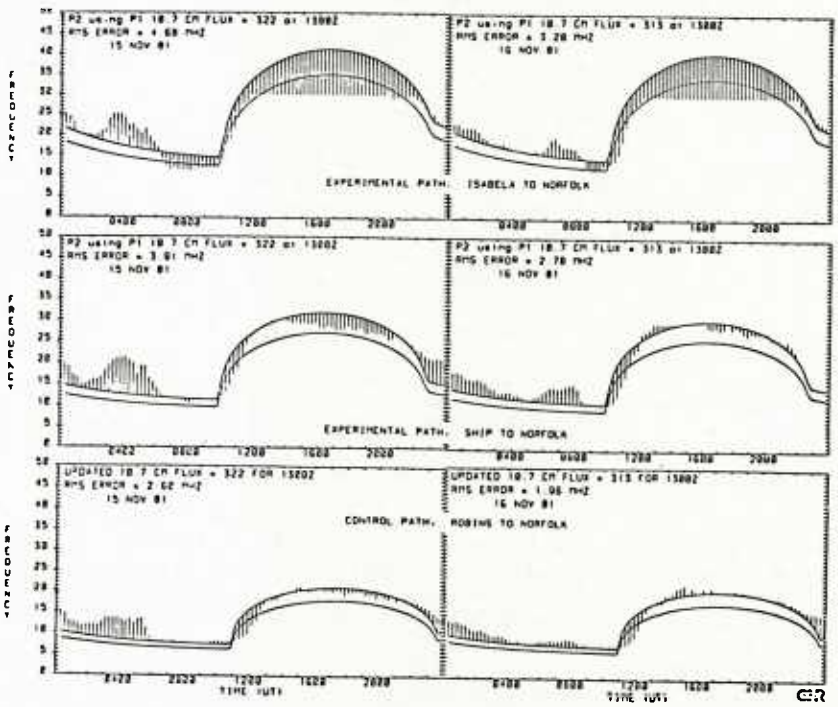

Figure 9: A comparison of the measured MOF with the updated model using a pseudo-flux derived from the "control path" which is designated to be Robins to Norfolk.

The goodness of this fit is indicated more dramatically in Table I. In this Table we have listed the rms error derived for the various model to observed MOF calculations for each path and each day. We note that the update closely approaches the absolute minimum obtainable with the model and the update yields a significant improvement in the rms error between the unupdated model and the measured MOF. Note also that in two instances in the Table, the 1300Z update and the absolute minimum possible are one and the same. These errors may be greatly improved upon by segmenting the update to shorter periods of time and using the shorter segments in time to provide information as to frequency selection.

TABLE I

RMS (MHz) ERRORS OF VARIOUS SITUATIONS

SITUATION \ SITE	ROBINS TO NORFOLK	SHIP TO NORFOLK	ISABELA TO NORFOLK
15 NOV 81			
5-DAY AVERAGE 10.7 CM FLUX	3.88	5.29	5.05
DAILY 10.7 CM FLUX	4.31	5.90	5.56
ABSOLUTE MINIMUM	2.60	3.88	4.34
1300Z UPDATE	2.60	3.91	4.68
16 NOV 81			
5-DAY AVERAGE 10.7 CM FLUX	3.76	4.66	4.34
DAILY 10.7 CM FLUX	4.35	5.42	5.07
ABSOLUTE MINIMUM	1.89	2.78	3.07
1300Z UPDATE	1.96	2.78	3.20

Hence, we have reached a point where our confidence has been fortified in the possibility that the model update approach may yield accurate frequency selection. In addition, note that if one could obtain more variability in the model itself, such as that produced by IONCAP, the possibility for fitting various features is greatly increased. We currently address this problem with MINIMUF by segmenting the model into shorter periods of time and performing an update on each segment.

3.2 The Application of the Model Update Technique to Frequency Sharing

We have established the idea that it may be possible to obtain a very accurate model computation of the expected MOF for circuits in an operational area without having to actively measure each circuit. In order to demonstrate the applicability of a model which is accurately predicting the MOF of the HF channel, we have constructed a case based on the MOF and FOT data first shown in figure 7. In figure 7 we examined the scaled MOF, LOF, and FOT; selected a number of frequencies one might have available from the maritime and mobile bands; and constructed a frequency assignment scenario to simulate communications to the three assets which were represented by the oblique sounder circuits indicated in the figure 7. In doing the construction for figure 7, we roughly prioritized the paths in order of importance where the ship was priority one; the Isabela circuit was priority two; and the control path, Robins, was priority three. Now an attempt is made to show that if one utilizes a model which has been updated by an oblique sounder, the possiblity exists that a frequency selection scenario similar to that constructed by knowing all the conditions might be possible. This demonstration is the essence of figure 10. In figure 10 an overlay of the measured MOF, LOF, and FOT is provided along with the updated MOF and computed FOT (.85 MOF) to further emphasize the success of the technique.

The general rules that were applied in this construction would be quite simple to implement on the computer. The highest priority channels were given frequencies first. Frequencies were selected that were closest to the computed FOT, but not exceeding the computed MOF. Lowest priority paths were given unoccupied frequencies as close as possible to the computed FOT. When higher priority frequencies were projected to drop below about 66% of the FOT, a frequency change was determined to be in order and lower priority circuits were appropriately shifted in frequency. During transition times, frequencies were maintained for at least an hour and the "66% of the FOT" rule was relaxed.

Using the overlay of the actual channel data, one may deduce potential problems or improvements that have been obtained. Upon first comparison of figure 7 and figure 10, the frequency scenarios are almost identical. Since the priority scheme has been strictly enforced in figure 10 due to the fact that one is constructing the frequency scenario based on a computer algorithm, there are some slight differences between the two. The most striking differences occur in the top portion of figure 10. In two instances, the computed frequency exceeded the measured MOF by a small amount for periods of time not exceeding three hours. In most other instances, however, the computed frequency remained quite close to the measured FOT indicating that communications would be highly reliable at those times.

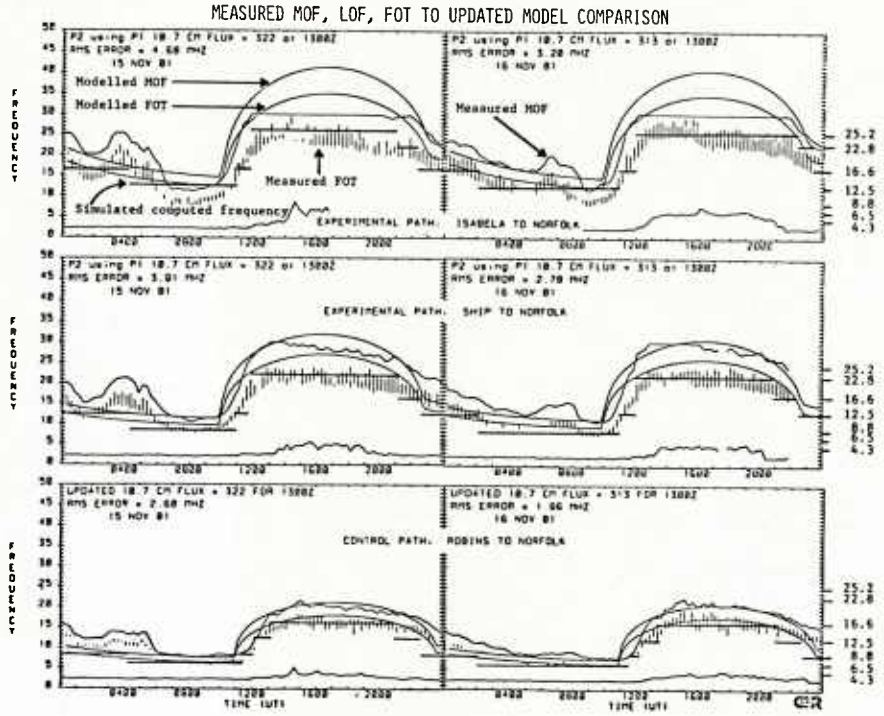

Figure 10: A simulated frequency selection scenario using updated model data.

The actual implementation of the priority structure and the rules for frequency sharing have not been implemented on the computer. This report is an exercise in determining the applicability of the model update technique to sharing frequencies as well as an exercise to determine the rules that should be followed in constructing a computer algorithm to do this. This indicates that the application of a highly accurate updated model to frequency management problems could provide a new scheme of frequency management based on the pooling of frequencies and the sharing of frequencies in the pool among a number of terminals.

Finally, figure 11 has been included to indicate the possibility that the reliability of the frequency selection by the computer might be increased by selecting a different criterion for the FOT as related to the MOF. In this figure, .75 x MOF was used to compute the FOT. We note that the computed FOT and the actual measured FOT are much more closely aligned here than in the previous figure where .85 of the MOF was used to compute the FOT. This .75 factor has been used in other systems (e.g., NOSC PROPHET system) to do different types of calculations. It is possible that further work in examining the FOT factor will lead to an improved algorithm for selecting shared frequencies.

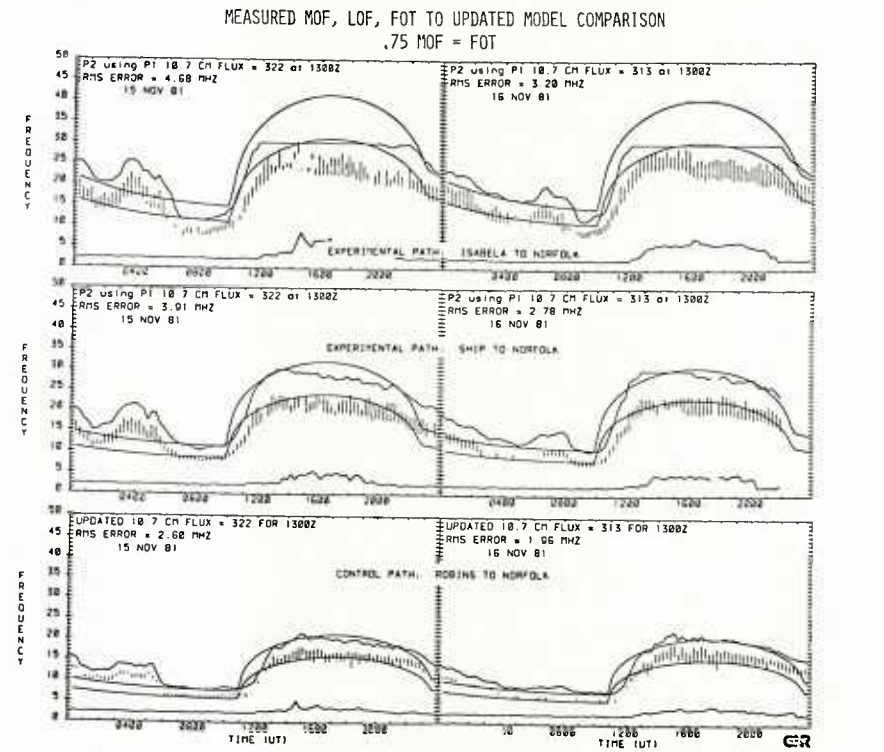

Figure 11: Updated model using a FOT = .75 MOF calculation

4.0 Conclusions

This report has presented work whereby a simple model of the maximum observed frequency, MINIMUF 3.5, has been updated by oblique sounder information in a very simple manner. If this technique can be substantiated over a wide range of geographies and situations, the applications to tactical situations appear to be quite broad indeed. The specific application of this technique to the method of sharing frequencies as obtained from a pool of frequencies has been discussed in this report. Simulations provided herein indicate that it is probably worthwhile a exercise to implement a computer based scheme to do frequency management from a frequency pool employing a simple model of a maximum observed frequency as driven by an oblique sounder circuit. The benefits to be accrued from this if successful, are wide ranging and can lead to a great increase in the efficient use of a very limited number of HF frequencies. NRL Code 4180 will be pursuing this effort in order to impact automated HF resource management systems of the future .

BIBLIOGRAPHY

AMES, J.W., and R. D. Egan, 1967, "Digital Recording and Short-Term Prediction of Oblique Ionospheric Propagation", IEEE Transactions on Antennas and Propagation, Vol. AP-15, No. 3, pp 382-389.

BECKWITH, R.I., and Narayana, Rao, 1975, "Real Time Updating of Maximum Usable Frequency Predictions for HF Radio Communication", IEEE Transactions on Communications, pp 286.

FENWICK, R.B., and T.J. Woodhouse, 1979, "Real-Time Adaptive Frequency Management", Special topics in HF Propagation, AGARD, CP-263.

ROSE, R.B., 1981, "PROPHET and Emerging HF Prediction Technology", IES '81, Washington, D. C.

ROSE, R.B., and J.N. Martin, 1978, "MINIMUF 3: A Simplified MUF Algorithm", NOSC TR-186, San Diego, CA.

ROSE, R.B., and J.N. Martin, 1978, "MINIMUF 3.5", NOSC TR-201, San Diego, CA.

UFFELMAN, D.R., 1981, "HF Propagation Assessment Studies Over Paths in the Atlantic", NRL Memorandum Report 4599, Naval Research Laboratory, Washington, D. C.

UFFELMAN, D.R. and L.O. Harnish, 1981, "HF Systems Test for the SURTASS Operation of February 1981", NRL Memorandum Report 4600, Naval Research Laboratory, Washington, D. C.

UFFELMAN, D.R., and L.O. Harnish, 1982, "Initial Results from HF Propagation Studies During SOLID SHIELD", NRL Memorandum Report 4849, Naval Research Laboratory, Washington, D. C.

DISCUSSION

P.Bradley, US

Please, will you include a map showing the observational paths, their lengths and midpoint separations in the published paper. The correlation of one path with another must diminish with separations.

Author's Reply

You have pointed out a deficiency in my presentation. I don't know these numbers precisely. The total path lengths for the 3 paths are between about 1000 and say 1600 km. The midpoint separations are of course less than this. A report is now available which has this information and I suggest you contact the co-author D.R.Uffelman to get this information and a copy of the report.

T.Jones, UK

(1) In a recent comparison of measured MUF and MINIMUF 3 reported by your laboratory (1982) considerable disagreement was noted. The results you presented today seemed to indicate that the agreement can be quite good – is this because you included correction for solar flux variations, etc?

(2) In Europe we often find that if the MUF is high (or low) in the morning it does not necessarily follow that the same sense of deviation is present in the afternoon. Clearly caution has, therefore, to be exercised in applying force fitting at one time during the day.

(3) Point to point oblique sounding gives information only about that particular circuit. Years ago oblique ground backscatter was considered as a possible tool for determining the ionospheric parameters at remote locations. With the advent of modern chirp sounding techniques has any thought been given to these methods in recent years?

Author's Reply

With respect to the first point, I can only say that considerable disagreement has been shown to exist on occasion especially during disturbed periods. We compensate for this by updating more often. The data points which you refer to correspond to only 1 update over a whole 24 hour period, I believe.

With respect to point No.2, I totally agree. Caution is imperative!

With respect to the final point, I think that it is safe to say that little consideration has been given to OTH radar backscatter as a means to achieve channel sounding without "handshaking". I suspect this is due to the fact that such systems are costly and typically require large power-aperture products. They are also pulse systems (generally, or perhaps exclusively) and create more interference problems than would a chirp (CW) sounder.

THE DEVELOPMENT OF AN IONOSPHERIC MODEL THESAURUS AND USER'S GUIDE

JOHN M. GOODMAN
Ionospheric Effects Branch
E.O. Hulburt Center for Space Research
Naval Research Laboratory
Washington, D. C. 20375

ABSTRACT

This paper describes the preliminary progress on the development of a comprehensive survey of ionospheric models - both physical and empirical -- which have been, are, or would be employed to evaluate the operation of military radiowave systems. Also to be contained in the survey are forecasting/prediction techniques and propagation effects models together with an evaluation of each based upon available documentation. This work is authorized and funded by the Naval Research Laboratory and promulgated under the aegis and guidance of the NATO-AGARD EPP.

1.0 INTRODUCTION

Ionospheric modeling has been pursued along a variety of lines since the existence of the ionosphere was verified by experiments in the first part of the 20th Century. Physical and experimental approaches to modeling, taken together, now provide a good basic picture of the electron density structures which exist along with the intrinsic variabilities as a function of geographic (and geomagnetic) coordinates as well as time. Modeling used for forecasting and prediction typically utilizes the insertion of indirect driving functions such as solar activity (i.e., sunspot number) and magnetic activity indices to describe the influence of both electromagnetic and corpuscular flux from the sun. As the interaction of the magnetosphere with the solar wind and the interplanetary magnetic field has become better understood and as the coupling between the magnetosphere and its various regions within the ionosphere has become more refined, forecasting methods have been suggested which take into account storm-time variablity of specified parameters in the ionosphere. Although many of these forecasting methods are promising, most have not been fully tested for utility and additional experimental verification is of utmost importance if credibility is to be established. In any case, these ionospheric parameters are typically chosen out of some need to characterize system vulnerabilities in some way. These systems are largely those which fall in the category of C^3I or C^3I-CM; abbreviations which stand for command, control, communication and intelligence in the first case, and for corresponding countermeasures in the second instance. The modeling thrust depends quite naturally upon the system involved. By and large we are concerned with systems which employ electromagnetic waves. Indeed, that is the primary interest of the NATO/AGARD EPP organization. Very crudely speaking, the lower ionospheric characterization may be of more importance to long wave systems, the lower and intermediate ionosphere may be of primary interest to MF and HF systems, and the total ionosphere is of importance to earth-space VHF/UHF/SHF systems. Nevertheless, the full ionospheric characterization is usually involved for most system applications owing to the coupling of the various ionospheric layers.

The general response of the ionosphere to solar flares has been known for some time and the details are now being examined both theoretically and experimentally. Within the last decade the mean morphological behavior of ionospheric inhomogeneities and the driving functions, have become rather fully investigated although more effort is required at high latitudes. Much of the success in ionospheric irregularity specification and modeling has been derived from ground-based scintillation studies, in-situ studies using satellite probes, and from advances in the area of computational physics modeling. Cause and effect relationships have been established in certain cases which may ultimately lead to further improvements in short-term forecasting based upon more direct driving functions.

The field of ionospheric modeling .... and I think it does represent a field because of the large number of workers who are involved in this area .... may be compartmentalized on a variety of ways. Basic understanding of ionospheric behavior derives principally from first-principles physical modeling although experimental approaches have produced some surprises. Equatorial scintillation of satellite signals is a clear case-and-point. Empirical or climatological modeling approaches have been exploited most by the user community principally because the systems themselves (or some variant) may provide the data base for modeling. There is, at this point, a bifurcation in the model classification with radiowave propagation models coming into play. Propagation models involve the ionosphere either implicitly or explicitly depending upon the construction of the model. As indicated previously, an ionospheric model may be constructed from a theoretical basis but this approach requires detailed knowledge of the global aeronomy (ionospheric physics and chemistry) as well as the interaction of the earth's dynamic atmosphere with a hierarchy of solar and terrestrial influences to describe the situation fully. This is a difficult problem but significant strides have been made despite a paucity of funds to promulgate the effort. On the other hand, an ionospheric model may be constructed by compiling data which details the ionospheric "personality" on a global and long term basis using a variety of sensors such as rocket and satellite probes, incoherent scatter radar, Faraday rotation polarimetry, scintillation measurements, group path and phase path measurements of satellite transmissions, partial reflection experiments, field strength measurements, satellite and terrestrial ionosonde, oblique incidence ionosonde, and a number of others. Radiowave propagation models using either of these two approaches have (or may be) developed. Since the interaction of radiowaves with a magneto-ionic medium is fairly well understood, and since the properties of the particular radiowave system may be specified, it is purely a mechnanical procedure to deduce system effects. However, the estimation of system effects using this procedure is only so good as the basic model. Hence, great care must be taken to indicate the limitations of the models, the zones over which they have been tested, and so on.

Because of the lack of assurance that specified ionospheric models are accurate for a particular application, "direct" radiowave propagation models have been generated and these are often broken down further so that they may be region-specific. Such models may be based solely upon any one of the sets of sensor data indicated above such as ionosonde or scintillation measurements to mention only two examples. These ad-hoc models are dangerous to use in regions or epochs for which they were not designed to apply and furthermore they often lack flexibility since they may not "anticipate effects rooted in physics". (It is noteworthy that some theoretical models are region specific as well). There are some exceptions, of course, and hybrid propagation models - incorporating physical insight - have been introduced which have had relatively good success.

Out of a need to characterize the ionospheric "channel" in quasi-real-time (of major importance to some users), a series of models are now being exploited by applying updated "driving parameters". These approaches have been successful in some instances where the major portion of the channel parameter variability takes the form of a slowly-varying or d.c. bias. This technique has been applied in refining model estimates of the maximum-usable-frequency (MUF) for example. Small-scale or short term variabilities create considerable risk to such approaches both in term of complexity and cost however.

The need for modeling for both system design and operation is fairly well established; these needs are varied and the degree of accuracy depends upon the applications involved. This paper constitutes a progress report on the development of an ionospheric model thesaurus and user's guide which upon completion will provide to the community of developers and users a basic document for assessing the current state-of-the art. Moreover, it is hoped that it may provide a stimulus for greater utilization of existing models by architects and users of various systems and will motivate scientists in their efforts to provide more practical models which take the customer needs more fully into account.

2.0 PURPOSE AND SCOPE OF STUDY

The purpose of this paper is to outline the progress of an on-going NRL project to compile information pertinent to existing ionospheric and ionospherically-sensitive radiowave propagation models. The total effort is supported in part through ongoing basic research programs but is principally directed toward applied research goals for support of HF and satellite communication/surveillance systems. The motivation for the study is derived from the author's affilation with the Electromagnetic Wave Propagation Panel (EPP) of the Advisory Group for Aerospace Research and Development (AGARD) under the aegis of the North Atlantic Treaty Organization (NATO). The NATO/AGARD official interest is in the development of an "Ionospheric Model Thesaurus and User's Guide". The primary stimulus for the effort derived from the author's participation at the NATO/AGARD meeting held in Ottawa Canada in 1978 which covered "Operational Modeling of the Aerospace Propagation Environment" [Soicher, 1978]. The program became officially sanctioned in 1981.

There are, of course, a myriad of ionospheric models as well as radiowave propagation models which have been developed over the years. The first phase of the study undertaken in development of the "Ionospheric Model thesaurus and User's Guide" is to identify the most current active models. In order to accomplish this task it was necessary to undertake a comprehensive literature search to obtain a data base. A set of references has been developed as a result of this search. At this time the bibliography is incomplete and work is continuing. Another approach, and the principal subject of this paper, is to obtain the necessary information more directly, either through questionaires or interviews. Two questionaires have been developed for this purpose and they have been forwarded to the "ionospheric constituency". The mailing list included the attendees at recent NATO/AGARD conferences, and selected individuals in the IEEE, AGU, and URSI standard mailing lists. The scope of the effort outlined in this manuscript is basically limited to reporting the results of the questionaires. However, a brief synopsis of current activities related to ionospheric prediction, mapping, and assessment, as well as propagation model development is included. The discussion concludes with a brief outline of future plans in connection with preparation of an AGARDOGRAPH.

The reader is referred to an NRL report [Goodman, 1982] which describes the status of the effort as of July 1982 and which includes copies of the questionaires forwarded to selected model developers and users.

3. STATUS OF THE EFFORT

3.1. Literature Search

A bibliography search has been initiated and of this writing has revealed more than 800 reports, papers, and other documents pertaining to ionospheric and radiowave propagation modeling. This basic reference list is in a continuous process of update since new documents are released at a rate of approximately 48 per year since 1973. Figure 1 is a graph showing the rates at which model-related documents have appeared over the years since 1955. These basic data were obtained from a two tier literature search which was augmented by publication lists provided on returned questionaires and a computer search of journal articles. The primary (first) tier literature search emphasized government or government-sponsored reports, and review of the following publications: J. Geophys. Res., J. Atmosph. Terrest. Phys., Radio Science, IEEE journals, AGARD publications, COSPAR publications, URSI abstracts and IES conferences. Assignment to the first tier is naturally biased by the author's view as to which article constitutes information either directly or indirectly related to modeling. Articles captured in this primary search are only part of the total bibliography however. In addition relevant articles cited as references within this primary group (or tier) are assigned to the second tier provided they are not repetitious. The second tier is also contained in the bibliography. As of this writing, references contained within the second tier have not been reviewed to form a third tier. It was concluded that more than two tiers would not be necessary since the "take" decreases rapidly owing to repetitions in the citations.

The complete bibliography is contained in the NRL report referred-to earlier [Goodman, 1982]. Naturally, the author assumes full responsibility for any oversights and welcomes the readership to provide corrections (either deletions or additions) to the basic list.

3.2 Responses to Questionaires

In order to obtain data regarding models, a set of two questionaires was mailed to a limited set of scientists and radiowave propagation specialists. The contents consisted of a short form requesting basic reference lists as well as R&D needs/operational requirements, and a long form requesting detailed information about specific codes.

Forty (40) individuals from twenty-six (26) different organizations responded to the questionaires as of this writing. These individuals, who were not necessarily the custodians of code, primarily regarded themselves as developers of models by a large margin. Figure 2 gives a breakdown of the responses from both developers and percentage users of ionospheric models.

No editing of the respondee identification of him/her-self as either a developer or a user was attempted. Although such editing is tempting, it was avoided to allow for the identification of a perception problem in the domain of the user-customer relationship. For example, some respondees correctly suggest that the ultimate user is the "white hat" in the Fleet (a Navy example) who must use equipment which is dependent upon the ionospheric channel, a medium this user knows little about. In this instance, the echelon above the ultimate user is the developer or system architect and the echelon above this is the sponsor/funding agency contact. Other respondees, specifically scientists who regard themselves as developers, view the sponsor/funding agency as the customer and ultimate user. However this view is usually an erroneous one if we define model utility in terms of its specific impact on system development or operation. As some respondees point out, if the intent of model development is to advance one's knowledge of the ionosphere, however, the ultimate user may be the scientific community at large with the sponsoring agency being a necessary intermediary. In this instance a scientist may regard himself as both a user and developer of models. Thus, a misinterpretation of the term "user" suggests that we should consider the following bifurcation of terms: the scientific-user and the systems-user. Typically the systems-user is implied when referring to the term "user" alone.

There are also users of "long-term" models and another category of users for which model development and application is of more immediate concern. The former category contains system designers as well as architects who are responsible for an a-priori evaluation of system performance. This responsbililty includes definition of the degree of system robustness required; i.e., the margins over which systems must be designed to adapt. In the latter category we naturally include the ultimate user in the operational arena, but we may also include those managers who are in need of immediate band-aid fixes for inadequately designed systems. Inadequacy of design is, of course, not always a result of the non-recognition of potential problems which have been identified in R&D efforts many years before, although it may be. It is sometimes a result of a changing operational environment which necessitates greater system performance than previously envisioned. More often than not the design requirements are directly related to the perceived threat within a specified warfare area. Unfortunately these perceptions change from time-to-time. Because the environment of the ultimate user is so dynamic, user requirements may have a short-fuse and this necessitates a flexibility of response by the R&D community. This argues for a broadly-based R&D program to achieve a specified goal. In the area of ionospheric research and model development, this is no less true.

One of the problems encountered in the questionaire data was the obvious imbalance. As of July 1982 we note that thirty seven (37) of the forty (40) responses were from the U.S. with the foreign responses being from Canada, UK and FRG. Of the twenty-six (26) organizations responding (some clearly with multiple respondees), the mix was almost equally divided between U.S. Government, University or University-affiliated laboratories/institutes, and industrial/other.

It is clear, and was certainly anticipated, that the response to the questionaires would be weighted toward the U.S. This is no doubt a natural consequence of the bias in the mailing list utilized. It is also noteworthy that greatest organizational responses came from NRL and AFGL within the U.S. This is not necessarily related to activity in modeling development or use by these organizations but is probably a combined result of the fact that the author is affiliated with the former organization and that there exists an historically strong interest in NATO/AGARD activities by individuals in the latter organization. Even so, the questionaire contributions by AFGL and NRL are certainly not complete from first-hand knowledge of work being conducted by these two U.S.-DoD laboratories.

Obviously there are problems involved in the application of a questionaire approach to obtain information. One of these involves the "procrastination syndrome" which is handled best by direct contact or telephone. Another is related to the psychology of the questionaire approach itself with many individuals being biased against such activity. Another problem, mentioned previously, is related to the "sampling algorithm" employed, i.e., the mailing list. Steps have been undertaken to alleviate the "sampling" problem. This involves literature search, a time-consuming exercise at best.

Since the time at which the NRL report [Goodman, 1982] on this subject was issued, additional responses have been received from a number of non-U.S. scientists. Of particular note are comments provided by Dr. H. Albrecht of FRG and Dr. P. Bradley of the U.K. Information concerning additional modeling efforts within the U.S. have also been provided by a variety of sources.

3.3. Models Described in Questionaire Responses

Table 1 contains an abbreviated list of models obtained in the questionaire response identified by category. Details are contained in the NRL report cited earlier [Goodman, 1982].

TABLE I: Models Cited in Returned Qustionaires
Identified By Category

HF PROPAGATION	IONOSPHERE
AMBCOM	ARL:UT
ANTCAP/SETCOM	AURORAL DYNAMIC IONOSPHERE
ARMY PROPHET	DMSP THERMAL PLASMA DENSITY
IONCAP	F REGION SERVO
JONES/STEPHENSON RAY TRACING	IONOS
NRL IONOSPHERIC MODEL	LOW/MID-LAT F REGION
RADARC	POLAR F
WIDEBAND HF	SPECTAL COMPONENTS OF foF2
	S3 EMPIRICAL F-REGION
	S3 ELECTRON TEMPERATURE
	UTAH STATE H-LAT
	YTCHIU
LONG WAVE PROPAGATION	**NUCLEAR EFFECTS**
EARTH-IONOSPHERE WAVEGUIDE	SIMBALL
WAVE HOP PROPAGATION	WESCOM
VLFACM	
SCINTILLATION	**OTHER**
ALBRECHT	NEC
AFGL SCINTILLATION OCCURRENCE	
BASU	
FANGS PLOT	
INDIAN SUB-CONTINENT	
IONO4	
WBMOD	

Upon inspection of Table 1 it is clear to any worker in the field (of Ionospheric Physics) that there are many other models which are not listed. In addition there are numerous radiowave propagation models, sub-models, and computer codes not listed but known to exist. Identification of these models is in progress and the final AGARDograph will take up this matter in some detail.

3.4 Other Models Identified Through Literature Search and Personal Contact

Of particular interest are models which have been developed by Raytheon based upon vertical and oblique ionospheric sounding data [Brink, 1982]. The earlier effort in software development for the monostatic HF propagation scenario was termed the Worldwide Ionospheric Modeling (WIM) program [Raytheon, 1976]. The WIM code has been described by Elkins and Gibbs [1977] of RADC. More recent efforts at Raytheon have generalized the ionospheric model for the case of a bi-static propagation geometry; this code is termed Realistic Oblique Matching Simulation (ROAMS). Full documentation of ROAMS has been provided to NRL [Raytheon, 1981a; Raytheon, 1981b].

One of the objectives of the effort embodied in this paper is to evaluate as well as enumerate various ionospheric and radiowave propagation models. While the effort was underway, another effort was initiated by the U.S. DoD Electromagnetic Compatibility Analysis Center (ECAC) [See Velie and Rigler, 1981] for NADC. The ECAC study is based upon the need (requirement) for analysis and prediction both in the near and long term. Of the numerous models evaluated, there were several which have been identified earlier. They are naturally propagation-oriented, but ionospheric properties are contained within these models which are basically empirical in nature. The following listing are models (codes) of interest in the present context.

TABLE II: MODELS EXAMINED BY ECAC

MODEL NAME	CODE NAME	DEVELOPER
High Frequency Communications Assessment Model	HFCAM	ECAC
HF Electromagnetic Compatibility	HF EMC^2	NOSC
HF Maximum Usable Frequency Evaluation	HF MUFES-4	ITS
Ionospheric Comm Analysis and Prediction Program	IONCAP	ITS
Minicomputer Model for Predicting the MUF in HF Comm	MINIMUF	NOSC
Propagation in the Earth-Ionosphere Waveguide I	MODE CONVERSION	NOSC
Propagation in the Earth-Ionospheric Waveguide II	MODESRCH	NOSC
Effect of Nuclear Burst on HF Communications	NUCOM	SRI
Program for the Analysis of Comm Satellite Systems	PACSS	ESD
Propagation Forecasting and Assessment System	PROPHET	NOSC
Quiet-Time Lowest Usable Frequency	QLOF	NOSC
HF MUFES-4 Ionospheric Propagation Model	RADARC	NRL
Satellite propagation Model	SATPROP	ECAC
Sudden Ionospheric Disturbance Grid	SIDGRID	NOSC
HF Skywave propagation Model	SKYWAVE	ITS
VLF and LF Propagation Model	VLF/LF	ECAC
X-Ray Flare and Shortwave Fade Duration Model	XRAY FLARE	NOSC

The ECAC study identified "principal models" based upon their specific requirements. They included IONCAP and MINIMUF from the above list.

TABLE III: MODELS DEVELOPED BY NAVAL OCEAN SYSTEMS CENTER

MODEL	SYSTEM	ACTION	STATUS
Flare detection	All hf, vlf; navagation and comm	hf comm-freq shift; reroute traffic	operational
Flare detection	all hf,vlf; nav/com	hf comm-freq shift; reroute traffic	operational
SID GRID	all hf	hf comm freq shift; reroute traffic	operational
SPA/vlf	vlf nav; Omega	phase correction factor	developed
SPA inversion	all hf,vlf	estimate x-ray flare size (independent of satell.);feed sid grid	in progress
PCA/vlf	vlf navig	phase correction factor for transpolar circuits	developed
PCA/hf	all polar hf	hf comm-advice; signal strength loss-freq shift	developed
PCA/vhf	all polar satellite	vhf comm-advice; signal loss	developed
QLOF	all hf	hf comm-normal operations; freq management	operational
LOF split	covert hf systems	opt freq selection against known rcvrs	operational
MINIMUF-5	all hf	hf comm-normal ops; freq management	operational
15 min update to MINIMUF using auroral E fields	all hf	correct MUF est. (real time) minimize errors to approx 1 MHz (feeds MINIMUF)	inprogress
RAYTRACE	all hf	hf comm-normal ops; antenna selection	operational
Launch angle multipath using quasi parabolic	all hf	hf comm-normal ops; antenna selection	operational
Polar & auroral ionosphere	all hf vhf satellite	hf comm-normal ops; polar circuits	in progress
Earth's magnetic field variations (ground)	ASW & any magnetically sensitive	corrections for field changes D_{st} and AE	in progress
Mixing shock front from auroral disturbances	all hf	hf comm-midlatitude (feeds MINIMUF)	in progress
Scintillation grid	vhf/uhf satellite comm	advisory-dB fade probability based on location	operational
Omega correction factors	Omega vlf	correction factors	operational
HFFIELDS	hf	diurnal MUF/LUF predictions with simplified field strength approximations	operational
Ionospheric storm	hf	opt freq selection to propagation changes	in progress
Ionogram	hf	optimum frequency selection	operational
Missing shock front from auroral disturbances	all hf	hf comm-midlatitude (feeds MINIMUF)	in progress
Scintillation grid	vhf/uhf satellite comm	advisory-dB fade probability based on location	operational
Omega correction factors	Omega vlf	correction factors	operational
HFFIELDS	hf	diurnal MUF/LUF predictions with simplified field strength approximations	operational
Ionospheric storm	hf	opt freq selection to propagation changes	in progress
Ionogram	hf	optimum frequency selection	operational

Rose [1981] has described the Navy-developed PROPHET system since its inception. The current version of PROPHET, which is based upon mini-computer technology, features over 15 HF prediction and assessment models. The NOSC efforts also include scintillation and long-wave modeling. Earlier versions of PROPHET included SOLRAD-PROPHET, the purpose of which was to exploit the real-time data retrieved from the two Navy SOLRAD HI satellite systems. Subsequently CLASSIC PROPHET was developed for the purpose of multi-station HF prediction while principally serving the needs of the HF-DF community. To serve the needs of the SIGSEC and COMSEC communities, the Tactical Prediction Module (TPM) was developed. A current development is embodied in ADVANCED PROPHET, the purpose of which is to maintain a test-bed for basic and exploratory research in forecasting technology. The success of the PROPHET concept is exhibited in spinoffs which satisfy certain short-term needs of the operational community. They include: FAA-PROPHET, FOTACS, and COPS-MOD. The PROPHET technology is also contained in the Army PROPHET Evaluation System, (APES). Table III is a listing of models contained within the ADVANCED PROPHET architecture [Rose, 1981].

4.0 REQUIREMENTS FOR IONOSPHERIC MODELING

4.1 Official Requirements

Both official and unofficial requirements were solicited from respondees to the questionaires. Within the U.S., official requirements were identified within the Department of the Army and these dealt principally with the provision for radio propagation technical services (in general) and with HF system performance predictions and analysis (in particular).

The U.S. Air Force and U.S. Navy official requirements were not formally identified through the questionaire approach. General R&D objectives promulgated by the services typically outline the needs in these areas in broad terms. The general "Military Requirements for Satellite Data" are contained in a Joint Chief of Staff unclassified report MJCS 251-76 dtd 31 Aug 1976. Currently the U.S. Navy has no officially-documented Operational Requirement (OR) relating to solar-terrestrial or ionospheric modeling/monitoring. The view is held by staff under the Chief of Naval Operations (CNO) that Navy requirements are adequately covered by national resources including systems operated by the Dept. of Commerce (NOAA/SEL/SESC), the National Aeronautics and Space Administration (NASA), and the Air Force (AWS/AFGWC/SESS).

(It is noteworthy that Navy requirements in these areas were quite close to formalization in the late seventies when a Draft OR entitled "Environment Prediction and Assessment System" was "tabled" by CNO with the comment that such a system was..."nice to have"...but not affordable in view of sister service and national assets already in place.)

The U.S. Air Force, on the other hand, has promulgated a Statement Of Need (SON) -- as equivalent to the Navy OR document -- called IONSON which reflects the need for ionospheric monitoring in specific terms. In addition, another SON for solar/environmental monitoring, termed SEMSON, is now in process. Official requirements of NATO allies and organizations such as the SHAPE Technical Center are now being solicited.

4.2 Unofficial Requirements

Unofficial needs of the user communities are typically contained in mission statements of various government laboratories and other institutions/agencies. Such needs for ionospheric modeling have been identified for the organizations listed in Table IV. The listing is clearly incomplete and a more thorough follow-up is planned. Again, responses from non-U.S. organizations will be solicited.

TABLE IV: ORGANIZATIONS WHICH HAVE INDICATED UNOFFICIAL NEEDS IN IONOSPHERIC/PROPAGATION MODELING

USACEEIA/CC-EMEO/Ft. Huachuca, AZ/USA
U.S. Air Force Avionics Laboratory/Wright-Patterson AFB, Ohio/USA
Air Force Geophysics Laboratory/Hanscom AFB, MA/USA
Applied Physics Laboratory (JHU)/Laurel MD/USA
Centre for Radio Science/London, Ontario/Canada
Los Alamos National Laboratory/Los Alamos, NM/USA
Naval Intelligence Environmental Sciences (NISC)/Wash. D.C./USA
Naval Research Laboratory/Wash. D.C./USA
Naval Ocean Systems Center/San Diego, CA/USA
RCA/Astro Electronics Division/Princeton, NJ/USA
Southwest Research Institute (SWRI)/San Antonio, TX/USA

4.3 General Commentary On User Needs

There has been an almost continuous dialogue at scientific colloquia, various topical conferences, and at focussed NATO/AGARD meetings concerning the matter of user or customer needs. This stems, at least in part, from the urge for "scientific self preservation". We are well aware of the "publish or perish" admonition in academia and in other scientific institutions. In view of diminishing basic research resources relative to the size of the current ionospheric constiuency, the analogue to this admonition is "technology- transfer or perish". In any case there has been a concern in the scientific community in recent years vis-a-vis relevancy of basic research and this concern was heightened by the

enactment of the Mansfield Amendment by the U.S. Congress in the past decade. This precipitated numerous studies in the U.S. DoD and elsewhere to focus-in on the use of ionospheric research for example. Another activity of interest was a workshop [Donnelly, 1979] held in Boulder in 1979 to address Solar-Terrestrial Predictions. In addition there have been three (3) Ionospheric Effects Symposia held in 1975, 1978 and 1981 dealing with ionospheric models and scientist-user dialogue problems among other things [Goodman, 1975, 1978, 1981].

5.0 ORGANIZATIONAL ACTIVITIES OF IMPORTANCE TO IONOSPHERIC PREDICTION AND MODELING

Of importance in the general radiowave propagation and ionospheric modeling areas are activities of various domestic and international organizations designed to foster cooperative research and promote understanding. They include ITU/CCIR, IEEE, URSI, COSPAR, AGU, IAGA, IUGG and SCOSTEP. Study group 6 of CCIR deals with international standards and issues relating to ionospheric radiowave propagation; CCIR activites are of major importance in the context of the current study. Various study groups of URSI and COSPAR also deal with ionospheric measurements and modeling efforts. Of particular interest is the development of the International Reference Ionosphere [Rawer,1981]. COSPAR Conferences are a good source of material relating to ionospheric/space research as well as ionospheric modeling [Mendillo, 1976; Checcecci, 1978; and Wernik, 1981].

Propagation prediction services and related R&D are provided by a number of organizations both with the U.S. and elsewhere within the U.S. They include NOAA Space Environment Laboratory and its Space Environmental Services Center (SESC) [Williams and Leimbach, 1982], the Institute for Telecommunication Sciences, the U.S.A.F. Air Weather Service and its Global Weather Central (AFGWC) [Thompson and Secan, 1979, Tascione et al, 1979], and the U.S.Army Communications-Electronics Engineering Installation Agency [Merkel, 1981]. Non- U.S. activities have been described in the Proceedings of the Solar Terrestrial Prediction Workshop [Donnelly, 1979] and are not detailed herein.

6.0 DISCUSSION

6.1 Recent Reviews of Ionospheric Modelling and Predictions

A review of recent (1978-1980) progress in development of ionospheric modeling has been given by Westerlund [1981]. Of interest are reviews of E and F Region dynamics (Section 3), ionospheric aspects of plasma instabilities (Section 5), influence of the ionosphere on radio systems (Section 6), morphological models of the ionosphere (Section 7), ionization and chemistry, (Section 8), stratospheric-mesopheric-ionosphere interactions, (Section 9), and finally, ionospheric sounding techniques and networks (Section 11). Of particular relevance to this paper were the following: Section 5 (parts dealing with spread F and scintillation), section 6 (all, but especially the parts dealing with forecasting), section 7 (all, but especially the part dealing with profiles of electron density), and section 11 (all).

Another useful source of recent progress in ionospheric predictions is due to Davies [1981]. His review is based in large part upon the proceedings of the Solar-Terrestrial Predictions Conference held in Boulder, Colorado in 1979 [Donnelly, 1979]. Nisbet [1978] has reviewed operational physical models of the ionosphere and Kohnlein [1978] has reviewed electron density models.

6.2 Some Thoughts on Categorization and Utilization of Models

Davies [1981] in his review of ionospheric forecasting breaks modeling into two classes: empirical and physical. Included within the empirical model class are numerical maps of ionospheric characteristics. Davies indicates the virtue of combining both classes in some instances.

Nisbet [1978], in his review of operational physical models of the ionosphere, defines three basic classes: mean morphological, dynamic, and forecasting. He maintains that the forecasting class is closely related to the mean morphological class of models. Using Nisbet's recipe, certain physical models could belong to either the mean morphological class or the dynamic class; whereas certain empirical models could belong to either the mean morphological or forecasting class. It is worth noting that almost any physical or empirical model and can be used as a tool in forecasting, although that may not be the original intent. They can certainly be useful in system design studies which require ionospheric vulnerability analyses to be performed.

Predictions based upon physical models, other than those used for system design, may not be useful in relation to quasi-adaptive empirical models. Most certainly, short term forecasting requirements depend heavily upon the empirical approach having been suitably modified to allow update through injection of remotely-sensed ionospheric parameters. However, some empirical models suffer over areas where the original data sets for model construction are sparse. For near-term forecasting the most advisable approach is to utilize an empirical mean morphology augmented by a physical model to extrapolate the model (or make it more accurate) in regions which are represented by an inadequate data set (i.e., over ocean areas or some portions of the Southern Hemisphere). For removing biases in this quasi-empirical approach, it must be made adaptive and one approach might be to inject the model with "fresh" data, from sounders, for example. In addition, certain modules must be added to account for time-varying solar and magnetic activity (or substorm) influences. (It has been recommended that sunspot number and magnetic activity indices be replaced by more physically meaningful parameters. Solar flux in the ultraviolet and x-ray bands and the Akasofu parameter should provide improvement in predictions).

As an example of this approach, NRL, in collaboration with NOSC, is testing specified mean morphological propagation models which have the capability for real-time update and may incorporate variable external source functions (i.e., solar, geomagnetic substorm). The models being used are MINIMUF and IONCAP, the source of model update is a sounder (oblique, vertical incidence and topside) data, and the external source functions are parameters K_p and 10.7 cm solar flux (or sunspot number). The approach has shown promise but is yet to be validated in the context of being operationally useful. (See companion paper by Uffelman et al [1982]).

Recently Rush et al [1982] have examined the use of theoretical models to improve the prediction of ionospheric parameters in regions of the earth inaccessable to ground-based measurements. The authors indicate that with further study it may be possible to significantly improve global maps of foF2 especially in the Southern Hemisphere and in the equatorial regions by use of theoretical model extrapolation of experimental data. It is remarked, however, that this improvement still is not sufficient for real-time applications. Quasi-real time update is still required for such applications.

It is important to understand that certain classes of ionospheric variability are currently impossible to forecast irrespective of the complexity and elegance of the model being used. These include as a minimum: TID's and spread F (plumes). These phenomena introduce important perturbations on various C^3I systems. Physical models may provide better insight regarding the likelihood of occurrence of these phenomena and even a rough estimate of their properties (i.e., time duration, spatial extent, magnitude, etc.), but it is unlikely to yield an answer for a particular point in space-time. The only solution visualized at this time is real-time mapping with good spatial and temporal resolution, perhaps from space itself. The fusion of data from networks of sounding stations or polarimeters may be useful for producing snapshots of the ionosphere but these "pictures" would be of limited clarity because of finite number of stations in the networks - a consequence of both economics and global topography. It would be ideal if a satellite-borne remote sensing device could "map" the ionosphere and produce snapshots of ionospheric "weather" similar to those obtained to estimate "tropospheric weather" patterns. Current approaches using topside sounders such as the Japanese ISS-B [RRL, 1981] produce "time-exposures" too large to be useful in the short-term context. Satellite-borne scanning devices have offered considerable promise, but are limited in application at present. DMSP mosaics of the auroral zone luminosity have yielded significant information about auroral phenomena but the developments cannot be followed on the sunlit side of the earth. It is speculated [Rust and Bernstein, 1981] that x-ray imaging may be used to partially resolve this problem but benign non-auroral properties cannot be examined by this technique. Huffman et al [1981] have suggested that ionospheric and auroral measurements are possible by using vacuum ultraviolet techniques. Support for this suggestion may be found in the OGO-4 and the STP S3/4 satellite experiments. NRL scientists are also interested in exploring the feasibility of producing UV images of the earth from either a highly elliptical or nearly synchronous satellite platform [Meier, 1981]. For the present, however, regional morphological mdels which are amenable to quasi-real time update (via oblique sounders, for example) must suffice for short-term forecasting. This is the approach followed by NRL to support certain fleet exercises and DoD programs. A similar approach has been followed by AFGWC through its AF4D ionospheric model development.

7.0 FUTURE PLANS

This effort is continuing. The next step is to provide, along with the identification of all available models, a brief description of the model (or an abstract of the referenced paper if a computer code is not available). We also intend to provide detailed information about selected models including data extracted from questionaires. The final step is to assess the merits of each class of models (and in some cases specific models) in the context of user requirements. The process of assessment is yet to be determined. A better definition of specific user requirements is being pursued as a parallel effort.

8.0 ACKNOWLEDGMENTS

The author is grateful to all individuals who took valuable time to respond to the "Ionospheric Model Thesaurus and Users Guide" questionaire. The EPP of NATO/AGARD is also acknowledged; specifically Dr. Jules Aarons of Boston University (AFGL at the initiation of this program), and Dr. Hans Albrecht of FGAN in FRG. This work was supported by the Office of Naval Research.

9.0 REFERENCES

BRINK, D.L. (Major, USAF), 1982, private communication

CHECCACCI, P.F. (Editor), 1978, Beacon Satellite Measurements of Plasmaspheric and Ionospheric Properties, IROE-CNR, Florence Italy.

DAVIES K., 1981 "Review of Recent Progress in Ionospheric Predictions" Radio Sci. 16(6), 1407-1430 (also appearing in Proceedings of IES '81).

DONNELLY, R.F. (Editor), 1979, Solar Terrestrial Proceedings, four volumes: Prediction Group Reports, Working Group Reports, Solar Activity Predictions, and Predictions of Terrestrial Effects of Solar Activity, U.S. GPO, Washington, D.C. 20402.

ELKINS, T., and J. Gibbs, 1977, "Coordinate Conversion Technique for OTH Backscatter Radar", RADC-TR-77-183.

GOODMAN, J.M. (Editor), 1975, Effect of the Ionosphere on Space Systems and Communications, U.S. GPO, Washington, D. C. 20402

GOODMAN, J.M. (Editor), 1978, Effect of the Ionosphere on Space and Terrestrial Systems, U.S. GPO, Washington, D. C. 20402.

GOODMAN, J.M. (Editor in Chief), 1981, Effect of the Ionosphere on Radiowave Systems, U.S.GPO, Washington, D. C. 20402.

GOODMAN, J.M., 1982, "A Survey of Ionospheric Models - A Preliminary Report on the Development of an Ionospheric Model Thesaurus and User's Guide", NRL Memorandum Report 4830.

HUFFMAN, R.E., D.E. Paulson, F.J. LeBlanc and J.C. Larrabee, 1981, "Ionospheric and Auroral Measurements from Space Using Vacuum Ultraviolet Emission" in Effect of the Ionosphere on Radiowave Systems , J.M. Goodman, (Editor in Chief) USGPO Washington, D.C. 20402

KOHNLEIN, W., 1978, "Electron Density Models of the Ionosphere", Rev. of Geophy and Spa. Phys. 16 (3).

MEIER, R., 1981, Private Communication

MENDILLO, M., (Editor), 1976, The Geophysical Use of Satellite Beacon Observations, Boston University, Boston, MA

MERKEL, M., 1981, "Propagation Prediction Services", Technical Memorandum EMEO-PED-TM-81-1 dtd April 1981.

NISBET, J., 1978, "Operational Physical Models of the Ionosphere" in Operational Modelling of the Aerospace Propagation Environment, H. Soicher (Editor), AGARD-CP-238-Vol 1, Tech Edit and Reprod. Ltd., London.

OSSAKOW, S.L., M.J. Keskinen, and S.T. Zalesak, 1982, "Ionospheric Irregularity Physics Modeling", NRL Memorandum Report 4741.

RAWER, 1981, "International Reference Ionosphere IRI 79", WDC-A for STP pub. (edited by J.V. Lincoln and R.O. Conkright), Dept. of Commerce NOAA, EDIS, Boulder, CO, USA 80303.

Raytheon Report, 1976, "Worldwide Ionospheric Modelling Technique", ER76-4168.

Raytheon Report, 1981a, "User's Manual-Realistic Oblique Automatic Matching Simulation", ER81-4010.

Raytheon Report, 1981b, "Realistic Oblique Automatic Matching Simulations", EA81-4059.

ROSE, 1981 "PROPHET - An Emerging HF Prediction Technology" in Effect of the Ionosphere on Radiowave Systems, J.M. Goodman (Editor), USGPO, Washington, D.C.

RRL, 1981, "Atlas of Ionospheric Critical Frequency (foF2) obtained from Ionosphere Sounding Satellite-b Observation (Part 3), January to June 1978", Radio Research Laboratories, Japan.

RUSH C.M., M. PoKempner, D.N. Anderson, and F.G. Stewart, 1982, "The Use of Theoretical Models to Improve Global Maps of foF2", NTIA-Report 82-93.

RUST, D.M. and P. Bernstein, 1981, "Application of X-ray Imaging Techniques to Auroral Monitoring" in Effect of the Ionosphere on Radiowave Systems, J.M. Goodman (Editor-in-Chief) USGPO Wash., DC 20402

SOICHER, H.(Editor), 1978, Operational Modeling of the Aerospace Propagation Environment, AGARD-CP-238, Vol 1, Ottawa Conference, Tech. Edit. and Reprod. Ltd., London.

TASCIONE, T.F., T.W. Flattery, V.G. Patterson, J.A. Secan, and J.W. Taylor Jr., 1979, "Ionospheric Modeling at Air Force Global Weather Central", in Solar-Terrestrial Predictions Proceedings: Vol 1, edited by R.F. Donnelly, USGPO, Washington, D. C. 20402.

THOMPSON, R.L. and J.A. Secan, 1979, "Geophysical Forecasting at AFGWC", in Solar-Terrestrial Predictions Proceedings: Vol. 1, edited by R.F. Donnelly, USGPO, Washington, D.C. 20402.

UFFELMAN, D.R., L.O. Harnish, and J.M. Goodman, 1982, "The Application of Real-Time Model Update by Oblique Ionospheric Sounders to Frequency Sharing", companion paper presented at this conference.

VELIE, E.R., and S. Rigler, 1981, "NAVAIR Analysis and Prediction Model Evaluation and Capability Improvement Program", prepared for NAVAIR Development Center (NADC), Warminster, PA, 2 Volumes.

WERNIK, A.W. (Editor), 1981, Scientific and Engineering Uses of Satellite Radio Beacons, Polish Scientific Publishers, Warsaw, Poland (Conference held in 1980).

WESTERLUND, S., 1981, "Ionospheric Radio and Propagation", Chapter 8 of Review of Radio Science 1978-1980, edited by S.A. Bowhill, URSI publication, Brussels, Belgium.

WILLIAMS, D.J. and H. Leinbach, 1982, Letter and attached Laboratory Fact Sheet (R43:DJW/HL dtd Feb 16, 1982), U.S. Dept. of Commerce NOAA/ERL.

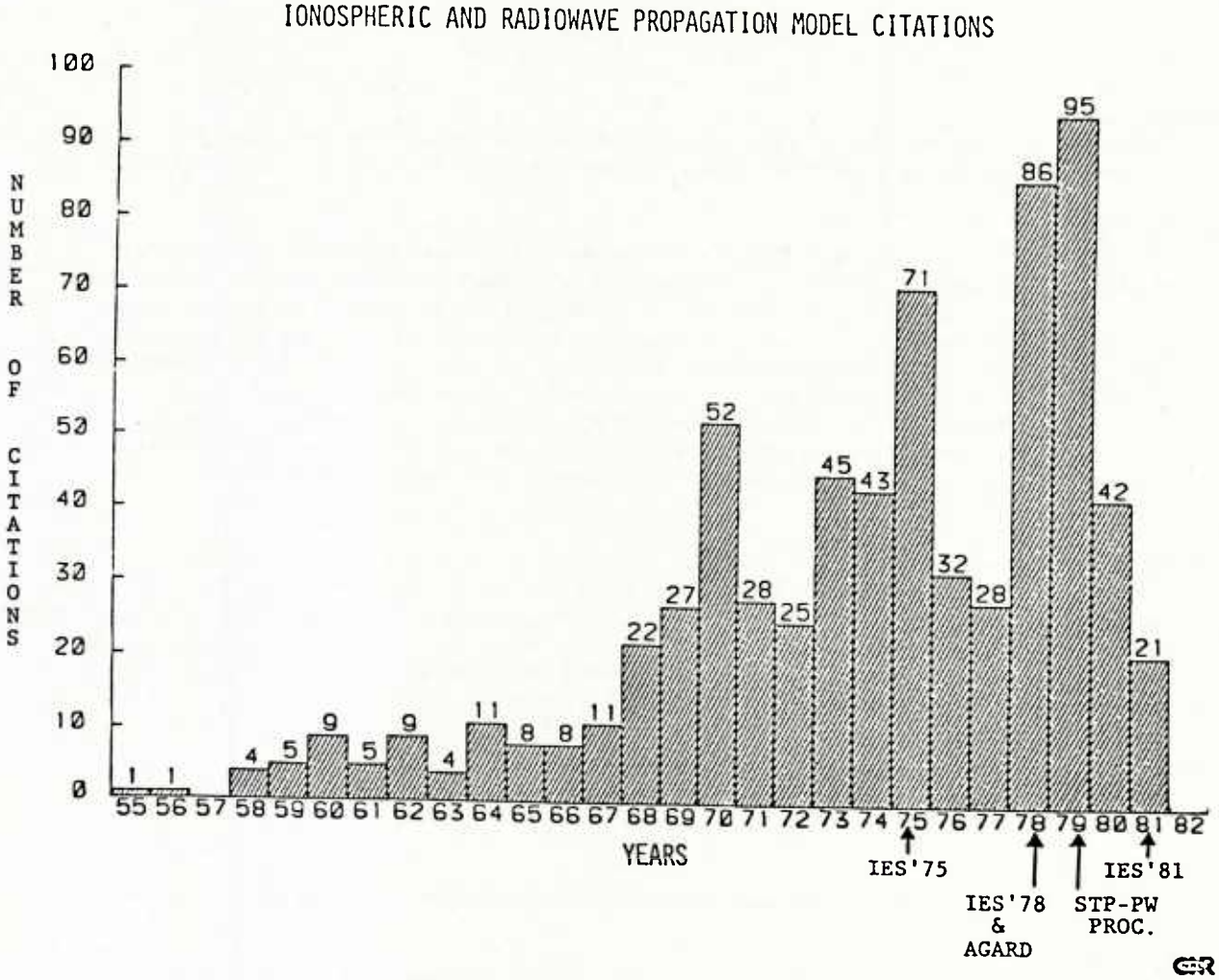

Fig.1 Time history of reports and papers which have been identified as relating to ionospheric modelling or radiowave propagation modelling

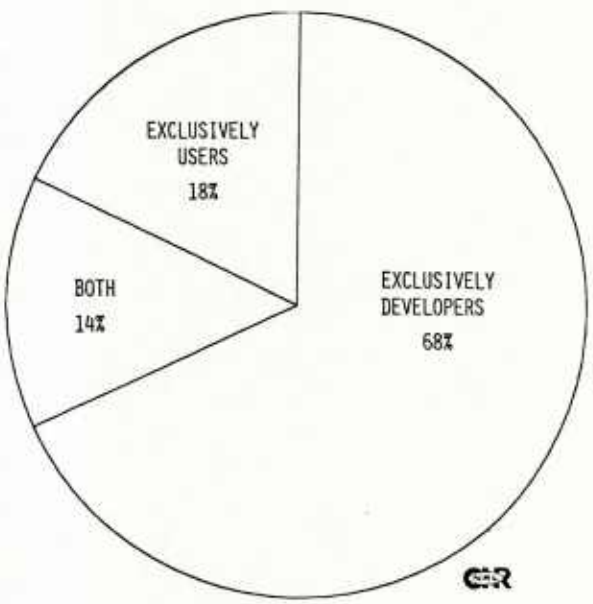

Fig.2 Breakdown of respondees to questionnaire requesting identification as user or developer of models

DISCUSSION

S.Segner, US

How wrong can we go in the US Army by starting with the PROPHET model towards developing HF pooling concepts? (We are copying the NOSC developed APES software onto our USAREUR – ATFES ADP systems.)

Author's Reply

This is a difficult question to answer. First of all it depends upon the use to which the model is directed. If the PROPHET models are to be used in a mobile environment or for disadvantaged users it has considerable merit. Most models are basically inadequate. Therefore it makes sense to start with a model (in this case you are talking about a propagation model) which is simple to operate, easy to maintain, and so on. Since, as I have said in the earlier paper one should always consider updating models with "fresh" data anyway to remove biases, the PROPHET models have a lot of charm. For the purpose you have indicated in your question, it would appear that you might wish to consider models which have more elegance; perhaps, say, ITS-78 or IONCAP to give some USA-developed examples. This is because you presumably have a large computer at your disposal. The US Army has had considerable experience with these models. You might contact the group at Ft Huachuca, for example.

G.H.Hagn, US

In regard to Mr Segner's question, it is important to keep in mind the fact that models useful for the HF system design may not be as useful as other models for actual frequency selection. Presumably, models which are relatively simple (e.g., PROPHET) which use very current information for their input may be better for near-real time frequency forecasting. Whereas, more comprehensive models, which predict monthly performance based on longer range prediction (e.g., IONCAP), may be more appropriate for system design.

Author's Reply

I agree fully.

P.A.Bradley, US

Do you know of any work in progress aimed at modelling ionosphere Doppler dispersion?

Author's Reply

I can't think of any first hand examples. I think a group at Huntsville, Alabama is doing some work in this area as is a propagation group in Japan. Also Dr L.S.Wagner at NRL is now conducting a series of measurements on the West Coast of the US using a wideband (1 MHz bandwidth) approach. He also has a narrowband sounder. I understand that he is obtaining very interesting layer height (doppler) effects.

SUMMARY OF SESSION III-A

TERRESTRIAL PROPAGATION (GROUND AND TROPOSPHERIC MODES)

by

Ing. en Chef L.Boithias
Session Chairman

This session consisted of eight contributed papers which may be classified as follows:

(1) *Long distance propagation influenced by ground characteristics*
with two papers:

14 – Medium Wave Groundwave Propagation Model – Numerical and Experimental Results by A.Fer and A.Hizal
15 – Multiple Knife Edge Diffraction by P.McManamon and L.Vogler

These two papers dealt mainly with diffraction propagation for MF (paper 14) and UHF (paper 15). The purpose was to obtain a reliable predicting method. In both approaches computers were required to perform calculations.

(2) *Long distance propagation influenced by atmosphere characteristics*
with three papers:

16 – VHF/UHF Propagation Studies on Long Over the Horizon Salt Water Radio Paths by R.E.Grantham and W.P.Lonc
17 – Modelling of Interference Due to Ducting at Frequencies above 19 Hz, by J.Dijk, J.Neessen and J.Van Tiggelen
18 – Statistical Study of Elevated Ducts Extension by B.Strauss and J-L.Dumas.

The first of these papers discussed the influence of tropospheric scatter and ducting on propagation. The other two papers studied ducts from a theoretical and radioelectrical point of view in paper 17 and from a purely meteorological point of view in paper 18.

(3) *Scattering by hydrometeors and reflectivity*
with two papers:

19 – Hydrometeors Multiple Scattering – A Numeric Simulation by N.Spanjaard and J.Lavergnat
20 – Bistatic Radar Reflectivity in the Ranges 11–30 GHz by D.G.Charlton, A.Holt and B.Evans

Both papers were theoretical. The first one pointed out the errors resulting from neglecting multiple rain drop scattering and the second one pointed out the errors resulting from the Rayleigh approximation in the calculation of reflectivity.

(4) *Long range interference due to propagation*
with one paper:

21 – Overshoot Interference on Microwave Radio Links Due to the Co-Existence of Multipath fading and Trans-Horizon by J.E.Doble

This paper pointed out the possible enhancement of interference by overshoot on radio links due to the fact that the same meteorological conditions are responsible for deep fades on a hop and, simultaneously, of high reception level from a distant station.

MEDIUM WAVE GROUNDWAVE PROPAGATION MODEL-NUMERICAL AND EXPERIMENTAL RESULTS

A.F. FER and A. HIZAL

Electrical Engineering Department
Middle East Technical University
Ankara - TURKEY

SUMMARY

Two computer models incorporating two different groundwave propagation analysis techniques are investigated. The first model is a perturbation technique based on the approach by King Maley and Wait and represents an extention of the previous results to take into account an n-section propagation path. The second model is the integral equation solution for irregular and inhomogeneous terrain based on the formulation by Ott. (i.e. PROGRAM WAGNER)

The results from the two approaches are compared with each other as well as the results from Millington formula for multisection paths and knife edge diffraction for mountainous regions. Limited amount of experimental data is also compared with computed values for ground wave propagation from Trabzon Broadcast transmitter over the Eastern Anatolian mountain ranges.

Computer modelling for the study of ground wave propagation is seen to present an economically advantageous tool in the design of MF communication links.

1. INTRODUCTION

In the design and planning of radio communication systems, the study of electromagnetic wave propagation is of primary importance. The theoretical modelling of the propagation medium while facilitating the prediction of expected quality of transmission, and the evaluation of alternative schemes, may provide a better insight into propagation phenomena that will be helpful in the selection of various design parameters. This report describes two computer models for ground wave propagation over inhomogeneous paths with terrain irregularities.

Groundwave propagation along multisection paths have been investigated both numerically and experimentally by King and Maley [1], and King et.al. [2] for flat terrain profiles and by Ott [3] for irregular and inhomogeneous grounds. For flat grounds the integral expressions developed by King et.al [2] based on the perturbation technique have been proven to be accurate [4] and can be used for propagation paths oblique to the land sea boundaries. For irregular terrain and continuously changing surface impedance, the integral equation method by Ott [3] as incorporated in PROGRAM WAGNER is suitable.

In the present work a groundwave propagation study in the Marmara and West Black sea region of Turkey is made in order to assess the performance of PTT's MF coastal maritime communication systems from the propagation point of view. Three techniques to predict ground wave propagation characteristics have been implemented. The first is based on the approach by King et.al. [1], and represents an extention of their model to n-section paths. The second is an integral equation solution based on the formulation by Ott [3]. The third is the semiempirical formula due to Millington [5] as recommended by the the CCIR in Recommendation 368-2. The computed results for the attenuation function obtained by the three techniques are compared within the context of the MF propagation study for maritime communication in the Marmara and Western Black Sea regions. A further comparison is made between experimental results and the results of the integral equation technique and Millingtons formula in the Eastern Black Sea region. The heights of the mountains encountered in this region being of the order of ten wavelengths have suggested the consideration of knife edge diffraction techniques and the results obtained in this way have also been presented.

2. THEORY

For the two-section propagation path shown in Fig.2, King et.al. [1] [4] have developed a formula in elliptical co-ordinates for the attenuation function $F(d,z,z_1)$ using the compensation theorem and the method of stationary phase integration (e.g. [7]):

$$F(d,Z,Z_1) = F(d,Z) + \left(\frac{id}{\lambda}\right)^{\frac{1}{2}} \int_0^{\theta_1} \left(\frac{Z-Z_1}{\eta_0}\right) F(r,Z)\, F(R,Z_1)\, d\theta \qquad (1)$$

where

$\theta_1 = \mathrm{Cos}^{-1}\{(2x_1/d)-1\}$, $r = (d/2)(1 - \mathrm{Cos}\theta)$, $R = d-r$

$\eta_0 = \sqrt{\mu_0/\varepsilon_0}$: Intrinsic impedance of free-space.

$Z = \eta/\eta_0 \sqrt{\eta_0^2 - \eta^2}$: Surface impedance of the land for the vertical polarization.

$\eta = \sqrt{i\omega\mu_o/(\sigma + i\omega\varepsilon)}$: Intrinsic impedance of land

For the sea Z and η are to be replaced by Z_1 and η_1, respectively.

$$F(r,Z) = 1 - i\sqrt{\pi p}\; e^{-p}\, \mathrm{erfc}\;(i\sqrt{p}) \tag{2}$$

is the Sommerfeld attenuation factor. $\mathrm{erfc}(z) = (2/\sqrt{\pi}) \int_z^\infty e^{-t^2}\, dt$ is the complementary error function and $p = (-ikr/2)(Z/\eta_o)^2$ is the numerical distance. Formula (1) has been proved to be very accurate when the source (A) and the observation point (B) are several wavelengths away from the coast. Expression (1) is easy to integrate numerically using Gaussian-quadrature. To obtain a formula amenable for iteration the reciprocity theorem may be used in the original compensation formula by replacing $F(r,Z)F(R,Z_1)$ in (1) by $F(R,Z)F(r,Z,Z_1)$. But it is found that such an iteration scheme is not necessary and (1) is quite accurate.

For the three-section paths King, et.al. [2] have developed a formula similar to (1) which contains the two-section result given by (1) in the integrand. It may be seen that such an n-section formula is desirable when the propagation study involves a geography such as in Fig.1 with many islands and peninsulas, and the major source of the inhomogeneity in the path consists of transitions from land to sea or vice versa.

Although an n-section formula has not appeared previously, it is a straightforward procedure to develop it using the electromagnetic compensation theorem [7]. To facilitate the description of the method consider a 4-section path. Referring to Fig.3, the mutual impedance change may be expressed by,

$$Z'_{AB} - Z_{AB} = \iint_S (Z' - Z)\, \vec{h}_{At} \cdot \vec{h}'_{Bt}\, ds \tag{3}$$

where $\vec{h}_{At}$ and $\vec{h}'_{Bt}$ are the tangential magnetic fields due to unit currents at A and B, the latter being open circuited. The primed situation refers to the case where the second land portion S exists. We have $Z = Z_1$ and $Z' = Z_2$ and S is the surface between θ_1 and θ_2. The unprimed situation refers to the case where only land (Z) and Sea (Z_1) exists. When (3) is evaluated in elliptical co-ordinates and invoking the stationary phase-approximation one obtains,

$$F_{AB} = F(d,Z,Z_1) + \left(\frac{id}{\lambda}\right)^{\frac{1}{2}} \int_{\theta_1}^{\theta_2} \left\{\frac{Z_1 - Z_2}{\eta_o}\right\} F(r,Z,Z_1)\, F(R,Z_1,Z_2)\, d\theta \tag{4}$$

where $|\vec{h}_{At}| \propto F(r,Z,Z_1)$ and $|\vec{h}'_{Bt}| \propto F(R,Z_1,Z_2)$

$\theta_o = \mathrm{Cos}^{-1}\{(2x_1/d) - 1\}$, $\theta_2 = \mathrm{Cos}^{-1}\{(2x_2/d) - 1\}$

$\theta_1 = \mathrm{Cos}^{-1}\left[\{2(x_2 + x'_2)/d\} - 1\right]$ • $F(d,Z,Z_1)$ is given by (1).

$F(r,Z,Z_1)$ and $F(R,Z_1,Z_2)$ are also given by (1) with the replacement of the set $\{d,Z,Z_1\}$ by $\{r,Z,Z_1\}$ and $\{R,Z_1,Z_2\}$, respectively, calculation of (4) is made numerically, evaluating the integral by the Gaussian quadrature method. The procedure may be extended to a 6-section path by taking a four section path consisting of land-sea-land-sea and considering a third land section as a perturbation on the four section path. By considering further land sections in the same way referring to Fig.4 the attenuation function for an n-section path (with n even) may be found as,

$$F_{AB} = F(d,Z,Z_1,Z_2,Z_1,\ldots,Z_{n/2},Z_1) + \left(\frac{id}{\lambda}\right)^{\frac{1}{2}} \cdot \int_{\theta_1}^{\theta_2} \left\{\frac{Z_1 - Z_{n/2}}{\eta_o}\right\} F(r,Z,Z_1,Z_2,\ldots,Z_{(\frac{n-2}{2})},Z_1)\, F(R,Z_1,Z_{n/2})\, d\theta \tag{5}$$

where

$$\theta_1 = \mathrm{Cos}^{-1}\left\{\frac{2x_1}{d} - 1\right\}, \qquad \theta_2 = \mathrm{Cos}^{-1}\left\{\frac{2x_1}{d} - 1\right\}.$$

In this equation $F(R,Z_1,Z_{n/2})$ is given by eq.1, and $F(r,Z,Z_1,Z_2,\ldots,Z_{(\frac{n-2}{2})},Z_1)$ is given by an expression for F_{AB} with (n-2) sections.

It is clear that with n large, this procedure provides the solution of the original integral equation for the attenuation function and does not provide an advantageous scheme. However for n small the solution is an approximation which is numerically advantageous. It is evident that considerably longer computer time is needed in cases where $n \geq 4$ compared with the two section path case, for the calculation

of the attenuation function. Theoretical and experimental investigations made by King and Maley [4] have revealed that these formulas developed for perpendicular incidence can be used for oblique incidence to the land-sea boundary up to about 70° from the normal. Consequently in the calculations presented Eq.(5) is used, with flat ground approximation. Once the attenuation function is computed the vertical electric field can be calculated from

$$E_A = -i \frac{L_A I_A}{\lambda} \cdot \eta_o \frac{e^{-ikd}}{d} \cdot F \qquad (6)$$

where L_A is the effective height of the transmitter antenna, I_A is the antenna current and F is the attenuation function.

When the propagation path involves inhomogeneities as well as an irregular terrain an integral equation solution is called for. Hufford in his classic paper [8] developed an integral equation for predicting the field strength of a radio wave over irregular terrain. A numerically feasible way to calculate the field strengths over a realistic smoothly varying, inhomogeneous terrain has been developed by Ott and Berry [6],[9]. A computer program based on the integral equation, known as PROGRAM WAGNER, had been tested previously for various irregular terrains and the numerical results were compared with measured values. PROGRAM WAGNER has been implemented in our computer facility IBM 370/145 and used for the paths presented in this work.

3. NUMERICAL RESULTS

In the present work a groundwave propagation study in the Marmara and Black-Sea region of Turkey is made in order to assess the performance of PTT's MF coastal maritime communication systems from the propagation point of view. In Fig.1, the region of interest and the location of the station are indicated. To the West of Istanbul (Çatalca Plain) where the station is located, the ground is mostly flat with small hills up to about 200 meters. The ground in this region may be assumed to be moderately wet. The other characteristics of the terrain in the Marmara region are: the existence of Marmara Island about 670 meters high, Kapıdağ Peninsula about 780 meters high, Gemlik Peninsula about 900 meters high, Istanbul-İzmit path almost flat with hills about 400 meters high near İzmit. To the south of the Dardanelles is placed the Biga peninsula where there are hills up to about 1700 meters for some propagation paths. In general the Marmara region has a climate which is a mixture of mediterranean and temperate climates, the ground in this region is moderately wet most of the year. Marmara and Aegean Seas are moderately salty while Black-Sea is considerably less salty.

We are interested in the attenuation factor in the sea sections of the paths, with a maximum total path length of about 400 km. Under these conditions flat ground modelling of the paths seems to be sufficient. Here we shall present the result of computations for the attenuation factor in various propagation paths indicated in Fig.1. For two of the paths with a second land portion, the flat-ground and the irregular-ground (i.e. those obtained by PROGRAM WAGNER) results will be presented. All the numerical results are for f=500 kHz (λ =600 m).

a) Two-section flat-ground paths

For the Black-Sea region near İstanbul we have chosen three paths for which the land portion is assumed to have $\varepsilon_r = 15$, $\sigma = 0.008$ mho/m and the sea has $\varepsilon_r = 80$ and $\sigma = 3$ S/m. x_1, the distance of the transmitter to the coast for the three-paths, are $x_1 = 15$ km, 20 km, and 35 km, respectively The results are shown in Fig.5.

For the Marmara-Sea which is more salty than the Black-Sea we shall assume $\varepsilon_r = 80$ and $\sigma = 4$ mho/m. We have chosen four paths described by the sets 1: $\{x_1 = 32.5$ km $\varepsilon_r = 15, \sigma = 0.01\}$, 2: $\{x_1 = 25$ km $\varepsilon_r = 15, \sigma = 0.01\}$, 3: $\{x_1 = 10$ km $\varepsilon_r = 8, \sigma = 0.002\}$ and 4: $\{x_1 = 70$ km, $\varepsilon_r = 15, \sigma = 0.008\}$. The results of the computations are shown in Fig.6.

b) Four-section flat ground paths

We shall describe four such paths: (i) $x_1 = 25$ km, $x_2 = 110$ km, $y_2 = 15$ km (Kapıdağ) $\varepsilon_r = 15$, $\sigma = 0.01$, $\varepsilon_{r2} = 8$, $\sigma_2 = 0.002$ mho/m, (ii) $x_1 = 12.5$, $x_2 = 52.5$, $y_2 = 18$ (Gemlik Bay), $\varepsilon_r = 8$, $\sigma = 0.002$, $\varepsilon_{r2} = 8$, $\sigma_2 = 0.002$, (iii) $x_1 = 35$, $x_2 = 117.5$, $y_2 = 12.5$. (Marmara Island), $\varepsilon_r = 15$, $\sigma = 0.001$, $\varepsilon_{r2} = 8$, $\sigma_2 = 0.002$, (iv) $x_1 = 3$, $x_2 = 120$, $y_2 = 130$ (Aegean Sea path 1) $\varepsilon_r = 15$, $\sigma = 0.01$, $\varepsilon_{r2} = 10$, $\sigma_2 = 0.008$. The results of the computations for the attenuation function beyond the second land portion in the sea are presented in Fig.7.

c) Comparisons with Millington's formula, knife edge diffraction and PROGRAM WAGNER results

For two selected paths (Paths 5 and Aegean (2)) results obtained by the perturbation technique are compared with results from Millington's formula [5], knife edge diffraction formulas [10] and the integral equation solution incorporated in PROGRAM WAGNER. PROGRAM WAGNER results are obtained by calculating the flat ground and topographic ground cases. PROGRAM WAGNER is first tested by repeating several test runs reported by Ott [6]. The terrain profile is taken into consideration with an accuracy of 25 m (λ/24). The field points were taken with λ/3 intervals at coastal boundary regions or in regions of rapid terrain variations. The ground constants for the paths are taken to be the same as those for the corresponding flat ground paths, since a detailed experimentally measured ground conductivity map of Turkey is not available. The terrain profile and the numerical results for the two paths under consideration are presented in Figs. 7 and 8. Results from the flat ground perturbation technique as well as Millington's

formula and knife edge diffraction formula are superposed on these curves. It is observed that on the Sea sections of the paths flat ground results do not deviate significantly from those of the topographic cases while on the land sections the attenuation functions for the two cases differ considerably. Results from the semiempirical Millington's formula are in good agreement with the flat ground results, as may be expected from the equivalence between the two techniques in the limiting case [7]. The simple knife-edge diffraction formulas on the other hand appear capable of predicting the trend of the "Shadowing" effect behind high hills even though they have tended to be rather pessimistic.

The results for these two cases display the "focusing" of the surface wave on the lit portions of concave hills which is a characteristic phenomenon that finds an explanation in terms of "whispering gallery" type of propagation [11].

4. COMPARISONS OF MEASUREMENTS WITH COMPUTED RESULTS

A series of signal strength measurements were made by the TRT (Turkish Radio and Television) to investigate the coverage area of its 300 kW broadcast transmitter in Trabzon operating at a frequency of 954 kHz. The expected coverage area situated in the northeastern corner of Turkey is a particularly mountainous region with peaks frequently higher than 3000 m. The severity of the terrain thus makes the flat earth approximations somewhat out of place and the ability of PROGRAM WAGNER to take into account the topographic details is called for. It is worth noting here that numerous comparisons between experimental data and computations have been reported and the range of validity for PROGRAM WAGNER has been fairly well indicated in the literature [12]. With such guidelines, the propagation path across the Eastern Anatolian mountain ranges appears to present a problem whose solution may not be feasible using this algorithm. However, the path profile indicated in Fig.9 is interesting as a case study to gain a better understanding of the capacity of the algorithm and to appreciate some of the numerical difficulties. Unfortunately the measurements by the TRT were taken with a view to determine the signal strengths in the main population centres in the region rather than to provide a basis for comparison with computer models, thus limiting the significance of the comparison over a given propagation path. The basic approach in tackling this particular propagation path has been to attempt to reduce the number of integration points by making apriori estimates of the behaviour of the attenuation function based on experience rather than to follow the strict guide lines of $\lambda/3$ step size. Thus the results shown in Fig.9 have been computed with $\lambda/3$ stepsize in regions where rapid fluctuations of the attenuation function are expected but with greater stepsize in regions where more stable behaviour is likely.

In Fig.9 it is observed that the general trend of the attenuation function is predicted, with the "focusing" effect on the lit portions of the slopes, and "shadowing" on the unlit side. The error between the measured and computed values at Çayeli and Artvin are 2 dB and 20 dB respectively. The general behaviour of the attenuation function seems to indicate that the numerical instabilities are not under control, and further computational work is necassary. Nevertheless this particular run completed in two hours of CPU time on an IBM 370-138 represents the arbitrarily assigned "limit of feasibility" for the purposes of the present study. The large amount of computer time is a basic limitation of the integral equation method. However the case under study is comparable with the Santa Rita Mountains path and the Dry Lake Nevada path tackled successfully by Ott [12], and it is evident that if a sufficient number of integration points are taken, PROGRAM WAGNER will yield accurate predictions.

For comparison results of PROGRAM WAGNER with flat ground approximation, Millington formula and knife edge diffraction have been included in Fig.9. It may be observed that with these methods errors of 16 dB, 19 dB and 4.1 dB are observed respectively between computed and measured values in Artvin and errors of 3.5 dB, 9.5 dB, and 10.5 dB are found for Şavşat. (Note that the measured value of 0.02 for the attenuations function at Şavşat is not visible in Fig.9)

5. CONCLUSIONS

The studies reported here have indicated the usefulness of computer models in ground wave field strength predictions. Formulas (1), (4) and (5) are simple and numerically efficient expressions that give accurate results when terrain features do not involve high hills and the propagation path is no more than 70^{0} to the coastline.

Millington's formula is shown to be capable of giving comparable results to the perturbation technique which reduces to the same in the limiting case. It is however no easier to apply to a multi section path, than the perturbation technique with the wide availability of the computer.

Knife edge diffraction formulas, generally used for VHF and above appear to give results with a fair degree of accuracy in mountainous terrain, with remarkable simplicity.

The integral equation solution incorporated in PROGRAM WAGNER and extensively tested against measured results represents the most accurate available computer model. The penalty of large computer time requirements for the integral equation technique may however render its applications unfeasible while theoretically an accurate solution may be achievable. It is therefore thaught useful to accumulate experience in a veriety of approaches to make calculations with appropriate techniques depending on the degree of accuracy, efficiency and available computing facilities with due regard to the special features of the terrain in consideration.

REFERENCES

[1] King,R.J. and Maley,S.W., 1965, "Model Experiments on Propagation of Groundwaves Across an Abrupt Boundary at Perpendicular Incidence", Radio Science Vol.69 D., No.10, pp.1375-1381.

[2] King, R.J., et.al., 1966, "Groundwave Attenuation Along Three Section Mixed Paths", Proc. IEE, Vol.113, No.5, pp.747-751.

[3] Ott, R.H., 1979, "Theories of Groundwave Propagation Over Mixed Paths", Terrain Profiles and Contours in Electromagnetic Wave Propagation, AGARD Conf. Proc. No.269.

[4] King, R.J. and Maley, S.W., 1966, "Model Experiments on Propagation of Groundwaves Across and Abrupt Boundary at Oblique Incidence", Radio Science, Vol.1, pp.111-115.

[5] Millington, G., 1949 "Ground wave propagation over inhomogeneous smooth earth", Proc. IEE, Part III, Vol.96, pp.53-64.

[6] Ott, R.H., 1971, "A New Method of Predicting HF Groundwave Attenuation Over Inhomogeneous, Irregular Terrain", OT/ITS Research Report 7, Institute of Telecommunication Sciences, Bo.Co., U.S.A.

[7] Monteath, G.D., 1973, "Applications of the Electromagnetic Reciprocity Principle", Pergamon Press.

[8] Hufford, G.A. 1952, "An integral equation approach to the problem of wave propagation over an irregular terrain", Quarterly J.Apply. Math., 9, pp.391-404.

[9] Ott, R.H., Berry, L.A., 1970, "An alternative integral equation for propagation over inhomogeneous irregular terrain", Radio Science, 5, No.5, pp.767-771.

[10] Assis, M.S. DE, 1971, "A simplified solution to the problem of knife edge diffraction over rounded obstacles",, IEEE, Trans, AP, pp.292-295.

[11] Ott, R.H., 1975, "Analysis of ground wave propagation over irregular, inhomogeneous terrain", Electromagnetic Wave Propagation Involving Irregular Surfaces and Inhomogeneous Media, AGARD Conf. Proc., No.144.

[12] Ott, R.H., "Ground wave propagation over irregular, inhomogeneous terrain: Comparisons of calculations and measurements at frequencies from 121 kHz to 50 MHz", Terrain Profiles and Contours in Electromagnetic Wave Propagation, AGARD Conf. Proc. No.269.

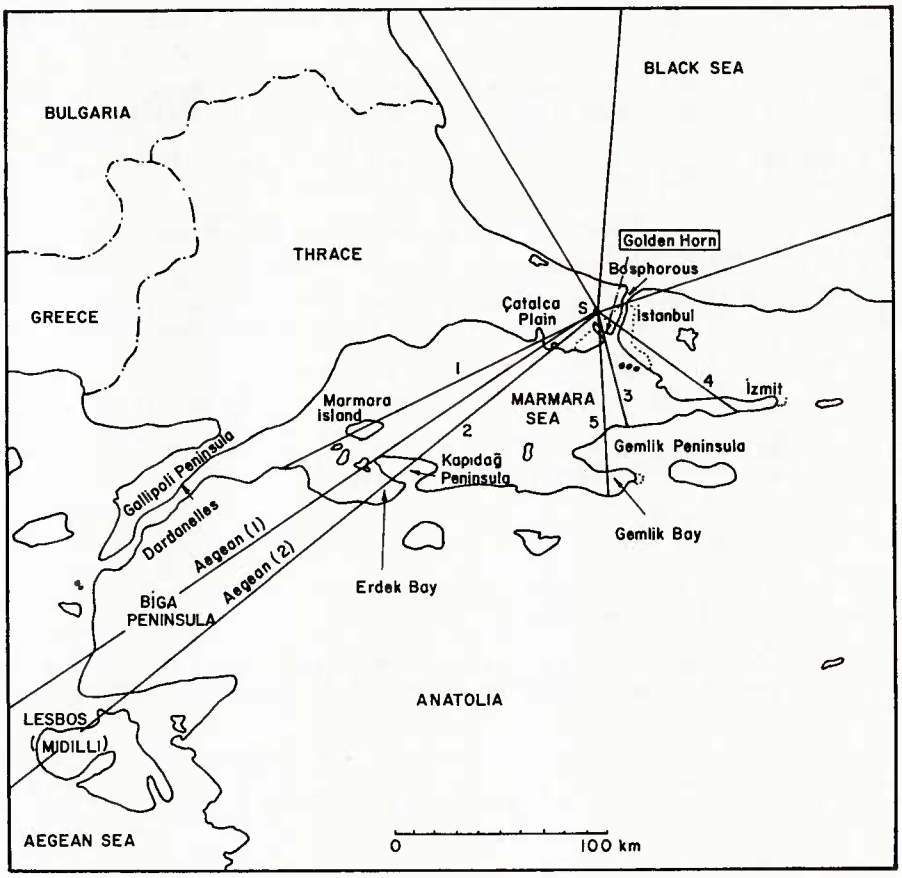

Fig.1. Geography of the Marmara region showing propagation paths.

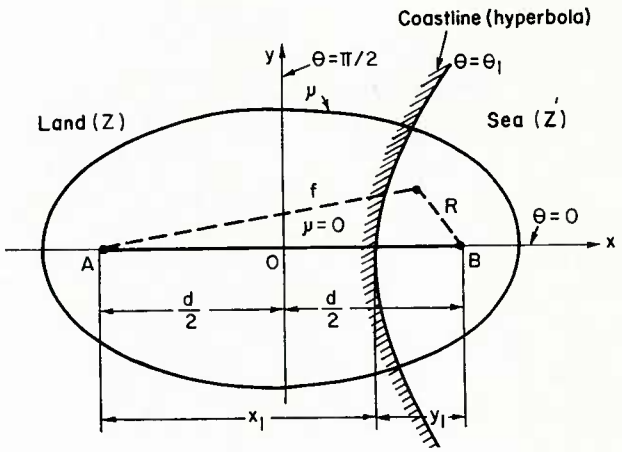

Fig.2. Transmitter receiver geometry in elliptical coordinates.

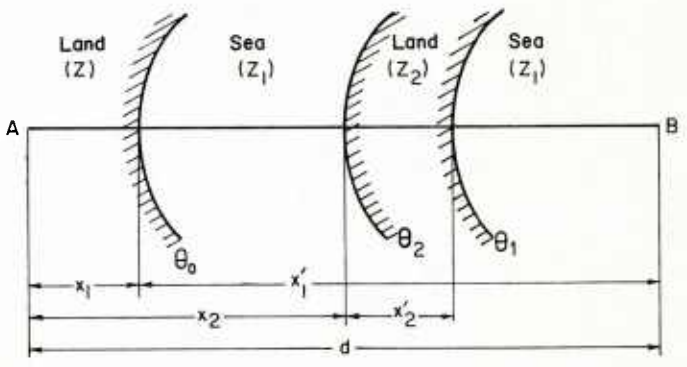

Fig.3. Geometry for a four section path. (Perturbation technique)

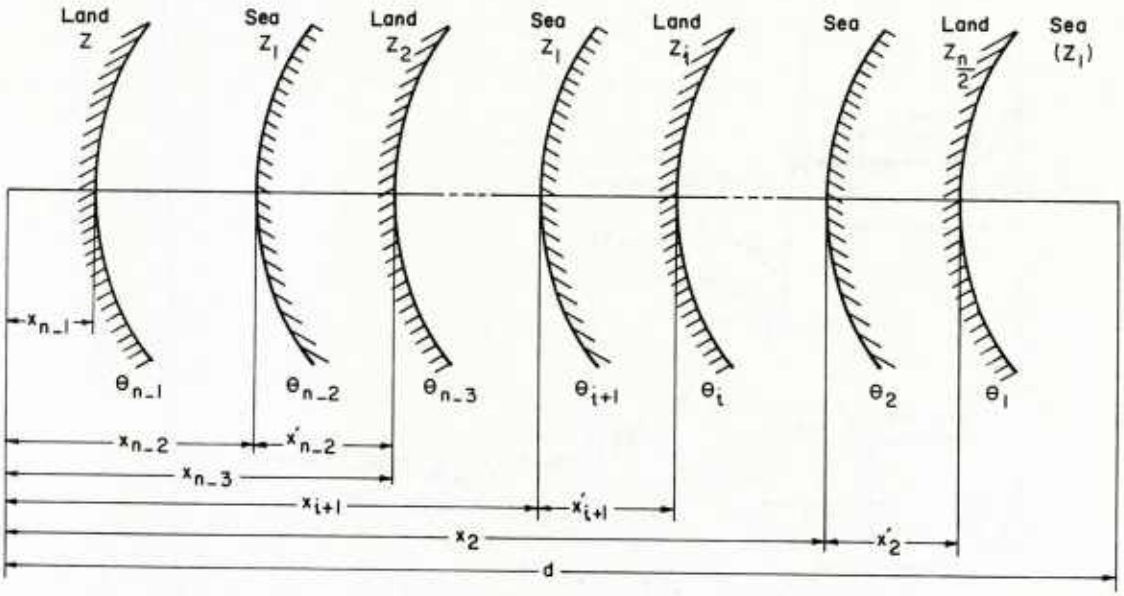

Fig.4. Geometry for an n-section path (Perturbation technique).

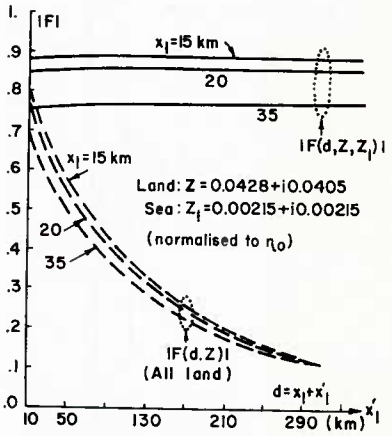

Fig.5. Two section path results for the Black Sea paths.

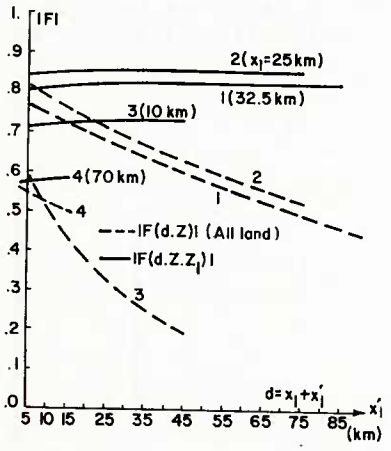

Fig.6. Two section path results for the Marmara paths.

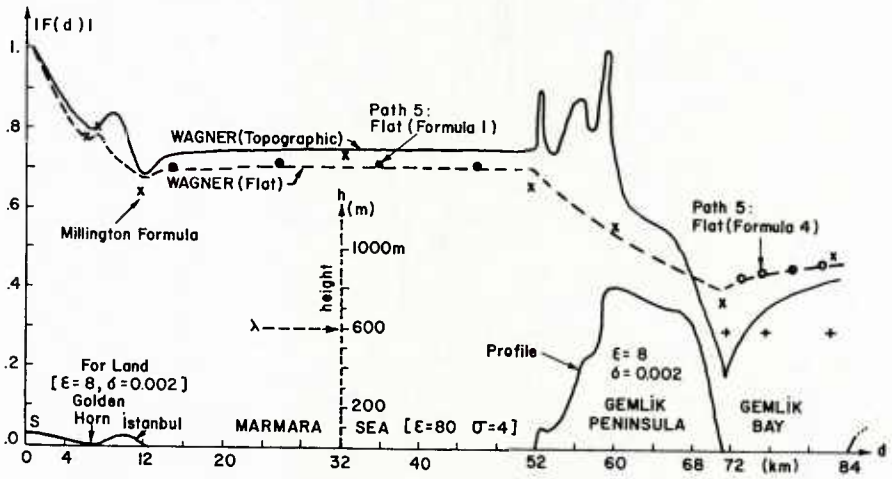

Fig.7. Gemlik path (Path 5) (x-Millington formula,+-knife edge diffraction) Inset showing path profile, v-showing knife edges considered.

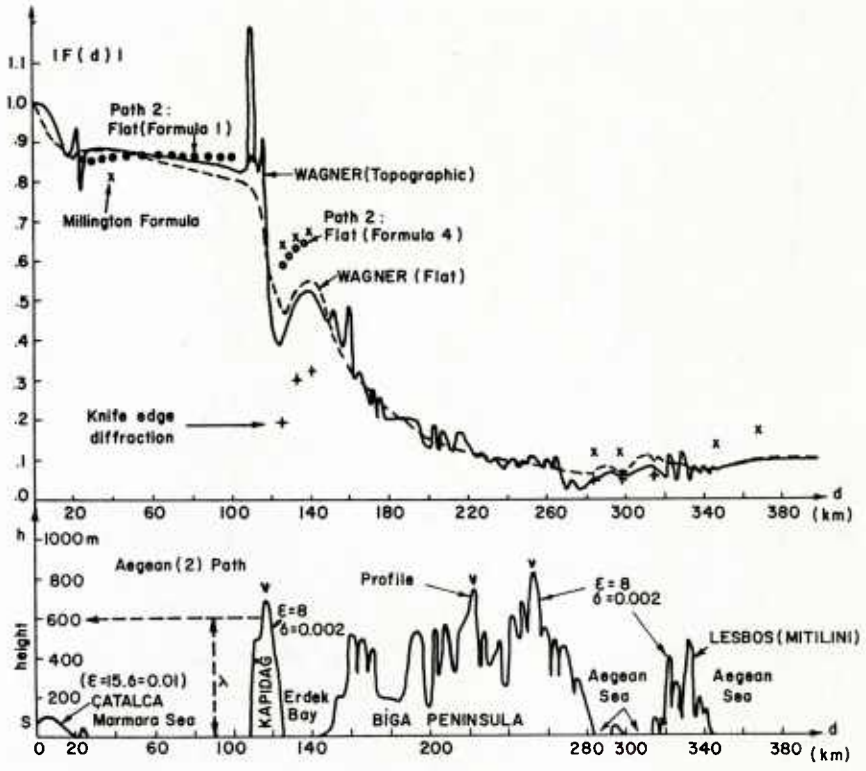

Fig.8. Kapıdağ path (Path Aegean 2). Path profile in lower portion. v indicating knife edges considered.

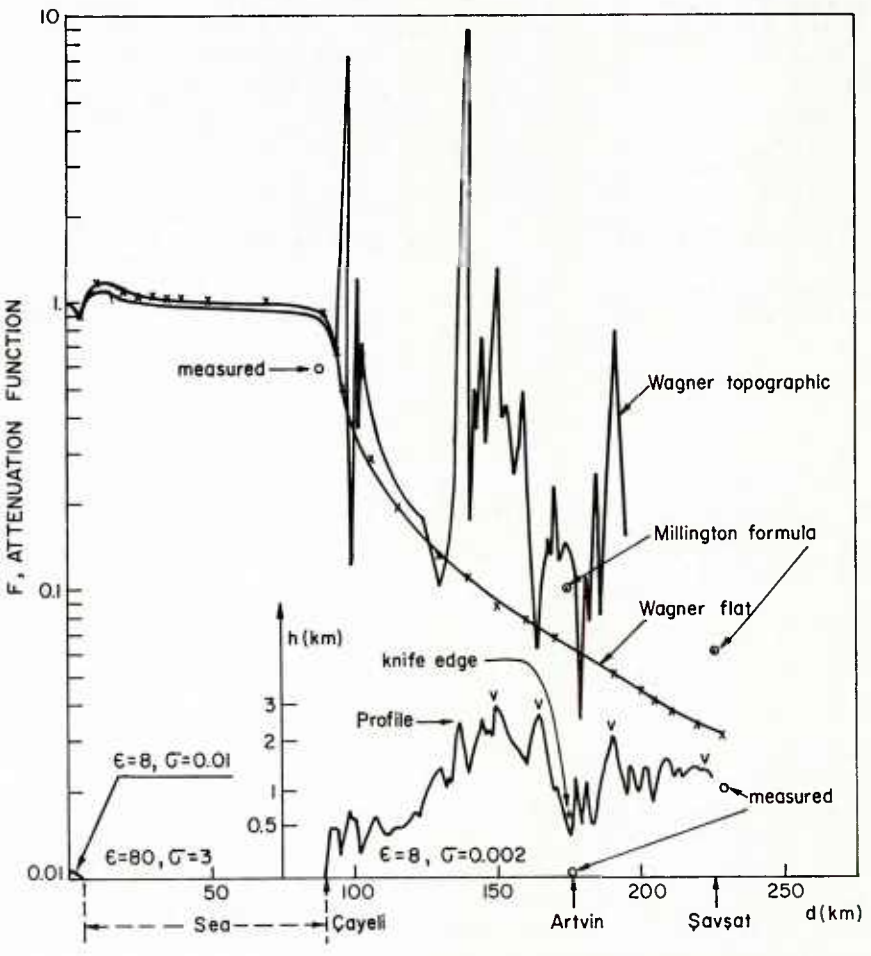

Fig.9. Trabzon-Şavşat path. Inset showing path profile, v indicating knife edges considered.

DISCUSSION

J.Arnbak, Ne

I should like to make a brief historical comment on the model adopted by Messrs Fer and Hizal for a flat multi-section ground. This model was first suggested and developed by Bremmer and described in an extensive paper in Physica (1955) in English. Some 10 years later, similar results were published in the US by King et al., and these results are the basis of your (and many other) publications. Professor Bremmer is much too modest to insist on being the first to develop the multi-section ground model. To my knowledge, he has only once – giving an invited survey paper at the AGARD EPP meeting in the Hague in 1974 – hinted at this. However, in the special issue of Radio Science published in 1980 in order to pay tribute to Professor Bremmer, his early work was recorded as an inspiration for subsequent modelling of multiple ground sections in propagation studies.

Author's Reply

I must say that I am indeed sorry for being unaware of the historical background relating to the origins of our work, and that I appreciate your comments with gratitude. Thank you.

H.J.Albrecht, Ge

It may be suggested that the agreement between measured and theoretical results, may be improved by maintaining the natural variability of ground parameters, as, e.g., for the two Aegean paths (1) and (2). Appropriate relationships have been published in the past; they may readily replace the rather idealised, constant ground parameters.

Author's Reply

This type of modification in the model is not possible in the present version of our program but I must say we intend to work along this valuable suggestion. However, due to unavailability of data we have difficulties in knowing the actual ground constants along the propagation path. Thus we must also consider that an important source of errors is lack of measured information on ground conductivity. Thank you.

L.W.Barclay, UK

The majority of this paper is a valuable comparison of different theoretical prediction methods. The measured results shown in Figure 9 are for very difficult terrain involving high mountains and steep gradients. I hope it will be possible for Dr Fer to obtain more experimental results in the future so that it will be possible to establish the merits of the various methods in more moderate circumstances.

Author's Reply

We are planning to undertake a new series of measurements over sea in the near future. We are also in possession of another set of measurements for Western Turkey where the terrain is not as severe. I do hope that comparisons with these measurements will enhance our understanding of the strengths and weaknesses of the models. However, I would like to mention that we consider that reliable data collected by other workers in other countries may also be necessary and useful to test the models described here. Thank you.

A COMPUTATIONAL MODEL FOR MULTIPLE KNIFE-EDGE DIFFRACTION

L.E. Vogler and P.M. McManamon
Institute for Telecommunication Sciences
National Telecommunications and Information Administration
U.S. Department of Commerce
325 Broadway
Boulder, Colorado 80303, USA

SUMMARY

Interference and frequency-sharing studies involving terrestrial communication networks and between terrestrial and satellite earth-stations require calculations of tropospheric radio propagation loss to the horizon and beyond.

The modeling of terrain features has been limited by the difficulties in applying knife-edge diffraction theories to actual path profiles. Previous exact theory accounted for, at most, two knife-edges on a path. In this paper the derivation of a multiple knife-edge attenuation function is described. This exact multiple integral is then transformed into a series suitable for numerical evaluation. The series solution has been implemented as a computer program capable of calculating the attenuation over a path consisting of up to ten knife-edges.

A comparison of theoretical attenuation calculations with observed measurements is presented for a 15-km path containing 5 knife-edges. The significance of atmospheric refractivity on multiple knife-edge diffraction is discussed, and a means of using this to provide information about the statistical distribution of propagation loss over specific paths is suggested.

1. INTRODUCTION

Sharing of the same frequency allocation by microwave radio links and satellite communication earth stations usually involves consideration of radio paths near line-of-sight limits and beyond. The terrain profiles for such paths are often very irregular, since these particular paths are not intended for communications but result from unrelated radio station site locations. These paths often present complex patterns of obstacles due to terrain, and in some cases, the terrain obstacles may have been favored for site-shielding benefits. It is usually necessary to estimate the path loss along such complex paths to determine if sharing criteria can be satisfied. Fresnel-zone line-of-sight models are not appropriate for this purpose. Since interference signal levels at potential victim receiver sites must be rather low, path losses must be carefully calculated.

Obstacles often can be treated as approximately equivalent to knife-edge obstacles, especially at shorter wavelengths. Unless the path contains large portions of calm water, the terrain features of an actual path are very seldom smooth, rounded obstacles at microwave frequencies.

Single knife-edge diffraction theory has been found to give good agreement with observed measurements of propagation over paths consisting of essentially one isolated hill (Kirby et al., 1955). Similarly, a double knife-edge theory has been developed and shows excellent agreement with recent test measurements (Ott, 1979). Multiple knife-edge theory for more than two knife-edges has not been available up to now, although recently suggested approximations have been compared with observed data (Meeks and Reed, 1981).

It is the purpose of this paper to present an exact expression for the multiple knife-edge (MKE) attenuation function. This equation, in the form of a multiple integral, has been transformed into a series which is amenable to computer implementation. The implementation has been partially verified by comparing its results with known values.

This work uses some basic results pertaining to propagation over irregular terrain obtained by Furutsu (1963). The expression from which the multiple knife-edge attenuation function was derived is a generalized residue series for the propagation of radio waves over smooth, rounded obstacles. Details of the derivation can be found in a paper by Vogler (1981).

2. THE MULTIPLE KNIFE-EDGE ATTENUATION FUNCTION

Figure 1 shows the path profile consisting of a series of rounded obstacles for which Furutsu (1963) derives the attenuation function for propagation over irregular terrain. The obstacles are characterized by radii of curvature, a_m; diffraction angles, θ_m; electromagnetic parameters, q_m; and separation distances, r_m. The quantity q_m is a function of the radius and electrical ground constants of the m^{th} obstacle, and the wavelength λ and polarization of the wave.

The attenuation of field strength relative to free-space, A, over a total path distance, r_T, for a path having N obstacles is given by

Rice, P.L., A.G. Longley, K.A. Norton, and A.P. Barsis (1967), Transmission loss predictions for tropospheric communication circuits, Vol. 1, NBS Tech. Note 101 (revised), U.S. Dept. of Commerce, NTIS Access. No. AD687-820.

Vogler, L.E. (1981), The attenuation of electromagnetic waves by multiple knife-edge diffraction, NTIA Report 81-86, National Telecommunications and Information Administration, Boulder, CO 80303, NTIS Access. No. PB82-139239.

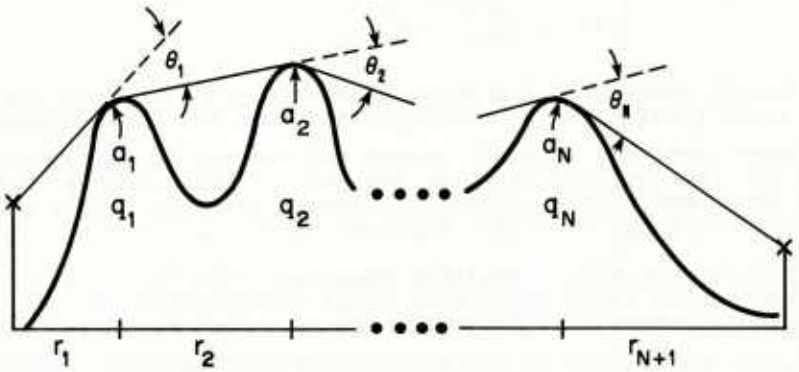

Figure 1. Representative path profile and geometry for equation (1).

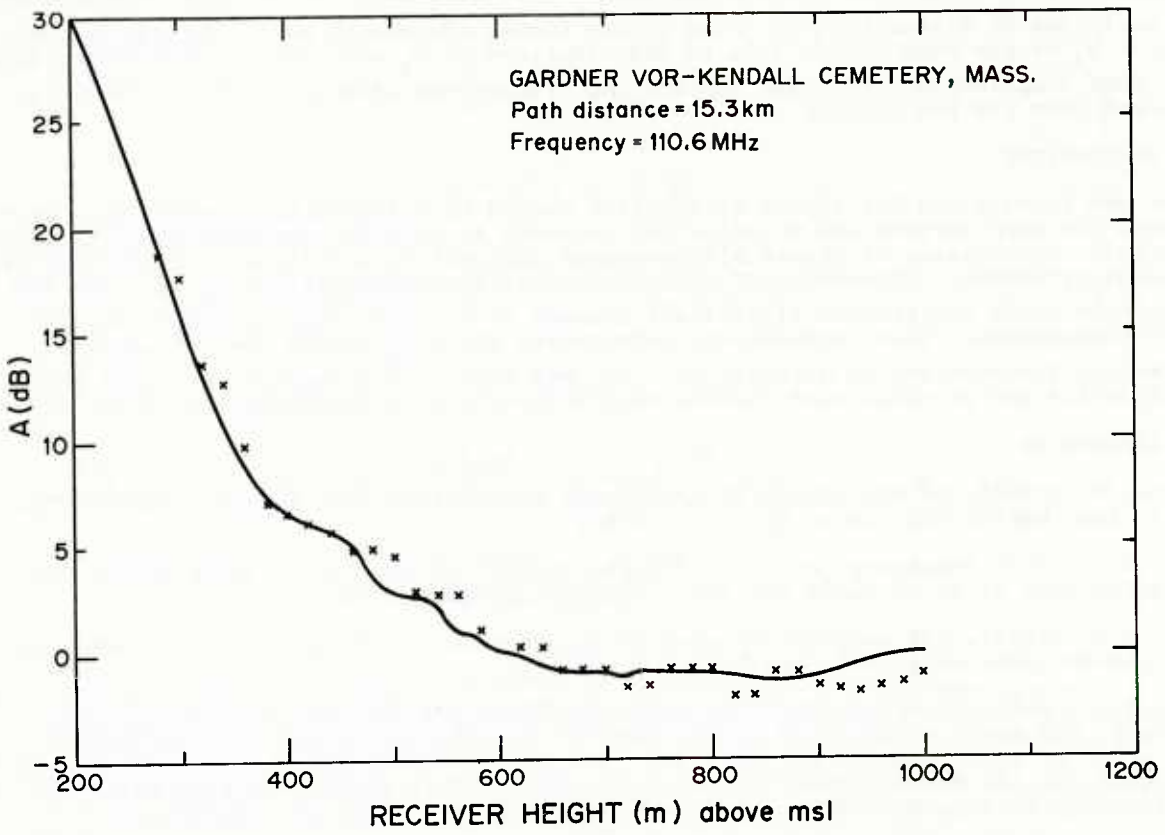

Figure 2. Comparisons of theoretical (solid line) and measured data (points) diffraction loss for a 5 knife-edge path. Measured data from Meeks (1982).

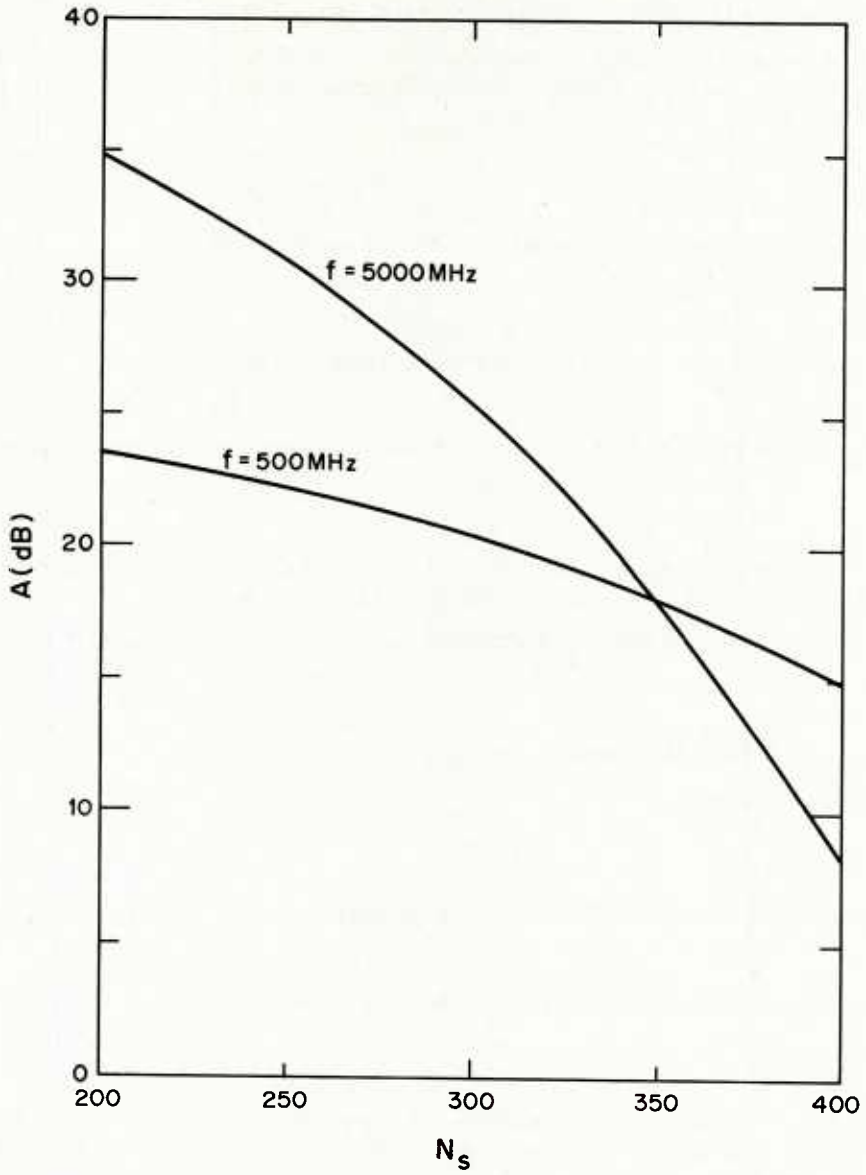

Figure 3. Diffraction loss in dB versus surface refractivity, N_s, for 80-km path on the earth's surface with 7 knife-edges.

DISCUSSION

M.Y. van der Scheur, Ne

(1) There are several approximation methods which estimate the MKE diffraction situation by a sequence of single knife edge diffractions (e.g. Millington/Eppstein-Peterson, . . .). Do you have any information concerning the differences in the results between your method and these approximations?

(2) Because the allocation of knife edges in a somewhat complicated terrain profile is a rather critical phase, it is interesting to examine the terrain profile from which the results from Figure 2 have been derived. Can you show us the profile?

Author's Reply

(1) Comparisons have not been made yet.

(2) We have the profile but I did not bring it with me. We will send you a copy.

D.Davidson, US

What assumptions are made in the model about transverse dimensions of the knife edges?

Author's Reply

The knife-edges are assumed to be perfectly absorbing. The usual semi-infinite half plane is assumed.

K.A.Hughes, UK

(1) It would be interesting to compare results from your model with those using Deygout's method which is usually reckoned as one of the most accurate for multiple knife-edge paths.

(2) Have you noticed whether the accuracy of your method is dependent on the number of knife-edges treated on the path?

Author's Reply

(1) We hope to compare our method with that of Deygout as well as others.

(2) This is described in our report.

S.Segner, US

What is the effect of foliage on knife edge? Have your measurements included modelling for foliage?

Author's Reply

The paper has not considered foliage, but has concentrated only on obstacles.

G.H.Hagn, US

In response to Mr Segner's question about propagation over wooded hills or mountain ridges on frequencies above 1 GHz, Mr L.G.Sturgill of Atlantic Research Corp found that scalar knife edge diffraction provided a good fit to his Thailand data on frequencies between 1 and 10 GHz. Prof. A.H.LaGrone, University of Texas (Austin), has also obtained similar results; however, he noted that the height of the equivalent knife-edge required to fit that data was a function of frequency below about 1 GHz.

On paths involving multiple ridges, there can be considerable energy reaching the receiver by non great-circle paths. This complicates the interpretation of the measured and predicted results. Perhaps scale models can provide a more controlled check of your predictions. Have you considered the use of scale models? Do you have any comment on non-great-circle propagation in terrain rough enough to provide paths over multiple ridges and on the applicability of your model in such cases?

Author's Reply

The paper considers multiple knife edge diffraction. Scale models are not a subject considered in the paper. The MKE algorithm can easily be applied to non-great-circle paths as well as great-circle paths.

R.Larsen, UK

Some comments to follow the previous questions about frequency and radius of curvature. I wonder if you are aware of the laboratory scale-modelling experiments carried out by Ken Hacking of the BBC? His results demonstrated that diffraction over rounded hills may depend on both the radius of curvature of the crest of the hill and also on the roughness of the surface. I note that a curve on one of your graphs is for a frequency of 5 GHz. Our own measurements and calculations of diffracted signals at this frequency suggested that radius of curvature and

surface roughness effects were very important for the situations that we studied. This makes me wonder whether the knife-edge approximation that you have used will be of much value at such frequencies.

Author's Reply

These are excellent points. The application of interest in our work involved terrain features which were clearly sharp knife-edge like obstacles. Hence, our interest in a method of calculation. Rounded obstacles still present a computational challenge and, of course, the radius of curvature relative to the wavelength is quite important. We believe the MKE algorithm is useful but only for terrain profiles which are clearly knife-edge in the view of a skilled analyst.

VHF/UHF PROPAGATION STUDIES ON LONG OVER THE HORIZON SALT WATER RADIO PATHS

Richard E. Grantham, M. Sc., P. Eng. (VE1AI)
Maritime Telegraph and Telephone Company Ltd.
P.O. Box 880
Halifax, N.S., Canada

Dr. W.P. Lonc, S.J. (VE1SMU)
Professor - Physics Department
Saint Mary's University
Halifax, N.S., Canada

SUMMARY

Received Signal Levels have been monitored and recorded over a number of long range (200 KM) salt water radio paths for the past year and a half. Preliminary anlysis of the data reveals that mean signal levels received are higher than anticipated and that a usable path can be established with 1KW ERP levels.

The propagation is characterized by short deep fades and there are only rare occasions when the signal drops below usable limits for extended periods. The type of fading reported by Wickerts and Nilsson (1973) has been observed.

A strong seasonal effect has been recorded. Path reliability approaches 100% during the summer and as low as 50% during the winter.

The fast fading effect can be reduced significantly with space diversity reception and the reliability could exceed 95% with simple diversity arrangements. Space and frequency diversity, if required, would offer near 98% reliability for voice communications.

Circular polarization appears to suffer less from fast fades than linear polarization and observations are continuing in this area.

The differences in performance between UHF (400) and VHF (140) are not pronounced. Certainly not to the degree as observed over land paths.

This paper outlines the nature of both short term and long term path tests being conducted, and describes the preliminary observations based on initial analysis of the data collected.

1. INTRODUCTION

Until recently the residents and staff of Sable Island have not had reliable communications services. One HF Teletype circuit and one MF marine telephone circuit were used to provide both data and voice communication services to and from the Island. These services were not of the quality or reliability required to serve the Island and proved to be inadequate with the increase in off-shore oil exploration in the Sable Island region.

Maritime Telegraph and Telephone Company Limited (MT&T) recognized the need to offer its services to the Sable Island area and has since become the prime provider of communications services to this region.

Sable Island is located in the Atlantic Ocean off the eastern coast of Canada. The island is approximately 200 KM east of the coast of the province of Nova Scotia. (Fig 1)

The Island is a crescent shaped sand bar some 20 KM long and less than 1 KM wide at the widest part. There is a weather station and an upper air station maintained on the Island which is staffed by employees of the Atmospheric Environment Services (AES) branch of the Canadian Government. The Island has become more prominent recently as it is located in an area of increased oil and gas exploration. The exploration results have been positive and activity in the region is steadily increasing.

Our initial investigation to provide service to the area was to attempt the establishment of a VHF path from the mainland to Sable Island - a distance of approximately 200 KM.

Normal sources of information used by MT&T for path calculations, such as Bullington and Okamara, appeared to be somewhat lacking in their treatment of long over-the-horizon salt water paths. This lead us to conduct our own investigation through actual testing. Initial results from a 4 day test, in November 1979, encouraged us to establish a permanent installation in December of 1980. It should be noted that cost was a significant factor and circuit requirements in 1980 were minimal. VHF spectrum assignment availability seemed sufficient to meet initial demand.

The initial short term results yielded signal levels in excess of what was anticipated and it was decided to record the signal level continuously to observe and study the long term performance of VHF (and later UHF) radio over a 200 KM salt water path.

A request was made to the Department of Communications (DOC) of the Canadian Government for research assistance. Through this request a grant was established for Saint Mary's University (SMU) of Halifax, N.S., to assist us in the collection and analysis of data from this and similar radio paths.

2. SYSTEM DESCRIPTION

The path from Sable Island to Nova Scotia was established using standard off-the-shelf commercial grade FM radio equipment. Effective Radiated Power (ERP) levels were kept within reasonable limits (1 KW) to preclude reuse of the assigned channel, over too wide an area.

Initial VHF paths were established between Sable Island and Seaview, N.S. and between Sable Island and Halifax, N.S. Later, a second VHF site at Arichat (18 KM from Seaview) was established. Also a UHF path was established between Sable Island and Halifax and a UHF path will be established, in October /82, between Sable Island and Arichat, N.S. All radio receivers on the NS coast are equipped with chart recorders and continuous data has been recorded for 1 1/2 years.

The Nova Scotia coastline is shown in detail, in Fig. 2, at the Seaview and Arichat sites. Bearings to Sable Island are indicated. Figure 3 indicates the direction of bearings from Sable Island to the receiver sites on the mainland. Figure 4 shows the coastline at the Saint Mary's University site.

The equipment used on the Sable-Island Seaview link was manufactured by Canadian Motorola and consists of their standard MICOR, 100 watt, continuous duty, duplex base stations. The antennas consist of a pair of phased 6 element yagi antennas, manufactured by Sinclair Radio Labs of Canada. The ERP for this path was established at 1100 watts. The path loss, according to Bullington, was calculated as 173dB and recevied signal estimated at 0.3 microvolts.

All antennas have an unobstructed view of the horizon.

3. PATH OBSERVATIONS

Received signal levels are much higher than anticipated. Signal levels of 10 microvolts or more are common. There are periods of sustained high level received signal and also long periods during which the received signal level suffers from rapid deep fades. There are only very rare instances when the signal suffers a sustained fade (below 0.2 Microvolts) for a long period (minutes to hours).

As reported by Wickerts and Nilsson at AGARD in 1973 (Wickerts and Nilsson et al 8), received signals across or along over-water radio paths were divided into three different types - A, B and C. Signal A is characterized by a low mean signal level with rapid superimposed fading. Signal type B has a higher mean level with less rapid fading but deeper minima than signal type A. Signal type C is a stable very high signal, which sometimes has deep fading minima of short duration.

For the duration of our monitoring period we have observed similar types of signals and Fig 5 is a good representation of this observation. This data is from December 24, 1980 and in one day it can be noted that all three types of signals were received. From 0001 hours local time, December 24, to 0800 hours of the same day, signal type A (low mean, very rapid fades) was received. From 0800 hours to 1800 hours, signal type C (high signal level, a few deep fades) was received; and from 1800 hours to 2200 hours, Signal type B (higher mean than A with slower fading, deeper minima) was received.

There are long periods during the winter months where signal types A and B persisted with occasional periods of type C signal being received. During the warmer month, however B and C type signals dominate, with only very rare occurances of type A being recorded.

No attempt is being made here to explain the mechanisms producing each type of received signal. It is interesting to note however that similar results were observed and that further study may be beneficial.

It should be noted that the speed of the chart recorder was very slow. Only fades greater than one half second were recorded, and more than one fade per minute produced a solid band trace on the chart recordings.

3.1 Propagation Statistics for Sable to Seaview - 142.605 MHz, vertically polarized.

The Received Signal level for the VHF telephone link from Sable Island to Seaview, on 142.605 MHz, (vertical polarization) has been recorded on a continuing basis from December 23, 1980. Each 24 hour-segment of the original chart-recording was examined visually, and an estimate made of "percentage usable time" with reference to a 0.2 microvolt datum line, as well as with reference to the fading behaviour. The estimates are qualitative, and represent what is thought to be a "worst case" interpretation of the data. The daily estimates were then averaged for each calendar month (Fig. 6). The monthly averages were then averaged for a 12-month period, resulting in approximately 75% for the "percent usable time" on this link. This is thought to be a "worst case" value.

On the basis of several experiments in which chart-recordings were made at higher feed-speeds, so that the signal's transition-rates could be observed to within 1 second, it was noted that much of the fading was short-lived, (1 second or so), suggesting the conclusion that estimates of usability, as obtained from the normal feed-speed recordings (18"/24 hrs), tended to be too pessimistic for a period of time marked by frequent fast-fading. (Signal Type A and B) Evidently, this correction factor would not apply to periods of time during which there was long-term fade of the signal below the 0.2 microvolt datum. (Severe A Type Signal)

Hence, the actual value for the "percent usable time" average over one year is thought to be perhaps as much as 10% higher, which means that the "Percent usable time" average over one year could be as high as 85%.

Note that during the summer months the reliability exceeds 90%, illustrating the shift from A type signal to C type signal during this period.

3.2 Time-occurrence of fading on the Sable to Seaview - diversity observations

Observations, with associated statistics, were made at Seaview and Arichat of the time-occurrence of fast fades for purposes of possible diversity configurations to improve the "percent usable time" on this link. Several configurations of the experiment were employed, as described below. Higher speeds were used on chart recorders to allow detailed examination of the received signal levels. Samples of a few hours each were taken.

3.2.1 Comparison of the signal at Seaview and Arichat on 142.605 MHz. This constituted a simple one-variable diversity experiment, where the geographical separation between receiver sites is 18 KM and is the only significant difference between the two sites. It was found that a significant number of fades at Seaview were not coincident with fades at Arichat, thereby suggesting that diversity could be useful.

It was observed that the drop-out time due to fading could have been reduced at Seaview by a factor of about 2, with this diversity arrangement. Recent additions to the experimental installation have included space diversity reception between Seaview and Sable Island and although no winter season data has been recorded, the reliability of the path during the summer of 1982 indicates 95% reliability.

3.2.2 Comparison of the signals at Seaview at two different antenna heights, at 142.605 Mhz, vertical polarization. In general, the experiment indicated that the difference in antenna heights was also clearly associated with some non-coincidence between fading events. It was estimated that of a total of 30 fades in the primary channel (called MTT#1), connected with the top-most antenna on the microwave tower at Seaview, only 5 fades were fully coincident with fades in the second channel (called MTT#2), connected with an antenna at the mid-point of the tower. In addition, it was estimated that perhaps another 10 fades in the MTT#1 channel were in partial coincidence with fades in the MTT#2 channel. Here again, indicating that a substantial improvement is possible even with single site space diversity.

3.2.3 Comparison of signals at Seaview at two different frequencies and two different polarization. This experiment entailed signal strength measurements for two channels:MTT#2(142.605MHZ,vert.pol.) and SMU(147.995MHZ,hor.pol.). The antennas associated with these receivers are within 2 meters of each other, at the mid-point of the tower. A cursory visual examination of the data indicated that perhaps fewer than 50% of the fades in the two channels coincided significantly. Inasmuch as this experiment is a function of at least two variables--frequency and polarization--the differences in fading behaviour cannot be persuasively ascribed to either one of the variables exclusively.

3.2.4 Comparison of signals at Seaview combining three variables: frequency, antenna height, and polarization. This experiment, combines two of the observations above. In other words, there are three signals being monitored: one on MTT#1 (142.605MHz vert.pol.), antenna on the top of the tower; one on MTT#2(142.605MHz vert. pol.), antenna at the mid-point of the tower; and one on SMU(147.995MHz, hor.pol.), antenna at the mid-point of the tower. The configuration of the experiment was determined primarily from the equipment (receivers and antennas) already in place. In general, it was observed that there was no full coincidence of fading among the three channels. In particular, of 22 fades in the MTT#1 channel, there was only one fade from the remaining channels in full coincidence with MTT#1, and perhaps 5 fades which were in partial coincidence. The observation indicates the substantial improvement that would be obtained by use of both frequency and space diversity.

Based on the short term observations of these diversity arrangements, continuing efforts are being made during the latter part of 1982 and into 1983, to record received signal levels on a number of diversity arrangements.

4. PROPAGATION STATISTICS FOR SABLE TO SEAVIEW ON 142.605HMz, VERTICALLY POLARIZED, VS SURFACE WEATHER

A preliminary attempt has been made to correlate the observed propagation on the Sable to Seaview path with the available surface meteorological or "met" data. In particular, only two features of propagation will be examined: noticeable attenuation, marked by relatively gradual transitions; and enhancements, marked by relatively sudden transitions. For example, the "data panel" (Fig. 7) for May 1 note the pronounced attenuation (gradual) during the early part of the day, taking into account the fact that the charts for Seaview and Arichat are associated with FM receivers (limiting occurs above 10 microvolts). The "data panel" for May 11, (Fig. 8) on the other hand, exhibits a sudden enhancement, again, during the early part of the day.

In attempting to correlate propagation behaviour with surface "met" data, it should be noted that the "met" data could, perhaps, be of limited significance. For example, on Sable Island, the "met" data is gathered at a point approximately 1.5km east of the beacon site, whereas the propagation path of interest is to the west and presumably depends on "met" factors in the line of the path. Similarly, for the Canso Straits area, the "met" data is obtained at Eddy Point, which is approximately 30km transverse to a line joining Sable and Seaview, and approximately 20km transverse to a line joining Sable and Arichat. For the Halifax area, the "met" data from Shearwater represents conditions approximately 2km transverse to a line joining Sable and SMU. Of the three cases, only the last one represents a relevant sampling of the surface "met" conditions along the acutal propagation path. However, even in this case, the data is less then ideal as the met date is collected near one end of the path. Therefore the surface "met" data for Sable Island may not always appear to correlate with the propagation from Sable because the propagation is presumably determined to a large extent by the "met" conditions west of the antennas; in particular, it is presumed that the conditions near the water from the Island to the horizon are the dominant factors. Hence, any discontinuity in propagation may or may not be accompanied by a discontinuity in the Sable Island "met" conditions measured, and may not necessarily exist in the exact line of the path.

With these preliminary considerations in mind, an examination of the data panels for May, June, July(part), and October, suggests that there is no clear-cut correlation between the propagation data recorded and the "met" data obtained. Occasionally, however, there is correlation, such as for June 20 (Fig 9). Here, there is a correlation between rain on Sable Island and gradual attenuation at all three receiving sites. Since there is no concomitant precipitation reported at either Eddy Point or Shearwater, then it would appear that precipitation at the beginning of the path is the significant factor.

If the sudden enhancements are examined, such as for early and later parts of June 20, there appears to be no corresponding discontinuity in the "met" data at any of the sites, except perhaps the discontinuity in "cloud amount" and "cloud ceiling" for Sable and Shearwater. However, even here, the correlation exists (perhaps) for the discontinuity in the early part of the day, but does not exist for the discontinuity towards the end of the day.

Examining the data for May 11 (fig. 8), sudden enhancements again occur: in the early part of the day for all four monitors, and the later part of the day for the 3 monitors in the Seaview-Arichat area. There is perhaps some correlation between the first enhancement and the "cloud ceiling/cloud amount" data for Sable, but similar discontinuities in "cloud ceiling/cloud amount" for Sable later in the day are not accompanied by enhancements. Regarding attenuation effects, which begin around 10AM in the Seaview/Arichat data and around 1PM or so in the Halifax data, the only precipitation reported is a light rain in the Shearwater data; there is no rain reported at either Sable Island or Eddy Point.

In general, and by way of a very tentative and approximate statement, it was observed that there is some correlation, for the four months in question, between precipitation at Sable and gradual attenuation in propogation. Regarding the sudden enhancements, however, there appears to be no correlation whatsoever. These observations are made on the basis of a cursory visual examination of the original data panels. It is again noted that the "met" data represents "surface" weather conditions only.

5. COMPARISON OF SIGNALS FROM HORIZONTALLY AND CIRCULARLY POLARIZED ANTENNAS ON SABLE AT 147.950MHz AND 147.850MHz RESPECTIVELY. The experiment was performed to enable a preliminary look at the possibility of significant differences in fading between plane (horizontal) and circular polarization on the Sable to Halifax path. It should be noted that the channel involving circular polarization consisted of one circularly polarized antenna: the one on Sable. The receiving antenna at SMU on this channel (147.850MHz) was horizontally polarized, it being assumed that this arrangement would give some indication of a difference between the two channels. It is also being assumed that the difference in frequency between the two channels is not significant for this test.

The experiment, consisting of some 20 observations, each of approximately 5 minutes duration, and these observations were made during the latter part of April and the early part of May, 1981. In general, it was observed that there was a noticeable difference between the two channels in terms of fading behaviour, and that the signal from the circularly polarized antenna on Sable had noticeably less fading associated with it than the signal from the horizontally polarized source. Continuous recording of circular polarized signals will begin in late 1982.

6. COMPARISON OF SIGNALS ON VHF AND UHF ON THE SABLE TO HALIFAX PATH. Experiments to compare VHF(147.950MHz) and UHF(431.950MHz) reception on the Sable to Halifax path have also been conducted. Horizontal polarization was used on both channels.

The experiment compared the signal strength at SMU for both channels, and represents reception at antennas located within a couple of meters of each other. In addition, some further data was obtained at various times during the winter of 1981-2; some of this data is in the form of chart recordings, and some as occasional listening tests.

In general, it has been observed that the UHF signal has been more intense and noticeably less marked by "Type A" fast fading than the VHF signal. This was especially apparent during the winter, during which time the VHF signal at SMU was not detectible, whereas the UHF signal was almost always detectible. There is a difference in antenna gains which might account for much of the difference in intensity. However, this does not account for all of the difference observed. UHF monitoring and recording of results will be increased in 1982-83 with additional paths being established and monitored over a long term.

7. CONCLUSIONS

On the basis of these observations, it is conculded that there is a marked seasonal dependence of signal strength on VHF between Sable and the Canso Straits area, going from almost 100% usability in the summer months, to perhaps 50% in the winter. A "worst case" average value for the year appears to be in the order of 75%. If account is taken of the fact that most of the fades are relatively fast, (1 second or so in duration), then the average value for the year could possibly be as high as 85%. This value is predicted on single-channel reception, i.e. without diversity.

It could be concluded that fast-fades on VHF for the Sable to Seaview/Arichat path show noticeable dependence on geographical separation, antenna height, and some combination of frequency and polarization. Hence, a multi-channel receiver system, in a diversity configuration, should show a marked decrease in fast-fading in the combined system. Reliability during the summer approaches 100%. Annual reliability could exceed 95%.

On the basis of these observations and surface weather it can be concluded that the available surface weather data shows no correlation with the propagation data, especially in reference to sudden enhancements in signal level. There could be, however, some non-insignificant correlation with precipitation (as reported for the surface), but a more detailed analysis of the "data panels" is required and is being continued. Presumably, given the relatively large geographical area, there could be precipitation events (localized) along the propagation paths which would not be observed at the weather-report sites.

In reference to possible dependence on linear polarization, the VHF data for the Sable to Canso Straits path does not exhibit any readily discernable difference. The comparison, of course, is complicated by the fact that the two MTT receivers are accessed after limiting. Hence, on the basis of the recorded data, polarization is not a major concern. It should be noted, however that the data is begin examined in such a way that short-term depolarization effects--in the order of a few seconds--would not be apparent in the course of a cursory examination of the data. Hence, depolarization could be present, but on a very short time-scale. Circular Polarization appears to offer some improvement over linear or plane polarization.

Concerning VHF compared with UHF, it could be concluded that UHF on the Sable to Halifax path is also less prone to fast-fading than is the VHF. The UHF performance appears as good as VHF and is now being recorded over a long term over two paths.

8. RECOMMEDATIONS FOR CONTINUED STUDY

1. Continue data acquisition on VHF for the Seaview, Arichat, and Halifax sites, to obtain improved statistics.
2. Undertake a more detailed analysis of the available data to obtain some quantitative indication of the correlation between discontinuities in propagation and discontinuities in surface weather.
3. Obtain upper-atmosphere data for 1981 (especially the summer) for the Sable Island area, with a view to correlating temperature inversions with sudden enhancements in propagation.
4. Perform more detailed observations on possible depolarization events on both VHF and UHF.
5. Obtain vertical-profile weather data on the west end of Sable Island to enable detailed discussion of "duct-assisted" propagation over the Sable to Nova Scotia mainland path.
6. Monitor diversity systems to determine extent of fast-fade compensation.
7. Measure time occurrences of A, B and C type signals in an attempt to correlate occurrences of each type with potential controlling mechanisms, and upper air weather correlation.

REFERENCES

1. David P. and Vogue J., "Propagation of Waves", Oxford, Pergamon Press, 1969.

2. Kerr Donald E., "Propagation of Short Radio Waves", Toronto, McGraw-Hill Book Company Inc., 1951.

3. Kirke H.L., "Calculation of Ground-Wave Field Strenght Over a Composite Land and Sea Path." Proc. Inst. Radio Engrs., 37, (1949).

4. Millington G., "Ground-Wave Propagation Over an Inhomogeneous Smooth Earth", Proc. IEEE, 96 Pt. III, (1949).

5. Millington G., "Ground-Wave Propagation Over an Inhomogeneous Smooth Earth, Part 2: Experimental Evidence' And Practical Implications", Proc. IEEE, 97 Part. III, # 48, (1950).

6. RCA, "Point-to-Point Radio Relay System 44 MHz to 13,000 MHz", RCA Service Company, 1972.

7. Sofaer E. and Stark J.W., "Tropospheric Radio Wave Propagation Over Mixed Land and Sea Paths", Proc. IEEE, 113 # 8 (1966).

8. Wickerts S. and Nilsson L., "The Occurence of Very High Field Strenghts At Beyond the Horizon Propagation Over Sea In The Frequency Range 60-5000 MHz.", AGARD Conference Proceedings, CP = 127, 14.1 to 14.15, (1973).

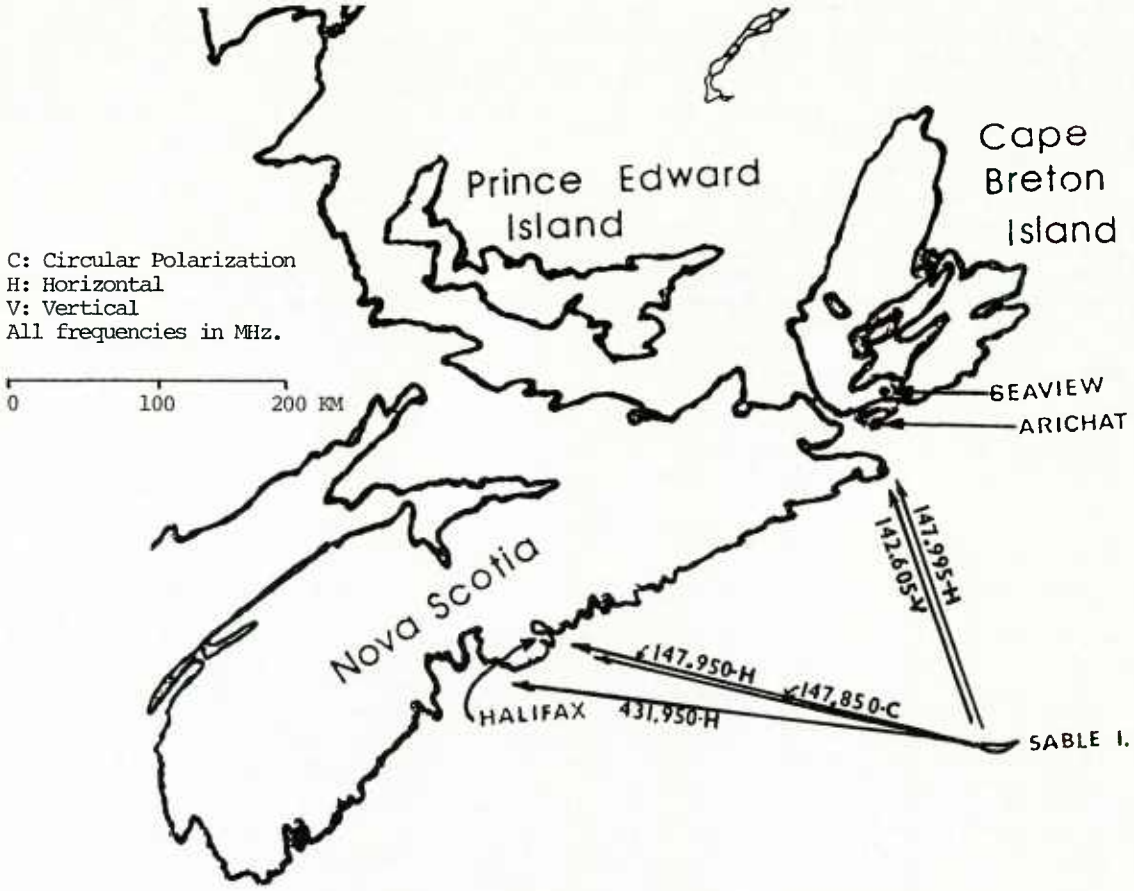

Figure 1: General coastline features and orientation of transmission paths.

Figure 2: Coast-line features of the Seaview-Arichat area, and location of antenna sites.

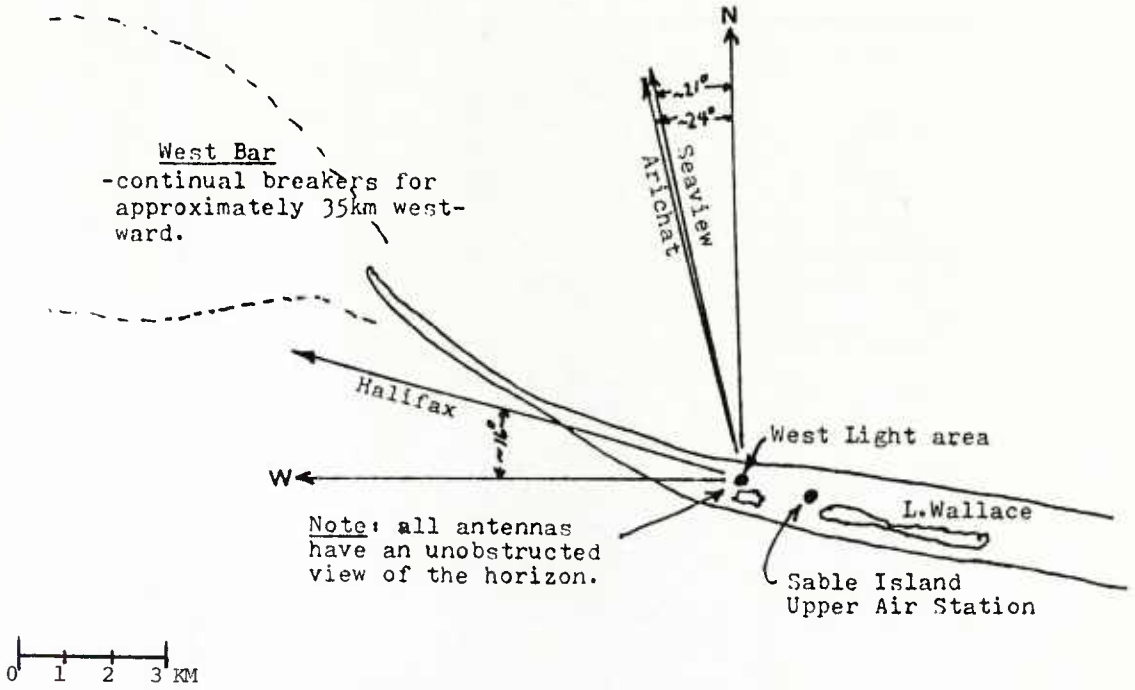

Figure 3: General features of the west end of Sable Island

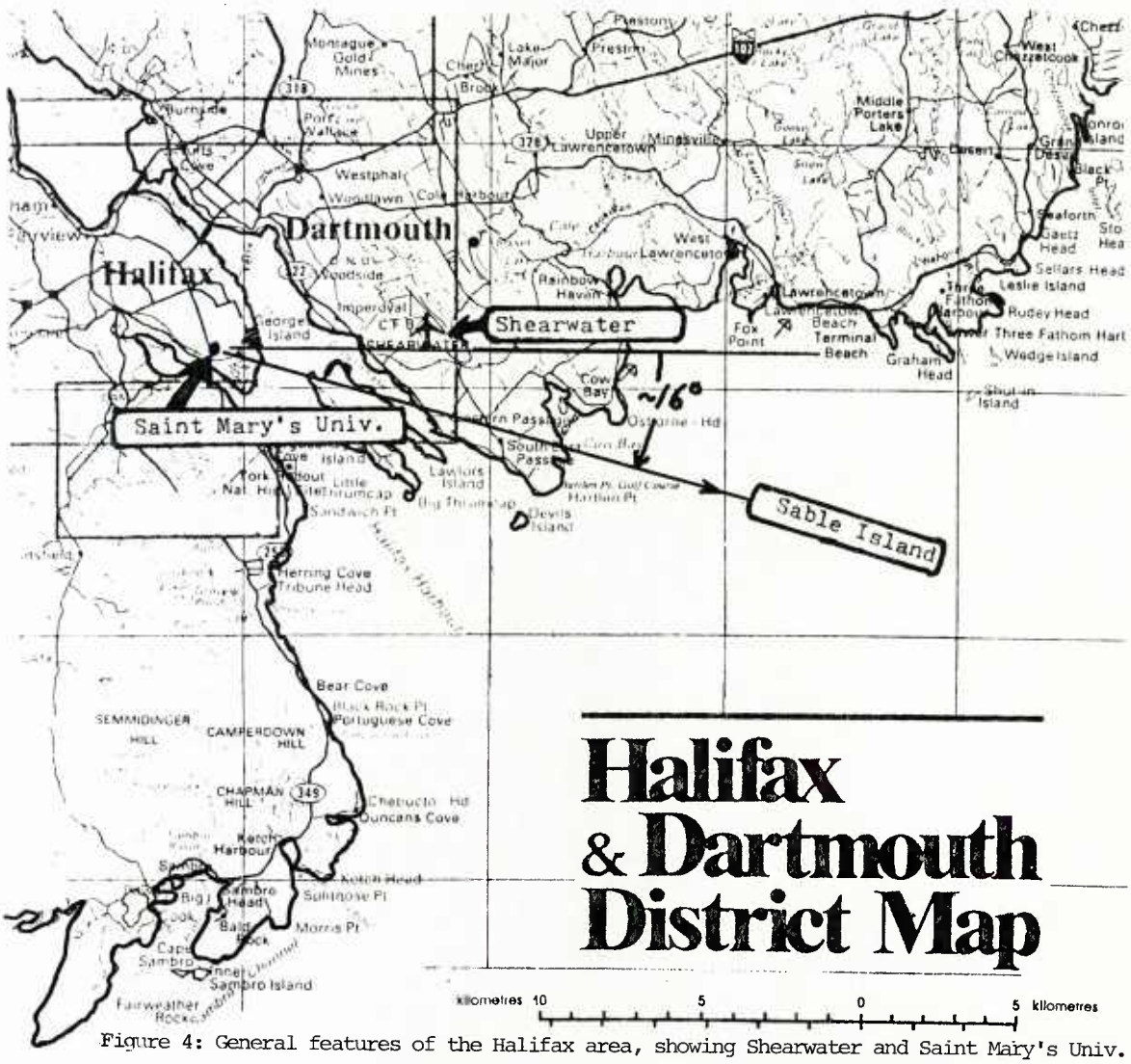

Figure 4: General features of the Halifax area, showing Shearwater and Saint Mary's Univ.

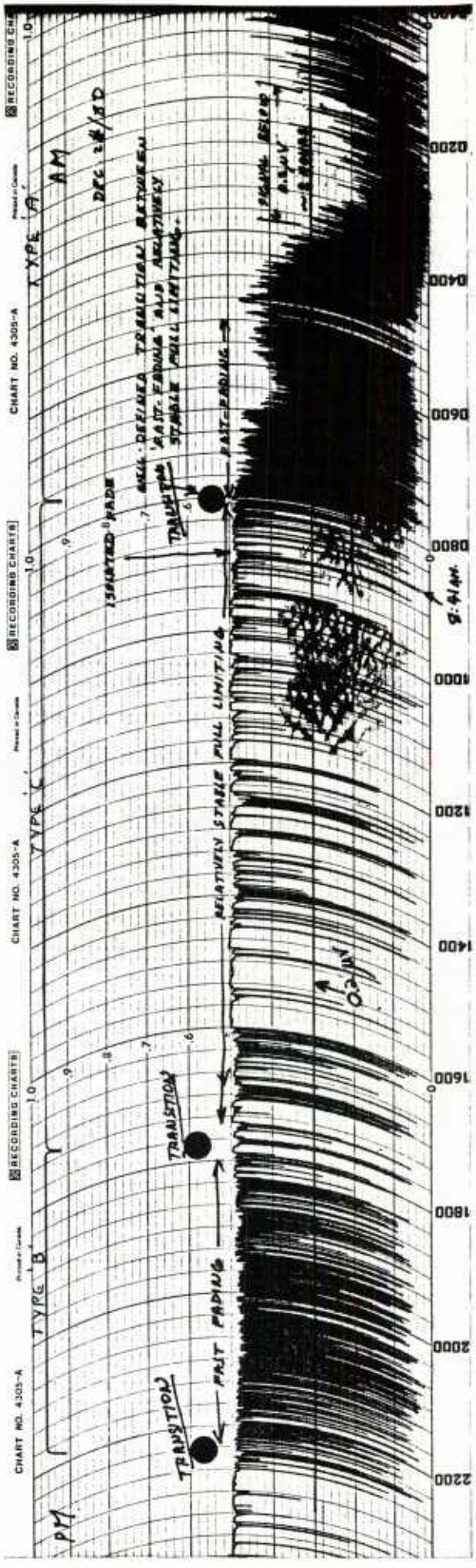

Figure 5: Received Signal Level at Seaview - 24 Dec 1980
142.605MHz (V)

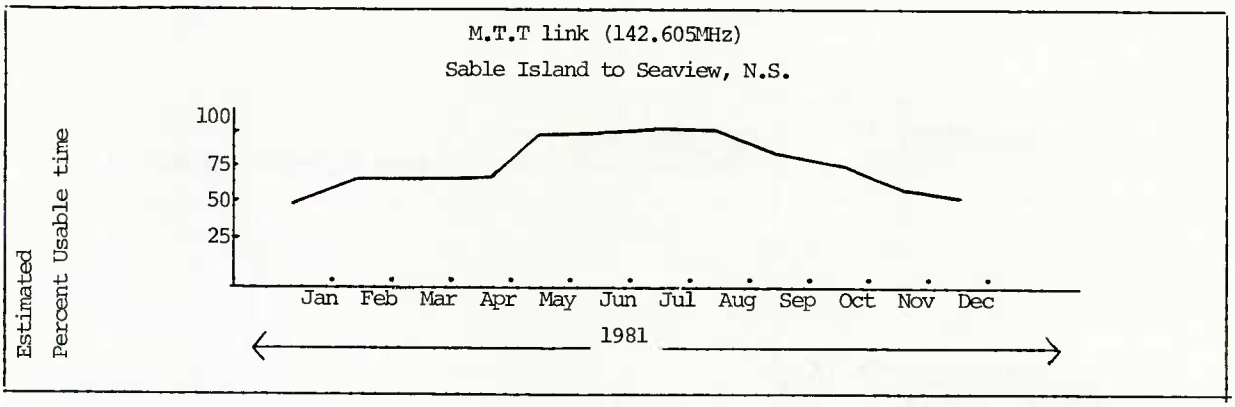

Figure 6: Monthly averages of signal strength at Seaview, as estimated from chart recordings.

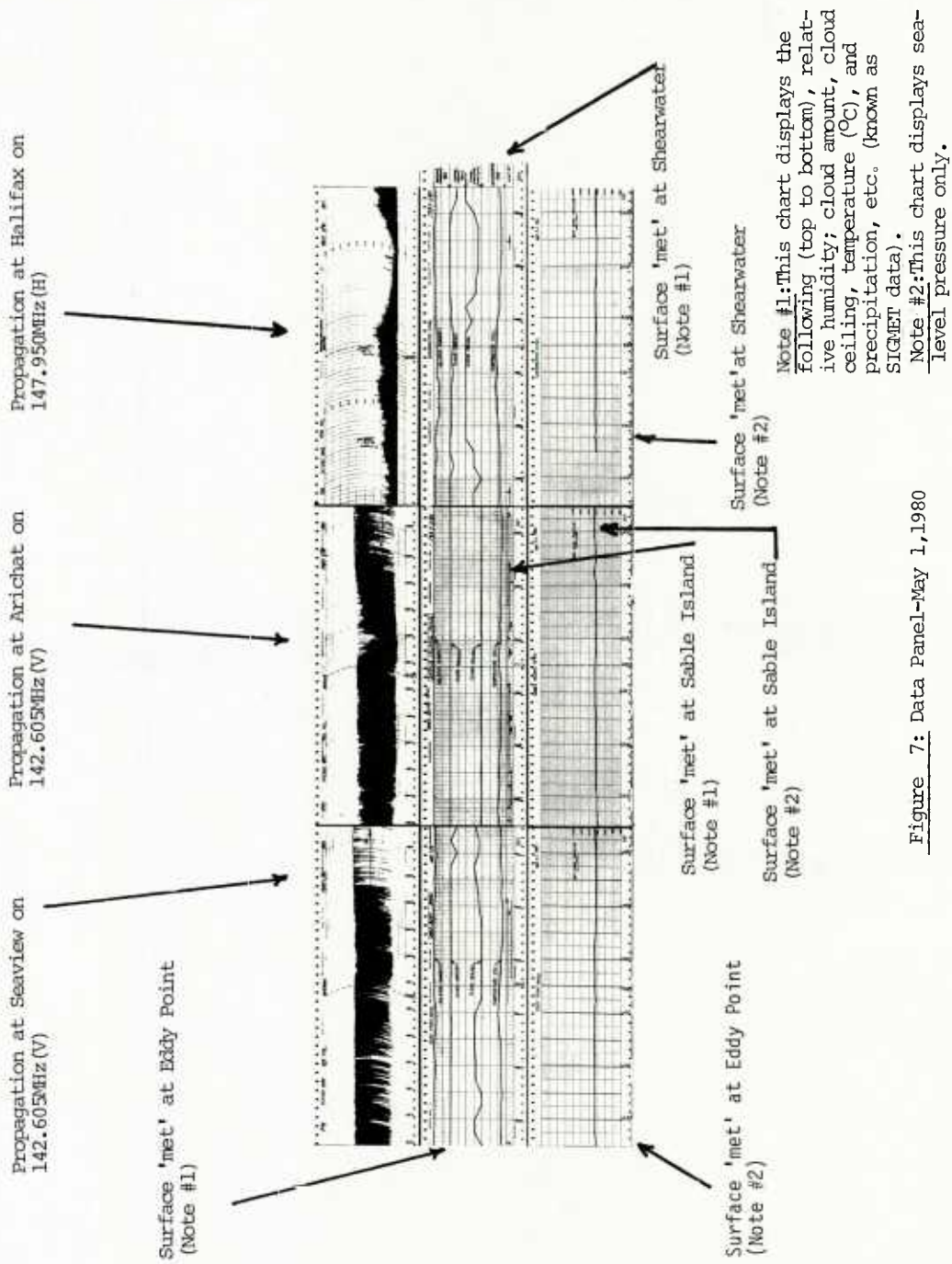

Figure 7: Data Panel-May 1,1980

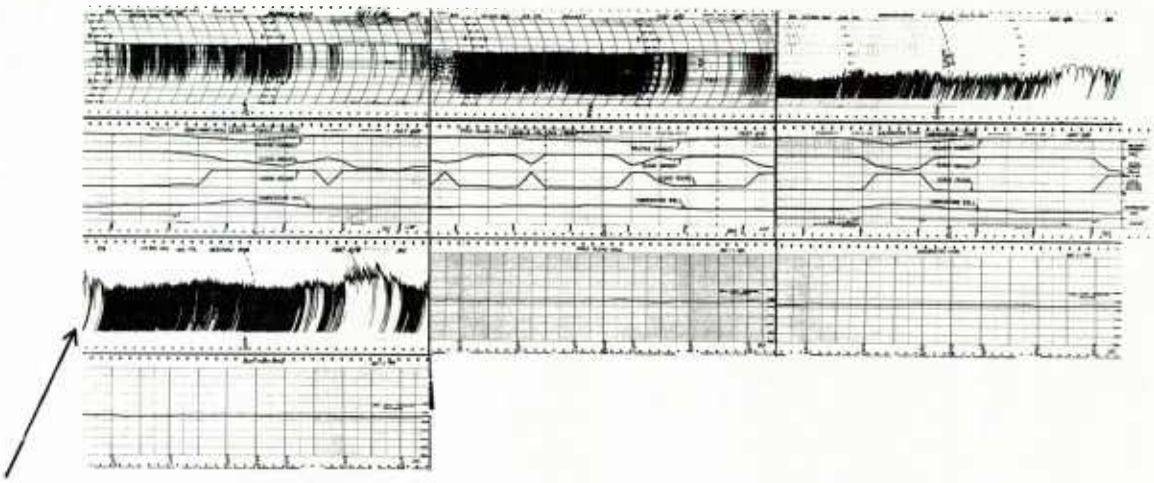

Figure 8: May 11/81 data panel

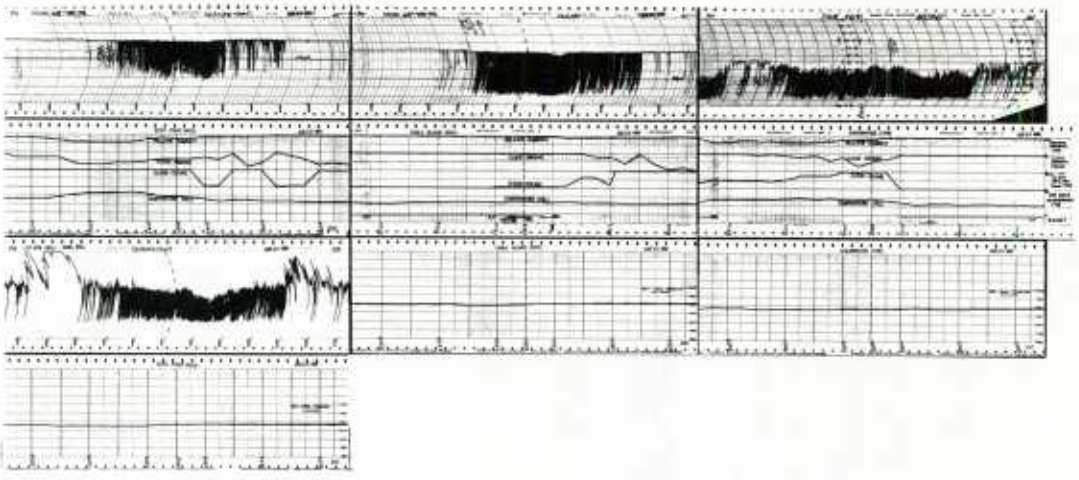

Figure 9: June 20/81 data panel

DISCUSSION

J.Arnbak, Ne

Did you correlate the signal strength with sea state and/or wind speed?

Author's Reply

Not yet. We have been looking for the cause of the sharp transitions that occur between the "types" of fading. I feel that wind speed may be of importance in its influence at the surface or near the surface in the centre of the path. We will be looking at wind speed this winter, but do not expect to correlate with the sea state until later.

J.T.Ong, UK

Could you give us details of the transmitter height? i.e. What is the value of k-factor when the path is grazing (zero clearance)?

I have sympathy for you since we have come across this problem before. The problem is one of too low a value of equivalent k-factor in the winter months, and ducting and significant variation of k-factor in the summer. A distribution of the equivalent k-factor is what is needed to obtain a reasonable estimate of the "slow fading" (i.e. the mean or median value without the fast fading). The path in question is approximately 90 km in length using low-band/highband VHF and employing 1 kw with stacked and bayed Yagis.

Author's Reply

On Sable Island the antennas at VHF are at various heights, the highest being 60 metres. At Seaview the antenna is approximately 200 metres above sea level. On the Halifax/Sable path the antennas are much lower. At UHF antennas are at 30 and 10 metres and are now switched every second with each antenna being fed in turn. The path is obviously blocked by earth curvature, since the path is 200 km. The distribution of k is unknown. However, the amount of slow fading is minimal (less than 5%).

R.Larsen, UK

Can you tell us the heights of your aerials and the scatter angles of the paths that you measured?

Author's Reply

Sable Island antenna heights vary for each of the radio paths. Sable/Seaview heights are 170 ft and 600 ft above sea level, respectively. The path length is 125 miles. I will contact you directly with additional path details and the geometry of the other paths we are monitoring.

T.B.Jones, UK

Have you correlated the times of fast fading on the VHF link with auroral activity? The local magnetometer would be a good indicator of radio aurorae in the vicinity of your circuit.

Experiments in Europe show strong auroral reflection at VHF during 16.00--24.00 hr especially at the equinoxes.

Author's Reply

No attempt has been made to correlate the fading with auroral activity. Because we are operating in a Northern climate, this might be an interesting investigation. Thank you for your suggestion.

MODELLING ON INTERFERENCE DUE TO DUCTING AT FREQUENCIES ABOVE 1 GHZ

J. Dijk and J. van Tiggelen
University of Technology
Den Dolech 2, Eindhoven
Netherlands

J. Neessen
Dr. Neher Laboratories (PTT)
St. Paulusstraat 4, Leidschendam
Netherlands

SUMMARY

In this paper a theoretical basis and the numerical tools are presented for the calculation of the fieldstrength due to ducting in beyond-the-horizon microwave links. The main aim of the paper is to contribute to the understanding of the propagation phenomena involved and to provide some physical basis for the predictive techniques to be considered for the evaluation of mutual interference between radio communication systems, operating at frequencies above 1 GHz.

1. INTRODUCTION

With the increasing demand for radio frequency bands -a natural limited resource-, it is quite certain that frequency sharing as a means of efficient utilization of frequency bands will become of increasing importance in future radio communication systems.

A dominant cause of interference originates from ducting, in particular in the frequency bands above 1 GHz. Due to certain refractive index profiles along the radio path, severe enhancements of signal level may occur at distances up to several hundreds, even thousands, of kilometers away from the transmitter. It is clear that such propagation phenomena may put severe limitations on the spatial reuse of frequency bands.

For the determination of the area, inside which harmful interference between radio communication systems may occur, co-ordination procedures are laid down in the Radio Regulations. The size of the co-ordination area depends severely on the propagation data, included in CCIR-Reports (CCIR, 1982). However the present CCIR predictive techniques on signal levels due to ducting include engineering formulae, which relation to the results from the elctromagnetic wave theory is not sufficiently clear.

It is very difficult to understand the phenomena involved from the geometrical optics. The principle reason for this is that the full wave description can not be reduced to the ray optics around the caustics, which normally occur under ducting conditions. For instance the ray optics can not sufficiently explain the frequency dependence of the fieldstrength during such conditions.

In this paper some results of theoretical work are presented, which can be used for the evaluation of the existing predictive techniques. In particular attention will be paid to the dependency of signal levels due to ducting on the frequency, path length and terminal heights.

2. THEORETICAL BASIS

Let us consider a flat earth, with the troposphere above characterized by the modified refractive index profile m(z) as sketched in fig. 1. Starting from the Maxwell-equations we can derive the scalar, source-free, Helmholtz equation:

$$\nabla^2 E + k^2 m^2(z)\, E = 0 \qquad (1)$$

with $k=2\pi/\lambda$, the wave number.

In his book 'The wave-guide mode theory of wave propagation' Budden (Budden, 1961) presents a lot of discussions on solutions of the equation above applied to propagation of waves in stratified media. From that it follows that it is useful to seek for the following solutions:

$$E_y(x,z) = \phi(z)\, e^{-ikx\cos\alpha} \qquad (2)$$

which corresponds to a horizontally polarized plane wave. Substituting equation (2) in it, equation (1) changes into:

$$\frac{d^2\phi(z)}{dz^2} + k^2\{m^2(z) - \cos^2\alpha\}\,\phi(z) = 0 \qquad (3)$$

In geometrical optics the parameter α corresponds to the grazing angle of the rays at z=0.

The preceding differential equation can only give the appropriate solutions, if the boundary conditions are known. Away from the caustics one can divide the solutions of equation (3) into an upwards and a downwards travelling wave, indicated by $\phi_u(z)$ and $\phi_d(z)$. In fact the following boundary conditions have to be considered (Hartree, 1946):

a) For $z\to\infty$ only an upwards travelling wave exists, because the transmitter is always in the neighbourhood of the earth surface:

$$\lim_{z\to\infty} \phi_d(z) = 0 \qquad (4)$$

b) For z=0 the downwards and the upwards travelling wave are related to each other by the Fresnel-reflection-coefficient of the earth surface according to:

$$\phi_u(0) = R\,\phi_d(0)$$

Assuming solutions $\phi(z)$ of the following type:

$$\phi_d(z) = \phi_d(0)\, e^{+ikz\sin\alpha}$$

$$\phi_u(z) = \phi_u(0)\, e^{-ikz\sin\alpha}$$

it follows that:

$$\frac{1}{\phi(z)}\left.\frac{d\phi(z)}{dz}\right|_{z=0} = ik\sin\alpha\ \frac{1-R}{1+R} \qquad (5)$$

Using equation (3) it turns out that only for specific values of α -the so called eigenvalues- a solution $\phi(z)$ exists which meets the boundary conditions (4) and (5). Each eigenvalue α_n is associated with a solution $\phi_n(z)$, corresponding to the n-th mode. In order to account for the different excitation values of the different modes, the fieldstrength of equation (2) has to be multiplied by a term C_n, called the excitation factor for the n-th mode. The resulting fieldstrength is the sum of the fieldstrengths of the discrete modes according to:

$$E_y^t(x,z) = \sum_{n=1}^{\infty} C_n\ \phi_n(z)\, e^{-ikx\cos\alpha_n} \qquad (6)$$

The excitation factors C_n can be derived, if a particular source is considered. It is appropriate to assume an infinite horizontal linear antenna at x=0 and $z=z_T$ -the height of the transmitter-, carrying a current I into the positive y-direction. In this case the excitation factor C_n becomes (Budden, 1961):

$$C_n = - \frac{Z_o I \phi_n(z_T)}{2 \cos\alpha_n \int_o^\infty \phi_n^2(z)dz} \qquad (7)$$

with $Z = 120\pi\ \Omega$, the characteristic impedance of free space.

If the fieldstrength E_y^t according to equations (6) and (7) is normalized to the free space value E_y^o originating from the antenna above, it follows that:

$$\frac{E_y^t}{E_y^o} = \sqrt{\lambda x}\, e^{ikx}\, e^{i\pi/4} \sum_{n=1}^{\infty} \frac{\phi_n(z_T)\ \phi_n(z)}{\cos\alpha_n \int_o^\infty \phi_n^2(z)dz}\, e^{-ikx\cos\alpha_n} \qquad (8)$$

This equation gives the normalized fieldstrength at a height z above the surface and distance x from the transmitter. Although this result has been derived for a particular antenna, it can be argued that in general equation (8) applies to point sources because of the normalization included.

An important term in equation (8) is $\cos\alpha_n$. The eigenvalue α_n is complex and so $\cos\alpha_n$ consists of a real and an imaginary part. The real part contributes to the phase only, while the imaginary part contributes to the attenuation of each mode. So at the height of the receiver $z=z_R$ the amplitude of the normalized fieldstrength can be written as:

$$\left|\frac{E_y^t}{E_y^o}\right| = \sqrt{\lambda d}\left| \sum_{n=1}^{\infty} \frac{g_n(z_T)\ g_n(z_R)}{\cos\alpha_n}\, e^{+kd\ \mathrm{Im}(\cos\alpha_n)}\, e^{-ikd\ \mathrm{Re}\ (\cos\alpha_n)} \right| \qquad (9)$$

with $g_n(z) = \dfrac{\phi_n(z)}{\left(\int_o^\infty \phi_n^2(z)dz\right)^{\frac{1}{2}}}$, the normalized height-gain function

d = distance between transmitter and receiver

The specific attenuation γ (dB/km) is proportional to the term $-\mathrm{Im}(\cos\alpha_n)$ according to:

$$\gamma = - \frac{20000\ k\ \mathrm{Im}(\cos\alpha_n)}{\ln 10} \quad (\mathrm{dB/km})$$

3. NUMERICAL METHOD

The determination of the eigenvalues α_n is the main problem in the mathematical procedures required to solve differential equation (3). Only for some simple refractive index profiles m(z) it is possible to calculate the eigenvalues analytically.

If $m^2(z)$ shows a linear dependence on z, which physically is associated with an infinitely high duct or with ordinary diffraction, differential equation (3) can be solved in terms of Airy-functions. This case, first solved by Booker and Walkinshaw, is extensively described in the book of Budden (Budden, 1961).

If $m^2(z)$ shows a parabolic dependence on z, physically associated with a duct with finite height, equation (3) can be solved in terms of Whittaker functions. Other profiles of $m^2(z)$ can only be solved numerically, unless one uses approximation methods such as the "comparison equation method" (Rotheram, 1974).

During World War II Hartree e.a. (Hartree, 1946) have solved equation (3) numerically, using a fifth-root-profile. They used boundary condition (5) in the form $\phi(0)=0$, equivalent with R=-1, and then solved equation (3) until they were able to check for boundary condition (4). This procedure has been used in our calculations too. Using an estimate of the eigenvalue α and using boundary condition (5) with (11) differential equation (3) is

numerically solved until one can check for boundary condition (4). But this latter check has turned out to be not a simple one. In general the upwards travelling wavecomponent increases exponentially for increasing z, while the downwards travelling wavecomponent decreases exponentially. So the downwards travelling component is ultimately "masked" by the upwards travelling component. To avoid this difficulty it has turned out to be necessary to solve equation (3) in the complex z-plane, choosing for such a path that the properties of the upwards and the downwards travelling wavecomponents are interchanged. This method can only be used if the refractive index profile m(z) allows analytic continuation into the complex z-plane. For a value of z great enough to allow for a check on boundary condition (4), say for z=z', one can use the property of $\phi(z)$ that different $\phi(z')$'s calculated for different estimates of α form an orthogonal grid of (Real part α, Imaginary part α). Therefore the value of α given by this grid for $\phi(z')=0$ seems to be a better estimate of α. If the first estimate of α is not too bad, a fast convergence to the exact value of α is ensured by this method, which is similar to the Newton-Raphson method.

Once an eigenvalue α_n has been found it is quite simple to solve equation (3) by a path along the real z-axis in order to find the height-gain function $\phi_n(z)$. Serious difficulties on the other hand are to be expected by solving the integral in equation (8), because in general $\phi_n(z)$ diverges for great values of z. This difficulty again can be avoided using a path in the complex z-plane instead of the real z-axis. The integration has to be done very accurate, because the integral in general is given by the small sum of large positive and negative contributions.

This entire procedure has been included in a computer program, using double precision numbers. The differential equations are being solved using the numerical method of Numerov; the required integration is done using the Simpson-method.

4. RADIOMETEOROLOGICAL ASPECTS

It is clear that the solutions of the differential equation (3) depend on the assumptions made for the modified refractive index profile. In fact such profiles depend severely on the radiometeorological conditions for the locations considered. For instance such conditions may differ significantly between land and sea. It is well known that interference conditions are worse on over-sea paths. Therefore we have chosen for a refractive index profile, which may exist during periods that the evaporation processes are dominant.

For the calculations it is assumed that the modified refractive index profile is according to a logarithmic linear function, which can be written as (Rotheram, 1974):

$$m(z) = 1 + \frac{z - (z_d+z_o)\ \ln(\frac{z+z_o}{z_o})}{r_e} \qquad (10)$$

with: z_d : the duct height
z_o : the hydrodynamic roughness of the sea
r_e : the effective radius of the earth

This profile m(z) shows a logarithmic dependence on z for $z<<z_d$, due to the evaporation process above the sea level. It gives a linear dependence of m(z) as a function of z for $z>>z_d$.

5. RESULTS OF THE CALCULATIONS

For all calculations presented in this paper the modified refractive index profile of equation (10) has been assumed. However it has to be stressed that the solution of equation (3) is possible for all functions m(z) which are regular functions of z including refractive index profiles corresponding to elevated layers. For any function m(z) the solution of equation (3) is according to equation (9).

The calculations are concentrated on frequencies between 1 and 40 GHz which are of main interest for the frequency sharing by the space and terrestrial fixed services. In fig. 2, 3 and 4 the specific attenuation is presented as a function of the duct height z_d assuming r_e=8500 km and z_o=0.00015 m. These calculations are done for the dominant first modes.Furthermore it is assumed that the earth reflection coefficient R = -1, which is appropriate in cases where reflection occurs at the "flat" sea for small grazing angles.

The general structure of the curves in fig. 2, 3 and 4 shows that the specific attenuation drops rapidly around a defined duct height, which in turn increases with decreasing frequency. Furthermore it turns out that this "cut-off" duct height increases with increasing mode number, indicated by the parameter n. This general structure is very similar to that in guided structures as wave guides and optical fibres.

In the fig. 5 to 10 the normalized height-gain functions are presented for defined duct heights, frequencies and modes. The curves can be understood in combination with curves of specific attenuation in the fig. 2 to 4. Low values of the specific attenuation correspond to a good trapping of the waves below the duct height and so the leakage of less energy into heights above the duct height, resulting into low values of the height-gain functions above the duct height. This behaviour of the height-gain function relative to the specific attenuation applies for relatively high values of the specific attenuation too, occurring simultaneously with high values of the height-gain function above the duct height.

The preceding results are obtained assuming a flat sea (R = -1). The boundary condition in equation (5) allows for other values of R as occurring due to the roughness of the sea surface. It is well known (Ament, 1953) that due to the roughness of the sea the value of the specular reflection coefficient R_s is reduced according to:

$$R = R_s \, e^{-2k^2 \Delta h^2 \sin^2 \psi} \qquad (11)$$

with: Δh : the r.m.s. value of the roughness of the sea surface
ψ : the grazing angle at the sea surface

It has been demonstrated by Arnbak that the grazing angle ψ can be substituted by the eigenvalue α_n (Arnbak, 1971).

In order to demonstrate the general impact of the roughness of the sea surface on the specific attenuation, fig. 11 shows the specific attenuation as a function of the frequency with Δh as a parameter. It is very clear that effects of the roughness of the sea are not negligible at the higher frequencies (f> 10 GHz).

Let us consider a particular path geometry in order to demonstrate the use of the results obtained so far. Because of running fieldstrength measurements on an actual over-sea-path between Rockanje (Netherlands) and Martlesham (United Kingdom) the following values of the link parameters are used:

z_T = 72 m
z_R = 32 m
d = 191 km
f = 11.365 GHz

Using the computer program mentioned above it is possible to calculate all the terms included in equation (9). The normalized fieldstrength as a function of the duct height is shown in fig. 12 for R=-1 and for a sea surface with a moderate roughness of Δh=0.5 m. Furthermore one can see the effect of the roughness of the sea, leading to a degradation of signal levels by about 10 dB.

6. COMPARISON WITH MEASURED DATA

As it has been explained before, the preceding theory presents the tools to calculate the fieldstrength as a function of the duct height for a particular path geometry. Such an approach allows for the derivation of the fieldstrength statistics, if the duct height statistics are known.

As an example of such calculations we consider an actual path, on which long term fieldstrength measurements were performed (B.T.I., 1982). The measured data are compared with the predicted ones, using the fieldstrength versus duct height relation of the same path according to fig. 12 and the duct height statistics as derived from data reported by Fischer (Fischer, 1982). In fig. 13 the measured and predicted data are shown.

Fig. 13 shows some agreement between predicted and measured data. Differences can be explained easily by the limited accuracy of the duct height statistics used, the concurrence of large duct heights and small surface roughness and the occurrence of other duct types. However the theoretical results obtained so far seem to provide a basis for the evaluation of fieldstrengths due to ducting.

7. COMPARISON WITH THE CCIR PREDICTIVE TECHNIQUES

In Report 569 the CCIR (CCIR, 1982) presents a method to predict the statistics of the attenuation A due to superrefraction and ducting, in excess of the free space loss:

$$A = -10 \log d + \gamma_d d + A_c \quad \text{(dB)} \qquad (12)$$

with: d : the path length (km)
γ_d : the specific attenuation due to ducting (dB/km)
A_c : the coupling loss (dB)

The values of the specific attenuation γ_d and A_c are given for defined time percentages in the range between 1% and 0.001%.

Using the theory as presented above, it is possible to derive an engineering formula similar to equation (12). The attenuation follows from equation (9) by:

$$A = 20 \log \left| \frac{E_y^o}{E_y^t} \right| = -24.8 + 10 \log f - 10 \log d + \gamma_d d - \left[g(z_T) + g(z_R) \right] \quad \text{(dB)} \qquad (13)$$

with: f the frequency (GHz)
d the path length (km)
γ_d the specific attenuation (dB/km)
g(z) the height-gain function (dB)
z_T the height of the transmitter (m)
z_R the height of the receiver (m)

In fact this formula is valid for each mode. It has been shown before -see fig. 12- that in general a particular mode is dominant for a defined duct height. Therefore equation (13) presents a close approximation to equation (9).

The comparison of equation (12) and (13) shows some significant differences:

a) Equation (13) includes a term 10 log f, which results from the cylindrical radiation of energy instead of spherical radiation in the case of free space.
b) Equation (13) does not include the coupling loss. This results from the use of the full wave solutions instead of the geometrical optical approximation.
c) Equation (13) includes the height-gain functions to account for the influence of the heights of the transmitting and receiving terminal.

These differences are of importance and have to be considered when evaluating predictive techniques on the basis of measured data on links with different path geometry and operating frequencies.

8. CONCLUSIONS

Using the Maxwell equations as a basis the theory is presented for the calculation of the fieldstrength in beyond-the-horizon microwave links during ducting conditions. This full wave description contributes to the understanding of the propagation phenomena involved and explains some general characteristics of experimental results which can not be understood from the geometrical optics.

The theory enables to derive a general engineering formula with parameters which values depend on the refractive index profile, the frequency and the path geometry. This engineering formula includes elements, which differ from existing predictive formulae, and provides a better basis for the evaluation of measured data in experimental links.

It is important to consider the effect of the surface roughness, because the presented theory shows clearly that at frequencies above about 10 GHz the signal enhancements due to ducting may be reduced significantly.

Although in this paper a logarithmic-linear refractive index profile -representative for the ground based duct due to evaporation- is assumed, the theory presented allows for calculations with other profiles which are a regular function of the height above the earth surface.For instance the computer program developed enables for the calculation of the fieldstrength during conditions of elevated ducts.

9. ACKNOWLEDGEMENT

The authors are indebted to Prof. J. Arnbak of the Eindhoven University for his encouraging support and his guidance through the mathematical difficulties. Furthermore the authorities of the Department of Electrical Engineering of Eindhoven University and the Dr. Neher Laboratories of the Netherlands Postal and Telecommunications Services are acknowledged for their support of the cooperation.

REFERENCES

1) AMENT, W.S., 1953, "Toward a Theory of Reflection by a Rough Surface", Proc. IRE, January 1953.
2) ARNBAK, J., 1971, "Wave propagation in a duct with an irregular boundary, Part I", Danish Defence Research Establishment, Report FOFT 1971/28.
3) B.T.I., 1982, private communications.
4) BUDDEN, K.G., 1961, "The wave-guide mode theory of wave propagation", Logos Press/Prentice-Hall Inc..
5) CCIR, 1982, "The evaluation of propagation factors in interference problems between stations on the surface of the earth at frequencies above about 0.5 GHz", Report 569-2, Volume 5, to be published.
6) FISCHER, K.E., "VHF-, UHF- and SHF-propagation limitations in the marine atmosphere", to be published.
7) HARTREE, D.R. e.a., 1946, "Practical methods for the solution of the equations of tropospheric refraction", in Proc. of a conf. on meteorological factors in radiowave propagation held by the Physical Society and The Royal Meteorological Society. Publ. by The Physical Society, London.
8) ROTHERAM, S., 1974, "Radiowave propagation in the evaporation duct", Marc. Rev., First quarter 1974.

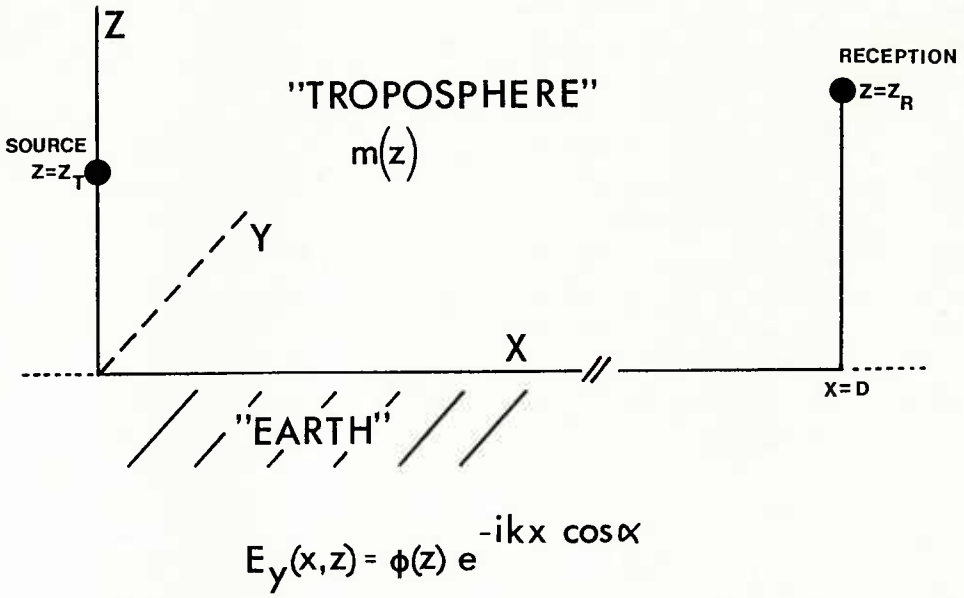

Fig.1 : Definition of the coordinate system.

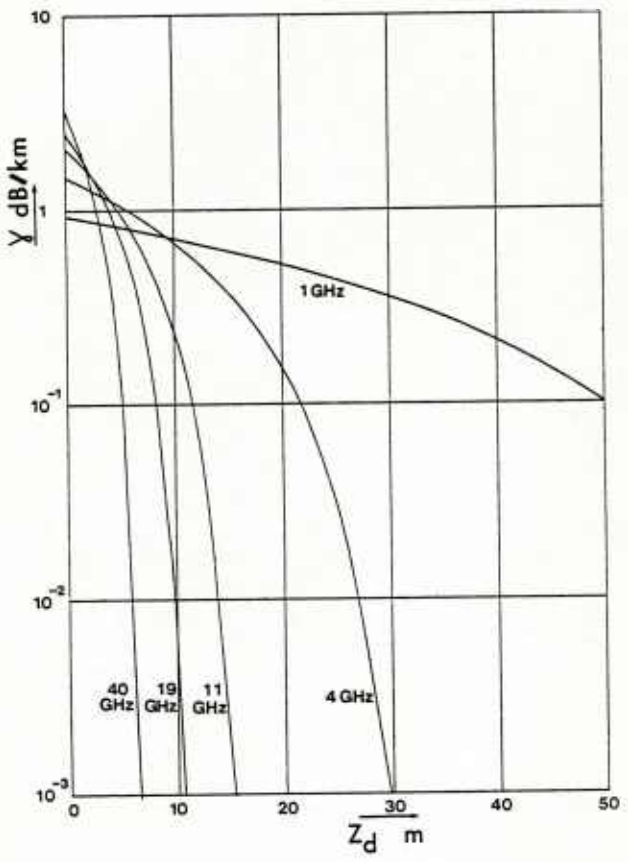

Fig.2 : Specific attenuation γ as a function of the duct height z_d for the 1st mode.

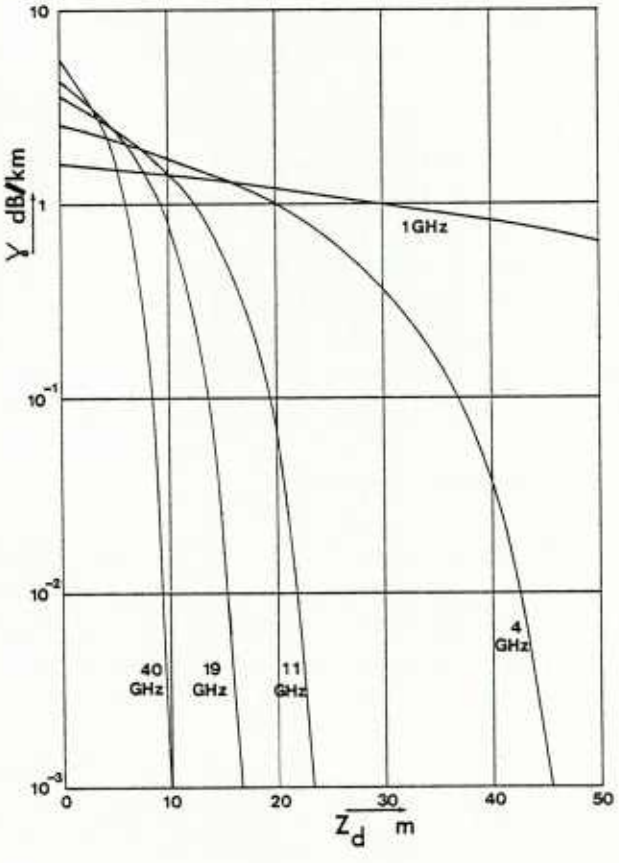

Fig.3 : Specific attenuation γ as a function of the duct height z_d for the 2nd mode.

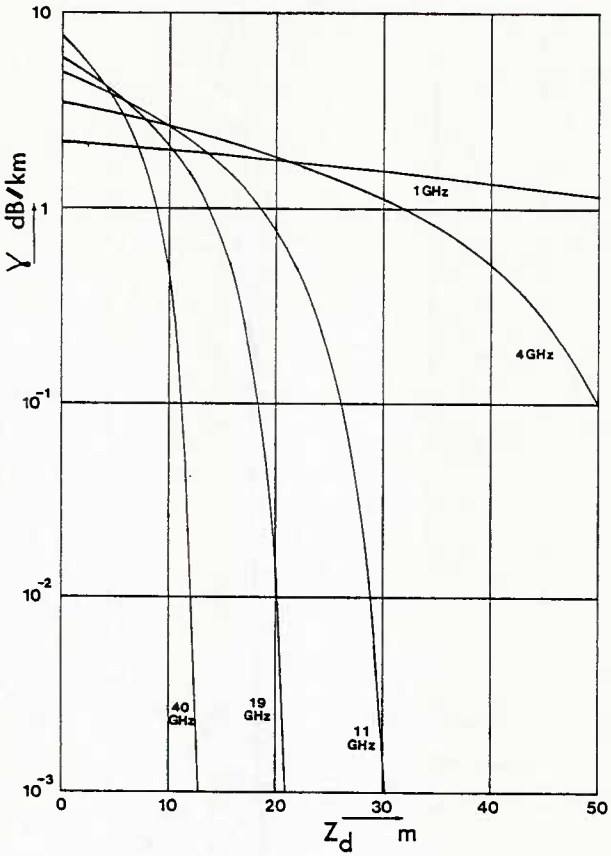

Fig.4 : Specific attenuation γ as a function of the duct height z_d for the 3rd mode.

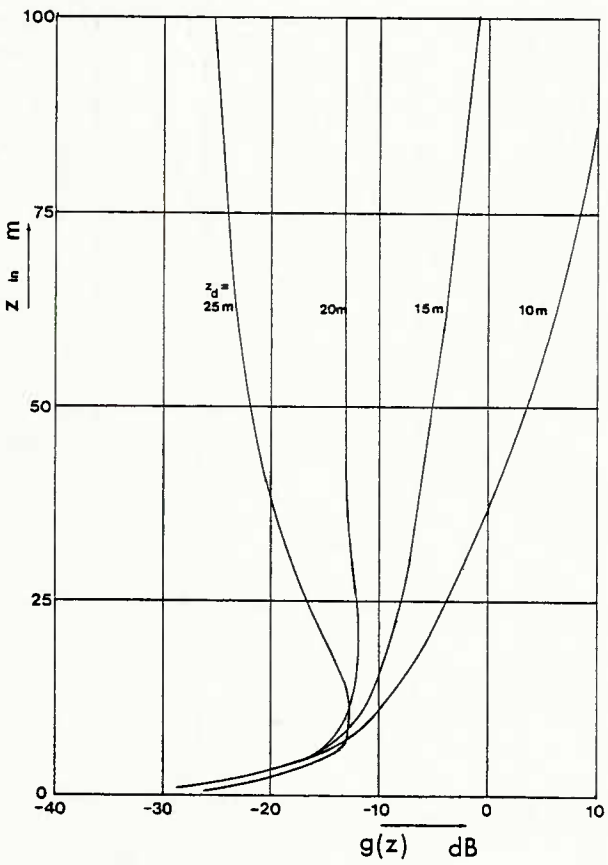

Fig.5 : The normalized height-gain function g(z) as a function of the height z. f = 4 GHz ; 1st mode.

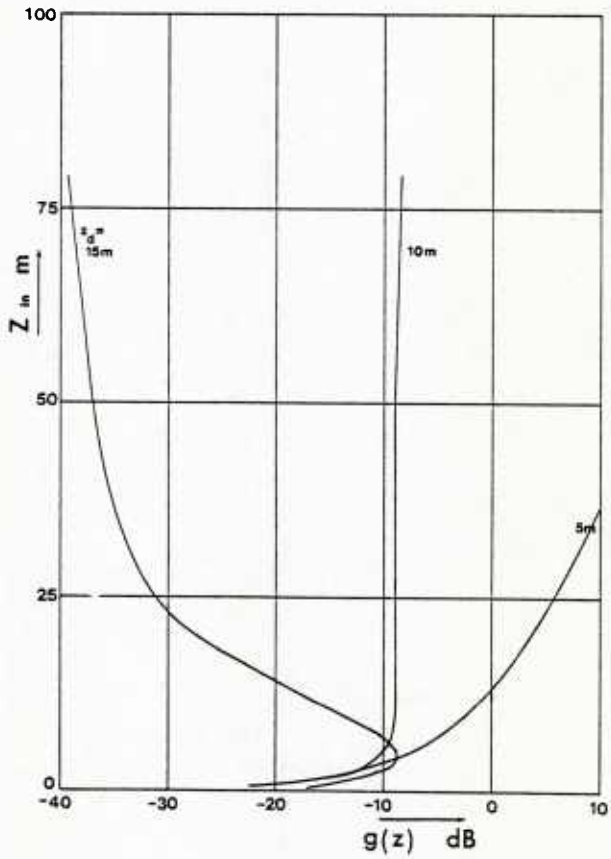

Fig.6 : The normalized height-gain function g(z) as a function of the height z. f =11 GHz ; 1st mode.

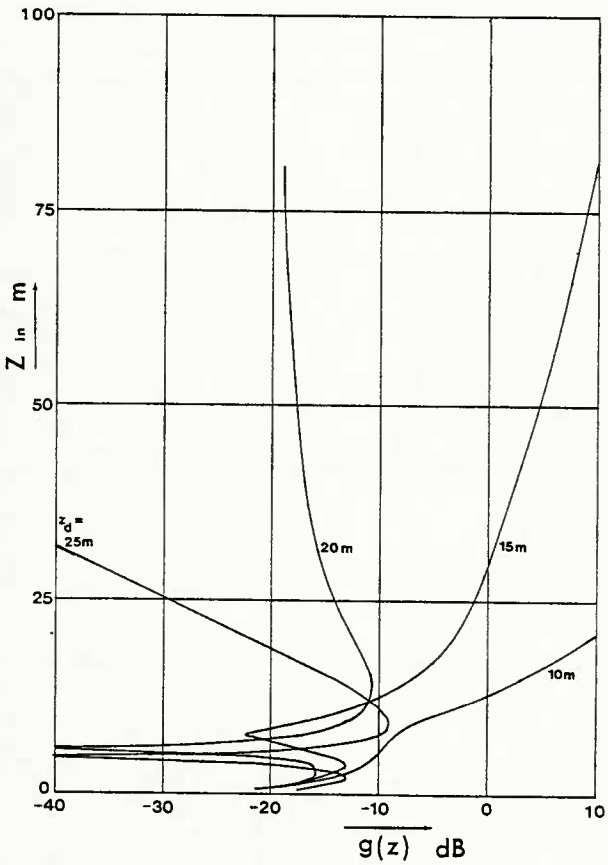

Fig.7 : The normalized height-gain function g(z) as a function of the height z. f =11 GHz ; 2nd mode.

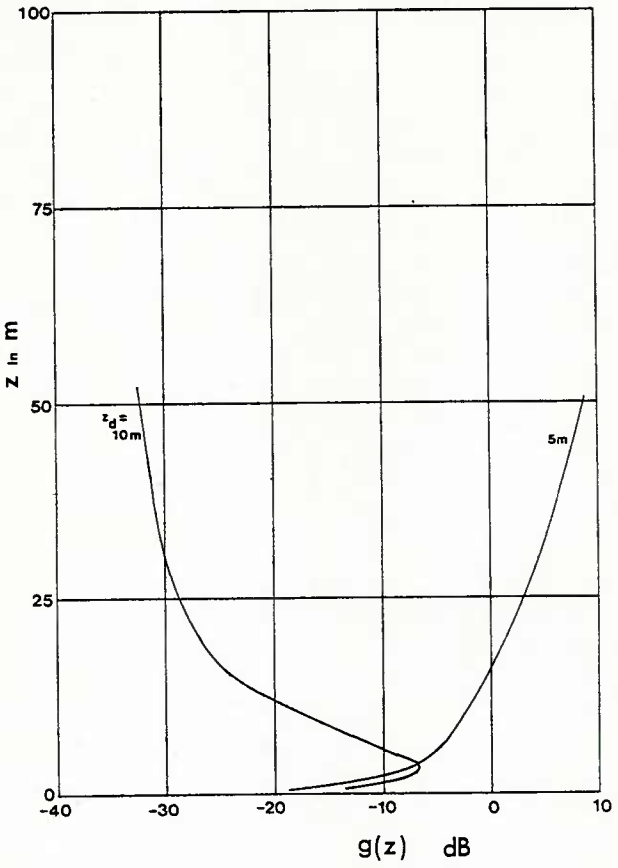

Fig.8 : The normalized height-gain function g(z) as a function of the height z. f = 19 GHz ; 1st mode.

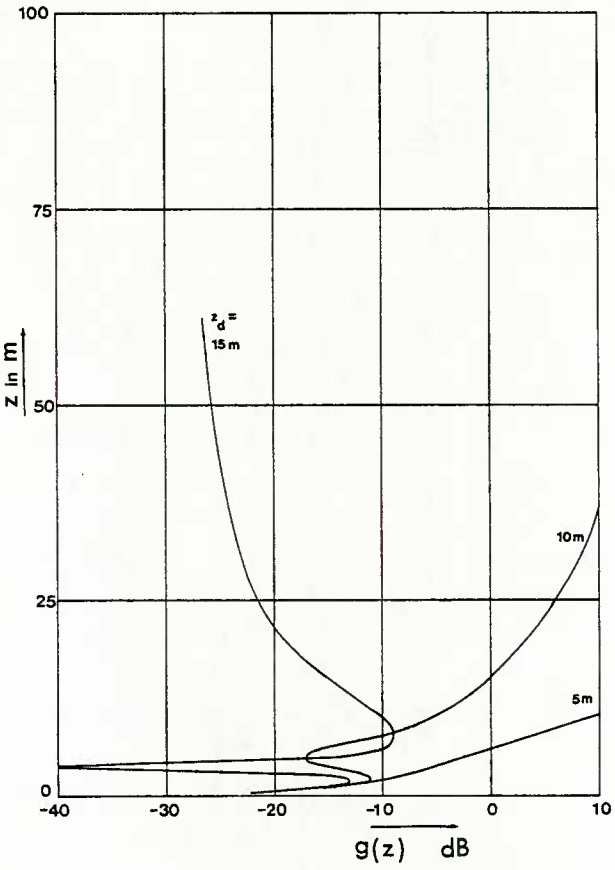

Fig.9 : The normalized height-gain function g(z) as a function of the height z. f = 19 GHz ; 2nd mode.

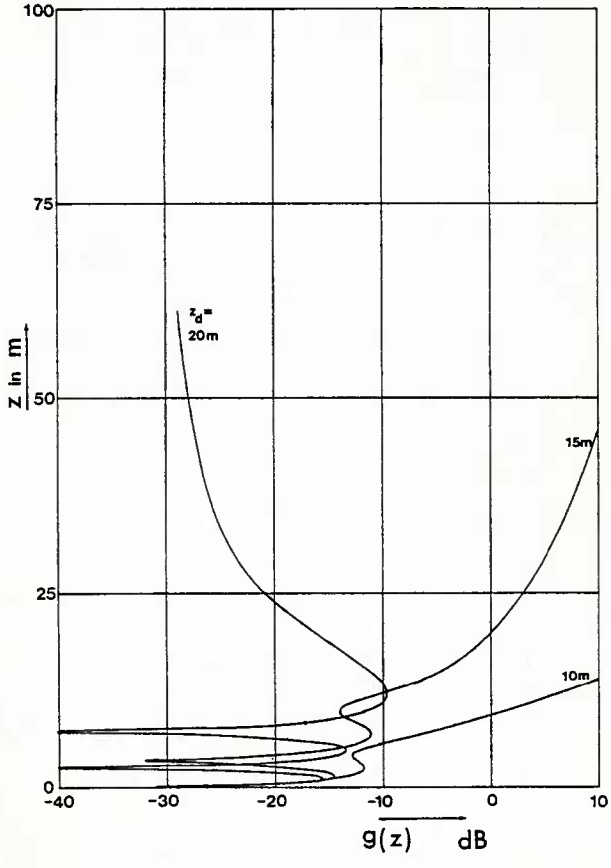

Fig. 10 : The normalized height-gain function g(z) as a function of the height z. f = 19 GHz ; 3rd mode.

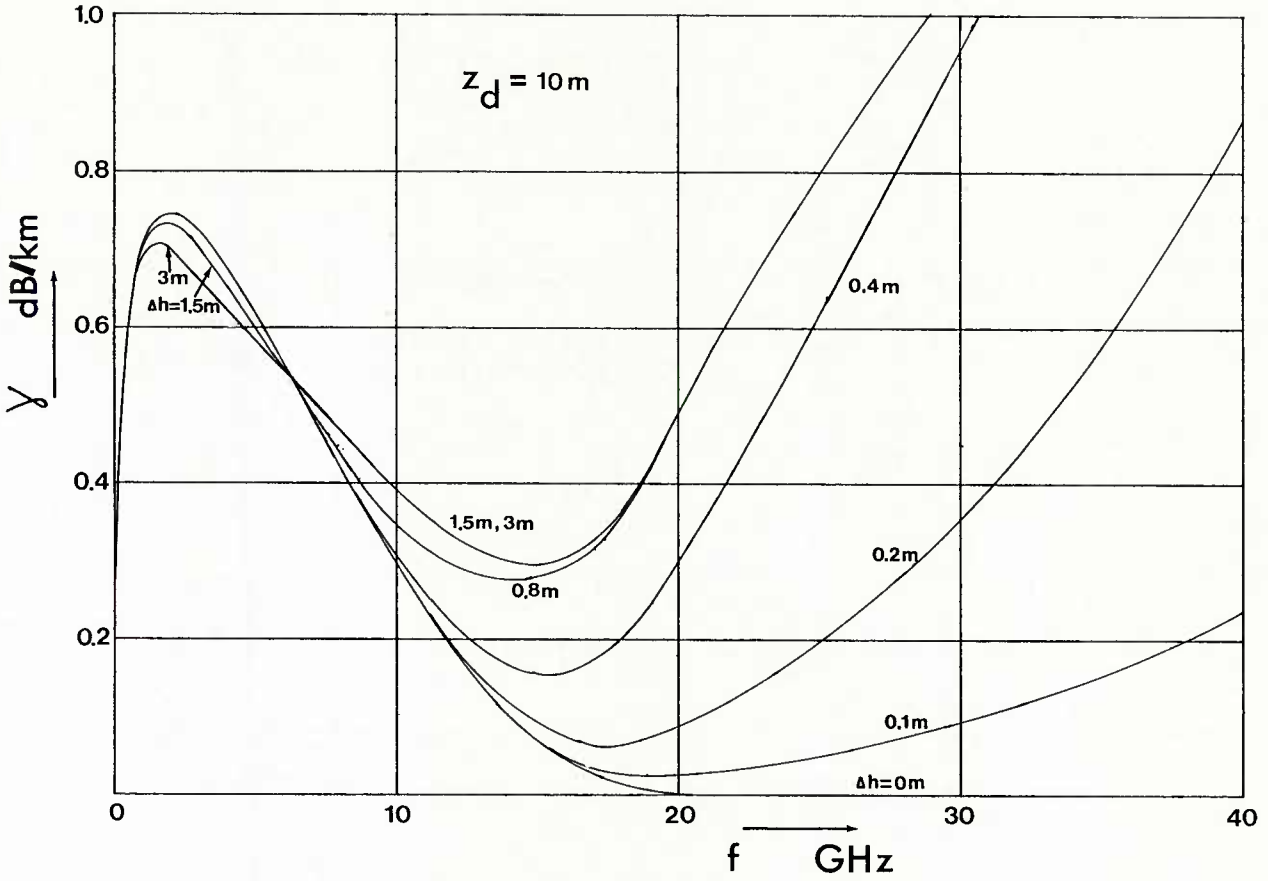

Fig.11 : The specific attenuation γ as a function of frequency with the surface roughness as a parameter.

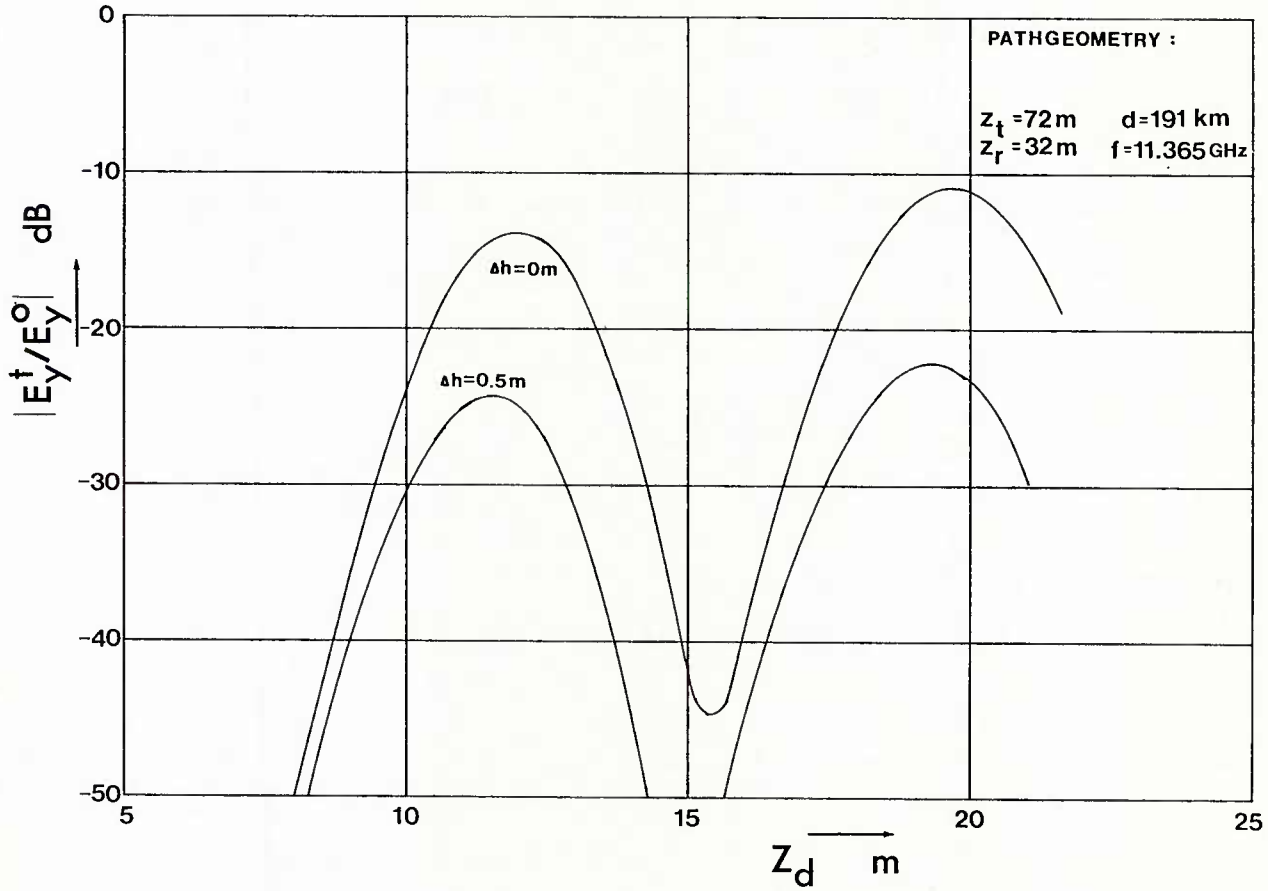

Fig.12 : The fieldstrength relative to free space as a function of the ductheight for the microwave link Rockanje-Martlesham.

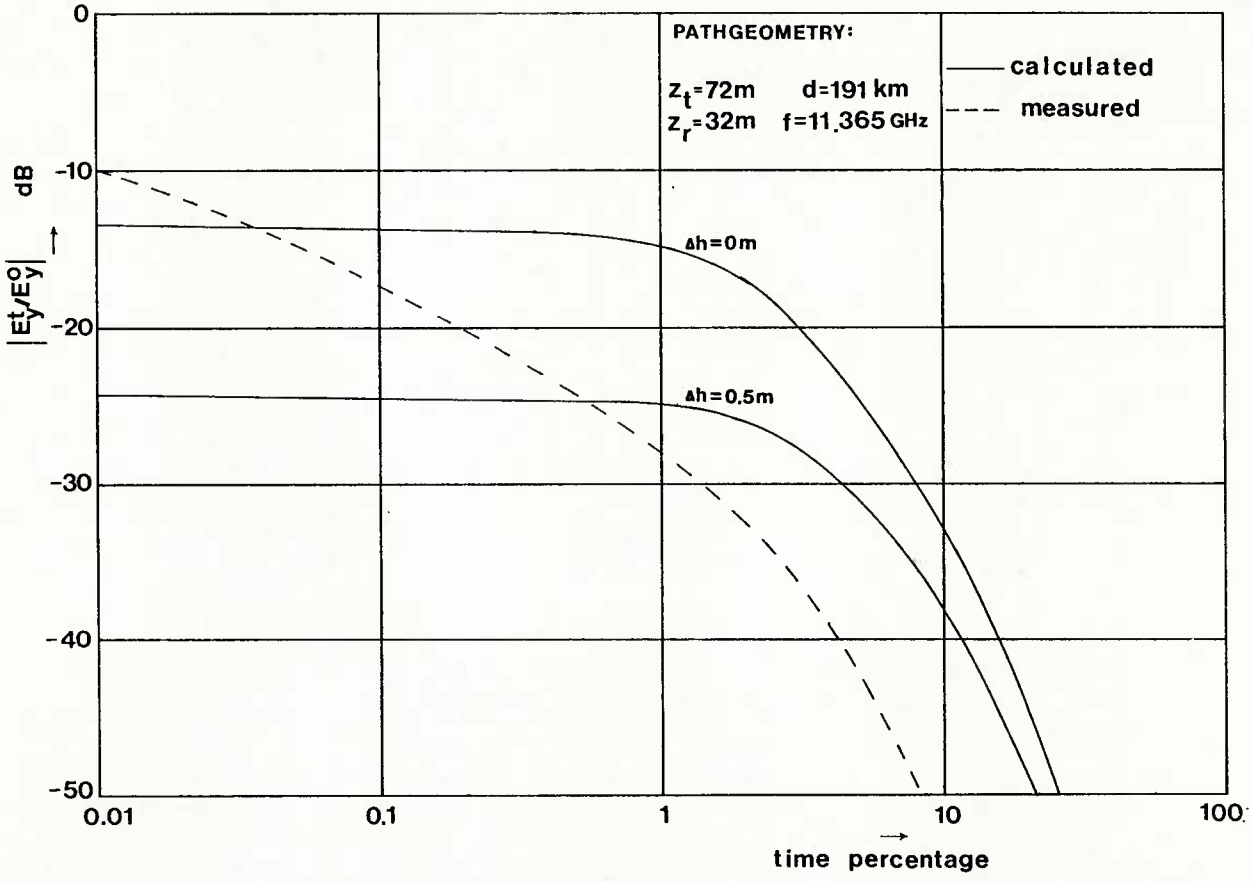

Fig.13 : A comparison between the predicted and measured cumulative distribution of the fieldstrength relative to free space for the microwave link Rockanje-Martlesham.

DISCUSSION

J.T.Ong, UK

Should the factor Δh be defined in accordance with Beckman as the standard deviation of terrain height rather than the rms value? I was thinking of applying this model to coastal areas.

Author's Reply

In our paper the parameters Δh relates to the rms value of the roughness of the sea. So this definition is different from that used by the CCIR Report 569 to indicate the roughness of land, including coastal areas. Our conclusions relate to over sea path and can not directly be applied to coastal areas.

D.Davidson, US

In your Figure 13, your calculated curves are flat to the left of 1% of time. The statistics of duct height are not given. Is it assumed, in view of the duct height influence on the field, that a constant duct height prevails for $t < 1\%$?

Author's Reply

The duct height statistics are derived from data reported by Fisher (see Reference 6). Applying these data, it's possible to calculate the statistics of the field strength using Figure 12. It turns out that a duct height corresponding to the second mode is smaller than 0.01%. Therefore the curve of fig.13 is flat for time percentages $< 0.01\%$.

L.Boithias, Fr

Pour définir l'atténuation linéique en dB/km on doit supposer un régime guidé homogène c'est à dire un guide infini. Ce concept ne s'applique donc pas dans une zone de couplage à chaque extrémité du trajet considéré. Dans le guidage troposphérique quel est l'ordre de grandeur de la longueur de ces deux zones?

Author's Reply

In principle, the concept of the specific attenuation of the total field-strength according to Equation (13) can be used, if the field strength corresponding to one particular mode is dominant. From the presented Figures 2 and 10, it can be derived easily that such condition is met for path length exceeding 100 km and terminal height of practical interest. These path geometries are of main interest in CCIR Report 569, consequently Equation (13) is applicable in that context.

STATISTICAL STUDY OF ELEVATED DUCTS EXTENSION.

B. Strauss and J-L. Dumas

Service Météorologique Métropolitain
2 av. Rapp 75340 PARIS cedex 07

Summary. The spatial extension of elevated ducts is studied using meteorological radiosonds soundings. A limited extension of a duct to the sounding station is found in about 85% of the cases.

INTRODUCTION.

This paper is intended to present a study of spatial extension of elevated ducts. The first steps have consisted in using the existing data, that means the radiosonds soundings, to their best. These measures are characterized by a bidaily occurence and a spatial density adjusted to the needs of the meteorological forecast, that is a distance of about 500 to 1000km between two points of measurement.

The 12 hours period between two measures obviously prohibits any study of the temporal evolution. In the same way 500km is too much to make a little scale study of the spatial structure, on the other hand it allows a statistical study of the simultaneous occurences of ducts between adjoining stations. This aspect is studied in the present work. (Surface ducts were not analysed in consideration of their greater variability).

Used datas.

Two five-years series of measures, one for each studied area, were used.

The first area, in the near Atlantic, includes the following stations: Brest, Bordeaux, and Point Romeo (fixed ship 47N and 17W). The distances between two stations are: Brest Bordeaux 480km
Brest Romeo 970km
Bordeaux Romeo 1280km. The study period runs from 1965 to 1969, with two daily observations at 00H and 12H. The total number of soundings is 3652.

The second area, in occidental Mediterranée, includes Nîmes, Alger and Ajaccio. The study period runs from 1958 to 1962, which gives also 3652 soundings (excluding Ajaccio with only one daily sounding at 12H).

For each sounding the refractive index profile was computed using meteorological data P,T,U.

Results.

Tables 1 to 3 illustrate the results. A lower frequency of ducts in Méditerranée than in Atlantic was found (on an average and for a given station the ducting frequency is 5% in Atlantic against 2.5% in Méditerranée). Therefore the Ajaccio data, in a too low number, but also the Alger data were not very usable.

The statistical results on spatial extension are to be understood in the following way (the Atlantic area is only considered): when a duct is observed in a station, ducting frequency in a 1000km forward station (possibly at a different altitude) is 16%. This result can be precised by distinguishing Point Romeo, where the frequency is 14%, from Brest and Bordeaux (neighbouring coast-stations) with a frequency of 18%.

An opposite expression of the results, may be more usable, consists in stating that a duct is located in a 200km radius in 84% of the cases (or 86% and 82% when the two area are distinguished).

This work was only an approach of the problem by using an availabla data set. It is intended to carry it on with a set of more recent and numerous data using every WMO station of the studied areas and daily brought up to date. More precise statistics will be then possibly achieved, and the problem of the distribution of altitudes between coexistings ducts approached.

Tab 1.	Bordeaux	Brest	Romeo	All
Ducts Number / cases number	136 / 3582	145 / 3570	223 / 3533	
(1)	93	103	178	374
(2)	15	22	25	62
(3)	3	3	3	9
(2)+(3)	18	25	28	71

(1): duct at the station only
(2): duct at two stations
(3): duct at the three stations.

Tab 2.	Nimes	Alger	Ajaccio
Ducts number	55 / 3633	105 / 2880	36 / 1819
At only one station	41	96	
At the two	3	3	

Tab 3 same as tab 1, but in percent frequency.

	Bordeaux	Brest	Romeo	All
Duct frequency	3.8	4.1	6.3	4.7
(1)	83.8	80.5	86.4	84.0
(2)+(3)	16.2	19.5	13.6	16.0

DISCUSSION

M.P.M.Hall, UK

Your statistics are interesting, and it would be good to relate them to those obtained by Dr Dougherty in the USA and by other authors in Europe.

The statistics are somewhat sensitive to the criterion for a duct. You do not mention yours. To use 157 N/km may be too severe if data are obtained over wide height intervals (as is all that is normally available from radiosondes). It would be useful if you could comment on the criterion used and the data intervals.

Relative to this, it would be useful to know the duct thickness, since this too is a major parameter for ducting studies.

Réponse d'auteur

La résolution verticale des mesures de radio-sondes est de l'ordre de 30 m. Il est certain que les ducts d'épaisseur inférieure échappent à la statistique.

Une solution consisterait à abaisser le seuil pour la sélection des couches minces (<50 m par exemple) en dessous de -157 N/km. Mais le choix du nouveau seuil, pour ne pas être hasardeux, demanderait l'examen d'un fichier de mesures de plus haute résolution, dont nous ne disposons pas. Ceci nous a conduit à nous en tenir au critère des -157 N/km.

L'épaisseur des ducts n'était pas prise en compte dans le fichier exploité ici, mais le sera dans le fichier constitué au jour le jour, ainsi d'ailleurs que l'altitude.

LA DIFFUSION MULTIPLE PAR LES HYDROMETEORES : UNE SIMULATION NUMERIQUE

N. SPANJAARD et J. LAVERGNAT
CNET/CRPE, 38-40 rue du Général Leclerc
92131 ISSY-LES-MOULINEAUX, FRANCE

RESUME

Dans le cadre d'un projet de balise embarquée sur satellite et émettant à des fréquences égales à 20, 30, 40 et 90 GHz, nous nous sommes intéressés à l'influence des hydrométéores sur la propagation des ondes millimétriques. Après une revue sommaire des effets principaux, une attention particulière a été portée sur ceux dus à la diffusion multiple. En effet, à ces fréquences la longueur d'onde est voisine des dimensions caractéristiques des noyaux diffusants : en conséquence le rapport entre les sections efficaces de diffusion et d'absorption est de plusieurs ordres de grandeur supérieur à celui qui concerne les ondes de fréquences inférieures à 10 GHz.

L'essentiel du travail présenté consiste en une étude théorique du problème. Après avoir passé en revue et critiqué les principales approches analytiques, nous présentons les résultats préliminaires d'une simulation numérique. Celle-ci assimile les hydrométéores à des diffuseurs de Rayleigh.

1 - INTRODUCTION

Les systèmes de télécommunications par satellite actuellement opérationnels, tel que le réseau mondial Intelsat, ou devant être mis en service prochainement, tels que le réseau européen Eutelsat ou le réseau national français Télécom I, fonctionnent dans des gammes de fréquences inférieures à 15 GHz. Malgré le développement de techniques permettant une utilisation maximale des bandes de fréquences allouées (réutilisation de fréquences, concentration numérique des conversations, accès multiple par répartition dans le temps...) l'accroissement de la demande en circuits téléphoniques et la mise en exploitation de nouveaux services (transmissions de données, téléconférence,...) imposeront l'emploi de bandes de fréquences plus élevées. Il importe donc d'étudier les caractéristiques particulières que présente la propagation des ondes millimétriques dans l'atmosphère, et en particulier les effets causés par la présence d'hydrométéores sur le trajet de propagation.

Si nous nous bornons pour le moment à ne considérer que des particules de faibles dimensions par rapport à la longueur d'onde, nous pouvons utiliser l'approximation de Rayleigh dans le calcul de la diffusion d'une onde électromagnétique par une particule. Nous constatons alors que la section efficace de diffusion σ_s est approximativement proportionnelle à V/λ^4 et la section efficace d'absorption σ_a à V, si V et λ sont respectivement le volume de la particule considérée et la longueur d'onde. La part de l'onde diffusée par la particule s'accroît donc avec la fréquence. Cette caractéristique n'est pas propre à l'approximation de Rayleigh mais s'étend, en tout cas, aux autres types de diffuseurs modélisant les hydrométéores. On s'attend donc à ce que les effets diffusifs soient plus marqués pour les ondes millimétriques que pour les ondes centimétriques. Plusieurs conséquences peuvent être d'importance pour les télécommunications : l'affaiblissement, le déphasage, la dépolarisation, les scintillations d'amplitude et de phase, et la diffusion latérale. L'évaluation quantitative de ces phénomènes ne peut malheureusement pas se déduire simplement de ce qui a été fait aux plus basses fréquences. En effet, les effets de diffusion augmentant, la probabilité d'observer de la diffusion multiple n'est plus à négliger, et ceci d'autant plus que les dimensions des hydrométéores, leur distance de corrélation et la longueur d'onde deviennent du même ordre de grandeur. Bien entendu la diffusion multiple n'introduit pas de nouvelles perturbations en elle-même, mais sa présence les accroît. Il est donc fondamental d'évaluer si ce surcroît est important ou négligeable, par exemple dans le calcul d'un bilan de liaison ou dans celui des interférences entre liaisons voisines. Cette évaluation est cependant difficile à effectuer parce qu'elle ne peut être réalisée correctement que si l'analyse du problème posé par le diffusion multiple a été menée suffisamment loin.

Pour des raisons mathématiques dont la discussion dépasse le cadre de cet article, il n'existe pas jusqu'à présent de théorie complète de la diffusion multiple. Seules des théories partielles existent, ne répondant bien souvent qu'à des cas particuliers bien précis. En ce qui concerne les hydrométéores, quelques tentatives ont été faites, mais aucune n'a encore conduit à une estimation quantitative des différents effets attendus.

On peut classer les différentes méthodes d'étude de la diffusion multiple en trois grandes classes :

a) La théorie du transfert radiatif (CHANDRASEKHAR S., 1950) qui est essentiellement phénoménologique et ne fait intervenir à l'aide des paramètres de Stokes que les flux d'énergie incidents et diffusés. Cette méthode ne permet donc de calculer que les énergies.

b) Une méthode analytique globale consistant à exprimer pour chaque diffuseur la valeur du champ incident et celle du champ diffusé puis d'appliquer le principe de superposition à l'ensemble aléatoirement distribué des particules diffusantes et enfin à appliquer les moyennes statistiques permettant d'obtenir les moments successifs des solutions (FRISCH U., 1968 ; TWERSKY V., 1962). L'ambition de cette méthode, qui a déjà fait l'objet de simulation par la méthode de Monte Carlo (OLSEN R.L., KHARADLY M.M.Z. et CORR D.G., 1976), est de passer d'équations différentielles aléatoires à des équations différentielles ordinaires sur les moments. Cela n'est pas sans difficultés et en fait seules des approximations sont possibles. Le formalisme de la "T matrix" introduit par Waterman (WATERMAN P.C., 1969) facilite l'obtention des solutions au moins pour la partie cohérente du champ diffusé. Ce formalisme n'a cependant pas encore fourni de résultats applicables au cas concret qui nous préoccupe.

c) Une méthode intermédiaire (UCSINSKY B.J., 1977) utilisant une formulation proche de l'optique géométrique aboutit à des équations différentielles sur les moments dont la résolution pose à nouveau des problèmes de sommation de séries à termes séculaires. De plus, il est difficile de relier les coefficients de ces équations aux propriétés microscopiques des diffuseurs.

Nous présentons ici une méthode simple de simulation, facile à mettre en oeuvre, et permettant de mettre en évidence certains aspects particuliers de la diffusion multiple. Nous exposerons les principes élémentaires sur lesquels s'appuie cette simulation, puis nous détaillerons sa mise en oeuvre pratique sur calculateur, enfin nous fournirons les premiers résultats obtenus.

2 - DESCRIPTION DE LA METHODE DE SIMULATION

Par souci de simplicité nous nous sommes restreints au problème bidimensionnel d'un ensemble pseudo-aléatoire et discret de diffuseurs de Rayleigh répartis à l'intérieur d'un rectangle.

Ainsi qu'il est classique dans les problèmes de diffuseurs discrets, on séparera les champs en champ incident et champ diffusé. Considérons tout d'abord un diffuseur isolé illuminé par un champ excitateur d'amplitude complexe $\vec{E}_e$. Sous l'action du champ incident, le diffuseur prend un moment dipolaire complexe :

$$\vec{p} = g \vec{E}_e \tag{1}$$

Le champ diffusé $\vec{E}_d$ à la distance d et dans la direction $\vec{u}$ (figure 1) est alors :

$$\vec{E}_d = \frac{k^2}{4\pi\varepsilon_o} g \frac{e^{-ikd}}{d} \left[\vec{E}_e - (\vec{E}_e.\vec{u})\vec{u}\right] \tag{2}$$

Plaçons nous maintenant dans le cas d'un ensemble pseudo-aléatoire de N gouttes soumis à un champ incident $\vec{E}_o$. La géométrie du problème est décrite figure 2. Soient $\vec{u}_{\alpha\beta}$ le vecteur unitaire porté par l'axe $\alpha\beta$, $d_{\alpha\beta}$ la distance séparant le diffuseur α du diffuseur β, et x_α l'abscisse du diffuseur α. Appelons $\vec{E}_\alpha$ la valeur du champ excitateur appliqué à la particule diffusante α. Ce champ peut s'écrire comme la somme du champ incident $\vec{E}_o e^{-ikx_\alpha}$ et des champs diffusés par les autres diffuseurs. Il vient alors :

$$\vec{E}_\alpha = \vec{E}_o e^{ikx_\alpha} + \frac{k^2}{4\pi\varepsilon_o} \sum_{\substack{\beta=1 \\ \beta\neq\alpha}}^{\beta=N} g_\beta \frac{e^{-ikd_{\alpha\beta}}}{d_{\alpha\beta}} \left[\vec{E}_\beta - (\vec{E}_\beta.\vec{u}_{\alpha\beta})\vec{u}_{\alpha\beta}\right] \tag{3}$$

Cette équation linéaire est de la forme :

$$\vec{E}_o + \sum_{\beta=1}^{N} \bar{\bar{f}}_{\alpha\beta}(\vec{E}_\beta) = \vec{0} \tag{4}$$

où $\bar{\bar{f}}_{\alpha\beta}$ traduit le couplage entre les particules α et β et $\bar{\bar{f}}_{\alpha\alpha}$ le déphasage du champ incident pour la particule α. La prise en compte de la polarisation fait que $\bar{\bar{f}}_{\alpha\beta}$ est un opérateur 2 x 2 dont le module est inversement proportionnel à la distance entre les diffuseurs α et β, le module de $f_{\alpha\alpha}$ étant égal à 1. On notera en outre l'absence de symétrie : $\bar{\bar{f}}_{\alpha\beta} \neq \bar{\bar{f}}_{\beta\alpha}$. La résolution du système linéaire (4) fournit la valeur du champ excitateur pour chaque diffuseur. Il suffit alors de sommer tous les champs diffusés par chaque diffuseur pour obtenir l'amplitude et la phase du champ diffusé total au point d'observation.

Le problème se résume donc à inverser l'opérateur linéaire $\bar{\bar{f}}$ de l'équation (4). Sans difficultés de principe, c'est cependant un calcul très lourd, très exigeant en capacité mémoire et en temps. Pour atténuer cet inconvénient il est tentant de procéder à des approximations. La plus évidente consiste à annuler $\bar{\bar{f}}_{\alpha\beta}$ pour des diffuseurs α et β suffisamment éloignés. C'est ce que nous avons fait. L'objet de cet article est la justification de cette approximation. En effet, le module des opérateurs $\bar{\bar{f}}_{\alpha\beta}$ ne décroît que de façon proportionnelle à la distance séparant les diffuseurs. Il n'est donc pas évident qu'une telle troncature soit satisfaisante. Il faut noter qu'en soi une telle approximation ne simplifie pas les problèmes posés par la résolution du système d'équations (4). Elle ne sera efficace que si elle entraine une modification de la matrice $\bar{\bar{f}}$ qui réduise son stockage en mémoire et facilite son inversion. L'idéal est d'obtenir une matrice bande ; cela revient à réduire (4) à une équation tronquée de la forme :

$$\vec{E}_o + \sum_{\beta=\inf(1,\alpha-n)}^{\beta=\max(N,\alpha+n)} \bar{\bar{f}}_{\alpha\beta}(\vec{E}_\beta) = \vec{0} \tag{5}$$

Remarquons que l'on peut toujours réduire l'équation (4) à une telle forme. Cette réduction ne sera équivalente à l'annulation des opérateurs $\bar{\bar{f}}_{\alpha\beta}$ pour des diffuseurs suffisamment éloignés que si la numérotation des diffuseurs a été faite judicieusement. L'indice de troncature n sera d'autant plus faible que la numérotation sera mieux faite. Ce nombre est l'écart maximal dans la numérotation entre deux diffuseurs au delà duquel ils peuvent être considérés comme suffisamment éloignés pour qu'on puisse négliger $\bar{\bar{f}}_{\alpha\beta}$.

3 - MISE EN OEUVRE DE LA SIMULATION

La mise en oeuvre de la simulation se déroule selon les étapes suivantes :

a) choix d'une distribution de diffuseurs : nous avons cherché à simuler la pluie sur deux dimensions. Nous avons donc considéré, pour une intensité de pluie donnée, la concentration de points dans un rectangle conduisant à la même distance minimale moyenne entre deux diffuseurs que dans le cas à trois dimensions. Le tirage est effectué par choix aléatoire des coordonnées de chaque diffuseur en excluant les diffuseurs trop près les uns des autres afin d'imposer un module inférieur à 1 aux opérateurs non diagonaux $\bar{\bar{f}}_{\alpha\beta}$. Si tel n'était pas le cas, l'approximation de Rayleigh serait injustifiée et la matrice $\bar{\bar{f}}$ pourrait être mal conditionnée. Les diffuseurs sont des gouttes sphériques de pluie dont le rayon est soit fixé par le programmeur, soit aléatoire selon la distribution de Marshall-Palmer.

b) numérotation des diffuseurs : les diffuseurs sont répartis dans un rectangle de longueur parallèle à l'axe des x et double de la largeur. Les diffuseurs sont numérotés dans le sens des x croissants. Ceci permet de penser que la valeur de l'indice de troncature de l'équation (5) sera approximativement proportionnelle à la racine carrée du nombre total de diffuseurs.

c) calcul des coefficients des équations (4) : les coefficients de diffusion sont évalués pour des gouttes d'eau sphériques selon la théorie de Rayleigh. L'onde incidente se propage dans la direction de l'axe des x et son champ électrique est parallèle à l'axe des y. Dans le cas présenté ici, la longueur d'onde a été choisie égale à 3 millimètres.

d) inversion du système d'équations (4) : cette inversion, qui est ici pratiquée par approximation successive à partir du développement limité de 1/1+x, est, comme nous l'avons vu, un point délicat de la simulation. Le nombre de gouttes, N = 180, a été limité par la capacité mémoire du calculateur dont nous disposions. Ce nombre est évidemment faible,

mais permet d'effectuer exactement la résolution de (4) et donc de pouvoir jauger la validité des résultats issus des approximations (5) pour différentes valeurs de l'indice de troncature.

e) calcul du champ diffusé au niveau de l'observateur : ce champ est calculé par sommation en amplitude et phase des champs diffusés par chaque goutte. La difficulté de cette sommation tient à ce qu'elle doit être faite en tenant compte des phases. Pour éviter des erreurs purement numériques, la phase des champs diffusés a été développée selon la distance des diffuseurs au centre du rectangle.

f) moyenne glissante de la puissance du champ diffusé : le champ diffusé se présente sous la forme d'un système de franges d'interférence. Le caractère granulaire provient naturellement du faible nombre de gouttes utilisé. Sans pouvoir encore le justifier rigoureusement, il nous a semblé qu'une moyenne angulaire devrait se rapprocher d'une moyenne purement statistique. Ce "lissage" a dont été effectué sur une largeur de 1 degré par pas de 1 centième de degré.

4 - RESULTATS

Les résultats que nous présentons ont tous été obtenus pour une distribution pseudo-aléatoire donnée de gouttes, c'est-à-dire que nous n'avons pas effectué de moyenne statistique sur plusieurs tirages de gouttes. Nous présentons d'abord, calculés sans avoir effectué de moyenne glissante, les amplitudes du champ diffusé par une distribution de gouttes correspondant à une intensité de pluie égale à 100 mm/h, les rayons étant distribués selon la loi de Marshall-Palmer. L'observateur est situé à 20 km du milieu diffusant qu'il voit sous des angles compris respectivement entre 88,6 et 89 degrés (figure 3a) et 89,6 et 90 degrés (figure 3b). Les courbes représentent l'amplitude en décibels du champ calculé par diffusion simple, par diffusion multiple sans troncature de l'équation (4), et par diffusion multiple avec un indice de troncature égal à 20. Nous pouvons constater d'une part la présence d'un système de franges d'interférence rendant impossible toute comparaison directe, et d'autre part l'évanouissement du champ diffusé dans la direction 90 degrés lors du calcul par diffusion simple. Ceci est une conséquence directe de la forme du diagramme de diffusion obtenu par la méthode de Rayleigh.

Nous présentons donc désormais des résultats obtenus après avoir effectué une moyenne glissante. Afin de rendre sensibles les effets liés à l'aspect multiple de la diffusion malgré le nombre restreint de gouttes considérées, nous avons placé les gouttes à l'intérieur d'un rectangle de dimensions égales à 50 x 100 cm, et nous avons choisis des rayons de gouttes tous égaux à respectivement 1,45 et 1,55 mm, ce qui correspondrait à l'effet qu'auraient des distributions aléatoires exponentielles de rayons de moyennes respectivement égales à 0,8 et 0,85 mm. Afin d'étudier l'influence de l'indice de troncature, nous nous sommes intéressés à l'influence de la direction d'observation entre 2,5 et 87,5 degrés. Nous avons calculés les valeurs en décibels de la puissance du champ diffusé pour des angles d'observation compris entre 2,5 et 87,5 degrés par pas de 2,5 degrés et nous avons effectués une régression non linéaire à trois paramètres avec pour fonction modèle une fonction de la forme :

$$P = 10 \log (a \cos^{b}\theta + c) \qquad (6)$$

où a, b et c sont les constantes déterminées par la régression.

La figure 4 illustre un calcul effectué pour un rayon de gouttes égal à 1,55 mm, l'observateur étant situé à 20 km du milieu diffusant. Les points représentent les valeurs calculées par la simulation et les lignes les courbes fournies par la régression. Pour comparer les résultats de la simulation effectués avec différents indices de troncature, nous avons calculé les courbes de régression pour les résultats fournis par la diffusion simple, la diffusion multiple et la diffusion multiple tronquée. Nous avons alors calculé l'écart quadratique moyen d'une courbe à une autre. Les figures 5a et 5b illustrent ces rapports pour deux distributions et deux rayons de gouttes différents ; nous y avons aussi représenté le rapport c/a des constantes de l'équation (6) sous forme logarithmique, montrant "l'isotropisation" de la diffusion. Les échelles sont normalisées à l'écart quadratique moyen entre les valeurs simulées et la courbe de régression pour la diffusion multiple non tronquée d'une part, au rapport c/a pour la diffusion multiple non tronquée d'autre part. En abscisse nous avons porté l'indice de troncature. Ces courbes montrent qu'il paraît raisonnable d'adopter un indice de troncature égal à 30 pour un rayon de goutte égal à 1,45 mm et un indice égal à 50 pour un rayon de goutte égal à 1,55 mm. Il paraît effectivement normal que l'indice de troncature doive augmenter avec le pouvoir diffusant des particules.

5 - CONCLUSION

Bien que cette méthode de simulation repose sur des concepts simples, elle a pu nous fournir une première estimation qualitative des effets de la diffusion multiple. Nous avons ainsi constaté un affaiblissement de la dépendance angulaire de la diffusion latérale. Nous pouvons donc nous attendre à ce que celle-ci soit sensiblement plus importante que ne le laissent prévoir les calculs basés sur le modèle de la diffusion simple. Nous avons aussi déterminé, pour la numérotation adoptée, un ordre de grandeur pour l'indice de troncature, ce qui permettra à l'avenir d'augmenter le nombre de gouttes. Enfin le modèle est suffisamment simple pour pouvoir tester ultérieurement l'influence d'un certain nombre de paramètres tels que la distance corrélation de goutte à goutte.

BIBLIOGRAPHIE

CHANDRASEKHAR, S., 1950, "Radiative Transfer", Clarendon Press, Oxford.

FRISCH, U., 1968, "Wave propagation in random media" dans "Probabilistic Methods in Applied Mathematics", ed. par Bharucha-Reid, Academic Press, New York and London.

OLSEN, R.L., KHARADLY, M.M.Z. et CORR, D.G., 1976, "On certain theories of multiple scattering in random media of discrete scatterers", Radio Science, 11, 1, p. 21-37.

TWERSKY, V., 1962, "On scattering of waves by random distributions", J. Math. Phys., 3, 4, p. 700-715, p. 724-734.

UCSINSKY, B.J., 1977, "The elements of wave propagation in random media", Mc Graw-Hill International Book Company.

WATERMAN, P.C., 1969, "Scattering by dielectric obstacles", Alta Frequenza, 38, p. 348-352.

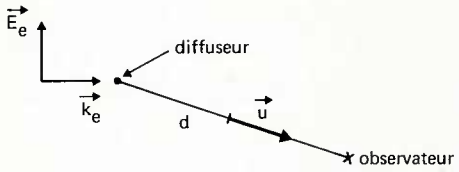

Figure 1

Géométrie de la diffusion causée par un diffuseur

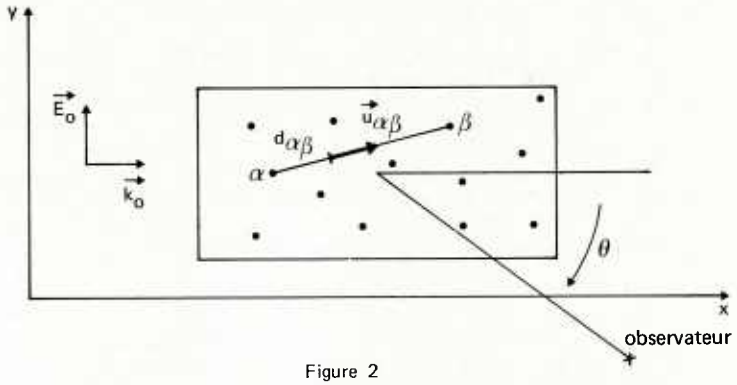

Figure 2

Géométrie de la diffusion causée par un ensemble de diffuseurs

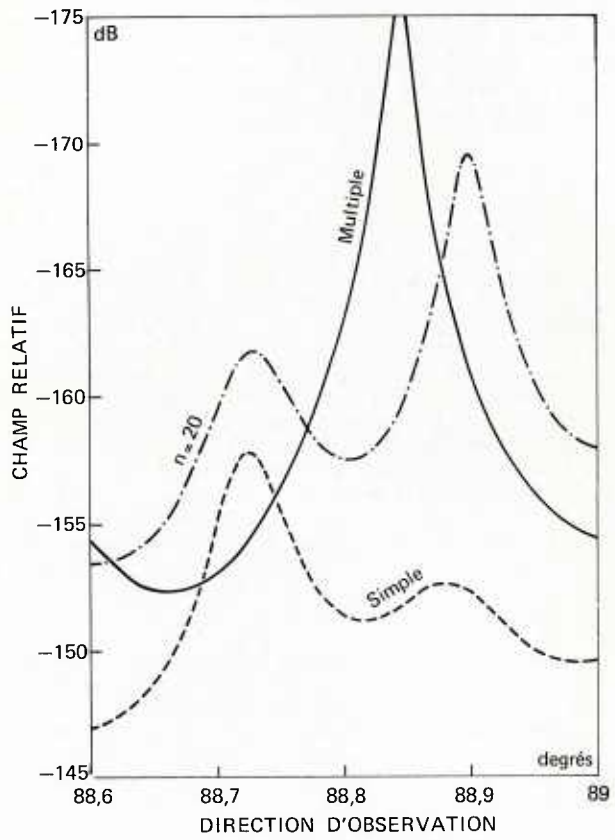

Figure 3a

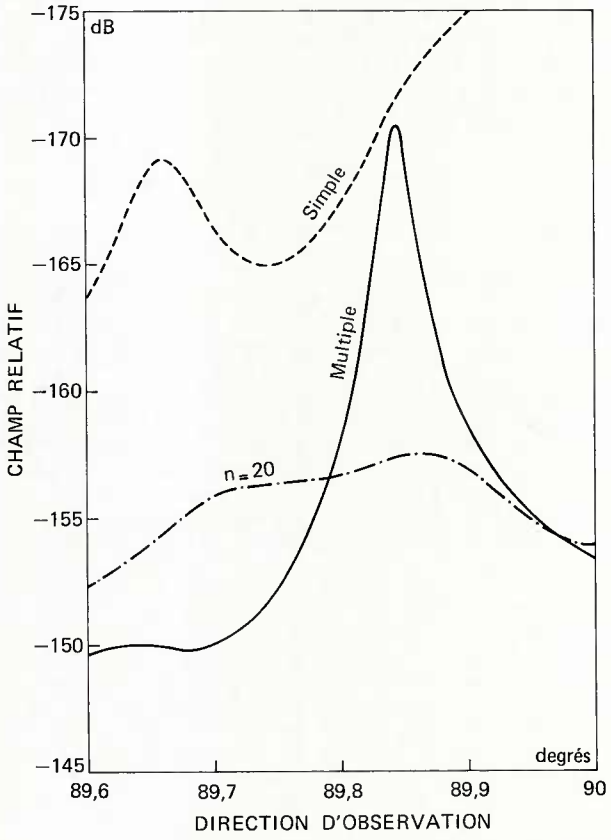

Figure 3b

Valeurs du champ diffusé à 20 km dans la direction θ.
La concentration et les rayons des gouttes correspondent à une intensité de pluie égale à 100 mm/h.

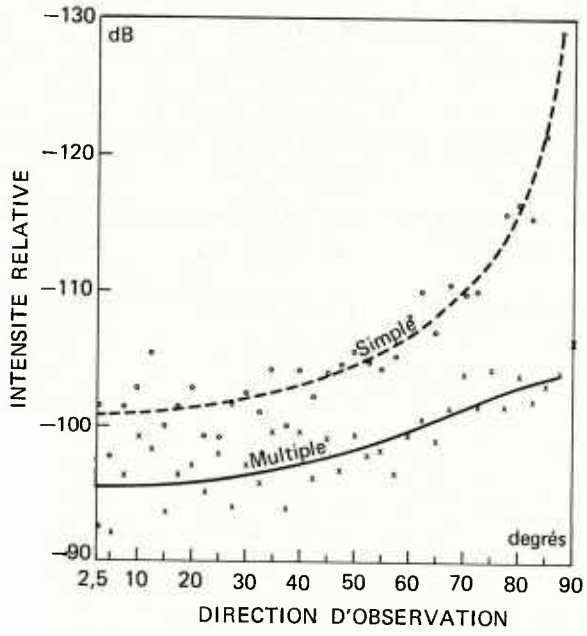

Figure 4

Intensité du champ diffusé à 20 km dans la direction θ.
Les points représentent les valeurs calculées par simulation et les traits pleins les courbes de régression.
Les gouttes sont réparties a l'intérieur d'un rectangle de dimensions 50 x 100 cm
et leurs rayons sont tous égaux à 1,55 mm.

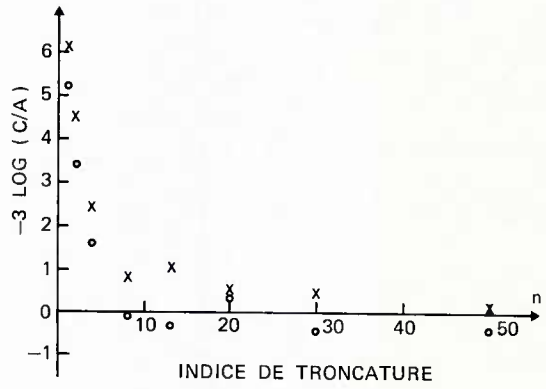

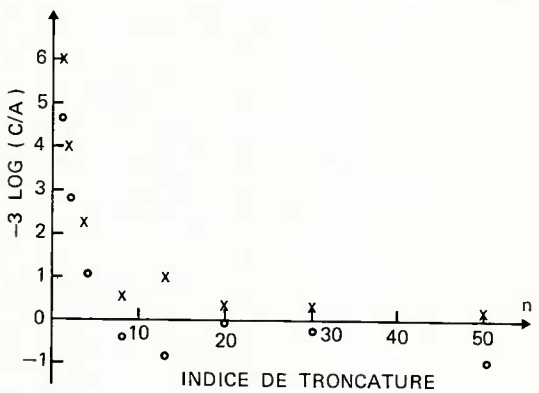

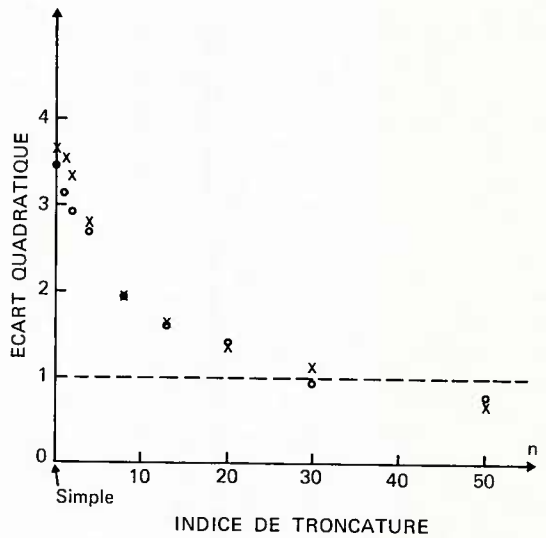

Figure 5a

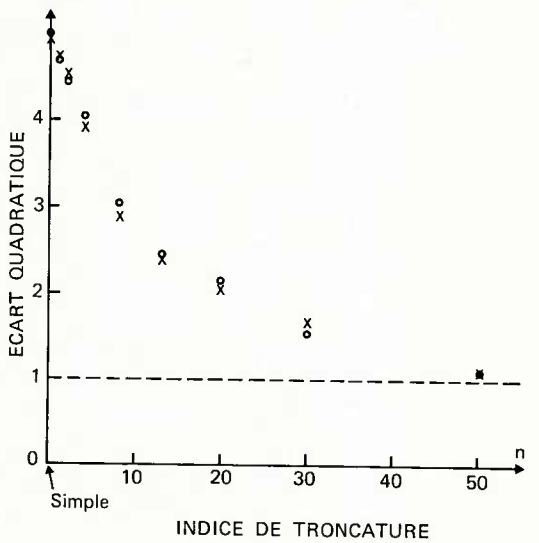

Figure 5b

Ecarts quadratiques par rapport à la courbe de diffusion multiple exacte et évolution du rapport c/a.
Les gouttes sont réparties à l'intérieur d'un rectangle de dimensions 50 x 100 cm
et leurs rayons sont tous égaux à 1,45 mm (fig. 5a) et 1,55 mm (fig. 5b).
Les valeurs sont normalisées par rapport aux valeurs déduites du calcul de diffusion multiple exacte.

DISCUSSION

J.Arnbak, Ne

The presence of interference lines in your results would seem to suggest that the phase of the scattered field is (too) important.

Have you considered applying the *random-phase approximation* known from nuclear scattering theory?

Réponse d'auteur

Nous avons présenté une méthode de simulation en nous efforçant d'exclure le maximum de considérations théoriques.

BISTATIC RADAR REFLECTIVITIES IN THE RANGE 11-30 GHz

by

D.G. Charlton*, A.R. Holt* and B.G. Evans†
Departments of Mathematics* and
Electrical Engineering Science†
University of Essex,
Wivenhoe Park,
COLCHESTER CO4 3SQ,
U.K.

ABSTRACT

In this paper we present bi-static scattering cross-sections and reflectivities for the scattering of microwaves by raindrops. We compare exact results for spheroids (obtained by the Fredholm integral equation method), with exact results for spheres (obtained using Mie Theory), and approximate calculations for spheroids using Rayleigh Theory. Results are given for several frequencies in the range 11-30 GHz, and for both a terrestrial and a satellite path. The Rayleigh approximation is found to give significant errors in certain cases. The results have implications for the calculation of interference between communication systems.

INTRODUCTION

One possible mechanism causing interference between microwave/millimetre wave communication systems, whether terrestrial or satellite, is scattering due to precipitation on the propagation path. The most likely configurations are interference between paths to two neighbouring satellites, and between a terrestrial and a satellite link. Such scatter is termed "bi-static" scattering, the bistatic angle being the angle through which the transmitted beam is deflected when being scattered towards the receiver of the other system. It is anticipated that the form of precipitation that contributes most to such interference is rain, and we confine our attention to rain-scatter in this paper, but the melting band or even the ice regions could give important contributions in some weather situations. Until recently investigation of the effects of rain at microwave/millimetre wave frequencies has been limited mainly to forward scattering (for prediction of the attenuation and cross-polarisation of propagation links) and to backscattering (for calculation of radar reflectivities). However calculation of bistatic scattering is no more difficult than calculation of forward or backward scattering.

Since polarisation diversity is now employed in both propagation and radar systems, the simple spherical model shape for raindrops (adopted for all early calculations) is completely inadequate, since it predicts no differential scattering in the forward and backward directions. Real raindrop shapes can be very complex, since drops are believed to vibrate as they fall, and the larger drops may become concave on their lower surfaces. However the spheroidal model appears to give an adequate description, and calculations using this model have given good agreement with experiment (Howell R.G., and Thirlwell J. 1981). Since there are so many unknowns, such as size distribution, mean drop shape etc., refinements of this model are unnecessary - differences between scattering from Pruppacher - Pitter form raindrops, and spheroidal drops have been shown to be small (Oguchi T. 1977). Bistatic scattering from such raindrops have been studied at 34.8 GHz. (Awaka J., and Oguchi T. 1982).

The foundation work on rain-scatter interference is the paper of Crane (Crane R.K. 1974) who considered an effective reflectivity for the common scattering volume and an effective propagation distance through the rain. He used the Rayleigh approximation for spheres to model the bistatic reflectivities. Recently we have presented some calculations of bistatic cross-sections and reflectivities at 11.7, 20 and 30 GHz, (Charlton D.G. et al. 1982), comparing the spheroidal model with the spherical model, and also with the Rayleigh approximation for spheroids. Although we found that the difference in drop cross-sections between the spherical model and the spheroidal model is generally not more that 3 dBs, there were cases where the error was greater than this, notably for a satellite path. In this paper we present further calculations of bistatic reflectivities and individual raindrop cross-sections at 11.786, 14.455, 17.5 and 30 GHz.

THEORY

We assume that raindrops may be approximated by oblate spheroids of semi-axes a, a, b, which are related to the drop-size by the approximate formula (Pruppacher H.R. and Pitter R.L. 1971)

$$b/a = 1 - \bar{a}$$

where $\bar{a}$ is the radius in cm of a sphere of equal volume.

We further assume that the rain consists of drops of the size distribution proposed by Marshall and Palmer (Marshall J.S. and Palmer W. 1948)

$$n(\bar{a}) = 8000 \exp(-4.1 R^{-0.21} \bar{a})$$

where $n(\bar{a})\, d\bar{a}$ is the number of drops in the size range $(\bar{a}, \bar{a} + d\bar{a})$, and R is the rainfall rate in mm/hr.

Suppose now that a plane electromagnetic wave $\underline{E}_i(\underline{r}) = \hat{\underline{e}}_p \exp(i\underline{k}_i \underline{r})$, of unit intensity, wave-vector $\underline{k}_i$ and polarisation vector $\hat{\underline{e}}_p$ is incident on a single raindrop of equal volume $\bar{a}$. The total field then consists of the incident field, and a scattered field $\underline{E}_s(\underline{r})$ which has the asymptotic form

$$E_s(\underline{r}) \sim \underline{f}(\underline{k}_i, \underline{k}_s, \hat{\underline{e}}_p, \bar{a}) \frac{\exp(ikr)}{r} + O(1/r^2).$$

Here $\underline{k}_s$ is the wave-vector in the scattered direction, and

$$|\underline{k}_i| = |\underline{k}_s| = k = 2\pi/\lambda$$

where λ is the wavelength.

The quantity $\underline{f}$ is the vector scattering amplitude. The total bistatic cross-section which describes the total power scattered from a single scatterer is defined as

$$\sigma_{bp}(\underline{k}_i, \underline{k}_s, \hat{\underline{e}}_p, \bar{a}) = 4\pi |f(\underline{k}_i, \underline{k}_s, \underline{O}_i, \bar{a})|^2$$

This includes power scattered into both (orthogonal) polarisations.

For an assemblage of scatterers, we define the reflectivity factor

$$z_p = \int \sigma_{bp}(\bar{a})\ n(\bar{a})\ d\bar{a}$$

In general z_p will depend on the particular geometry of the scattering process being considered. The theory has been summarised by Charlton et al (1982)

RESULTS

The scattering geometry assumed in these results is that of Charlton et al (1982). The raindrops are assumed to be falling with their axes of symmetry all aligned and vertical. A particular direction is defined by two angles (θ,ϕ) where θ is measured from the axis of symmetry of the drop and ϕ is measured from the plane containing the axis of symmetry and the incident direction.

The raindrops are assumed to be subject to an incident plane wave propagating in the direction $\underline{k}_i$ making an incident angle θ_i with the axis of symmetry of the drop. We define vertical and horizontal polariations, in any direction, as $\hat{\underline{e}}_\theta$, $\hat{\underline{e}}_\phi$ respectively.

The comparisons shown here are between reflectivities/scattering cross-sections calculated exactly for spheroids and spheres, using Fredholm Integral Method (Uzunoglu N.K. et al 1977; Holt A.R. 1980) and Mie theory respectively, and approximately for spheroids using the Rayleigh approximation.

Figures 1 and 2 show scattering patterns for individual drops. In figure 1 we compare the patterns for three spheroidal drops ($\bar{a}$ = 0.125, 0.150, 0.175 cm) around the resonance region at a frequency of 14.455 GHz. The polarisation is horizontal, the incident angle 90^o and we show the plane given by $\theta = 90^o$.

The patterns, which are plotted on a logarithmic (dB) scale are of similar shape. The direction of maximum scattered power is forward for $\bar{a} < 0.125$. In figure 1 we notice that at $\bar{a} = 0.125$ cm, the forward power just exceeds the backward, and for larger drops the maximum scattered power is in the backward direction, until $\bar{a} \sim 0.32$ cm where the maximum again switches to the forward direction. The patterns for the three drops vary. In the scattering plane shown the variation in intensity between patterns for adjacent drop sizes, can vary by up to 4dB.

Figure 2 shows an example of the more varied patterns arising from larger drops at higher frequencies. Here the geometry is similar to that of figure 1, with a drop size of 0.325 cm at a frequency of 30 GHz.

The other results in this paper indicate the scattering patterns due to rain. These patterns are formed from considering a unit volume of rain and integrating over $\bar{a}$ the product of the power scattered in a given direction and the assumed drop-size distribution. In this study we assume a Marshall-Palmer drop-size distribution.

Figure 3 shows a comparison of scattering patterns predicted for a satellite path for a rain rate of 20 mm/hr. The angle of elevation is 30^o and the graph shows the scattering in the vertical plane $\phi = 0,\pi$ of a vertically polarised wave. The first point of interest is that the Rayleigh approximation shows nulls that are neither aligned with the polarisation vector nor complete (i.e. of 0 magnitude). The reason for the non-alignement is that the direction of the dipole induced in the drop is modified by the shape of the scatterer so that it does not quite line up with the polarisation vector. A complete null is not shown due to the plotting process. Since no calculated point lies in the exact direction of the null the curve fitting process results in the depth being taken as that at the nearest point (points are spaced at 5^o intervals). This will also affect the exact position of the null though this will be very close to that shown. The modification of the dipole direction does not occur in the geometry of the other figures due to symmetry arguments.

The exact sphere and spheroid give very similar patterns varying by no more than 1.5 dBs. However the pattern due to the sphere is, in fact, symmetrical about the propagation direction while the pattern due to the spheroid is not.

Further scattering patterns are shown in figures 4-6. These give the scattering patterns at 17.5 GHz for the same geometry as figure 1. The Rayleigh approximation generally underestimates the scattering, though not substantially, except in the directions near parallel to the polarisation vector. Here the Rayleigh theory erroneously predicts a null. For the higher rainfall rate (40 mm/hr) a comparable pattern for spheres is also shown. In this case the pattern due to the spheres does not approximate the spheroid pattern any more accurately than the Rayleigh theory except in the region of the null. Here it gives quite good agreement, far better than the Rayleigh approximation.

Finally figure 7 shows the variation with rain rate of the scattering in four directions due to rain. The geometry here is the same as that for figure 1. The directions chosen are forward, backward and at 45^o from both forward and backward. The rain rate varies from 1 to 50 mm/hr. At 1 mm/hr the backward is actually less than the forward though this is indistinguishable on the graph. At 5 mm/hr the backward has already overtaken the forward scattering.

This calculation of bistatic cross-sections is the first stage in a study of interference between communication systems due to rain scatter - the main previous study so far being the work of Crane (Crane R.K. 1974), who inter alia assumed the validity of the Rayleigh approximation. The factors which will have to be taken into account include the scattering geometry (which affects the common volume), beam patterns, overall weather situations (e.g. rain "cell", or widespread rain), attenuation within common volume.

CONCLUSION

We have presented results for scattering both by individual raindrops and rain for several frequencies, drop-sizes and rain rates. Comparisons have been drawn between the scattering patterns arising from spheroidal drops, calculated exactly and using the Rayleigh approximation, and those for equivolume spheres.

It has been found that the use of the Rayleigh approximation will result in serious errors occurring for scattering in the region around the direction of the incident polarisation vector. As the frequency increases the Rayleigh theory will be found to be increasingly inaccurate in all directions.

The approximation by equivolume spheres, however, models the scattering near the polarisation vector much more accurately. Though in general it does not appear to give substantially better results than the Rayleigh approximation at frequencies below 17.5 GHz for rain rates below 40 mm/hr.

ACKNOWLEDGEMENTS

One of us (D.G. Charlton) acknowledges the receipt of an SERC Case award and sponsorship from British Telecom. All calculations were performed on the PDP-10 computer at Essex University. The help of the computing centre staff is gratefully acknowledged.

REFERENCES

AWAKA J. and OGUCHI T, 1982. "Bistatic radar reflectivities of Pruppacher and Pitter form raindrops at 34.8 GHz", Radio Science, vol. 17(1) pp 269-78.

CHARLTON D.G., HOLT A.R. and EVANS B.G., 1982. "A comparison of the bistatic cross-section and reflectivities of spherical and spheroidal raindrops at microwave frequencies". To be published.

CRANE R.K., 1974. "Bistatic scatter from rain". IEEE Trans. A.P., vol AP-22, pp 312-320.

HOLT A.R., 1980. "The Fredholm integral equation method and comparison with the T-matrix approach" in "Acoustics, Electromagnetic and Elastic wave scattering: Focus on the T-matrix approach" ed Varadan (New York: Pergaman Press).

HOWELL R.G. and THIRLWELL J., 1981. "Slant path depolarisation measurements at 12 and 14 GHz carried out at Martlesham Heath using OTS satellite". Int. Conf. Ant. & Prop. York, UK, IEE Conf. Proc. 195, pp 55-61.

MARSHALL J.S. and PALMER W., 1948. "The distribution of raindrops with size", J. Meteorology vol 5 pp 165-166.

OGUCHI T., 1977. "Scattering properties of Pruppacher and Pitter form raindrops and cross polarisation due to rain: calculation at 11, 13, 19.3 and 34.8 GHz". Radio Science vol 12(1) pp 45-51.

PRUPPACHER H.R. and PITTER R.L., 1971. "A semi-empirical determination of shape of cloud and raindrops". J. Atmos. Science vol 28 pp 86-94.

UZUNOGLU N.K., EVANS B.G. and HOLT A.R., 1977. "Scattering of electromagnetic radiation by precipitation particles and propagation characteristics of terrestial and space communications systems", Proc. IEE vol 124 pp 417-424.

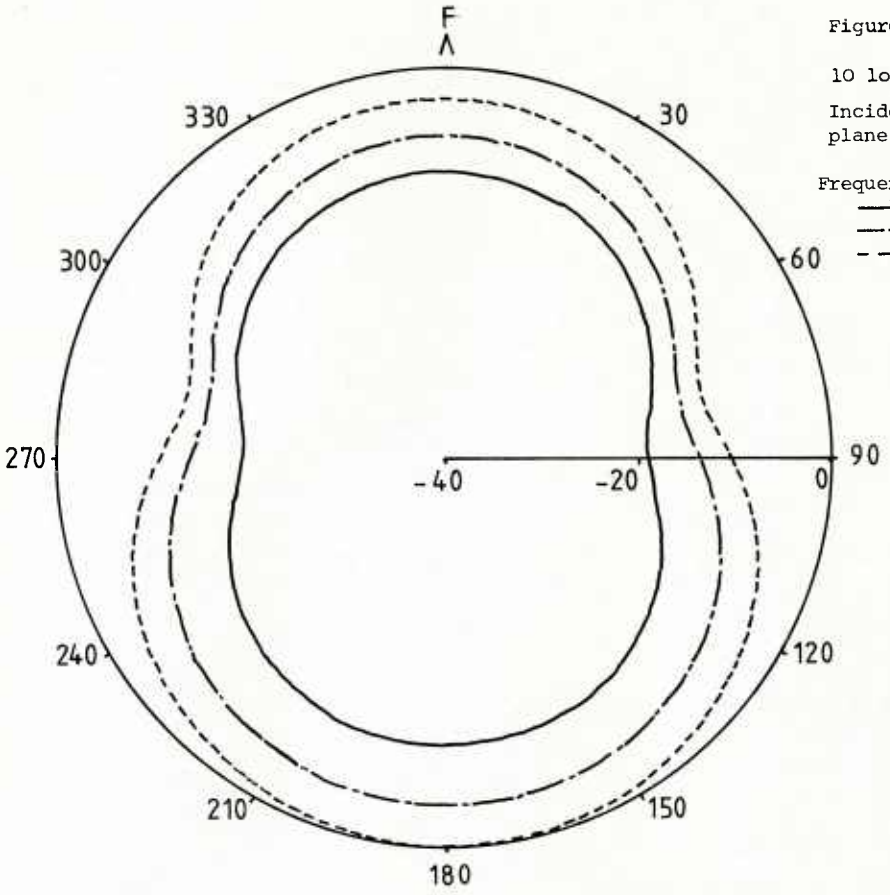

Figure 1

$10 \log_{10} |f|^2/|f_{max}|^2$ for three drops.
Incident direction and scattered plane perpendicular to drop axis

Frequency = 14.455 GHz
——— = 0.125 cm
—·—·— = 0.150 cm
– – – = 0.175 cm

Figure 2

$10 \log_{10} |f|^2/|f_{max}|^2$ for $\bar{a}$ = 0.325 cm.
Frequency = 30 GHz
Same geometry as in Figure 1.

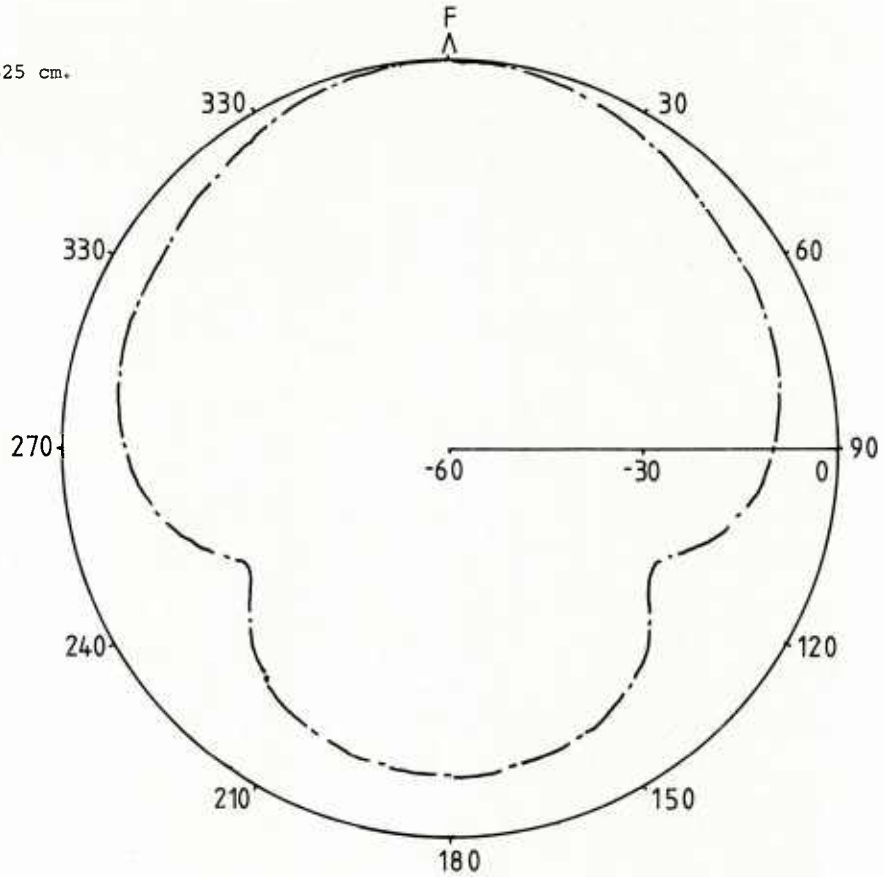

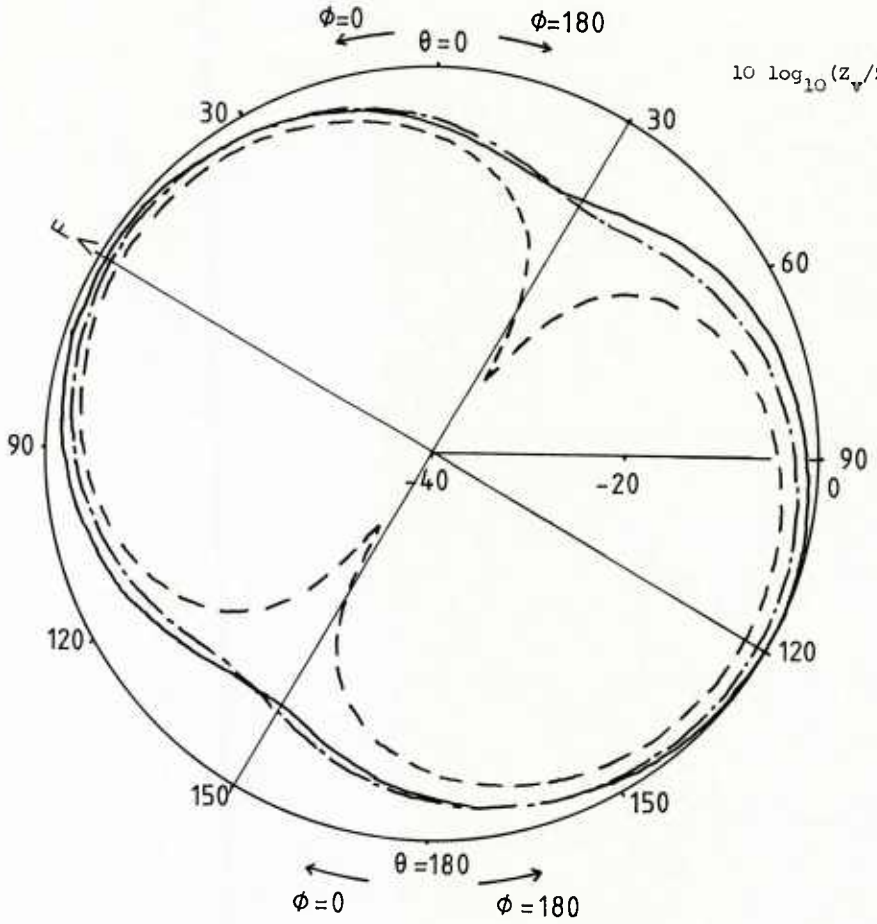

Figure 3

$10 \log_{10}(Z_v/Z_{v\ max})$ for a rain rate of 20 mm/hr.
Vertically polarised wave incident at 60° to drop axes.
Scattered plane vertical
Frequency = 11.7 GHz
—·— Exact spheroid
— — — Rayleigh spheroid
——— Exact sphere

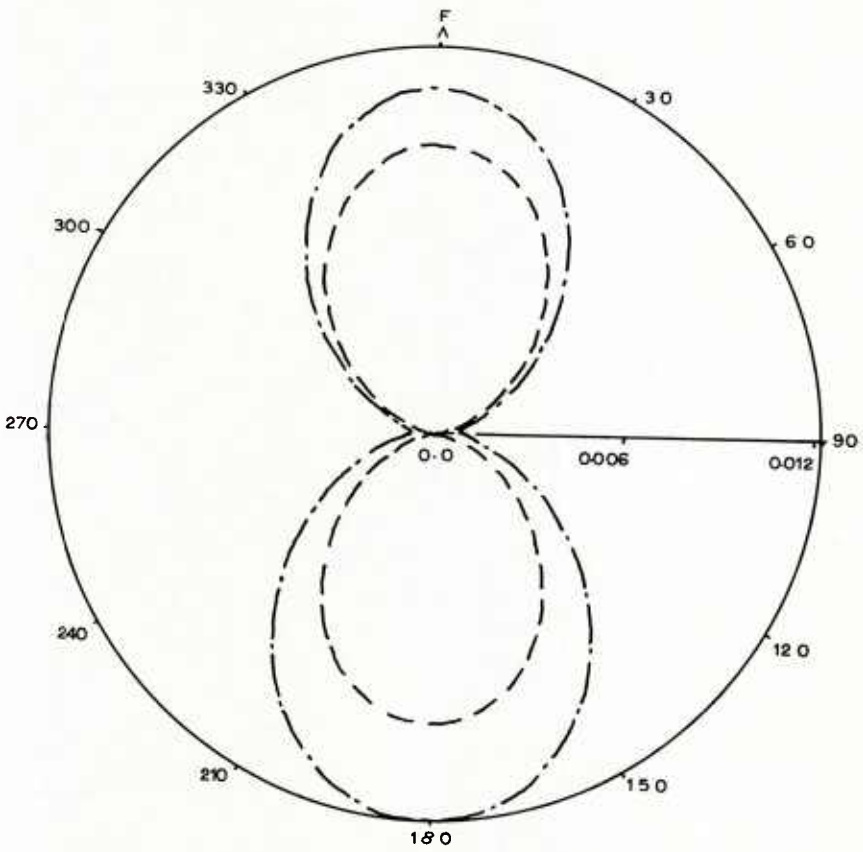

Figure 4

$Z_H/4\pi$ for rain rate 5 mm/hr.
Same geometry as in Figure 1.
Frequency = 17.5 GHz
—·— Exact spheroid
- - — — Rayleigh spheroid

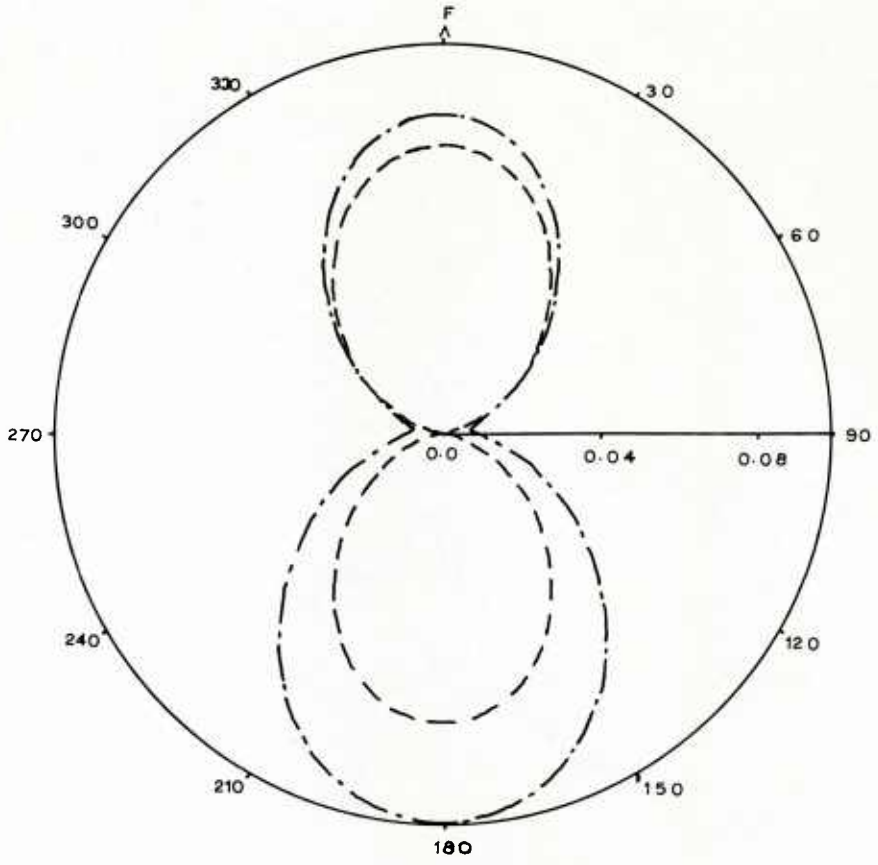

Figure 5

$Z_H/4\pi$ for rain rate of 20 mm/hr.
Same geometry as in Figure 1.
Frequency = 17.5 GHz
——·—— Exact spheroid
— — — Rayleigh spheroid

Figure 6

$Z_H/4\pi$ for rain rate of 40 mm/hr.
Same geometry as in Figure 1.
Frequency = 17.5 GHz
——·—— Exact spheroid
- —— — Rayleigh spheroid
———— Exact sphere

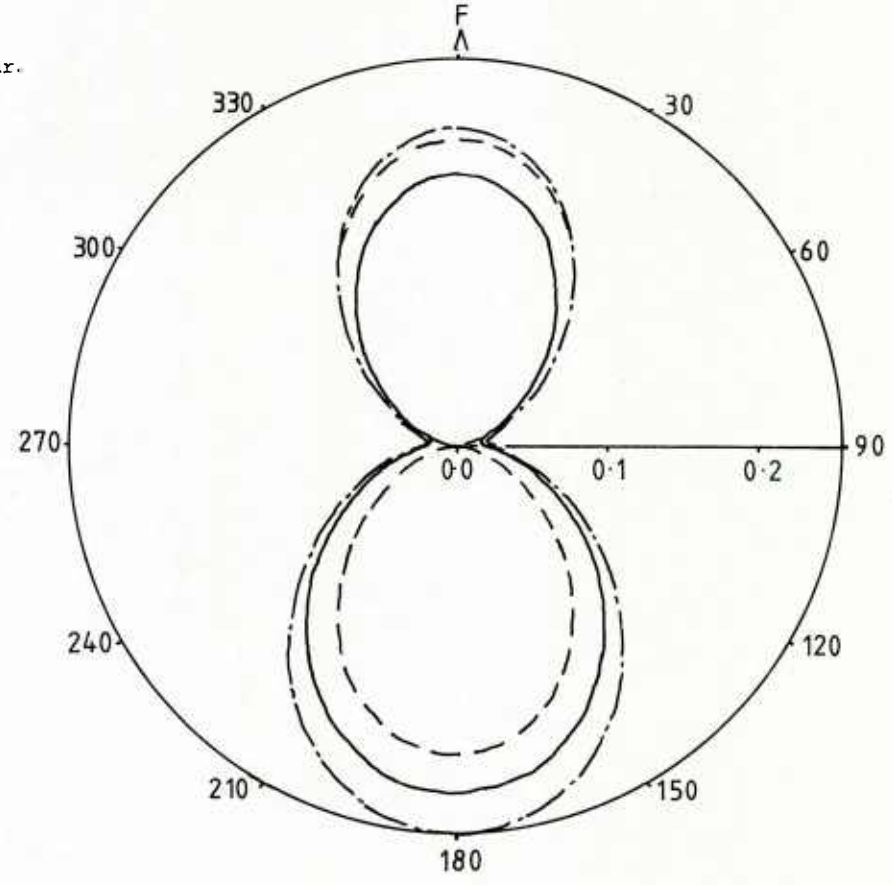

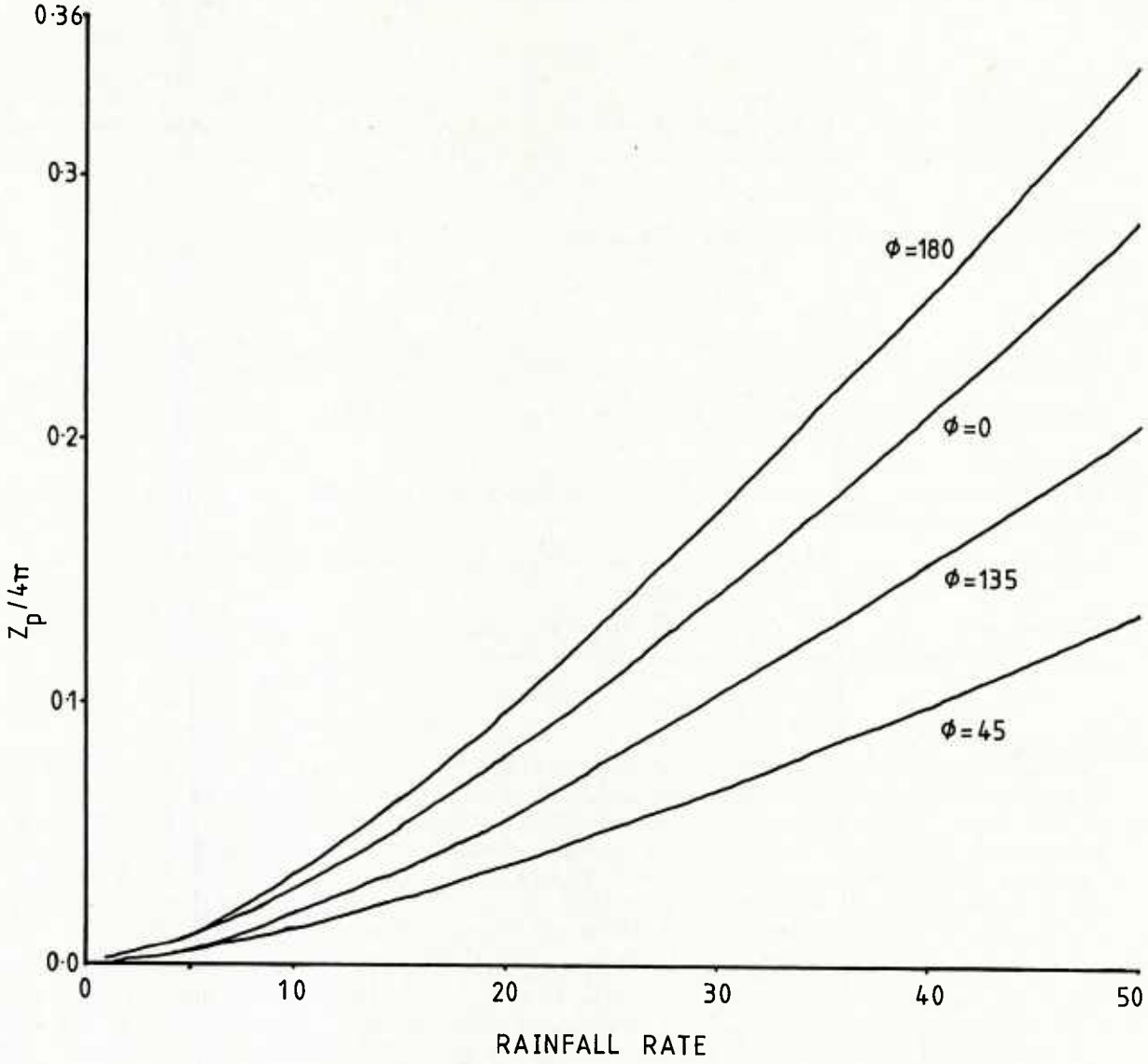

Figure 7

Variation of $Z_H/4\pi$ with rain rate. Frequency is 17.5 GHz $\theta = 90^\circ$ for all curves. Exact spheroid calculations used.

DISCUSSION

S.Segner, US

At a 1973 AGARD meeting, the late Mr Fansler and I gave a paper on coordination distance as a result of rain scatter and troposcatter. The US Army and FAA spent a year trying to match coordination distance model against measurements. How do you see your work affecting Appendix 28 and 29?

Author's Reply

Hopefully within a year better modelling will be available.

R.K.Crane, US

Comment: At the higher frequencies (above 15 GHz) the simultaneous occurrence of attenuation and scattering complicates the modelling process. Snow may be a more important cause of interference than rain.

Question: Will you consider scattering by snow and will you consider the role of attenuation in your future work?

Author's Reply

At higher frequencies substantial attenuation will occur especially for high rainfall rates. At these frequencies, non-attenuating particles may be more significant.

We have performed some calculations for ice. However, as there is no generally accepted model for snow it is difficult to perform calculations for this medium.

It is intended to continue this investigation in order to calculate interference fields and at this stage we would hope to take into account the attenuation along the interference path.

B.G.Evans, UK

As co-author of the paper, I would like to comment on the last two questions. Firstly, in terms of our work leading to an improvement of the CCIR coordination distance calculation, I think that ultimately we will be able to propose an improved method. At the moment we have addressed the scattering problem and shown that the true scattering pattern can lead to interference fields below those calculated with the present model in certain interference directions. We are working on other aspects of the model which may lead to further improvements in modelling the common-volume and until this has been done we would not propose a definitive improved model. But to answer your question, I feel that the indications are that the present model overestimates interference fields.

Secondly, I would agree with Prof. Crane that for higher rainfall rates the path attenuation factor would swamp all others in the millimetre interference field calculation. However, for low rainfall rates and for ice hail and melting band scatterers the interference due to precipitation scatter will be significant. We have already performed a limited calculation on hail and ice and plan to extend them in the future. We are also setting up an experiment at 34 GHz to measure the interference fields and to verify the theoretical models that we have discussed.

T.Sullivan, US

The problem of rain scatter interference between satellite networks is very interesting. This is perhaps a more serious problem than those involving terrestrial paths. In particular, the portion of the effective scattering volume that is composed of the "bright band" in earth-to-space paths might be significantly larger than that for terrestrial paths. Work that I have done in applying the CCIR model at 17 GHz indicates that there may be situations, such as light rain or snow conditions, where the net interference to a "victim" satellite may exceed that which is present during clear sky conditions.

Author's Reply

We would agree that precipitation scatter could cause significant interference between adjacent satellites and that at the higher frequencies the ice and melting band scatterers could play an increasingly important role. We have not as yet fully investigated bistatic scattering from these particles but intend to do so. When we have done this work we will apply our model to the adjacent satellite interference problem. It does not surprise me that your calculations at 17 GHz indicate significant effects.

D.Davidson, US

In the practical coordination of earth stations many of us have been able to coordinate situations by taking into account beam averaging, that is, the variation of the antenna gain (pattern) over the scattering volume, which may be quite large.

Author's Reply

We are in the process of looking at this point at the moment. We hope to be able to calculate an "effective volume" which takes into account a Gaussian beam pattern for both beams.

The gain is not only quantity that may vary throughout the volume. If the common volume is a large distance from the transmitter and receiver it is quite large and the rain fall through out the volume may not be constant affecting the scattering cross-section and attenuation.

OVERSHOOT INTERFERENCE ON MICROWAVE RADIO LINKS DUE TO THE CO-EXISTENCE OF MULTIPATH FADING AND TRANS-HORIZON PROPAGATION

J E DOBLE

British Telecommunications Research Laboratories
Martlesham Heath
IPSWICH
IP5 7RE
UK

SUMMARY

Periods of meteorological conditions which lead to multipath effects on line-of-sight systems can also be those during which anomalous trans-horizon propagation is present. The coexistence of these two effects can give rise to increased system sensitivity to overshoot interference from one section of a microwave route into subsequent sections, or into other systems. Current overshoot interference calculations treat these two effects as uncorrelated and the degree to which this assumption is in error has been estimated from independent measurements on transhorizon links (comprising overland, oversea and mixed paths) and terrestrial links terminating in the same area.

A method of estimating the probability of outage due to this cause is suggested. It makes use of the CCIR models for multipath fading and transhorizon propagation together with an empirically determined weighting factor of the order of 50 times.

1 INTRODUCTION

An extensive programme of measurements has been carried out at the British Telecommunications Research Laboratories (BTRL) to determine extent of enhanced transhorizon propagation phenonema. This work was initiated to estimate the severity of interference from terrestrial microwave systems into satellite communication ground stations and the results have formed a significant input to the revision of CCIR Study Group 5 Report 569. However, it was also realised that there could be some correlation between the periods of enhanced transhorizon propagation and those of multipath fading on line-of-sight systems. Such correlation would have considerable implication for current methods of calculating overshoot interference levels in which complete statistical independence of the two phenonema is assumed.

This contribution describes the basis of determination of an empirical factor that enables an estimate to be made of the shortfall in the current method of overshoot interference calculation.

2 THE RADIO PATHS (See Figure 1)

2.1 The Line-of-Sight Paths

The initial phase of the study made use of fading records obtained from an experimental digital link operating between Stoke Holy Cross, near Norwich, and Mendlesham, 22km north-west of BTRL. This link was closed down at the end of 1980. The details of the link were:-

Path length 40.5km
Frequency 11.115 GHz
Transmitter antenna height 55.4m above ground, ground height 65m asl.
Receiver antenna height 39.6m above ground, ground height 56m asl.

Since the closure of this link a new digital link has been established between Swaffham, to the west of Norwich, and Mendlesham. Details are:-

Path length 50.3km
Frequency 6.275 GHz
Transmitter antenna height 64.5m above ground, ground height 59m asl.
Receiver antenna height 63.8m above ground, ground height 56m asl.

2.2 The Transhorizon Paths

Rockanje-Martlesham
Path Length 190.8km (178.1km sea, 12.7km land)
Frequency 11.365 GHz
Transmitter antenna height 67m above ground, ground height 5m asl.

Rockanje is situated just to the south of the Europort complex in The Netherlands, about 400 metres from the coast. The flat, sea-level land of this area is very typical of a large part of The Netherlands and Belgium. The path crosses an area of the North Sea which is frequently subjected to atmospheric ducts resulting from the advection of warm, dry, continental air over the cooler, moist air above the

sea's surface. The short land section at the UK end of the path is flat countryside with no major obstructions.

Climatological data show that atmospheric conditions in this area are significantly influenced by the North Sea environment, and although the path is divided for prediction calculations, it can normally be considered as an "over-sea" path.

Staxton Wold - Martlesham
Path length 262.6km (186.6km land, 76km sea)
Frequency 11.425 GHz
Transmitter antenna height 52km above ground, ground height 175m asl.

The link from Staxton Wold, Yorkshire, provides an interesting situation for the comparison of predicted and measured signal levels. The CCIR co-ordination prediction procedures define this as a mixed land and sea path in the proportions shown, but experience suggests that the coastal land areas are more appertaining to the marine environment. Activity caused by advection, radiation and subsidence have all been observed, confirming this path as a complex propagation situation.

Sparsholt Firs - Martlesham
Path length 199.9km over land
Frequency 11.405 GHz
Transmitter antenna height 62m above ground, ground height 233m asl.

Sparsholt Firs radio station is high on the downs on the Oxfordshire-Wiltshire border. The path topography varies from rolling downland in the west to the flat land of East Anglia. The anomalous propagation observed over this path results from "radiation-night" effects and occasionally from low-level subsidence inversions. All the receivers at BTRL have similar antennas on a thirteen metre high tower, representing the centre height of a small earth-station parabola. The minimum detectable signal levels are approximately -105 dBm at the receiver input, and data is only recorded during periods when the signals are enhanced above this threshold by atmospheric ducting.

3 THE BASIC PREMISE

The premise on which the study was based was that there would be a degree of correlation between the incidence of multipath and transhorizon events, but within any joint event there would be no correlation of the fine structure of signal variations. For the purpose of the study a joint event was defined as, multipath fading in excess of 25 dB existing concurrently with transhorizon signals rising to within 25 dB of free-space values (for the transhorizon path).

4 DERIVATION OF A CORRECTION FACTOR BETWEEN THE BASIC PREDICTIONS AND THE MEASURED RESULTS

4.1 Basic Prediction of Outage

In order to determine the outage due to overshoot interference using the traditional approach, two characteristics are required. The first is the multipath fading prediction and that used here is the BT fading model:-

$$F_{0.1} = -28 + 35\text{Log } D + 8.5\text{Log } F - 14\text{Log } \sigma_i - G \text{ dB}$$

Where $F_{0.1}$ is the fade depth exceeded for 0.1% of the worst month

D is the path length in km
F is the frequency in GHz
σ_i is the terrain roughness factor in milliradians
G is an empirically determined geographical factor

This expression can be rearranged to the form shown in CCIR report 338, but that given above is found to be more convenient to use The $F_{0.1}$ value derived is that for the worst month and the characteristic is assumed to follow a 10dB/decade slope for cumulative probabilities of the order of 1% and less.

The second characteristic is that for enhanced transhorizon propagation and the method advocated in CCIR Report 569 is used. This is the best model available but is a prediction for the average-year. Its use here as a worst-month prediction is the approach used in the UK in the absence of any published data relating worst-month to average-year figures.

Both characteristics, as they apply to the wanted and transhorizon paths detailed below, are plotted in figure 2.

Since in the current approach to the overshoot problem the two effects are considered uncorrelated the joint, cumulative, probability contours of wanted and transhorizon path attenuation can be constructed by taking the product of the individual probabilities. If the characteristic representing the minimum

carrier-to-interference ratio that the system can tolerate is then superimposed on this family of joint statistics then the probability of outage (carrier-to-interference ratio less than 15 dB) can be determined by taking the contour that has the same exclusion area as the system characteristic. This method is depicted in figure 3, where it is clear that the $p = 6 \times 10^{-3}\%$ contour most nearly meets the above criterion. Note, the system characteristic in this presentation is linear whereas the probability contour is not; there is room for error at this point.

4.2 Prediction of Outage Based on Observed Events

Events in which multipath fading on the Stoke Holy Cross to Mendlesham Link was observed to exceed 25 dB, during the sixteen month period commencing 19 June 1979 were noted. A search through the records of the transhorizon links was then made to identify any periods that could be designated "joint events" within the limits laid down in the basic premise. This search revealed 46 multipath events on the line-of-sight link, 49 periods of transhorizon-path enhancement for the oversea path and 5 periods for the overland paths. The data yielded two joint-events for the oversea situation and one for the overland. The probability of such joint events as calculated from the uncorrelated multipath and transhorizon characteristics is $7 \times 10^{-4}\%$. To register three such events (14 hours total) in a sixteen month period, ie $1.2 \times 10^{-1}\%$, is an indication that the current method of prediction is inadequate for the particular case considered and raises doubts regarding its general accuracy.

As a pointer to the degree of correlation that exists between the two phenomena, on a day-to-day basis, between 1 April 1980 and 30 September 1980 there were 25 days during which there was enhancement of the oversea transhorizon path to within 25 dB of free-space. During the same period there were 28 days during which there was multipath fading in excess of 25 dB, and 15 of the days contained both effects, a very high degree of correlation. See Figure 4.

NB. Because of the time shift between the occurrence of the two effects, only one of the days contained a joint event as defined in section 3.

From the more severe of the oversea events cumulative distributions of path loss for the six-hour duration were plotted (figure 5). These distributions were then used to construct joint-probability contours on the following basis.

i. The loss figures recorded for the transhorizon path were decreased by 10 dB to take account of experimental results which suggested that the level of interference received at the aerial heights typically used on terrestrial links would be 10 dB greater than those indicated in the experiment which simulates the height of satellite communication ground-station aerials.

ii. The paths of the links involved were assumed to be aligned.

iii. The individual probabilities were multiplied together since the two parameters were considered to be uncorrelated within the joint event (see section 3).

iv. The product of the probabilities was multiplied by 0.008 in order to convert from the six-hour event to worst-month values.

The joint-probability contours so produced are shown in figure 6, together with the system-tolerance characteristic. Comparing figure 6 with figure 3 shows a very significant difference between the two approaches.

4.3 The Ratio of Outage Predictions From the Different Approaches

This difference in outage probability was expressed as a ratio of the joint-probability contours that just grazed the system characteristics. As figures 3 and 6 indicate, this is not strictly correct for all attenuation values but was considered acceptable within the limits of the available data. The ratio so determined was found to be 50. On carrying out a similar exercise for the overland situation, the ratio was again found to be close to 50. At this point the results were published (DOBLE, J E, 1981) and also submitted to Study Groups 4, 5 and 9 of the CCIR, the intention being not so much to say that a weighting factor of 50 times should be applied to the current prediction method, but to sound a note of warning that a problem did exist in this area.

5 SUBSEQUENT INVESTIGATIONS

5.1 General Observations

Following the closure of the link between Stoke Holy Cross and Mendlesham, it was necessary to make a compromise and use data available from the 6 GHz link operating between Swaffham and Mendlesham, for comparison with the 11 GHz transhorizon results. It was realised that the situation was not ideal, but it was more important that the measurement terminals of the two systems should be close together. The expected difference in multipath fading at 6 & 11 GHz is only

2.2 dB for the worst month and it would not be too unreasonable to expect similar distributions of fading during an event, even though the fine structure of fading on a 6 GHz and an 11 GHz link operating over the same hop would not be correlated.

5.2 Measured Results

At the time of writing, the results from a six-month period have been examined and found to be very similar to those from the previous phase of study. The highest degree of correlation was again found to be for the situation involving an oversea interferer. This is to be expected since the multipath environment in East Anglia is dominated by ducting systems drifting in from the North Sea.

The most severe joint-event lasted for nearly six hours, commencing at 0014 hrs on 5 8 81. The relevant cumulative distributions are reproduced as figure 7. (The predicted path loss characteristic, ie free space attenuation and multipath fading, for the 6 GHz line-of-sight link is identical to that of the earlier reference link so that figures 2 & 3 can again be used). Comparing figures 6 & 8 strikingly demonstrates how similar these recent results are to those from the previous year. So once again there is a ratio of 50 between the measurement and prediction.

6 CONCLUSIONS

The study, which was based on results derived from propagation data rather than direct measurement of interference in a system, has clearly indicated that to assume that multipath and transhorizon-interference are uncorrelated in overshoot-interference evaluation can lead to significant errors. Normal planning procedures carried out by administrations would seek to ensure that possible interference situations were avoided by adjusting the relative alignment of the lines-of-shoot so that aerial directivities gave the required protection. However, with a dense network this may not always be possible and the probability of joint events of the nature described should be kept in mind. Such a situation may well arise in Europe where there are many administrations operating in common bands and in close proximity.

The apparent increase in susceptibility to transhorizon interference, by a factor of 50, derived from these results cannot be taken as applying to all locations. East Anglia, where the measurements were made, is the most severe multipath environment in the United Kingdom. However, it has been shown that there is a high degree of correlation, in general terms, between multipath fading and enhanced transhorizon propagation and there is no reason to believe that this should not exist elsewhere, although the severity of the individual effects may well be reduced. In order to give some idea of scale, the $F_{0.1}$ multipath-fade prediction for the Stoke Holy Cross to Mendlesham link is 27.7 dB and that for the Swaffham to Mendlesham link is 31.7 dB. In contrast a more general figure for the main UK network is found to be 19 dB. Some of the difference is due to the lengths of the test links, 40 & 50km respectively, and the remainder by the multipath environment. (The factor G in the prediction model in section 4.1 varies between +4dB in East Anglia and -2dB in the South and Midlands).

The conclusion is, therefore, in a situation where there is good alignment between the line-of-shoot of a link and an identified possible source of interference, then the correlation factor that will exist between multipath and transhorizon effects must be taken into account when estimating trans-horizon-interference induced outage.

Acknowledgment is made to the Director of Research of The British Telecommunications Research Laboratories for permission to publish this paper.

REFERENCE

DOBLE, J E 1981, "Interference on Microwave Digital Radio Links Due to Transhorizon Propagation", Electronics Letters, Vol. 17, No 12, P 399.

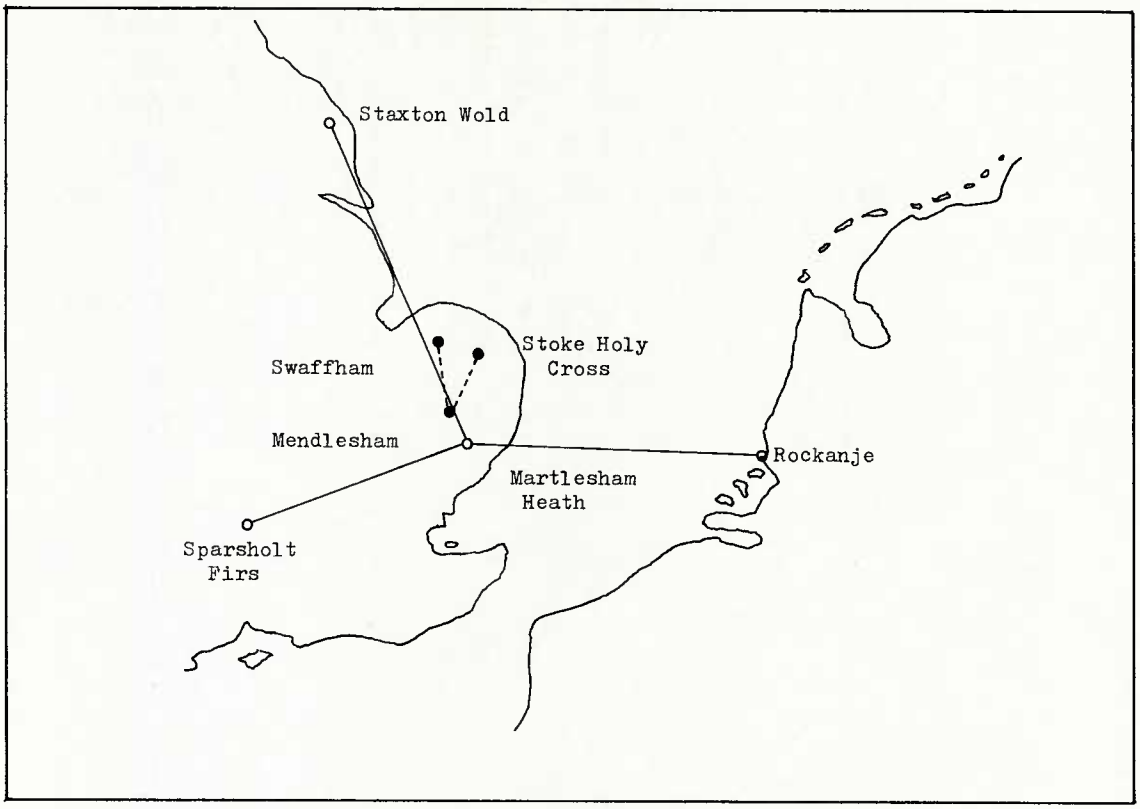

Figure 1. Location of Links Used in the Study

Figure 2

Predicted Cumulative-Distributions of Path Attenuation for:-

a. Rockanje to Martlesham
b. Stoke Holy Cross to Mendlesham

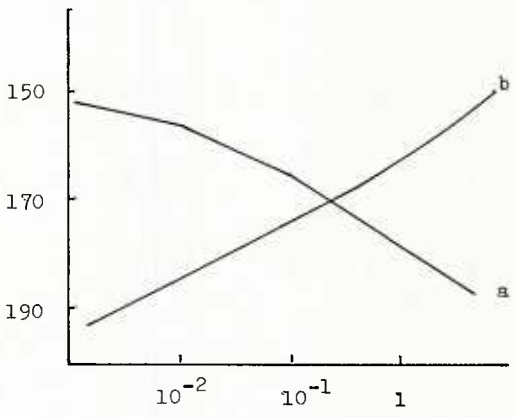

Abscissa: Percentage Time Attenuation on Wanted Path was Greater Than or Attenuation on Transhorizon Path was Less Than Ordinate Value.

Ordinate: Path Attenuation, dB.

Figure 3

Joint-Cumulative-Distributions of Carrier-to-Interference Ratios Derived on a Zero Correlation Basis from the Distributions of Figure 2.

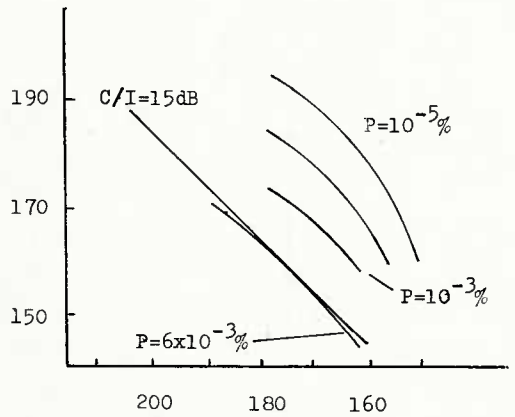

Abscissa: Attenuation on Transhorizon Path, dB.

Ordinate: Attenuation on Wanted Path dB.

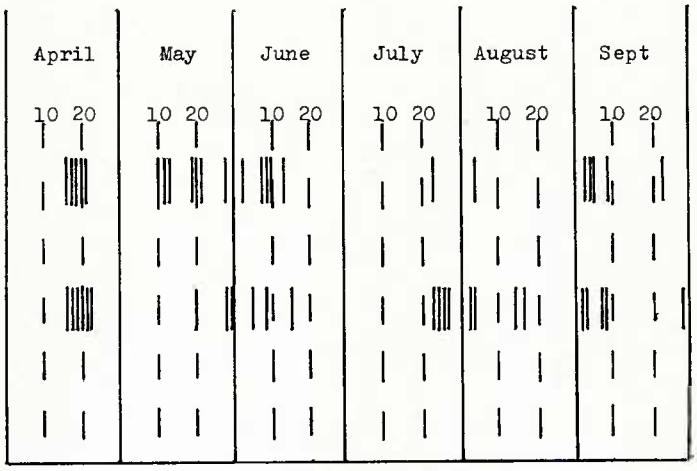

Figure 4

Correlation Between Enhanced Transhorizon Propagation and Multipath Fading on a Day-to-Day Basis, for Rockanje to Martlesham and Stoke Holy Cross to Mendlesham, Between 1/4/80 & 30/9/80.

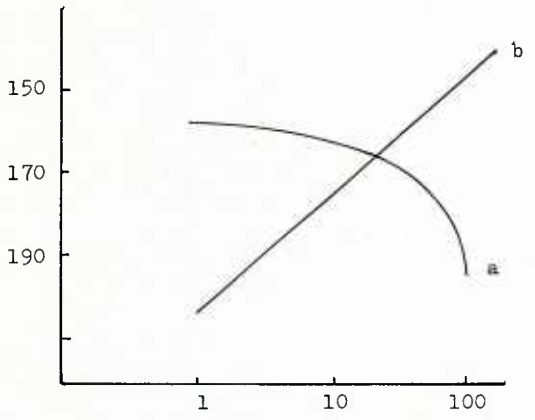

Figure 5

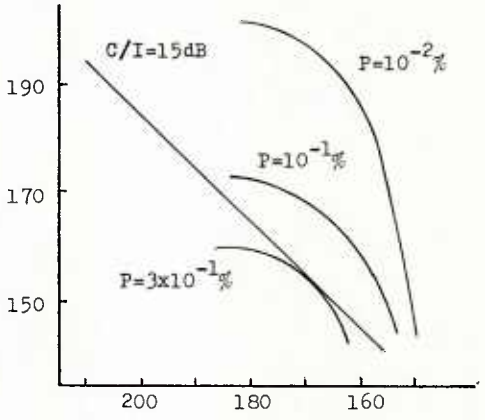

Figure 6

Figure 5/7. Cumulative-Distributions of Path Attenuations on (a) Transhorizon Path and (b) Wanted Path for Worst Events of 1980 & 1981 Respectively.

Abscissa: Percentage Time Attenuation on Transhorizon Path was Less Than or Attenuation on Wanted Path was Greater Than Ordinate Value.

Ordinate: Path Attenuation, dB.

Figure 6/8. Joint-Cumulative-Distributions of Carrier-to-Interference Ratio Derived on a Zero Correlation Basis from the Distributions of Figures 5/7.

Abscissa: Attenuation on Transhorizon Path, dB.

Ordinate: Attenuation on Wanted Path, dB.

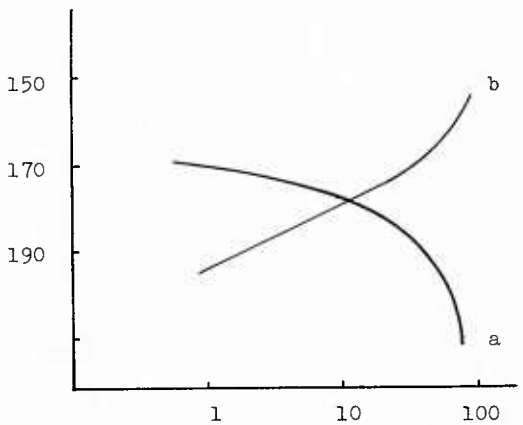

Figure 7

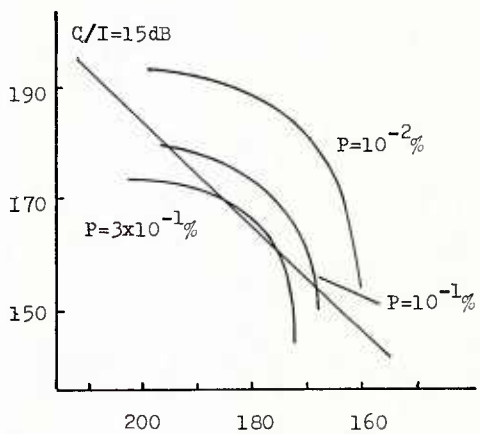

Figure 8

DISCUSSION

E.J.Holliman, US

Since your experimental data is in the general spectrum area once considered for digital computer-driven data exchange with ships, are you suggesting that this portion of the spectrum would be undesirable in a coastal-maritime environment?

Author's Reply

There could well be a problem in this area. However, the solution is not to be found in a shift of operating frequency since although there is evidence to suggest a reduction of transhorizon levels with increasing frequency, this may well be cancelled out by the increase in multipath fading (3.5 Log F term in the model). The answer must be the use of efficient diversity to hold up the wanted signal level and thus reduce outage to an acceptable figure.

H.J.Albrecht, Ge

Referring to possible effects of high-pressure areas of Western Continental Europe on duct formation – perhaps mainly on the Rockanje-Marlesham path – such conditions should occur rather regularly, i.e. for a number of consecutive days. If the short-term prediction method employed does not make use of this situation, an appropriate improvement is suggested.

Author's Reply

This aspect of prediction improvement will be covered by an input to SG 5 of CCIR in which I intend to relate worst-month to average-year statistics for transhorizon propagation (as far as UK experience is concerned).

J.T.Ong, UK

I have mentioned our experience with simultaneous occurrence of high interference levels with presence of multi-path fading/depression of wanted signal on LOS system during Dr Dougherty's presentation. I would just like to add that in such cases we take into account this factor in C/I predictions.

However, I am aware of a method of calculating C/I ratio assuming decorrelation (negative correlation) when 10 dB is added to the C/I ratio.

Author's Reply

I can see no way in which decorrelation of the two transmission effects can take place, and would appreciate further discussion with you on this aspect.

SUMMARY OF SESSION III-B

EHF PROPAGATION

by

Dr H.J.Albrecht
Session Chairman

This session concerned the effects of EHF propagation on frequency sharing, interference and system diversity, with emphasis upon the two first-mentioned areas.

The first paper by **J.Hopponen** and **D.Theobold** on system aspects of clear-air propagation above 40 GHz described a computer program to simulate the characteristics of a communication channel for the frequency range indicated. The program takes into account the transfer properties of the clear air mass and their effects upon communication channels, such as attenuation, signal delay and passband distortion. Atmospheric clear-air characteristics are represented by an appropriate filter function.

In another paper, **B.Evans** and **A.Holt** dealt with propagation constraints in the millimetre wave bands due to precipitation scattering; the frequency range extended up to 210 GHz. This contribution emphasized the need of and indicated an approach to establish simple scaling rules, to reduce the requirement of exhaustive and complex calculations. Their validity was discussed and evaluated.

The final paper of the session, by **B.Rembold**, **M.Wippich**, **H.Bischoff**, and **W.Frank**, concerned a millimetre-wave collision warning device for helicopters. In this case, the frequency range of maximum atmospheric attenuation around 60 GHz has been used. The contribution reported on experimental results obtained and discussed aspects of the frequency selection and radar cross-section on typical obstacles, such as wires.

With all papers presented in this session, the discussions after presentations served to augment the information contained in the contributions, themselves. Among the comments leading to an indication of possible future research the suggested comparison with characteristics and systems on optical frequencies predominated.

SYSTEM ASPECTS OF CLEAR AIR PROPAGATION ABOVE 40 GHZ

David M. Theobold and Jerry D. Hopponen
Lockheed Missiles and Space Company
Sunnyvale, California 94086 USA

SUMMARY

Communication links operating at frequencies above 40 GHz may be modeled using computer programs which treat both the atmosphere and communication hardware of the system in an integrated fashion. The principle mechanisms to be considered in the clear air mass are absorption by atmospheric gases and turbulence effects. Link degradations due to seasonal variations are treated.

Absorption by molecular oxygen and water vapor causes dispersive signal attenuation, phase delay, and noise due to random atmospheric emission. These quantities may be predicted for specific frequency bands and atmospheric conditions by employing a computer program for ray tracing. Examples of the variation of these effects illustrate their complex dependence on atmospheric conditions and ray path elevation angle. The characteristics of the atmospheric transfer function (both amplitude and phase) are of particular importance to questions of modulation distortion in high data rate systems. The atmosphere is viewed as an additional signal filter of the communication channel and the resultant signal distortion is quantified by predicting bit error rate degradation.

1. INTRODUCTION

The performance of a trans-atmospheric communication link for frequencies above 40 GHz can be assessed with the aid of accurate computer programs which model the transfer properties of clear air and characteristics of system components. Signal generation, propagation effects, and hardware distortions are modeled via frequency and time domain techniques. The goal of the simulation model is to assess the effect of combinations of various sources of degradation on a communication channel.

Several computer models have been integrated into an end-to-end simulation language. A description of the EHF atmospheric propagation model and the communication link model is presented in the following sections. Several examples are also given.

2. ATMOSPHERIC ABSORPTION MODEL

For frequencies above 40 GHz, the lower atmosphere exhibits transfer properties which are much different from those at lower frequencies. Attenuation, phase dispersion, and noise from the medium present constraints on system design which may be compounded by tropospheric turbulence, rain, fog, and clouds. In the 40 to 300 GHz range the small wavelengths (1 mm at 300 GHz) dictate careful consideration of not only the atmospheric filter but also of the system hardware as it relates to propagation phenomena.

Figure 1 depicts the attenuation coefficient as a function of frequency at the surface of the earth for clear air, rain, and fog. This broadband summary, taken from (Zufferey, C.H.,1972), shows that attenuation generally increases across the EHF band, with the exceptions due to the peaks in the clear air curve. It is apparent that, based on attenuation considerations alone, design of terrestrial links in the EHF band should include propagation effects. As discussed below, phase dispersion in some regions also begins to impact various modulation types which are used on EHF links. The survey presented here will focus on attenuation by the clear atmosphere, rain, and gain degradation by tropospheric turbulence, but the secondary treatment of phase effects should not minimize the importance of that aspect of the atmospheric filter.

In the EHF band, clear air transfer characteristics arise from absorption by molecular oxygen and water vapor. Figure 2 shows cumulative earth-to-space attenuation along a vertical path through a midlatitude summer atmosphere (solid curve) and a midlatitude winter atmosphere (dashed curve). The water vapor peaks at 22.235 and 183 GHz vary in proportion to the water vapor content of the atmosphere, whereas the peak absorption due to molecular oxygen (60 GHz and 118 GHz) exhibits an inverse temperature dependence. At sea level pressure, the oxygen resonance lines clustered around 60 GHz coalesce into an unstructured band having the appearance of a single line, as in Figure 1. At higher altitudes a fine structure of maxima and minima emerges (for both attenuation and phase: Liebe 1981) and may be manifest in detailed plots of trans-atmospheric filter characteristics. This comb-like structure is not shown in Figure 2. It is important to note that high altitude aircraft-to-aircraft (or aircraft-to-satellite) links in the 55-65 GHz band, which are shielded from the surface, must consider the effects of persistant oxygen absorption in the upper atmosphere.

Figure 3 shows clear air attenuation coefficients calculated for sea level conditions, typical of four climates, across the 50-70 GHz band using the formulation of Liebe et.al. (1977). Although some foreign gas broadening of the oxygen lines by water vapor does occur, the differences between the curves arise primarily because of the temperature dependence in the quantum mechanical expressions for oxygen absorbtion. For

a horizontal link operating near the band center, a subarctic winter atmosphere may yield over 6 dB/km more attenuation than a tropical atmosphere. Table 1 lists attenuation (dB/km) and phase dispersion (radians/km) for the 54-58 GHz band for both seasonal extremes. Although variations at the edges of this band are small per kilometer, integration of attenuation along an earth-to-space path may yield noticeable seasonal variations (see Figure 2).

Figure 4 presents calculated earth-to-space attenuation at 94 GHz as a function of surface elevation angle through four different atmospheres. For elevation angles above 30 degrees the figure shows that cumulative attenuation does not exceed 2.1 dB and shows a slight (in an absolute, not relative, sense) seasonal variation. A similar situation for 172 GHz is shown in figure 5, but at this frequency the seasonal variations (22.5 dB at 30 degees for the tropical atmosphere versus less than 3 dB for the subartic winter case) may make a significant difference in many applications.

Figures 2-5 show that at certain frequencies the transfer properties of the clear air mass may change considerably from season to season. Thus, the design of EHF systems may have to include consideration of atmospheric absorption and also of the seasonal variations. On a shorter time scale, rain and fog may seriously degrade a trans-atmospheric link, as shown by the curves in Figure 1. For system development purposes, rain attenuation probabilities for specific sites may be generated using the Crane Rain Model (1979).

Low elevation angle downlinks which employ large aperture antennas have been known to exhibit some gain degradation due to tropospheric turbulence (Theobold and Hodge, 1978). Based on a model developed at the Ohio State University, gain degradation due to turbulence-induced angle-of-arrival variations is regarded as a function of the receiving antenna beamwidth and the path elevation angle, as shown in Figure 6. For low elevation angles (long path lengths) gain degradtion, R, is shown to be on the order of one-half dB or greater for antenna beamwidths of less than a degree. Thus, tropospheric turbulence is an additional factor which may have to be included in the design of systems operating above 40 GHz, for which such narrow beamwidths are often utilized.

It is to be stressed that phenomena such as fog and rain, which are highly variable, are additional filters which add to the distortion caused by the slowly varying calm, clear air mass. For initial system design, only the latter filter is considered.

3. COMMUNICATIONS SIMULATION LANGUAGE

For inclusion of propagation effects in a computer simulation of the performance of a communication system, the atmosphere is treated as a dispersive filter with amplitude and phase characteristics dependent on the particular band of interest. For a specific frequency band, satellite or aircraft altitude, ground station, path elevation angle, and atmosphere (i.e., atmospheric data profile), ray tracing is performed in order to obtain the calculated signal attenuation and phase delay. A computer disk file containing data for representative frequencies in the band is generated and subsequently used as the definition of the atmospheric filter in the communication model.

The integration of the atmospheric filter and the communication system model is via a communication simulation language, as distinguished from a simulation program. A simulation language is comprised of commands and data structures tailored to the signal environment which it models. A command for a simulation language to perform a function, such as convolution, is typically invoked by a single statement such as "CONVOLVE", whereas in a simulation program the user must encode primitive arithmetic functions and control statements to accomplish the desired operation. The language user only needs to employ commands which are tailored to communication systems analysis in order to solve certain design problems, thus removing a large programming burden.

The COMmunications SIMulation special purpose language (COMSIM) has been developed to model and analyze via computer simulation a wide class of baseband and passband communication systems. Implemented in the form of an interpreter/compiler, COMSIM provides the user with a means of passing simulated data or measured test signals through a system and examining waveforms and performance measures at any stage of the system. The language provides utilities to perform parametric studies by varying any descriptive or design parameter which is used to specify a node process. Node processes are simply the elementary signal definition points within the system where a waveform is either generated, modified, or measured. For example, in Figure 7, the nodes 1 through 8 define message generation (PNSEQ), modulation (MODLTR), baseband filtering (NYQUIST), atmospheric filtering (ATMOS), limiting (LIMIT), demodulation (DEMOD), bit synchronization (BITSYNC), and bit error rate calculation (BER). Each node is defined and connected to other nodes via the language commands.

COMSIM provides an ideal environment in which to perform system optimization, tradeoff, and performance analyses. It presents an interactive, user oriented, accurate means to perform extensive waveform analyses and is accessable to a non-programming communications or systems engineer. The language commands offer a wide variety of functions in addition to modeling communications devices. Waveforms may be observed with time or frequency plot commands inserted wherever desired between nodes of the

simulation. This is analogous to probing a test bench setup with an oscilloscope or spectrum analyzer. Other display facilities include:

Data Plots - Polar or Rectangular Format
Signal Space (vector) Plots
Eye Diagrams
Bit Error Rate Plots

Statistical measures such as average, rms, and deviations in amplitude and phase may be printed. Waveforms may be saved on disk file for later reference or use in iterative studies without regeneration.

The bandpass simulation in COMSIM utilizes the complex envelope representation of communication system waveforms. Either measured passband amplitude and phase (or delay) device characteristics or transfer function characteristics in the time or frequency domain are solicited by the language commands. Passband simulation is accompliched by inserting filters into the signal path through the communication channel. The language allows easy interactive changes to the parameters defining the communication channel under study, thus affording a means of isolating or at least identifying the effects of one or more system parameters.

The user, when satisfied that all node parameters are correctly specified, initiates the simulation by the RUN command. As each node of the system is executed, simulated input data is processed by the transfer characteristics of the node, producing an output waveform. Processing occurs either by multiplication or convolution in the time domain or by conversion via the Discrete Fourier Transform for operation in the frequency domain.

Iterative investigations may be performed without operator programming by using typical structural language statements such as FOR-NEXT and IF-THEN. Repetitive case analyses and measurements based upon the outcome of previous runs are readily accomplished. These features are made possible by a wide variety of functions, user variables, tests, and branchings which have been implemented in the COMSIM language structure.

4. ATMOSPHERIC FILTER MODEL

The atmospheric absorption and phase delay data which was generated for 54 to 58 GHz (Table 1) has been integrated into a COMSIM run in order to investigate the deleterious effects of the atmosphere on a biphase modulated communications system.

Typically, many thousand sample points in frequency are required in a passband simulation such as COMSIM. The atmospheric model which generates amplitude and phase delay characteristics takes less than one second to produce one point as a function of frequency. However, large amounts of time may be consumed in generating an atmospheric filter function if every sample point requires a separate computation. Atmospheric absorption and phase data is continuous and relatively smooth across passbands of interest, i.e. across 5 GHz at a center frequency of 56 GHz. For the data presented in Figure 8, a cubic spline was used to produce the large number of data points required by COMSIM (4096) from a small sample of points generated from the atmospheric model (18).

The simulated performance variation due to deviation of the interpolated points from the values which would have been generated by the atmospheric model is well within the expected error limits of the simulation.

5. BPSK SYSTEM SIMULATION

A Bi-Phase Shift Keyed (BPSK) pseudo-random signal with 0.25 gigabits per second data rate centered at 56 GHz was passed through the atmospheric filter described above. This signal was Nyquist filtered at a bandwidth of twice the data rate. Its input power spectrum is depicted in Figure 9.

This spectrum is perturbed as it passes through the atmospheric filter. Amplitude and phase degradation, primarily in the form of parabolic distortion is imposed upon the symmetric modulated waveform. The output power spectrum, shown in Fig. 10, exhibits the effects of distortion. Other propagation effects, such as multipath, would be imposed upon the waveform at this point in the simulation, if present.

The distorted waveform next passes into a BPSK demodulator and the bit error rate (BER) is calculated. The process by which this is performed assumes that white gaussian noise is added to the distorted waveform and a matched filter detects the resultant waveform. BER is calculated for varying amounts of additive noise and plotted in Fig. 11 as a function of one bit energy per one-sided noise spectral density (Eb/No) along with the theoretical values for Nyquist filtered BPSK. The Nyquist bandlimiting is expected to contribute approximately 0.5dB of BER degradation at (10)-5. Hence, most of the degradation observed in Fig. 11 is expected to be due to the effects of the atmosphere.

6. CONCLUSIONS

Transfer properties of the clear air mass for the EHF band may degrade the performance of communication channels by attenuating and delaying signals and introducing passband amplitude and phase distortions. The exact magnitude of the distortion due to the atmosphere is a function of the frequency band, the season of the year, the trans-atmospheric path elevation angle, and the altitude of both the transmitter and the receiver. Computer models of the atmospheric filter function may be incorporated into system simulation routines in order to identify propagation related problems and to aid in the design of mitigating techniques.

Computer simulation of communication link performance is a potentially useful design aid whose utility is enhanced by the creation of a simulation language. In contrast to a simulation program, a simulation language is more amenable to the needs of the engineer not familiar with programming practices and ultimately is a more cost-effective software tool.

As more and more use is made of the EHF band, it appears likely that the need for both accurate atmospheric filter prediction and rapid communication system simulation will increase.

REFERENCES

1. CRANE. R.K., 1979, "Prediction of Attenuation by Rain",ERT Report.

2. LIEBE, H.J., 1981, "Modeling Attenuation and Phase of Radio Waves in Air at Frequencies Below 1000 GHz",Radio Science, Vol. 16, No. 6, 1183-1199.

3. LIEBE, H.J., GIMMESTAD, G.G., AND HOPPONEN, J.D., 1977, "Atmospheric Oxygen Microwave Spectrum-Experiment Versus Theory", IEEE Trans. Ant. and Prop., AP-25(3), 336-345.

4. ZUFFEREY, C.H., 1972, "A Study of Rain Effects on Electromagnetic Waves in the 1-600 GHz Range",University of Colorado Report, reissued 1979 as a scientific report.

	SUBARCTIC WINTER		TROPICAL	
FREQUENCY GHz	ATTENUATION DB/Meter	DISPERSION Radians/M	ATTENUATION DB/Meter	DISPERSION Radians/M
54.00	.00250	.00101	.00218	.00078
54.25	.00295	.00106	.00255	.00082
54.50	.00348	.00111	.00297	.00085
54.75	.00409	.00116	.00345	.00088
55.00	.00479	.00120	.00398	.00090
55.25	.00556	.00123	.00457	.00093
55.50	.00643	.00126	.00520	.00094
55.75	.00737	.00128	.00579	.00094
56.00	.00835	.00129	.00657	.00093
56.25	.00937	.00128	.00726	.00092
56.50	.01039	.00126	.00794	.00089
56.75	.01141	.00122	.00857	.00086
57.00	.01239	.00117	.00919	.00081
57.25	.01334	.00111	.00975	.00077
57.50	.01423	.00104	.01027	.00071
57.75	.01509	.00096	.01075	.00066
58.00	.01587	.00087	.01119	.00060

Table 1. Attenuation and Phase Dispersion

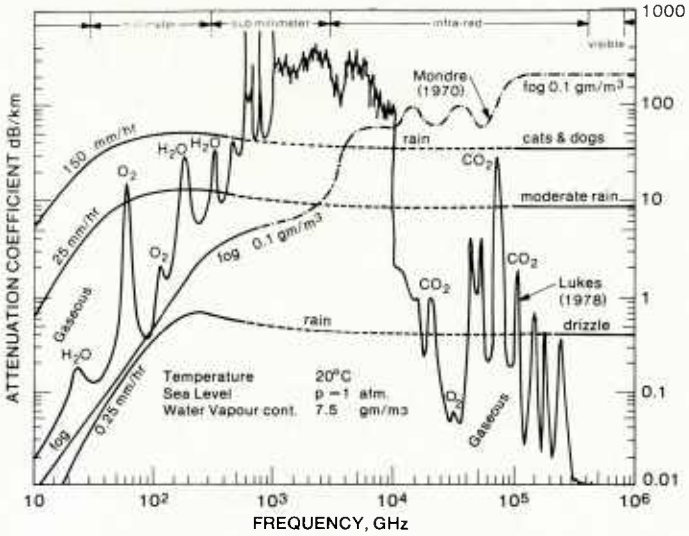

Fig.1 Attenuation coefficient as a function of frequency at earth surface

- VERTICAL EARTH-SPACE PATH
- OXYGEN AND WATER VAPOR EFFECTS

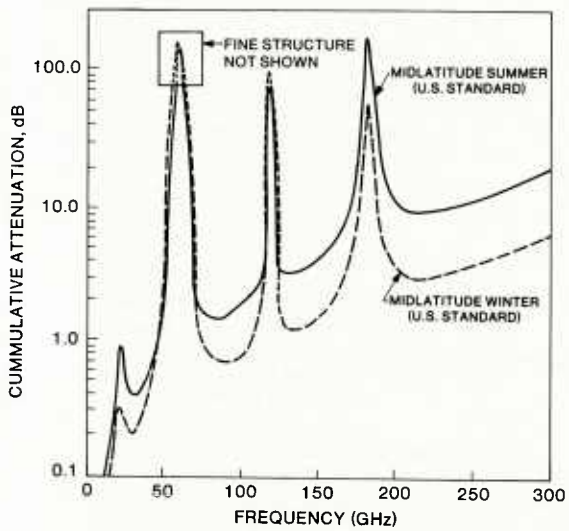

Fig.2 Cumulative earth-to-space attenuation along a vertical path

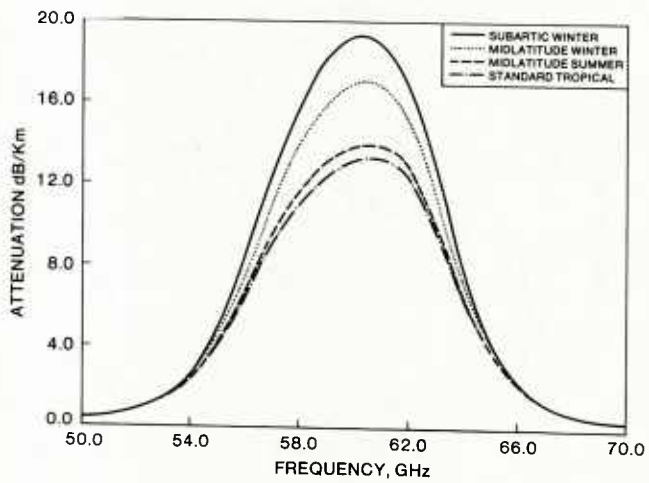

Fig.3 Sea level attenuation coefficients

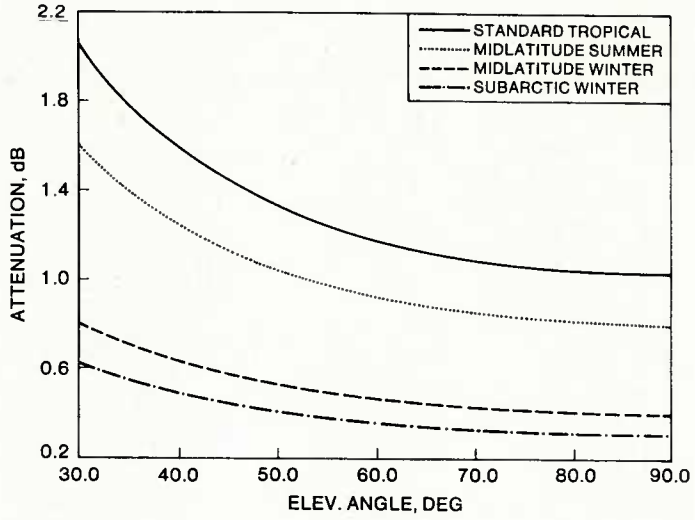

Fig.4 Earth-to-space attenuation at 94 GHz as a function of elevation angle

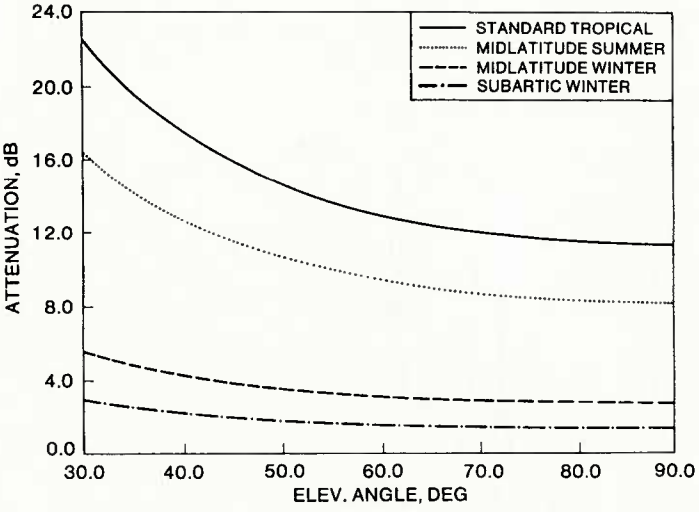

Fig.5 Earth-to-space attenuation at 172 GHz as a function of elevation angle

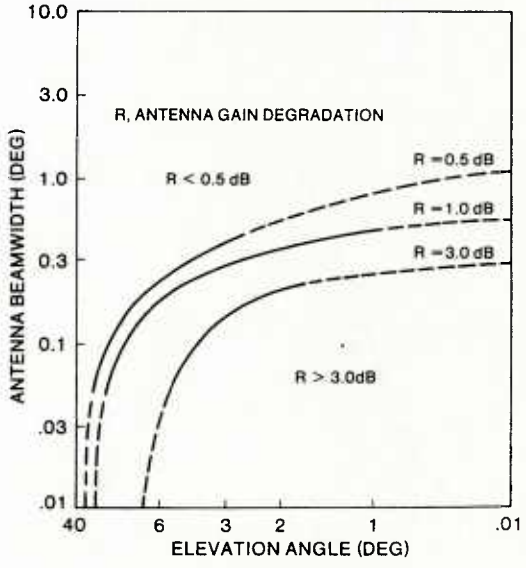

Fig.6 Gain degradation due to turbulence-induced angle-of-arrival variations

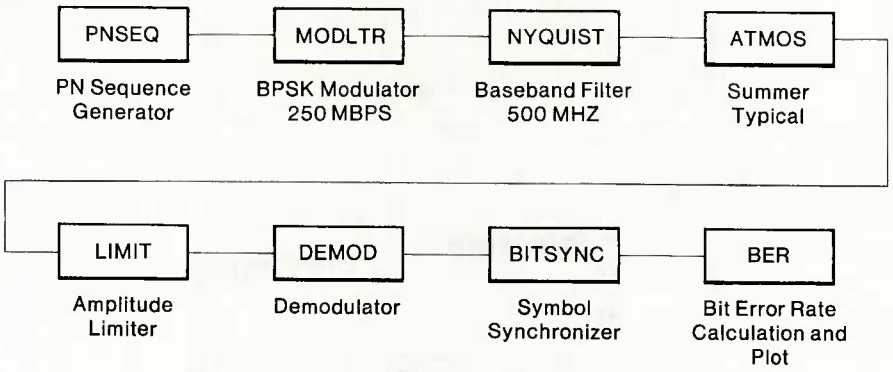

Fig.7 Block diagram of BPSK communication system simulation

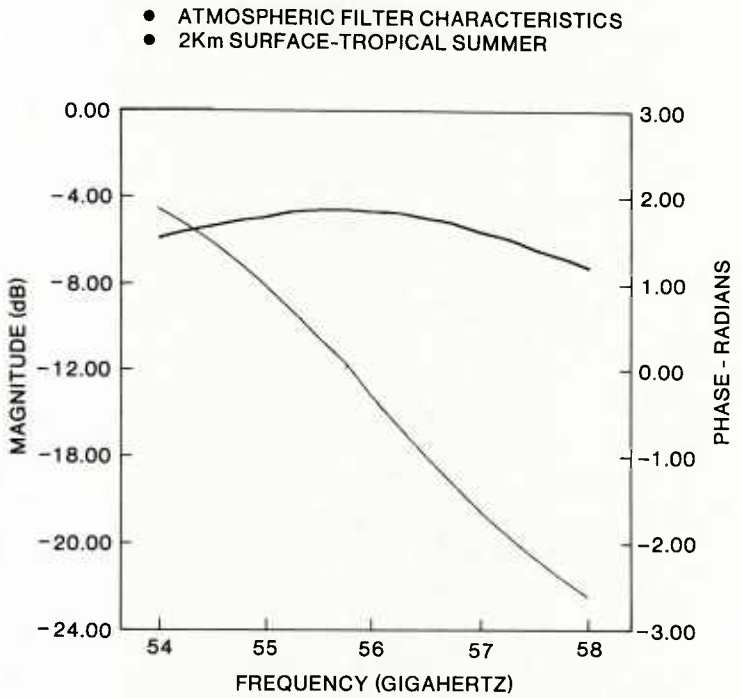

Fig.8 Atmospheric amplitude and phase filter characteristic

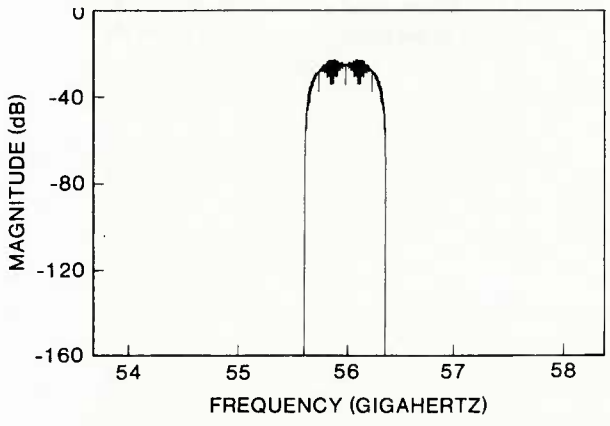

Fig.9 Power spectrum of Nyquist filtered BPSK signal

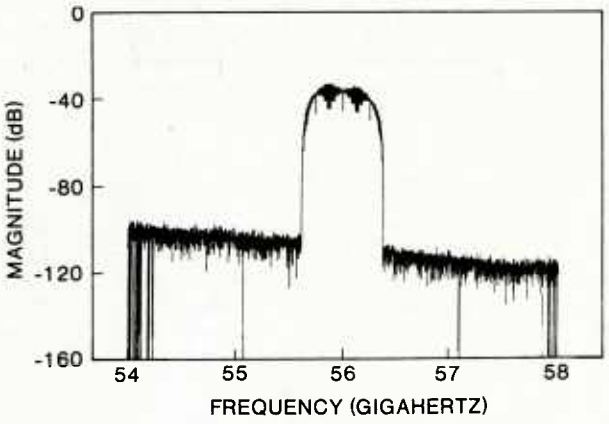

Fig.10 Power spectrum of BPSK signal after passing through an atmospheric filter

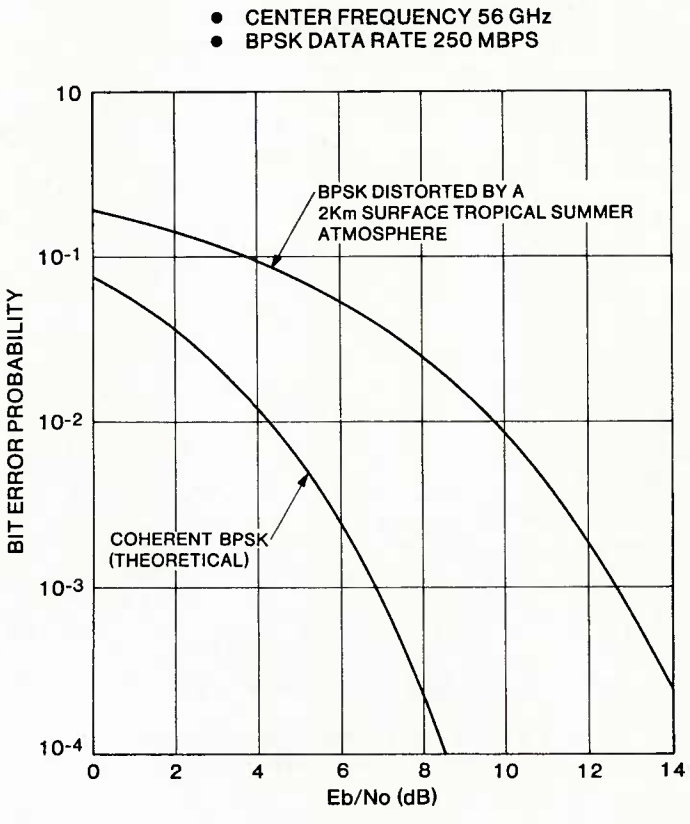

Fig.11 Bit error rate as a function of input Eb/No for a theoretical and distorted BPSK signal

DISCUSSION

D.J.Fang, US

(1) What's the essence of your simulator? Are the simulation processes similar to those marketed by Signatron Company for US Department of Transportation using delay lines and Rician statistical way to randomize signals?

(2) Another comment: BER from a measurement may be much worse than the results you simulated. Because once you lose sync, it takes time to restore. At COMSAT Labs we found this out when we performed an L-band ship-to-satellite experiment a couple of years ago. We published the finding in two IEEE papers.

Author's Reply

(1) This is a computer simulation utilizing uniformly spaced samples of the complex envelope representation of pseudo-random BPSK data.

(2) In general, we are interested in estimating the degradation of trans-atmospheric data links with adequate S/N to preclude loss of demodulator lock, typically operating with BER better than 10(−3).

J.Arnbak, Ne

With the strong amplitude variations shown in your slides, the modelling of carrier recovery in your synchronous demodulator is of crucial importance for the bit-error-rates. How was this done in your simulation package?

Author's Reply

Carrier recovery was by I−Q correlation to the modulated waveform, before filtering.

R.K.Crane, US

Your low elevation angle model includes only part of the problem. Have you neglected the fluctuations induced by turbulence?

Author's Reply

The integrated simulation model does not currently include turbulence effects. They are estimated separately for purposes of link margin requirements using an empirical model from Theobold and Hodge.

PROPAGATION CONSTRAINTS IN THE MILLIMETRE WAVEBANDS DUE TO PRECIPITATION SCATTERING

B.G. Evans and A.R. Holt
University of Essex,
Wivenhoe Park,
Colchester CO4 3SQ, U.K.

ABSTRACT

We present theoretically derived forward and backward scattering calculations for precipitation up to 210 GHz. Simple scaling rules are investigated for forward and backward directions which will allow scattering parameters at one frequency to be derived from other frequencies thus obviating the need for exhaustive and complex calculations. Predictions of propagation degradations for communication and radar systems operating in the millimetre wave bands are given

1. INTRODUCTION

The effects of precipitation scattering on the propagation of microwave radio and radar systems up to a frequency of around 30 GHz have been investigated in some depth in the literature [1-3]. Frequencies above this range, in the millimetre wave bands, although not in great use, are progressively becoming more used for both communication links and radar systems. Very little experimentation has been performed in these bands as it can be both complex and expensive. In this paper we look at the extension of theoretical prediction techniques used in the microwave range, to the millimetre wave range for assessing the likely degradations that will be imposed on future systems by precipitation scattering.

Communication systems concerned with the transmission of signals are likely to be most concerned with the attenuation of those signals. In addition more systems are using dual-polarisation, in which cross-polarisation becomes an important constraint. The other major constraint that can be imposed by precipitation in the media is bistatic scattering, which produces interference. We have dealt with the latter in other papers [4,5] and will concentrate on the former in this paper.

Systems involving radars and radiometers are becoming common in the millimetre wave range, particularly for military use. Here the effects of precipitation are to obscure or clutter the target or render guidance systems at error. The important aspect of the precipitation in these applications is the backscatter characteristics. Here again the use of multipolarisation radars would indicate that both reflectivity and differential reflectivities between polarisations should be investigated.

In this paper we present some results of our extension of theoretical scattering from precipitation into the millimetre wave range (up to 210 GHz). We investigate the validity of simple scaling rules for both forward and backward scattering which make theoretical prediction much easier. Finally we look at some applications of the work to future communication and radar systems that might be planned to work at these millimetre wave frequencies.

2. TRANSMISSION AND REFLECTION PARAMETERS

The theory of transmission in a precipitation filled medium has been well described elsewhere [6]. A brief summary is as follows:

If $f^F_{V,H}(\chi,\bar{a})$ are the forward scattering amplitudes for scattering of vertically/horizontally polarised electromagnetic waves incident at an angle χ to the axis of a precipitation particle of equivolumetric radius $\bar{a}$ (cm) then we may define propagation parameters $K_{V,H}$ where

$$K_{V,H} = K_o + \frac{2\pi}{K_o} \int_o^\infty f^F_{V,H}(\chi,\bar{a})\, n(\bar{a})\, d\bar{a} \qquad (1)$$

K_o being the wavenumber $(2\pi/\lambda)$ of the incident radiation, and $n(\bar{a})d\bar{a}$ the particle size distribution. For a precipitation segment of length L (cm) with particles all aligned we define

$$d_{1,2} = \exp(iK_{V,H}L) \qquad (2)$$

If E^n_V, E^n_H are the linearly polarised components incident on the n^{th} segment, then

$$\begin{pmatrix} E^{n+1}_V \\ E^{n+1}_H \end{pmatrix} = \begin{pmatrix} D^n_{11} & D^n_{12} \\ D^n_{21} & D^n_{22} \end{pmatrix} \begin{pmatrix} E^n_V \\ E^n_H \end{pmatrix} \qquad (3)$$

where $D^n_{11} = d_1 \cos^2\theta + d_2 \sin^2\theta$

$D^n_{22} = d_1 \sin^2\theta + d_2 \cos^2\theta$

$D^n_{12} = D^n_{21} = (d_1 - d_2)\cos\theta\sin\theta$

and θ is the apparent canting angle of the particles. The attenuation of linearly polarised waves passing through a region containing N segments is given as

$$A_{V,H} = 20\log_{10}\left|E^{N+1}_{V,H}/E^{1}_{V,H}\right| \text{ dB} \tag{5}$$

and for circularly polarised waves

$$A_{c} = 20\log_{10}\left|(E^{N+1}_{V} - iE^{N+1}_{H})/2E^{1}_{V}\right| \text{ dB} \tag{6}$$

For crosspolarisation the formulation depends on the orientation of the particles and for an all-aligned situation at angle θ the linear and circular crosspolarisations are given in Fig. 1.

In radar systems backward scattering is the important parameter and the measure of interest in the effective reflectivity from a volume of precipitation scattering which is defined by:

$$Z_{V,H} = \frac{\lambda^4}{\pi^5 |K|^2} \int_{o}^{Dmax} \sigma_{V,H}(D) N(D) dD \tag{7}$$

where $Z_{V,H}$ ($mm^6 m^{-3}$) is the reflectivity for vertical or horizontal polarisation, λ is the wavelength, $K^2 = \left|(n-1)/(n+2)\right|$, n is the complex refractive index of the particle, D is the equivalent diameter of the raindrop and the back-scatter cross-sections of the particles are:

$$\sigma_{V,H}(D) = \left| f^{B}_{V,H} \right|^2 \tag{8}$$

with $f^{B}_{V,H}(D)$ being the backward scattering amplitudes.

In order to resolve targets with greater accuracy radar systems are progressively turning to the use of multi-polarisations and hence the depolarisation on the backscattered signal is of importance. For linear polarisations the quantity of differential radar reflectivity Z_{DR} is defined by

$$Z_{DR} = 10\log\left(\frac{Z_H}{Z_V}\right) \text{ dB} \tag{9}$$

For circular polarisation radars an equivalent parameter C_{DR} can be defined (7).

In this brief account of the major forward and backward transmission parameters we have not addressed the problem of multiple-scattering effects which could be significant above 100 GHz for propagation (8).

3. EXTENSION OF SCATTERING THEORY TO THE MILLIMETRE WAVEBAND

In the previous section we have presented transmission and reflection characteristics through a rain-filled medium. It will be noted that all of these parameters are dependent upon the forward and backward scattering amplitudes of the particles ($f^{F}_{V,H}(\chi,\bar{a})$ $f^{B}_{V,H}(\chi,D)$) being available. In order to calculate these quantities one needs to know the shape, size and refractive index of the particles. For raindrops and ice crystals information is available (6,9,10) to enable such calculations to proceed. The solution of electromagnetic scattering from dielectric particles involves sophisticated mathematical theory, is complex and time consuming to evaluate numerically. A review of the techniques which have been successfully applied to the problem is to be found in reference (11). We have developed one of these techniques which we have called the Fredholm Integral Method (F.I.M.). Whilst in principle many of the techniques can be extended to yield results in the millimetre wave range, in practice there are considerable difficulties. We have thus developed a specific extenstion to the F.I.M. technique to enable us to calculate into the millimetre wave region for raindrops and ice crystals. A brief summary of the method extension follows.

F.I.M.

This method employs a volume integral equation formulation and obtains the scattering amplitudes by determining the internal field. The solution is in fact obtained for the Fourier transform of the internal field. The method is stable, and convergence is guaranteed. Part of the calculation is independent of the refractive index of the scatterer, and thus the method can be very efficient in applications. It is, however, in practice limited to regular shapes such as spheroids, ellipsoids, finite circular cylinders, and infinite cylinders of elliptic or rectangular cross-section.

Modified F.I.M.

The volume integral equation describing the scattering of a plane wave, of wave vector $\underline{K}_o$, by a scatterer of volume V and dielectric $\varepsilon(\underline{r})$ is

$$\underline{E}(\underline{r}) = \underline{J}_o \exp(i\underline{K}_o \cdot \underline{r}) + \int_V G(\underline{r},\underline{r}^1) \cdot \gamma(\underline{r}^1)\, \underline{E}(\underline{r}^1) d\underline{r}^1 \tag{10}$$

where

$$G(\underline{r}\underline{r}^1) = \left(\underline{1} + \frac{1}{K_o^2} \underline{\nabla}\underline{\nabla}\right) \exp \frac{(iK_o|\underline{r}-\underline{r}^1|)}{4\pi|\underline{r}-\underline{r}^1|} \tag{11}$$

$$\gamma(\underline{r}) = K_o^2 (\varepsilon(\underline{r})-1) = K_o^2 n_o^2(\underline{r}) \tag{12}$$

$$\mathbf{J}_\Lambda = \mathbf{1} - \underline{\bar{K}}_\Lambda \underline{\bar{K}}_\Lambda \text{ for any subscript } \Lambda. \tag{13}$$

$\mathbf{1}$ denotes the unit tensor, and dyadic quantities are in bolder type.

The dyadic scattering amplitude for scattering in the $\underline{K}_s$ direction is

$$f(\underline{K}_s,\underline{K}_o) = \frac{1}{4\pi} \mathbf{J}_s \cdot \int_V \exp(-i\underline{K}_s.\underline{r}) \boldsymbol{\gamma}(\underline{r}) \mathbf{E}(\underline{r}) d\underline{r} \tag{14}$$

The scattering parameters can thus be determined from knowledge of the field inside the scatterer only.

Equation (10) is extremely difficult to solve directly since the Green's function is singular, so in the FIM we iterate the equation and deal with the singularity analytically. This results in a pair of equations.

$$\int \underline{dk}\, \mathbf{K}(\underline{K},\underline{K}).\mathbf{C}(\underline{K},\underline{K}_o) = \mathbf{J}_o \mathbf{U}(\underline{K},\underline{K}_o) \tag{15}$$

$$f(\underline{K}_s,\underline{K}_o) = \frac{1}{4\pi} \mathbf{J}_s \int \underline{dK}\, \mathbf{U}(\underline{K}_s\ \underline{k})\, \mathbf{C}(\underline{K},\underline{K}_o) \tag{16}$$

Where $\mathbf{C}(\underline{K},\underline{K}_o)$ is the Fourier transform of the field inside the scatterer, $\mathbf{K}$ is a non-singular kernel and $\mathbf{U}(\underline{K},\underline{K})$ is the first Born term (as in the Rayleigh-Gans approximation). Equation (15) is a Fredholm integral equation of the first kind for the transform of the interior field.

We solve these equations by a Galerkin procedure - we approximate the integrations in (15) by numerical quadrature, thus converting this to a matrix equation. The process is very stable since a variational principle is satisfied.

The extension to the method (12) consists in expanding $\mathbf{C}(\underline{K}\ \underline{K}_o)$ as a Fourier series in the azimuthal angle of $\underline{K}$. This results for axi-symmetric scatterers in the main matrix becoming block-diagonal and in consequence, not only is the number of matrix elements reduced, but also we have only to solve a number of matrix equations whose dimension is far less than the original matrix equation. Thus the calculation can be extended to much larger values of $k_o \bar{a}$. The stages are:

(i) Calculation of a set of basic integrals dependent on k_o and particle shape parameters - but not on refractive index.

(ii) Calculation of the matrix elements.

(iii) Solution of a set of matrix equations and calculation of scattering amplitudes.

It is noted that one calculation of the matrix elements in stage (ii) suffices for all scattering amplitudes for any incident direction and/or polarisation. Since also the integrals in stage (i) do not depend on the refractive index of the scatterer, we can perform calculations for a given wavelength, and for a range of refractive indices very economically.

We have made calculations at 57, 94, 137 and 209.6 GHz using the method and present results in Table 3 for forward and backward amplitudes at 94 GHz for raindrops with an oblate spheroidal shape with axial ratio $b/a = 1-\bar{a}$, and water temperature 0^oC. Simple elevation rules already given by us (13) have been found applicable within the millimetre wave region for the forward direction.

Even with the simplifications made possible by our extended theory the numerical evaluation of scattering for size parameters $K_o\bar{a} \gtrsim 3$ is still exhaustive of computer time and storage. Since drops with $\bar{a} \backsim 0.25$ can still be important at high frequencies, $K_o\bar{a} \gtrsim 3$ is equivalent to frequencies above about 60 GHz. However, it should be noted that the differential amplitude $I_m(f_H^r - f_V^r)$ becomes small for large drops as the frequency increases.

4. FREQUENCY SCALING IN THE FORWARD DIRECTION

As exaplained in the previous section computations of scattering amplitudes at higher millimetre wave frequencies are exhaustive and thus we have examined simple scaling rules that would allow us to derive amplitudes from those frequencies already calculated by the exact (FIM) method.

First we examine scaling amplitudes for use in attenuation prediction e.g. proportional to $\mathrm{Im}(f_{V,H}^F)$. We have already reported (13) that a plot of K_o Im (f_H^F) against $K_o\bar{a}$ for horizontal polarisation incident at 90^o to the particle axis, produces points lying on a curve which is virtually independent of frequency. We show the computer generated graphs equivalent to this situation in Fig. 2, where the coincidence of the plots is remarkable. This leads us to the following rule for scaling:

$$\mathrm{Im}(f_H^F) = \frac{1}{K_o} \phi(K_o\bar{a}) \tag{17}$$

where ϕ is function which can either be tabulated or analytically determined from Fig. 2.

Using (17) we may obtain the approximate amplitudes at any frequency and have demonstrated the accuracy of the method in the previous publication (13).

We had until recently been unable to scale for vertical polarisation with similar accuracy. Our best results had been obtained by using $K_o b$ as the abscissa instead of $K_o\bar{a}$. However, we have found that by multiplying K_o Im (f_V^F) by a shape dependent parameter $(a/b)^{0.45}$ and plotting against $K_o\bar{a}$ we obtain similar coincidence of different frequency curves as for horizontal polarisation. The results are shown in Fig. 3. This gives us a scaling rule for vertical polarisation:

$$\text{Im}\ (f_V^F) = \frac{1}{K_o}\left(\frac{a}{b}\right)^{-0.45} \Psi(K_o\bar{a}) \tag{18}$$

It has further been noticed, by overlaying Figs. 2 and 3, that $\phi(K_o\bar{a}) \simeq \Psi(K_o\bar{a})$ for $K_o\bar{a} \lesssim 3$, and this would lead to a simple rule for differential attenuation (useful in crosspolar prediction) scaling.

We next investigate the scaling of amplitudes for use in phase shift prediction e.g. proportional to Re $(f_{V,H}^F)$. Again for horizontal polarisation plotting K_o Re (f_H^F) against $K_o\bar{a}$ yields reasonable coincidence of plots with frequency for $K_o\bar{a} \lesssim 1.5$ (Fig. 4). For vertical polarisation a similar picture emerges as seen in Fig. 5, but for $K_o b > 1.5$ the curves rapidly diverge. It would appear again that within this restricted particle size region the vertical and horizontal scaling functions, although not so well ordered as before, are closely related indicating that differential phase also may be scaled simply, viz.

$$\text{Re}\ (f_H^F) = \frac{1}{K_o}\gamma(K_o\bar{a}) \quad , \qquad \text{Re}\ (f_V^F) = \frac{1}{K_o}\beta(K_o b) \tag{19}$$

5. FREQUENCY SCALING IN THE BACKWARD DIRECTION

In general we have noticed that backscatter amplitudes are always more sensitive to changes in shape, frequency etc. than forward. It has thus proved difficult to scale backscatter amplitudes in the same way as with the forward cases. We show in Fig. 6 a linear plot of K_o Im (f_H^B) as a function of $K_o\bar{a}$. It will be noticed that for $K_o\bar{a} \simeq 1.6$ the function changes sign. However, the surprising feature is that the amplitudes remain quite constant with frequency.

In Figs. 7-8 we show a plot of K_o^2 times the horizontal and vertical backscatter cross section σ_H, σ_V as a function of $K_o\bar{a}$. For $K_o\bar{a} \lesssim 1.0$ there seems to exist a fairly well ordered scaling relationship:

$$\sigma_{H,V} = \frac{1}{K_o^2}\Omega_{H,V}(K_o\bar{a}) \tag{20}$$

beyond $K_o\bar{a} \simeq 1.0$ the function becomes much more ill-conditioned. However, this demonstrated that for the backward direction it still looks possible to scale, but in this case with cross-sections rather than amplitudes.

Differential backscatter cross section (σ_H/σ_V) is shown in Fig. 9 as a function of $K_o\bar{a}$. This quality shows changes of sign which appear to occur at size parameters which are reasonably independent of frequency, although the sizes of the peaks and troughs is dependent on frequency. One point to notice is that the dual polarisation ZDR technique would fail for frequencies above around 25 GHz since rainfall distributions could occur for which zero ZDR was returned from heavy rainfall.

6. TRANSMISSION (COMMUNICATION) ASPECTS

We have demonstrated in the previous sections the possibility of scaling the scattering amplitudes for individual particles. In order to demonstrate the accuracy of this rule, we show in Table 2 a selection of scaled against exactly calculated attenuations for various rainfall rates within the millimetre region. The agreement is seen to be very good. In performing these calculations we have found that it is not sufficient to calculate amplitudes at intervals of 0.025 cm, as is the practice below 30 GHz. It is preferable to use the size parameter $K_o\bar{a}$ as integration variable, and then use intervals of 0.05. Care needs to be taken in using a wide enough range of $K_o\bar{a}$ at the higher frequencies if accurate results are to be achieved.

Results presented herein relate to a water temperature of 20°C. Checks at 0°C have indicated similar agreement although the function ϕ is not identical to that for 20°C.

In Table 3 we show a selection of attenuations calculated for various rainfall rates within the millimetre range. Previous calculations have used the Mie sphere approximation at these frequencies and we have found this to yield good approximations to attenuation in the higher millimetre range.

In addition to the scaling of attenuation we have shown that it is also possible that differential amplitude and differential phase may also be scaled in a similar manner. This will allow crosspolarisation to be scaled. As yet we have not obtained numerical data on such scaling and the accuracy remains to be evaluated.

Exact calculations allow us to assess the crosspolarisation, however, and we present some results in Fig. 10 of crosspolarisation versus attenuation. Notice that crosspolarisation has reduced significantly from that at lower frequencies due to the reduction in both differential amplitude and phase. This reduction continues with frequency for linear polarisation but for circular polarisation, is still some 20 dB worse on average.

7. REFLECTION (RADAR) ASPECTS

For the first time we have demonstrated that backscatter cross sections of raindrops may be scaled. It should thus be possible to scale reflectivity (Z) in the same manner as attenuation in the forward path. This will enable the effects of precipitation on millimetre wave radar systems to be investigated. As yet we still have to demonstrate the accuracy of the scaling rule for this application, but the indication is that it should be good.

Future radar systems will almost certainly employ multiple polarisations in order to improve resolution of

targets. Hence the effect of precipitation on the backscatter signal as a function of polarisation state (Z_{DR} or C_{DR}) is also of interest. In order to demonstrate likely effects we have performed a calculation for linear polarisation at 94 GHz of Z and Z_{DR}. The results are shown in Table 4 and represent the amount (in dB's and in percentage terms) by which Z_H and Z_{DR} are underestimated with various rainrates on the path. The backscatter in this case is caused by a single raindrop; values do not seem to be dependent on the size of the target raindrop. It will be seen that errors in reflectivity are much greater than errors in differential reflectivity. Such errors become very large as the rain path-length is increased at this frequency. It would appear that differential polarisation techniques may be more accurate in determining radar backscatter signatures in this range than single polarisation parameters. However, it has to be noted that the differential backscatter oscillates in sign across the size-parameter range and hence cancellation effects will occur at high frequencies which may make the Z_{DR} measurement no longer useful. We have to investigate the case of circular polarisation which is slightly more complex.

8. CONCLUSIONS

We have demonstrated the accuracy of scaling basic scattering parameters of raindrops in the forward direction. Attenuation may thus be calculated in the millimetre range, without the necessity of exhaustive single particle scattering calculations. Although we have dealt herein with raindrops, the case for ice particles remains to be investigated. We have shown the possibility of scaling differential attenuation and phase and hence crosspolarisation but the accuracy has still to be determined.

It has been shown that scaling in the backward direction is possible via backscatter cross-sections and that this is good within the millimetre range. Some effects of rain on the path of single and dual polarisation millimetre radars have been presented. Using the scaling method it should be possible to assess the effects of precipitation on radar systems throughout the millimetre range.

9. REFERENCES

1. OGUCHI, T. (1981) 'Scattering from hydrometeors - a survey', Radio Science 16, no. 5.

2. OLSEN, R.L. (1981) 'Crosspolarisation during clear-air conditions on terrestrial links - a review', Radio Science, Vol. 16, no. 5, 609-647.

3. UZUNOGLU, N.K., EVANS, B.G. and HOLT, A.R. (1977) 'Scattering of electromagnetic radiation by precipitation particles and propagation characteristics of terrestrial and space Communication Systems', Proc. IEE 124 (4).

4. CHARLTON, D.G., HOLT, A.R. and EVANS, B.G. (1982) 'A comparison of the bistatic cross-section and reflectivities of spherical and spheroidal raindrops at microwave frequencies'. Proc. IEE. part F (in press)

5. CHARLTON, D.G., HOLT, A.R. and EVANS, B.G. (1982) 'Bistatic radar reflectivities at 11/14 and 20/30 GHz', This conference.

6. EVANS, B.G. and HOLT, A.R. (1980) 'A review of theoretical prediction techniques of transmission parameters for slant path, earth-space communications', AGARD Conf. prop. effects in space-earth paths, London, Conf. Proc. no. 284.

7. TORLASHI, E.C., HUMPHRIES, R.G. and BANGE, B.L (1982) 'Circular polarisation for precipitation measurements'. URSI Symp. on multi-parameter radar measurements of precipitation, Bournemouth, U.K.

8. (1981) URSI Workshop report: 'Effects of the lower atmosphere on radio propagation at frequencies above 1 GHz', Radio Science 16, no. 5.

9. RAY, P.S. (1972) 'Broadband complex refractive indices of ice and water', J. Applied Opt. 11.

10. PRUPPACHER, H.R. and PITTER, R.L. (1971) 'A semi empirical determination of the shape of cloud and raindrops' J. Atmos. Sci. 28.

11. HOLT, A.R. (1982) 'The scattering of electromagnetic waves by single hydrometeors', Radio Science 17, no. 5.

12. HOLT, A.R. and EVANS, B.G. (1980) 'The scattering of millimetre waves by precipitation particles' URSI Comm. F. Symp. Canada.

13. EVANS, B.G. and HOLT, A.R. (1981) 'Frequency scaling at millimetre wave frequencies', IEE. Int. Conf. Antennas and Prop. York, U.K.

Table 1 Forward and Backward scattering amplitudes for raindrops at 94 GHz

$\bar{a}$ (cm)	f_V^F		f_H^H		f_V^B		f_H^B	
0.02	0.2980E-02	0.9038E-03	0.3047E-02	0.9411E-03	0.2786E-02	0.4172E-03	0.2852E-02	0.4447E-03
0.04	0.1786E-01	0.1941E-01	0.1819E-01	0.2094E-01	0.2100E-01	0.8819E-02	0.2160E-01	0.1015E-01
0.06	0.1511E-01	0.5422E-01	0.1288E-01	0.5733E-01	0.2317E-01	0.2604E-01	0.2139E-01	0.2794E-01
0.08	0.1949E-01	0.8905E-01	0.1498E-01	0.9516E-01	0.1008E-01	0.5097E-02	0.9588E-02	0.3335E-02
0.10	0.2008E-01	0.1394E+00	0.9575E-02	0.1479E+00	0.5533E-02	- 0.3746E-01	0.1162E-01	- 0.3945E-01
0.12	0.2069E-01	0.1926E+00	0.4929E-02	0.2045E+00	0.2886E-02	- 0.4931E-01	0.9139E-02	- 0.4574E-01
0.14	0.1927E-01	0.2626E+00	- 0.3060E-02	0.2725E+00	- 0.2180E-01	- 0.9289E-02	- 0.2407E-01	- 0.1051E-01
0.16	0.2193E-01	0.3287E+00	- 0.1317E-01	0.3478E+00	- 0.4650E-01	0.3109E-01	- 0.5668E-01	0.2210E-01
0.18	0.2392E-01	0.4085E+00	- 0.2514E-01	0.4325E+00	- 0.3475E-01	0.4729E-01	- 0.3330E-01	0.3651E-01
0.20	0.2381E-01	0.4958E+00	- 0.4175E-01	0.5217E+00	0.2401E-01	0.3186E-01	0.3107E-01	0.3902E-01

FREQUENCY (GHz)	RAIN-RATE (mm/hr)	A_H (dB/km) SCALED	EXACT
30	15	3.38	3.49
	45	9.98	10.1
	105	21.7	21.5
94	15	10.6	10.9
	45	21.4	22.2

Table 2 Accuracy of Scaling attenuation

FREQUENCY \ RAINRATE (mm/hr)	5	15	25	55	105
30	0.9	3.0	3.9	8.8	17.0
57.3	2.9	7.5	11.3	20.4	32.2
94	4.6	10.3	14.6	24.3	35.9
137	5.4	11.2	15.4	24.4	34.6

Table 3 Millimetre wave attenuation (vertical polarisation) dB/km as a function of rainrate (temp. 0°C)

Z_H

Rainrate (mm/hr)	5		10		50		100	
L(km)	dB	%	dB	%	dB	%	dB	%
0.1	0.09	(2.0)	0.23	(5.1)	1.47	(28.7)	2.83	(47.9)
0.3	0.26	(5.8)	0.69	(14.6)	4.41	(63.8)	8.49	(85.8)
0.5	0.43	(9.5)	1.14	(23.2)	7.35	(81.6)	14.1	(96.1)
1.0	0.86	(18.1)	2.29	(41.0)	14.7	(96.6)	28.2	(99.8)

Z_{DR}

Rainrate (mm/hr)	5		10		50		100	
L(km)	dB	%	dB	%	dB	%	dB	%
0.1	0.005	(0.1)	0.01	(0.3)	0.08	(1.8)	0.15	(3.4)
0.3	0.014	(0.3)	0.04	(0.9)	0.24	(5.3)	0.46	(10.0)
0.5	0.02	(0.5)	0.06	(1.4)	0.40	(8.7)	0.76	(16.1)
1.0	0.05	(1.1)	0.12	(2.8)	0.80	(16.7)	1.53	(29.2)

Table 4 Amount in dB's by which Z_H, Z_{DR} are underestimated

Radar frequency = 94 GHz
M-P Rainrate

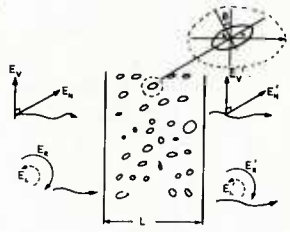

$$\begin{pmatrix} E_V' \\ E_H' \end{pmatrix} = R^{-1}.T.R.\begin{pmatrix} E_V \\ E_H \end{pmatrix} \qquad R = \begin{pmatrix} \cos\theta & \sin\theta \\ -\sin\theta & \cos\theta \end{pmatrix}$$

$$\begin{pmatrix} E_R' \\ E_L' \end{pmatrix} = C^{-1}.R^{-1}.T.R.C.\begin{pmatrix} E_R \\ E_L \end{pmatrix} \qquad T = \begin{pmatrix} e^{jkv(=)L} & 0 \\ 0 & e^{jkH(=)L} \end{pmatrix}$$

$$C = \frac{1}{\sqrt{2}}\begin{pmatrix} 1 & 1 \\ j & -j \end{pmatrix}$$

$$X_{V_H} = 20 \log \left| \frac{E'_{H\,IV}}{E'_{V,H}} \right|$$

$$X_c = 20 \log \left| \frac{E_L'}{E_R'} \right|$$

Figure 1. Formulation of cross-polarisation (XPD)

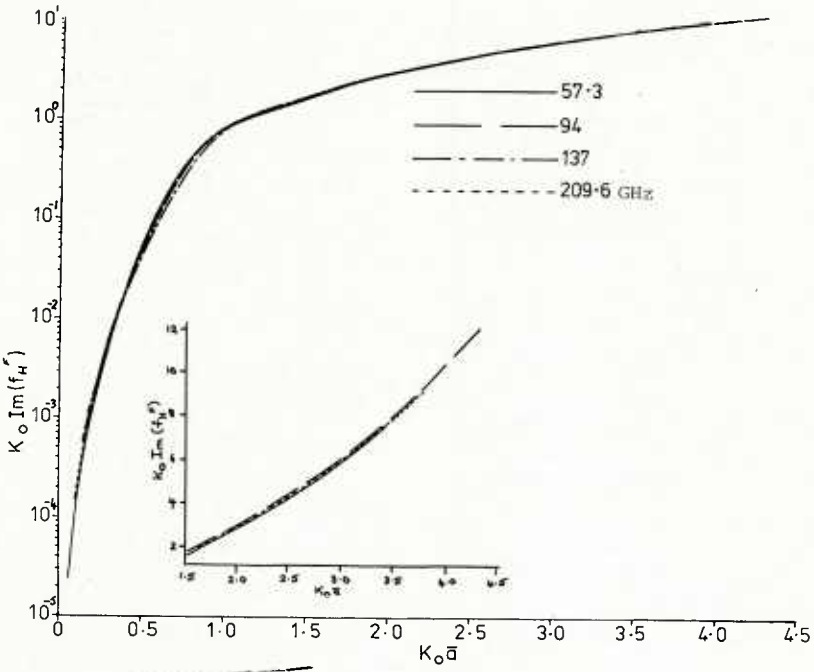

Figure 2. Horizontal polarisation - $K_o \mathrm{Im}\,(f_H^F)$ as a function of $K_o \bar{a}$. (inset linear scale)

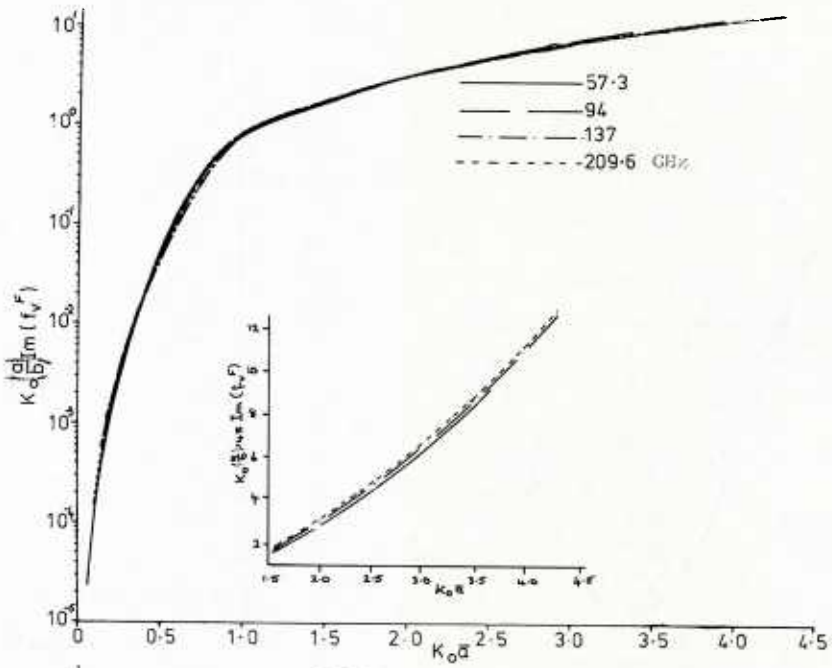

Figure 3. Vertical polarisation - $K_o \times \left(\frac{a}{b}\right)^{0.45} \times \mathrm{Im}\,(f_V^F)$ as a function of $K_o \bar{a}$ (inset linear scale)

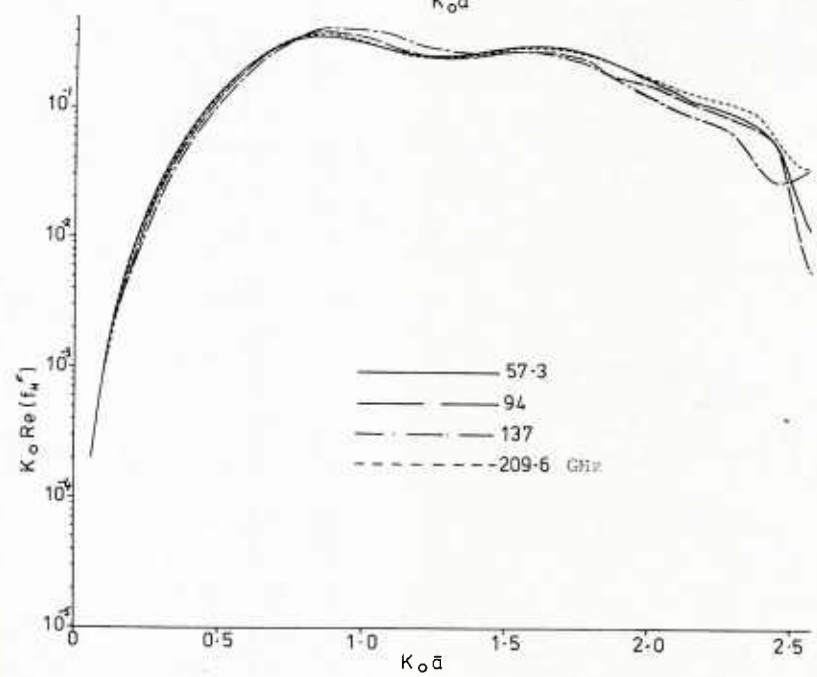

Figure 4. Horizontal polarisation - $K_o \mathrm{Re}(f_H^F)$ as a function of $K_o \bar{a}$.

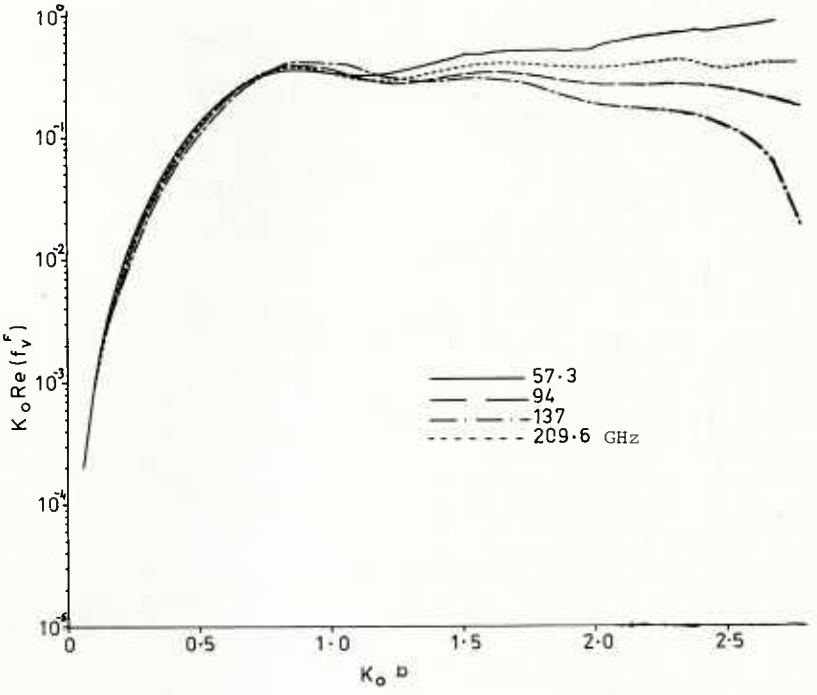

Figure 5. Vertical polarisation - $K_o.Re\ (f_V^F)$ as a function of $K_o b$.

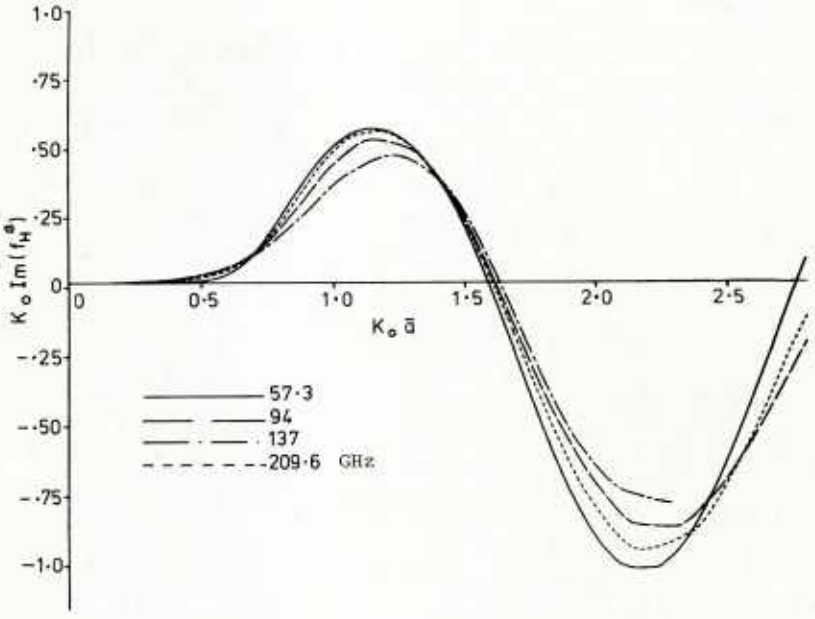

Figure 6. Horizontal polarisation - $K_o\ Im\ (F_H^B)$ against $K_o \bar{a}$ plotted on a linear scale.

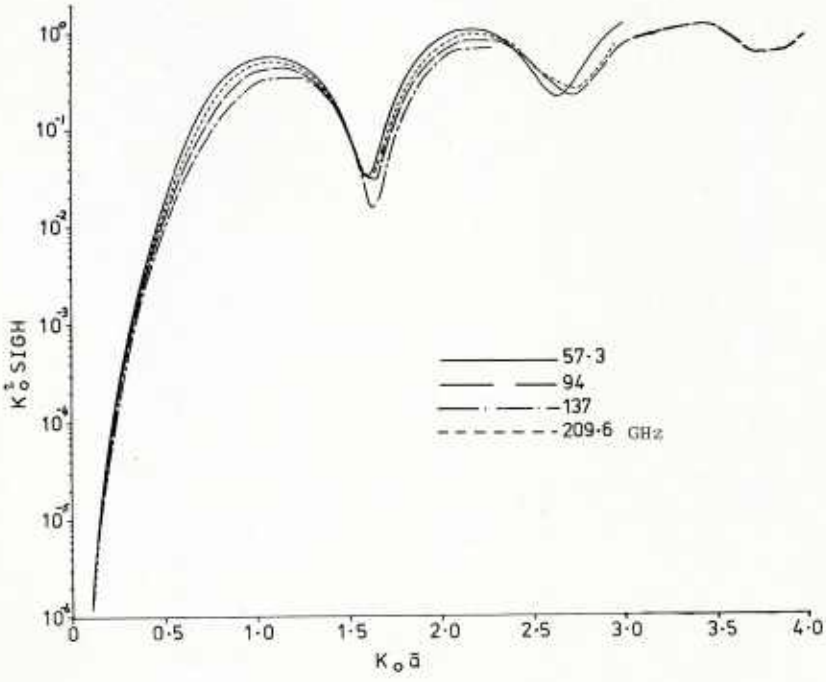

Figure 7. Horizontal polarisation - $K_o^2 \sigma_H$ as a function of $K_o \bar{a}$

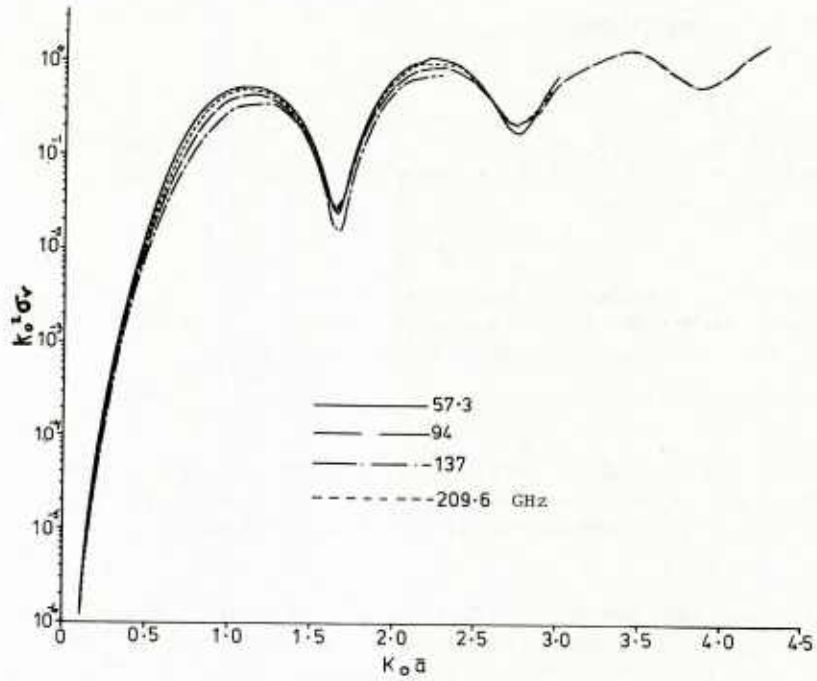

Figure 8. Vertical polarisation - $K_o^2\,\sigma_V$ as a function of $K_o\bar{a}$

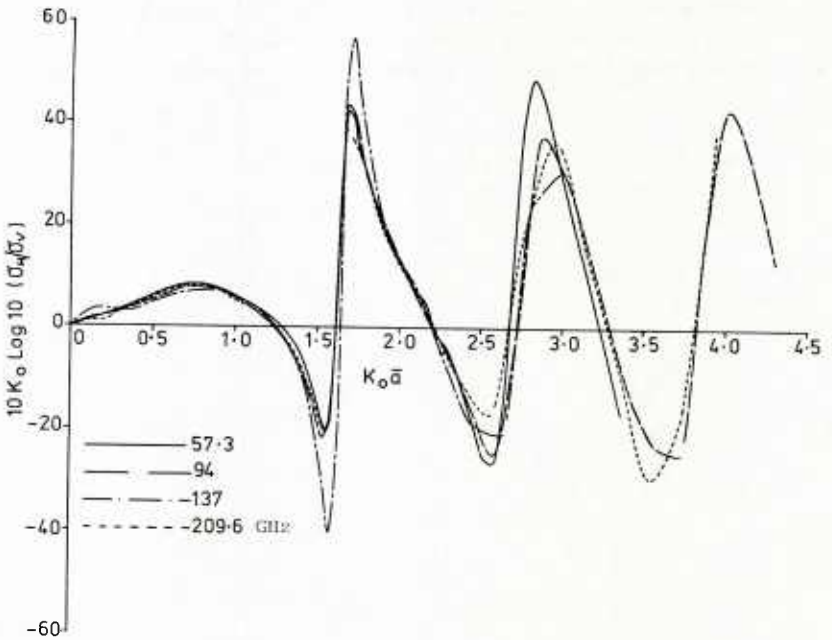

Figure 9. Differential backscatter cross-section 10log (σ_H/σ_V) as a function of $K_o\bar{a}$

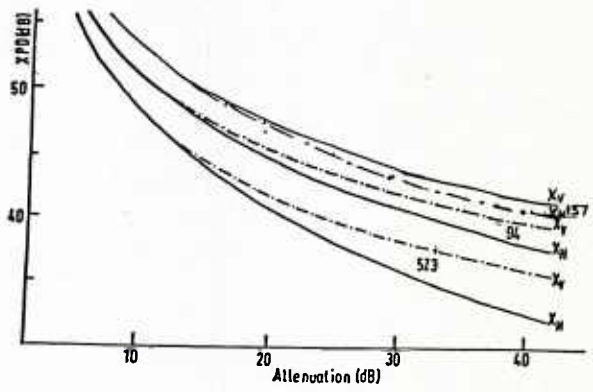

Figure 10. Crosspolarisation versus attenuation for linear polarisation in the millimetre range.

DISCUSSION

M.B.White, US

Will you comment upon the applicability of these scaling techniques into the optical wavelength domain? The ka's are about comparable and the basic problems of optical and mm radars are about the same for fog/clouds and rain, respectively.

Author's Reply

The scaling techniques can be applied into the optical region, although we haven't done so. However, exact calculations in the optical region are much easier as the refractive index of the particles and their sizes are not large. So, yes, we could do exact calculations for fog and cloud particles or apply a scaling technique.

R.K.Crane, US

The restriction $k\bar{a} \lesssim 1.5$ for backscattering is quite restrictive when considering meteorological targetst at the higher frequencies. Interest in frequency scaling should be for an ensemble of drops rather than single drops. Do the deviations from perfect scaling still occur when integrated over the entire drop size distribution?

Author's Reply

The restriction $k\bar{a} \lesssim 1.5$ is not as restrictive as might first appear as the size range $\bar{a}$ is restricted as k is increased into the millimetre wave range. I agree that the integration over a drop-size distribution is the most important aspect and we have demonstrated the accuracy of doing this in the forward direction for attenuation. We find that the accuracy is very good. As yet, we have not checked the equivalent accuracy for reflectivity in the backward direction. However, indications are that it will be as good. In general, the integration over a number of drops tends to smooth out the inaccuracies that may be present in single drops. This is fortunate for systems prediction.

A MM-WAVE COLLISION WARNING DEVICE FOR HELICOPTERS

B. Rembold, H. G. Wippich,
M. Bischoff, W. F. X. Frank
AEG-TELEFUNKEN
Geschäftsbereich Hochfrequenztechnik
7900 Ulm/Do.
Federal Republic of Germany

SUMMARY

Using the frequency slot of maximum atmospheric attenuation around 60 GHz a short range collision warning device for helicopters has been developed. The system consists of a pulsed radar sensor using semiconductors exclusively, a fast scanning mechanism and a display. First measurements showed that high voltage transmission lines having diameters of about 20 mm could be detected at a distance of more than 400 m.

INTRODUCTION

The application of the mm-wave region for short-range radar purposes is investigated since several years. A comprehensive survey of already realized systems can be found in /1/.

In general the frequencies chosen for mm-wave radar are within the windows of the atmospheric attenuation, for instance 35 or 94 GHz /2, 3/. For some applications however even the frequencies of maximum attenuation, i. e. 24 GHz, 60 GHz, and 120 GHz with clear-air attenuation factors of about 0.2, 16, and 4 dB/km respectively may be recommended, if the related system has to cover only small ranges, e. g. 0.5 - 2 km max: The additional atmospheric attenuation helps to prevent interception and interference. The location of radiation sources is quite difficult, and as an economic effect the same frequencies can be reused for different communication links or radar systems. Furthermore the system parameters are less dependent of changed weather conditions.

The present paper describes a mm-wave radar sensor for helicopters. The radar operates in the frequency band around 60 GHz. The chosen frequency constraints the operational radar range - nearly independent of radar-cross section - within margins of 500 - 1000 m. The aim of the radar is to detect small obstacles, for instance wires of high voltage transmission lines or similar objects being in the vicinity of the radar, in order to avoid collisions.

As an all solid state device this radar system is rather light weight. Because the emitted peak power is only 3 W no dangerous hasards have to be expected by the operators.

First measurements have shown that high voltage transmission lines can be detected in a distance of several hundred meters.

SYSTEM ASPECTS

A most important system parameter is the lateral resolution, given by the relation of antenna diameter D and wavelength λ. For our purposes a relation of 40 is chosen, which corresponds to half power beamwidth of 1.6°. Because helicopters move in lateral direction also, the field of view must cover an azimuth angle of $\vartheta_A = \pi$ ($\pm 90^{\circ}$), while in the direction of elevation only an angle range of $\vartheta_E = \pi/6$ ($\pm 15^{\circ}$) is necessary. An other given system parameter is the image repetition rate 1/T of the scanning mechanism, which should reach 1 Hz. All parameter-resolution, field of view and repetition rate-determine the angular scanner velocity

$$\omega = \frac{\vartheta_A \cdot \vartheta_E}{T} \cdot \left(\frac{D}{\lambda}\right)^2 \qquad (1)$$

which furthermore strongly affects the mechanical stability requirements of the system: As it can be shown, the stored mechanical energy E of the rotating antenna is proportional to $\omega^2 \cdot D^4$, and after inserting eq. (1) even proportional to D^8! That means a 10% increase of D doubles the mechanical effort.

Thus in contrast to other radar systems the antenna scanning time is not given by the pulse propagation (and integration) time for each angle cell, but by inertial forces of the rotating mirror. As the radar has to cover only a small range of several hundred meters, the Pulse Repetition Frequency (PRF) can be very high (250 kHz). Because of the atmospheric attenuation, no ambiquous ranges must be taken into account. Another system aspect is, that this radar needs no MTI capability. Even non moving obstacles have to be detected. Therefore a simple non coherent pulse radar has been developed, which reduces the RF-effort considerably.

FREQUENCY SELECTION

The selection of radar frequency is a result of a trade off of different aspects:

- For a collision warning system only small to moderate radar ranges are necessary. A maximum distance of 500 - 1000 m need not to be exceeded.
- The detection of very small obstacles - for instance wires, having a diameter of 3 mm - requires high operation frequencies, the wavelength of which has to be equal or smaller than the circumference of the smallest wires to be detected. However, if this condition is fulfiled, the radar cross section will no longer increase with growing frequency.
- In order to reduce the antenna aperture high frequencies should be chosen.
- Components cost and reliability lead to lower frequency solutions.
- The system behaviour should not depend of different weather conditions.
- Mutual interference of different radars has to be prevented.

The considerations gave raise to take a frequency being situated in the vicinity of the 60 GHz atmospheric attenuation maximum. The high attenuation of about 15 dB/km does not affect the radar properties within a range of several hundred meters. Otherwise mutual interferences are prevented. Furthermore the radar can not be detected and jammed from distances exceeding several kilometers.

RADAR CROSS SECTION OF WIRES

One of the most important application of this radar is the detection capability of small wires. In order to claim the system parameters an expression for the radar cross section of wires is desired having sufficient accuracy. Known formulas /4, 5/ describing the radar cross section of thick, metallic circular cylinders with finite length suppose a plane incident field. In reality, because of the finite distance between radar source and wire, phase and amplitude of incident field change along the wire, thus the plane wave assumption is not valid.

In order to get a handy formula considerations have been made which define the radar cross section of an infinite wire as the geometrical mean of the radar cross sections of an infinite plane and a sphere having the wire's diameter:

$$\sigma = \sqrt{\sigma_{p\infty}} \cdot \sqrt{\sigma_s} = \sqrt{R^2\pi} \cdot \sqrt{\pi d^2/4} = \pi d R/2$$

The formula is valid for wavelengths which are lower than the wire circumference πd. As a special result the radar cross section increases with growing distance R between radar and wire, thus reducing the R^4 dependence of received radar power down to R^3. Fig. 1 shows measured reflection cross sections of wire samples using this radar. Distance of measurement was fixed to 16 m, which is just outside the nearfield region of the 20 cm parabol antenna. The tested wire samples have a length of about 1 m thus being 2 times longer than the 3 dB beam diameter at this distance. As shown the agreement of theoretical and measured data is quite sufficient.

BLOCK DIAGRAM

The block diagram of the experimental incoherent pulse radar for 60 GHz is plotted in Fig. 2. A crystal controlled time base generates the 125 kHz PRF. Triggered by this signal a pulse modulator drives a thermostatted gunn-pulse-oscillator with 20 ns output pulsewidth and 28 dBm peak output power. A likewise thermostatted pulsed impatt-oscillator is synchronized by the gunn-oscillator. Output pulsewidth is 20 ns too and peak output power is 36 dBm. A 40 dB gain parabolic dish antenna with vertical polarisation is fed via a circulator. The received signal is transmitted to a balanced mixer via an RF-STC. The mixer LO-power is generated in a temperature compensated gunn-oscillator with 15 dBm cw-output power and is fed to the mixer via a circulator.

The mixer is followed by a low noise IF amplifier, an IF-STC and a bandpass-filter of 100 MHz bandwidth. After a second stage of preamplification the signal is formed into a videopulse by an log-amplifier-limiter. In order to get enough output power for display the signal is amplified and fed into the display processing unit.

SCANNING-ANTENNA AND -MECHANISM

With an image-repetition rate of 1/s a sector of $\pm 90^\circ$ in azimuth and $\pm 15^\circ$ in elevation can be covered. Assuming an antenna half-power-beam-width of less than 2° leads to a minimum of 15 lines to be scanned. The parabolic dish antenna may not be scanned that fast with reasonable mechanical effort due to the extreme forces resulting from this scanning scheme.

Instead, in this development a mechanical polarisation twist antenna scanning mechanism was used which consists of a fixed parabolic dish and a movable plane mirror. The mirror rotates at 900 rounds per minute (rpm) swinging its second axis from 37.5° to 52.5° every second in order to twist the vertically incident beam from the parabolic dish between -15° and 15° in elevation. The high centrifugal forces arising from the rotational movement of the mirror are compensated for using suitable compensating masses.

In the block-diagram (Fig. 2) the antenna drive and the drive control are shown. The position of the mirror (i. e. the actual direction of the beam) is related to the output signal of a shaft encoder and serves as an input to the central control unit for signal display. A detected obstacle thus appears on the display in a space sector related to the position of the rotating mirror.

DISPLAY

For the display of the detected obstacles a flight-qualified multifunction display is employed with a 5" x 5" screen. The scanning sector of ± 90° in azimuth and ± 15° in elevation is divided into 80 x 15 picture cells. These cells are inscribed by symbols corresponding to the distance of the obstacles. In this manner all three coordinates are displayed on a two-dimensional screen. The image is written at a rate of 100 Hz flicker-free and is up-dated line by line reflecting the actual changes in the scene.

DESCRIPTION OF MM-WAVE FRONT-END

The realization of the mm-wave components applied has been performed using rectangular waveguide technique for the transmitter part and planar technique for the receiver part - with not taking into account the local oscillator. The construction of this oscillator is shown in fig. 3 /6/. The gunn-diode is placed at the bottom of a reduced height waveguide section. The resonator, operating in the TE_{013} mode, has an unloaded Q-factor of about 10.000. This is obtained by silver plating and diamond tooling of the cavity. The cavity backshort consists of an invar and a copper part. Optimizing the related lengths an additional temperature compensation is obtained. Frequency drift typically is about 100 kHz/°C, but values as low as 10 kHz/°C can be achieved by a proper choice of the temperature compensation and nitrogen filling of the cavity. Because pulling is only some MHz at 15 dB return loss, no isolator is necessary. The output power is about 10 mW.

The construction of the pulsed gunn-oscillator for the transmitter is similar to that of the LO, the high Q-resonator, however, is replaced by a backshort. Frequency stability against temperature variations is given by heating up the device to a constant temperature. The achieved output pulse power amounts to 0.7 W.

The pulsed impatt-oscillator /7/ consists of a rectangular waveguide resonator and the impatt-diode itself, being soldered on a copper-stub. This stub is taken to vary the diode height with respect to the waveguide by means of a collet, which is fixed in the bottom of the waveguide. Further matching can be achieved using the variable backshort. Bias supply is performed with a commonly used coaxial low-pass filter.

As it is well known, the output pulse of non stabilized impatt-oscillator has a considerably high chirp rate, resulting from the heat-up process within the diode crystal during pulse. In order to reduce the necessary synchronisation power the chirp must be reduced by a proper pre-forming of the bias pulse. To this end a pulse-synthesizer /8/ has been developed,which assembles the bias pulse from 10 invidually adjustable subpulses. As a result the chirp can be droped down to 50 MHz.

For the receiver part fin-line technique is used /9, 10/. This allows to combine the STC-PIN-attenuator and the balanced mixer on one substrate only, as shown in fig. 4. The local oscillator power is fed to the diodes via a transition from an asymmetrical fin-line to a coplanar line, working in a similar way to a "probe-type" transition from standard waveguide to coaxial line. For proper operation, a short is placed a quarter wavelength away from the transition. Additionally, this short allows a final adjustment of the LO input match. The signal path consists of a symmetrical unilateral fin-line. Schottky-barrier beam lead diodes are placed at the junction between fin-line and coplanar line. A microstrip IF low-pass filter is connected to the coplanar line.

In front of the mixer signal input a PIN-attenuator is embedded using series stubs in the fin-line. The series stubs are designed in such a way, that in the case of high attenuation, a parallel resonant circuit is formed by the stub and the diode parasitics. For the case of low attenuation, a rather low impedance results in series to the line. The parallel resonant circuit limits the bandwidth of the attenuator. This disadvantage, which is not important here, is compensated by an increased dynamic range of the attenuation and by an inherent DC isolation from the residual circuit because two diodes are used. The attenuation can be adjusted between 1 and more than 30 dB. The measured conversion loss of the PIN-attenuator/mixer-unit amounts to about 7 dB at the radar frequency. Fig. 5 shows the complete mm-front end including the mounted antenna feed. Fig. 6 gives a scope of the opened radar sensor.

EXPERIMENTAL MEASUREMENTS

First field experiments in order to detect high voltage transmission lines and other obstacles using the 60 GHz radar have been performed. Fig. 7 shows the measurement scene with a 110 kV and a 10 kV transmission line. The wire bundle diameters are 21.7 mm and 8.1 mm respectively. The fig. 8 a-c shows the reflected signals from this high voltage line (110 kV) in different distances. The strong peaks left and right are the reference signals.

In every case the beam center is directed perpendiculary to middle of the three line planes. Because the beam-diameter increases with growing distance, only the first figure (8a) shows sharp reflections of the both lines. The other figures inhibit reflections also from top and bottom line planes. The signal reflected from the low voltage transmission line is shown in fig. 9. The figures 10 and 11 demonstrate the reflection behaviour of a transmission line pylon and of a bush without leaves in distances of 240 m and 210 m respectively.

CONCLUSION

An incoherent 60 GHz pulse radar for helicopter collision avoidance purposes has been developed having the following data:

frequency	59,1 GHz
pulse power (incl. losses)	3 W
pulse length	20 nsec
PRF	125 kHz or 250 kHz
antenna gain	40 dB
half power beamwidth	1.6^{o}
receiver noise figure (incl. losses, SSB)	13 dB
receiver bandwidth	100 MHz
field of view (azimuth x elevation)	180^{o} x 30^{o}
image repetition rate	1/sec

First test results demonstrate the feasibility of this radar. High voltage transmission lines having wire diameters of about 20 mm have been detected at a distance of more than 400 m.

REFERENCES

/1/ Johnston, St. L.: Millimeter Wave Radar. Arteck House, Inc., Washington, 1980.

/2/ Lindner, K.; Plattner, A.: GERA- ein 35 GHz-Pulsdopplerradar hoher Auflösung. Techn. Mitteilungen AEG-Telefunken 68 (1978) 6/7, pp. 255-258.

/3/ Barth, H.; Bischoff, M.: A 90 GHz-FM-cw-Radar Transmitter, Symp. Dig. IEEE MTT-S (1979), Orlando, pp. 75-78.

/4/ Kerr, D.E.: Propagation of short radio waves, Bd. 13, MIT Rad Lab, 1951.

/5/ Meyer, E.; Kuttruff, H.; Severin, H.: Experimentelle Bestimmung des Radar-Streuquerschnittes zylindrischer Metallkörper. Z. f. angew. Physik 11 (1959), Heft 1, pp. 1-6.

/6/ Bischoff, M.; Schroth, J.: A 64/4 GHz Down converter for a 60 GHz satellite communication System. Symp. Dig. 9th EuMC 1979, Brighton, pp. 608-613.

/7/ Kasper, E.; Barth, H.; Freyer, J.: Gepulste Silizium-Impatt-Dioden für Millimeterwellenoszillatoren. ntz 34 (1981) pp. 768-774.

/8/ Barth, H.; Wippich, H.G.: Ein gepulster Impatt-Oszillator bei 90 GHz mit Chirp-Kompensation. Wiss. Berichte AEG-Telefunken 54 (1981) 4/5, pp. 193-196.

/9/ Menzel, W.; Meinel, H.; Rembold, B.; Schmidt, L.P.: Millimeter-wave planar integrated components for frequencies up to 110 GHz. MSN, Vol. 12, No. 1o, October 1982

/10/ Menzel, W.; Callsen, H.: Integrated fin-line components for radar and radiometer applications. Military Microwave, London, 1982.

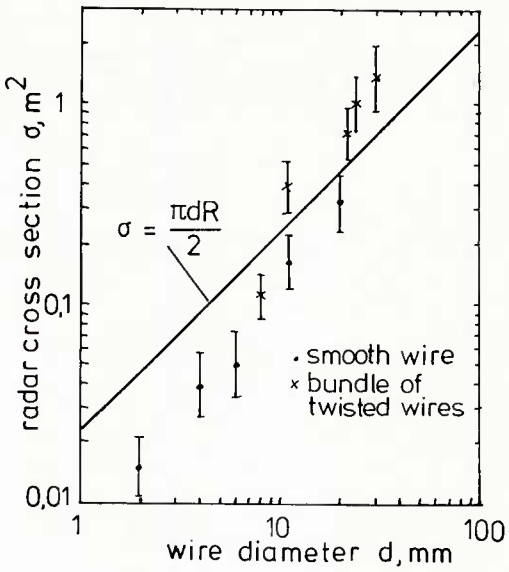

Fig. 1: Measured radar cross-section of straight wires with different diameters.

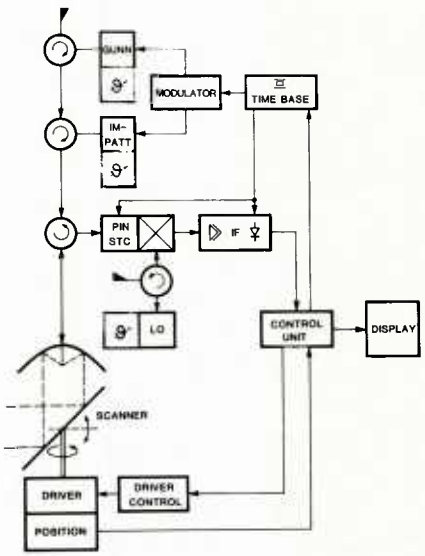

Fig. 2: Block diagramm of realized 6o GHz pulse radar.

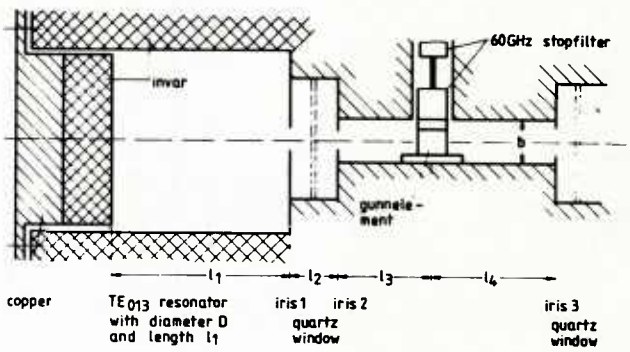

Fig. 3: Cross-section of temperature compensated Gunn-oscillator.

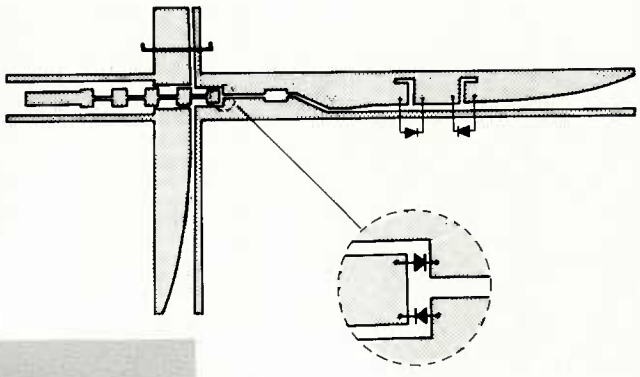

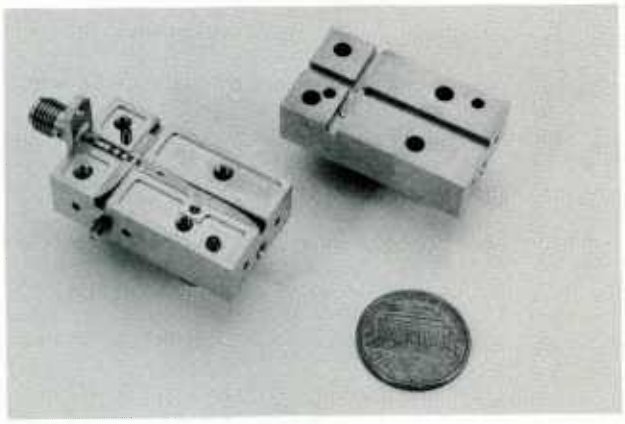

Fig. 4: Layout and opened split block of fin-line receiver front-end incl. mixer and PIN-attenuator

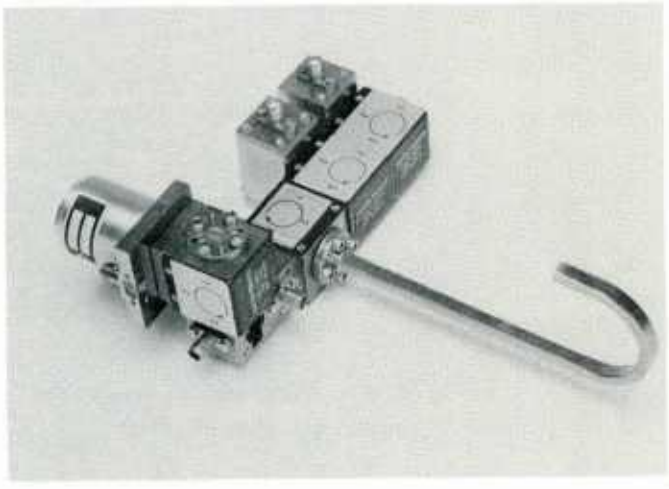

Fig. 5: 6o GHz transmitter-receiver front-end

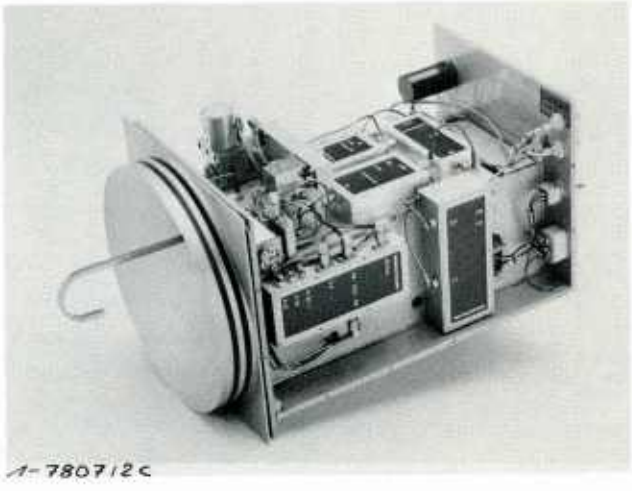

Fig. 6: Complete radar sensor without scanner and cover

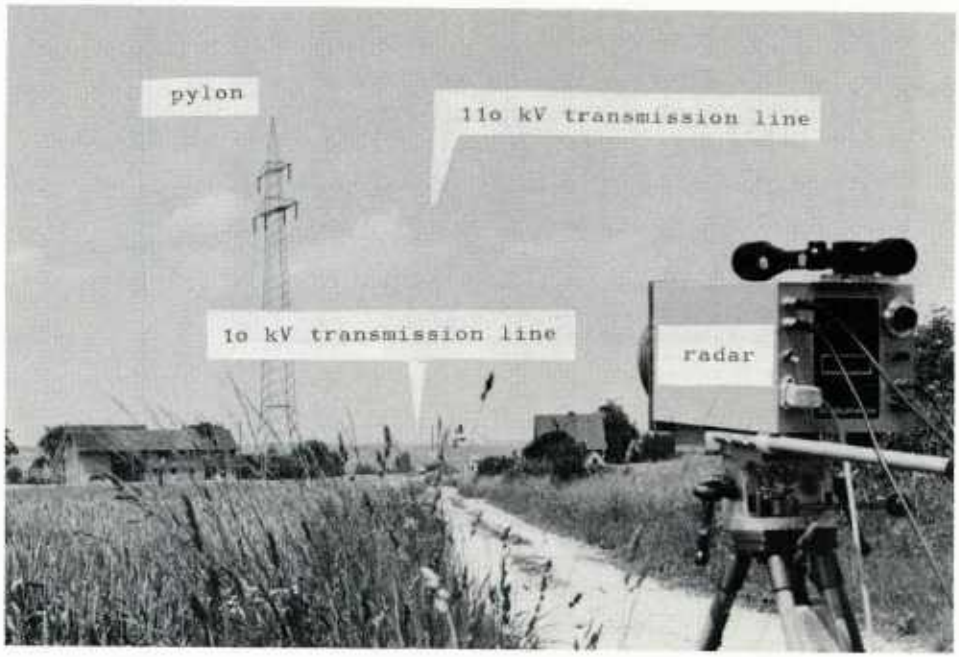

Fig.7: Measurement scene with a 110 kV and a 10 kV transmission line.

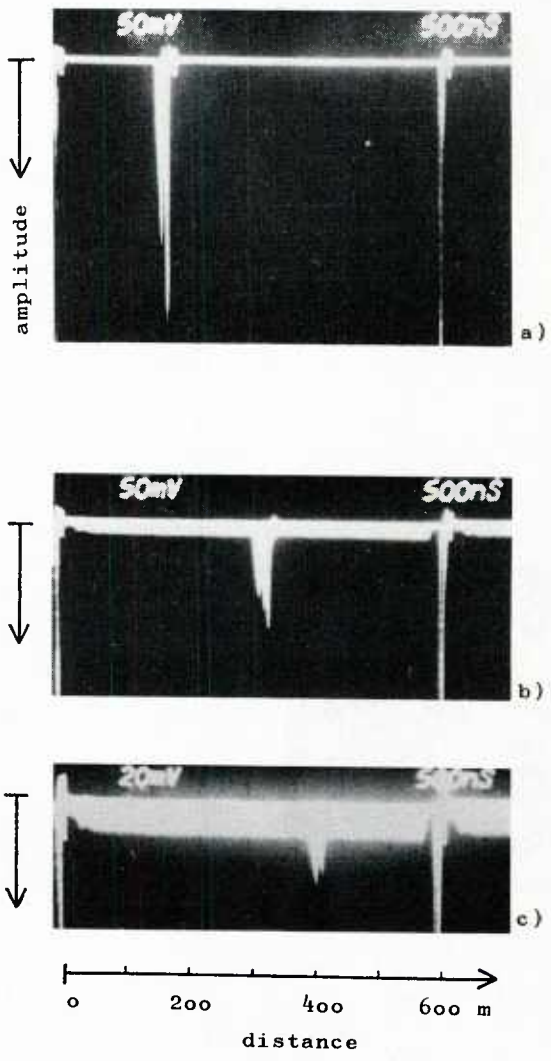

Fig. 8: Reflected signals of a 110 kV transmission line, wire diameter 21.7 mm.

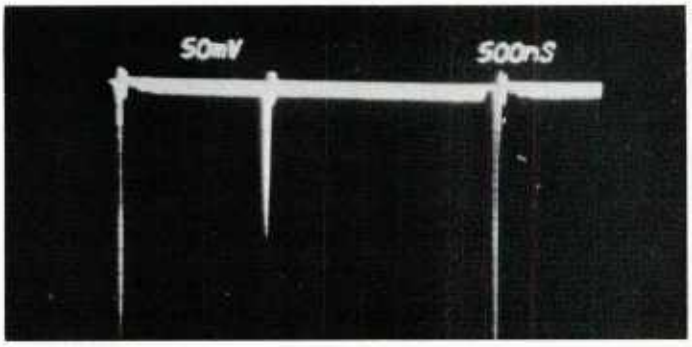

Fig. 9: Reflected signal of a 1o kV transmission line, wire diameter 8.1 mm, distance 24o m.

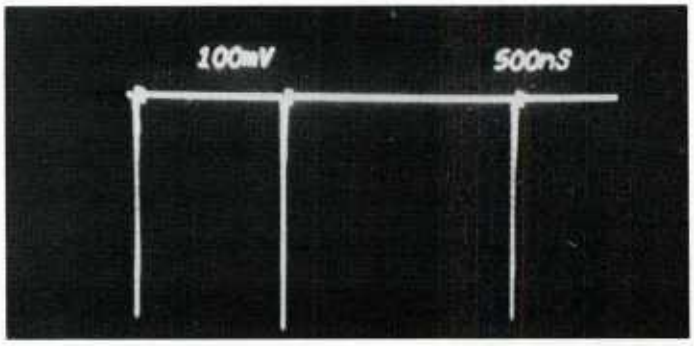

Fig. 1o: Reflected signal of a pylon, distance 24o m.

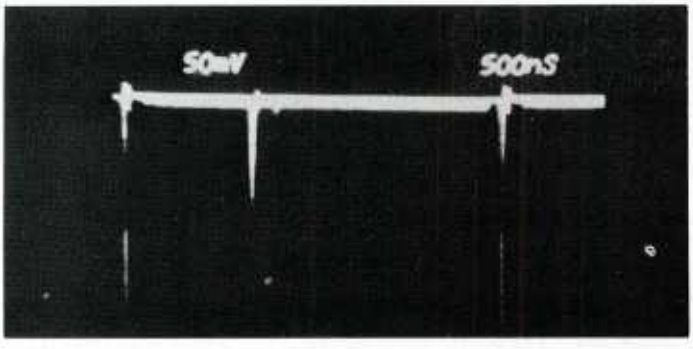

Fig. 11: Reflected signal of a bush without leaves, distance 21o m.

DISCUSSION

E.J.Holliman, US

Is the MM Collison Warning Device locked in azimuthal scan with the rotor blades of the helicopter?

Author's Reply

No because the rotor blade rotation is too slow. Our scanner is planned to rotate with 900 rpm.

M.B.White, US

Will you point out what you consider to be the principal advantages of the MM lidar system, as compared to the competitive CO_2 laser approach?

Author's Reply

- No degradation in operation caused by adverse weather condition (e.g. fog).
- No constitution of hazards.
- Low weight and volume (no need for high voltage power supply).

A.J.Simmons, US

(1) Thin wires are better reflectors of horizontal than vertical polarization. Your antenna rotates its polarization as it scans. Can you comment?

(2) Horizontal wires scatter strongly primarily at normal incidence; more weakly at other angles. Does this present a problem to your system?

Author's Reply

(1) For circumference to wavelength ratios greater than 1 the reflection behaviour becomes increasingly independent of polarization. For 8 mm diameter for instance the ratio is about 5.

(2) Measurements have shown that due to the grating effect of wire bundles additional reflections occur besides the normal incidence, having nearly the same amplitude.

SUMMARY OF SESSION IV

PROPAGATION ALONG SPACE-EARTH PATHS

by

Mr M.P.M.Hall
Session Chairman

The session comprised five papers covering different aspects of studies being conducted on space-earth propagation. All but one dealt with effects of the troposphere.

The first paper, by **Dr L.Schwab** and **Dr A.Simmons**, covered basic modelling of attenuation due to rain on space-earth paths. This is perhaps the most essential problem for such paths, and this paper described a major contribution in the current study progress towards establishing a widely accepted prediction method that may be applied worldwide. The paper went on to use the prediction model to assess worldwide service coverage at 20, 30 and 45 GHz.

The next paper, by **Dr D.Davidson** and **Dr T.Tang**, discussed the prospects for reducing the effects of rain attenuation by using two terminals at the ground operating in diversity mode. The measurements presented showed that, in regions where attenuation due to rainfall is most severe, e.g. Florida in the USA, diversity mode operation is likely to provide major improvements at frequencies greater than 20 GHz so long as the site spacing was at least 15 km. Provided the elevation angle is high, the baseline orientation is unimportant. Without such diversity, fades of 10 dB were encountered for periods from 0.4 to 10 minutes, whereas diversity operation reduced these periods to 0.04 to 2.4 minutes.

The paper by **R.Howell**, **Dr J.Thirlwell** and **Dr D.Emerson** produced useful statistical data on the relationship between cross-polar coupling and attenuation on space-earth paths operated at 11 and 14 GHz. It brought out the effect of polarization and departures from the current CCIR model, and quantified the range of values that may be encountered.

The paper by **Dr E.Vilar** and **J.Haddon** introduced a very different aspect, namely the use of spectral analysis of amplitude scintillations in the troposphere as a remote sensing tool on a 12 GHz space-earth path for the derivation of refractive index structure constant, C_n^2, the turbulent path length and the dominant eddy size. It is also important to evaluate the wind speed across the path.

The final paper by **Dr D.Fang** and **Dr C.H.Liu**, described how the intensity and percentage of time for which scintillations were observed on 4 GHz space-earth paths increased significantly with sunspot number. Peak-to-peak levels of intensity up to 14 dB were observed on many evenings, the event being most common at about 22 hrs (local time). Cumulative distribution plots were presented for worst month and annual data.

Discussion of these papers was lively and wide ranging, covering propagation and applications to systems.

A PREDICTOR MODEL FOR EHF COMMUNICATION SATELLITE SYSTEM AVAILABILITIES IN THE PRESENCE OF RAIN* †

LEONARD M. SCHWAB AND ALAN J. SIMMONS
Massachusetts Institute of Technology, Lincoln Laboratory
Lexington, Massachusetts

SUMMARY

As the trend toward utilization of higher operating frequencies for future MILSATCOM systems continues to develop, the need for clearer understanding and prediction of global rain attenuation effects becomes more pronounced. Rain attenuation of millimeter waves has a major effect upon link availability which, in turn, is the major element of system availability. A computer-based tool for assessing the effect of rain attenuation upon availability has been developed to aid in selecting fundamental MILSATCOM parameters such as satellite subpoint and operating frequency as well as secondary parameters such as design margin and antenna radiation patterns.

A numerical model for predicting system availability of a geo-stationary communications satellite system operating in the EHF bands (up to 50 GHz) has been formulated and programmed. The model computes link availability using Crane's eight-region world-wide rain rate model. The link availability, A_L, is computed for a specific value of system link margin provided as an input to the program along with specified values of operating frequency (in GHz), and satellite subpoint. The up- or downlink availability is contour plotted on a Mercator projection of the world. Example calculations show that average availabilities in the 98-99% range can be achieved in most regions of the earth with modest link margins (6-12 dB). Because of the inverse correlation of rain intensity and duration, the effective availability is greatly increased if a relatively short waiting time is permissible.

1. INTRODUCTION

As is well known, rain attenuation can severely affect communication links operating in the EHF bands. For satellite links in the 20, 30 and 45 GHz bands, the system designer must allow sufficient margin to permit communication for a high percentage of the time. The regions of the earth with which military communications will be required in the future are relatively unpredictable, so military satellite communications systems should be designed to give high link availability from any region on the earth's surface visible from the satellite. Fortunately, in contrast to commercial satellite communications systems which demand outage times of less than one hour per year (link availability greater than 99.99%), many military communications systems are useful with somewhat lower values of availability. This can, it turns out, be achieved with modest link margins from almost everywhere on the earth.

In order for the system designer to determine the required link margin to achieve a desired level of availability for a global communications system, a rain model for the earth is required, as well as a model relating expected attenuation with rain rate and satellite elevation angle. The latter is a function of terminal position as well as of satellite location. We have developed a computer model which includes all these parameters and permits one to make plots of constant availability contours on the earth for specified values of link margin at a variety of frequencies. The initial use of this parametric approach to numerically solve for link margin contours was derived at Lincoln Laboratory and is described in [Schwab, 1980]. The global rain attenuation model used is due to Crane** [Crane, R. K., 1978a,b; Crane, R. K., 1980] and is briefly described in the next section of this paper. The third section describes how the rain model was used with the earth-satellite geometry to produce contour maps of availability. The fourth section presents some results for various frequencies, and the final section presents some conclusions as well as some suggested techniques for effectively improving link margins.

2. RAIN MODEL

2.1 Rain attenuation

The expected value of rain attenuation for a particular terminal-satellite path is associated by a semi-empirical formula with the point rain rate at the terminal, the

---

*This work has been sponsored by the Defense Communications Agency.

†"The U.S. Government assumes no responsibility for the information presented here."

**Crane has recently [Crane, R. K., 1982] developed a new rain model (the so called two-component model) which attempts to model more closely the physics of rain. The older empirical model gives reasonably close agreement with his newer model and so can still be used for the purpose of our study.

melting layer height above the terminal, and the satellite elevation angle. The formula used is

$$L(dB) = H \csc \theta \cdot \alpha(F) \cdot \gamma(D) \cdot R_p^{[\beta(F) - \delta(D)]}; \quad \theta \geq 10^0 \qquad (1)$$

where H is the height of the melting layer (0°C isotherm) in km

θ is elevation angle (in degrees)

$\alpha(F)$ and $\beta(F)$ are frequency dependent coefficients which relate specific attenuation (i.e., attenuation in dB/km) to the point rainfall rate

R_p is the point rainfall rate in mm/h

$\gamma(D)$ and $\delta(D)$ are factors which empirically account for the average rain rate along the path given a particular point rain rate at the terminal. (D is the surface projection along the ground of this propagation path. $D = H \cot \theta$)

The height, H, of the 0°C isotherm depends on both the season of the year and the geographical region. The values of H associated with different regions of the world will be discussed in the next section.

For purposes of computation, the values of the various parameters in (1) were approximated by appropriate polynomials, which were fit to Crane's empirical curves. These expressions are

$$\alpha(F) \simeq 1 - \exp[.115F' - 2.02(F')^2 - 1.01(F')^3] \qquad (2)$$

$$\beta(F) \simeq 0.9[1 + 3.8408\ F' - 21.810(F')^2 + 48.80\ (F')^3 - 39.7(F')^4] \qquad (3)$$

where $F' = F(GHz)/100$, and (2) and (3) are valid in the range $5 \leq F \leq 50$ GHz

$$\gamma(D) \simeq 1 + p - 0.23\ p^2 + .0215\ p^3 \qquad (4)$$

where $p = D/4.5$, D in kilometers

$$\delta(D) \simeq q - 0.98\ q^2 + 0.446\ q^3$$

where $q = D/22.5$.

These functions are plotted in Figs. 1 and 2. In the use of these formulas, D is restricted to values less than 22.5 km, which corresponds to an elevation angle of 10° for a typical melting layer height, H, of 4 km. The model does not apply for elevation angles below 10°. In cases where $H > 4$ km and D is greater than 22.5, the values of γ and δ for $D = 22.5$ were used.

With these formulas, we are in a position to determine the attenuation, given a value of rain-rate, R_p, and a value of H. These can be associated with regions of the earth and with a probability of occurrence. To the attenuation due to rain must be added the normal attenuation due to water vapor and oxygen absorption, as will be described below.

2.2 Climate Regions

For the purposes of our global model, Crane's 8-region world model was used (see Fig. 3). The regions vary from a low-rain polar type (A) through a high-rain tropical type (H). Associated with each of the regions is a rain rate distribution as shown in Fig. 4. From Fig. 4 may be obtained the percentage of time a given value of point rain rate is exceeded, and this value used in (1) to obtain the probability that a certain value of attenuation will be exceeded. Clearly, the map shown in Fig. 3 may be subdivided somewhat finer. Our model is not intended, however, to predict precise values of availability for a particular location, but instead to give guidance on the values of margin required to give general levels of availability anywhere on earth. For this purpose the eight-region model, with the wide spread in rain rate probability, as shown in Fig. 4, is satisfactory.

In order to use the eight-region model, the map shown in Fig. 3 was digitized by setting a 2.5° longitude x 2.5° latitude grid on the Mercator projection of the rain region map,

and associating a rain region with each point where the grid lines crossed. This table of 8352 points was stored in computer memory. The data file covers +70°N to -70°S in latitude. All points north of +70° and south of -70° are in region A, and in fact are hardly visible from a synchronous equatorial satellite, since we restricted our plots of the field of view from one satellite to points on the earth with 10° or greater elevation angle. The locus of such points in longitude λ and latitude ϕ for at satellite located over the equator a latitude λ_s is given by the solutions of the equation

$$\lambda = \pm \cos^{-1}\left(\frac{\cos(71.43^{\circ})}{\cos \phi}\right) + \lambda_s \qquad (6)$$

Clearly, $|\phi| \leq 71.43°$. When $\phi = 71.43°$, $\lambda = \lambda_s$, i.e. the point directly north of the satellite at latitude 71.43° views the satellite at a 10° angle.

The curves in Fig. 4 were approximated by fitting a number of exponential functions of the form

$$f_y = \exp[k_o + k_1 R_p + k_2 R_p^2 + k_3 R_p^3] \qquad (7)$$

to each of the curves, where f_y is the fraction of the year the rain rate is exceeded, R_p is the point rain rate.

A number of points were selected on each of the curves in Fig. 4 and a set of four constants, k_i, associated with each contiguous set of four points. The appropriate constants were then chosen for a particular value of R_p to calculate f_y. For example, if we want to find f_y for a particular value of R_p, we find the four consecutive data points R_{p1}, R_{p2}, R_{p3}, R_{p4} for which a set of constants k_0, k_1, k_2, k_3 has been calculated, and for which $R_{p2} \leq R_p \leq R_{p3}$. We use this set of constants in (6) to calculate f_y. The only exceptions to this method of calculation are made near the ends of the curves. At the low rain rate end of the curve, the data is extended to zero rain rate by linear extrapolation, to reach zero rain rate at 100%, which should be an upper bound to the real data. At the high rain rate end of the curve, values of rain rate for times less than 10^{-5} year were set equal to the values for 10^{-5} year. Both of these portions of the curves are normally outside the region of interest.

2.3 Melting Layer Height

The average height, H, of the melting layer is approximated by two polynomials, one for the regions A-D, and the other for regions E-H. A basis of $\sin^2\phi$, ϕ being the latitude, is used. The formula is

$$H \simeq 4.8[1 + a_2 \sin^2\phi + a_4 \sin^4\phi + a_6 \sin^6\phi + a_8 \sin^8\phi] \qquad (8)$$

where

	REGIONS A, B, C, D	REGIONS E, F, G, H
a_2	0.15498931	- 0.276000
a_4	-1.54759303	3.705036
a_6	-0.87194405	-14.212189
a_8	1.47241242	12.032159

Figure 5 shows a plot of these values.

2.4 Clear-Sky Attenuation

To the loss due to rain calculated by use of (1) is added the attenuation due to clear air, primarily due to water vapor and oxygen. The attenuation is assumed to follow a simple cosecant law

$$A(\theta) = A(90^{\circ}) \csc \theta, \ \theta \geq 10^{\circ} . \qquad (9)$$

For the zenith attenuation, A(90°), we chose the attenuation of a standard atmosphere, (7.5 g/m^3 at 20°C) based on Fig. 2 of [Crane, R. K., 1971]. The zenith attenuation curve was approximated by two polynomials, one for the region below 22 GHz, the other, above 22 GHz as follows:

$$A(90^0)_{dB} \approx \exp(C_1F + C_2F^2 + C_3F^3 + C_4F^4) - 1 \qquad (10)$$

where F is in GHz and

	7 GHz < F ≤ 22 GHz	22 GHz < F ≤ 50 GHz
C_1	-0.00617564	0.13030320
C_2	0.00432368	-0.00816987
C_3	-0.00044445	0.00015648
C_4	0.00001358	-0.00000074

Figure 6 shows a plot of points based on (10).

3. PROCEDURE FOR OBTAINING AVAILABILITY CONTOUR MAPS

The approach used to calculate link availability was to start with an assumed communications link margin, M, between a satellite and terminal located at the subsatellite point, then to calculate the allowable rain attenuation for each point on the earth in the satellite field of view and finally to associate a probability of occurrence with this value of rain attenuation. The allowable maximum rain attenuation associated with a point on earth is given by

$$L(dB) = M - L_{cs}(dB) - L_{sr}(dB) \qquad (11)$$

where

L_{cs} is the assumed value of attenuation by the normal atmosphere given by (9)

L_{sr} is the additional slant range path loss to the point in question as compared to the range to the subsatellite point.

Given the frequency, satellite location, and a point on the earth, the parameters H, θ, α, γ, β, δ L_{cs} and L_{sr} may be then calculated, and the value of L from (11) may be used in (1) to obtain R_p, the maximum allowable point rain rate. The probability of occurrence is then obtained by using the rain-rate probability curve appropriate for the climate region. This value of rain-rate probability is thus also the probability of being able to communicate, or availabilty of the link. Having the availability at each point in the latitude-longitude grid, it is easy to plot contour lines of constant availability.

4. TYPICAL RESULTS

Figures 7 through 12 give typical results. Shown are calculations for three values of frequency, and two values of margin at each frequency. These plots show the view of the earth from a single satellite. Another version of the program shows the entire earth as viewed from a constellation of satellites. Figures 7 and 8 show availability at 20 GHz for 6 and 12 dB margin for a satellite located over the Atlantic Ocean. Areas with availability less than 99% are shaded. As might be expected, these areas occur at low elevation angles at low latitudes. What might not be expected is that a very large area of the earth has availability greater than 99% with only 6 dB margin, and essentially all the visible earth with 12 dB margin. These results are typical for any satellite location.

Figures 9 and 10 show selected plots for 30 GHz, with margin of 12 and 18 dB respectively, with similar results as for 20 GHz. At 18 dB margin, most of the temperate regions of the world exhibit availability in excess of 99%.

Figures 11 and 12 are for a frequency of 45 GHz with 12 and 18 dB margin and show that availability of 98% in most of the world can be obtained. As another example, Fig. 13 shows the coverage area for 98% availability for a constellation of four equi-spaced geostationary satellites with 12 dB margin at 45 GHz. Note that with a four-satellite constellation, there is overlapping coverage in the equatorial region, and in fact, a station on the equator can always find a satellite at an elevation angle of 38° or above. This improves the low availability which is observed in these regions in Fig. 12 when only a single satellite is considered.

5. CONCLUDING REMARKS

By means of a computer model making use of Crane's global rain model, worldwide availability of satellite to earth links can be graphically portrayed. Results obtained with the model show, for example, that with a four-satellite geostationary configuration, coverage of almost all the world can be obtained with 99% availability

with link margins of 6 dB at 20 GHz and 12 dB at 30 GHz, and 98% availability with 12 dB margin at 45 GHz. (By link margin is meant the signal/noise margin for a link to a terminal at the subsatellite point with no allowance for atmospheric attenuation). The model can be used at other frequencies in the 7 to 50 GHz region, and for other values of availability and margin. Its main utility is to permit the system designer to estimate minimum values of margin required to achieve a desired availability, and thus to be able to size terminal and satellite antennas, receivers, and transmitters. The model is not expected to give exact results for a particular location of a terminal, but instead, gives a global estimate, which should be useful for a mobile military satellite communications system.

Other than the direct approach of increasing link margin, the only other way of increasing availability that has been suggested is by means of diversity techniques. Site diversity has been shown to be useful in increasing availability for fixed-rate terminals, but cannot be used for mobile terminals. The mobile terminal user is thus forced to wait for the rain to diminish or stop before communicating. Fortunately, there is a strong inverse correlation between rain rate and duration, i.e.,the heavier the rain, the shorter it lasts. Thus one can consider trading off average waiting time for the rain to diminish vs link margin. In a recent study by Rafuse [Rafuse, R. P., 1980], he introduced the parameter D_T/D_R, where D_T is the number of thunderstorm days and D_R the number of rainy days per year for a particular location. Using this ratio, the following result was obtained:

$$M_2/M_1 = \left[1 + 0.2\ T\ e^{3.7\ D_T/D_R}\right]^{0.5} \qquad (12)$$

where M_1 is the actual system margin in dB in the absence of rain

M_2 is an effective system margin in dB

T is the waiting time in minutes.

An interpretation of this formula is that if one can wait a time, T, then the availability may be calculated using the effective margin, M_2, rather than the actual margin, M_1. Typical values of availability calculated on this basis for a specific location, Crawford Hill, New Jersey are shown in Fig. 14. One can see that for a system margin of 10 dB at 30 GHz, the probability of having zero waiting time is about .992. The probability of incurring a waiting time of 10 minutes or less is about .999. The value of D_T/D_R varies with climate region, between 1 and 0, so if T = 10 minutes, $M2/M_1$ varies between 1.7 for regions of very little thunderstorm rain to 9 for regions where the rain occurs almost entirely in thunderstorms.

References

Crane, R. K., 1971, "Propagation Phenomena Affecting Satellite Communications Systems Operating in the Centimeter and Millimeter Wavelength Bands", Proc. IEEE, 59, pp. 173-188.

Crane, R. K., 1978a, "Rain Attenuation Predication", Doc. F5/003 submitted to CCIR Special Preparatory Meeting.

Crane, R. K., 1978b, "A Global Model for Rain Attenuation Prediction, IEEE Eascon'78 Record, pp. 391-395.

Crane, R. K., 1980, "Prediction of Attenuation by Rain", IEEE Trans. Comm., COM-28, p. 1717-1733.

Crane, R. K., 1982, "A Two-Component Rain Model for the Prediction of Attenuation and Diversity Improvement", Report published by Thayer School of Engineering, Dartmouth College under NASA Contract No. NASW-3506.

Rafuse, R. P., 1980, "Rain-Outage Reduction by Data Storage in EHF SATCOM Systems", Project Report DCA-10, Lincoln Laboratory, M.I.T.

Schwab, L. M., 1980, "A Predictor Model for SHF and EHF MILSATCOM System Availabilities in the Presence of Rain", Technical Note 1980-15, Lincoln Laboratory, M.I.T.

In the addition to the above references, material in this report was abstracted from the following Lincoln Laboratory reports.

Frediani, D. J., 1979, "Technology Assessment for Future MILSATCOM Systems: The EHF Bands", Project Report DCA-5, Lincoln Laboratory, M.I.T.

Schwab, L. M., 1981, "World-Wide Link Availability for Geostationary and Critically Inclined Orbits Including Rain Attenuation Effects", Project Report DCA-9, Lincoln Laboratory, M.I.T.

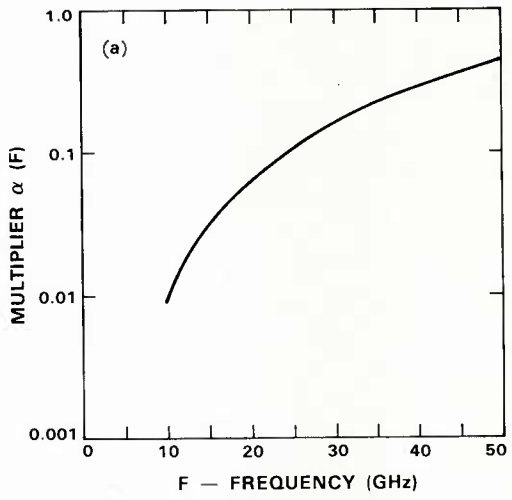

Fig. 1a. Polynomial approximation to $\alpha(F)$ vs frequency.

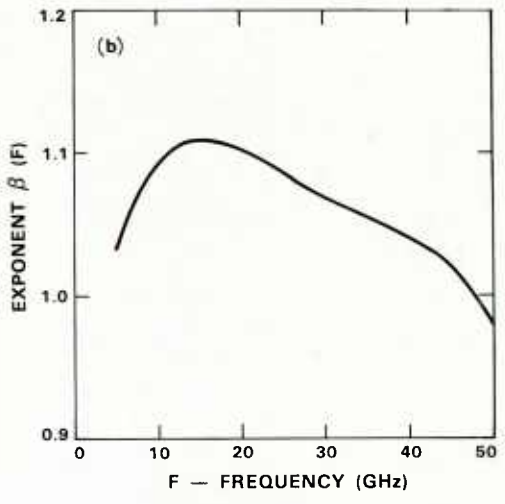

Fig. 1b. Polynomial approximation to $\beta(F)$ vs frequency.

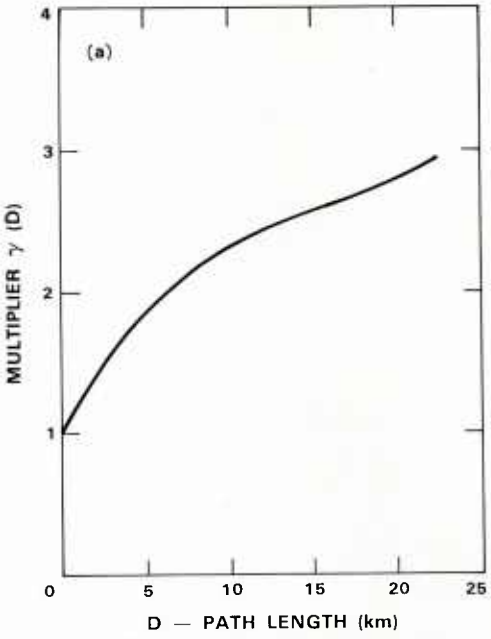

Fig. 2a. Polynomial approximation to $\gamma(D)$ vs path length.

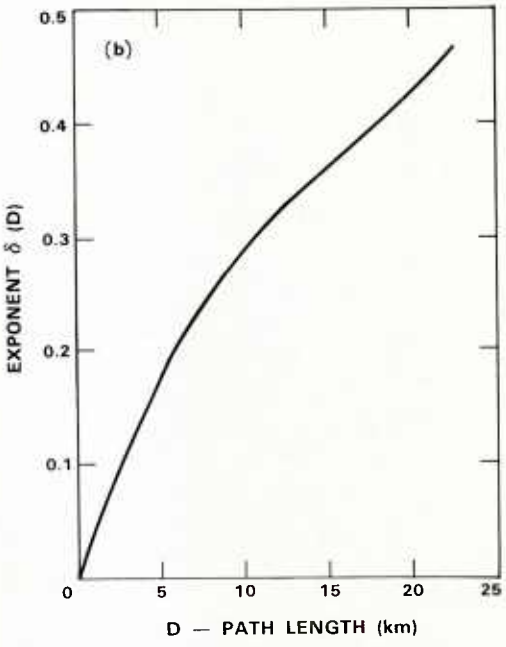

Fig. 2b. Polynomial approximation to $\delta(D)$ vs path length.

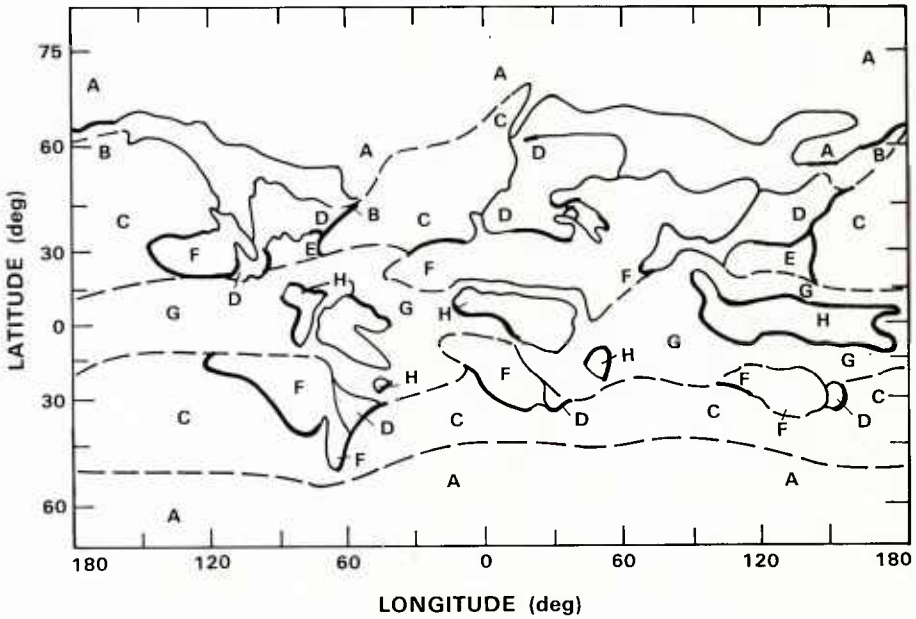

Fig. 3. Rain rate climate regions.

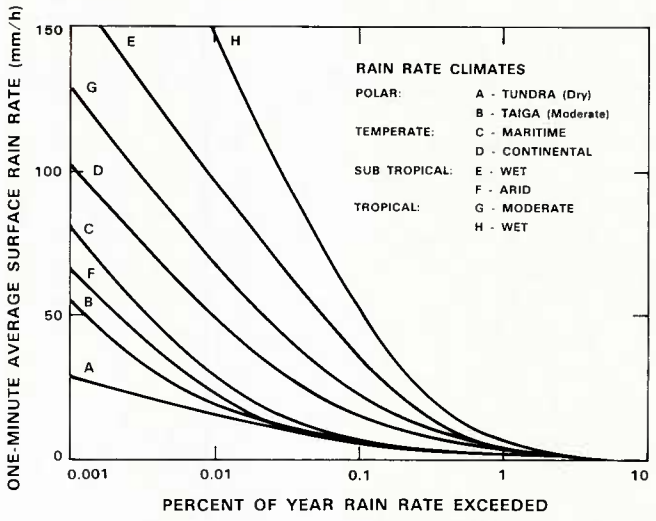

Fig. 4. Rain rate distributions.

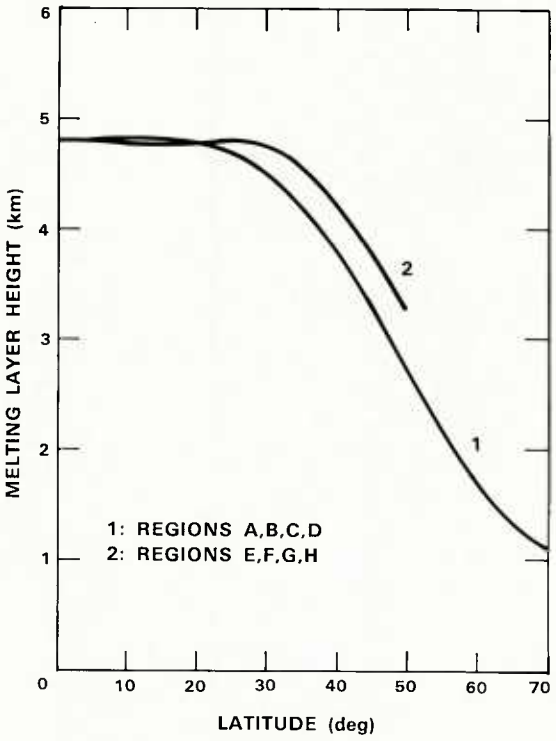

Fig. 5. Polynomial approximations to melting layer height vs latitude.

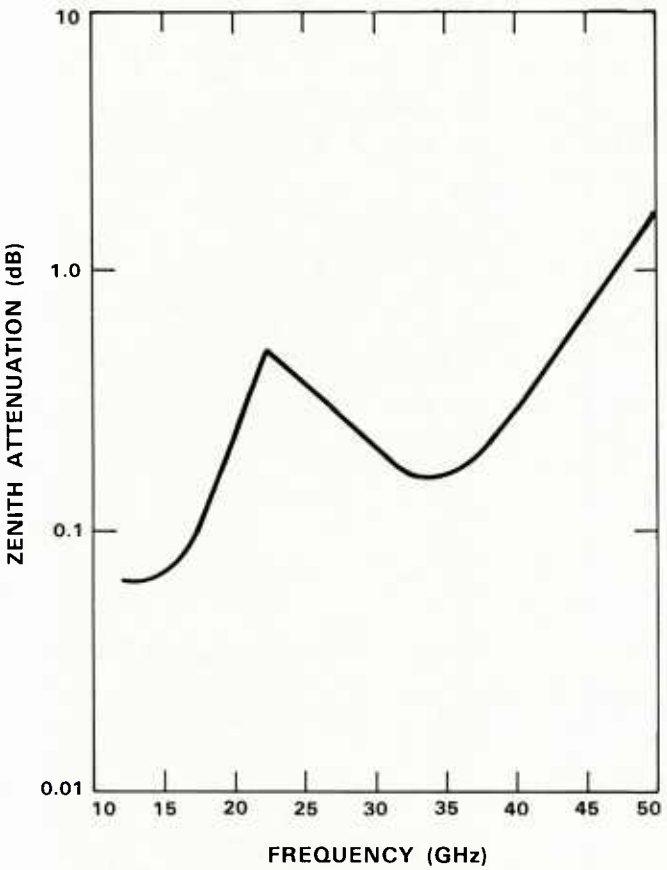

Fig. 6. Polynomial approximation to zenith attenuation vs frequency. Humidity = 7.5 g/m^3 (43% relative humidity at 20°C)

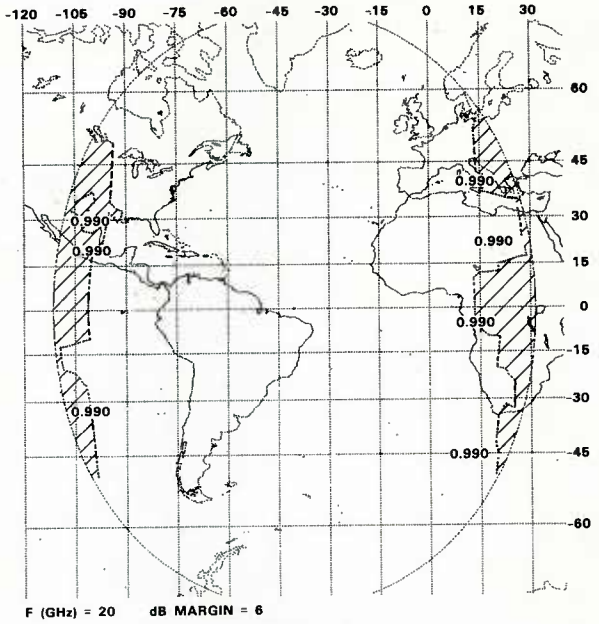

Fig. 7. Region of availability >99%, F = 20 GHz, Margin = 6 dB.

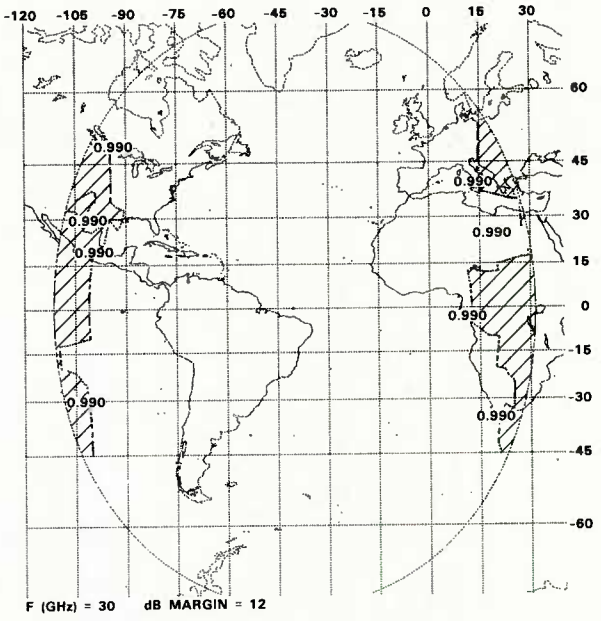

Fig. 9. Region of availability >99%, F = 30 GHz, Margin = 12 dB.

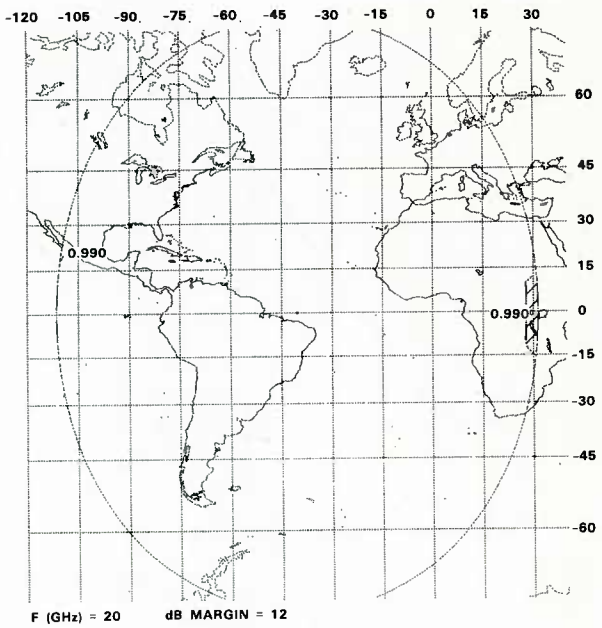

Fig. 8. Region of availability >99%, F = 20 GHz, Margin = 12 dB.

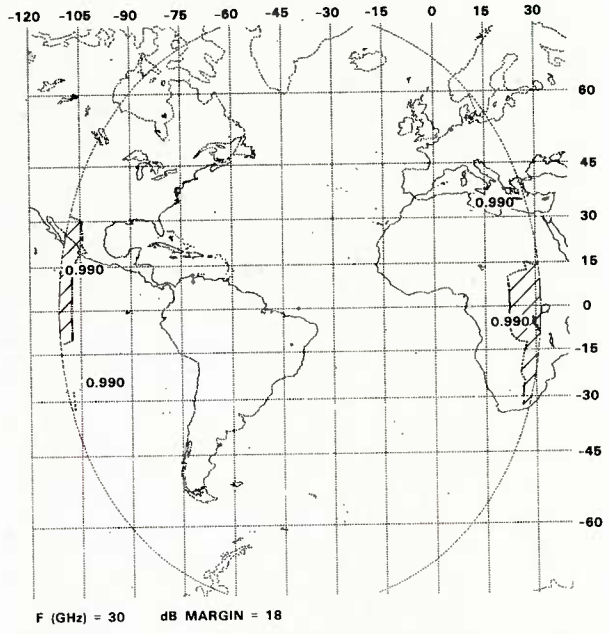

Fig. 10. Region of availability >99%, F = 30 GHz, Margin = 18 dB.

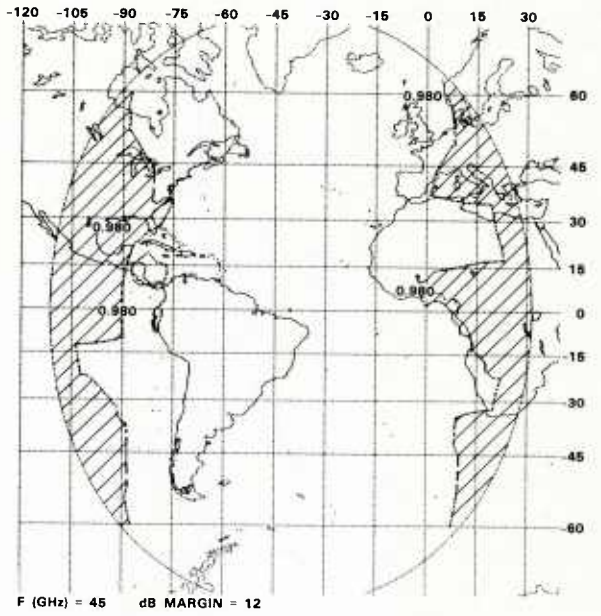

Fig. 11. Region of availability >98%, F = 45 GHz, Margin = 12 dB.

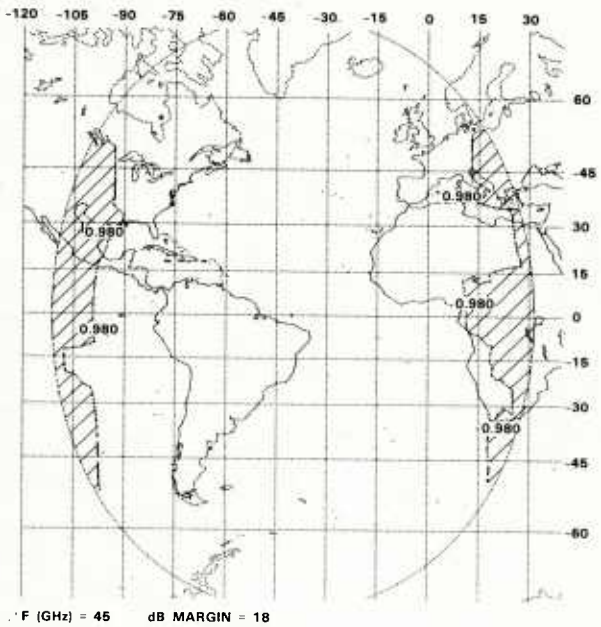

Fig. 12. Region of availability >98%, F = 45 GHz, Margin = 18 dB.

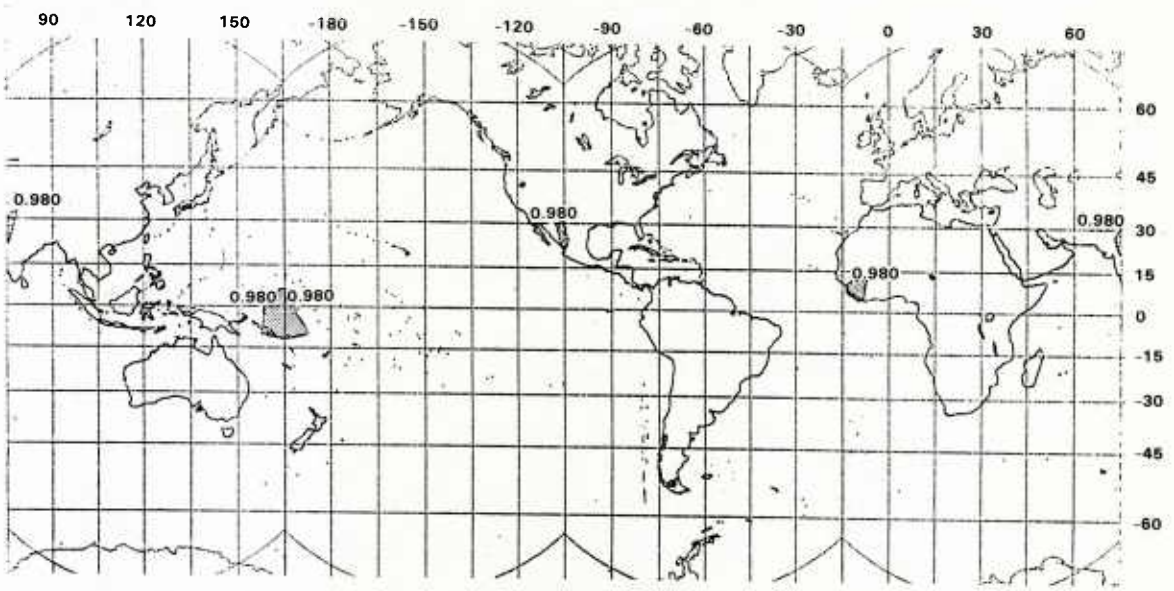

Fig. 13. 98% availability coverage, four geostationary satellites, F = 45 GHz, Margin = 12 dB.

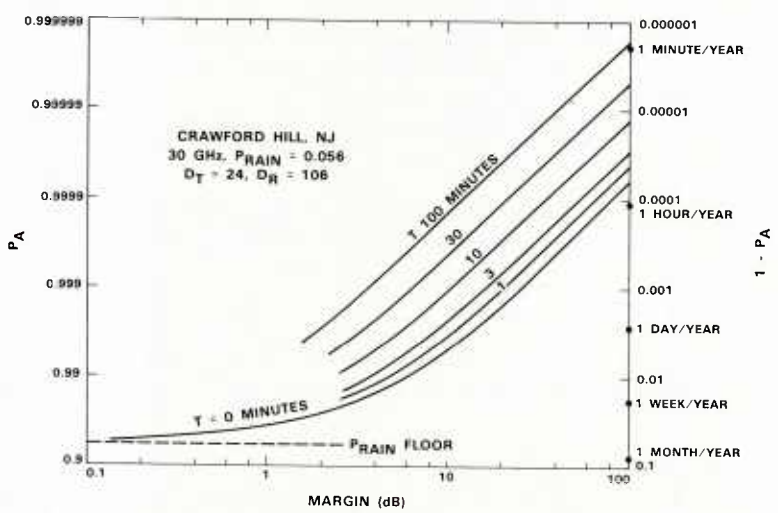

Fig. 14. Availability vs margin and waiting time for Crawford Hill, New Jersey at 30 GHz.

DISCUSSION

M.B.White, US

Isn't the elimination of seasonal effects a rather gross assumption? In a similar model of cloud optical propagation statistics, we have to consider temporal variations of cloud cover on a finer than seasonal scale in order to adequately describe optical communication system performance.

Author's Reply

One could modify the model so that it could be used on a seasonal or even a monthly basis. For our purposes, which were to establish guidelines for system designers, such detail was thought unnecessary. We did attempt to be conservative and weigh the summer months in the temperate zone somewhat more heavily in our annual average.

J.Arnbak, Ne

The representation of availability (or reliability) *worldwide* for a fixed margin *worldwide* does not really reflect modern system design principles and the related need for local propagation data.

Modern resource sharing principles (TDMA slot extension, MBA gain enhancement, etc.) and the possibility of assigning individual link gains in multi-user systems would benefit from a different presentation of your valuable predictions (i.e., not assuming a fixed margin).

Author's Reply

You're quite right that allocation of extra satellite resources to areas of low availability is a useful strategy. Our model permits one to do this by making calculations for different values of margin until adequate values of availability were found. It was simpler computationally to fix the margin and let availability vary over the earth's surface. It is however possible, by running the program many times, to obtain a presentation where availability is fixed and the variation of required link margin is plotted on the map. This presentation would permit one to allocate resources a priori. A more interesting idea might be to try to adjust margin on a dynamic basis, i.e. increase the energy transmitted only to those areas where it was actually raining.

B.C.Evans, UK

(1) Have you allowed for the attenuation of the melting band in your model? This would be a significant contribution at the higher frequencies.

(2) Have you allowed for the altitude of the Earth-Stations? This would again affect the rain-path length as in some countries it is improbable that Earth-Stations will be located at sea level.

Author's Reply

(1) No.

(2) We assumed that the earth stations were always at sea level. This worst-case assumption is suitable for bounding the problem.

D.J.Fang, US

You talked about margins in your paper. From the system impact point of view, margins may be of the transmitter as well as the receiver. But once you introduce the margins of the receiver, your conclusions may change accordingly and significantly. The system people consider G/T as a whole, rather than attenuation alone. For different earth stations, there are different G/Ts, and under precipitation condition, not only signal fade, but also sky noise temperature increases. This severely degrades G/T. As a result, the assessment of precipitation for EHF communications may be more complicated than those you have addressed.

Author's Reply

The effect of precipitation on G/T can be taken into account separately. Our approach has been to use a worst-case value of G/T in all our link margin assumptions; that is, we calculate G/T for the case when it is raining.

A.Fer, Tu

Will the model take into account cross polarization effects which may limit system availability through lack of isolation between orthogonally polarized channels when a frequency re-use system is used?

Author's Reply

We have not included prediction of cross polarization effects in our model. The *loss* due to polarization conversion is small and is implicitly contained in the data base used to generate the original semi-empirical model.

L.Boithias, Fr.

Si on tient compte:

(a) des pourcentages de temps d'indisponibilité très élevés considérés ici (entre 1% et 2%)

(b) de l'influence prépondérante des gaz atmosphériques sur l'atténuation.

(c) de l'augmentation du bruit (non étudiée ici) due aux nuages, est-il nécessaire de calculer l'atténuation due à la pluie? En outre la méthode de calcul proposée semble criticable et les données pluviométriques au voisinage de 1% du temps sont peu fiables.

Author's Reply

The results shown were for 98–99% availability, but the model can also be used for higher values, if desired. It is probably true that below 95% availability, the effect of rain is negligible, but it is a factor at 98 to 99%. We have done the best we could with the available data, and have tried to present a conservative or worst-case approximation.

M.P.M.Hall, UK

This model has given most useful predictions of the area of the world that can be covered on the operating margin mentioned. However, it should be noted that considerable variability about predicted levels is to be expected when examining specific paths. Perhaps a measure of this variability is a matter which those of us engaged in prediction of attenuation will have to give more attention in future.

DIVERSITY RECEPTION OF COMSTAR 19/29 GHZ SATELLITE BEACONS IN CONVECTIVE RAIN CLIMATE OF FLORIDA, 1978-1981

D.Davidson and D.D.Tang
GTE Laboratories Incorporated, Waltham MA 02254

S.C.Bloch
University of South Florida, Tampa FL 33620

Tampa, Florida (28°N, 82.5°W), has about 90 thunderstorm days per year, nearly all in summer, dominated by events tending to occur in afternoon or early evening. Results of 19-GHz downlink rain-attenuation diversity studies involving site separations of 11, 16 and 20 km and reception at high elevation angle (about 57°), are reported for a period of 29 months, including three rainy seasons. Despite marked month-to-month differences, long-term measurements with the two larger spacings indicates that for separations above about 15 km diversity performance is not sensitive to spacing or orientation. During a fourth rainy season, using a 29-GHz beacon and the 16-km spacing, performance was similar to that predicted by scaling the 19-GHz results of the previous seasons. For rain climates like Tampa's, some form of site diversity will be required for high-reliability SHF satellite links. The diversity data may be helpful in designing schemes for resource-sharing among numbers of TDMA links.

1. INTRODUCTION AND BACKGROUND

Three sites in Florida (Tampa Triad, Figure 1) received 19-GHz vertically polarized beacon signals from COMSTAR satellites from April 1978 through August 1980. (Table 1.) Separations were: Lutz(L)-Sweetwater(S), 11 km; Sweetwater-University of South Florida(U), 16 km; Lutz-Sweetwater, 20 km. SU and LS baselines are almost at right angles to each other.

Reception was confined to D-2 beacon during its lifetime, followed by D-3, with respective elevation angles 55° and 57°. At these elevation angles, signal attenuation during rain is produced in an interaction region close to each site.

For part of the reporting period, one or more sites each had two rain gauges, one a capacitance rain-rate gauge, the other a standard tipping-bucket (0.254 mm) gauge.

Particulars of the COMSTAR beacon emissions have been given by Cox and Arnold[1982]. Early SHF diversity results using radiometry were reported by Lin et al [1980].

About 60 percent of the annual rain falls during the period June-September. As May too was an important rain-producing month in the 1978-1979 experience in Tampa, the summer season has been taken in some of our work to include five months in the years 1978-1980.

COMSTAR satellite D-4, launched February 1981, was maneuvered to 127°W in May to replace aging D-1 which had previously been moved to about 95°W for paired operation with D-2 (also aging). Only the 29-GHz beacon of D-4 survived into summer 1981. Because only two 29-GHz receivers were available, diversity data collection involved just the SU pair for summer 1981. The elevation angle to D-4 about 31°. Choice of SU was based on two factors: the relative diversity improvements noted for the three pairs in the preceding years, and the coincidence of SU baseline's orientation with direction to D-4. (See Table 1.)

This paper summarizes diversity reception results for the Tampa Triad with emphasis on potential outage reduction ('diversity advantage') and sensitivity to station separation.

As in many other sub-tropical areas, in a sampling of two or three consecutive years Tampa's annual rainfall may show large deviations from long-term means. This is shown in Figure 2 which displays the monthly means and extremes for the period 1935 through August 1981. The unusual rainfalls of May, August, September 1979 are paralleled in the beacon rain attenuation experience.

2. 19-GHz CUMULATIVE ATTENUATION DISTRIBUTIONS, TAMPA: 29 months

Distributions

Attenuation distributions were prepared by scaling analog recordings at 2-dB intervals within the receiver's 30-dB dynamic range. Beacon was acquired by phase lock of the 19-GHz (V) signal; loss of lock could occur for a fade of around 30 dB. In 1981, the switch to 29 GHz involved the same attenuation range.

Figure 3 shows the cumulative 19-GHz single-site and diversity distributions for Tampa for the 29-month period. Data collection in the summer of 1980 was shortened because D-3 beacon was turned off at end of August to conserve spacecraft battery.

Principal Conclusions Regarding Diversity (1978 - 1980)

The following conclusions may be drawn from the 29-month distributions of Figure 3:

1. Distributions for individual sites are very much alike, indicating that observed month-to-month differences tend to be reduced.

2. The shortest pair (LU, 11 km) was the poorest diversity performance.

3. Very little difference in diversity performance appears between the SU (16-km) and the LS (20-km) pairs, indicating an insensitivity to separations greater than about 15 km.

4. With the high elevation angles used to view D-2 and D-3 beacons, baseline orientation is unimportant, at least for lengths above about 15 km. This result should facilitate diversity site selection since 12/14 or 20/30 GHz satellite system service to southeastern USA, because of attenuation alone, will involve orbit location choices giving high elevation angle.

5. Beyond an attenuation of about 10 dB, distribution curves for individual sites show little slope. This characteristic arises from the steep rainfall onset for most summer convective rain cells in Tampa, as discussed elsewhere [Tang, Davidson and Bloch, 1981]. Because of this characteristic in the attenuation distributions, attempting to provide system downlink fade margins in excess of 10 dB at 19 GHz in Tampa's type of rain climate will likely be unproductive. There are of course other reasons why downlink attenuation margin greater than 10 dB may be impractical, especially since the associated uplink attenuation margin would have to be around 20 dB or more.

6. For rain climates like Tampa's (e.g. other locations along the coast of the Gulf of Mexico, or locations along the southeast Atlantic coast, typified by Rain Climate G, [Crane, 1980], link outages (annual) of 0.01 percent with 10-db fade margins cannot be achieved with single-site operation; some form of diversity must therefore be considered for high-availability applications like trunking systems. (Note: Florida has been reclassified into Rain Climate N according to CCIR Draft Report 563-1 (Mod F). See CCIR Doc. 5/5049-E (10 September 1981). Only one other rain climate, Rain Climate P, is defined that exceeds N in rainfall intensity. Rain Climate N is characterized by rain rates 5, 35, and 95 mm/h for 1, 0.1, 0.01% of an average year, respectively.)

7. Three-site diversity operation is very effective.

Other aspects of diversity performance can be gleaned by transforming attenuation distributions to display a measure of diversity effectiveness or improvement.

3. DIVERSITY IMPROVEMENT

Definitions

Diversity improvement can be measured either by the ratio of outage times at given attenuation level ('diversity advantage'), or by noting the reduction in attenuation for a fixed percentage of time ('diversity gain'). For distributions having small change in percentage time occurrence for large changes in attenuation, the only practical measure is diversity advantage. (Tampa diversity gains are very large or indeterminate for attenuations of 10 dB or more. See NASA Propagation Effects Handbook, [Ippolito et al, 1981].) Diversity advantage is a criterion regularly used in the telephone industry to evaluate diversity.

Diversity advantage, here identified by the symbol I, is shown in Figure 4 for each of the three dual-diversity configurations for the 29-month period, as well as for triple-diversity. As reference the (geometric) mean single-site attenuation probability (at specified attenuation level) is chosen. If P_1 and P_2 are the cumulative single-site probabilities then the diversity advantage, I, is

$$I = (P_1 P_2)^{1/2}/P_{12} \qquad (1)$$

where P_{12} is the joint (diversity) probability. (Extension to a three-site combination is obvious. Other references that may be employed are the arithmetic mean single-site probability, and the smaller probability).

If rain attenuation is uncorrelated at two sites (correlation coefficient $\rho=0$), then

$$I = 1/(P_1 P_2)^{1/2} \qquad (2)$$

which is a simple form, arising from our choice of reference.

If fading is perfectly correlated $P_{12} = P_1$ or P_2, whichever is smaller; then I can still be greater than unity with our definition if $P_1 < P_2$.

Figure 4 shows clearly that there is little difference between baselines SU and LS over the 29-month period. At the 10-dB level, uncorrelated fading would lead to I≈333; actual LS and SU values are about I=10.

Diversity Advantage, Month by Month

Table 2 lists the measured 10-dB diversity advantage (at 19 GHz) for the 29-month period. These figures represent the reduction in outage over mean single-site operation, and are useful in projecting performance of particular systems.

The competing performances of LS and SU stand out. But it is also clear that in isolated rainy months, such as August 1978 and August 1980, diversity can be disappointing. This is undoubtedly due to the prevalence of organized bands of rain cells, often seen in local weather radar scans. The entries for May 1979 are virtually all due to one extraordinary event, that of May 8, that lasted unabatedly for about 15 hours. (Details will appear in Tang, Davidson and Bloch [1982].)

Application to Link Resource-Sharing

Acampora [1981] proposed a SHF TDMA link resource-sharing scheme to provide additional downlink reception slots, from a reserve pool, for rain-affected stations. Two critical parameters were identified: α, the ratio of number of hours in a year to the number of thunderstorm hours per year in a region; and β, manifesting the conditioned correlation of thunderstorm attenuation events for a given pair of stations in a climate region.

Acampora's correlative index is expressed via

$$P_{12} = k P_1 P_2 \qquad (3)$$

where P_1 and P_2 are single-site annual probabilities of given attenuation, P_{12} is the annual joint probability of that attenuation, and $k = \alpha\beta$.

In Figure 4, for SU, $P_1 \approx P_2 \approx 0.0025$, while $P_{12} \approx 0.0002$. Thus k=32. On average, there are 88 thunderstorm days in Tampa, and estimating an average of 4 hours per thunderstorm period gives $\alpha = 25$, which is close to Acampora's assumed $\alpha = 24$. (Here a thunderstorm period is one in which thunderstorms have a high expectancy within the locality.) Then $\beta \approx 1.3$, which is close to what Acampora identifies as a most favorable geographic condition: $\beta=1$. Note that β can be usefully related to the diversity advantage as defined earlier by

$$\beta = 1/(\alpha I \sqrt{P_1 P_2}) \qquad (4)$$

or

$$\beta = I(\rho=0)/\alpha I \qquad (5)$$

Spacing Dependence

The dependence of diversity advantage I on site spacing S may be expressed through a power law:

$$I = c P_s^{\,d} \qquad (6)$$

For the Tampa Triad 29-month operation at high elevation angle

$$c(S) = -0.405896 + 0.295135\ S - 0.00727\ S^2 \qquad (7)$$

and

$$d(S) = 1.70103 - 0.32722\ S - 0.010194\ S^2 \qquad (8)$$

These are valid only for spacing S between 11 and 20 km. Coefficient c continuously increases with S, while d has its maximum near 16 km, indicating a diminishing contribution as separation is increased.

Of particular interest for comparison with the Florida measurements are diversity results for a two-year period in Japan at 19.5 GHz with the CS satellite using 19-km separation. [Otsu et al, 1982.] These are shown in Table 3 along with our results for the LS pair (20-km). The diversity advantages are within 15-18% of the Tampa SU values. However, the Tokyo sites had much lower individual outage percentages at the attenuation levels listed.

4. ATTENUATION SEVERITY WITHIN LOCAL TIME BLOCKS

To indicate the temporal nature of downlink rain attenuation, 1979 summer 19-GHz data (both single-site and diversity) were grouped according to six-hour local time blocks: 00-06, 06-12, 12-18, 18-24 hours (Eastern Standard Time). See Figures 5 and 6. The 00-06 h time block shows the least outage percentage. For the individual sites, the six-hour block with maximum outage was between noon and 18 h. Maximum outage was as high as ten times the minimum outage. Inter-site differences within the worst time blocks can be appreciable. With diversity, the time blocks of maximum outage differed according to diversity combination: For LS, maximum outage occurred in 06-12 h; for LU, 12-18, much like a single site; for SU, 18-24 h; and finally, for LSU, 12-18 h, reflecting the influence of the LU combination. Note, too, that in some time blocks, especially 18-24 h, LU (smallest separation) outperformed SU and was about as good as LS.

Indicated also in the figures are the 00-24 h outage percentages. Note that L and S had almost identical outage percentages.

These results indicate that even with the significant overall diversity performance, a satellite downlink operating in southeastern USA could experience difficulty in a particular summer during the post-noon period.

5. 29-GHz DIVERSITY, SU BASELINE, SUMMER 1981

Attenuation distributions for S, U and SU for the entire summer period are shown in Figure 7. Diversity advantages are shown in Figure 8 for the individual months and for the whole period. The plot for July 1981 shows a steep transition between 12 and 14 dB attenuation because July was an unusually dry month, and most of the attenuation events were low but one event caused sudden severe loss of lock.

Of interest are predictions of SU (29-GHz) summer distributions made by scaling up 19-GHz results of prior years. Employing the basis of the Crane [1980] model but with rain rates from Dutton and Dougherty [1979], and adjusting for the different elevation angle used in 1981, the scale-up factor averages about 3.57 for the range of attenuation involved. Note that path-averaged rain rates producing up to 30-dB attenuation at 29 GHz at an elevation angle of 57° are less than about 25 mm/h. Clearly then, since extreme rain rates in convective storms reach 75-120 mm/h in Tampa, a 29-GHz link is sensitive to the onset and waning phases of a convective storm and would be noticeably affected during widespread rain and "debris" of convective systems [Crane, 1982].

Figure 9 shows the 29-GHz SU attenuation distribution for June through August 1981, along with four synthesized distributions: (1) Summer 1980 19-GHz SU distribution scaled up to 29 GHz; (2) Summer 1979, scaled up similarly; (3) a scaled-up 29-month 19-GHz SU distribution unadjusted for seasonal dilution, and (4), the same as (3) but adjusted by a factor reflecting the average fraction of rainy months in the 29-month period. [Summers of 1979 and 1980 in these distributions included May through August; May 1979 was an extremely rainy month, Figure 2.] In the region below 12 dB, the 1981 SU percentages are higher than the higher predictions, but are fairly close beyond that level. These high percentages for relatively low attenuation stem from the strong influence of weaker disturbances. A cull of the individual 1981 attenuation events at S and at U revealed that well over 50% of the events had attenuations significantly under 30 dB, and 12% (U) and 20% (S) of the events with weak attenuation were unaccompanied by on-site rainfall.

Prediction curves like those in Figure 9 have only limited value in suggesting the range of compensation that would be needed in an uplink power-control scheme. Experience both at Tampa and at GTE Laboratories in Waltham, Massachusetts measuring the dynamic attenuation-ratio during the course of numbers of rain events showed that the ratio can often have such wide scatter that power control within the narrow limits demanded in high-performance systems may be difficult to achieve. [J.E.Allnutt, private communication, 1981.] Thus, site diversity and link resource-sharing are alternatives to uplink power management in the 20/30-GHz satellite bands.

6. FADE DURATIONS

Lin [1974] has shown that rain fades are characterized statistically by log-normal distributions. An important parameter is the mean fade duration at specified attenuation. Figure 10 shows mean 19-GHz fade durations as a function of attenuation for the three Tampa sites for the period each site was operational, encompassing between 400 and 600 rain events per site. The three distributions are nearly alike, and are representable by a power-law dependence on attenuation. Standard deviations of the logarithm of mean fade duration are also alike, but are practically independent of the attenuation level. Thus for Tampa, while the mean 10-dB fade duration was two minutes, one standard deviation encompassed the range 0.4 to 10 minutes.

Diversity fade durations are not so simply represented. Figure 11 shows the diversity results as a function of attenuation. The dependence is bilinear, possibly indicating a change in rain regime. The LSU data, lying all below 10 dB in attenuation, show essentially one slope.

With the two longer separations, mean fade duration was around 0.3 minute, with SU slightly better than LS. The range corresponding to one standard deviation was 0.04 - 2.4 minutes. Thus, at 19 GHz at the 10-dB level in Tampa, with high elevation angle to the satellite, the diversity advantage I ≈ 10, and fades are typically one-sixth as long as at a single site.

For the two-site combinations the slope break point for mean fade duration is at about the 10-dB level, while for three sites it occurs at 4-dB conceivably because thunderstorm rain very rarely hits all three sites at once.

For the pairs, the mean fade duration is inversely dependent, approximately, on the square of attenuation, while with triple diversity a cubic inverse dependence is a good description. Seemingly therefore, the exponent is representable by the order of the diversity (number of sites involved).

7. CONCLUSIONS AND ACKNOWLEDGEMENTS

Site diversity with spacings of at least 15 km will be required if high-reliability SHF links are to be designed for USA's southeast coast and the coast of the Gulf of Mexico, according to the evidence of 29-month's reception of the COMSTAR 19-GHz beacons and reception at 29 GHz during the summer of 1981. To keep attenuation as low as possible for these regions, the satellites to be employed should be positioned to provide high-elevation-angle reception, for which case the data indicate that baseline orientation is unimportant. The intense rain events cluster in the afternoon and early evening of the summer months. Fade durations (10-dB level) in these periods typically ranged from 0.4 to 10 minutes, with reduction to 0.04 to 2.4 minutes with diversity. Tampa Triad data should be useful in assessing the feasibility of TDMA link-resource sharing for mitigating rain attenuation effects among single sites in an area. The Tampa data may be scaled to estimate attenuation severity at other SHF frequencies and to explore potentials of frequency diversity using the lower bands with a hybrid, more complex, satellite.

Tampa Triad operations were made possible through the kind cooperation and agreement of the University of South Florida and the General Telephone Company of Florida. The experiment was sponsored in part by GTE Satellite Corporation. The 1981 summer continuation was supported partly by Jet Propulsion Laboratory, California Institute of Technology (Contract 956078), within the framework of NASA's SHF Propagation Experiment, under the leadership of Dr. L. J. Ippolito.

REFERENCES

Acampora, A.S., (1981), Rain margin improvement using resource sharing in 12-GHz satellite downlinks, Bell Sys. Tech. J., 60(2), 167-192.

Cox, D.C., H.W. Arnold, (1982) Results from the 19- and 29 -GHz COMSTAR satellite propagation experiments at Crawford Hill, Proc. IEEE 458-488.

Crane, R.K., (1980), Prediction of attenuation by rain, IEEE Trans. COM-28(9,II), 1717-1733.

Crane, R.K., (1982), A two-component rain model for the prediction of attenuation and diversity improvement. Report prepared under NASA Contract NASW-3506, Environmental Research and Technology Inc., Concord, MA 01742.

Dutton, E.J., H.Dougherty, (1979), Year-to-year variability of rainfall for microwave applications in the USA, IEEE Trans. COM-27(5), 829-832.

Ippolito, L.J., R.D.Kaul, R.W.Wallace, (1981), Propagation Effects Handbook for Satellite Systems Design, NASA Reference Publication 1082, NASA Headquarters, Washington DC 20456.

Lin, S.H. (1974), Statistical Behavior of Rain Attenuation, Bell Sys. Tech. J., 52(4), 557-581.

Lin, S.H., H.J.Bergmann, M.V.Pursley, (1980), Rain attenuation on earth-satellite paths - Summary of 10-year's experiments and studies, Bell Sys. Tech. J., 59(2), 183-228.

Otsu, Y., K.Kosaka, K.Muranaga, N.Ishida, A.Iso, T.Isumisawa, (1982), Japanese Domestic Satellite Communications Systems Experiments, Microwave Journal, 25(1), 67-80.

Tang, D.D., D.Davidson, S.C.Bloch, (1981), Diversity reception of a 19-GHz satellite beacon signal during intense rainy periods in Florida, Proceedings of 2nd IEE International Conference on Antennas and Propagation, 13-16 April 1981, York (UK).

Tang, D.D., D.Davidson, S.C.Bloch, (1982), Diversity reception of COMSTAR satellite 19/29 GHz beacons with the Tampa Triad. Submitted for inclusion in forthcoming special issue of Radio Science on results of the CTS and COMSTAR beacon experiments.

TABLE 1

Particulars of the Tampa Triad and COMSTAR 19/29-GHz Beacons

Pair	Spacing	Baseline orientation (at northern site)
LU	11 km	157.4° TN
SU	16	244.4
LS	20	209.9

(Angle between LU and SU baselines: 93.7°)

COMSTAR Satellite and Position		Elevation Angle	Azimuth (TN)	Operational Period
D-1	128°W	30.9°	245.2°	5/76 - 8/78
D-2	95	54.6	205.2	7/76 - 8/78
D-3	87	57.0	189.4	9/78 - 8/80
D-4	127	31.7	244.4	5/81 - 8/81(*)

(*) D-4's 19-GHz beacon failed on May 18.

TABLE 2

COMPARISON OF DIVERSITY ADVANTAGE
AT 10-dB ATTENUATION LEVEL, TAMPA TRIAD

Month	LS			LU			SU			LSU		
	1978	1979	1980	1978	1979	1980	1978	1979	1980	1978	1979	1980
January	X	7.5	∞	X	∞	∞	X	∞	∞	X	∞	∞
February	X	5.8	15.7	X	6.1	8.6	X	17.0	∞	X	∞	∞
March	X	∞	22.9	X	∞	6.9	X	∞	4.0	X	∞	∞
April	∞	∞	∞	∞	∞	38.0	2.6	∞	22.4	∞	∞	∞
May	3.3	7.9	17.8	2.2	3.5	3.6	2.0	5.5	36.1	5.6	14.1	41.6
June	∞	∞	10.1	∞	9.2	16.0	∞	∞	27.7	∞	∞	∞
July	72.0	16.6	13.0	21.0	12.0	4.9	174.0	5.4	39.1	∞	∞	∞
August	3.8	12.0	4.8	2.6	6.0	4.4	6.8	26.0	7.1	9.6	60.0	∞
September	5.6	18.0	X	11.5	6.0	X	∞	80.0	X	∞	80.0	X
October	∞	∞	X	∞	∞	X	∞	∞	X	∞	∞	X
November	NR	∞	X	NR	∞	X	NR	∞	X	NR	∞	X
December	9.8	∞	X	6.4	∞	X	∞	∞	X	∞	∞	X

NOTE: NR = No Rain; X = System Not in Operation.

TABLE 3

Comparison of Diversity Improvement, Florida and Japan

Parameter	Tampa Triad	Japan (Tokyo area)
Station Pair	Lutz/Sweetwater	Yokosuka/Sugita
Spacing, km	20	19
Satellite(s)	COMSTARS D2,D3	CS
Elevation (°)	57,55	48
Frequency, GHz	19.04	19.5
Period, months	29	24
Dates	Apr '78 - Aug '80	Apr '78 - Mar '80
Level	<--Diversity Advantage[1],I-->	
10 dB	9.6	7.8
12.5	13	11
15	15	12.3

(1) Referred to mean (geometric) single-site probability.

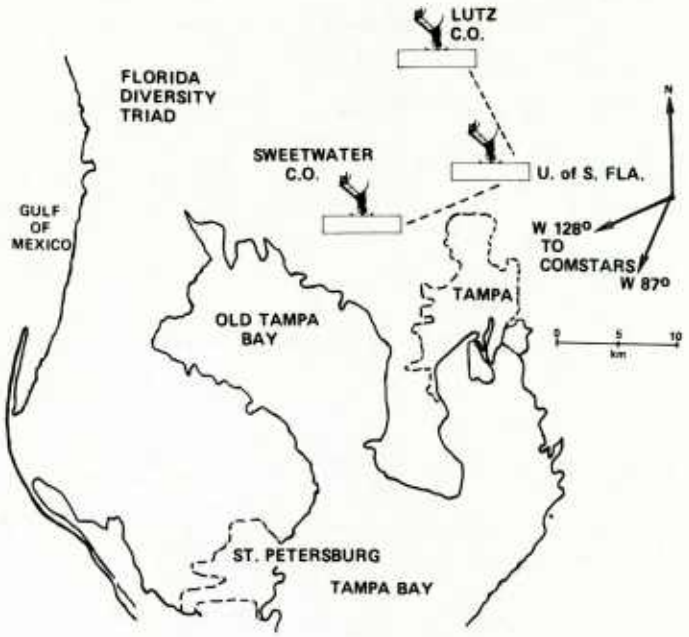

Figure 1. Map showing location of Tampa Triad.

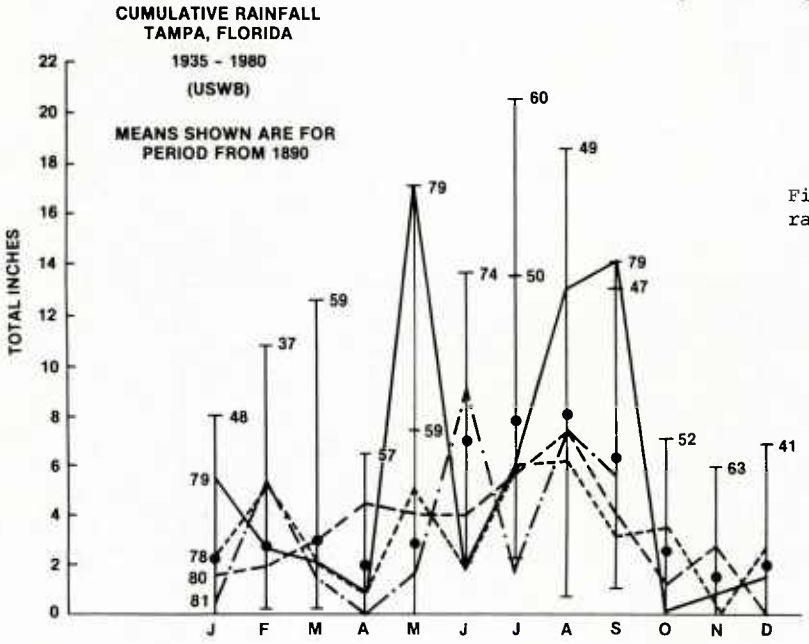

Figure 2. Means and extremes of monthly rainfall, Tampa.

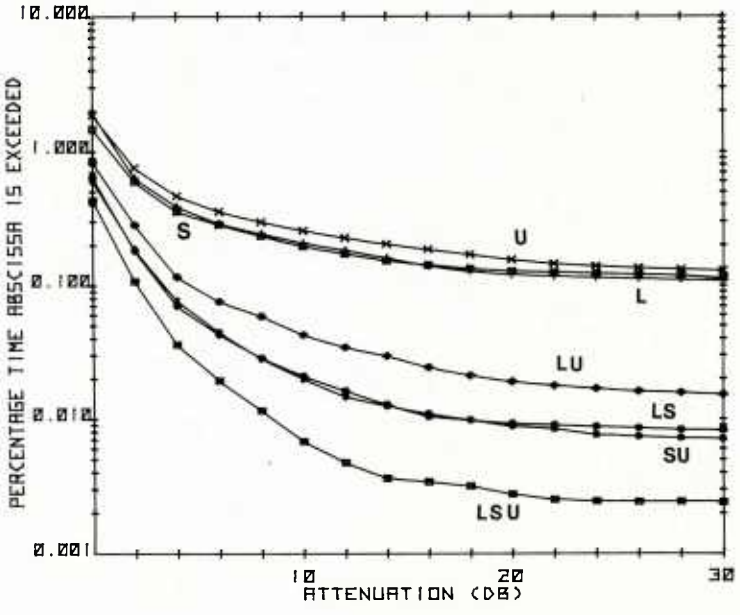

Figure 3. 19-GHz attenuation distributions, Tampa Triad, 29 months.

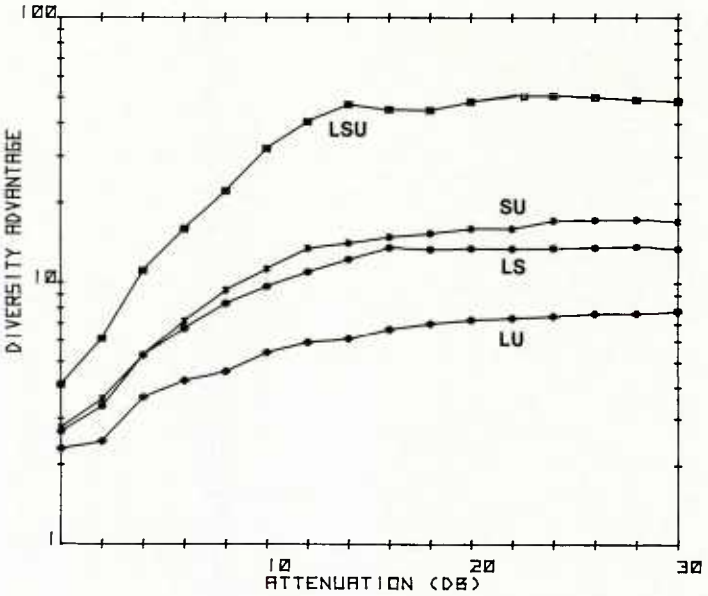

Figure 4. Diversity advantage, 29 months (1978-1980), Tampa Triad.

Figure 5. Time block distribution of attenuation, (U,S,L), summer 1979.

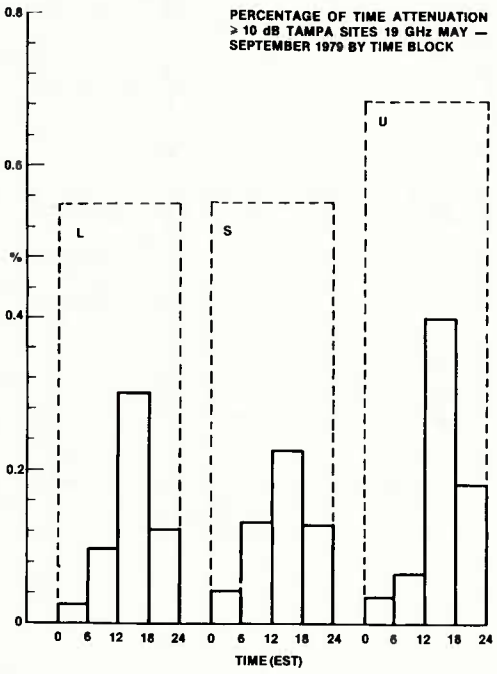

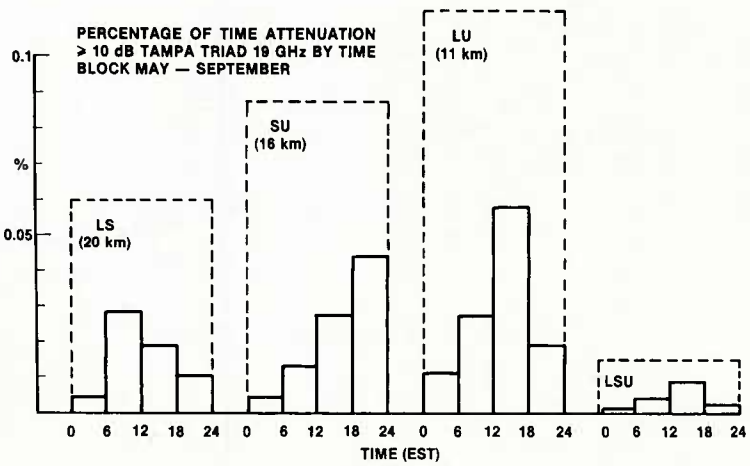

Figure 6. Time block distribution with diversity, summer 1979.

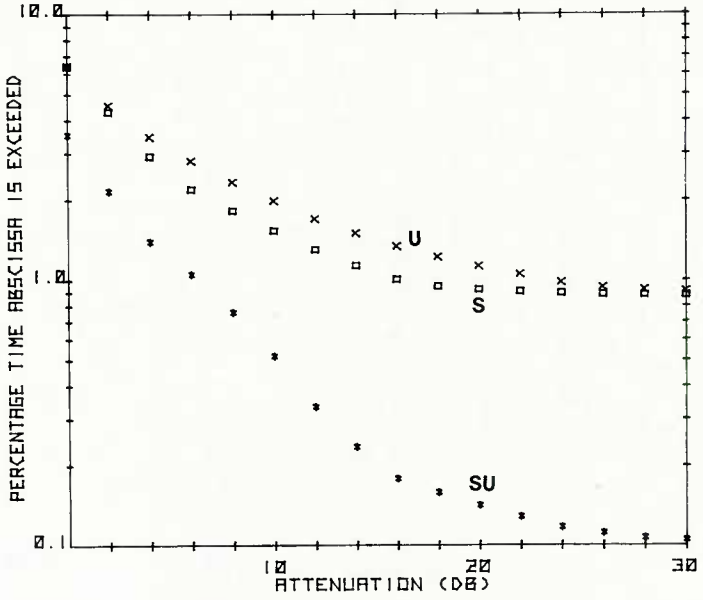

Figure 7. 19-GHz S, U, and SU distributions, June-August 1981.

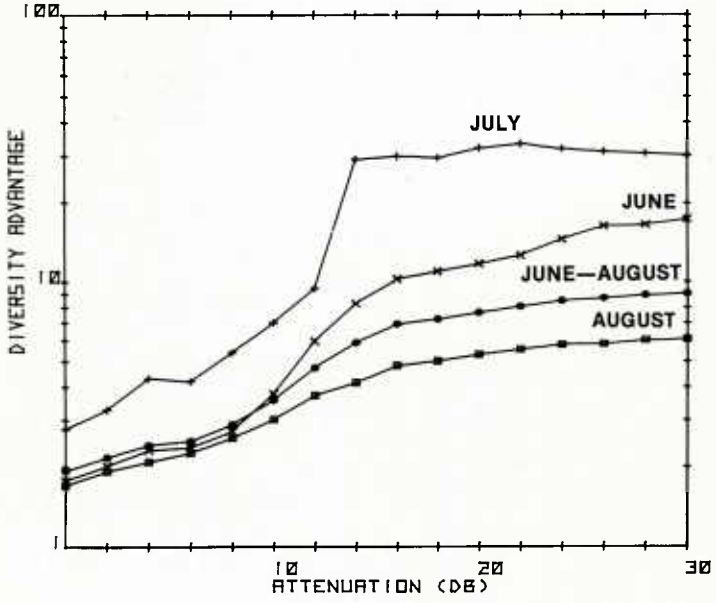

Figure 8. SU diversity advantage, 29-GHz, summer 1981.

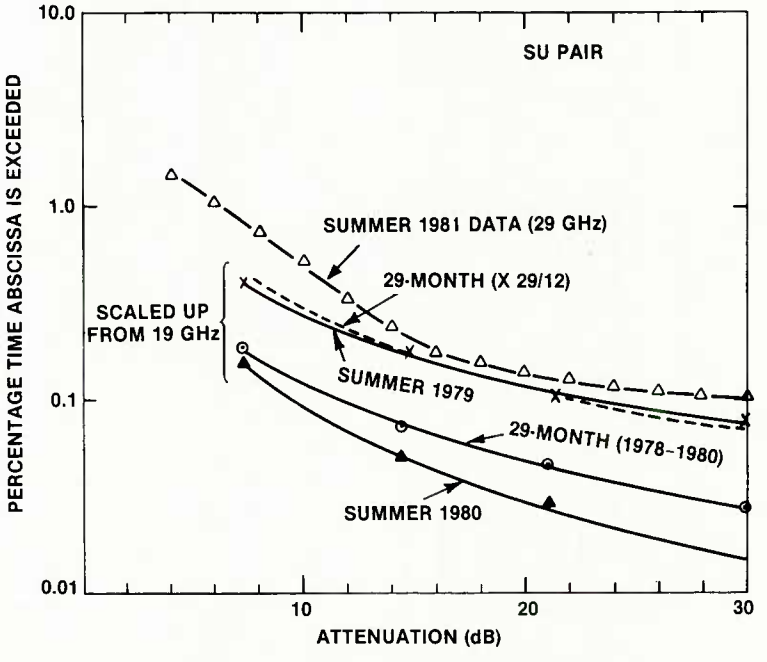

Figure 9. SU summer distribution, and predictions based on prior seasons.

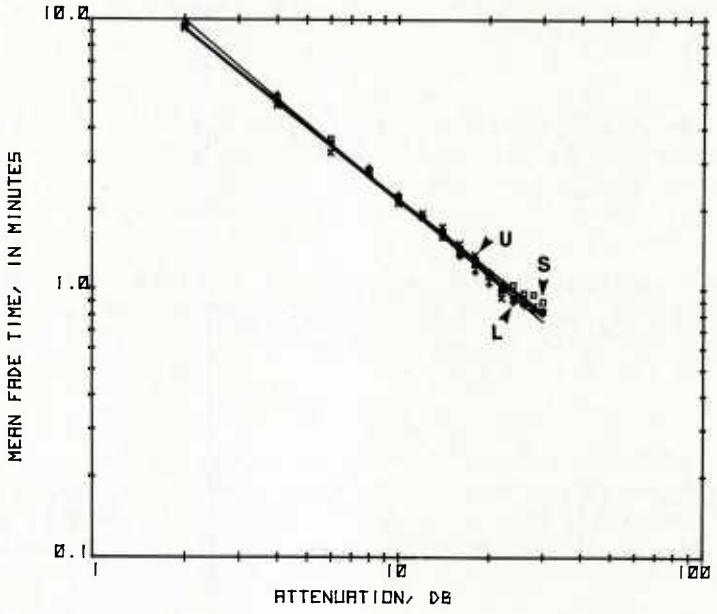

Figure 10. Mean fade duration, single sites, Tampa, 1977-1980.

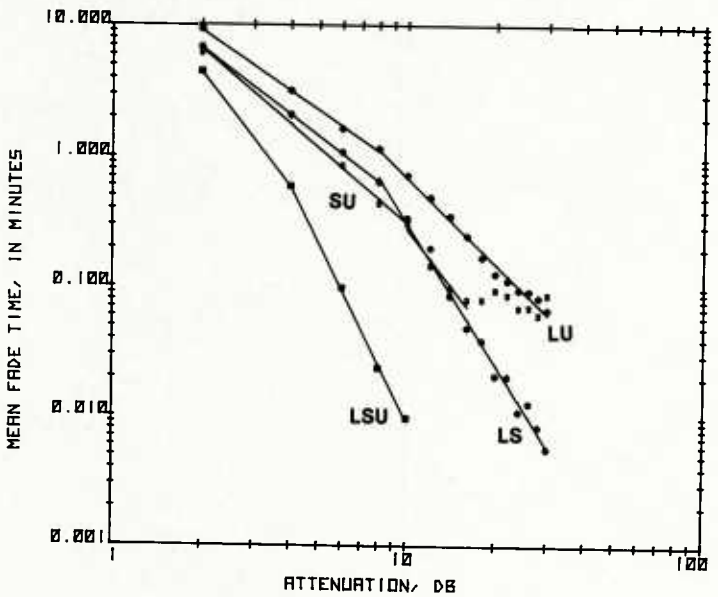

Figure 11. Mean fade duration, diversity, Tampa, 1978-1980.

DISCUSSION

M.P.M.Hall, UK

Your studies show that some form of diversity will be required for high-reliability SHF satellite links in a rainy climate such as Tampa, i.e. the region showing most intense rain within the USA. Would you like to comment on the need to use spaced site diversity in a region having somewhat less intense rain, for instance, other parts of the USA and N.W. Europe?

Author's Reply

A lot depends on the outage probability of a single-site as I mentioned in my oral presentation, with reference to Japan. But diversity advantage measured in other parts of the USA, for example by Bell Labs using radiometry at a number of locations, comes out to about 10 or so, for attenuations (equivalent) of about 10 dB in this same part of the SHF Spectrum. From those figures on 0.01% (annual) rain rates in N.W.Europe that I have seen, I doubt that site diversity would be needed in the 20/30 GHz band.

As to comparison of attenuation experience with predictions, such as Crane's Models (or the CCIR) for rain climates, our measurements in the Tampa and Boston areas, are within the variability associated with models, and these are quite large for the small outage fractions.

E.J.Holliman, US

Recently during the telecast of a professional football game at Tampa by satellite, the cameras showed an increasing rain fall which began to affect visibility. The television picture rapidly degraded as the rain increased and soon failed. When the telecast resumed in 30 minutes with only a light rain, the announcer said the picture failed because of the effects of rain on the satellite terminal. Was this a demonstration of the susceptibility of the satellite link to rainfall?

Author's Reply

The earth station involved is located 115 km north of Tampa, so it is highly unlikely that rain was simultaneously interacting with the earth-space link, and in any case, that link is in C-band, which is virtually unaffected by rain, especially at the elevation angle for this station. I suspect that the outage occurred on the feeder or back-haul link from Tampa to the earth station, perhaps in the local pickup right at the Tampa Stadium, or else in one of the hops. A 30-minute outage suggests that the trouble may have been in the video pickup equipment or cables.

SCINTILLATION MODELLING AND MEASUREMENT. A TOOL FOR REMOTE-SENSING SLANT PATHS

E. Vilar and J. Haddon*
Department of Electrical and Electronic Engineering
Portsmouth Polytechnic
Anglesea Road, Portsmouth, Hamshire, U.K.

*Now at Plessey Avionics, Westleigh, Havant, U.K.

ABSTRACT

The use of spectral analysis of amplitude scintillations as a remote-sensing tool of a slanted path is investigated in order to derive values of C_n^2, turbulent path L, and dominant eddy size. Relevant propagation aspects are reviewed and extended, a layer model analysed in detail, and experimental results are presented and discussed. The limitations of the remote-sensing technique are also discussed, particularly the use of cross-path wind v_t. The remote-sensing of v_t is briefly outlined and relevant antenna aperture effects are also considered.

1. INTRODUCTION

Since 1978 a research programme has been under way at Portsmouth Polytechnic to investigate amplitude and phase scintillations induced in microwave signals propagating through the atmosphere along slant paths. The experimental investigation has mainly used the 11.786 GHz B1 propagation beacon of the Orbital Test Satellite (OTS) received at an elevation of 31°, although provision exists for reception of the telemetry beacon TM operating at 11·575 GHz. Because of the high elevation angle, the experimental results and subsequent theoretical modelling are valid above about 5 degrees of elevation below which ray bending and multipath effects occur (e.g. Kaul R. et al, 1980).

The research has been focused along experimental and theoretical lines. The experimental work has the objective of obtaining long-term reliable statistics of the parameters which characterise the scintillation process from the point of view both of the systems application and also remote sensing of the turbulent atmosphere traversed by the wave. Details of the intensity of the process from the spectral and probabilistic aspects as well as some details about the measurement system can be found in the literature (Haddon J. et al, 1980 (a) and (b), Vilar E. et al, 1981, Haddon J. et al, 1981). Preliminary findings on the variability and non-stationarity of the scintillation statistics and a detailed analysis of this phenomenon have also been published (Moulsley T.J. et al, (a) 1981, (b) 1982).

This paper is concerned with the use of experimentally obtained amplitude scintillation spectra which together with a specially developed model of propagation through a slanted path, allow one to derive amongst other parameters a path-integrated value for the turbulence intensity characterised by the refractive index structure constant C_n^2. In addition, an effective turbulent path is also derived. An important item is the cross-path wind speed and although in this paper the comparison between some of the theoretical and experimental results is carried out using values of the wind speed derived from meteorological soundings, nevertheless a technique is discussed to derive this parameter using only propagation measurements.

2. REMOTE-SENSING BY SPECTRAL ANALYSIS

2.1 Theoretical Background

A radio link between the earth and a satellite includes a path through the atmosphere. This path has a complex structure which includes the planetary boundary layer, clouds, and the free atmosphere which generally exhibits a layered structure (Anderson A.D., 1956). The atmosphere affects the parameters of the wave amplitude phase and polarisation in both deterministic and random manner. In the deterministic case we could include attenuation due to scattering and absorption by particulate media, mainly rain, and the cross-polarisation generation effects. The wave also exhibits random fluctuations of amplitude and phase known as scintillations both across the receiver aperture (spatial structure) and in time. These scintillations are caused by random fluctuations of the atmospheric refractive index $n(\underline{r},t)$ due to turbulent mixing of air masses of different temperatures and humidities. Although the random structure of the electron content of the ionosphere causes scintillations too, because they follow a λ^2 dependence they are experienced below about 4 GHz (Taur R.R., 1974) with strong diurnal and seasonal trends, and this only for low latitudes. In order to put the theoretical techniques detailed in the next sections into perspective we now review basic relevant concepts although a wide literature exists on scattering leading to the scintillation phenomenon. There are also review papers (Wheelon A.D. 1959, Lawrence R.S. et al 1970, Ishimaru A. 1977, Prokhorov A.M. et al 1975, Fante R.L. 1975, Rino C.L. 1976), and the work of Ishimaru (Ishimaru A. 1978) is of special relevance to remote sensing.

From the wave propagation point of view the random medium is characterised by a refractive index $n(\underline{r},t)$ which is a stochastic function of space and time. The instabilities or eddies of the turbulent flow are characterised by inner, outer and integral scales or sizes ℓ or the turbulence namely ℓ_o, L_o and L_n. Under conditions of isotropic turbulence, the intensity of the fluctuations of the refractive index associated with scale sizes within the range $\ell_o - L_o$ can be well modelled by a three dimensional spectrum of the fluctuations $S(\kappa)$ at least for values of κ greater than $2\pi/L_o$. This spectrum reflects the three dimensional fluctuations of the wind velocity and was studied by Komogorov leading to a $\kappa^{-11/3}$ dependence of $S(\kappa)$. Experimental results seem however to indicate a range of values about that slope and furthermore the -11/3 slope is only a special case of the model

$$S(\kappa) = \frac{\Gamma(n-1)}{4\pi^2} \sin\frac{\pi(n-3)}{2} \; C_n^2 \, \kappa^{-n} \quad , \; 3 < n < 5 \qquad \ldots\ldots (1)$$

associated with the homogeneous (stationary) field $n(r)$ with a structure constant or intensity of the

fluctuation characterised by the parameter C_n^2. Although equation (1) is only valid for the region $1/L_o \lesssim \kappa \lesssim 1/\ell_o$ (inertial sub-range) where turbulence is fully developed, for convenience it is necessary to complete the range of $\kappa < 1/L_o$ with a spectrum which has a finite value in that region. This modified model, which we can write as

$$S(\kappa) = \frac{\alpha(n) e^{-(\kappa/\kappa_m)^2}}{(1 + L_o^2 \kappa^2)^{n/2}} \qquad \ldots\ldots (2)$$

with $\kappa_m = 5{\cdot}91/\ell_o$ (Tatarski V.I. 1961) and $\alpha(n)$ a constant determined below, not only satisfies a physical requirement of a finite mean square value of refractive index fluctuation, $< \Delta n^2 >$, which is in agreement with long-term observations of phase fluctuation in line of sight and interferometric paths (Barton D.K. 1971), but also allows convergence of a variety of integrals which appear in turbulence theory. Details of the physical significance of the above models in connection with input range $\kappa < {}^{2\pi}/_{L_o}$, the inertial sub-range ${}^{2\pi}/_{L_o} - {}^{2\pi}/_{\ell_o}$, and the dissipative region $\kappa > {}^{2\pi}/_{\ell_o}$ will not be discussed here and can be found in many works on turbulence (e.g. Tennekes H.T. et al, 1972) and references quoted above. An example of the use of equation (2) relevant to this paper is the relation between $< \Delta n^2 >$ and C_n^2 under the above assumption of homogeneity, that is a finite $< \Delta n^2 >$ exists and therefore it can be written in terms of the integrated spectrum

$$< \Delta n^2 > = \lim_{r \to 0} \frac{4\pi}{r} \int_0^\infty \kappa\, S(\kappa) \sin(\kappa r)\, d\kappa \qquad \ldots\ldots (3)$$

Substitution of (2) in (3) leads to the solution (Haddon J. 1982)

$$< \Delta n^2 > = \frac{\alpha(n)\, 2\pi}{L_o^{3-n}} \Gamma\left(\frac{3}{2}\right) U\left(\frac{3}{2}, \frac{5-n}{2}, \frac{1}{\kappa_m^2 L_o^2}\right) \qquad \ldots\ldots (4)$$

with U (a, b, c) the confluent hypergeometric function. A solution of (3) has also been obtained by Strohbehn (Strohbehn J.W., 1968). Because L_o will be at least one metre of more (usually tens of metres) (Gage K.S., 1979, Crane R.K. 1980, Vilar E. et al 1978) and ℓ_o less than about 10 millimetres (Zimmerman S.P. 1966, James P.K. 1980), then $\kappa_m \ell_o \geq 600$ and asymptotic expansions may be used for U. For the important case of $n > 3$ we get,

$$\alpha(n) = \frac{< \Delta n^2 > L_o^{3-n}\, \Gamma\left(\frac{n}{2}\right)}{2\pi\, \Gamma\left(\frac{3}{2}\right) \Gamma\left(\frac{n-3}{2}\right)}, \quad n > 3 \qquad \ldots\ldots (5)$$

For large values of κ both the general Kolmogorov and the modified spectrum should agree and thus using equations (1), (2) and (5) we get,

$$C_n^2 = \frac{2\pi}{\sin\frac{\pi}{2}(n-3)} \frac{\Gamma\left(\frac{n}{2}\right)}{\Gamma(n-1)\, \Gamma\left(\frac{3}{2}\right) \Gamma\left(\frac{n-3}{2}\right)} L_o^{3-n} < \Delta n^2 >, \quad 3 < n < 5$$

$$= 1{\cdot}92\, L_o^{-2/3} < \Delta n^2 >, \qquad n = {}^{11}/_3 \qquad \ldots\ldots (6)$$

The result of equation (6) for n = 11/3 agrees with that obtained elsewhere (Ishimaru A. 1978). We can also now readily relate $\alpha(n)$ and C_n^2

$$\alpha(n) = \frac{\Gamma(n-1)}{4\pi^2} \sin\left[\frac{\pi}{2}(n-3)\right] C_n^2, \quad 3 < n < 5$$

$$= 0{\cdot}033\, C_n^2 \qquad n = 11/3 \qquad \ldots\ldots (7)$$

Although the above relations are useful for practical work, inclusive of feasibility studies, they assume homogeneity within a region of constant C_n^2 or $< \Delta n^2 >$, and furthermore the form of the spectrum for $\kappa \lesssim 1/L_o$ is only at best a rough approximation.

A second aspect of importance within this paper is the subject of amplitude scintillations both in spectral form and as a variance. Under the convenient assumption of homogeneity and isotropy of the turbulence, the correlation function of the amplitude fluctuations at the receiver plane between two points ρ units of distance apart is the Hankel transform of the weighted refractive index spectrum

$$C_A(\rho) = 2\pi^2 k^2 L \int_0^\infty \kappa\, J_o(\kappa\rho)\, S(\kappa)\, f(\kappa)\, d\kappa \qquad \ldots\ldots (8)$$

Under the assumption of constant cross path wind of magnitude v_t then time lag and distance may be interchanged using $\rho = v_t \tau$ and invoking frozen turbulence. The weighting function $f(\kappa)$ acts as a high pass filter on the spectrum $S(\kappa)$ in the sense that only wavenumbers which are greater than or approximately equal to $\sqrt{2\pi/\lambda L}$ will contribute to the value of the integral. This implies that turbulent eddies with sizes $\sqrt{\lambda L}$ or less will contribute to the scintillation. The variance of the scintillation $\sigma^2(A)$ is then obtained from (8) when ρ (or τ if applicable) is zero. That is

$$\sigma^2(A) = 2\pi^2 k^2 L \int_0^\infty \kappa\, S(\kappa)\, f(\kappa)\, d\kappa \qquad \ldots\ldots (9)$$

which in the special case of n = 11/3 and the model of equation (1) leads to the familiar result

$$\sigma^2(A) = 0{\cdot}307\ C_n^2\ k^{7/6}\ L^{11/6}$$

$$= (20\ \log_{10}\ e)^2\ C_n^2\ k^{7/6}\ L^{11/6}\ (dB)^2 \qquad \ldots\ldots (10)$$

This of course assumes a constant C_n^2 along the path and this aspect is discussed further in sections 2.3 and 2.4. The spectral density of $W_A(\kappa)$ of the scintillations can be obtained by Fourier transforming equation (8) and deriving the results either by numerical integration (Tatarski V.I. 1961) or in analytical form (Ishimaru A. 1978). In addition, the correlation function $C_A\ (v_t\ \tau)$ can be well modelled by an exponential cosine auto-correlation (Bendat J. 1958) and this can be used to full advantage to derive parameters such as rate of zero crossings and integral scales of the turbulence (Vilar E. et al 1978); in this case the corresponding spectrum resembles that of white noise low-pass filtered by an R-C network. The main difference between this model and the one derived from the Kolmogorov spectrum $S(\kappa)$ (Tatarski or Ishimaru) is that in a logarithmic scale the roll-off at high Fourier frequencies is -2 instead of -8/3. In general and consistent with a variable $n \neq 11/3$, one observes variable slopes associated with the parameter n-1.

Another aspect from the remote sensing point of view is the decrease in measured variance brought about by an antenna of finite aperture D. Because the wavefront is crinkled across this aperture, the amplitude of the field collected in the feeder is the superposition of many contributing terms randomised by a spatial term. The greater this randomisation the greater the chances of a destructive composition occurring in the feeder and thus as the aperture increases the amplitude fluctuations of the signal fed into the receiver decrease. This aspect is further discussed in Section 3 and then in Section 4 to outline its positive implications as a tool for remote sensing. However the discussions in this paper assume a point receiver and whenever required the intensity can be corrected accordingly. In our case and for the 2·4 metre antenna the smoothing factor of the variance is very close to 1 and therefore the variance experimentally observed has not been corrected.

2.2 Variability of the Scintillation Intensity

The study of equation (10) suggests the possibility of determining one of the parameters if the others are known. For example, if an experiment derives statistics of the variance $\sigma^2(A)$ and if an effective turbulent path is assumed, then values of C_n^2 could be determined. The problem is that although the experimental investigation of these amplitude scintillations reveals the expected general form of the spectrum, there is a great variability not only in integrated values (variance) but also in the frequency independent region of that spectrum and in the slopes (Haddon J. et al 1980). Figure 1 shows the envelope and the 90 and 95% limits of experimental spectra. The variability of the slopes, theoretically -8/3, could be thought of as being consistent with the variability of the exponent n leading in turn to the variability of $\sigma^2(A)$. To look into this aspect, if the model of equation 2, with $\alpha(n)$ as given by equation (7), is used in equation (8) and Tatarski's spatial filter function

$$f = 1 - \frac{\sin(\kappa^2 L/k)}{\kappa^2 L/k} \qquad \ldots\ldots (11)$$

is used, then after a set of lengthy calculations involving changes of variables, solving the integrals in terms of the function U(a,b,c), taking limits and series expansions of U as well as allowing for simplifications arising from $L_o >> \sqrt{\lambda L}$ and $(L_o\kappa_m)^2 >> 1$, one finally obtains the general expression,

$$\sigma^2(A) = \alpha(n)\ \pi^2 k^2 L\ L_o^{n-2} \left[\frac{\Gamma\left(\frac{n-2}{2}\right)}{\Gamma\left(\frac{n}{2}\right)} + \Gamma\left(\frac{2-n}{2}\right) \left(L_o\kappa_m\right)^{2-n} - \frac{2}{n-2} \right.$$

$$\left. - \frac{kL_o^2}{L}\ \Gamma\left(-\frac{n}{2}\right)\left(\frac{L}{kL_o^2}\right)^{n/2}\left[\left(\frac{k}{L\kappa_m^2}\right)^2 + 1\right]^{n/4} \sin\left[\frac{n}{2}\tan^{-1}\left(-\frac{\kappa_m^2 L}{k}\right)\right]\right]$$

$$L_o^2\kappa_m^2 >> 1\ ,\ \sqrt{\lambda L} << L_o\ ,\ \kappa_m = 5{\cdot}91/\ell_o \qquad \ldots\ldots (12)$$

This expression is general and can be used to investigate the behaviour of the scintillation variance with inner and outer scales ℓ_o and L_o as well as the spectral slope n. This function is shown in Figure 2 for the indicated values of some of the parameters relevant to our OTS experiment. Before we discuss these results we note that a numerical integration has been carried out (Strohbehn J.W., 1968) but an analytical solution is preferable in order to investigate the influence of the parameters. Also it is worth noting that if in equations (11) and (12) the minus sign is changed to plus we obtain expressions for the variance of the phase fluctuations. However, although this may seem useful for a quick estimate of the variance of phase fluctuations, because the spatial function f now emphasizes the contribution due to refractive index fluctuations with low wavenumber components, as a result the variance obtained is heavily dependent on L_o and the model chosen for $S(\kappa)$ in the low wavenumber range.

Turning now to Figure 2 one notes that for values of L_o of several tens of metres one could expect a maximum scintillation for values of n in the neighbourhood of 3·3; this maximum is rapidly smoothed when L_o is about 10 or 20 metres. Changes in the outer scale L_o affect the variance for spectral slopes greater than 3 and the reverse occurs for the inner scales ℓ_o. Further study of equation (12) indicates that variations in path length L tend to displace the curves vertically leaving the overall shape unchanged. Although Figure 2 reflects a mathematical expression, not all values of n are physically realisable and many experimental results show reasonable agreement with the Kolmogorov value 11/3 = 3·67. At that slope, Figure 2 shows that the variance is not only dependent on n but is also heavily dependent on L_o. If we look at equation (6) we see that even small variations in $< \Delta n^2 >$, and even assuming a fixed turbulent path L, a large range of values of L_o and slopes n will lead to a wide range of variances in $\sigma^2(A)$. This is experimentally verified in the results of Figure 3 showing a large dispersion of values although there is a clear correlation coefficient of 0·625. The variance values shown have been derived after integration

of a set of spectra selected from a total of 140. Although after a least squares fitting of the results the observation of the spectral slope $-(n-1)$ of the amplitude scintillation spectra would lead to values of $\sigma^2(A)$, and vice versa, the large dispersion appears to rule out remote sensing using solely the variance; more parameters have to be introduced as explained in the next section.

2.3 Variance and Spectral Density Approach

From the results of the previous section it is clear that an attempt to derive experimental information about the refractive index structure constant by observations of the variance of amplitude fluctuations does not lead to clear results due to the uncertainty not only of the effective turbulent path but also of the scale L_o and slope n. More parameters are required if amplitude scintillations, as observed by any receiving system, are to be used to full advantage. These parameters can be supplied by direct on-line analysis of the temporal spectrum $W_A(\omega)$, and furthermore a high resolution of that spectrum is not required. These parameters are the asymptotic values of the spectrum for very low and very high Fourier components, and the corner frequency ω_c related to the cross-path wind and the Fresnel frequency ω_o.

If one assumes that the medium along the turbulent path is uniform in that not only is $< n^2 >$ constant but also the eddy structure along that path is constant, this makes C_n^2 independent of height. Under these conditions expressions have been derived (Ishimaru A., 1972) giving both a complex analytical solution to the spectrum and also, perhaps of more interest here, the asymptotic expressions for low and high Fourier components ω, and the corner frequency ω_c. For the 11/3 case for example we recall

$$W_A^{\,o} \equiv \lim_{\omega \to o} W_A(\omega) = \frac{2{\cdot}765}{\omega_o}\,\sigma^2(A)$$

$$W_A^{\,\infty} \equiv \lim_{\omega \to \infty} W_A(\omega) = \frac{7{\cdot}13}{\omega_o}\,\sigma^2(A)\left(\frac{\omega}{\omega_o}\right)^{-8/3} \qquad \ldots\ldots (13)$$

in which ω_o is a constant called the Fresnel frequency, of value $v_t\sqrt{k/L}$, which is the ratio between the transverse velocity and the dominant eddy size $\sqrt{\lambda L}$. ω_o determines the shape behaviour of the spectrum. The corner frequency or intercept of the two asymptotes in a log-log plot is related to ω_o by

$$\omega_c = \left[\frac{2\,\Gamma\left(\frac{n-1}{2}\right)\,\Gamma\left(\frac{n+3}{2}\right)\,\sin\left[\frac{\pi}{4}(5-n)\right]}{\sqrt{\pi}\,\Gamma(n/2)}\right]^{1/(n-1)}\omega_o \qquad \ldots\ldots (14)$$

$$= 1{\cdot}43\,\omega_o\ ,\ (n = 11/3)$$

It is now clear that a strategy can be devised to use a least squares fit for the two parts of the spectrum, equation (13), or to determine the slope $(n-1)$, from which ω_o can be determined using equation (14). If v_t is known then we determine an effective path L. If in addition we have a general expression similar to (13) involving the generalised slope n then measurements of the variance will lead to estimates of C_n^2. Unfortunately an earth-space path and even a line of sight path is far from homogeneous although one may often revert to that assumption to simplify the calculations. One finds that C_n^2 can vary by more than one order of magnitude between the ground and the top of the boundary layer.

An approach to this problem in the past has been to postulate a profile of the refractive index structure constant. Fried and Cloud (Fried D.L. et al, 1966) have used the model

$$C_n^2(h) = C_{no}^2\,h^{1/3}\exp(-h/h_o)\ ,\ h_o = 3{\cdot}2\ k_m \qquad \ldots\ldots (15)$$

and derived an analytical solution to equation (8). Tatarski (Tatarski V.I., 1961) has taken the variability of C_n along the propagation path coordinate z and the variance is then given in terms of an integrated $C_n^2(z)$, that is

$$\sigma^2(A) = 4\pi^2\,k^2\int_0^\infty \kappa d\kappa S(\kappa)\int_0^L C_n^2(z)\,\sin^2\left(\frac{z\kappa^2}{2k}\right)dz \qquad \ldots\ldots (16)$$

Various models can be used and the exponential $C_n^2\exp(-z/z_o)$ is often invoked, leading for the 11/3 value of n to the result

$$\sigma^2(A) = 0{\cdot}53\,C_n^2\,k^{7/6}\,z_o^{\,11/6} \qquad \ldots\ldots (17)$$

which shows a great dependence on the parameter z_o and is consistent with the fact that since in equation (16) z appears in the integrand, not only will eddies furthest away have the strongest impact on the amplitude scintillations, but also the value of the integral will be very sensitive to the choice of the profile.

2.4 Layered Structure

2.4.1 Theoretical Study

In order to avoid the choice of a particular C_n^2 profile we suggest in this paper an alternative model which takes into consideration the fact that the atmosphere exhibits a layered structure (Anderson A.D., 1956), that a slant path goes through regions of more or less intense turbulence, and that within each region turbulence can be considered homogeneous.

To develop the theoretical expressions we start by considering the atmosphere as a series of layers of uniform but different C_n^2. That is we take $C_1^2 \equiv C_n^2(z)\ z_o \leqslant z < z_1$, $C_2^2 \equiv C_n^2(z)\ z_1 \leqslant z < z_2$, and so on. We further assume that within each layer only forward scattering exists. Under these conditions the second integral of equation (16) becomes a sum of integrals and the i'th term is given by

$$\int_{z_i-1}^{z_i} C_i^2 \sin^2\left(\frac{z\kappa^2}{2k}\right) dz = \frac{C_i^2}{2}\left[\left(z_i - \frac{\sin\frac{z_i\kappa^2}{k}}{\frac{\kappa^2}{k}}\right) - \left(z_{i-1} - \frac{\sin\frac{z_{i-1}\kappa^2}{k}}{\frac{\kappa^2}{k}}\right)\right] \quad \ldots\ldots (18)$$

By using the $S(\kappa)$ model of equation (2) we get

$$\sigma^2(A) = \pi^2\, \alpha_i(n)\, k^{(6-n)/2} \sin\left(\frac{n\pi}{4}\right)\left(z_i^{n/2} - z_{i-1}^{n/2}\right), \quad \sqrt{\lambda z} \ll L_o, \ldots \quad \ldots\ldots (19)$$

where the brackets after α emphasize the n dependence as given by equation (7) and the suffix i refers to the i'th layer. If N layers are present, then equation (19) must be summed between 1 and N. A particularly interesting case is that of a single layer of thickness $T = z_2 - z_1$ where z_1 is the distance to the base of the layer. Calling y z_1/z_2 we get, for the variance,

$$\sigma^2(A) = \pi^2\, \alpha(n)\, k^{(6-n)/2} \sin(n\pi/4)\, \Gamma\left(-\frac{n}{2}\right) z_2^{n/2}\,(1 - y^{n/2}) \quad \ldots\ldots (20)$$

In addition, the square brackets of equation (18) become

$$1 - \frac{\sin\frac{\kappa^2 L}{k}\cos\frac{\kappa^2}{k}\left(z_1 + \frac{T}{2}\right)}{\frac{T\kappa^2}{2k}} \equiv f_\ell(\kappa) \quad \ldots\ldots (21)$$

which means that we have introduced the wave filter $f_\ell(\kappa)$ in the integral of equation (9). This function is identical to that obtained to model ionospheric scintillations within a turbulent layer (Wernick A.W. et al, 1974).

For the spectral density we note that the correlation function for the ith layer has the same expression as equation (8) if we substitute $f(\kappa)$ for the $f_\ell(\kappa)$ above discussed. Invoking the 'frozen' turbulence within the layer in which the crosspath wind is v_ℓ, the expression for the temporal spectrum is

$$W_A(\omega)_i = 4\int_o^\infty \cos\omega\tau\, C_A(\tau)_i\, d\tau$$

$$= 8\pi^2 k^2 \int_o^\infty \cos\omega\tau\, d\tau \int_o^\infty \kappa\, d\kappa\, S(\kappa)\, J_o(\kappa v_t \tau) f_\ell(\kappa) \quad \ldots\ldots (22)$$

Integrating in relation to τ and recalling that the layer filter function introduces a cut-off in the wavenumber at $\kappa \sim \omega/v_t$ we get

$$W_A(\omega)_i = 8\pi^2 k^2 L \int_{\frac{\omega}{v_t}}^\infty \kappa\, S(\kappa) \frac{f_\ell(\kappa)}{(\kappa^2 v_t^2 - \omega^2)^{1/2}}\, d\kappa \quad \ldots\ldots (23)$$

The asymptotic results for $\omega \to 0$ and $\omega \to \infty$ are now given by

$$W_A^o = \frac{4\,\alpha(n)\pi^2}{\omega_o} k^{(6-n)/2}\, \Gamma(-(n+1)/2) \sin((1+n)\pi/4) z_2^{n/2}(1-y^{n/2})$$

$$\omega \ll \omega_o \quad \ldots\ldots (24)$$

$$W_A^\infty = \frac{4\,\alpha(n)\pi^2}{\omega_o} k^{(6-n)/2}\, \Gamma\left(\frac{1}{2}\right)\Gamma((n-1)/2) z_2^{n/2}(1-y)\left(\frac{\omega_o}{\omega}\right)^{n-1}/\Gamma(n/2)$$

$$\omega_o = v_t (k/z_2)^{1/2} \qquad \omega \gg \omega_o \quad \ldots\ldots (25)$$

and the suffix i has been dropped as the y variable has been introduced and therefore we refer to the i'th level $z_i - z_{i-1}$. The low and high frequency asymptotes meet at a corner frequency ω_c whose value is dependent not only upon the slope n but also on the layer thickness. Equating (24) and (25) we get

$$\omega_c = \omega_o\, A\, B \quad \ldots\ldots (26)$$

where $A = \left[(1-y)/(1-y^{(1+n)/2})\right]^{1/(n-1)}$

$$B = \left[\Gamma\left(\frac{1}{2}\right)\Gamma\left(\frac{n-1}{2}\right) / \Gamma\left(\frac{n}{2}\right)\Gamma(-(n+1)/2)\sin(\pi(1+n)/4)\right]^{1/(n-1)}$$

For a very thick layer such as a uniform atmosphere for $n = 11/3$ and by making $y \to 0$ we get $\omega_c = 1{\cdot}43\ \omega_o$ in agreement with the result of equation (14). For a very thin layer ($y \to 1$) we obtain for $n = 11/3$, $\omega_c = 1{\cdot}04\ \omega_o$, and for other values of n that factor is close to 1 so that the corner frequency is just the Fresnel frequency ω_o.

Expression (26) is very important in that it links a measurable quantity, the corner frequency, to atmospheric parameters such as the dominant eddy size or 'most efficient scattering eddy' which is of the same order as the Fresnel zone size $\sqrt{\lambda z}$, the height of the layer z, and its refractive index structure constant.

In practice, as Figure 1 shows, the spectrum of amplitude scintillation is found to be extremely variable, especially so for frequency components below the corner frequency. Thus the determination of ω_c by visual inspection of the spectrum is not usually straightforward. An alternative method of determining ω_o is to

make use of expressions (24) and (25) for the low and high frequency asymptotic values of the amplitude scintillation spectrum and the variance (20). One readily finds that

$$\omega_o = \alpha_1(n) \frac{\sigma^2(A)}{W_A^{\,o}(\omega)} \qquad \omega << \omega_c \qquad \text{..... (27)}$$

$$\omega_o = \alpha_2(n) \left[\frac{W_A^{\,\infty}}{\sigma^2(A)} \frac{(1-y^{n/2})}{(1-y)} \omega^{(n-1)} \right]^{1/(n-2)} \qquad \omega >> \omega_c \qquad \text{..... (28)}$$

where $$\alpha_1(n) = \frac{4\,\Gamma(-(n+1)/2)\,\sin\left[(1+n)\pi/4\right]}{\Gamma\left(\frac{n}{2}\right)\sin(n\pi/4)}$$

$$\alpha_2(n) = \left[\frac{\Gamma\left(\frac{n}{2}\right)\Gamma\left(-\frac{n}{2}\right)\sin(n\pi/4)}{4\,\Gamma\left(\frac{1}{2}\right)\Gamma\left(\frac{n-1}{2}\right)} \right]^{1/(n-2)}$$

It can be seen that the ratio of variance to spectral density for ω smaller than ω_c is independent of the layer thickness. Both relationships assume that the medium is homogeneous and isotropic within the region (z_i, z_{i-1}) (whether a thin layer or uniform atmosphere) and that the effects of the antenna aperture on the slope $-(n-1)$ of the spectrum can be neglected. This assumption is correct for our experimental results but it is known that the antenna diameter may affect the slope.

Equations (7), (19) and (24) to (28) are the key to the remote sensing of the parameters C_n^2, T (layer case), $\sqrt{\lambda L}$ and L. Two models are assumed for a slanted earth-space path of elevation θ. These are:

(a) Slab model, that is a single thick layer of height $h = L \sin\theta$ with a uniform C_n^2 and effective turbulent path L, within which there is a constant transverse wind velocity v_t.

(b) Thin layer model, that is a layer of thickness $T << h = z \sin\theta$ moving with velocity v_t and mostly responsible for the observed scintillation. z is the slant path distance to the layer.

Expressions (27) and (28) can then be computed for the limiting cases of:

(i) $z_1 \to 0$ and $z_2 = L$ that is $y \to 0$ for a slab model

(ii) $z_2 - z_1 = T << z_1$ that is $y \to 1$ for a thin layer model.

Operating we obtain

$$\omega_o = \alpha_1(n) \frac{\sigma^2(A)}{W_A^{\,o}(\omega)} \quad \omega << \omega_o \text{ for the slab and thin layer case} \qquad \text{..... (29)}$$

$$\omega_o = \alpha_2(n) \left[\frac{\omega^{(n-1)}\, W_A^{\,\infty}(\omega)}{\sigma^2(A)} \right]^{1/(n-2)} \quad \text{for the slab model} \qquad \text{..... (30)}$$

$$\omega = \alpha_2(n) \left[\frac{\omega^{(n-1)}\, W_A^{\,\infty}(\omega)}{\sigma^2(A)} \cdot \frac{n}{2} \right]^{1/(n-2)} \quad \text{for the thin layer model} \qquad \text{..... (31)}$$

$\omega >> \omega_o$; $\omega >> \omega_c$

The frequency ω_o can then be determined for both models by either visual inspection and using (26) or by a linear fit of the high frequency estimates to derive the spectral slope (n-1) and then using the expressions (29) to (31).

In practice, due to the extremely variable nature of the spectrum, as shown in Figure 1, obtaining the corner frequency by visual inspection or using the low frequency part of the spectrum is not usually very precise. However the high frequency region of the spectrum is generally well defined and the computed spectral estimates have a better statistical reliability. Accordingly expressions (30) and (31) were used in subsequent analysis.

Having determined ω_o, $\sqrt{\lambda L}$ and L can be readily obtained if we know v_t (this aspect is discussed in the following sections). The distance L may be interpreted as either the slab thickness (effective turbulent path) or the distance z to the scattering layer, depending upon the model used.

As regards the intensity of the refractive index spectrum, equation (20) can be solved for C_n^2 for the slab case. For the thin layer case we have to consider the thickness T which is unknown; however we can still solve for the product $C_n^2 T$. We get for the two models

$$C_n^{\,2} = \alpha_3(n)\, \sigma^2(A)\, k^{(n-6)/2}\, L^{-n/2} \qquad \text{..... (32)}$$

$$C_n^{\,2} = \alpha_3(n)\, \frac{2}{n}\, k^{(n-6)/2}\, z^{(2-n)/2}\, \sigma^2(A) \qquad \text{..... (33)}$$

where the variable $\alpha_3(n)$ is readily found to be

$$\alpha_3(n) = \left[\frac{1}{4}\,\Gamma\left(-\frac{n}{2}\right)\,\Gamma\,(n-1)\,\sin\frac{n\pi}{4}\,\sin\left(\frac{\pi}{2}\,(n-3)\right)\right]^{-1} \qquad \ldots\ldots (34)$$

2.4.2 Experimental Results

In order to determine the dominant eddy size, distance to the scattering layer and C_n^2T, the transverse wind velocity of the medium to the propagation path is required. For a dual antenna facility, estimates can be made of the transverse wind velocity by using temporal correlation techniques and spaced antennas. However the ground station at Portsmouth has only at present a single antenna capability so that another method was required to determine wind velocities quite apart from locating possible layers.

Facsimiles of radiosonde ascent data were obtained from two meteorological stations in southern England, Larkhill and Crawley. The most complete set of radiosonde data was that obtained from the Crawley site with is situated south of Gatwick Airport and is about 44 miles away from Portsmouth in a north easterly direction. Despite the distance of Crawley from Portsmouth, it was felt that for heights above one kilometre or more, the Crawley data would give a reasonable estimate of conditions above Portsmouth. The reasoning behind this is that the atmosphere above the turbulent boundary layer tends to be homogeneous in a horizontal plane. Therefore wind speed and direction in a plane might be expected to change relatively slowly with small distances compared with the dimensions of the weather systems. The radiosonde ascent data were given as a temperature-pressure graph against which were displayed dry bulb and dew point temperatures as a function of atmospheric pressure. Atmospheric pressure may be interpreted in terms of height above sea level by assuming a standard atmosphere. Radiosonde ascents were available for the months of June to September 1980 and the ascents were made at midnight and noon of each day. Wind speed and direction were given at 100 mbar pressure intervals starting at 900 mbar (0·99 km) and ending at 100 mbar (16·21 km). For each pressure interval (height) the wind velocity perpendicular to the propagation path v_t may be obtained from wind speed V and direction.

As described in the previous section, ω_c and therefore ω_o were obtained from the values of the amplitude scintillation spectrum in the frequency dependent region. This procedure was carried out for the slab and thin layer atmospheric profiles. The corner frequencies so derived for each model were always found to be within a few percent of each other and to agree very well with the corner frequencies derived by inspection from plots of power spectra. This good fit of theory would support the view that the amplitude scintillations of the received beacon are caused primarily by scattering from turbulent eddies and not another process such as scattering from water droplets.

Having obtained the corner ω_c and Fresnel frequencies ω_o, for each spectrum the quantity $\sqrt{\lambda L}$ or $\sqrt{\lambda z}$ was then estimated. Initially a path averaged v_t was used and this quantity was obtained by simply averaging the v_t's obtained at equipressure intervals of 100 mbar. However, the use of the path averaged transverse wind velocity was found to give unrealistically large effective path lengths with equivalent heights above the tropopause of about 10 km. Accordingly, an alternative method was used for choosing v_t. For each pressure interval or height h, the transverse wind velocity was determined and the corresponding Fresnel frequency ω_o was calculated using the distance or path z given by h/sin Θ. Comparison of this ω_o with that obtained from the spectrum of amplitude scintillations for that day was then made and the transverse wind velocity selected was the one that gave the closest match in Fresnel frequencies. That wind velocity selected was then used for subsequent calculations and the values obtained for $\sqrt{\lambda L}$ or $\sqrt{\lambda z}$ as well as L and z were found to be reasonable. It should be noted that the method of choosing V just described implicity assumes a layer model interpretation. However, a slab model can still be made to fit the data, although it is less realistic since a uniform v_t is assumed throughout the slab. In practice, of course, v_t varies with height.

Under the assumption that the layer model is a realistic one, an attempt was then made to correlate layer height with features of the temperature profiles which might indicate the presence of layers. Features considered were temperature inversions and maxima in dew point temperatures. The approach of the dew point temperature towards that of the dry bulb temperature may indicate the possible existence of cloud. Heights of these features were then obtained using a standard atmosphere and plotted against their inferred heights obtained from the spectral data. This scatter diagram is shown in Figure 4. The vertical bars represent the thickness of the feature obtained from the temperature profiles. The horizontal bars represent the range of thin layer heights obtained from the amplitude scintillation spectra of that day. The centre of each of the data ranges has been arbitrarily marked by a dot. It can be seen that there is a definite linear correlation between temperature profile features that might be indicative of layers, and their inferred height from spectral data. Table 1 summarizes the results and the comparison shows that the mean corner frequencies derived with both models are within 4% of each other. The Fresnel frequencies for each model tend to be more variable; their means are within 29% of each other. Despite this, the mean transverse correlation length (of order $\sqrt{\lambda L}$) is almost identical and just under 11 metres. Consequently the mean effective slant path, the slant path distance to the layer, the slab height and layer height for both models are very similar.

Histograms of the tabulated quantities are shown in Figures 5 to 7. The one about corner frequencies for both profile models. Figure 5, appears to be similar and asymmetrical or skewed. The histogram of Fresnel frequencies for both models is also asymmetric and it appears that there is a greater probability of higher frequencies occurring for the thin layer model. The results for the dominant eddy size $\ell_c \simeq \sqrt{\lambda L}$, whose values are derived from the Fresnel frequency data, would appear to show symmetry in the sense that the 10% and 90% limits are approximately equidistant from the mean. Figure 5 shows also the histogram of slant path distances, or slab, or layer heights, and it is interesting in that thin layers would appear to occur almost uniformly between 0·5 and 4·5 km in height. Figure 6 shows the results for C_n^2 and C_n^2T derived from a selection of a class interval (either 2^n or 4^n) which is linear in a logarithmic scale. These histograms appear to be fairly symmetrical. For the purpose of comparison the various 'C_n^2' obtained under n's other than 11/3 have been brought to the 11/3 exponential dependence so that both numerically and in terms of dimensions they may be compared.

Histograms of the variance of the spectra of amplitude scintillations and their slopes are shown in Figure 7 The one on variances was prepared using a class interval linear on a logarithmic scale and is remarkably symmetrical. This indicates a log-normal distribution for the variance and is in agreement with results to appear in literature (Moulsley T.J. et al, 1982) using a different and much greater data bank. As regards the spectral slopes, about 78% lie between -2·5 and -3·5 and this implies a wavenumber exponent of the refractive index spectrum in the range -3·5 and -4·5 with a mean of 3·95 and which can be compared with the theoretical estimate of -11/3 = -3·66.

3. ANTENNA APERTURE EFFECTS

The relationships given in the previous sections for the variance and spectrum of the amplitude scintillations apply to point antennas. For a finite antenna some correction may be necessary to allow for antenna aperture effects or smoothing. Aperture smoothing effects depend upon the ratio of the effective antenna diameter to the transverse correlation length of the amplitude scintillation. If the antenna diameter D is less than the correlation length then fluctuations in the incident wavefront are effectively correlated over its area and the aperture acts as a point receiver. If the antenna dimensions are larger than the correlation length then the incident wavefront fluctuations are essentially uncorrelated so that the signal delivered by the antenna output is a spatial average of the wavefront fluctuations. The observed signal fluctuations are then smaller than those expected for a point antenna. This subject has been partly dealt with in the literature (e.g. Crane R.K. et al, 1979, Van Weert, M.J.M., 1975) and results are usually derived by numerical integration of the spatially filtered spectrum. Although beyond the intended scope of this paper, and as part of a programme of related studies, analytical solutions have been derived for both the variance and the asymptotic value of the spectrum normalised to the point receiver; one finds

$$\frac{\sigma_A^2(D)}{\sigma_A(O)} = 3{\cdot}86\ (x^2+1)^{11/12} \sin\left[\frac{11}{6}\ \tan^{-1}\left(\frac{1}{x}\right)\right] - 7{\cdot}08\ x^{5/6} \qquad \ldots\ldots (35)$$

$$\frac{W_A^{\circ}(D)}{W_A^{\circ}(O)} = 2(x^2+1)^{7/6} \sin\left[\frac{7}{3}\ \tan^{-1}\left(\frac{1}{x}\right)\right] - 4{\cdot}66\ x^{4/3}$$

with $x = 0{\cdot}0584\ \frac{k}{L}\ D^2$

For plane wave propagation the transverse correlation length is of the same order as the Fresnel size $\sqrt{\lambda z_2}$. Equations (35) can be used not only to correct for the measuring values of the zero aperture case but also as an alternative approach to a cross-correlation technique of a dual-antenna system to measure effective cross-path wind speed v_t.

4. DISCUSSION AND CONCLUSIONS

This paper has dealt with the use of spectral analysis of amplitude scintillations for the purpose of remote sensing the turbulent atmosphere using a satellite path. Theoretical models have been revised and various new theoretical expressions have been specially developed. A layered atmosphere has also been theoretically investigated and the resulting expressions have been used to derive turbulence parameters using experimental results. The procedure which was followed has been given in detail.

The values of the parameters derived using the remote sensing technique presented in this paper have been summarised in Table 1 and discussed in Section 2.4.2. Although the number of experimental results is sufficiently high to derive reasonably reliable mean and standard deviations of the parameters, the data set is too small to fit the histograms shown in Figures 5 to 7 into an analytical model. For example C_n^2 and C_n^2T appear to have a symmetrical distribution on a logarithmic base but this is not as conclusive as in the case of $\sigma^2(A)$ which is log-normally distributed. As regards the choice of model, the thin layer model is probably more realistic than the slab model. This is because the slab model assumes a uniform velocity profile throughout its thickness, which is generally not the case in practice, particularly on a slanted path. However, the slab model may be thought of as an equivalent terrestrial line of sight case that would give the observed amplitude scintillation spectrum.

The theory and methods presented in Section 2 assume knowledge of the cross-path wind v_t. Clearly and as pointed out before, this can be obtained using two antennas receiving the same satellite beacon frequency and using cross-correlation techniques. Alternatively, two antennas could be used, one of small diameter operating as a point receiver and the second of diameter D giving 'smoothed' scintillation values. In this case the ratio of the variances for the two antennas would be proportional only to the ratio $D/\sqrt{\lambda z}$. The quantity $\sqrt{\lambda z}$ could be estimated directly and thus the distance z to the scattering layer. Corner frequencies derived from simultaneously obtained spectra could then be used to obtain transverse wind speeds; the other quantities such as C_n^2 and C_n^2T would then follow immediately.

5. ACKNOWLEDGEMENTS

The authors wish to acknowledge the contribution of their colleagues P. Lo and T.J. Moulsley to the overall satellite project, as well as that of colleagues in the Power Group for the use of the mobile data processing unit. One of the authors is grateful to the U.K. Science and Engineering Research Council (SERC) for a research studentship. The project has been financed by SERC and Portsmouth Polytechnic.

6. REFERENCES

Anderson, A.D., 1965, 'Free Atmospheric Turbulence', Aerology Branch Atm. and Astroph. Div., U.S. Naval Res. Lab. Rep. 4753.

Barton, D.K., 1971, 'Interferometer Phase Measurements: Comparison with Theory', IEEE Trans AP Vol. 19, July 1971.

Bendat, J., 1958, 'Principles and Applications of Random Noise Theory', John Wiley.

Crane, R.K., 1980, 'A Review of Radar Observations of Turbulence in the Lower Stratosphere', Radio Sci., Vol. 15, No. 2.

Fante, R.L., 1975, 'Electromagnetic Beam Propagation in Turbulent Media', Proc. IEEE, Vol. 63, No. 12.

Fried, D.L., 1967, 'Aperture Averaging of Scintillation', J. of the Opt. Soc. of America, Vol. 57, No. 2.

Gage, K.S., 1979, 'Evidence for a $k^{-5/3}$ Law Inertial Range in Mesoscale Two-Dimensional Turbulence', Jour. of Atmos. Sci., Vol. 36, No. 10.

Haddon, J., Lo, P., Moulsley, T.J., Vilar, E., 1980, 'Spectra of Amplitude Scintillations in X-Band Satellite Down-Link', Electronics Letters, Vol. 16.

- 1980, 'Statistical Intensity of Amplitude Scintillations on Earth-Space X-Band Link', Electronics Letters, Vol. 16.

- 1981, 'Measurements of Microwave Scintillations on a Satellite Down-Link at X-Band', IEE Conf. Ant. and Prop., York (U.K.).

Haddon, J., 1982, 'A Study of Microwave Scintillations on a Satellite Down-Link at X-Band', PhD Thesis, Portsmouth Polytechnic (U.K.).

Ishimaru, A., 1972, 'Temporal Frequency Spectra of Multi-Frequency Waves in Turbulent Atmosphere', IEEE Trans AP, Vol. 20, No. 1.

- 1977, 'Theory and Application of Wave Propagation and Scattering in Random Media', Proc. IEEE, Vol. 65, No. 7.

- 1978, 'Wave Propagation and Scattering in Random Media', Vols. I and II, Academic Press Inc.

James, P.K., 1980, 'A Review of Radar Observations of the Troposphere in Clear Air Conditions', Radio Sci., Vol. 15, No. 2.

Kaul, R., Wallace, R., Kaimal, G., 'Propagation Effects Handbook for Satellite Systems Design', NTIS Rep. N80-25520.

Lawrence, R.S., Strohbehn, J.W., 1970, 'A Survey of Clear-Air Propagation Effects Relevant to Optical Communications', Proc. IEEE, Vol. 58, No. 10.

Moulsley, T.J., Haddon, J., Lo, P., Vilar, E., 1981, 'Measurement and Modelling of the Probability Density Function of Amplitude Scintillations on an X-Band Satellite Down-Link', Electronics Letters, Vol. 17.

Moulsley, T.J., Vilar, E., 1982, 'Experimental and Theoretical Statistics of Microwave Amplitude Scintillations on Satellite Down-Links', To appear in IEEE Trans AP.

Prokhorov, A.M., Bunkin, F.V., Guchelashisly, V.I., Shiskov, V.I., 1975, 'Laser Irradiance Propagation in Turbulent Media', Proc. IEEE, Vol. 63, No. 5.

Rino, C.L., 1976, 'Ionospheric Scintillation Theory - A Mini-Review', IEEE Trans AP, Vol. 24.

Strohbehn, J.W., 1968, 'Line-of-Sight Wave Propagation Through the Turbulent Atmosphere', Proc. IEEE, Vol. 56, No. 8.

Tatarski, V.I., 1961, 'Wave Propagation in a Turbulent Medium', Dover Publ. Inc.

Taur, R.R., Fall 1974, 'Ionospheric Scintillations at Frequencies Above 1 GHz', Comsat Tech. Rev. Vol. 4, No. 2.

Tennekes, H.T., Lumley, J.L., 1972, 'A First Course in Turbulence', MIT Press 1972.

Van Weert, M.J.M., 1975, 'The Influence of Frequency and Receiver Aperture on the Scintillation Noise Power', AGARD Conf. Proc. 159, Paper 12.

Vilar, E., Matthews, P.A., 1978, 'Summary of Scintillation Observations on a 36 GHz Link Across London', IEE Conf. Ant. and Prop. London.

Vilar, E., Moulsley, T.J., Haddon, J., Lo, P., 1981, 'Scintillation Statistics on a Satellite Down-Link at X-Band', URSI 20th General Assembly, Washington.

Wernick, A.W., Chu, C.H., 1974, 'Ionospheric Irregularities Causing Scintillation of GHz Frequency Radio Signals', J. of Atm. and Terr. Phy., Vol. 36.

Wheelon, A.D., 1959, 'Radio Wave Scattering by Tropospheric Irregularities', Jour. of Res. NBS, Vol. 630, No. 2.

Zimmerman, S.P., 1966, 'Parameters of Turbulent Atmospheres', Journal of Geophysics Research, Vol. 71, No. 10.

Quantity		Sample Number	Mean	Standard Deviation	Percentage Limits not Exceeded 10%	90%
Fresnel Frequency	(a)	82	0·334	0·192	0·107	0·596
f_o (Hz)	(b)	82	0·471	0·265	0·139	0·829
Corner Frequency	(a)	82	0·431	0·222	0·137	0·724
f_c (Hz)	(b)	82	0·448	0·230	0·155	0·753
Transverse Correlation	(a)	59	10·90	2·90	7·06	14·25
Length ℓ_c(m)	(b)	66	10·84	3·25	6·46	14·44
Effective Path Length L (km)	(a)	59	4·989	2·568	1·957	7·954
Distance z (km) to layer	(b)	66	5·045	2·721	1·639	8·174
Height	(a)	59	2·570	-	1·008	4·097
h (km)	(b)	66	2·598	-	0·844	4·210
C_n^2 ($m^{-2/3}$) x 10^{13}	(a)	59	1·792	2·934	0·132	2·946
C_n^2 T($m^{1/3}$) x 10^{10}	(b)	66	3·204	3·331	0·601	6·671
C_n^2($m^{-2/3}$) x 10^{13} (T = 250 m)	(b)	-	12·82	-	2·403	26·68

Table 1: Quantities derived from radiosonde ascent wind velocity profiles and spectra of amplitude scintillations assuming

(a) a slab model (uniform thickness),

(b) a thin layer model of thickness T.

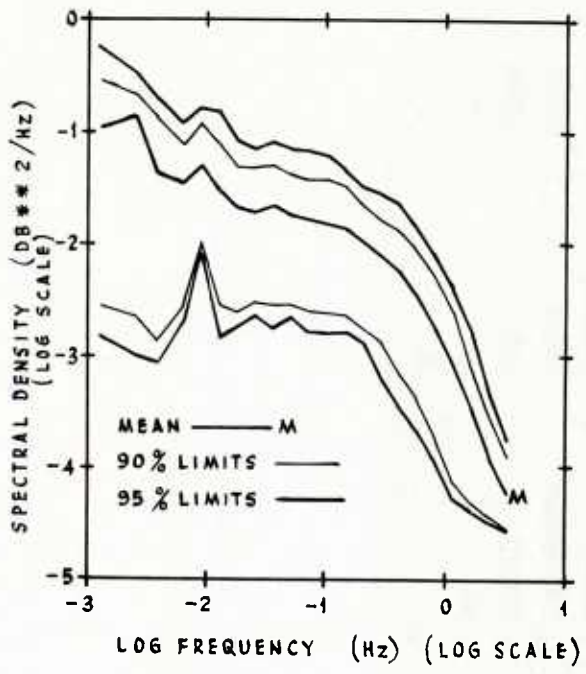

Figure 1: Experimental Results of Spectra and Limits.

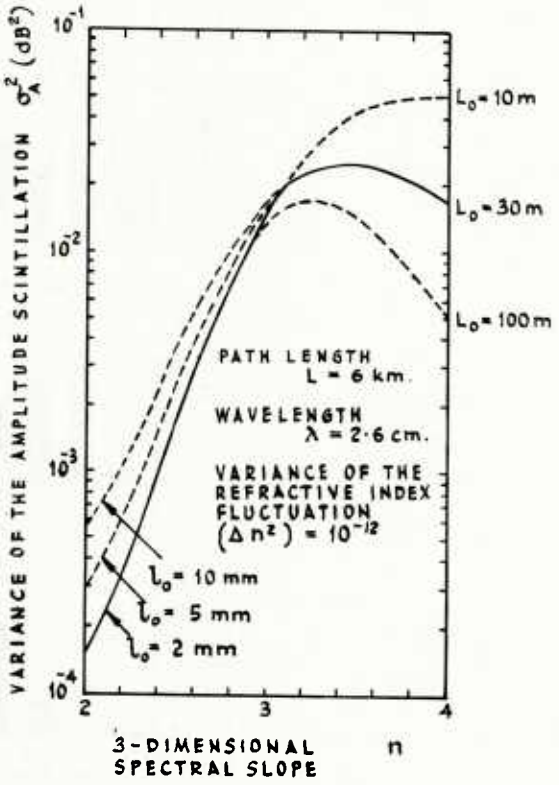

Figure 2: Dependence of the Variance of Amplitude Scintillation upon L_o, ℓ_o and the Spectral Slope n.

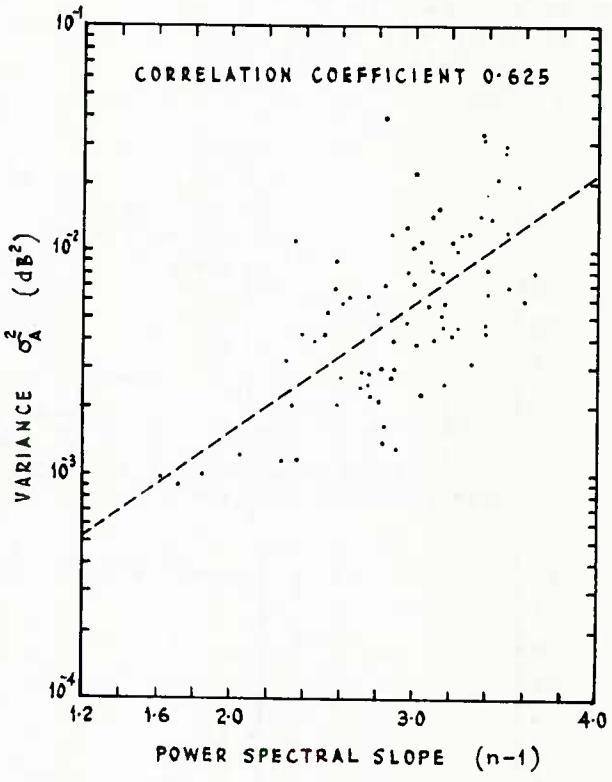

Figure 3: Correlation Between Variance of the Amplitude Scintillation Obtained from Power Spectra and the Slope of the Spectrum at Higher Frequencies.

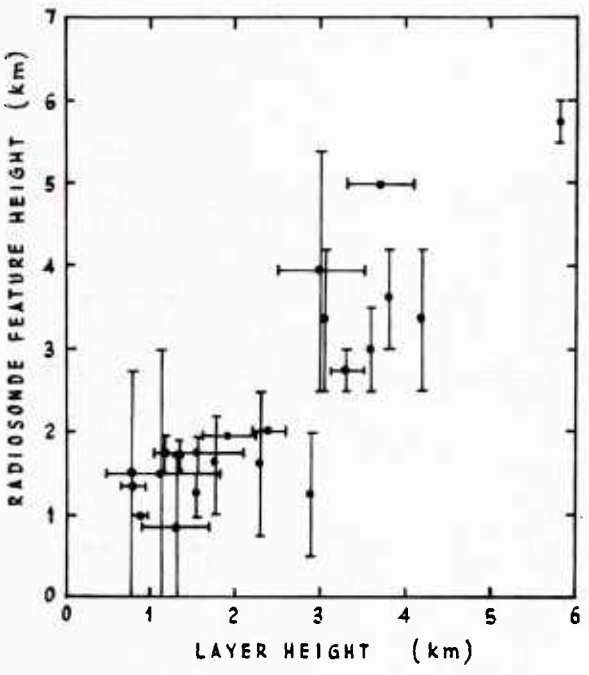

Figure 4: Correlation of Radiosonde Temperature Profile Feature Height with the Inferred Scattering Layer Height.

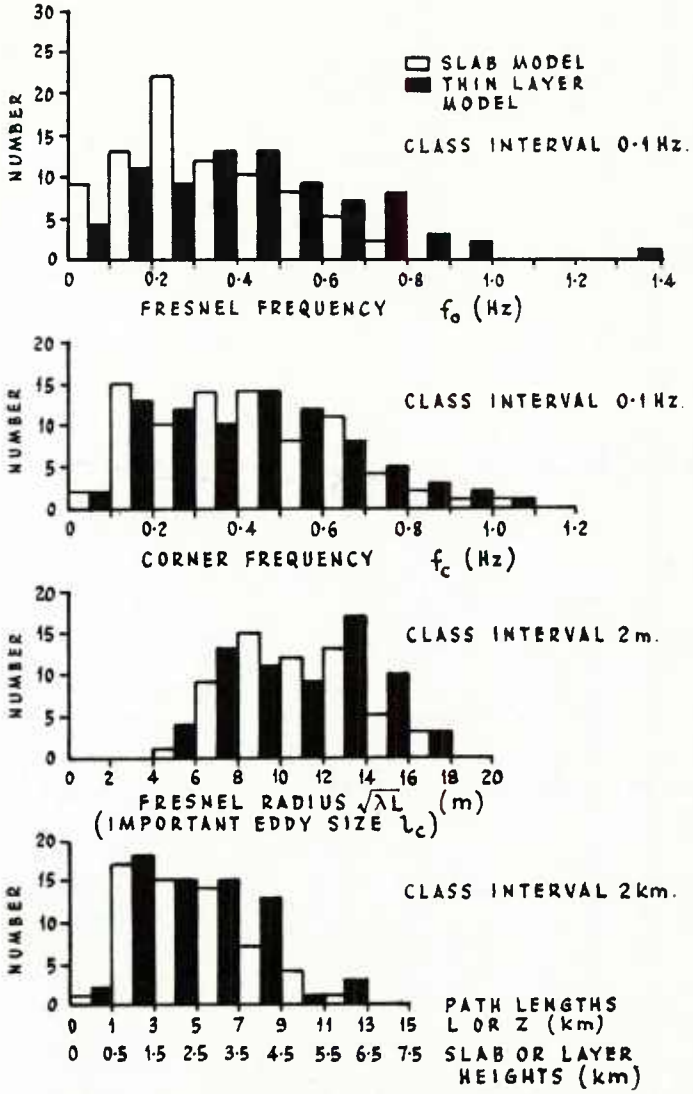

Figure 5: Histograms of Fresnel and Corner Frequencies, Fresnel Radius, and Effective Path Lengths and Heights for the Slab and Thin Scattering Layer Models.

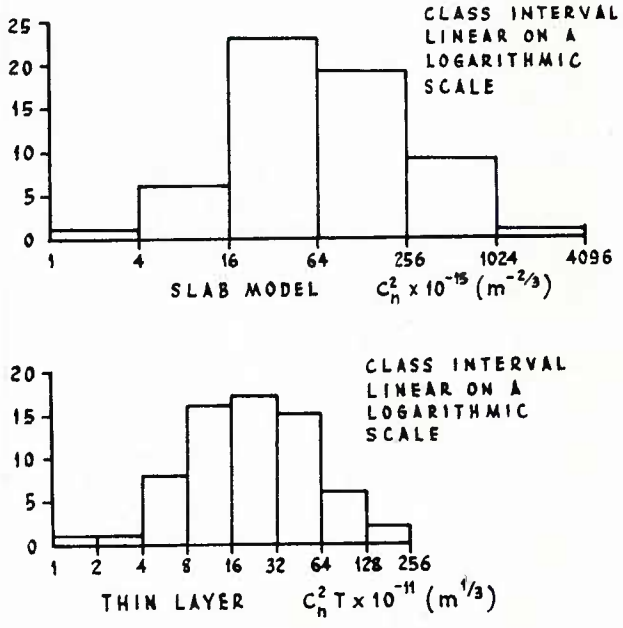

Figure 6: Histograms of Refractive Index Structure Constant C_n^2 (slab model) and $C_n^2 T$ (thin scattering layer model).

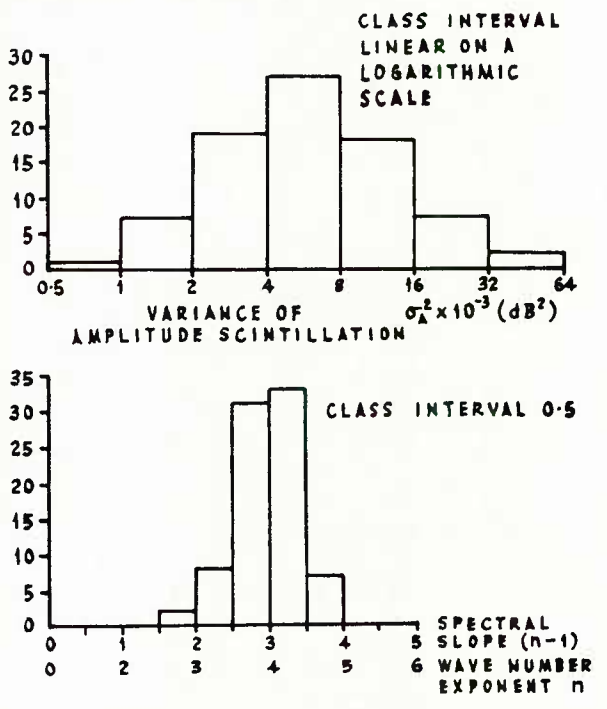

Figure 7: Histograms of the variance $\sigma^2(A)$ derived from Power Spectra, and of the Slopes n-1, (n).

DISCUSSION

D.J.Fang, US

I have no problem with your basic approach of assuming Kolmogorov type of spectrum for studying scattering of waves due to troposphere turbulent irregularities, but, I do have some reservations about the title of your paper, "A tool for remote sensing". You are certainly aware of the fact that signal scattering (or scintillations) can be produced by tropospheric irregularities other than Kolmogorov type of turbulent structures. Gravity wave is the leading candidate in this regard. It would be risky to lump the gravity-wave type of signal fluctuations into fluctuations produced by Kolmogorov type of irregularities. Would you agree?

Author's Reply

In my opinion you raised several questions.

- I would agree that the word "turbulent" should preceded "slant paths" in the title. The question of short titles is a common one and in a session on radio meteorology perhaps the ambiguity would not arise.
- I am not sure whether you question the concept of remote sensing, but in my understanding it implies the determination of the value of an observable by other means than direct in-situ measurements. This leads me to the intended message of the paper: if you have an operational ground station, then, with help of a "turbulence" propagation model, a coarse type of spectral analysis of the scintillations, and a small amount of data processing, you can derive very important turbulence parameters. We have done just this in our experiment and the results presented are very reasonable and agree with those of Bell Labs* in so far as the existence of turbulent layers; that is, the chances are that you will encounter a heavily turbulent layer (cloud probably) responsible for most of the scintillation observed. Please note Figure 4 of the paper and the excellent correlation between feature heights (layers?) obtained by meteorological observations and "remotely sensed" feature heights.
- This last point I think answers your question about gravity waves (G.W.) which play a small part in the overall forward scattering process discussed in the paper. I am sure that G.W. could be introduced in the model, but I am not so sure whether they would reflect the effects observed.

* Cox, C.P. and Arnold, H.W. "Results from the 19 and 28 GHz Comstar Satellite Propagation Experiments at Crawford Hill" Proc. IEEE Vol.70, May 1982.

LONG TERM CROSS-POLAR STATISTICS AT 12 AND 14 GHz ON A 30° SLANT-PATH

R.G. Howell, J. Thirlwell, D.J. Emerson
British Telecom

SUMMARY

Slant-path propagation measurements relevant to the design of dual-polar satellite systems are reported. The measurements were made on a 29.9° elevated slant-path during the period July 1978 to September 1981 using the Orbital Test Satellite (OTS) in conjunction with a 6.1 m off-set Cassegrain aerial located at Martlesham Heath near Ipswich (UK). Co-polar and cross-polar circularly polarised signals at a frequency of 14.5 GHz were transmitted to the satellite. These signals were down-converted to 11.8 GHz and re-transmitted to the ground together with an 11.8 GHz circularly polarised beacon signal. In addition measurements were made on an 11.6 GHz linearly polarised telemetry carrier transmitted by the satellite.

Cumulative statistics of the cross-polar discrimination (XPD) for the 11.6 and 11.8 GHz signals are presented and the XPD statistics for the 14.5 GHz signal estimated. The statistical significance of the depolarisation produced by high altitude ice crystals is discussed. The relationship XPD = U - V log CPA proposed by the CCIR to relate XPD to the co-polar attenuation (CPA) (dB) for rain is investigated and values for U and V obtained. The dependence of depolarisation on the type of polarisation (linear compared to circular) is studied and compared with theory.

1. INTRODUCTION

Dual polarisation techniques have been proposed as a means of increasing the capacity of satellite systems. In order to efficiently design such systems information is required on the propagation characteristics of the atmosphere; in particular the attenuation and depolarisation produced by rain and other hydrometeors.

The launch of the Orbital Test Satellite (OTS) in May 1978 (ESA, 1978) enabled data to be collected in the 12 and 14 GHz frequency bands. This paper reports the results of such measurements carried out at the British Telecom Research Centre at Martlesham Heath near Ipswich. The measurements were made during the period 1st July 1978 to 30th September 1981.

2. THE MARTLESHAM HEATH SITE

Martlesham Heath is located at 52.06N, 1.29E ie approximately 8 km E of Ipswich in East Anglia and 11 km from the coast of the North Sea. The terrain below the slant-path is mainly flat agricultural land at about 15 m above sea level. The OTS path crossed the coast at a slant range of 16 km and a height of 8 km. The local weather is maritime temperate and is characterized by fronts moving in from the Atlantic on the prevailing westerly airstream and convective rain in the summer. The total annual rainfall is lower than most other places in Britain (547 mm), however the incidence of heavy rain is about average.

3. THE OTS PROPAGATION EXPERIMENT

OTS carries a 5 MHz transponder (module B) which is primarily designed for slant-path propagation research. Two circularly polarised signals at a frequency of 14.455 GHz and separated by 5 kHz were transmitted from Martlesham and received by module B of the satellite. One of these signals, B2, was co-polar and the other, B3, was cross-polar with respect to the satellite receive aerial. These signals were transponded to 11.793 GHz and re-transmitted to earth using circular polarisation. Comparison of the relative level of these signals allowed the up-path cross-polarisation discrimination (XPD) to be determined.

A circularly polarised beacon (BO), at 11.786 GHz, was also transmitted by the satellite, allowing the down-path XPD and fade to be determined. Subtraction of the down-path fade from the total fade experienced by the transponded up-path co-polar signal enabled the up-path fade to be determined. Finally, measurements made using the satellite's linearly polarised telemetry carrier at 11.575 GHz allowed the down-path XPD and fade for linear polarisation to be determined. This signal ($\overline{TM}$) was polarised at 11.8° anti-clockwise from the horizontal on reception at Martlesham.

OTS was located at 10°E, giving elevation and azimuth bearings at Martlesham of 29.9° and 169° respectively.

4. THE EXPERIMENTAL EQUIPMENT AND MEASUREMENT TECHNIQUE

The signals were transmitted and received from the satellite using a 6.1 m diameter steerable offset Cassegrain aerial which was program-tracked to an accuracy of $\pm$ 0.01°. The aerial 3 dB beamwidths were 0.32° and 0.25° at 11.6 and 14.5 GHz respectively. A high pressure air blower was used to prevent the accumulation of water or snow on the feed window. Static cross-polar cancellation (EVANS, B.G..., 1977) was used in both the transmit and receive paths (linear and circular).

Narrow band phase-locked receivers capable of measuring the co-polar signal level and the relative amplitude and phase of the co- and cross-polar signals were used for the measurements on BO and $\overline{TM}$. These receivers locked onto the co-polar signal and the cross-polar signal was extracted by a coherent demodulation technique. This enabled measurements to be made on very low level cross-polar signals without problems of acquisition or loss of lock.

Because of the 5 kHz difference frequency, two separate phase-locked loops were used to acquire the transponded up-path signals. The co-polar loop pre-tuned the cross-polar loop to approximately the correct frequency and then the cross-polar loop acquired B3 when the latter was at a sufficiently high level.

The output time constants of the co-polar and cross-polar channels were 50 ms and 3 s respectively. The co-polar measurement range was +5 dB to -20 dB relative to the nominal clear sky level. The XPD could be measured over the range 10 to 60 dB.

Sky-noise radiometers aligned along the OTS slant-path and operating at 12.1 and 14.8 GHz were used to establish the zero for the attenuation measurements and to correct the recorded data for variations in the satellite EIRP as follows. Provided there was no significant fading, the outputs from the radiometers were converted to attenuation and the attenuation recorded from the corresponding receiver set to the same value. This gives the path attenuation relative to a vacuum. At the start of a fade this correction process was discontinued and the receivers remained calibrated to the EIRP applicable at the start of the fade. Since the radiometers are reasonably accurate at low levels of attenuation and the change of satellite EIRP was negligible over the duration of a typical fade this process significantly improved the accuracy of the fade measurement.

The attenuation data used in this paper is the attenuation in excess of the fine weather value. This was derived from attenuation as measured above by subtracting a small amount (0.1 dB at 11.8 GHz and 0.2 dB at 14.5 GHz) to allow for the attenuation due to atmospheric water vapour and oxygen.

The data were logged on a minicomputer at a rate of 2 samples per second with chart recorders for 'quick look' and back up.

4. THE RESULTS

4.1. General Description

The full programme of measurements (ie 14.5 GHz up-path and 11.6 and 11.8 GHz down-path) terminated on the 30th September 1981, however, measurements on the 11.6 GHz linearly polarised beacon continued until the 30th November 1981. The measurements reported in this paper refer to the full programme of measurements. It should be pointed out that a very severe rain storm occurred on the 23rd November 1981 which reduced the XPD of the linearly polarised signal to 16.2 dB together with an attenuation of 20 dB. This was one of the most severe events recorded at any time.

During the thirty-nine months of the full measurement programme the most severe events (XPD < 15 dB) occurred in the months May to December inclusive. The lowest XPD measured in the months January to April inclusive was 17 dB.

Some of the most significant cross-polar events are listed in Table 1.

TABLE 1

DATE	MINIMUM XPD		
	14.5 GHz	11.6 GHz	11.8 GHz
21 6 1978	*	25.4	15.4
31 7 1978	12.2	20.4	11.8
3 8 1978	15.0	27.2	17.2
13 12 1978	*	22.6	15.4
20 9 1979	10.2	24.4	16.6
20 9 1979	13.6	28.0	20.0
17 6 1980	14.6	29.0	21.0
17 6 1980	15.2	26.4	19.4
17 6 1980	14.8	27.0	19.2
19 9 1980	13.2	22.8	13.8
19 9 1980	12.0	22.0	15.0
20 9 1980	12.0	23.2	13.8
7 5 1981	12.6	22.2	11.6
2 6 1981	*	15.6	10.2

*Data not available

The data has been accumulated into an event list using thresholds of 4 dB attenuation at 14.5 GHz and/or 20 dB XPD on any signal. In section 4.5 it is shown that the XPD of the linearly polarised 11.6 GHz signal is about 8 dB greater than that of the circularly polarised 11.8 GHz signal. Hence the statistics obtained for the linearly polarised signal are valid for XPDs up to about 28 dB.

It is well known that depolarisation on slant-paths can be caused both by rain and/or high altitude ice crystals (COX, D.C..., 1982). The event list has been divided into 129 individual events each of which has been broadly classified as being caused by rain, a mixture of ice and rain, or predominantly ice. Of the 129 events 38 can be classed as either ice or a mixture of ice and rain and 11 are classified as predominantly due to ice. Refering to the measurements on the circularly polarised 11.8 GHz signal the lowest XPDs recorded during the 11 ice events were:- 15.8, 20.4, 20.0, 24.6, 22.8, 23.4, 21.8, 25.6, 20.8, 19.6 and 15.8 (mean = 21.0 dB). These values can be compared with those for the 11 most severe rain events which produced lowest XPDs at 11.8 GHz of :- 15.4, 11.8, 17.2, 15.4, 16.6, 19.2, 13.8, 15.0, 13.8, 19.6 and 10.2 (mean = 14.5 dB). Thus the results indicate that rain is by far the most significant cause of depolarisation for XPDs $\leq$ 15 dB, cf. six cases for rain and none for ice.

4.2. Cumulative Statistics of XPD

There are significant gaps in the 14.5 GHz data records because of equipment faults and operational constraints. Statistical results will therefore be presented in terms of the 11.6 and 11.8 GHz measurements. The 14.5 GHz statistics can, however, be inferred from data derived from concurrent 11.8/14.5 GHz measurements. These measurements (HOWELL, R.G..., 1981) indicate that on average the XPD of the circularly polarised 14.5 GHz signal is 2 dB less than that of the 11.8 GHz circularly polarised signal.

Since the period of the full programme of measurements was 1st July 1978 to 30th September 1981 it is not possible to produce three separate calendar years of cumulative distributions (C.D.s) for this data. The data has therefore been divided into years running from 1st Oct to 1st Oct. This allows the year to year variability to be seen over three separate years.

Figure 1 shows the 11.6 GHz data. For the reasons discussed above the data can be considered valid up to XPDs of about 28 dB. The curves are shown as a broken line beyond this level. It can be seen from this figure that the year to year variability for percentage times less than 0.01% can be as much as 5 dB and below 0.001% this increases to about 8 dB. This shows the importance of measuring for several years if a reasonable measure of the long term statistics is required.

Figure 2 shows the corresponding C.D.s for the circularly polarised 11.8 GHz signal. The curves are again shown as broken lines above the selection threshold level.

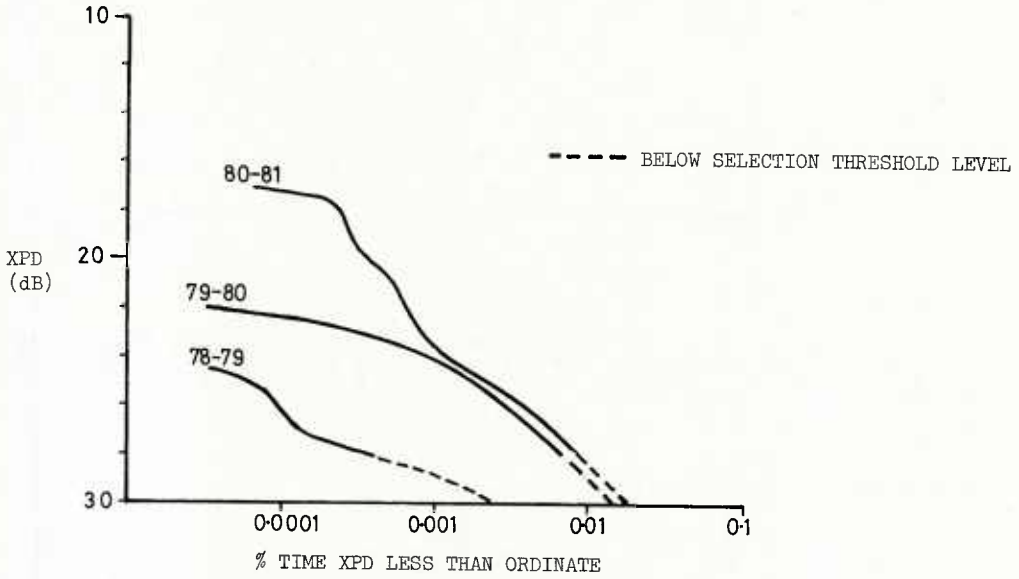

FIG.1 YEARLY (1st OCT - 1st OCT) CUMULATIVE DISTRIBUTIONS OF XPD FOR THE 11.6 GHz LINEARLY POLARISED SIGNAL

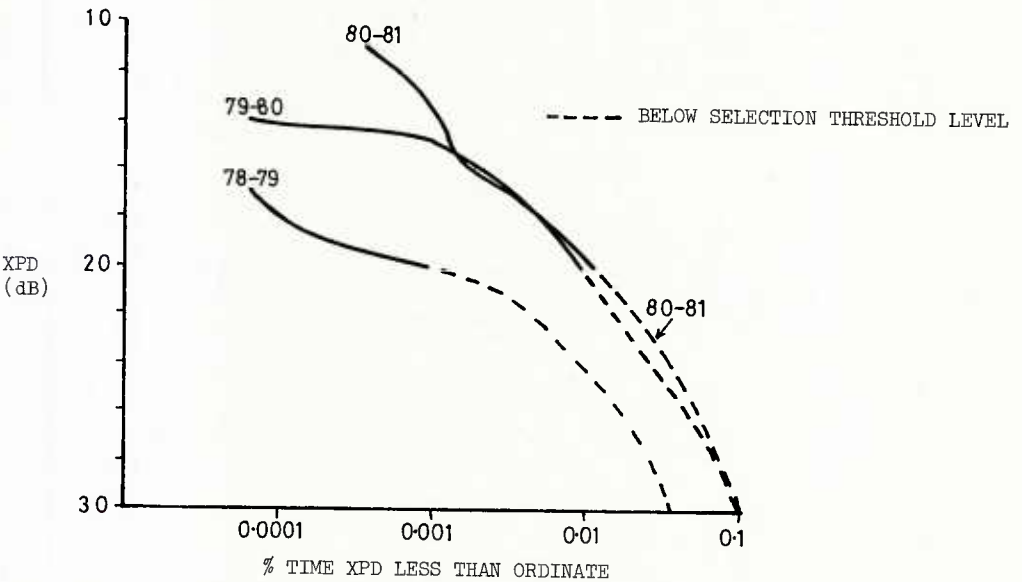

FIG.2 YEARLY (1st OCT - 1st OCT) CUMULATIVE DISTRIBUTIONS OF XPD FOR THE 11.8 GHz CIRCULARLY POLARISED SIGNAL

The data presented in figures 1 and 2 are not exactly concurrent in that some minor events are included in one and not the other (due to the non-availability of data), however, both sets of data include all the major events. Thus a comparison between the two sets of C.D.s is valid. It can be seen from this comparison that the XPD of the circularly polarised signal is consistently of the order of 8 to 9 dB worse than that of the linearly polarised signal. This is confirmed by an analysis of concurrent data as discussed in section 4.5 below.

Figure 3 shows the C.D.s for the 11.6 and 11.8 GHz signals for the total period 1st July 1978 to 30th September 1981. For the reasons explained earlier it would be misleading to present the C.D.s of

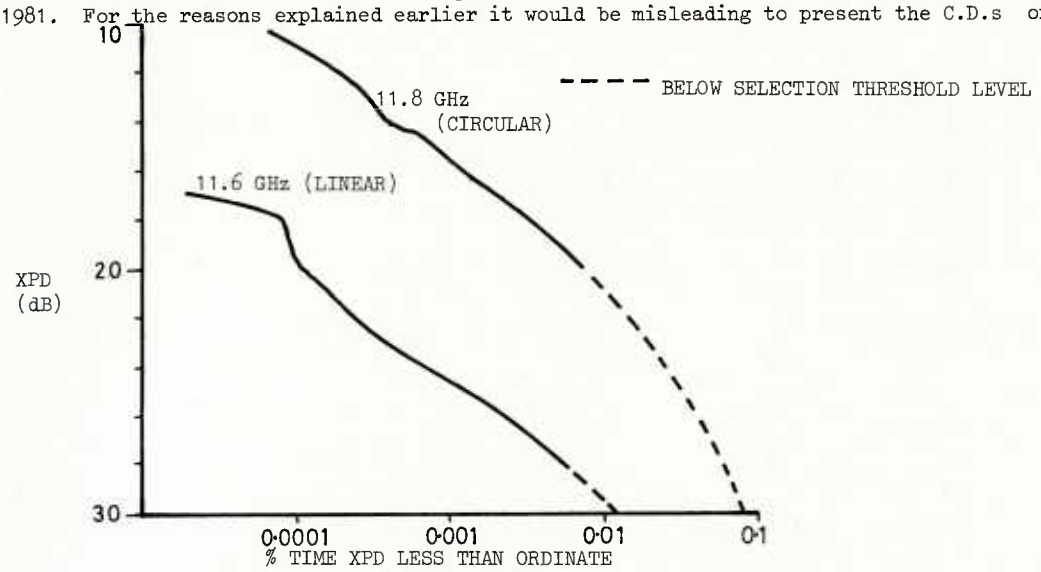

FIG.3 CUMULATIVE DISTRIBUTIONS OF XPD FOR THE PERIOD 1st JULY 1978 - 30th SEPTEMBER 1981

14.5 GHz XPD and the best estimate for this data can be obtained by subtracting 2 dB from the 11.8 GHz data. Hence in the long term for 0.01% of the time, and for the path and polarisation characteristics described earlier, the XPD can be expected to be less than about 29, 20 and 18 dB for the 11.6, 11.8 and 14.5 GHz signals respectively. The corresponding figures for 0.001% of the time are 24.5, 15.5 and 13.5 dB.

4.3. Joint Measurements of XPD and Attenuation

A large amount of slant-path attenuation data is either available or can be inferred from radiometric measurements (THIRLWELL, J..., 1981), rain cell modelling etc. It would therefore be of considerable use if a functional relationship between XPD and attenuation could be established. There is both theoretical and experimental evidence (NOWLAND, W.L..., 1977; ZUFFEREY, C., 1976) that such a relationship could be used and a semi-empirical relationship is included in the CCIR Green Book (CCIR, 1978). It is well known that no such relationship exists for the case of ice depolarisation, however, there is evidence from both our results and the work of others (SCHLESAK, J.J..., 1981) that at least in the 12 and 14 GHz bands, rain is the dominant cause of depolarisation for the small percentages of time. In order to investigate this relationship concurrent XPD and attenuation data has been analysed. The number of data samples falling in 1 dB by 1 dB class intervals of XPD and attenuation were calculated. The median and 10% and 90% percentile values of XPD were then calculated for each 1 dB class interval of attenuation. The results are shown in figures 4,5 and 6 for the 11.6, 11.8 and 14.5 GHz signals respectively. The total number of minutes of

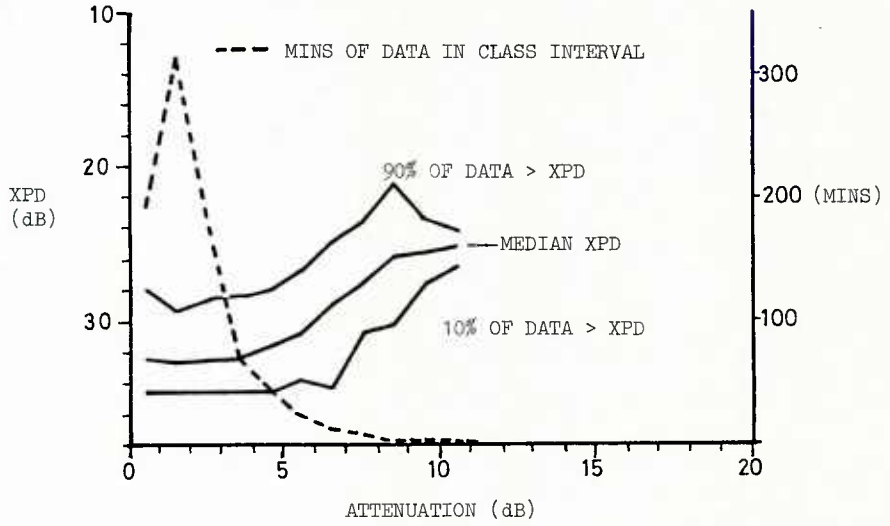

FIG. 4 STATISTICAL RELATIONSHIP BETWEEN XPD AND ATTENUATION FOR THE 11.6 GHz LINEARLY POLARISED SIGNAL

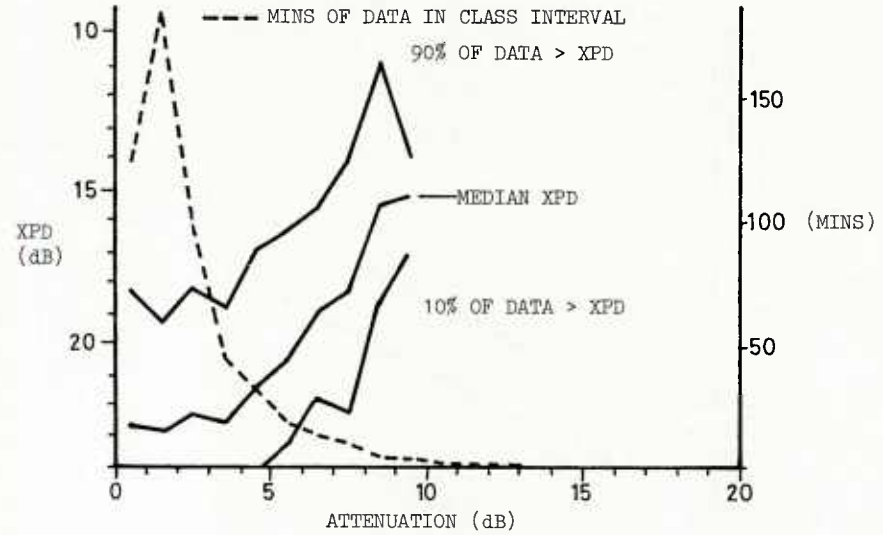

FIG. 5 STATISTICAL RELATIONSHIP BETWEEN XPD AND ATTENUATION FOR THE 11.8 GHz CIRCULARLY POLARISED SIGNAL

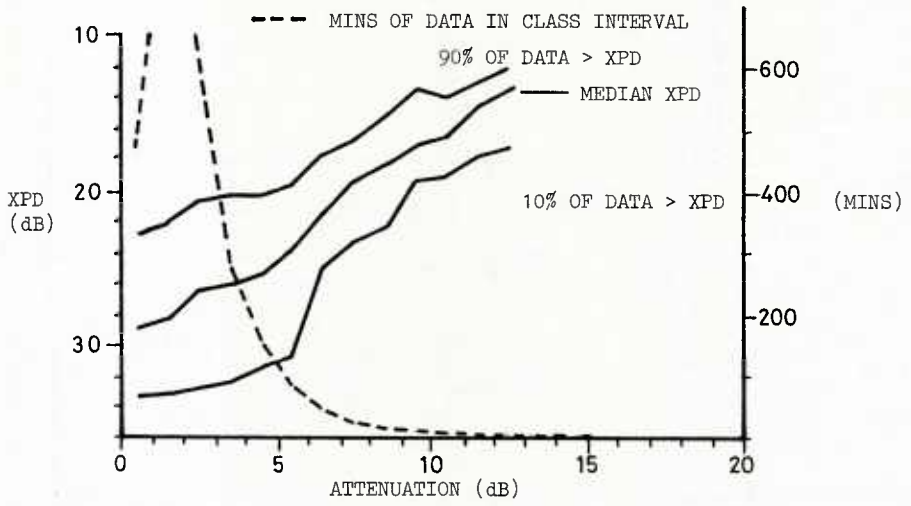

FIG. 6 STATISTICAL RELATIONSHIP BETWEEN XPD AND ATTENUATION FOR THE 14.5 GHz CIRCULARLY POLARISED SIGNAL

data in each attenuation class interval used in calculating the median and percentile values is also shown. Data for which the total accumulated time in an attenuation class interval is less than 2 min is not included in the figures since the data from such a small sample cannot be considered statistically reliable.

The large spread in XPD for a given attenuation is typical of the results obtained from this type of measurement (COX, D.C..., 1982).

4.4. Comparison of the Results with the CCIR Semi-empirical Relationship

The CCIR relationship is of the form

$$XPD = U - V \log CPA.$$

Where XPD is the cross-polar discrimination due to rain and CPA is the co-polar attenuation due to rain. Since ice crystals produce very little attenuation the XPD data attributable to ice crystals can be eliminated from the analysis by plotting only XPD data which is associated with a fade of more than say 3 dB. The median values of XPD for attenuations above this value are shown in Figure 7 plotted as a function of log CPA. Least squares linear regression lines are also shown together with the lines calculated from the CCIR relationship.

It can be seen that in the case of the circularly polarised 11.8 and 14.5 GHz signals the agreement is very good giving best-fit relationships of:-

$$XPD_{11.8} = 33 - 18 \log CPA_{11.8}$$

and

$$XPD_{14.5} = 38.4 - 21.4 \log CPA_{14.5}$$

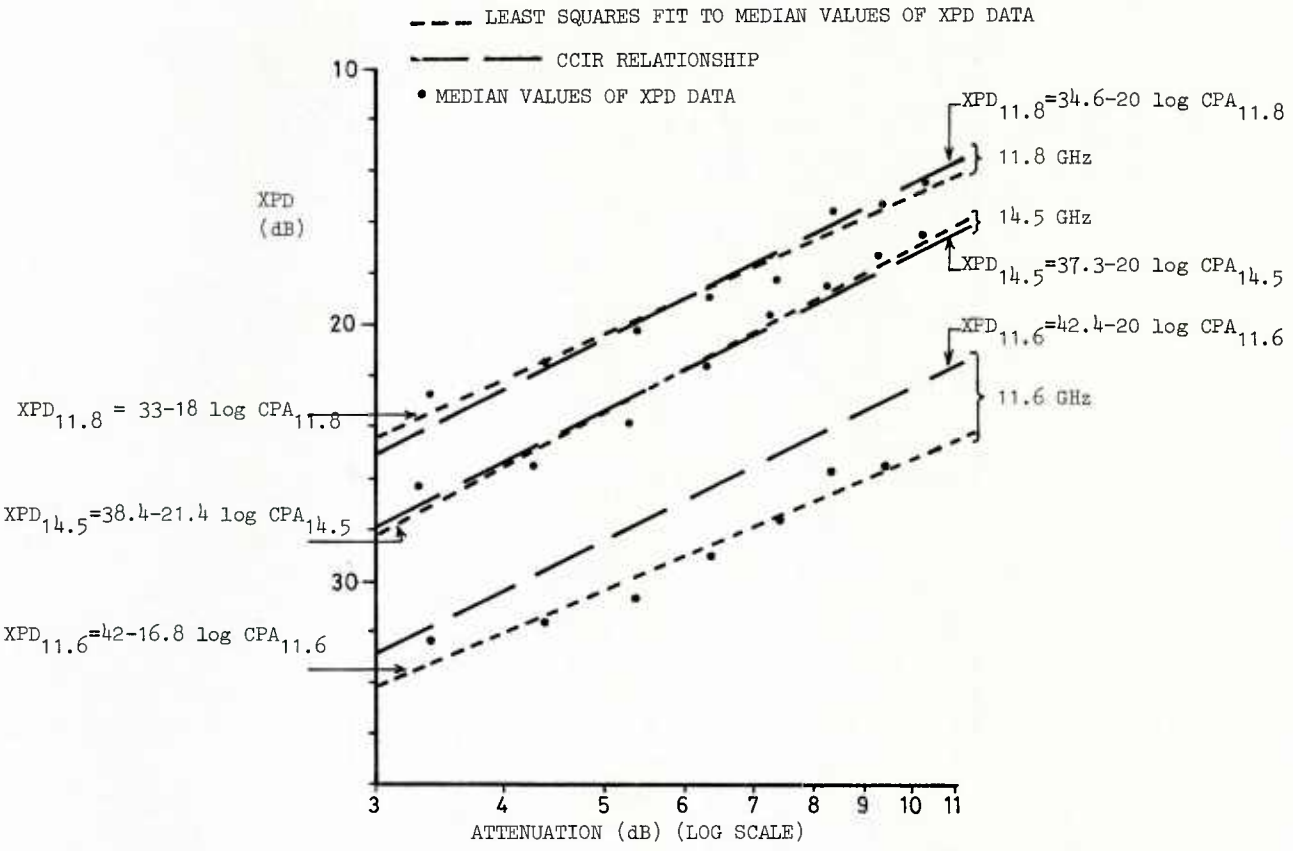

FIG. 7 COMPARISON OF THE MEDIAN VALUES OF THE XPD DATA WITH VALUES PREDICTED BY THE CCIR RELATIONSHIP

The 11.6 GHz data gives an XPD which is about 2 dB greater than that predicted by the CCIR formula. A systematic tilt in the mean value of the raindrop canting angle of about 2° - 3° would be one possible explanation of these results. The best fit relationship obtained from the 11.6 GHz data is:-

$$XPD_{11.6} = 42 - 16.8 \log CPA_{11.6}$$

It should be remembered that these formulae apply to the median of the long term data and that during an individual event the XPD corresponding to a given attenuation can vary over the range indicated in figures 4,5 and 6.

4.5. Polarisation Dependance of XPD

It is of considerable importance in designing a satellite system using dual-polar frequency re-use techniques to optimize the polarisation to give the best cross-polar performance ie lowest interference due to depolarisation. Hence the dependence of XPD on the type of polarisation (circular compared to linear and the orientation of the linear) is of interest.

Theory predicts an improvement factor for linear polarisation compared to circular polarisation of -20 log sin 2 (τ-θ) dB, where τ is the angle of the linear polarisation relative to the horizontal and θ is the tilt angle, relative to the horizontal, of the principle plane of the medium. In the case of the Martlesham measurements $\tau = 11.8^{\circ}$. Taking a value of θ of zero gives an improvement factor for linear polarisation of 7.9 dB.

Concurrent 11.8 and 11.6 GHz data was divided into 1 dB by 1 dB class intervals of 11.8 GHz XPD and 11.6 GHz XPD. The median and percentile values of 11.8 GHz XPD were then calculated for each class interval of 11.6 GHz XPD. The results are plotted in figure 8 together with the accumulated number of minutes of data in each class interval. The theoretical relationship discussed above is plotted in this figure as a broken line. The close agreement between the median value of the measurements and the theoretical prediction is apparent in this figure.

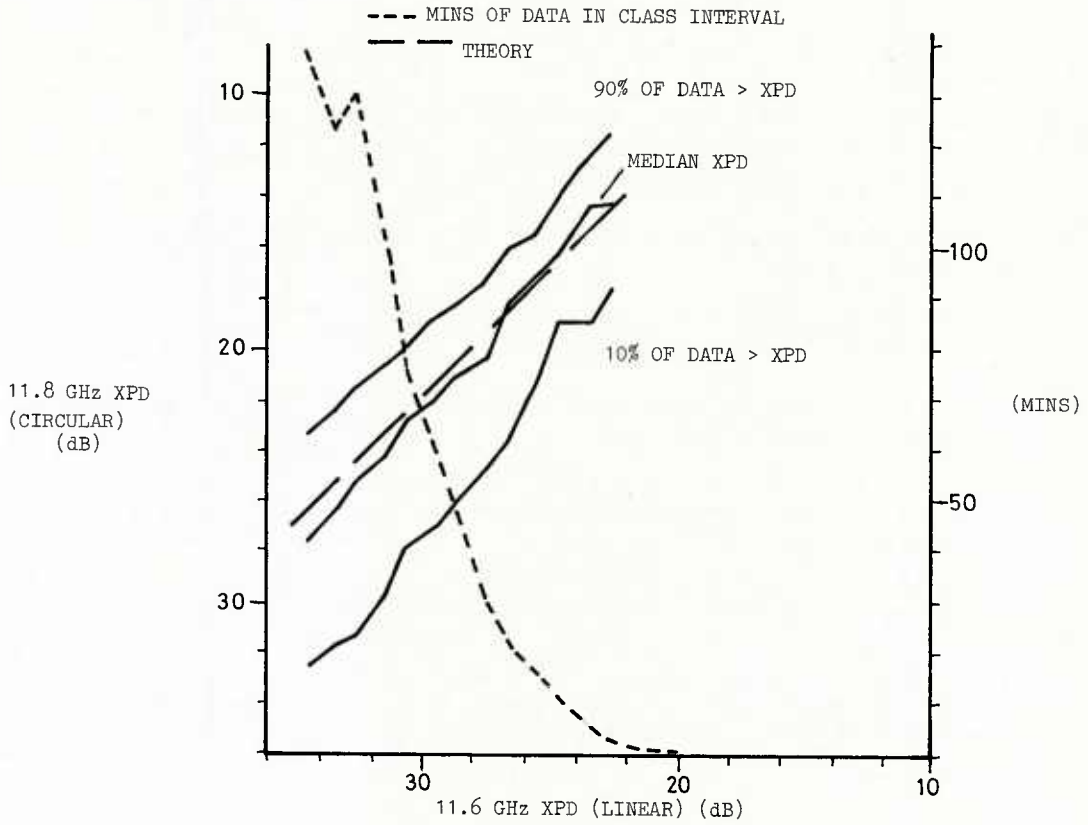

FIG. 8 STATISTICAL RELATIONSHIP BETWEEN THE XPD OF THE CIRCULARLY POLARISED 11.8 GHz SIGNAL AND THE XPD OF THE LINEARLY POLARISED 11.6 GHz SIGNAL

5. CONCLUSIONS

The results indicate that, for satellite links operating in the UK in the 12 and 14 GHz frequency bands, rain is the most significant cause of depolarisation for XPDs $\leqslant$ 15 dB.

During the measurement period the XPDs were less than the following values for 0.001% of the time:-

i. linearly polarised 11.6 GHz signal ..... 24.5 dB

ii. circularly polarised 11.8 GHz signal .... 15.5 dB

iii. circularly polarised 14.5 GHz signal ..... 13.5 dB (estimated)

The year to year variability in the cumulative distributions of XPD was up to 5 dB at the 0.001% level.

Joint measurements of XPD and attenuation showed a large spread in XPD for a given attenuation ($\sim \pm 4$ dB). Comparison of the median values of this data with a relationship proposed by the CCIR showed excellent agreement for the circularly polarised 11.8 and 14.5 GHz measurements. The best fit relationships to the data were:-

$$XPA_{11.8} = 33 - 18 \log CPA_{11.8}$$

and

$$XPD_{14.5} = 38.4 - 21.4 \log CPA_{14.5}$$

The 11.6 GHz data gave XPD values which were about 2 dB better than those predicted by the CCIR formula. The best fit to this data was:-

$$XPD_{11.6} = 42 - 16.8 \log CPA_{11.6}$$

Comparison of the XPDs for the circularly polarised 11.8 GHz and linearly polarised 11.6 GHz signals showed good agreement with that predicted by theory ie about an 8 dB higher XPD for the linearly polarised signal.

ACKNOWLEDGEMENT

The authors are indebted to their colleauges responsible for the day-to-day running of the propagation experiments described. Acknowledgement is made to the Director of Research of British Telecom for permission to publish this paper.

References

E.S.A, BULLETIN, May 1978, No 14.

EVANS, B.G. and THOMPSON, P.T., 1977, Use of cancellation techniques in the measurement of atmospheric cross-polarisation; Electron. Lett., 9, 447-448.

CCIR Green Book, 1978, Vol V, Report 564-1, Kyoto.

COX, D.C. and ARNOLD, H.W., May 1982, Results from the 19 and 28 GHz Comstar satellite propagation experiments at Crawford Hill; Proc. IEEE, Vol 70, No 5.

HOWELL, R.G. and THIRLWELL, J., April 1981, Slant-path depolarisation measurements at 12 and 14 GHz carried out at Martlesham Heath using the OTS satellite; IEE 2nd International Conference on Antennas and Propagation, York.

NOWLAND, W.L., OLSEN, R.L. and SHKAROFSKY, I.P., 1977, Theoretical Relationship between rain depolarisation and attenuation; Electron. Lett., 13, 676-678.

SCHLESAK, J.J. andSTRICKLAND, J.I., 1981, Circular cross-polarization measurements on earth-space paths at 11.7 GHz; Ann. Telecommunic., 36.

THIRLWELL, J. and HOWELL, R.G., April 1981, Slant-path attenuation measurements in the range 12-30 GHz using OTS and passive radiometers at Martlesham Heath; IEE 2nd International Conference on Antennas and Propagation, York.

ZUFFEREY, C., June 1976, Cross-polarisation measurements at 13 GHz on a slant terrestrial path: comparison between circular and linear polarisation; Colloquium on frequency re-use transmission experiment at 180 Mbit/s over the Jungfrau link, European Space Agency, Technical Centre of the Swiss PTT, Berne, Switzerland.

DISCUSSION

M.B.White, US

Do you have a physical explanation of why ice depolarizes less strongly than water droplets? At optical wavelength the situation appears to be exactly opposite.

Author's Reply

I think there is a problem in trying to make this comparison; namely, how can one compare an ensemble of ice crystals with an ensemble of water drops and be sure one is comparing "like with like"? I must emphasize that all our results are presented on a statistical basis, and we have found that statistically ice is less important than rain when one is considering the very low values of XPD or the small percentages of time.

A.Ochs, Ge

The relative importance of XPD caused by ice crystals and rain seems to depend on the climate. At our station at Darmstadt, Germany, which is farther away from the sea than Martlesham, ice depolarization has been observed less frequently than in your case.

Author's Reply

Thank you Dr Ochs for that information. This observation also agrees with the results obtained by Dr Olsen and his collegues in Canada. He has found the effects of ice depolarization to be more severe from ground stations near the coast than for those well inland.

C.H.Hagn, US

Can you comment on how to determine the angle to use in your formula for XPD improvements of linear polarization over circular polarization? For example, the orientation of ice particles in an electrified cloud may be difficult to determine.

Author's Reply

Yes, I agree that the principal axis of the depolarizing medium is difficult to determine and this is a general problem in trying to model propagation processes (namely, obtaining suitable values for the meteorological parameters such as raindrops canting angle distribution etc.). We have assumed an average value of zero degrees relative to the horizontal in determining the theoretical improvement factor.

B.G.Evans, UK

In answer to the question of whether you can ascribe an orientation angle to the propagation medium I would say that this is difficult because the population of particles will have a range of orientations. One can obviously ascribe a mean-averaged path angle "θ" for a particular event, but this has little physical significance. The angle will be constantly varying – as seen in the slides shown in the presentation an electric field discharge can orientate a population of ice crystals that would otherwise be random. I thus think that to talk about one angle "θ" is misleading. Authors tend to use a value "θ" that fits "long-term" measured data and this is the value that has been used in the linear vs circular transformation. It is not possible to look at a physical ice-cloud situation and ascribe to this an angle "θ" which ties up with the actual angle of the ice crystals.

M.P.M.Hall, UK

In addition to the useful information given to improve the model: XPD = U − V log CPA , it is good to see the inclusion of upper and lower deciles. These are likely to be equally important to the system planner.

K.A.Hughes, UK

As a result of your work, are you in a position to recommend more appropriate values for the parameters U and V in the CCIR prediction method?

Author's Reply

Yes – I have not presented the values for U and V which we have derived in my slides in order to keep the slides reasonably clear. The value can be found in the published paper.

FADING STATISTICS OF C-BAND SATELLITE SIGNAL DURING SOLAR MAXIMUM YEARS (1978-1980)

D. J. Fang
Propagation Studies Department
COMSAT Laboratories
22300 Comsat Drive
Clarksburg, Maryland 20871

C. H. Liu
University of Illinois at Urbana-Champaign
Urbana, Illinois 61801

ABSTRACT

From January 1978 to June 1980, scintillation experiments were conducted at the Hong Kong earth station. INTELSAT satellite signals at 4 GHz were received via both the Pacific Ocean Region (POR) and Indian Ocean Region (IOR) satellite-earth links. Severe intensity scintillations with peak-to-peak fluctuations up to 14 dB were observed on many evenings during the equinoctial period. This paper presents detailed statistics of the scintillating signals. The level of fluctuations based on the scintillation index is evaluated, and fading rates in terms of the coherence time are examined and correlated with the level of scintillation. Power spectrum densities are also assessed. The high-frequency asymptotes, i.e., the roll-off slopes at frequencies above the Fresnel frequency, as approximated by f^{-n}, are derived for different levels of fluctuations. For system applications, various cumulative statistics, including annual and worst-month statistics, diurnal variations, and sunspot cycle dependence are summarized.

INTRODUCTION

Since 1970, COMSAT Laboratories has been conducting C-band ionospheric scintillation measurements for INTELSAT using INTELSAT earth stations around the world. Early data established the existence of 4- and 6-GHz ionospheric scintillations and gross features, such as dependence on local sunset conditions, diurnal and seasonal patterns, geomagnetic boundaries, and magnitude of frequency (f) dependence. The gross features of 4/6-GHz ionospheric scintillations can be summarized as follows:

a. Scintillations occur in the geomagnetic equatorial region, mainly between 30° GMN and 30° GMS, and expand and contract as solar activities increase and decrease, respectively.

b. The frequency of occurrence of scintillation events has strong diurnal peaks. The probability of occurrence is greatest about 1 hour after local ionospheric sunset, and scintillations may last for hours until midnight.

c. The frequency of occurrence varies by season, with peak activity around vernal equinox and high activity at autumnal equinox.

d. An f^{-s} relationship with s between 1.5 to 2.0 exists between the 4- and 6-GHz scintillation amplitudes.

e. The power spectral densities of the scintillation generally exhibit a power law frequency dependence for spectral frequencies greater than the Fresnel frequency. An f^{-3} asymptotic dependence can be considered reasonable for weak scintillation events with peak-to-peak fluctuations below 4 dB.

All of these features have strong annual variations related to the 11-year sunspot cycles. Consecutive measurements at the Hong Kong earth station revealed that during solar minimum years, signal fluctuations never exceeded 1 dB peak-to-peak for more than 1 year, while during solar maximum years, scintillations occurred every evening around equinox, with fluctuations frequently exceeding 10 dB. (Taur, R. R., 1974 and 1976; Fang, D. J., 1980 and 1981; Fang, D. J., and Pontes, M. S., 1981).

This paper analyzes ionospheric scintillation data collected at the Hong Kong earth station from March 1977 to October 1978, and from November 1978 to June 1980, as the solar activities approached and exceeded the peak of the current sunspot cycle 21. The data provide further details of ionospheric scintillations that are unique in solar maxima years.

EXPERIMENTAL CONFIGURATIONS

Two geostationary satellites, five earth stations, and eight up/down-link signals were involved in the experiment. The two satellites, INTELSAT IV F8 Pacific Ocean Region (POR) and INTELSAT IV-A F1 Indian Ocean Region (IOR), were located at 174°E and 63°E, respectively. The five earth stations were Stanley, Hong Kong; Sentosa, Singapore; Si Racha, Thailand; Paumalu, Hawaii; and Padukka, Sri Lanka. Detailed information is given in Table 1. Only the Hong Kong earth station (HK) was used for data collection. At a 400-km altitude, the down-link paths for POR-HK and IOR-HK penetrate the ionosphere at 122.7°E, 20.3°N and 108.2°E, 20.4°N, respectively. The east-westward separation in the ionosphere is about 1,700 km, or about 1 hour geographical local time. Two beacons and six communications carrier signals were monitored at the Hong Kong earth station, as illustrated in Table 2. The lowest transmission path, from Si Racha to POR, has an elevation angle of approximately 8°. The elevation angles for all the other paths are more than 10°, which is well above the angle (~5°) at which tropospheric and multipath effects may degrade microwave signals (Fang, D. J., Tseng, F. T., and Calvit, T. O., 1982A and 1982B).

Table 1. Earth Station Information

Earth Station	Geographic Location		Geomagnetic Latitude	Antenna (Satellite)	Elevation Angle (deg)	Measurement Period
	Longitude	Latitude				
Stanley, Hong Kong	114°13'E	22°12'N	10.52°N	HK1(POR) HK2(IOR)	19.59 27.76	1977-1980
Sentosa, Singapore	103°50'E	01°15'N	10.36°S	SN1(IOR) SN2(POR)	42.78 11.31	1979-1980
Si Racha, Thailand	100°56'E	13°06'N	1.57°N	SR1(POR) SR2(IOR)	7.87 43.94	1977-1980
Paumalu, Hawaii	158°02'W	21°40'N	21.40°N	PA(POR)	49.05	1977-1978
Padukka, Sri Lanka	80°06'E	07°11'N	2.88°S	PD(IOR)	67.12	1977-1978

Table 2. Signals Monitored at Hong Kong Earth Station (HK)

Path	Frequency (MHz)		Nature
	Up-Link	Down-Link	
POR → HK1	None	3950 ± 2.5	POR Beacon
SN2 → POR → HK1	5977.5	3752.5	Communications Carrier
SR1 → POR → HK1	6227.5	4002.5	Communications Carrier
IOR → HK2	None	3950 ± 2.5	IOR Beacon
SN1 → IOR → HK2	6190.0	3965.0	Communications Carrier
SR2 → IOR → HK1	6103.75	3878.75	Communications Carrier
PA → POR → HK1	5940.0	3715.0	Communications Carrier
PD → IOR → HK2	6097.5	3872.5	Communications Carrier

The method of monitoring satellite signals for ionospheric scintillation studies can be briefly described as follows. For each carrier or beacon signal, a buffered output proportional to the automatic gain control (AGC) voltage is recorded. The input to each IF amplifier includes an attenuator, which is normally set at 5 dB; the amplifier gain is adjusted to accommodate the attenuation. The recorded data can thus be calibrated by changing the attenuation in 1-dB steps to provide a ±5-dB range for a scintillation experiment within ±0.5-dB accuracy. This accuracy limit is established because, even under clear sky conditions, the buffered IF output has small noise-induced variations.

OUTSTANDING FEATURES OF SCINTILLATIONS IN THE SOLAR MAXIMUM YEAR

From March 1979 to March 1980, ionospheric scintillations of over 1.0-dB peak-to-peak fluctuations at either IOR or POR links were observed at the Hong Kong earth station for about 100 evenings. In March 1980, scintillations occurred almost every evening, as shown in Figure 1. The frequency of occurrence (20 evenings in both April 1979 and September 1979) confirms the theory that scintillations have seasonal variations, with peaks at vernal and autumnal equinoxes.

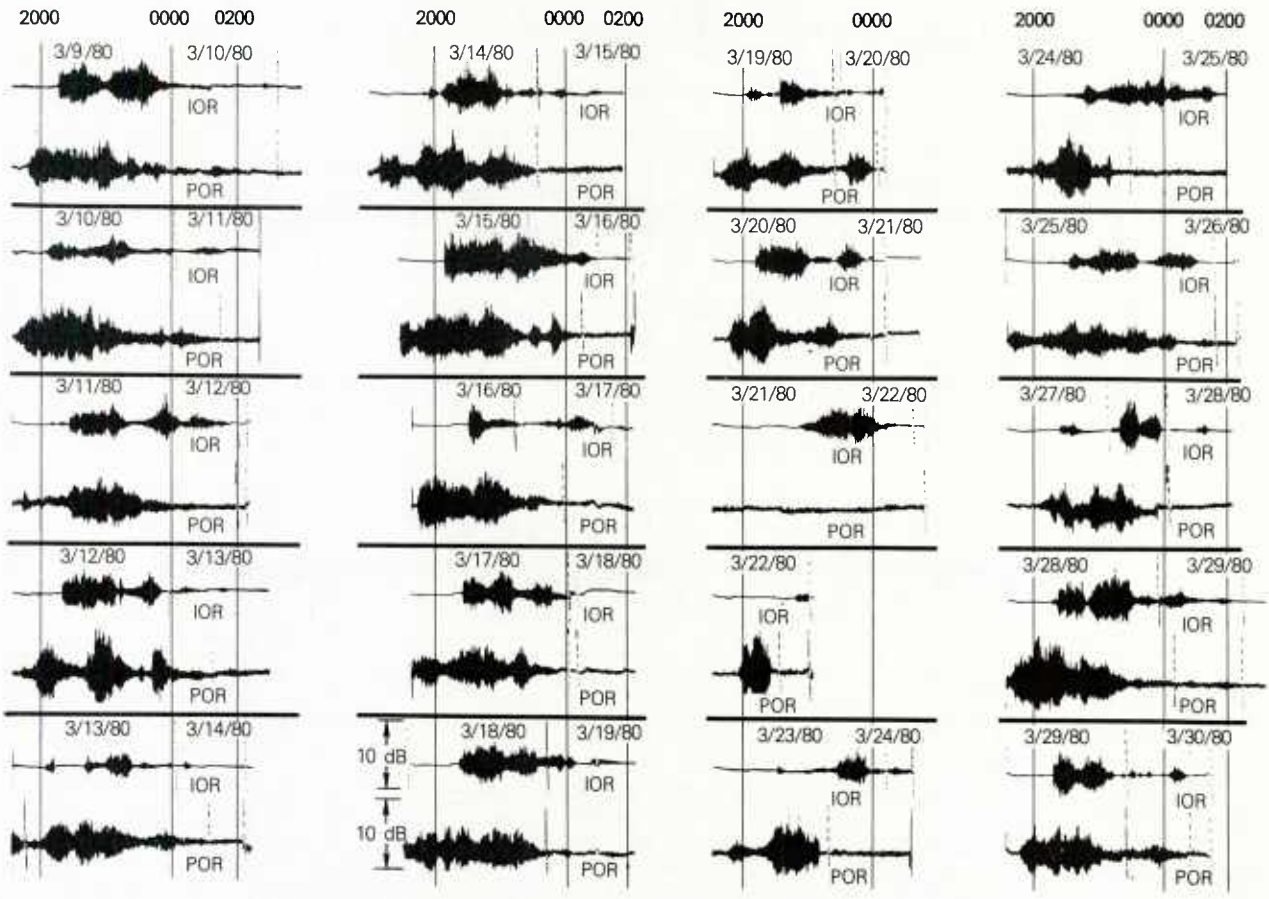

Figure 1. Monthly Glance at Ionospheric Scintillations in March 1980

Except for the evening of March 21, 1980, when the IOR link only scintillated, the monthly glance clearly suggests that scintillations usually occurred on both links and lasted from 3 to 5 hours in at least one link. This behavior had not been observed in earlier years when sunspot numbers were much lower (Fang, D. J., 1980). Obviously, ionospheric disturbances responsible for gigahertz scintillations are stronger, larger, faster, and of longer duration during years of high solar activity than during years of low to medium solar activity.

Figures 2 and 3 provide records of two ionospheric scintillation events in March 1979. The fluctuation patterns of the two carrier signals from the IOR satellite are well correlated, irrespective of the up-link paths (i.e., whether the signals are from Singapore or from Thailand). This is also true for the fluctuation patterns of the two POR satellite signals. This correlation has proved valid for data collected over the year, suggesting that ionospheric scintillations observed from an earth station are predominantly down-link phenomena.

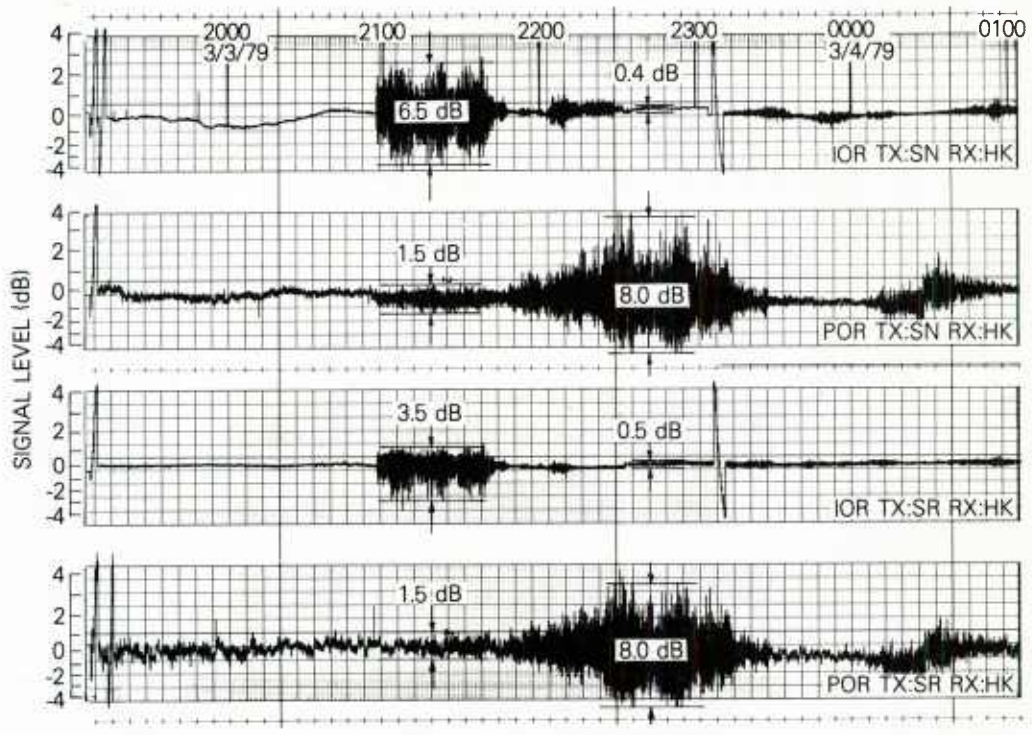

Figure 2. Records of Ionospheric Scintillation on March 3-4, 1979

Figure 2 shows that the IOR link scintillated before the POR link, which is rare for a year of maximum solar activity. Before 2200 hours local time, significant scintillation occurred in the IOR link, while the POR link had only low-level fluctuations. Furthermore, the IOR scintillation started suddenly without any precursor. These features are typical for years of low solar activity (Fang, D. J., 1980). IOR scintillation lasted almost an hour and then faded quickly. A separate and obviously uncorrelated scintillation event occurred along the POR link at about 2200 hours. The signal fluctuation enhanced itself gradually until it reached a magnitude of about 8 dB peak-to-peak. The event lasted slightly more than an hour and was followed by another minor event with peak-to-peak fluctuations of 3 dB.

Figure 3 represents the majority of events observed during solar maximum years. The following typical characteristics are noted:

a. Scintillations occurred on both links. Although the onset times of the two links were not simultaneous (they differed from a few minutes to 2 hours), the scintillations nevertheless overlapped for a significant length of time (from 20 minutes to several hours). The two links are separated at an F-max height (400 km altitude) of about 1,700 km, suggesting that ionospheric disturbances, which created irregularities causing ionospheric scintillations, may have scales on the order of at least 1,000 km.

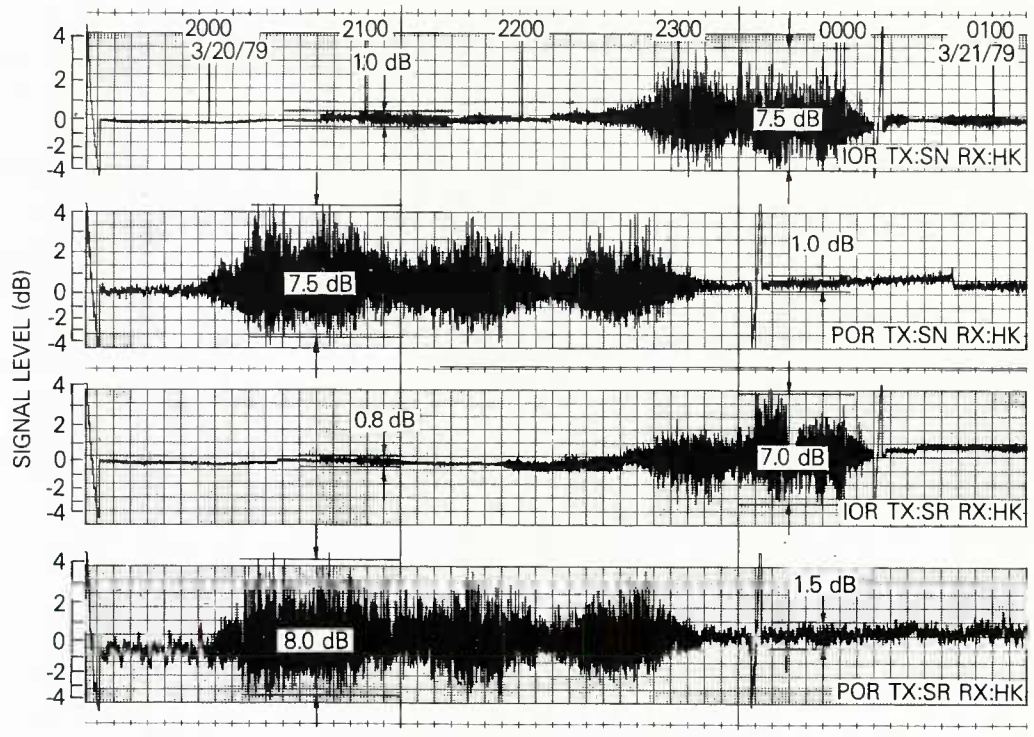

Figure 3. Records of Ionospheric Scintillation on March 20-21, 1979

b. Most scintillations did not erupt suddenly, but with a noticeable gradual increment of fluctuations as precursors. Frequently, the scintillations were intermittent for an entire evening; they were not confined to 2 to 3 hours as those observed in previous years. Individual fluctuation events lasting more than 2 hours along at least one link were common.

c. Because of the precursor, it is difficult to identify the exact onset time of a scintillation event. However, the majority of events, as represented by Figure 3, clearly show that the POR link scintillated much earlier than the IOR link, and the time delays of scintillations between the two links varied from a few minutes to 2 hours. This indicates that gigahertz scintillation is an ionospheric sunset phenomenon, and that the time delays are associated with the ionospheric sunset times at altitudes of 200 to 400 km, where F-region irregularities are known to be present under disturbed ionospheric conditions.

d. An extensive effort was made to correlate the scintillation patterns between the two links with a proper shift of time scale to accommodate the time delays. Detailed correlations between the links could not be established; hence, it was concluded that the scintillations along the two links were independent events. Recent observations by Aarons et al. (1980 and 1981) suggest that, although the disturbances may have a spatial scale as large as 2,000 km and a time scale of several hours, and travel with the ionosphere from east to west in line with the local sunset, the specific irregularities responsible for scintillations nevertheless exhibit much smaller spatial scales and are relatively short-lived.

FADING CHARACTERISTICS OF INDIVIDUAL EVENTS

To quantify the severity of signal fluctuations for individual events, scintillation indices S_4 are derived according to the following equation:

$$S_4^2 = \frac{\langle I^2 \rangle - \langle I \rangle^2}{\langle I \rangle^2} \qquad (1)$$

where I is the intensity of the signal (the signal level in linear scale after conversion from log scale in dB as shown in Figures 2 through 4) and < > indicates ensemble averages. These averages are performed based on an ergodic assumption, and each S_4 value is generated from either a 3.5- or a 1-minute segment of data sampled at 10 Hz.

The values of S_4 for IOR and POR links for the two events shown earlier are plotted in Figures 4a, 4b, 5a, and 5b, respectively. Consecutive 1-minute segments of data were used to further evaluate autocorrelation functions and their power spectrum densities. In such evaluations, the 1-minute sample size is no longer adequate; 3.5-minute segments of data must be used. Values of n of f^{-n}, which is the high-frequency asymptote, or the roll-off slopes of power spectrum densities, are plotted in Figures 4c and 5c. The decorrelation time, τ, in seconds, which is the time required for the normalized autocorrelation function to drop from unity to one-half, is plotted in Figures 4d and 5d. Selective power spectrum density profiles are shown in Figure 6, which also provides appropriate values of S_4, f^{-n}, and τ.

The level of S_4 never exceeds 0.5, as shown in Figure 4a, 4b, 5a, and 5b. Theoretically, it can be assumed that the scintillations observed were weak, and hence that the weak scattering theory [Rufenach, 1972; Singleton, 1974; Briggs and Perkins, 1963] developed earlier for VHF and UHF scintillations is still applicable. The validity of such an assumption remains to be determined.

Assuming a power law spectrum of refractive index fluctuations with the exponent equal p equal to 4, weak scattering theory predicts an f^{-3} high-frequency asymptote of the power spectrum density. Such a theoretical model is generally consistent with observed data of UHF ionospheric scintillations [Crane, 1976]. For scintillations at 4 GHz during years of low to medium solar activities, when peak-to-peak fluctuations never exceeded 4 dB, the power spectrum density had an f^{-3} asymptote [Fang, 1980]. However, in the present cases shown in Figures 4c and 5c, the values of n for f^{-n} are most frequently and significantly higher than 3. For the POR link, n's are generally between 4 and 5; for the IOR link, n exhibits wider fluctuations with a majority of cases ranging from 3 to 4.

The above finding is not surprising. Many measurements at gigahertz frequencies have revealed that the high-frequency asymptote can indeed be steeper than f^{-3} [Rino and Owen, 1981; Basu and Basu, 1981] when scintillations are intense. In particular, the L-band measurements at Ascension Island, which is located near the crest of southern equatorial anomaly, reported an f^{-6} relationship for many cases of strong scintillations [Basu and Basu, 1981]. Researchers have attempted to interpret the steepening of f^{-n} by various theories, most of which involve the concept of strong scattering and/or multiple scattering [Briggs, 1980; Yeh and Lin, 1982; Rino and Owens, 1981]. Thus, it is not clear whether these theories can be used to interpret the scintillations reported here with S_4 less than 0.5.

Most of the theories referred to in the preceding paragraph would produce a desired feature that the steepening of f^{-n} is a result of pronounced scintillations. This feature is also evident from Figures 4 and 5, which compared n with S_4 for either POR or IOR. On the other hand, when the tabulated values of n and S_4 are checked, the relationship between the two is not evident. Curves 1, 2, and 10 exhibit nearly the same intensity at $S_4 \sim 0.27$, yet the values of n differ considerably. Curve 6 represents more scintillations than that of curve 11, yet the latter case exhibits a steeper frequency asymptote. Curves 3, 4, 7, and 12 have low-level fluctuations, and the roll-off slopes are somewhat random. Examination of the curves, either for comparable S_4 (curves 1 and 2; curves 4 and 5) or for substantially different S_4 (curves 8 and 9; curves 10 and 12), reveals that the patterns and the roll-off behavior are, by all means, intuitively similar. There are indications that equatorial irregularities may have two component power-law spectra with a shallower slope for a scale larger than 1 km and a steeper slope for smaller sizes [Yeh and Liu, 1982]. Further investigations are under way to determine if the observed spectra can be better explained by the two component spectra.

Besides the steepening of the high-frequency asymptote, another effect often reported in the literature when the scintillation level increases is the low-frequency broadening for the power spectrum densities, i.e., the expansion of the Fresnel frequency [Basu and Basu, 1981; Rino and Owen, 1981]. There were also reports of the opposite findings, i.e., the reduction of the Fresnel frequency as scintillation increases [Rufenach, 1975]. If it is assumed that scintillations are produced mainly by irregularities with sizes smaller than the Fresnel size, that the height in the ionosphere where those irregularities are concentrated remains fixed, and that irregularities drift across the antenna receiver beam at a constant speed, then the weak scattering theory will not suggest any broadening. On the other hand, based on a certain physics on the evolution of scintillations and geometrical configurations of the irregularities, it is

possible to argue that correlation distances for irregularities could change, that height may increase or decrease, and that most importantly, the drift velocity may vary by a factor of 3. The weak scattering theory can then be used to explain either the broadening or narrowing of the power spectrum densities depending how the calculation is made. For $S_4 > 0.5$, the broadening, which is frequently observed, can be interpreted as a result of signal decorrelation in the multiple scattering processes [Yeh and Lin, 1982].

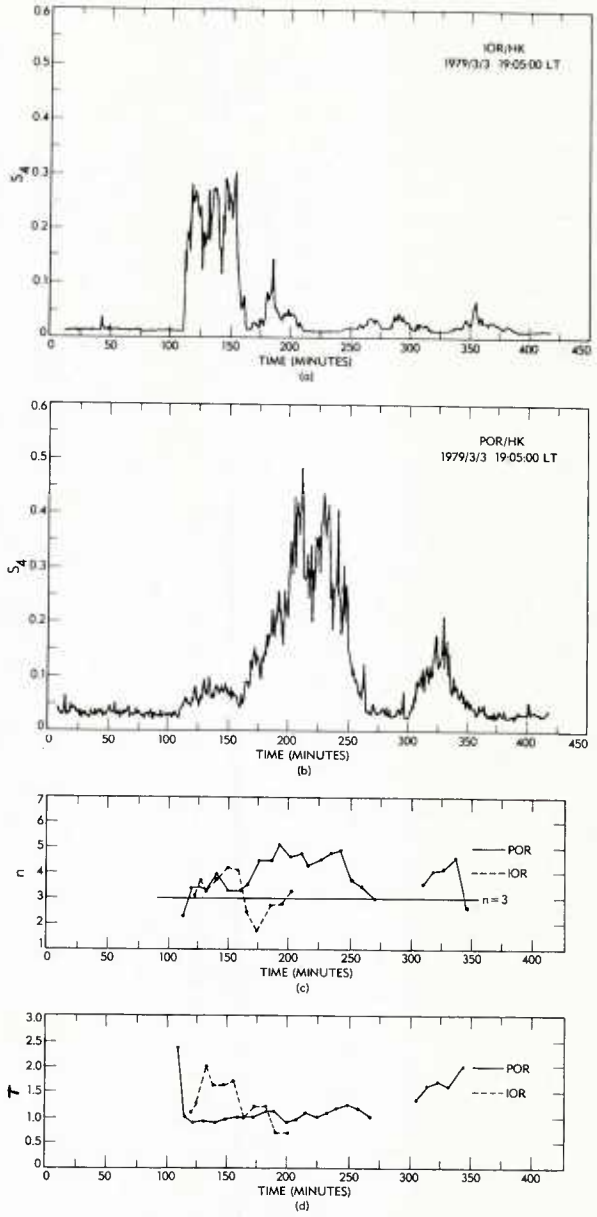

Figure 4. Signal Fluctuation Statistics for the Event Starting 19:05:00 Local Time on March 3-4, 1979

a. IOR Scintillation Index
b. POR Scintillation Index
c. Slope n of Power-Law Spectral Density (f^{-n}) Only
d. Decorrelation Time τ in Seconds

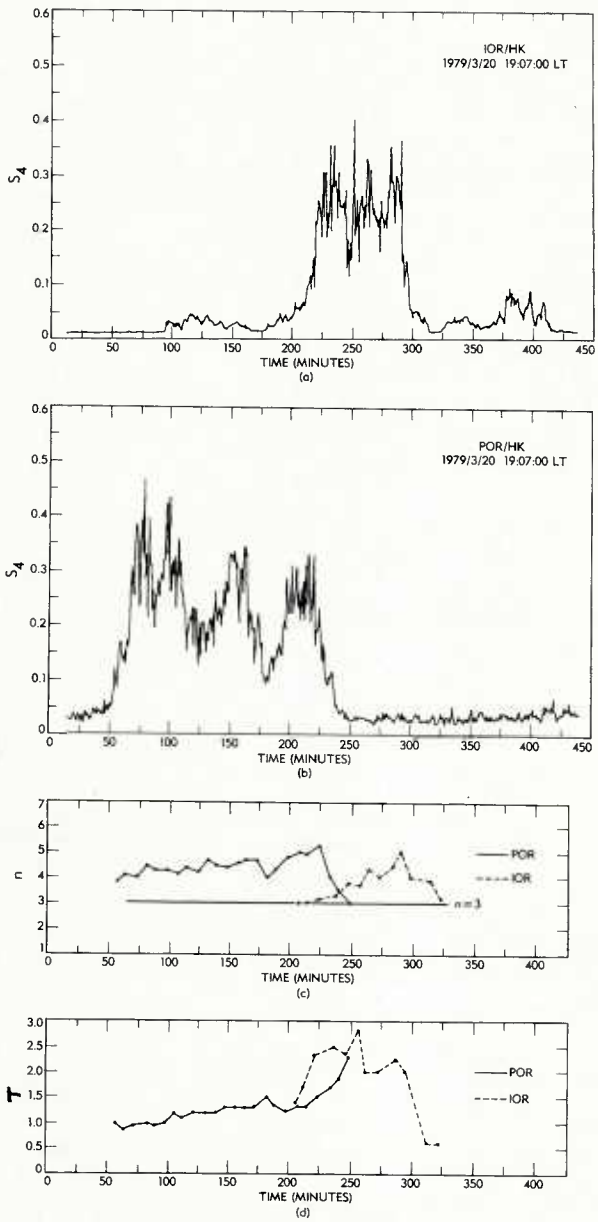

Figure 5. Signal Fluctuation Statistics for the Event Starting 19:07:00 Local Time on March 20-21, 1979

a. IOR Scintillation Index
b. POR Scintillation Index
c. Slope n of Power-Law Spectral Density (f^{-n})
d. Decorrelation Time τ in Seconds

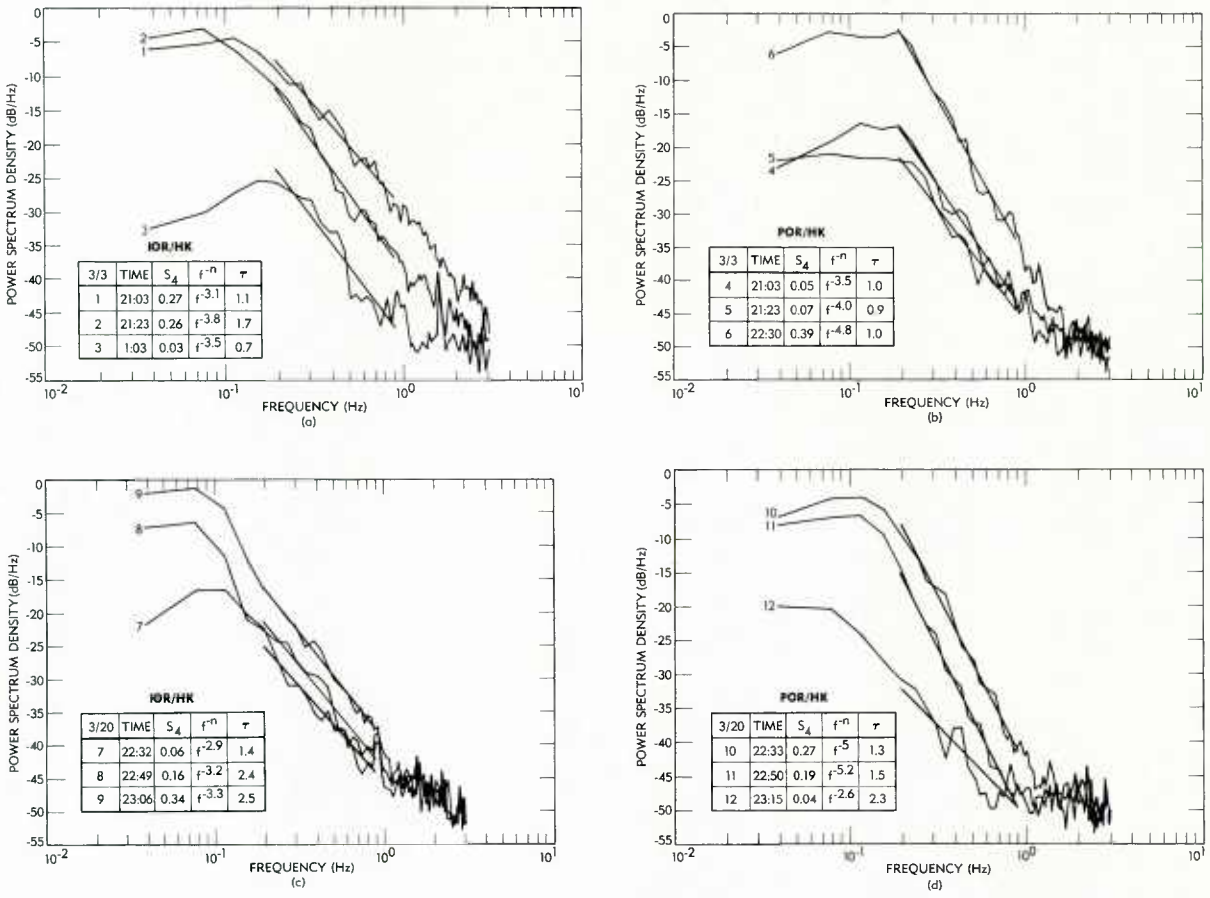

Figure 6. Power Spectra Densities and Roll-off Slopes in Straight Lines for March 1979

a. IOR, March 3-4; b. POR, March 3-4; c. IOR, March 20-21; and d. POR, March 20-21.

The present data contain examples of both spectrum narrowing and spectrum broadening, as shown in Figure 6c and 6d, respectively. In most cases, such as those shown in Figure 6a and 6b, the conclusion of whether the spectrum is broadening or narrowing is obviously subjective. For objectivity, the decorrelation time τ has been plotted as shown in Figures 4d and 5d.

The broadening effect will result in a decrease of τ, and vice versa. Most of the data in Figures 4d and 5d show that scintillations are correlated by a time scale of 1 to 2 seconds. The value of τ for the IOR from a 110- to a 160-minute period for the evening of March 3, and from a 200- to a 320-minute period for the evening of March 20 shows an obvious increase when signal fluctuation activity is in progress, suggesting spectrum narrowing rather than broadening. The POR patterns are similar, yet much milder. The most noticeable fact about the two figures is that decorrelation time for the IOR link is consistently higher than that for the POR link, if the data are compared on the basis of S_4. This point was also stressed in an earlier paper that studied the same phenomena in Hong Kong using a different data base [Fang and Pontes, 1981].

There is no apparent reason to assume that the irregularity configuration along the POR link is different from that of the IOR link, particularly in terms of height and drift velocities. The only differences between the two links are their respective elevation angles and angles between horizontal drift direction and propagation path. Based on Table 1, it can be deduced that the difference in elevation angles will result in a 20-percent difference in Fresnel size, and that the difference in relative angles will result in a 50-percent difference in transverse drift velocities. Both differences are additive and will suggest a 70 percent higher decorrelation time for the POR link than that for the IOR link. This is in direct contrast with the findings presented in this paper. A plausible explanation of this contradiction has yet to be offered. It may relate to the vertical drift velocity of the irregularities, an aspect often not considered in weak scattering modelings.

CUMULATIVE STATISTICS OF SCINTILLATION

For communications applications, the cumulative statistics (i.e., the percentage of time in a year, and in a worst month, that ionospheric scintillations exceed a given level) are crucial for link design. These statistics are needed to establish the system margins that ensure the desired link quality. Annual statistics of ionospheric scintillations are provided in Figure 7, where POR and IOR beacon signals are represented by solid and dashed lines, respectively. In addition to the four sets of annual statistics covering March 1977-March 1978, October 1977-October 1978, November 1978-November 1979, and June 1979-June 1980, statistics collected in two earlier measurements are also given: March 1975-March 1976 as measured in Hong Kong, and June 1976-June 1977 as measured in Taipei. It can be readily concluded that ionospheric scintillations are closely correlated with solar activities.

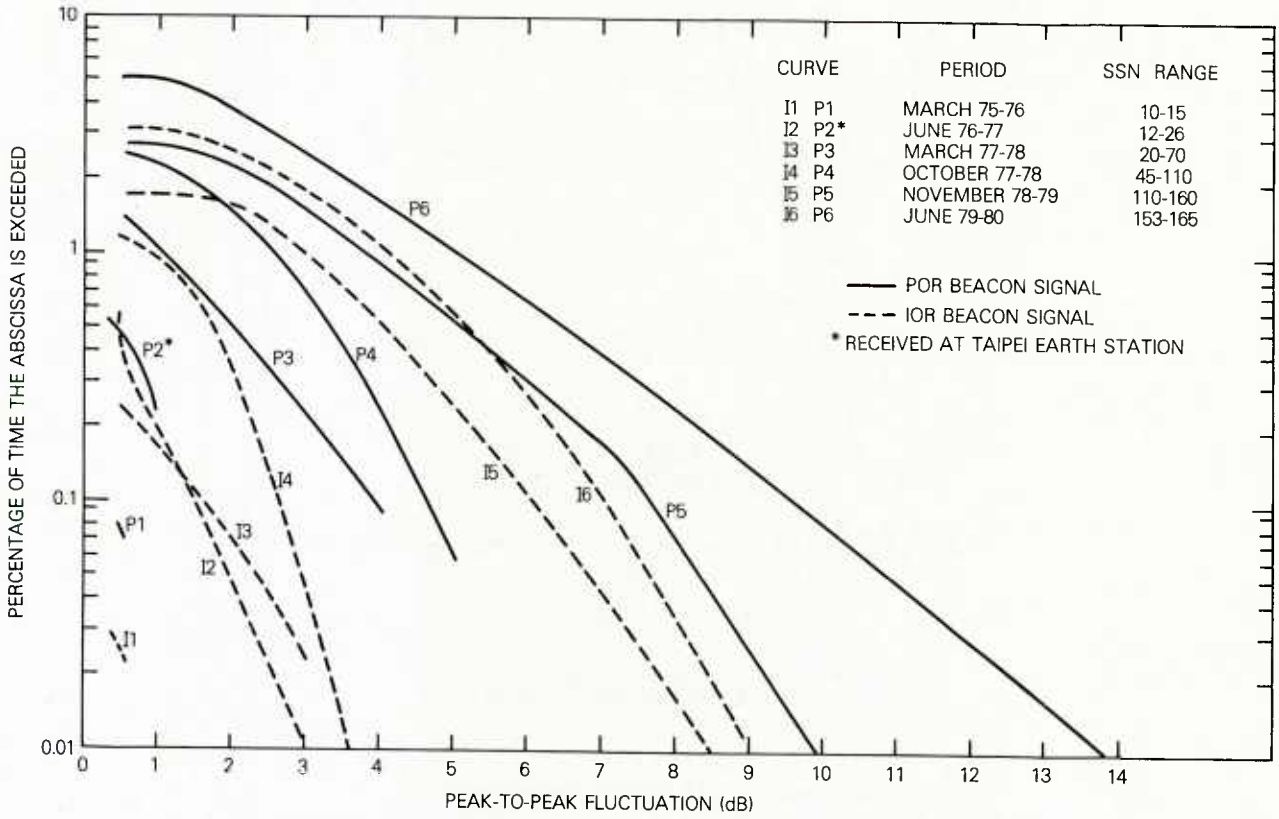

Figure 7. Annual Statistics of Ionospheric Scintillations at Hong Kong Earth Station

To examine this correlation further, the occurrence of scintillations was evaluated in terms of the percentage of time in a year during which peak-to-peak signal fluctuations exceeded 1.0 dB, as a function of the monthly averaged Zurich sunspot numbers for past and present INTELSAT ionospheric scintillation programs. For each program, upper and lower bounds of occurrence are established based on the maximum and minimum percentages of occurrence monitored in the multiple-carrier channels. The bounds of the abscissa are the maximum and minimum monthly sunspot numbers observed. Figure 8, which gives a summary plot, suggests a log-linear dependence of the scintillation occurrence on sunspot numbers for the years in which the maximum sunspot number is less than 70. A gradual saturation appears as the sunspot number exceeds 70.

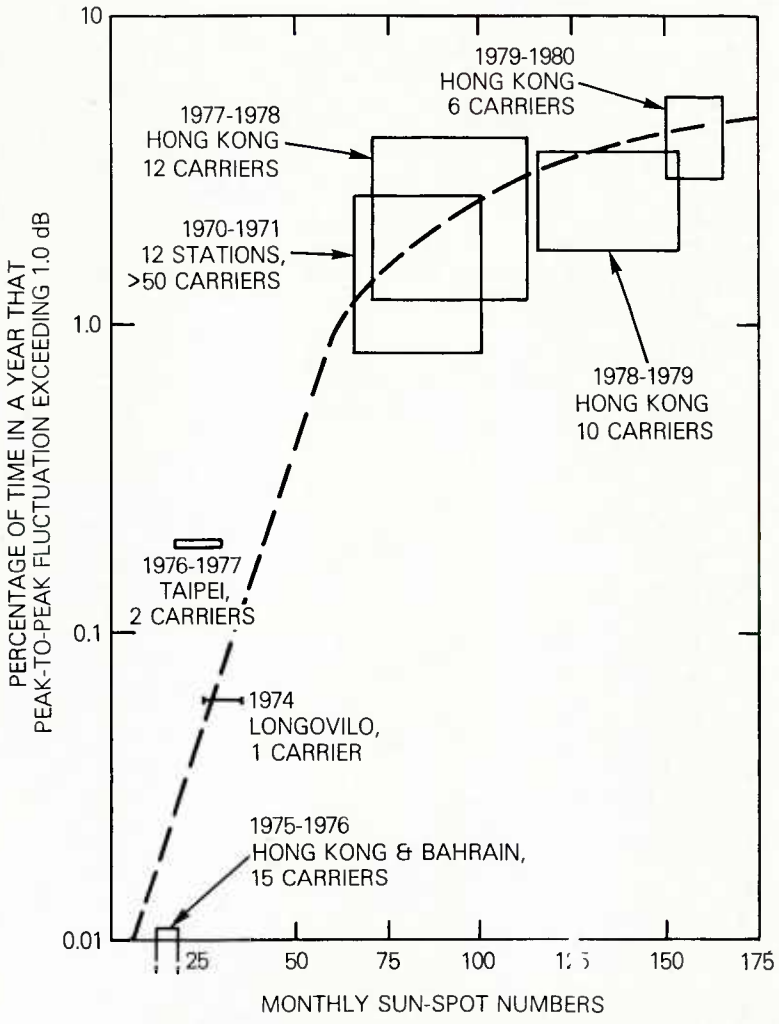

Figure 8. Dependence of 4-GHz Equatorial Ionospheric Scintillations on Monthly Averaged Zurich Sunspot Numbers

In digital communications systems, outages caused by the loss of synchronization and the time required to restore it are critical. To establish an outage condition, a typical CCIR criterion is that the mean 1-minute value of the bit-error rate should not be worse than 10^{-4} for more than 0.3 percent of the time in any month [Fang, D. J., Kennedy, D. J., and Devieux, C., 1978]. Consequently, in addition to annual statistics for ionospheric scintillations, worst-month occurrence statistics are also essential.

The worst month can be defined either as the worst calendar month or as the worst 30 days. The worst calendar month is a month in which the maximum minutes of peak-to-peak signal fluctuations are equal to or greater than 0.5 dB, the minimum detectable level of ionospheric scintillation. The worst 30 days is a continuous 30-day period covering major scintillation events with the highest magnitude of peak-to-peak fluctuations in the entire year. For years of low and medium solar activity, when the scintillation level is low to moderate, worst-month statistics for both definitions differ substantially; this would yield substantial differences in assessing the impact on a digital communications system [Fang, 1980]. In solar maximum years, such discrepancy does not exist. For either definition, March is the worst month for 1979 and for 1980. In both, ionospheric scintillations occurred almost every evening and maximum peak-to-peak fluctuations were registered.

The worst-month statistics for March 1980 are shown in Figure 9, along with annual statistics and "4.4/1 conversion" statistics for comparison. The 4.4/1 conversion is an engineering rule used when worst-month statistics are not available to convert annual statistics into monthly statistics, or vice versa. According to this rule, the annual percentage exceedance for a given scintillation level is multiplied by 4.4 to derive the

worst monthly percentage exceedance for the same scintillation level. Figure 9 shows that this rule generally underestimates scintillation by approximately 1 dB of the actual worst-month statistics.

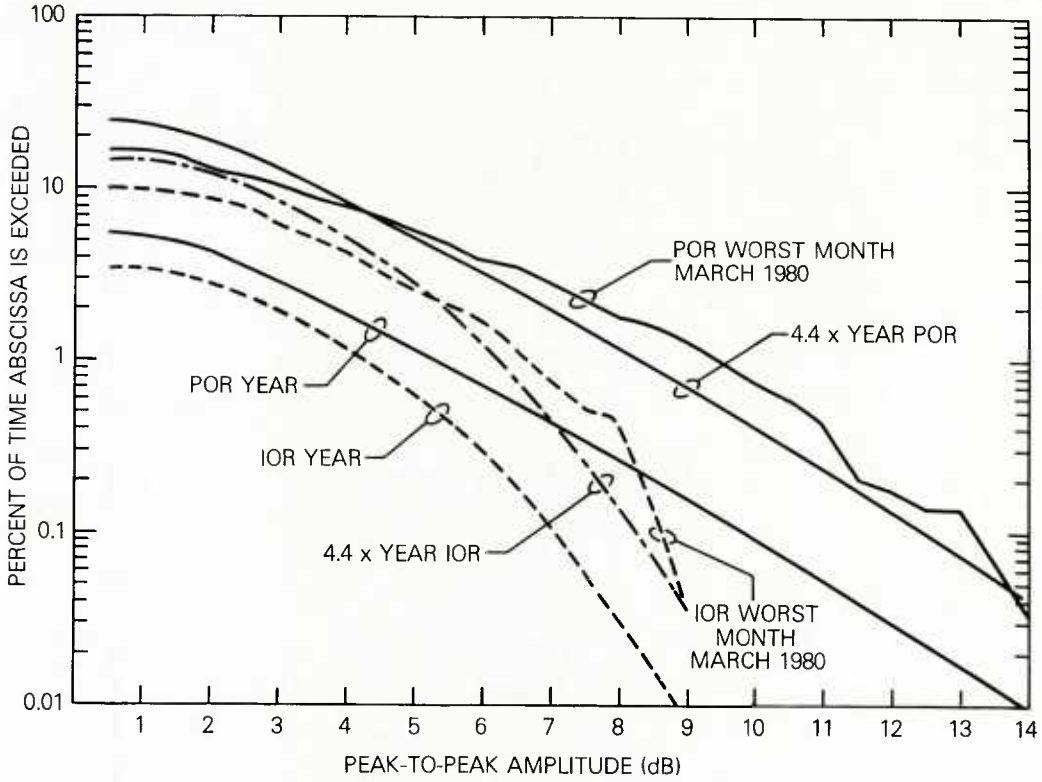

Figure 9. Worst-Month Statistics and 4.4/1 Conversion Statistics at Hong Kong Earth Station

The diurnal variation of ionospheric scintillation is shown in Figure 10, which clearly indicates that ionospheric scintillations occur after local sunset. For the POR link, activity starts around 1800 hours local time, increases drastically with time, and peaks between 2000 to 2200 hours. Activity decreases gradually through midnight, then drops off quickly in the early morning after 0200 hours. The pattern for the IOR link is similar, but has a time lag of approximately 1 hour.

Although a scintillation event can begin at any time in an evening, the fact that onset occurs only after local sunset suggests that the occurrence of an ionospheric event is directly associated with the local sunset condition in the ionosphere. Consequently, diurnal and seasonal variations of ionospheric scintillations should not be assessed against local time at the receiving station, but rather against a time differential relative to the local sunset time of the F-region ionosphere. A detailed modeling effort is in progress.

CONCLUSIONS

Ionospheric scintillation measurements at Hong Kong from 1977 to 1980 coincided with the solar maximum period of the current solar cycle 21. During 1979 and 1980, scintillations were observed for approximately 100 evenings, much longer than in previous years. Satellite beacon signals with maximum peak-to-peak fluctuations of 14 dB were observed. Simultaneous observations of signals from the POR and IOR satellites provided a rare opportunity to examine ionospheric scintillation on a scale of 2000 km. Scintillations frequently occurred on both links, usually with fluctuations starting first in the POR. The onset time delays varied from a few minutes to 2 hours. The S_4 index for all the scintillation events are below 0.5. Power spectra revealed that the high-frequency asymptote of f^{-n} with $n = 3$ is no longer valid. Values of n are consistently between 4 and 5 for the POR link and generally between 3 and 4 for the IOR link. Decorrelation times are between 1 to 2 seconds, increasing with the increase of S_4.

Solar cycle dependence is evident when cumulative statistics are compared for six consecutive 1-year periods. Worst-month statistics provide correction criteria for the empirical 4.4/1 conversion rule used for system engineering applications.

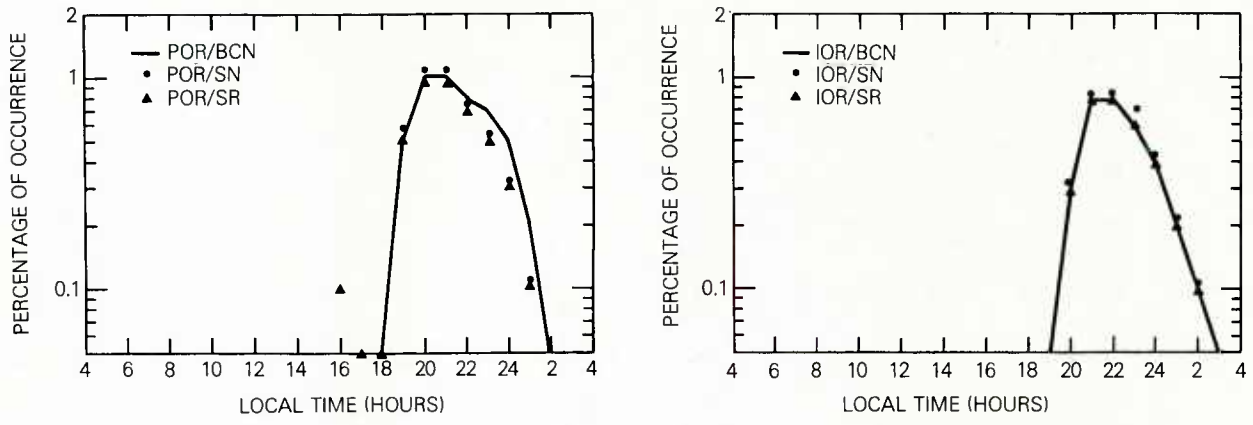

Figure 10. Diurnal Variations of Ionospheric Scintillations at Hong Kong Earth Station

ACKNOWLEDGMENT

This work is sponsored by the International Telecommunications Satellite Organization (INTELSAT) as well as by an internal corporate R&D program at COMSAT Laboratories. Views expressed in this paper are not necessarily those of the sponsors.

REFERENCES

Aarons, J., Mullen, J. P., Whitney, H. E., and McKenzie, E. M., 1980, "The Dynamics of Equatorial Irregularity Patch Formation, Motion and Decay," Journal of Geophysical Research, Vol. 85, pp. 139-149.

Aarons, J., Whitney, H. E., MacKenzie, E. M., and Basu, S., 1981, "Microwave Equatorial Scintillation Intensity During the Current Solar Maximum," Radio Science, Vol. 16, pp. 939-945.

Basu, S., and Basu, S., 1981, Equatorial Scintillations--A Review, Journal of Atmospheric and Terrestrial Physics, 43, 473.

Briggs, B. H., and Parkins, I. A., 1963, "On the Variation of Radio Star and Satellite Scintillations with Zenith Angle," Journal of Atmospheric and Terrestrial Physics, Vol. 25, p. 339.

Crane, R. K., 1976, "Spectra of Ionospheric Scintillation," Journal of Geophysical Research, Vol. 81, 1976, pp. 2-41 to 2-50.

Fang, D. J., 1980, "4/6 GHz Ionospheric Scintillation Measurements, AGARD Conference Proceedings No. 284, Propagation Effects in Space/Earth Paths, pp. 33-1 to 33-12.

Fang, D. J., 1981, "C-Band Ionospheric Scintillation Measurements at Hong Kong Earth Station During the Peak of Solar Activities in Sunspot Cycle 21," Proceedings of III Ionospheric Effect Symposium, Paper 3A-2, pp. 1-12.

Fang, D. J., Kennedy, D. J., and Devieux, C., 1978, "Ionospheric Scintillations at 4/6 GHz and Their System Impact," EASCON-78 paper, IEEE Pub. No. CH1352-4/78/0000-0385.

Fang, D. J., and Pontes, M. S., 1981, "4/6 GHz Ionospheric Scintillation Measurements During the Peak of Sunspot Cycle 21," COMSAT Technical Review, Vol. 11, No. 2, pp. 293-320.

Fang, D. J., Tseng, F. T., and Calvit, T. O., 1982A, "A Low Elevation Angle Propagation Measurement of 1.5 GHz Satellite Signals in the Gulf of Mexico," IEEE Transactions on Antennas and Propagation, Vol. AP-30, pp. 10-15.

Fang, D. J., Tseng, F. T., and Calvit, T. O., 1982B, "A Measurement of the MARISAT L-Band Signals at Low Elevation Angles On-board Mobile Aero," IEEE Transactions on Communications, Vol. COM-30, pp. 359-365.

Rino, C. L., and Owen, J., 1981, "On the Temporal Coherence Loss of Strongly Scintillating Signals," Radio Science, 16, pp. 31-33.

Rufenach, C. L., 1972, "A Power-Law Wavenumber Spectrum Deduced from Ionospheric Scintillation Observations," Journal of Geophysical Research, Vol. 77, pp. 4761-4772.

Singleton, D. G., 1974, "Power Spectra of Ionospheric Scintillations," Journal of Atmospheric and Terrestrial Physics, Vol 36, pp. 113-133.

Taur, R. R., 1974, "Ionospheric Scintillation at Frequencies Above 1 GHz," COMSAT Technical Review, Vol. 4, pp. 461-476.

Taur, R. R., 1976, "Simultaneous 1.5- and 4-GHz Ionospheric Scintillation Measurements," Radio Science, Vol. 11, pp. 1029-1036.

Yeh, K. C., and Liu, C. H., 1982, "Radio Scintillations in Ionosphere," IEEE Proceedings, Vol. 70, No. 4, pp. 324-360.

DISCUSSION

J.Arnbak, Ne

In your presentation, you stated that coding may provide a solution to digital communication by TDMA in the presence of ionospheric scintillations. Please explain how this should be carried out, considering the typical de-correlation time of 1.5 sec quoted by yourself. (This is many TDMA frames, and also much more than the delay of 400 msec allowed by CCITT for telephone circuits.)

Author's Reply

I meant coding together with interleave. The essence is the buffer size which really limits the bit transmission rate, as you mentioned.

H.Soicher, US

Are GHz scintillations prevalent at equatorial regions only?

Author's Reply

No, certainly it exists in the auroral zone. I should have mentioned that.

J.T.Ong, UK

There is significant evidence to indicate that the scintillations recorded are due to "ionospheric effects". However, it would be useful to look very selectively at simultaneous radiosonde data to see the effects of the troposphere.

Author's Reply

I agree. In fact the signature of ionospheric scintillation and tropospheric scintillations are separable. Their spectrum properties, their occurrence patterns and Fresnel sizes are very different. At 4 GHz, we do observe ionospheric scintillation, mixed with tropospheric scintillation. The magnitude of the latter is, however, much lower, say at most 3 dB peak-to-peak.

SUMMARY OF SESSION V

INTERFERENCE CONTROL AND INCREASE IN CHANNEL CAPACITY

by

Dr E.Lampert
Session Chairman

Only where interference between links separated either by geographical or frequency separation can be closely controlled, it is possible to increase the capacity of a network of links within a specified geographical/space area. The interference mechanisms between communication links have to be therefore closely modelled, which has been done in the papers by **Gott**, **Hughes** and **Lane**, **Sullivan**, and **Segner**. Based on these propagation data one can enter into the design of new systems and amendments to present systems. These aspects have been covered by **Niemeyer et al.**, **McManamon** and **Hanson**, and **Arnbak et al.**, who studied characteristics and improvement of antennas whereas **Galpin** and **Tou** have emphasized the signal design.

Gott clearly points out, as the ambition of the operator of HF-links is to use optimum frequencies of transmission from a propagation point of view, this leads to the well known situation that mutual interference of links is highly probable. Based on extensive measurements, he shows means of frequency planning which take these effects into account.

Hughes presents planning data for VHF links considering interference due to anomalous propagation conditions in particular ducting and scatter. This however restricts the model to certain climatic areas.

Segner describes methods and philosophies used in an US-Army development program using propagation data for the specific problems associated with military tactical frequency management. The paper therefore does not restrict itself to a particular frequency region. **Sullivan** discusses interference between links via satellites placed in the already very crowded geostationary orbit using a shared frequency band.

Niemeyer et al. present an approach to decrease the fading margin in VHF-LOS systems by using steerable narrow beam antennas in order to decrease the necessary amount of transmitted power.

McManamon and **Hanson** in their paper compiled sidelobe data of presently existing LOS SHF-High Gain Antennas and extracted models which can be used in calculation of interference as well as in the selection of the actual antenna system.

Arnbak et al. show means of improving the sidelobe characteristics of existing satellite ground antennas by installing auxiliary feeds and combining these signals with the main one.

In troposcatter systems mutual interference and that with LOS systems has always been a problem, which will increase because of digitalization and the requirement of maintaining the number of channels. **Galpin** in his paper therefore describes methods to restrict the bandwidth of the digitally modulated signal to a minimum considering also technical constraints in systems.

As multipath is one of the major sources of self-interference in a system, the communication engineer community is always looking for methods to suppress these effects. **Tou** describes the capabilities of Spread Spectrum Systems with respect to this effect emphasizing specular reflected components only.

NEW ASPECTS IMPROVING THE AVAILABIIITY OF DIGITAL LOS-RADIO RELAY LINKS DEDUCED FROM WIDE-BAND MEASUREMENTS AT 5 AND 15 GHz

M. Niemeyer, W. Schwarz, B. Sommer
Siemens AG
Hofmannstr. 51
8000 München 70
West Germany

SUMMARY

Multipath propagation causes interference on line-of-sight radio relay links and results in amplitude and envelope delay distortion of the received digital signals. The spectral behaviour of these multipath effects is of special significance.

This paper will first describe a frequency sweep method based on recordings of broadband amplitude distortions which were continuously performed over a period of two years. Measurements have been carried out on a 60 km path in the 5 and 15 GHz frequency range. The relative measuring bandwidth was 2 and 3 %, respectively.

The analysis of the records revealed two important results:
First, the statistical consideration of the long term experiments yields to a prediction about the availability of digital radio links as a function of the occupied bandwidth provided, that no additional diversity measures are used.
Second, the analysis of the determined coherence bandwidth allows a physical interpretation of the interference phenomena. The model of a dominating 3-path propagation found by these experiments could be proved with the aid of a high-directive, tracked antenna system (3 dB-beamwidth approx. 0.3 degree) in the 15 GHz frequency range.

The knowledge of the multipath mechanism during fading is the basis of a low-cost antenna system to improve the availability of wide-band digital radio links.

1. INTRODUCTION

Planning point-to-point ground based communications systems in the visual range (LOS, Line of sight) starts with making path profiles. Taking into consideration the bulge of earth and the refractive index of the air such a path profile, as shown in Fig. 1, indicates whether the planned LOS-section is suitable for transmission or not. Dependent upon the limited antenna beam width transmission energy is not exclusively reaching the receiving antenna over the shortest rectilinear path, but also over longer reflection paths, for instance the surface of the earth. The receive signal is than composed by vectorial addition of all partial waves being concerned.

The supervision of such signal components leads to amplitude and delay distortions as function of frequency caused by the different time delays. For the simplest case there are only two different dominant propagation paths. This may be illustrated by a two-path model. Fig. 2 shows the amplitude and time

delay distortions for two rays having a time delay of τ = 3.8 ns and an amplitude difference of Δa = 7.9 and 1.4 dB, respectively. This situation leads to typical amplitude variations with deep notches. The difference in frequency between two notches is called coherence bandwidth and may be calculated from the time delay τ as

$$B_c = \frac{1}{\tau} .$$

Those distortion influence the analog transmission technique, for instance FDM, only insofar as they introduce a reduction of the signal-to-noise ratio. If in a communications system large RF-bandwidths are needed with regard to the coherence bandwidth, the distortions may be compensated by sufficient high fading reserves and therefore lead only to increasing intermodulation noise.

In high speed digital systems, however, the error rate due to distortion cannot be influenced by improving the signal level. In addition one can generally say that multilevel modulation techniques used for getting a smaller RF-spectrum turn out to be much more sensitive to amplitude distortions with respect to two-level modulation techniques. Reduction of multipath effects is possible by using diversity euipment. But, the high investments for double links or additional receiver systems are disadvantageous.

The investigation of distortion caused by multipath propagation and their compensation by means of additional devices has been the major goal of our studies.

2. SPECTRAL INVESTIGATION ON A LOS-MEASURING LINK IN THE 5 and 15 GHZ FREQUENCY RANGE

2.1 Description of the Measurements

The data required for the statistical evaluation have been obtained by two long time experiments. The measuring link was running from Munich in north-east direction over a distance of 60 km. The path profile in Fig. 1 shows, that we have a rather unfavourable radio link hop, partially running over urban area as well as over wet low ground with various rivers. For reliable registration of the fading parameters caused by meteorological effects a frequency sweep technique has been used having the following characteristics:

- high sweep rate (10 Hz)
- large frequency range (100 MHz at 5 GHz and 400 MHz at 15 GHz)
- high dynamic range (more than 50 dB)
- continuous link supervision
- computer-aided data acquisition
- low-residual error of the measuring system.

The block diagram of the principal experimental set-up is shown in Fig. 3. While the transmit site was fairly simple realized, the receive site required a high sophisticated receiver synchronization and data recording. The measuring task principally includes the following steps

- all 30 seconds one sweep with a sweep time of .1 sec.
- temporary storage of the frequency and level information
- comparison of the new amplitude level with the previously stored level. If the difference exceeds a given level range the complete data will be stored.

Fig. 4 shows the relative receive level as function of frequency. While in the upper part of the figure the spectral propagation conditions were highly constant over several hours in the center part of the figure frequency-selective fading were registered, lasting approx. 10 minutes.

2.2 Extraction of the Model Parameters

At the beginning of our statistical evaluation the assumption of two-path model (Fig. 2) proved to be correct. With the aid of a computer-aided simulation a curve-fitting for each recorded data file has been made. The parameters of the two-path model have been varied such, that the squared deviation between the simulated function of propagation and the measured data became a minimum. The tight compliance of the measured values and the values being approximated is shown in Fig. 5. An error calculation has been made showing that the relative error for the important range of system-critical amplitude distortions ($A\,a > 5$ dB) was very low (~ 10 %), Fig. 6. Therefore the two-path model was applicable here.

2.3 Statistics of the Model Parameters

The automated time acquisition is also of great importance for the statistical evaluation. Besides the amplitude and frequency values the time data belonging to these values have been stored on each data file. Thus, it is possible to get information on the dwell time of certain propagation modes. Table 1 shows the various measuring conditions at 5 and 15 GHz.

Frequency	5 GHz	15 GHz
Time of record	Oct. 79...Apr. 80	Nov. 80...May 81
Measuring time	2436 h	3243 h
Number of data files	1501	3910

Table 1 Measuring conditions

The results were analyzed under different view aspects to get a comprehensive picture of the effective propagation mechanism at 5 and 15 GHz as there are

- the diurnal occurance of the frequency-selective fading
- the dwell time for classes of certain coherence bandwidths and amplitude distortions, relative to the overall measuring time (Fig. 7, Fig. 8)
- number of occurance and its mean dwell time of the classes defined above
- probability of occurance
- correlation between the mean receive level and the depth of the frequency-selective fadings
- probability of amplitude distortions assuming that a system with a certain bandwidth is being run on a communications link (Fig. 9)

The results shown in Fig. 9 seem to be of particular importance. They show a simple way of calculating the availability of digital LOS-systems, provided the maximum tolerable amplitude distortions were known. Considering for instance a QPSK-system with a data rate of 34 Mbit/s (bandwidth approx. 20 MHz) and tolerable amplitude distortions of 6 dB max. the communications Link under consideration will have a failure rate of 10^{-4}. Increasing the transmit power will not improve the availability. This can only be achieved with diversity techniques, adaptive equalizers or tracked antenna systems. The results in

Fig. 9 are in good agreement with those of Greenstein and Prabhu (1979) in [1]. For equal length of link and for a 45 Mbit/s-QPSK-system at 6 GHz (bandwidth: 24.6 MHz) a system availability of 10^{-3} is given.

Evaluating the measurements with respect to the different seasons (summer/ winter) the curves given in Fig. 9 showed an unessential displacement.

3. PHYSICAL INTERPRETATION OF THE MEASUREMENTS

In addition to statistical investigations the experiments should also deliver a reliable picture of the propagation behaviour on LOS-links in the microwave region. Reliable system planning requires that a true nature model of the tropospheric wave propagation is available.

3.1 Transmission Characteristics Deduced from the Measurements

Before a physical interpretation of the formation of the frequency-selective fadings is given, the most important results of the measurements should be summarized:

- frequency-selective fading has been observed only during short time intervals (30 to 60 minutes) in both twilight and night times
- selective fading appears only together with broadband low receiving levels
- the notch depth grows with decreasing mean receive level
- amplitude decrease appears not only in conjunction with selective fading (flat fading condition)

3.2 Three-Way Model

Change of amplitude level at the receiver site may rise from shadowing losses caused by the k-factor's deviation from nominal $k = 4/3$. This leads to slowly changing events which are not correlated to a certain day time. Ray reflections at inversion layers are of much greater influence on the LOS-propagation. Fig. 10. Such inversion may be produced near the soil (ground-based inversion) or in heights of up to 1000 meters above earth.
(Fehlhaber, L., Giloi, H. G. 1976, [2])

For the fading depth of the resultant receiving signal first of all the reflection characteristic of the inversion layer as well as the angle of arrival at the layer is responsable. Thus, in the case of ground-based layers mostly strong echo-signals occure with low differences of time delay to the direct radio path, causing heavy fadings with large coherence bandwidth (> 1 GHz).

Echo signals from high inversion layers usually have low amplitudes with great delay differences. For calculating the phase difference between the direct and the reflected path a geometrical model has been used, described by Ruthroff in [3].
The relation beween the radiation angle, the height of inversion layer, and the resultant coherence bandwidth may then be calculated. The results are graphically shown in Fig. 11 and Fig. 12 for different inversion heights.

Fig. 11 which represents the situation of our experimental link, shows that at 5 GHz for higher radiation angles inversion heights of 200 to 300 m were effective, whereas at 15 GHz for lower radiation angles 150 to 200 m came into consideration.

If we investigate the level of echo signals with high angle of arrival at the inversion layer we get additional loss of more than 10 dB, dependent upon the refractive index (J. Großkopf, 1970 [4]). In this case the echo signal has only minor effect on the resultant receive signal.

If the direct ray interferes with an additional echo signal (from a ground-based inversion layer) having a low delay time difference and nearly the same field strength as the direct ray, then the echo signal from the higher inversion layer will play a dominant role. It then causes heavy frequency selective fadings with small coherence bandwidth if the mean receiving level is low.

With this three-path model the results of our sweep experiments could be evidently interpreted in all respects.

4. EXPERIMENTS WITH CONTROLLABLE ANTENNA SYSTEMS

Several methods are well known and widely used to reduce the multipath effects. For instance space diversity together with various types of RF/IF-combining systems (E. G. Jarvis, 1977, [5]). Some of those systems have the disadvantage of being implemented with great expense (IF-combining with two independent receivers). Other systems use adaptive equalizers. Having in mind the severe ECM (Electronic Counter Measures) conditions in a military communications network we think that equalizers are not the optimum, although they may be effectively used in some commercial systems.

During the development of mobile military digital radio systems we were confrontated with the task of looking for a rather simple and cheap additional equipment working even under severe multipath conditions with sufficient availability. So we have concentrated our efforts upon studies on the antenna side. As mentioned in the introduction the main task is to flaten the frequency response in a broad communication channel, which is disturbed by fading.

In order to find a suitable antenna system several experiments with various antenna configurations have been made.
The first experiment at 15 GHz consisted of electronically shifting the beam of an antenna (diameter: 1.7 m, 3 dB-beamwidth: 0.9°) to ± 1°. Trying to improve the receiving level under fade conditions by tilting the major antenna lobe we almost failed completely. The explanation of this unexpected result was found to be the too small angle of arrival of the reflected ray (typical in the range of 0.1° to 0.4°) in relation to the antenna beamwidth. Thus, discrimination of that part of signal was not possible with the antenna in use.

For a second experiment at 15 GHz two smaller antennas (diameter: 0.6 m, 3 dB-beamwidth: 2°) have been installed at a vertical distance of approx. 90 wave lengths, fed via a 3 dB-power divider and phase shifters in each antenna branch, thus building an interferometer configuration. This configuration, shown in Fig. 13a, yields to an antenna diagram, shown in Fig. 13b with a 3 dB-beamwidth of

$$\vartheta_{3dB} = \arccos\left[1 - \frac{1}{8}\left(\frac{\lambda_0}{h}\right)^2\right] \qquad h/\lambda_0 > 50$$

(h ≙ vertical distance, λ_0 ≙ wave length)

and a null depth of

$$\vartheta_n = \arccos\left[1 - \frac{1}{2}\left(\frac{h}{\lambda_0}\right)^2 (2n-1)^2\right] \qquad h/\lambda_0 > 50$$

For n = 1 and h = 90 λ_0 , $\vartheta_{3\,dB} = 0.32°$ and $\vartheta_{n=1} = 0{,}64°$.

It is interesting to see that for large values of h/λ_0 the antenna diameter of the single antenna is of no influence. Changing the differential phase of the antenna signals I_1 and I_2 by $\pm$ 180° yields to the maximum beam shifting angle of

$$\Delta \vartheta = \pm \arccos \sqrt{1 - (\lambda_0/2h)^2}$$

and is for the example given above $\pm$ 0.32°.

Fig. 14 shows part of a typical RF-level record made at 15 GHz with that antenna system. Note a strong multipath fading of up to -40 dB. Changing the relative phase of the antenna signals automatically between -180° and +180°, thus rotating the antenna diagram to $\pm$ 0.32° causes RF-level improvements to over 30 dB. Continuous phase control would improve the receive level to only 5 dB under normal conditions.

From these experiments the following conclusions can be made:

a. an effective suppression of the multipath fading is possible if antenna systems with electronical beam steering are used. Hereby the first diagram null has to be orientated for one of the interfering incoming rays. It is of no importance whether this antenna system is implemented by the use of suitable multiple feed systems in a single antenna or by use of an interferometer (two antennas).

b. it is of of great importance that the antenna system has sufficient low 3 dB-beamwidth (typical lower than 0.5°) and is controllable in sufficient fine angle steps.

Condition (b) is the reason for the difficulty of developing effective antennas with several feeders (K.-P. Dombek, 1980, [6]). In mobile systems it also seems to be much better using two smaller antennas building an interferometer system than one very large antenna.

5. AN OPTIMUM ANTENNA SYSTEM REDUCING THE MULITPATH EFFECTS

Further studies were undertaken to find an automatic antenna tracking system also working under multipath conditions. Reducing the amplitude distortions caused by multipath ray interference optimum function will be obtained. Thus, if we consider a digital radio system with high bit rates and/or multi-level modulation types, the system must work over a relative broad bandwidth.

Fig. 15 shows the principle block diagram of an adaptive antenna system. Automatic antenna tracking is realized by modulating the phase shifters with a low-frequency ac-voltage thus causing low level modulation of the receive signal. By evaluating phase and frequency of the RF-amplitude modulation with respect to the modulating signal in a phase detector a failure signal and thus a criteria for antenna tracking is generated. This is a well known configuration (U. H. Gysel, 1980, [7]), However, our investigations have shown, that the generated controll criteria is not always sufficient to produce an effective reduction of the amplitude distortions over the entire RF-channel bandwidth. This disadvantage is eliminated with the aid of a further criteria, the eye opening. This criteria, deduced from the receiver between demodulator and regenerator, is fed into a special discriminator and then compared with the modulating signal in a second phase detector. The output of the detector forms

together with the output signal of the first phase detector the complete failure signal for further treatment in the integrator. This component then delivers the control signal for the phase shifters.

REFERENCIES

[1] GREENSTEIN, L. J., PRABHU, V. K.: Analysis of multipath outage with applications to 90 Mbit/s PSK-systems at 6 and 11 GHz. IEEE Trans. on COM 27, No 1, Jan. 1979, pp. 68 - 75

[2] FEHLHABER, L., GILOI, H. G.: Effects of nocturnal ground-based temperature inversion layers on line-of-sight radio links. AGARD Conf. Proceedings No 208, 1976, pp. 9-1 - 9-14

[3] RUTHROFF, C. L.: Multipath fading on LOS microwave radio systems as a function of path length and frequency. BSTJ Vol. 50, Sept. 1971, pp. 2375 - 2397

[4] GROSSKOPF, J.: Wellenausbreitung. Band I, Hochschultaschenbücher-Verlag, 1970

[5] JARVIS, E. G.: The use of phase-control height diversity for 11 GHz digital radio systems. Radio and Electr. Eng., Vol. 47, No 3, 1977, pp. 101 - 104

[6] DOMBEK, K.-P.: Minderung von Mehrwegeschwund durch adaptive Schwenkung der Antennencharakteristik. NTG-Fachberichte, Band 70, 1980, pp. 133 - 138

[7] GYSEL, U. H.: Elektronisches Raumdiversity System für Richtfunk-Anlagen. NTG-Fachberichte, Band 70, 1980, pp. 199 - 205

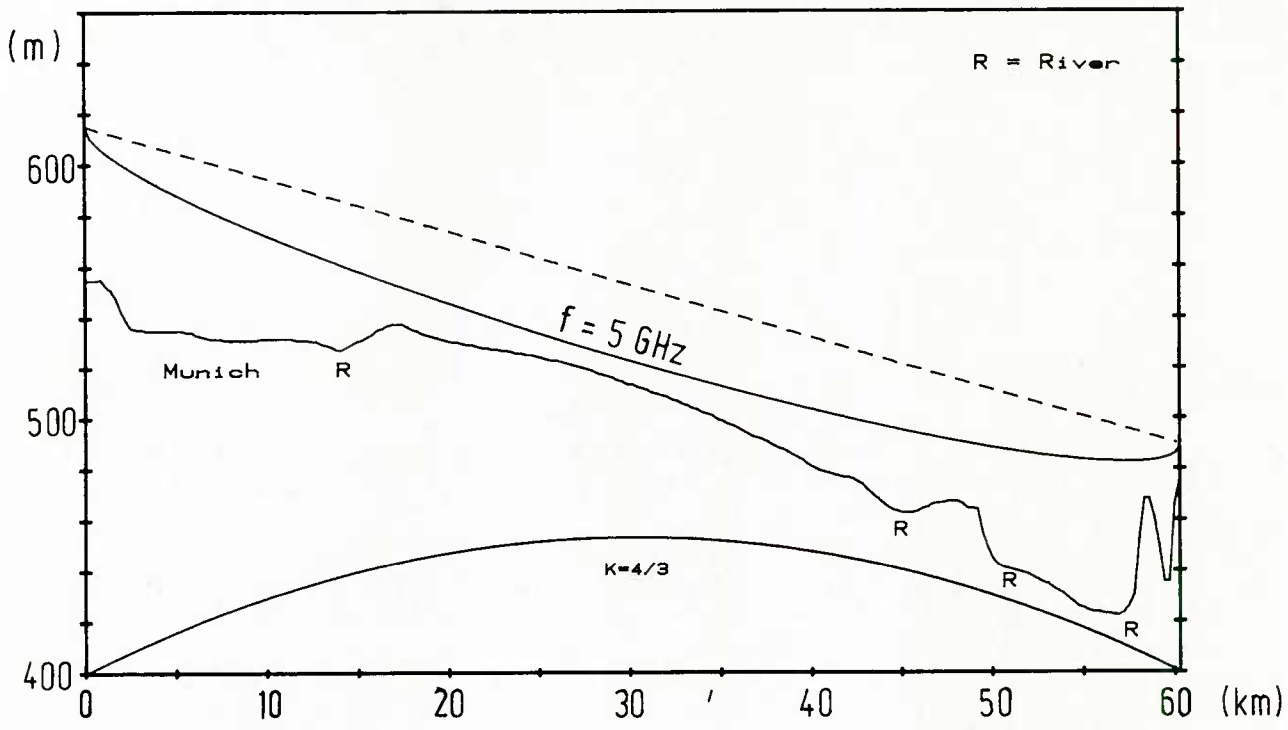

Fig. 1 Microwave Path Profile

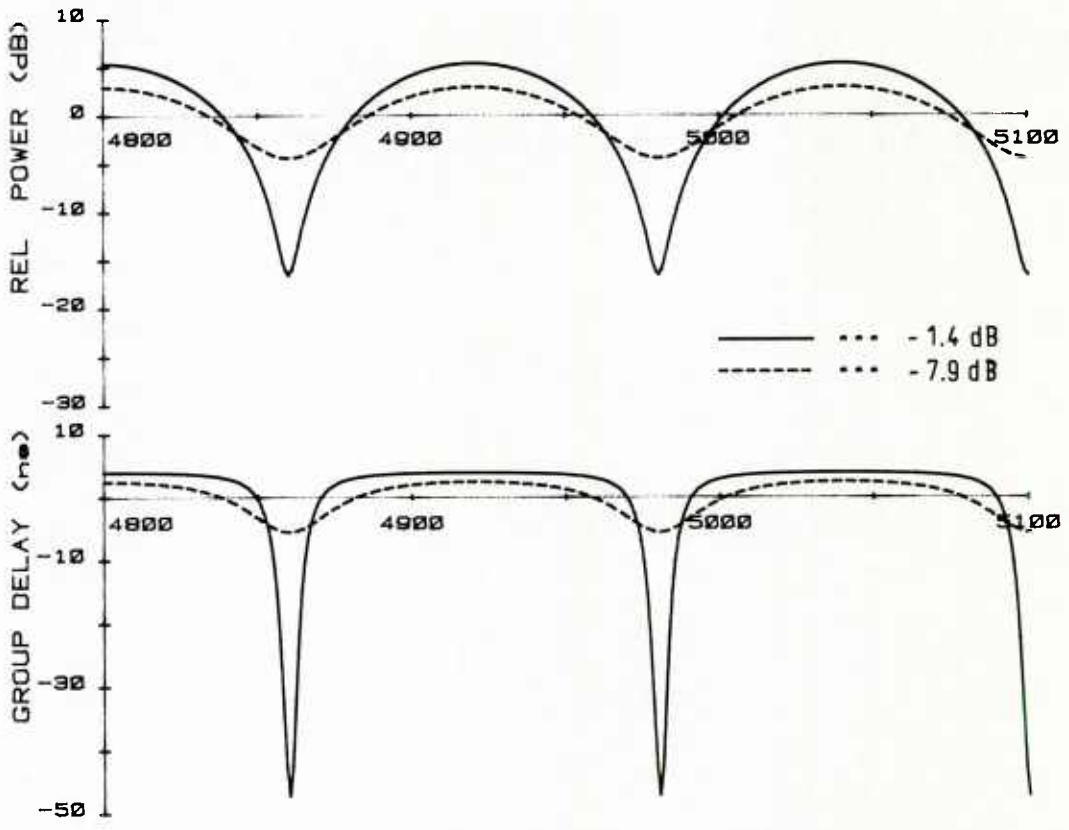

Fig. 2 Amplitude and Delay Distortion (2 Path Model)

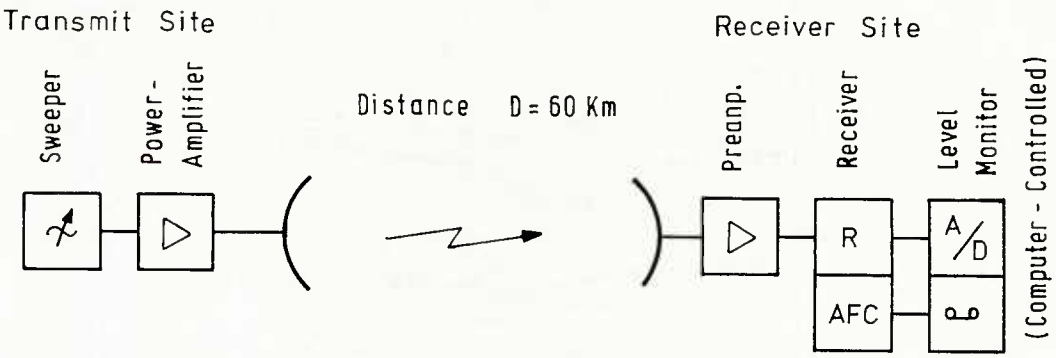

System Parameters :

Frequency	4,9 .... 5,0 GHz	14,8 .... 15,2 GHz
Path Loss (nominal)	142 dB	151 dB
Antenna Diameter	2 m	1,7 m
Beam Width (-3dB)	2,7°	0,9°
Transmitted Power	1 (10) W	10 W
Noise Figure	9 dB	8 dB
Dynamic Range	> 50 dB	> 50 dB

Fig. 3 Measuring System

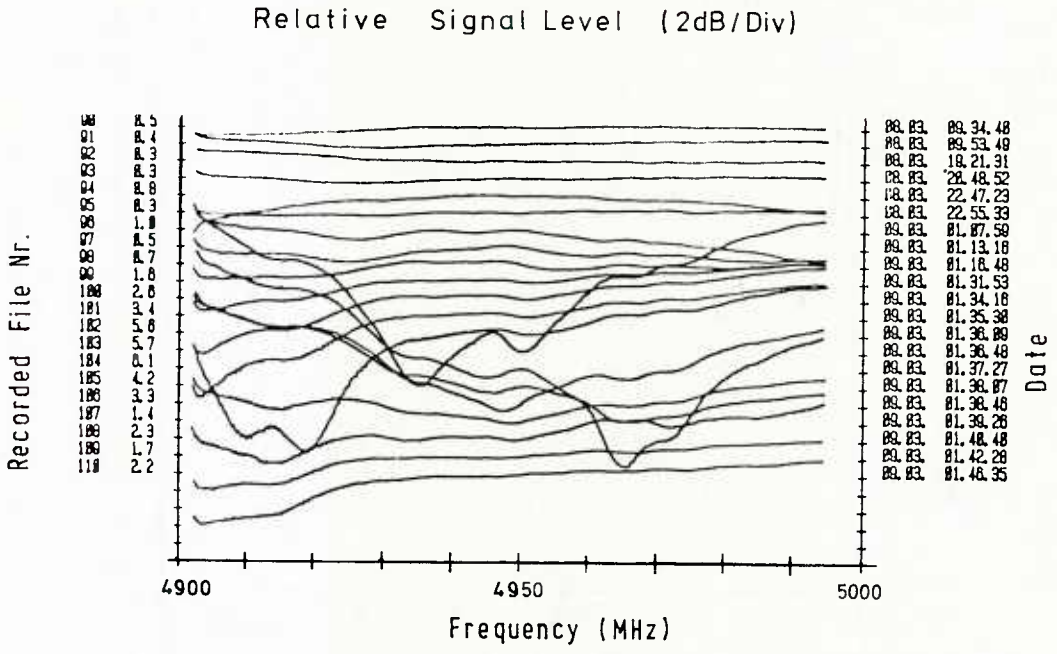

Fig. 4 Relative Amplitude of the Received Signal
(Frequency Selectivity of a Fade)

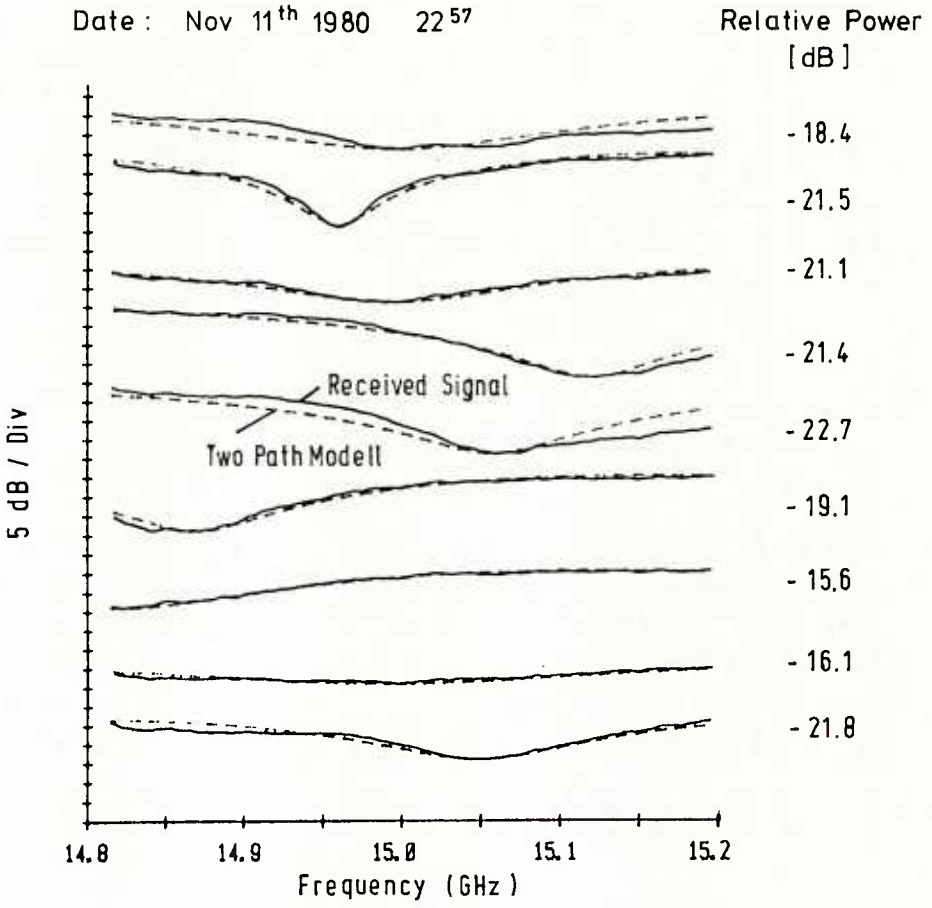

Fig. 5 Computer Simulation for a Two Path Modell
(Curve Fitting)

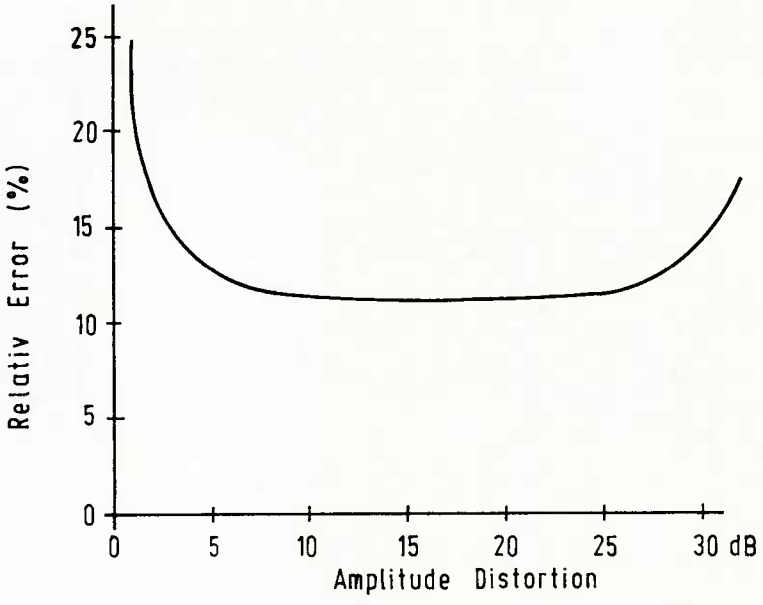

Fig. 6 Error - Function of the Fitting Method

Relative Dwell Time [%]

Notch Depth (dB)	Coherence Bandwidth B [MHz]			
	< 50	50...100	100...200	> 200
< 2	7,6	27,5	35,2	17,1
2...4	0,26	3,8	6,7	0,69
4...6	0,25	0,07	0,27	0,12
6...8	0,07	0,03	0,04	0,05
8...10	< 0,01	0,01	0,02	0,04
> 10	—	0,01	0,03	0,02

Evaluation Time : 2436 hours
(Oct.79... Apr.80)

Fig. 7 Model Parameter Statistics 5 GHz

Relative Dwell Time [%]

Notch Depth (dB)	Coherence Bandwidth B [MHz]			
	< 200	200... 500	500... 1000	> 1000
< 2	10,3	12,4	15,8	0,63
2...4	1,09	5,2	41,3	7,7
4...6	0,03	0,22	1,9	0,9
6...8	0,004	0,01	0,25	0,2
8...10	0,004	0,01	0,11	0,07
> 10	0,028	0,028	0,15	1,46

Evalution Time : 3243 hours
(Nov. 80... May 81)

Fig. 8 Model Parameter Statistics 15 GHz

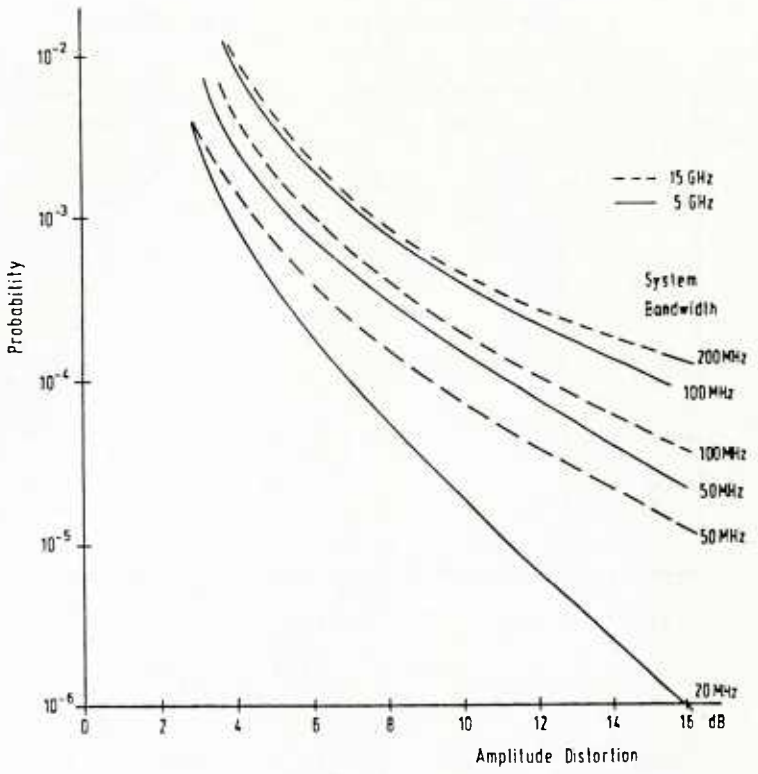

Fig. 9 Amplitude Distortion Statistics for Various System Bandwidths

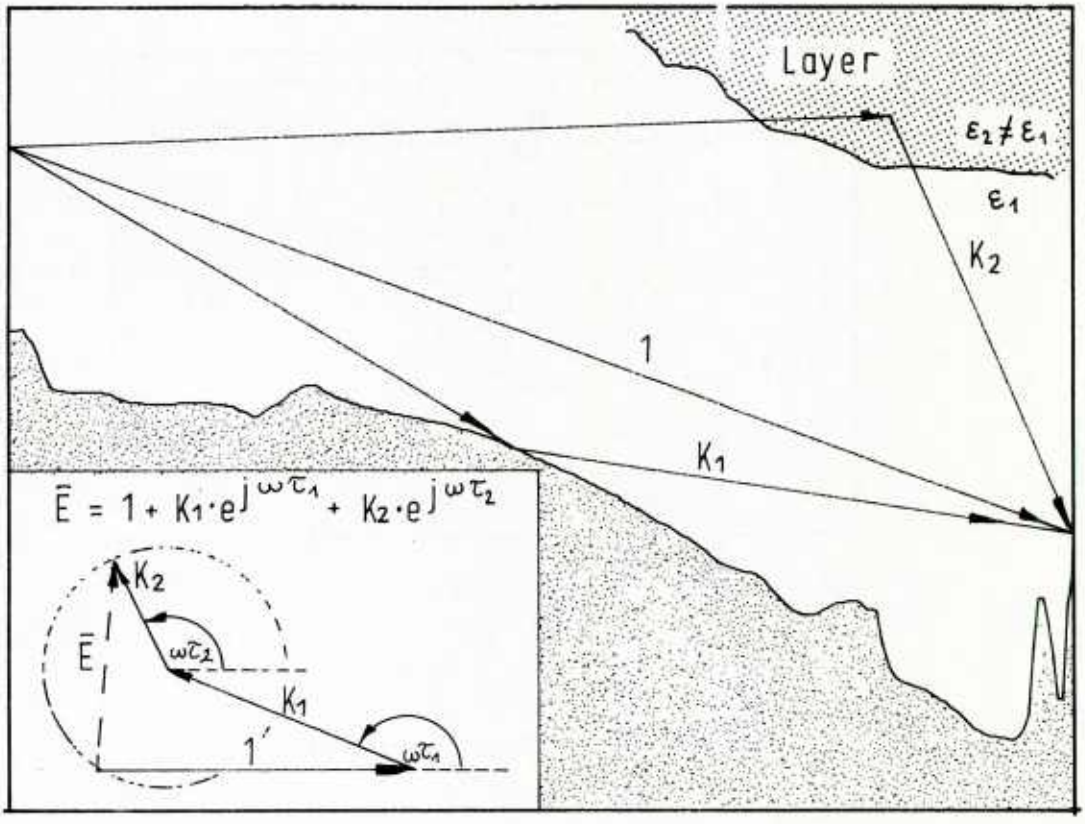

Fig. 10 Physical Interpretation of Measurements by 3-Path Model

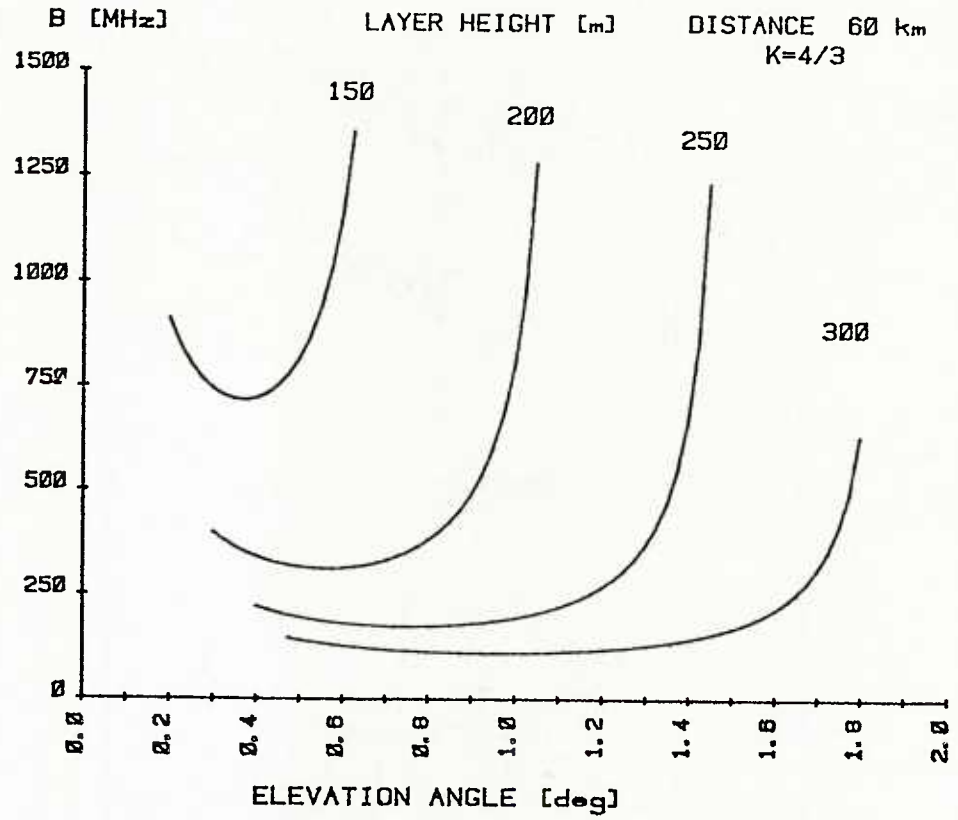

Fig. 11 Coherence Bandwidth as a Function of Elevation Angle for a 60 km LOS Path

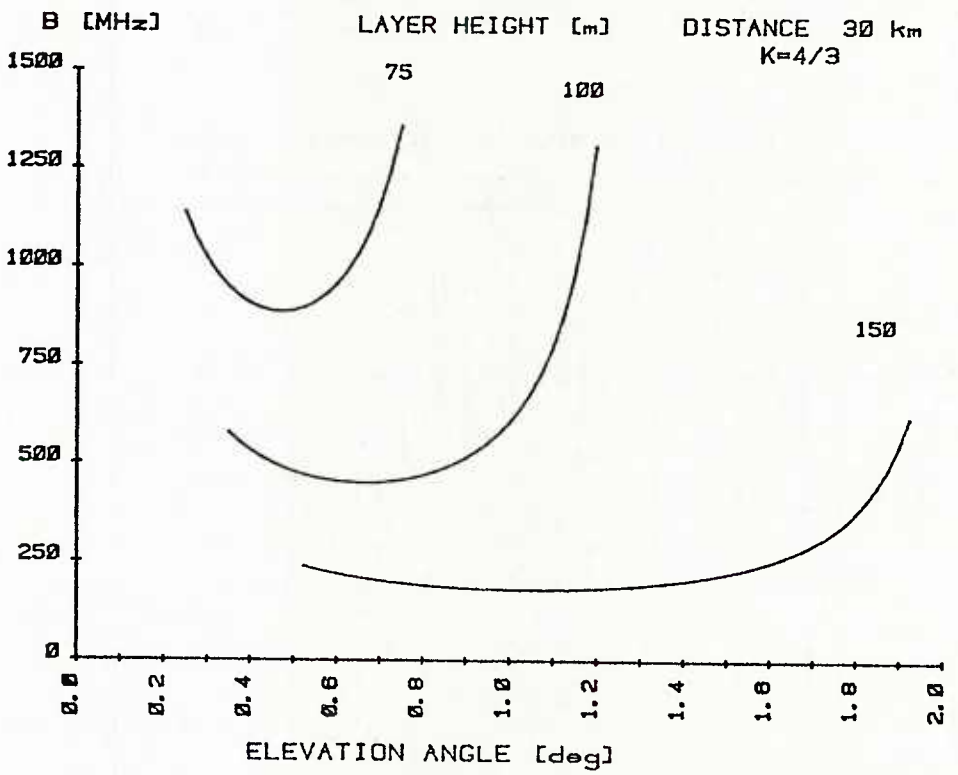

Fig. 12 Coherence Bandwidth as a Function of Elevation Angle for a 30 km LOS Path

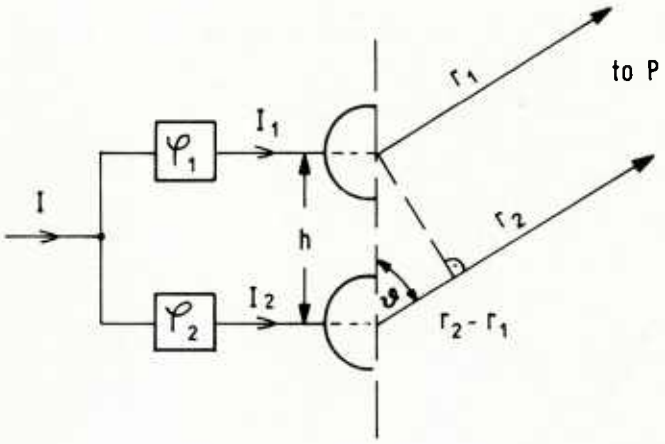

a. Principal Configuration

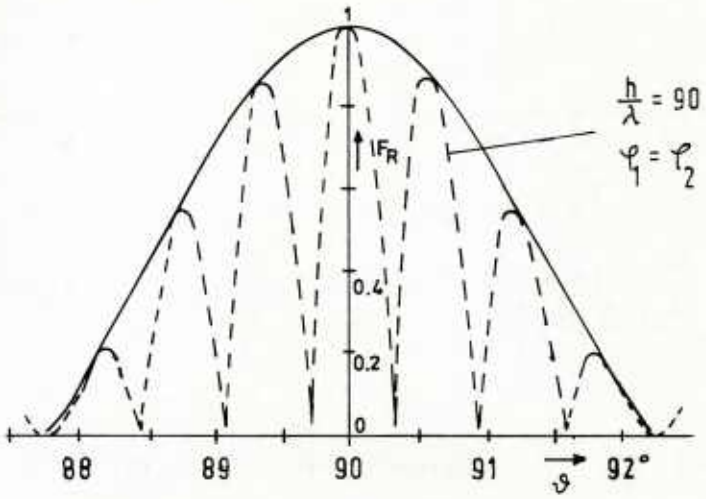

b. Antenna Diagram

Fig. 13 Experimental Interferometer System

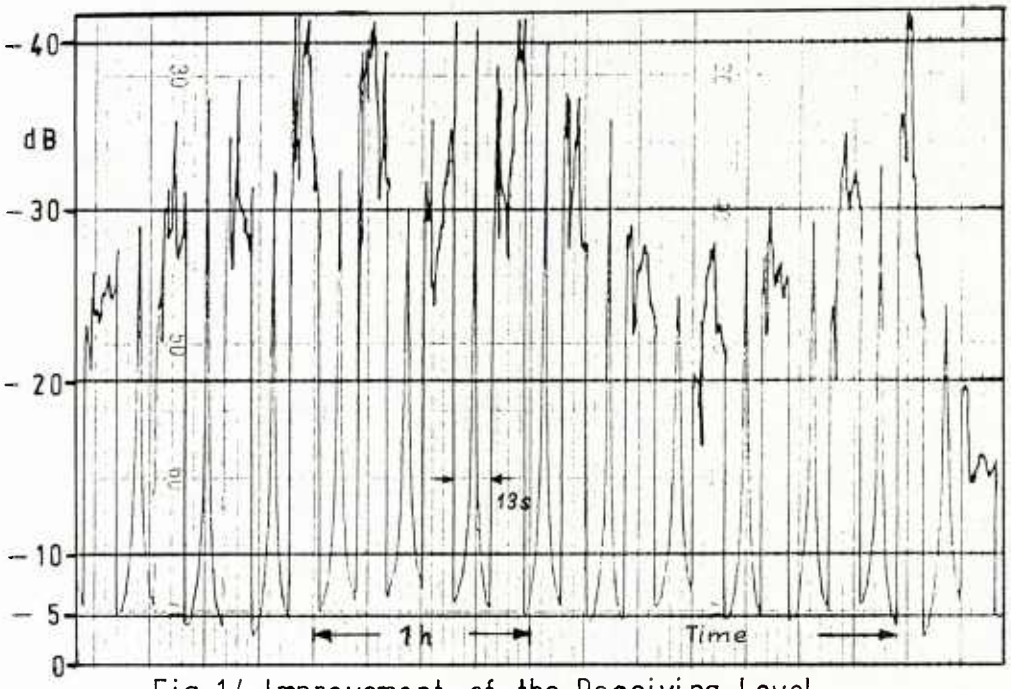

Fig. 14 Improvement of the Receiving Level

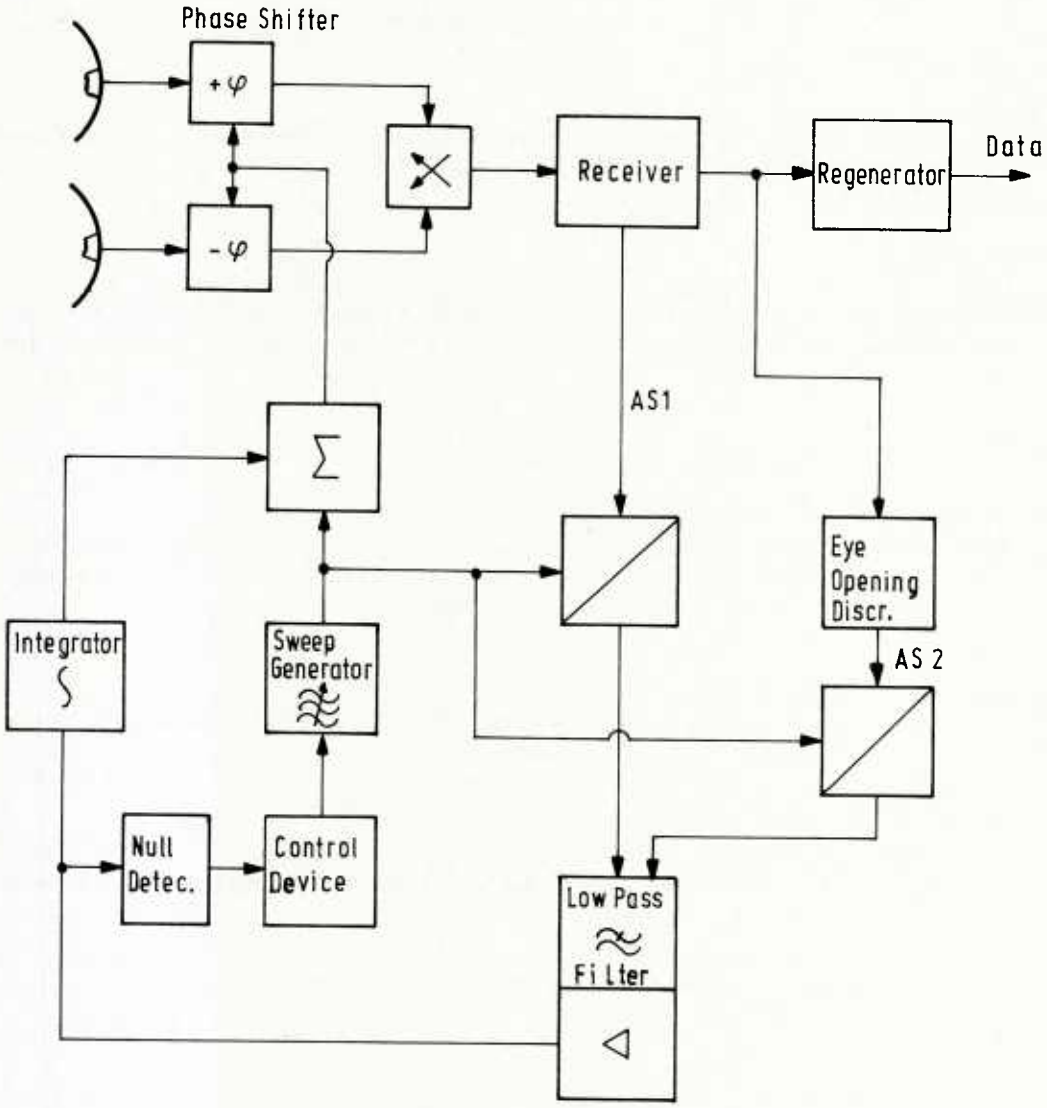

Fig.15 Antenna Tracking System

DISCUSSION

L. Boithias, FR

Votre système de correction utilise deux antennes et des circuits radiofréquence supplémentaires, ce qui peut soulever certains problèmes. Peut-on obtenir un résultat équivalent en opérant seulement des corrections en bande de base?

Author's Reply

In our system we use *one* receiver. For combining in the base band you must leave two independent receiver/demodulator systems. This is rather expensive. At base band there may exist problems of bit storage in a digital radio system. We also think, that combining in the RF-plane cancelling the delayed signal is more effective.

G.H.Hagn, US

Have you considered using more antennas than two?

Author's Reply

Additional antennas, their positioning and tracking is very complicated. We did not make any experiments with more than two antennas. Our measurements show that most of the time it is sufficient to have two antennas in the configuration shown in our paper, to cancel out the interfering signal.

J.T. Ong, UK

(1) I refer to fig.9 of your paper which shows unavailability for a digital system due to selective fading for various system bandwidths. What type of modulation is assumed? For low capacity system or for other (shorter) paths with higher system bandwidth flat fading unavailability could be significant. Should we therefore calculate the unavailability separately for flat and selective fading?

(2) Comment on Mr Hagn's question regarding the use of more than two antennas: I suggest this would produce one or very few main narrow beams against several grating lobes achieved using two antennas spaced many tens of wavelengths apart.

(3) Is the technique adopted in this paper similar to that described by Jarvis? The drawback of this technique up to recently is that it maximizes the RF signal which is not the best parameter to optimize. You have also used an output from the eye pattern. What we require is to cancel out the delayed signals.

Author's Reply

(1) The results, shown in the paper (Fig.9) consider only the amplitude distortion due to selective fading. There is no specific system nor specific modulation technique meant. But, if you consider a specific system you often know the maximum tolerable amplitude distortion and so you can use Fig.9 for an estimation of the availability of your system due to selective fading.

(3) It is correct that maximizing the RF-signal is not best. We blend out the unwanted signal. The eye-opening signal is only used in case of an absence of a unique criterion of the phase detector (Fig.15).

OCCUPANCY MEASUREMENTS ACROSS THE ENTIRE HF SPECTRUM

by

Geoffrey F. Gott, Ngiam F. Wong, and Santanu Dutta
Department of Electrical Engineering and Electronics
University of Manchester Institute of Science and Technology
Manchester
England

SUMMARY

The paper outlines the various aspects of a research programme into the characteristics of interference at HF, and gives measured results of occupancy across the entire HF spectrum. These occupancy values are given for several thresholds, and for the different HF user frequency allocations, as defined by ITU regulations. They are presented for day and night conditions, at times of the year corresponding to the winter and summer solstices, for a period of high sunspot activity.

1. INTRODUCTION

A programme of work exists at UMIST, supported by the Ministry of Defence, to investigate spectral occupancy within the HF band. The aim of the work has been to gain an understanding of interference from other HF users, which may in turn lead to improved communication via improvements in signal design and processing, and in operating procedures. The work has involved detailed investigations of spectral occupancy within frequency allocations used by aeronautical operators (Gott and Staniforth, 1978) and by fixed operators (Dutta, 1979; Dutta and Gott, 1982), and measurements of the correlation of interference spectra with range (Dutta and Gott, 1982). Also, measurements of spectral occupancy across the whole HF spectrum have been made (Dutta, 1979; Wong, 1981), and some results of this particular aspect comprise the essential content of this paper.

Using information gained from the interference studies, digital communication systems have been constructed which have shown improved operation in the presence of interference. These have included an aeromobile frequency agile system (Gott and Hillam, 1973; Gott and Hillam, 1979; Leonidou, 1980), an adaptive chirp system (Sepehri and Gott, 1982), and a robust sixth order diversity system incorporating automatic rejection of interference (Doany, 1981). An improved diversity combiner has also been constructed and evaluated on an HF Link (Gott and Dutta, 1979).

2. OCCUPANCY MEASUREMENTS

2.1 Initial results

Previously published work has examined the detailed occupancy of 50 kHz sections of the HF spectrum, with a resolution bandwidth of 100 Hz. Elementary parameters have been defined to characterise the interference, and these parameters have been usefully applied to the design of signals and signal processing techniques, and given some insight into the vulnerability of various signal formats to typical interference (Dutta and Gott, 1982).

The occupancy measurements have now been extended to cover the whole of the HF spectrum. An aim of this aspect of the work is to provide data which may be used in conjunction with frequency predictions, to advise HF operators on the typical congestion they may encounter, and how this may vary with threshold level, frequency, time, bandwidth, type of user allocation, and geographical location. Such information may also be useful to HF/VHF ground wave users, who may then choose operating frequencies to avoid severe interference from sky wave users, and also to study groups who are concerned with the determination of international frequency assignments.

Initially, occupancy measurements were made with the experimental system of figure 1, which was located at RSRE Pershore, in central England, a rural site with low urban noise level. The signals were received by an active wideband vertical aerial and applied to a spectrum analyser, whose vertical output signal was recorded onto magnetic tape for subsequent analysis in the laboratory. The analysis involved slicing the recorded spectra at various thresholds, and determining the probability of each threshold being exceeded. This quantity, termed congestion, thus gave the probability of being able to place a filter of bandwidth 1 kHz (the resolution bandwidth of the spectrum analyser) anywhere within the chosen section of the HF band, so that the output from the filter exceeded the given threshold. The results were presented as histograms of congestion against frequency, as shown by the example of figure 2. Here, the frequency axis is divided into 500 kHz increments, and average congestion is shown for each increment, for two threshold levels. Each threshold level is defined by the level of a calibration signal applied at the aerial terminals, and also in terms of received field strength.

Spurious modulation products were kept at a low value by analysing the HF spectrum in 2 MHz increments (subsequently sub-divided into 500 kHz increments in the analysis) using appropriate bandpass filters at the input to the spectrum analyser. Linearity was also checked by applying two sine waves, whose amplitudes exceeded the maximum amplitude encountered in the analysis, and observing that intermodulation products were below the noise level of the spectrum.

It was also ensured that the baseline of the recorded spectra was not the noise of the spectrum analyser and recording system. This was easily verified by disconnecting the aerial, and terminating the input to the spectrum analyser, which gave a lowering of the base line. The aerial noise appeared to be dominant when the predicted atmospheric noise level was low, but when it was high, atmospheric noise was dominant, when the level agreed approximately with published predictions (Dutta, 1979).

Spectral recordings were made twice yearly, at times corresponding approximately to the winter and summer solstices, when the diurnal variation in the predicted optimum working frequency is maximum and minimum, respectively. At these times, recordings were made at midday and midnight, corresponding to stable ionospheric conditions, and at dawn and dusk, as indicated on the typical frequency prediction curves of figure 3. The dawn recordings were made during the time of the predicted 'dawn dip', and the dusk recordings in the region of the transition.

Initially, for each solstice, results were taken daily over a period of five days, and it was observed that good agreement was obtained for results taken at equivalent times, but on different days, which was encouraging. Examples of congestion histograms are shown in figure 4.

The first and second columns are results taken on consecutive days during the winter of 1980, and show the good typical agreement. The third column gives results for the summer of 1980. These are a small sample from a large record of results (Dutta, 1979; Wong, 1981), in which each histogram is presented for five threshold levels, but for the simplicity of presentation, only results for two threshold levels are given here.

In general, the occupancy results have been taken using an active vertical aerial. A comparison between results taken with aerials of different polarisations is difficult, because of the need to formulate a precise basis of comparison. However, occupancy measurements were made every hour over a period of one day, alternately using active vertical and active horizontal aerials, whose isolation in polarisation had been verified to be in excess of 20 dB. The results indicated that the spectra, and congestion histograms, were highly correlated. From a practical viewpoint, this suggests that polarisation diversity is unlikely to give effective discrimination against sky wave interference (Dutta, 1979).

2.2 User defined occupancy

By ITU regulations, the HF band is divided into frequency allocations which are dedicated to specific users, or to groups of users, e.g., aeromobile, fixed, broadcast, etc. Presenting occupancy results with the frequency axis divided into 500 kHz increments will merge the congestion values for different types of user (although those increments which contain broadcast bands have well defined congestion peaks), and therefore, for more recent measurements, the frequency axis has been divided into the different user categories.

To achieve this, an improved computer controlled measurement system has been used. It essentially comprises the Hewlett Packard automatic spectrum analyser system, type 8581B, interfaced to a Racal communication receiver type RA1792, via the HPIB bus. This system is used for a variety of HF and VHF spectral observations. For the measurement of congestion for the different HF users, the communication receiver, operated without AGC, and having an IF bandwidth of 1 kHz, is stepped in 1 kHz increments through each user defined allocation, spending one second at each increment. Each 1 kHz channel is defined as occupied at a particular threshold level if the average signal value exceeds the threshold in the one second observation period. The receiver is used in preference to the spectrum analyser for these particular measurements, essentially because the filters are more selective, and a filter bandwidth of 1 kHz was chosen because measurements have shown that spectral occupancy observations are approximately statistically independent for frequency separations greater than 1 kHz (Dutta and Gott, 1982).

This measurement of occupancy across the whole HF spectrum takes several hours, and therefore only results corresponding to the stable ionospheric conditions that occur at about midday and midnight are taken. Even so, the measurement time exceeds the diurnal period of stability, and results for the whole spectrum are taken over three days and three nights, determining occupancy across one third of the HF spectrum at each session.

Examples of HF spectra are shown in figure 5. Tables 1 and 2 give corresponding congestion results for five threshold levels (as measured at the aerial terminals of the receiver), where the relationship between threshold and field strength is indicated in figure 2. For the night results, it is apparent that the lowest threshold (-117 dBm) intercepted the noise level at the lower part of the HF spectrum.

Obviously, congestion will be strongly dependent on the bandwidth of the resolution filter. Table 5 gives measured values of this dependence for several frequency allocations, where the frequencies chosen corresponded approximately to the optimum working frequency for a range of 1000 km. Those filters of bandwidths less than 300 Hz were spectrum analyser filters, and were incremented through the allocations in 1 kHz steps. Those filters of bandwidth 300 Hz and greater were communication filters, and were incremented in steps equal to their bandwidths.

The research programme is continuing to obtain spectral occupancy data, and it is anticipated that a record of such measurements will be made until at least the time of the next sunspot minimum. Results are presently being analysed, and the significance of the various experimental parameters is being investigated. True RMS measurements are also being made, and threshold levels are being referenced to predicted atmospheric noise levels. Also, efforts are being made to set up a second recording site, when simultaneous measurements of occupancy will be compared.

3. ACKNOWLEDGEMENTS

The authors wish to thank the Ministry of Defence and the Science and Engineering Research Council, who have both supported the work. The occupancy project was initiated by John Guest, formerly of RSRE, and Clive Harding, of RSRE, has given much help with the experimental work. The analysis of the results has been done in the Department of Electrical Engineering and Electronics at UMIST.

4. REFERENCES

DOANY, P., 1981; 'A wideband frequency hopping modem for HF data transmission', Ph.D. Thesis, UMIST.

DUTTA, S., 1979; 'Spectral occupancy on low angle and high angle HF links', MOD/UMIST report AT/2044/077, UMIST.

DUTTA, S., GOTT, G.F., 1982; 'Spectral occupancy at HF', IEE Conference 'HF communication systems and techniques', London.

DUTTA, S., GOTT., G.F., 1981; 'Correlation of HF interference spectra with range', Proc.IEE, vol.128, pt.F, no.4

GOTT, G.F., HILLAM, B., 1973; 'Improvements to HF FSK data transmission', AGARD Meeting 'Radio systems and the ionosphere', Athens.

GOTT, G.F., STANIFORTH, M.J.D., 1978; 'Characteristics of interfering signals in aeronautical HF voice channels', Proc. IEE, vol.125, no.11.

GOTT, G.F., DUTTA, S., 1979; 'Improved diversity combiners in HF interference', IEE Conference 'Recent advances in HF communication systems and techniques', London.

GOTT, G.F., HILLAM, B, 1979; 'Improvement of slow rate FSK by frequency agility and coding', Proc. IEE, vol.126, no.6.

HILLAM, B., 1979; 'FSK data transmission in HF interference', Ph.D. Thesis, UMIST.

SEPEHRI, M., GOTT, G.F., 1982; 'An adaptive chirp modem', IEE Conference 'HF communication systems and techniques', London.

WONG, N.F., 1981; 'Spectral occupancy at HF', M.Sc. Thesis, UMIST.

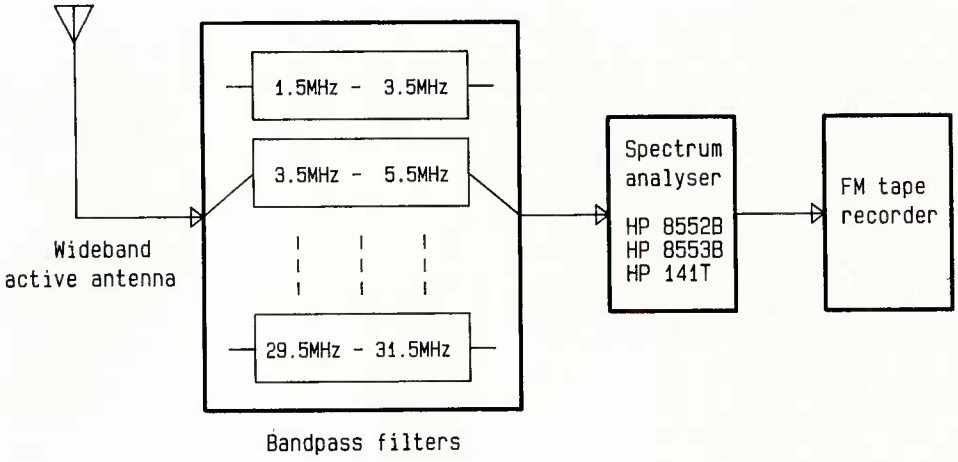

Figure 1 Initial experimental system

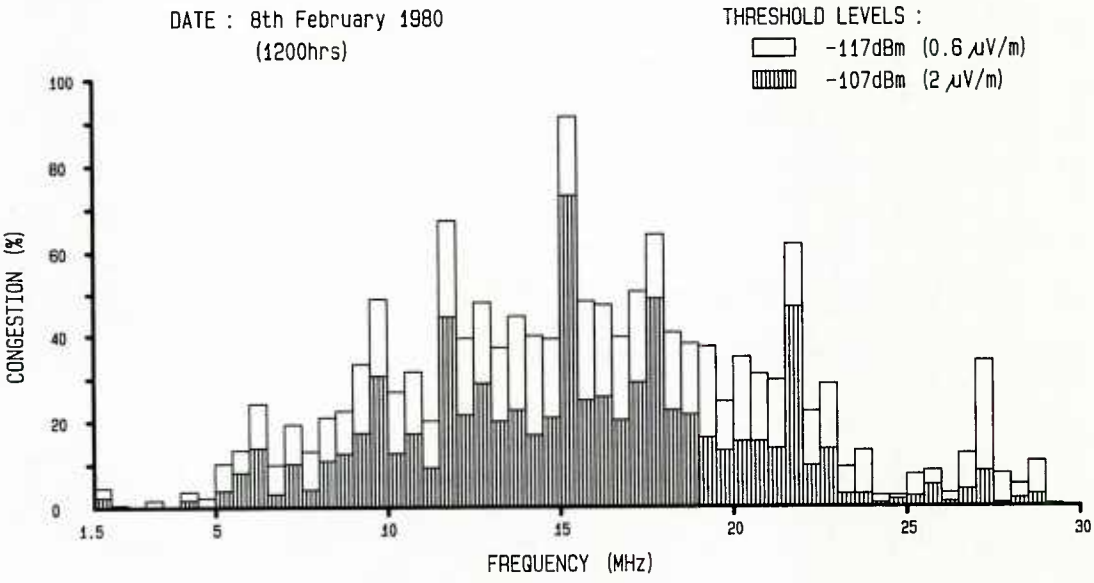

Figure 2 Example of congestion histograms

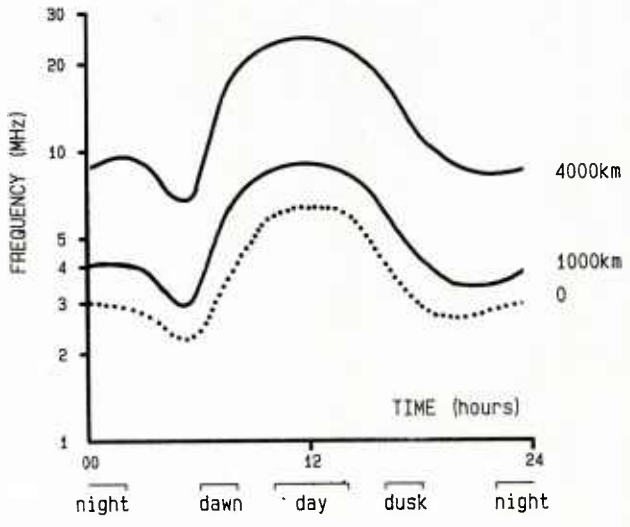

Figure 3 OWF curves

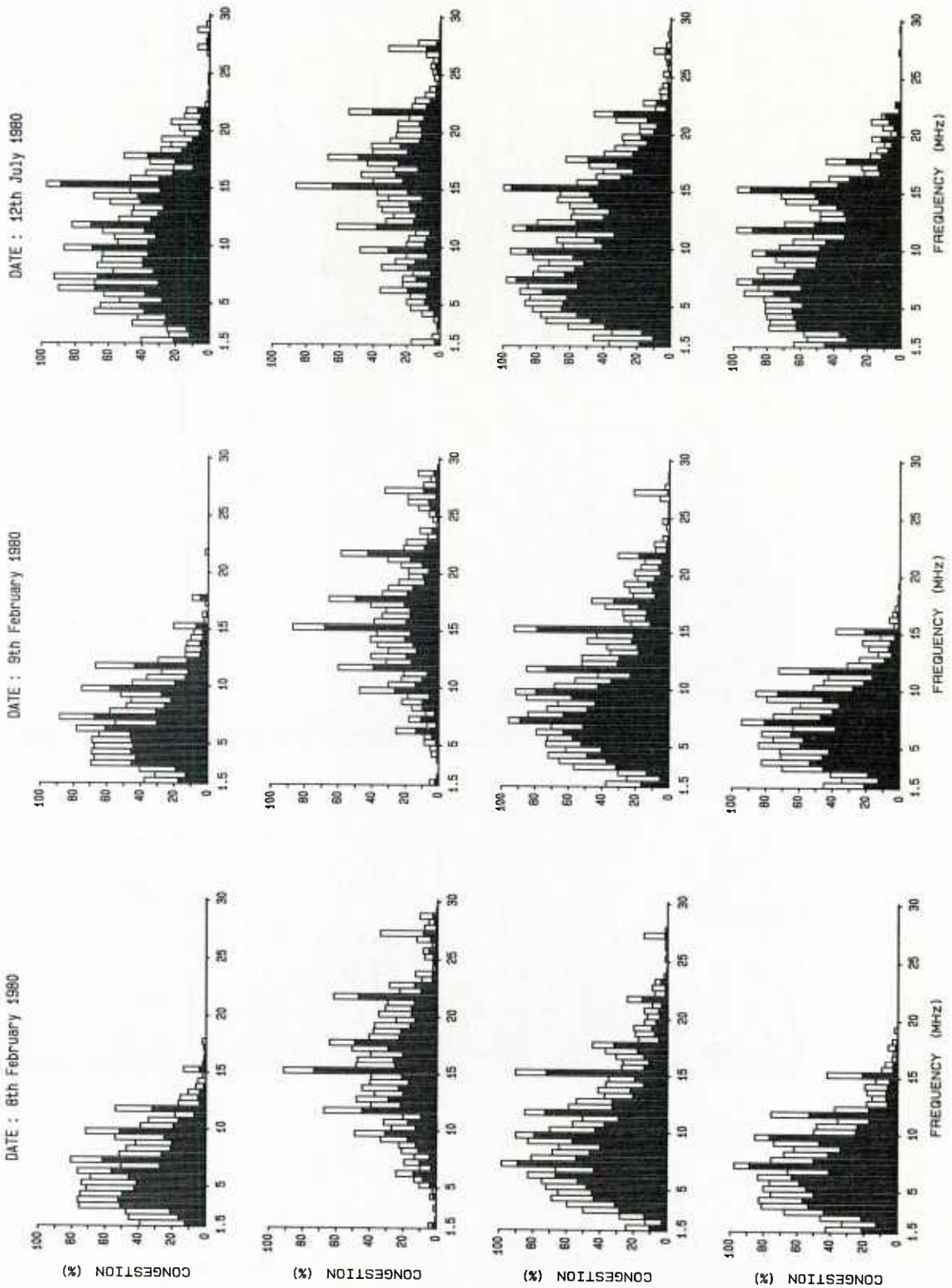

Figure 4 Examples of congestion histograms

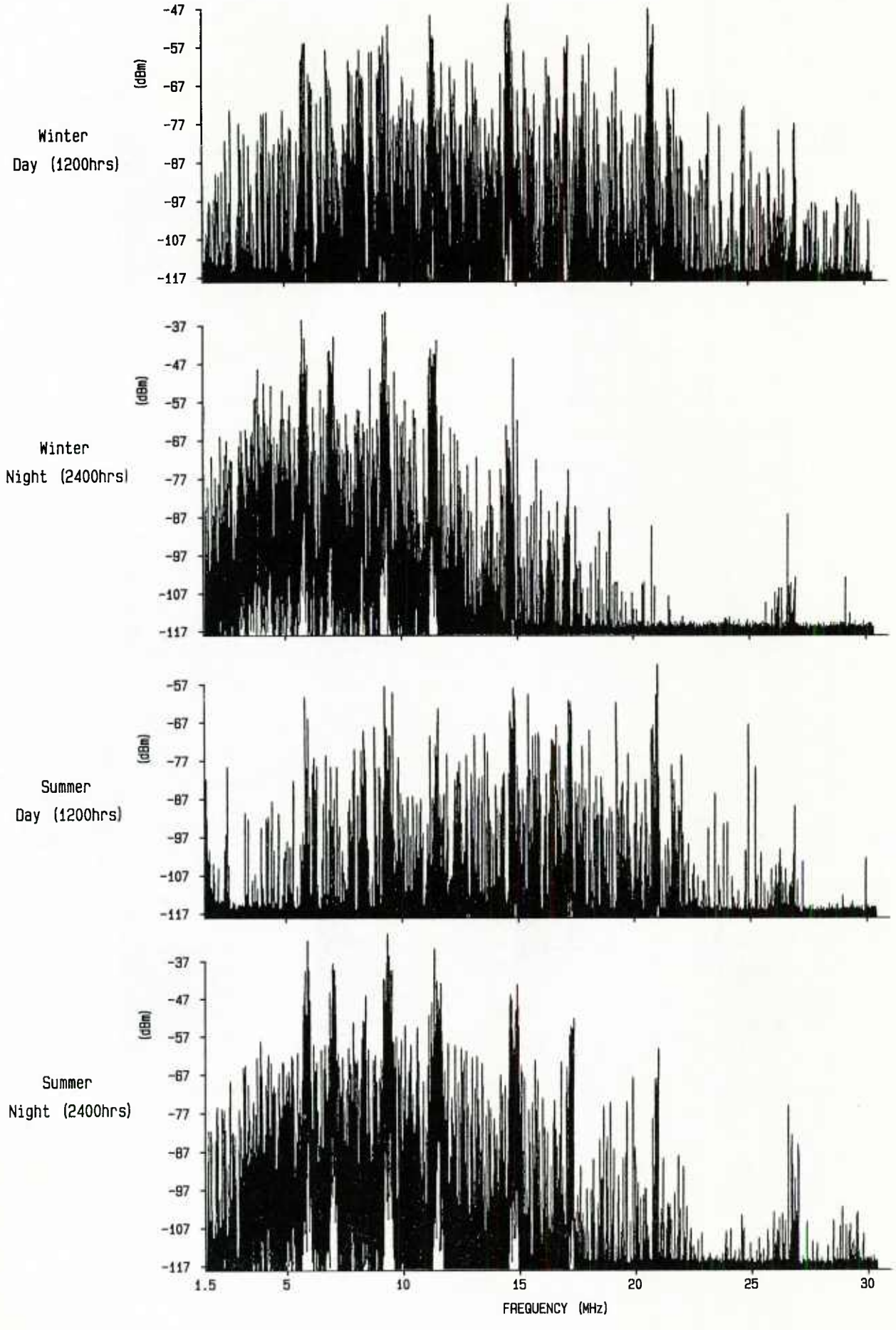

Figure 5 Typical spectra corresponding to winter and summer solstice conditions

	FREQUENCY RANGE (MHz)	USER	DAY CONGESTIONS (%)					NIGHT CONGESTIONS (%)				
			-117dBm	-107dBm	-97dBm	-87dBm	-77dBm	-117dBm	-107dBm	-97dBm	-87dBm	-77dBm
1	1.605 - 2.000	FIXED AND MOBILE	20	3	1	0	0	96	30	13	3	1
2	2.000 - 2.300	FIXED AND MOBILE	13	1	0	0	0	75	22	10	2	0
3	2.300 - 2.500	FIXED AND MOBILE	5	1	0	0	0	71	36	19	3	0
4	2.500 - 2.850	FIXED AND MOBILE	10	3	0	0	0	70	38	23	11	3
5	2.850 - 3.155	AEROMOBILE	5	2	0	0	0	76	31	17	6	2
6	3.155 - 3.200	FIXED AND MOBILE	25	19	5	0	0	100	79	49	26	9
7	3.200 - 3.400	FIXED, MOBILE AND BROADCAST	15	6	1	0	0	94	77	53	32	13
8	3.400 - 3.500	AEROMOBILE	2	0	0	0	0	80	34	19	10	4
9	3.500 - 3.800	FIXED AND MOBILE	13	4	0	0	0	97	83	61	27	6
10	3.800 - 3.900	FIXED AND MOBILE	2	1	0	0	0	99	80	58	35	16
11	3.900 - 3.950	AEROMOBILE	2	0	0	0	0	96	65	21	4	2
12	3.950 - 4.000	FIXED AND BROADCAST	0	0	0	0	0	100	98	88	71	42
13	4.000 - 4.438	MARITIME MOBILE	8	6	4	2	0	98	79	52	31	15
14	4.438 - 4.650	FIXED AND MOBILE	16	9	3	1	0	99	82	57	37	17
15	4.650 - 4.750	AEROMOBILE	1	0	0	0	0	94	57	20	6	4
16	4.750 - 5.000	FIXED, MOBILE AND BROADCAST	12	9	2	0	0	100	84	53	27	10
17	5.000 - 5.480	FIXED AND MOBILE	14	7	4	1	0	99	84	52	33	12
18	5.480 - 5.730	AEROMOBILE	26	2	1	1	0	96	61	24	14	4
19	5.730 - 5.950	FIXED	19	9	5	1	0	99	88	64	49	24
20	5.950 - 6.200	BROADCAST	72	49	31	16	5	100	100	94	80	51
21	6.200 - 6.525	MARITIME MOBILE	31	20	13	8	4	100	86	58	40	17
22	6.525 - 6.765	AEROMOBILE	10	5	3	0	0	100	64	23	10	2
23	6.765 - 7.000	FIXED	18	8	5	2	0	100	86	62	37	15
24	7.000 - 7.100	AMATEUR	68	42	19	6	0	100	94	56	27	14
25	7.100 - 7.300	BROADCAST	46	31	15	8	2	100	100	93	70	49
26	7.300 - 7.800	FIXED	29	14	7	3	1	100	87	66	51	25
27	7.800 - 8.195	FIXED	30	16	6	4	2	98	74	51	30	10
28	8.195 - 8.500	MARITIME MOBILE	36	19	11	8	3	92	55	31	17	7
29	8.500 - 8.815	MARITIME MOBILE	51	35	26	16	10	88	67	46	26	12
30	8.815 - 9.040	AEROMOBILE	26	15	8	2	0	57	27	12	3	1
31	9.040 - 9.500	FIXED	53	37	23	10	2	91	69	47	27	11
32	9.500 - 9.775	BROADCAST	94	79	55	34	16	100	100	100	93	77
33	9.775 - 10.000	FIXED	72	42	28	16	6	100	87	53	34	21
34	10.000 - 10.100	AEROMOBILE	22	11	2	0	0	59	24	8	3	2
35	10.100 - 10.600	FIXED	75	39	18	7	2	92	78	67	39	16
36	10.600 - 11.175	FIXED	55	32	18	9	3	75	51	37	20	7
37	11.175 - 11.400	AEROMOBILE	26	6	3	0	0	60	30	8	2	0
38	11.400 - 11.700	FIXED	67	42	24	11	2	75	53	36	19	8
39	11.700 - 11.975	BROADCAST	96	75	57	34	14	100	96	77	50	27
40	11.975 - 12.330	FIXED	78	53	30	18	6	73	48	24	11	3
41	12.330 - 12.800	MARITIME MOBILE	46	29	18	11	4	72	49	28	8	1

Table 1a Congestion values (February 1981)

	FREQUENCY RANGE (MHz)	USER	DAY CONGESTIONS (%) -117dBm	-107dBm	-97dBm	-87dBm	-77dBm	NIGHT CONGESTIONS (%) -117dBm	-107dBm	-97dBm	-87dBm	-77dBm
42	12.800 - 13.200	MARITIME MOBILE	64	45	29	19	8	56	38	26	14	1
43	13.200 - 13.360	AEROMOBILE	35	20	9	3	2	23	10	4	1	0
44	13.360 - 14.000	FIXED	63	41	22	11	4	39	24	12	0	0
45	14.000 - 14.350	AMATEUR	73	45	23	9	2	73	45	16	0	0
46	14.350 - 15.000	FIXED	84	52	32	17	5	34	19	6	0	0
47	15.000 - 15.100	AEROMOBILE	100	60	26	11	6	32	25	9	0	0
48	15.100 - 15.450	BROADCAST	100	99	93	77	51	77	55	34	0	0
49	15.450 - 16.000	FIXED	91	60	41	23	9	20	12	3	0	0
50	16.000 - 16.460	FIXED	100	54	33	18	7	12	6	4	0	0
51	16.460 - 17.000	MARITIME MOBILE	94	49	28	15	7	12	7	4	1	0
52	17.000 - 17.360	MARITIME MOBILE	99	66	46	30	15	11	5	1	0	0
53	17.360 - 17.700	FIXED	92	60	35	20	9	7	2	1	0	0
54	17.700 - 17.900	BROADCAST	100	100	98	91	64	20	10	4	2	1
55	17.900 - 18.030	AEROMOBILE	47	26	16	9	2	3	2	0	0	0
56	18.030 - 18.500	FIXED	61	42	24	11	3	1	1	0	0	0
57	18.500 - 19.000	FIXED	58	39	24	12	4	3	0	0	0	0
58	19.000 - 19.500	FIXED	55	37	21	10	4	7	1	0	0	0
59	19.500 - 20.000	FIXED	56	26	14	6	2	5	1	0	0	0
60	20.000 - 20.500	FIXED	60	37	20	9	5	5	3	0	0	0
61	20.500 - 21.000	FIXED	53	31	15	5	2	3	2	0	0	0
62	21.000 - 21.450	AMATEUR	73	31	11	4	1	18	7	2	1	0
63	21.450 - 21.750	BROADCAST	99	89	76	54	29	11	7	3	1	1
64	21.750 - 21.870	FIXED	79	54	31	20	5	0	0	0	0	0
65	21.870 - 22.000	AEROMOBILE	55	26	7	1	0	0	0	0	0	0
66	22.000 - 22.400	MARITIME MOBILE	66	35	16	7	1	3	1	1	0	0
67	22.400 - 22.720	MARITIME MOBILE	76	50	33	17	9	1	0	0	0	0
68	22.720 - 23.200	FIXED	41	23	12	5	1	0	0	0	0	0
69	23.200 - 23.350	AEROMOBILE	30	11	3	1	0	0	0	0	0	0
70	23.350 - 24.000	FIXED AND MOBILE	32	18	9	2	0	16	15	0	0	0
71	24.000 - 24.500	FIXED AND MOBILE	37	14	4	1	0	11	10	0	0	0
72	24.500 - 25.000	FIXED AND MOBILE	31	10	3	3	1	0	0	0	0	0
73	25.000 - 25.600	FIXED AND MOBILE	28	13	5	1	0	0	0	0	0	0
74	25.600 - 26.100	BROADCAST	38	18	8	4	2	0	0	0	0	0
75	26.100 - 26.500	FIXED AND MOBILE	47	17	3	1	0	0	0	0	0	0
76	26.500 - 27.000	FIXED AND MOBILE	43	16	6	1	0	0	0	0	0	0
77	27.000 - 27.500	FIXED AND MOBILE	94	61	23	5	0	6	2	1	0	0
78	27.500 - 28.000	METEOROLOGICAL AIDS	58	28	11	2	0	3	2	0	0	0
79	28.000 - 28.500	AMATEUR	21	8	3	0	0	18	0	0	0	0
80	28.500 - 29.000	AMATEUR	61	20	7	1	0	0	0	0	0	0
81	29.000 - 29.700	AMATEUR	7	3	2	0	0	2	2	0	0	0
82	29.700 - 30.000	FIXED AND MOBILE	4	2	1	0	0	0	0	0	0	0

Table 1b Congestion values (February 1981)

	FREQUENCY RANGE (MHz)	USER	DAY CONGESTIONS (%)					NIGHT CONGESTIONS (%)				
			-117dBm	-107dBm	-97dBm	-87dBm	-77dBm	-117dBm	-107dBm	-97dBm	-87dBm	-77dBm
1	1.605 - 2.000	FIXED AND MOBILE	38	7	1	0	0	88	24	4	0	0
2	2.000 - 2.300	FIXED AND MOBILE	45	4	0	0	0	100	25	7	1	0
3	2.300 - 2.500	FIXED AND MOBILE	37	4	2	1	1	100	35	14	3	0
4	2.500 - 2.850	FIXED AND MOBILE	36	3	1	0	0	100	41	16	6	2
5	2.850 - 3.155	AEROMOBILE	34	2	0	0	0	100	29	11	5	1
6	3.155 - 3.200	FIXED AND MOBILE	33	13	0	0	0	100	78	52	30	9
7	3.200 - 3.400	FIXED, MOBILE AND BROADCAST	28	3	1	0	0	100	75	49	29	12
8	3.400 - 3.500	AEROMOBILE	13	1	0	0	0	100	49	25	15	5
9	3.500 - 3.800	FIXED AND MOBILE	21	4	1	0	0	100	84	51	24	7
10	3.800 - 3.900	FIXED AND MOBILE	15	0	0	0	0	100	87	56	37	20
11	3.900 - 3.950	AEROMOBILE	12	0	0	0	0	100	63	22	8	4
12	3.950 - 4.000	FIXED AND BROADCAST	6	0	0	0	0	100	94	65	41	20
13	4.000 - 4.438	MARITIME MOBILE	22	4	2	1	0	100	86	54	33	18
14	4.438 - 4.650	FIXED AND MOBILE	31	9	2	1	0	100	91	54	35	17
15	4.650 - 4.750	AEROMOBILE	5	0	0	0	0	100	69	17	7	3
16	4.750 - 5.000	FIXED, MOBILE AND BROADCAST	14	4	1	0	0	100	96	51	25	14
17	5.000 - 5.480	FIXED AND MOBILE	12	4	1	0	0	100	76	42	26	12
18	5.480 - 5.730	AEROMOBILE	4	1	0	0	0	99	62	29	14	5
19	5.730 - 5.950	FIXED	16	8	3	1	0	100	83	54	37	19
20	5.950 - 6.200	BROADCAST	62	35	14	6	2	100	100	86	70	46
21	6.200 - 6.525	MARITIME MOBILE	21	12	6	2	1	100	73	40	28	17
22	6.525 - 6.765	AEROMOBILE	9	3	0	0	0	100	69	28	12	5
23	6.765 - 7.000	FIXED	24	11	5	1	0	100	75	42	26	14
24	7.000 - 7.100	AMATEUR	54	27	4	0	0	100	91	50	21	10
25	7.100 - 7.300	BROADCAST	24	14	3	1	0	100	92	72	50	31
26	7.300 - 7.800	FIXED	8	4	2	0	0	100	78	55	36	16
27	7.800 - 8.195	FIXED	20	11	5	1	0	100	80	43	26	13
28	8.195 - 8.500	MARITIME MOBILE	18	12	6	3	1	100	75	40	25	10
29	8.500 - 8.815	MARITIME MOBILE	36	23	12	6	1	97	68	43	26	11
30	8.815 - 9.040	AEROMOBILE	9	4	0	0	0	94	44	20	11	7
31	9.040 - 9.500	FIXED	18	9	4	0	0	99	65	41	23	9
32	9.500 - 9.775	BROADCAST	62	41	25	12	3	100	100	97	81	48
33	9.775 - 10.000	FIXED	33	22	10	3	1	97	67	47	32	17
34	10.000 - 10.100	AEROMOBILE	16	6	0	0	0	97	47	18	14	7
35	10.100 - 10.600	FIXED	21	12	6	2	1	99	63	35	16	5
36	10.600 - 11.175	FIXED	28	17	7	3	1	97	50	26	13	4
37	11.175 - 11.400	AEROMOBILE	32	18	6	2	1	97	40	14	4	0
38	11.400 - 11.700	FIXED	41	24	15	8	2	99	65	49	29	17
39	11.700 - 11.975	BROADCAST	74	53	31	17	7	100	100	100	88	56
40	11.975 - 12.330	FIXED	50	28	14	7	3	98	69	51	33	20
41	12.330 - 12.800	MARITIME MOBILE	41	24	12	5	1	87	37	20	10	3

Table 2a Congestion values (July 1981)

	FREQUENCY RANGE (MHz)	USER	DAY CONGESTIONS (%)					NIGHT CONGESTIONS (%)				
			-117dBm	-107dBm	-97dBm	-87dBm	-77dBm	-117dBm	-107dBm	-97dBm	-87dBm	-77dBm
42	12.800 - 13.200	MARITIME MOBILE	44	25	13	5	2	91	44	31	19	6
43	13.200 - 13.360	AEROMOBILE	19	9	1	0	0	84	35	22	9	4
44	13.360 - 14.000	FIXED	38	21	10	4	2	83	36	22	14	4
45	14.000 - 14.350	AMATEUR	37	21	9	4	0	96	63	30	13	3
46	14.350 - 15.000	FIXED	34	19	7	2	1	83	41	21	11	3
47	15.000 - 15.100	AEROMOBILE	51	23	10	5	2	100	59	42	27	16
48	15.100 - 15.450	BROADCAST	92	69	51	32	15	100	98	87	64	43
49	15.450 - 16.000	FIXED	46	25	11	6	2	78	45	27	14	6
50	16.000 - 16.460	FIXED	43	21	9	3	1	56	29	16	9	3
51	16.460 - 17.000	MARITIME MOBILE	32	14	6	3	1	31	16	9	4	1
52	17.000 - 17.360	MARITIME MOBILE	50	28	13	4	0	32	18	11	3	1
53	17.360 - 17.700	FIXED	55	32	14	5	2	35	17	7	2	1
54	17.700 - 17.900	BROADCAST	100	93	74	52	22	88	58	35	19	6
55	17.900 - 18.030	AEROMOBILE	36	19	10	5	2	11	2	2	1	1
56	18.030 - 18.500	FIXED	41	22	13	5	1	23	8	3	1	0
57	18.500 - 19.000	FIXED	48	23	11	4	1	17	4	1	1	0
58	19.000 - 19.500	FIXED	45	21	11	5	2	10	4	3	1	0
59	19.500 - 20.000	FIXED	31	17	9	3	1	6	1	0	0	0
60	20.000 - 20.500	FIXED	28	15	7	2	1	34	11	7	3	0
61	20.500 - 21.000	FIXED	24	13	5	1	0	24	5	3	1	0
62	21.000 - 21.450	AMATEUR	14	6	2	1	0	65	20	8	2	1
63	21.450 - 21.750	BROADCAST	95	71	47	24	10	80	56	39	23	10
64	21.750 - 21.870	FIXED	43	19	11	7	3	33	16	11	2	0
65	21.870 - 22.000	AEROMOBILE	8	3	2	0	0	15	5	2	0	0
66	22.000 - 22.400	MARITIME MOBILE	24	10	4	0	0	17	5	3	1	0
67	22.400 - 22.720	MARITIME MOBILE	27	14	7	3	1	22	5	3	1	0
68	22.720 - 23.200	FIXED	11	6	2	0	0	17	9	5	2	0
69	23.200 - 23.350	AEROMOBILE	6	3	1	0	0	6	1	0	0	0
70	23.350 - 24.000	FIXED AND MOBILE	12	5	1	0	0	9	1	0	0	0
71	24.000 - 24.500	FIXED AND MOBILE	5	2	1	0	0	4	0	0	0	0
72	24.500 - 25.000	FIXED AND MOBILE	2	2	1	0	0	2	1	0	0	0
73	25.000 - 25.600	FIXED AND MOBILE	1	0	0	0	0	0	0	0	0	0
74	25.600 - 26.100	BROADCAST	12	8	2	1	0	1	0	0	0	0
75	26.100 - 26.500	FIXED AND MOBILE	6	2	0	0	0	2	0	0	0	0
76	26.500 - 27.000	FIXED AND MOBILE	6	2	0	0	0	4	1	0	0	0
77	27.000 - 27.500	FIXED AND MOBILE	29	8	1	0	0	8	1	0	0	0
78	27.500 - 28.000	METEOROLOGICAL AIDS	18	7	1	0	0	9	3	1	0	0
79	28.000 - 28.500	AMATEUR	9	4	0	0	0	0	0	0	0	0
80	28.500 - 29.000	AMATEUR	1	0	0	0	0	0	0	0	0	0
81	29.000 - 29.700	AMATEUR	1	0	0	0	0	1	0	0	0	0
82	29.700 - 30.000	FIXED AND MOBILE	0	0	0	0	0	0	0	0	0	0

Table 2b Congestion values (July 1981)

SESSION	USER	RESOLUTION FILTER BANDWIDTH (Hz)	CONGESTION (%) -117dBm	-107dBm	-97dBm	-87dBm	-77dBm
DAY	AMATEUR 14.000 - 14.350MHz	300	37	13	5	1	0
		1000	52	31	12	3	1
		3000	67	39	19	10	3
		6000	97	66	29	17	5
	FIXED 14.350 - 15.000MHz	10	8	3	1	0	0
		30	12	5	2	1	0
		100	14	6	2	1	0
		300	23	9	3	1	0
		1000	48	25	8	3	1
		3000	75	43	15	4	1
		6000	96	66	33	14	3
	AEROMOBILE 15.000 - 15.100MHz	300	34	13	6	2	1
		1000	65	36	7	3	2
		3000	85	44	24	12	6
		6000	100	59	41	12	6
	BROADCAST 15.100 - 15.450MHz	300	92	66	43	24	9
		1000	92	73	50	30	13
		3000	100	90	74	58	37
		6000	100	100	95	88	59
NIGHT	MARITIME MOBILE 8.500 - 8.815MHz	300	99	44	23	11	4
		1000	100	87	56	29	14
		3000	100	99	76	49	27
		6000	100	100	94	81	60
	AEROMOBILE 8.815 - 9.040MHz	300	76	26	12	7	2
		1000	99	52	20	11	2
		3000	100	93	42	24	8
		6000	100	100	84	50	24
	FIXED 9.040 - 9.500MHz	300	81	33	15	6	2
		1000	100	74	42	20	7
		3000	100	99	76	45	25
		6000	100	100	92	73	43
	BROADCAST 9.500 - 9.775MHz	300	100	96	75	43	23
		1000	100	100	97	87	63
		3000	100	100	100	95	83
		6000	100	100	100	100	98

Table 3 Effect of bandwidth variation on congestion (July 1981)

DISCUSSION

P.A. Bradley, UK

I should like to compliment Dr Gott on this work which appears to hold considerable promise in yielding reference data for radio circuit and service planning to complement those given in CCIR Reports 322 and 258 for atmosphere and man-made noise in "quiet" channels. The strength of the approach lies in the combining of measurements within the different allocated bands, thereby leading to statistically stable results. Tests applied to the data of Tables 1 and 2 show that congestion (or occupancy) varies with the threshold (expressed in dBm) in accordance with a log-normal law. The frequency dependence of the threshold for 50% occupancy in the sound broadcasting and aeronautical mobile bands is the same, apart from a scaling factor of some 30dB consistent with the mean difference is effective radiated power of transmissions within these two services. This suggests a way ahead which might involve the geographical and temporal mapping of interference grades at a reference frequency, together with service-scaling factors and standard frequency conversion curves.

L.W. Barclay, UK

(Refers to compatibility contour map which is shown below)

May I make a suggestion for a way to apply these compatibility data for frequency management. If contour maps for predictions of the wanted signal field strength are prepared on the same axes as for compatibility, the 2 contour maps might be overlayed. This would allow a frequency manager to select frequencies giving adequate predicted wanted field strength with minimum expected compatibility problems. The prospect of frequency management in such a way may be a substantial advance on present methods.

Author's Reply

Thank you for the suggestion which I would like to pursue.

The contour map referred to is included here with a brief explanation. This particular map has been derived from measurements taken in frequency allocations of fixed users (including allocations shared by fixed users). For each allocation, congestion values were measured every hour, and graphs of congestion against time were plotted for a particular threshold level. Such graphs from all the fixed allocations form sections of a 3 dimensional surface, where z, y, and x correspond to congestion, frequency, and time respectively. The contour map has been determined from such a surface for a threshold level of 2μV/m. Congestion contours are indicated, and for simplicity of presentation, the contours have been made to appear continuous between the fixed allocations, i.e. across frequency ranges of other types of user. The contour map shows congestion at the time of the winter solstice of 1982, and is shown with examples of corresponding OWF curves.

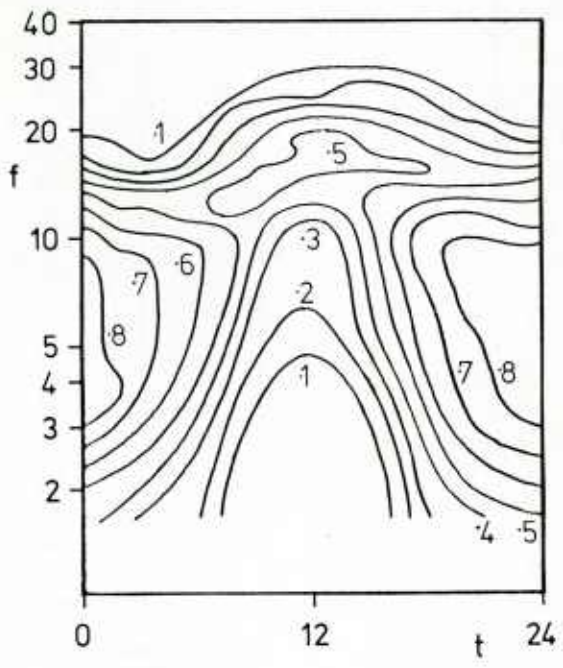

Contour map

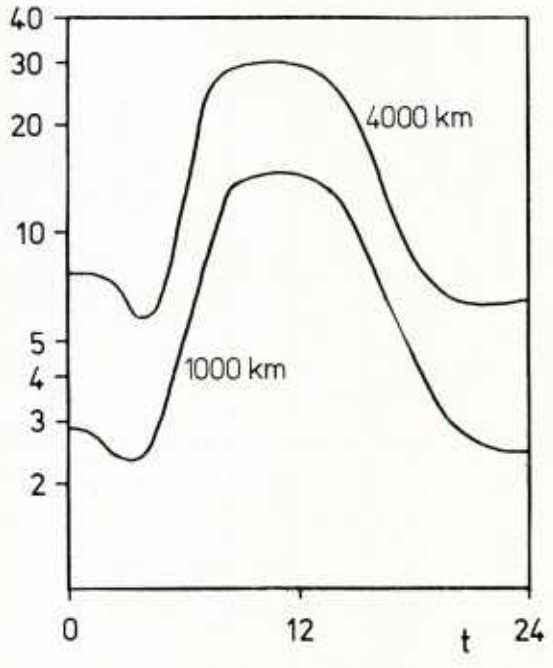

OWF curves

(axes: f(MHz) t(hours))

E.J. Holliman, US

The approach described is an outstanding step towards solving a difficult spectrum problem, and which will continue to become more serious. When one applies precise analytical sampling techniques to a dynamic environment of some 300 different types and classes of radio users, the measurement criteria must be carefully defined. The findings in this type analysis are more useful as a management tool. The pitfalls are in proper selection of the frequency of examination, and the comparison within a cell (or service user). Otherwise, the operational characteristics may create erroneous interpretations. Specifically, one sample each three days as stated is too low a sample rate. In view of the value of this type analytical process, is it planned to continue this effort?

Author's Reply

Thank you for the comments and question.

So far we have made detailed measurements of occupancy across the whole HF spectrum only at the times of the winter and summer solstices, and for each solstice the measurements have been made over a period of 3 days. We had observed previously that measurements made at equivalent times, and across equivalent frequency ranges, were very similar, even when such measurements were separated by several days. This good correlation applies to the results of the type presented in the paper, i.e. averaged across user allocations with a resolution bandwidth of 1KHz, and also to detailed conventional spectral observations, made across bandwidths of 50 KHz (and greater) using a resolution bandwidth of 100 Hz.

The present programme of observations was started at the time of the last sunspot maximum and will continue at least until the time of the next sunspot minimum.

PROPAGATION DATA FOR VHF PLANNING IN THE UK AREA

K A Hughes and J A Lane
Home Office
Directorate of Radio Technology
LONDON SE1 8UA

SUMMARY

Demand for VHF spectrum in the UK requires sharing of frequency bands by different services. Fundamental to the planning of shared bands is the prediction of the potential interference between the services for small percentages of the time. The most well established prediction method at VHF is probably that given in CCIR Recommendation 370.

As an aid to UK spectrum planning, the suitability of Recommendation 370-4 has been investigated for propagation paths within, or terminating in, the UK. Comparisons have been made between long-term measurements and predicted values of field strength using the Recommendation. For some categories of path, measured field strengths were found to exceed predicted values by some 10 dB; other categories however, show good agreement. The applicability of the Recommendation to current planning requirements is discussed in the light of the comparisons.

1. INTRODUCTION

The VHF spectrum encompasses a wide variety of radio communication services and the ever increasing demand for frequencies ensures that this situation will prevail indefinitely. In consequence, further work will be needed in the planning of the band, in which frequency sharing will play a dominant role. A fundamental aspect of the planning of shared bands is a knowledge of the propagation characteristics at the frequencies in question and the ability to predict field strengths occurring for given percentages of the time. In particular, the planning engineer is especially concerned with those enhanced signals, occurring for small fractions of the time and associated with "anomalous" propagation conditions, which may give rise to unacceptable interference.

A well established and widely used method of field strength prediction for use at VHF is that given by CCIR Recommendation 370 which is primarily intended for the estimation of the coverage areas of broadcasting stations. In addition to median field strengths, the method provides data corresponding to smaller percentages of the time for use in determining interfering field strengths, drawing a distinction between propagation paths over land and over sea.

In the planning of VHF services, a need arose to investigate the suitability of Recommendation 370-4 for propagation paths within or terminating in the UK. To this end, available measurements of field strength at VHF were reviewed and compared with corresponding predictions using the Recommendation. Two sets of measurement data were used in the study:

(i) A compilation of earlier measurements obtained at frequencies in or close to those of the Broadcast Bands I, II and III for paths over land and sea, giving the field strengths exceeded for 50, 10 and 1 per cent of the time;

(ii) Recent measurements made in five locations in South East England of two European Band II broadcast transmitters.

Where possible, the CCIR predictions took into consideration the terrain irregularity of the paths in the vicinity of the transmitters and also allowed for effects of local terrain obstructions at each of the receiving sites.

The present paper shows the results of the comparisons. The first set of measurements indicated that Recommendation 370-4 seriously underestimated the field strength for certain categories of path (by some 15-20 dB), whilst the recent measurements in South East England, although still generally exceeding the predictions, showed a somewhat closer agreement.

In the light of the comparisons, comments are expressed on the applicability of the Recommendation to current planning requirements, in the area of the UK.

2. CCIR RECOMMENDATION 370-4

The Recommendation offers a field strength prediction method applicable to broadcasting services at VHF and UHF. It additionally serves as the basis of a prediction method for the mobile services, found in CCIR Report 567-2. In essence, the method in the Recommendation comprises two sets of curves of field strength as a function of distance for various effective transmitter antenna heights. One set relates to VHF (30-250 MHz), the second set to UHF (450-1000 MHz).

The propagation curves represent field strength values exceeded at 50 per cent of locations for different percentages of the time, namely 50, 10, 5 and 1 per cent. The field strengths are adjusted for an e.r.p of 1 kW and correspond to a receiver antenna height of 10m above local ground level. For the smaller time percentages, distinction is drawn between propagation paths over land and over sea. The land path curves were prepared from data obtained mainly from temperate climates found in Western Europe and North America, whilst the sea path curves were prepared from data obtained mainly from the North Sea and Mediterranean

regions. The land path curves refer to a value of Δh^* = 50m, as do those applying jointly to land and sea paths; curves associated exclusively with sea paths however, correspond to a value of Δh < 10m.

The prediction method incorporates certain corrections that must be applied, where appropriate, to the values of field strength obtained from the curves. These corrections are discussed at length in Report 239-5, the most significant of which are:

(i) an allowance for values of Δh other than those to which the curves apply;

(ii) a correction based on terrain clearance angle to allow for terrain obscuration local to the receiving site;

(iii) a correction for predictions applying to percentages of locations other than 50 per cent;

(iv) a correction for mixed land/sea paths.

In addition, corrections are given for a change in receiver antenna height from 10m to 3m for different categories of environment, these being particularly relevant for the mobile services.

3. EARLIER MEASUREMENTS ON VHF TRANSHORIZON PATHS

3.1 Analysis of data

The study commenced using an available compilation of propagation data for VHF paths terminating in the UK, spanning the period from 1946-66. The data consisted of measurements of field strength, in the frequency range 41 to 203 MHz, documented as values exceeded for various percentages of the time. In total, 135 paths were monitored, and these were categorised into groups of either land or sea paths and with frequencies near to the 3 broadcast bands, viz:

	Land	Sea
Band I (40-70 MHz)	32	14
Band II (70-100 MHz)	25	11
Band III(150-205 MHz)	22	31

with an average measurement period between 1 and 2 years.

Details were available also of the transmitter and receiver sites and of the respective antenna heights; in the main, effective transmitter antenna heights fell broadly in the range 100-200m, whilst receiver antenna heights were consistently around 10m. Virtually all the paths were over-the-horizon, at distances between 100 and 500 km.

Since the field strengths in the data compilation were quoted relative to free space values, comparison could readily be made with corresponding values predicted from Recommendation 370-4. In the majority of cases, the appropriate value of Δh was computed for each path, either by use of a data bank of terrain height if the entire path lay within the UK, or by inspection of a map for those cases with the transmitter located overseas. Correction factors, as given by the Recommendation, could then be applied to the values of field strength obtained from the curves to allow for the differing values of Δh. It is noteworthy that such corrections are given only for frequencies above 80 MHz and consequently no allowance for Δh was made to the predictions for the Band I paths.

Similarly, corrections were applied to predicted values of field strength for the cases relating to mixed land/sea paths. The correction procedure, given in Report 239-5, applies only to the small time percentages for which separate curves are provided for land and sea paths. For the present study therefore, this correction was only appropriate for predictions made for field strengths exceeded for 1 per cent of the time.

The predicted and measured values of field strength were depicted graphically as a function of distance, drawing a distinction between Bands I, II and III, land and sea paths, and time percentages of 50, 10 and 1 per cent. In the main, measured values were found to exceed predictions typically by 10-15 dB and Figure 1 shows the case for Band II land paths. In order to quantify the comparisons, "best-fit" lines were constructed through the data. Although these have not been normalized to a single transmitter antenna height, the range in these heights is not large and consequently, the best-fit lines still give a useful indication of the variation of field strength with distance.

Comparisons between predicted values and those represented by the best-fit lines are depicted in Figure 2, where the differences are plotted as a function of distance for all cases under consideration. With the exception of median field strengths for land paths at Band I and for sea paths at Band III, measured values exceed those predicted over the distances considered; in some instances discrepancies of 20 dB are apparent.

* Δh defined as the inter-decile range of terrain height found between 10 and 50 km from the transmitter.

3.2 Discussion

Figure 2 indicates a tendency for the greatest discrepancies to occur at the shorter distances, implying that the Recommendation is least accurate in the near diffraction region. There appears, however, to be no consistent variation in the accuracy of the method with time percentage. The prediction method thus seems to find its greatest accuracy when applied to distances for which the dominant propagation mechanisms would be essentially tropospheric in nature, namely "scatter", or layer-mode propagation producing the occasional high signal in "anomalous" conditions. The result obtained for Band III land paths, at 1 per cent time, might seem to contradict the above argument, but the measurement values in this example displayed considerably greater variation than in the other cases, and consequently the comparison with predictions should be treated with some caution.

As described earlier, the predictions were corrected for variations in Δh, and in the cases of sea paths for 1 per cent time, for the proportion of land/sea within the total path. Since virtually all of the land paths, and many of the mixed paths, had values of Δh exceeding 50m, application of the correction factors in general reduced the values of field strengths from those derived directly from the curves in the Recommendation. In consequence, the general effect of applying the corrections was to increase the discrepancies between the measured and predicted data. Since, however, the correction factors involved were generally less than 6 dB, the apparent inaccuracies found in the CCIR method in this study could be only partly attributed to this aspect of the prediction method.

In these comparisons, no corrections were made for location variability. The possibility may exist though, that many of the receiver sites did not correspond to median locations but more appropriately represented locations receiving enhanced field strengths in comparison with median locations for a given percentage of the time. Reference to the location variability distribution given in Recommendation 370-4 indicates that field strengths predicted for "good" sites may typically be some 10 dB greater than those for median sites. Factors of this magnitude could therefore explain at least some of the discrepancies found in the present analysis.

In a similar study of UK transhorizon data at VHF, Owolabi and Lane (1973) also compared measured field strengths in Band I and Band III with corresponding values predicted by then current Recommendation 370-1. Their analysis revealed that the measured field strengths exceeded for 1 per cent of the time were significantly greater than those predicted, especially for Band III, but also to some extent for Band I. For median field strengths however, closer agreement was generally obtained. They also found that measured field strengths for 1 per cent time in Band III exceeded those for the same time percentage in Band I and suggested an explanation in terms of preferential enhancement of Band III transmissions due to coherent partial reflections from inversion layers situated at appropriate heights. In the present study, Figure 2 possibly shows evidence of a similar result when comparing the plots for Band I and Band III land paths, since the predicted field strengths are equal, apart from the Δh correction, in both cases.

4. BAND II MEASUREMENTS IN SOUTH EAST ENGLAND

4.1 Collection and anlysis of data

Since June 1981, signal strength measurements have been made at 5 sites in SE England using transmissions from broadcasting stations at Lopik (the Netherlands) and Aalter (Belgium) on frequencies of 92.6 and 98.6 MHz respectively. Figure 3 shows the locations of the transmitters and monitoring sites. The effective transmitter antenna height at Lopik is 280m, whilst that at Aalter is 130m; both transmitters operate with an e.r.p of 50 kW. Two of the receiver sites, Southminster and Wennington, are situated in rural areas, whilst the other three are located in suburban towns. Receiver antenna heights are 10m, with the exception of that at Chelmsford which is 30m.

From approximately 1 year of measurements, statistics have been derived for each path of the field strengths exceeded for 50, 10 and 5 per cent of the time, and it is these data which are the subject of a further evaluation of Recommendation 370-4.

As in the previous study, corrections were made to the values of field strength derived from the curves to allow for the actual values of Δh associated with the paths. In all cases, Δh was less than 10m, corresponding to correction factors ranging from 0 dB to +4 dB. In addition, an allowance was made for local terrain obscuration at each of the receiving sites. This correction is based on the terrain clearance angle which is measured between the horizontal at the receiver antenna and the line which clears all obstacles within 16 km in the direction of the transmitter. Since the angle can be above or below the horizontal, the correction can act to decrease or increase respectively the value of field strength initially obtained from the curves in the Recommendation.

Comparisons have been made between the measured statistical values and those predicted by Recommendation 370-4 and the results are shown in Figures 4a, 4b and 5 in terms of the differences for each frequency, receiver site and time percentage, drawing a distinction between predicted field strengths with and without corrections for Δh and receiver site clearance. In general, measured values exceeded those predicted, but, with the exception of the results relating to Chelmsford, the discrepancies are considerably smaller than those found in the previous study and are generally less than 10 dB. The large differences indicated for Chelmsford are attributed to the receiver antenna height of 30m compared with 10m used in the predictions. The influence of "height gain" on the measured values in this case will be discussed in section 4.2.4.

4.2 Discussion

4.2.1 Δh and receiver site clearance correction factors

With the exception of Wennington, Figures 4a, 4b and 5 generally indicate that the discrepancies between the measured and predicted field strengths are reduced by the application of correction factors for Δh and receiver site clearance. In some cases, the improvement is quite marked, e.g Sidcup for 92.6 MHz, but for others, it is non-existent or barely significant, e.g Chelmsford for 98.6 MHz, Stowmarket for 92.6 MHz. The height of the receiving site at Wennington is significantly lower than those of the other sites and, despite the surrounding low lying land, the terrain clearance angles on both propagation paths are of a greater magnitude than for the other monitoring sites. It is the corresponding correction factors for receiver site clearance which appear to cause the increased discrepancies indicated in Figures 4a and 4b for Wennington. Other cases exist in which the application of a correction for Δh without that for receiver site clearance, or vice versa, improves marginally the agreement between the measurements and predictions but it has not been possible to identify any overall pattern to the effects on prediction accuracy of applying either or both corrections.

4.2.2 Propagation path length dependence

In the previous study, there was evidence that the CCIR prediction method tended to be least accurate at the shorter distances, with the closest agreement occurring at distances approaching 500 km. Included in Figures 4a, 4b and 5 are the distances for each of the paths in the present study, together with the percentage of the total path length which was over sea. However, in this case no correlation appears to exist between the accuracy of the prediction method and path length.

4.2.3 Location variability

The results shown in Figures 4a and 4b, relating to those sites with a receiver antenna height of 10m, indicate that, after Δh and receiver site clearance corrections have been applied, the discrepancies between the measured and predicted values of field strength are significantly smaller for Sidcup and Stowmarket than for Southminster and Wennington. The first pair of sites relate to a suburban environment, with the antennas surrounded by housing estates and small industrial buildings, whilst the second pair is located in the rural environment, with few local obstructions, and with the sea in close proximity in the direction of the transmitters.
By undertaking further measurements of field strength in the immediate vicinity of each fixed site, it was confirmed that the antenna location in each case was representative of a median location within the area immediately surrounding the site. As a consequence, it is suggested that the differences shown above, between the two pairs of receiver sites, are due chiefly to the different nature of the site types, i.e rural and suburban.

Inspection of Figures 4a and 4b indicates that the discrepancies associated with the rural sites (Southminster and Wennington) are some 4-5 dB greater than those of the suburban sites (Sidcup and Stowmarket). A location variability distribution is given in Recommendation 370-4, from which the ratio of the field strength for a given percentage of receiving locations to that for 50 per cent of receiving locations may be derived. Although the distribution is not referred to any particular category of environment, it nevertheless may serve to illustrate that a factor of some 5 dB could arise between a "good" site, representative of 30 per cent of locations say, and an average or median site. By equating these two examples to the rural and suburban sites respectively, the differences observed in Figures 4a and 4b may be reconciled.

4.2.4 Variation in field strength with height(height gain)

As noted previously, the differences between the measured and predicted field strengths at Chelmsford were considerably greater than those found at the other sites. This result can be attributed to the receiver antenna height at Chelmsford of 30m, as compared with 10m used in the predictions. Comparison of Figures 4a and 4b with Figure 5 indicates that the discrepancies, and in turn the measured field strengths, at Chelmsford were perhaps some 5 to 15 dB greater than for the other sites, implying that a value of height gain for 10 to 30m may lie within this range of values.

Recommendation 370-4 discusses height gain, essentially in the range 3 to 10m, in terms of the change in median (time) field strength, but no information is provided however, for the height range of interest here.

The change in field strength with height will be sensitive to several factors, but, in particular, will vary with local environment. In suburban areas such as Chelmsford, the main result of changing the receiver antenna height from 10 to 30m would be to remove the majority of local obstructions from the propagation path, and the effect might be compared with moving the antenna to a "good" site from a median or poor site.

Since no further field strength measurements were taken at a height of 30m in the immediate vicinity of the Chelmsford site, the antenna location variability in this case cannot be quantified. However, the close relationship between height gain and antenna location variability must be borne in mind in a correct interpretation of the results.

4.2.5 Seasonal variation of received field strengths

By separating the measured field strength data into approximately three month periods, the seasonal variation of the values exceeded for 50, 10 and 5 per cent of the time was investigated. No well defined pattern was identified though, and considerable variation existed between the data associated with the 5 sites; differences were even found between the data for the two frequencies at each site. However, there was some evidence to suggest that the field strengths received in summer were, in general, higher than those in winter, consistent with the increased likelihood of enhanced signal levels due to stable anti-cyclonic conditions. Such conditions are not exclusive to the summer season alone, and many more measurements would be required before a significant trend could be established.

5. CONCLUSIONS

The foregoing has described how two sets of field strength measurements have been used to evaluate the effectiveness of the prediction method given in CCIR Recommendation 370-4 for propagation paths in the UK area. The study revealed that, in general, the CCIR method underestimated the field strength and that the magnitude of the discrepancy depended on several factors, the most significant of which were:

(i) Path distance: the earlier data set indicated that the method appeared to be least accurate just beyond the horizon;

(ii) Δh: in the main, application of correction factors to allow for variations in terrain irregularity, as quantified by the parameter Δh, improved the accuracy of the method;

(iii) Receiver site clearance: in most cases, application of correction factors to allow for terrain obstructions local to the receiver antenna in the direction of the transmitter, improved the accuracy of the method;

(iv) Environment type at receiver site: the measurements obtained in SE England indicated the effects of site variability on the accuracy of the method;

(v) Location and height of receiver antenna: the measurements obtained at Chelmsford demonstrated the influence of antenna height on received field strength, the so-called height gain interpreted in terms of antenna location variability within a suburban environment.

When using the prediction method for point-to-point paths, it is the factors relating to the receiver site and receiver antenna location which are considered to exert the greatest influence on its accuracy. For these cases, more information is required in the Recommendation in terms of location variability, both site location and antenna location, and defined for various categories of path and environment. In its absence however, the user is advised to quantify the site by measurements, in order to relate it to an average site for the local area.

For general planning purposes though, the Recommendation offers the user a convenient method of deriving good approximations of received field strength within a given area. For greater accuracy, an alternative method of quantifying terrain irregularity, other than by Δh as currently defined, might be beneficial and a distinction may have to be made between the curves of field strength relating to land and sea paths for all time percentages.

The value of Recommendation 370-4 rests largely in the fact that it is based on actual measurements and consequently reflects realistic propagation conditions. Nevertheless, the almost infinite variety of propagation paths encountered in practice demands that the user pays particular attention to the influential factors cited above in order to effect an accurate prediction using the Recommendation.

ACKNOWLEDGEMENTS

The authors acknowledge the permission of the Director of Radio Technology to publish the paper. The compilation of data analysed in Section 3 was undertaken by Mr P J Brice. Appreciation is expressed for the efforts of Mr R A Stewart and Mr J A Scratchley in the collection, processing and provision of the recent data used in the study, and thanks are conveyed also to Mr R J Hodges for help in the analysis. The advice and guidance of Mr L W Barclay throughout the study is also acknowledged.

REFERENCE

OWOLABI, I.E and LANE, J.A (1973), Transhorizon propagation on v.h.f. and u.h.f. radio links in the United Kingdom. Proc. IEE, 120, 2, 165-172.

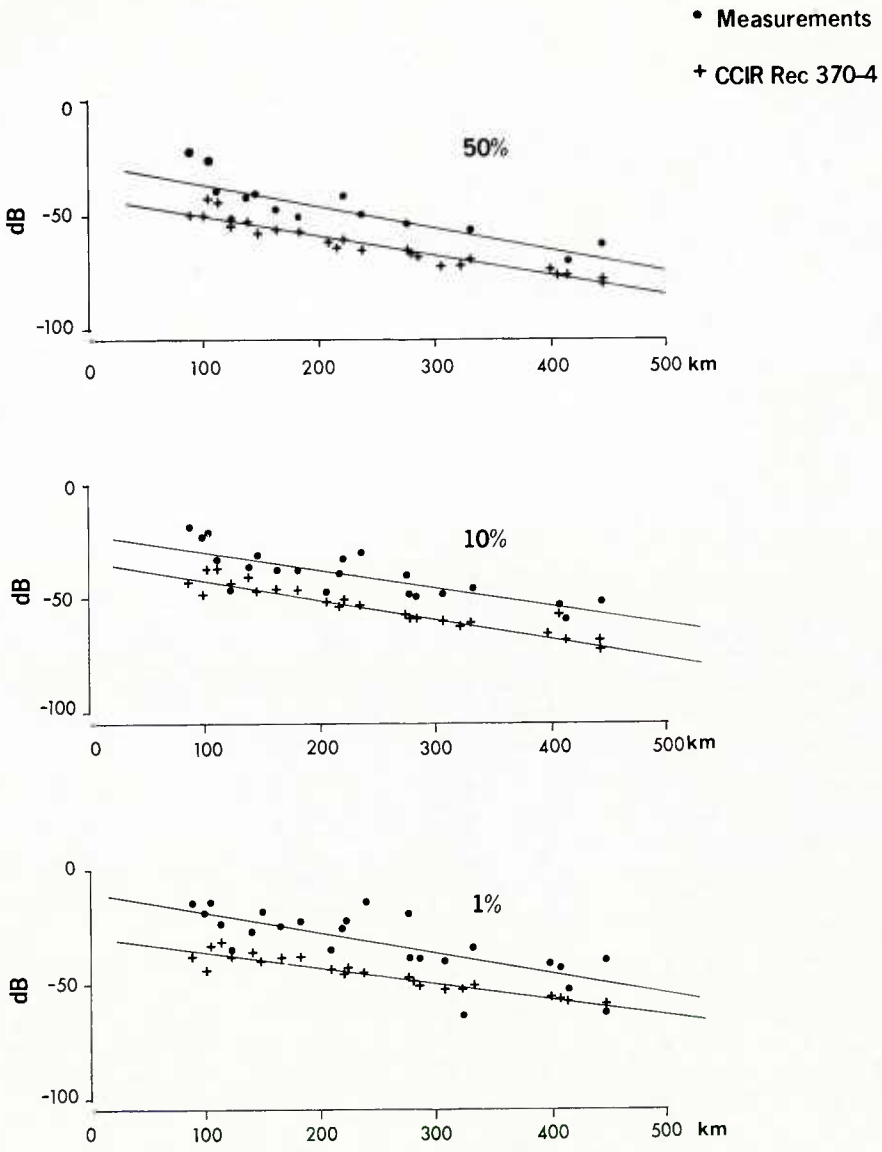

Figure 1: Band II Land Paths; Field Strength (dB relative to free space) exceeded for stated percentage of time as a function of distance (km)

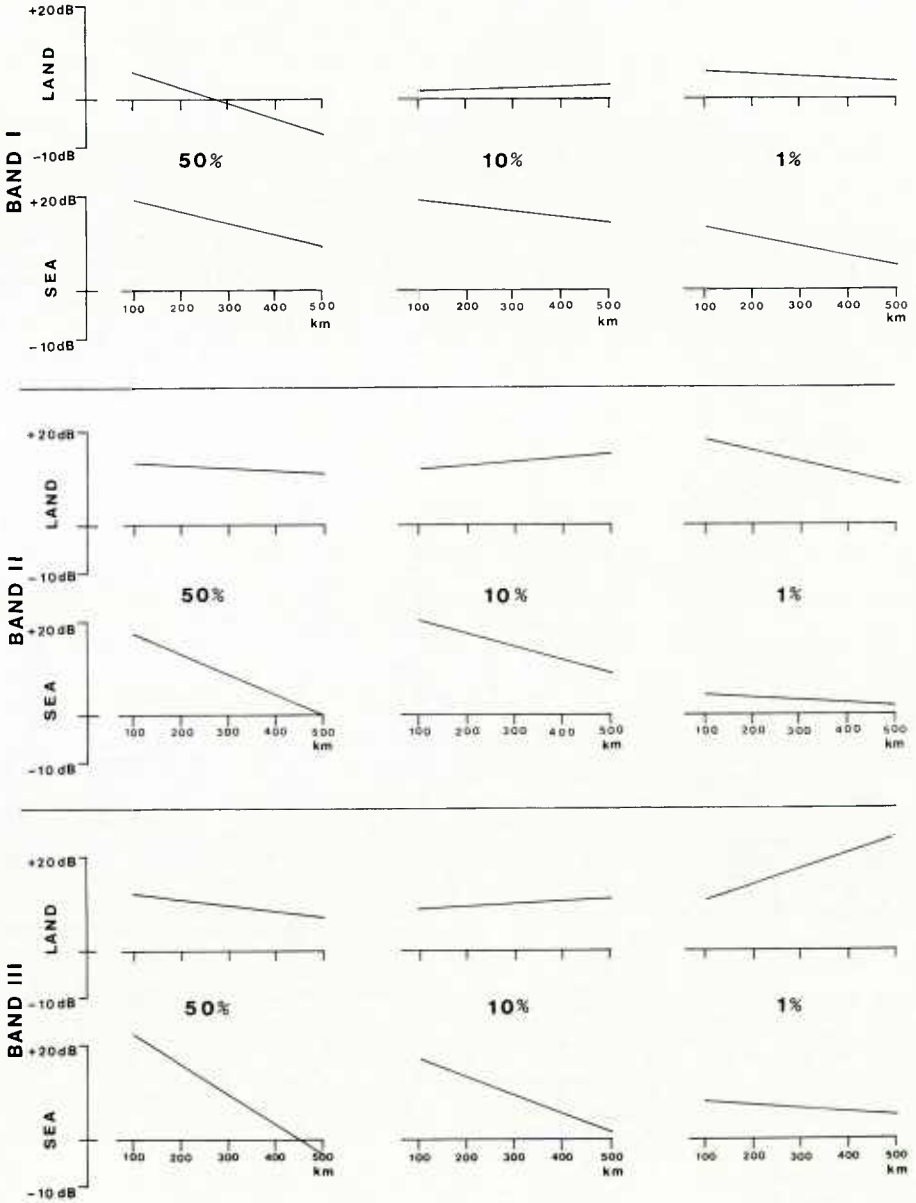

Figure 2: Difference (M–P) between Measured (M) and Predicted (P) Field Strength (dB) as a function of distance (km)

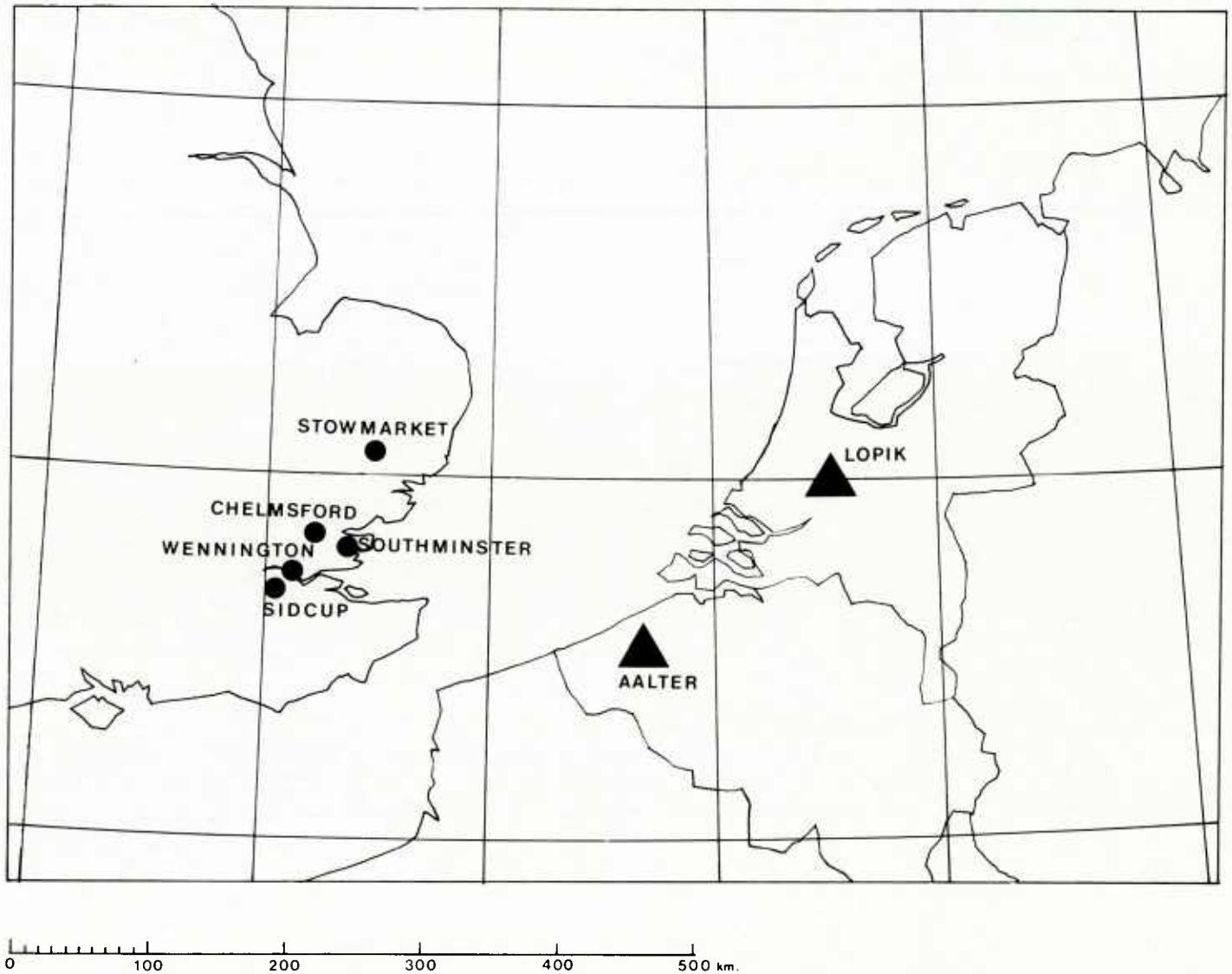

Figure 3: Locations of Transmitters ▲ and Receiving Sites ●

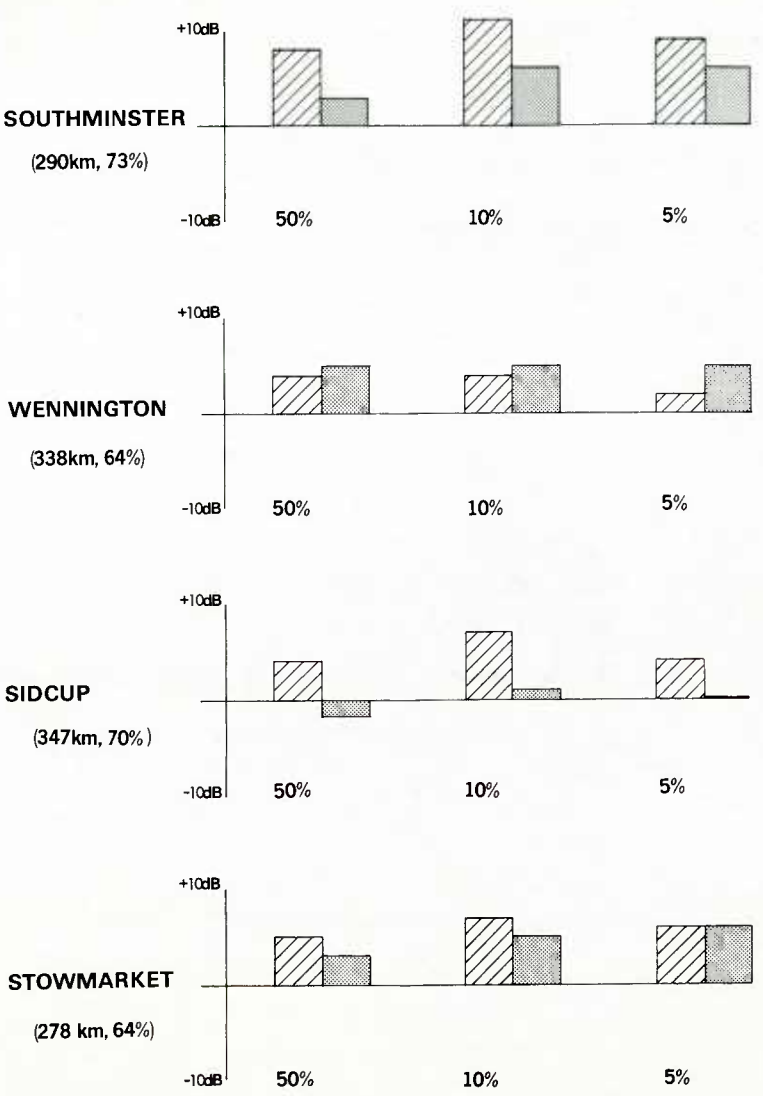

Figure 4a: Difference(M-P) between Measured (M) and Predicted (P) Field Strength (dB) at 92.6 MHz, without corrections ▨, with corrections ▩

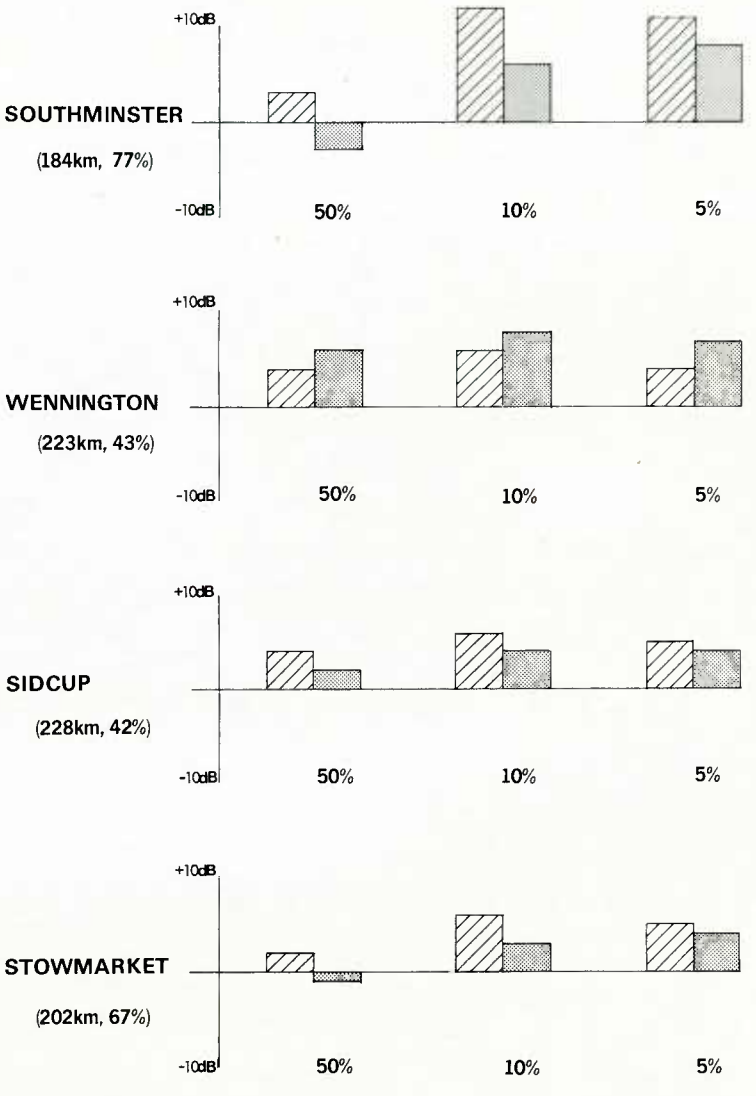

Figure 4b: Difference (M-P) between Measured (M) and Predicted (P) Field Strength (dB) at 98.6 MHz, without corrections ▨, with corrections ▩

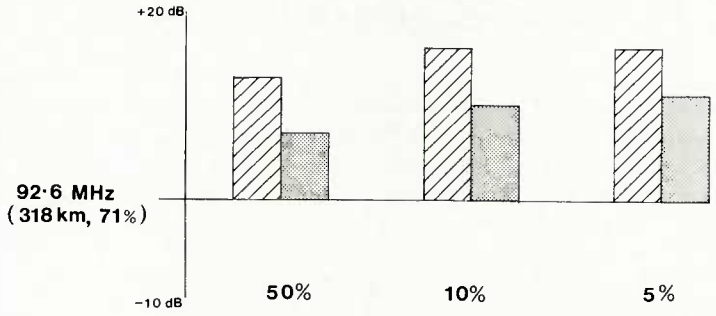

CHELMSFORD

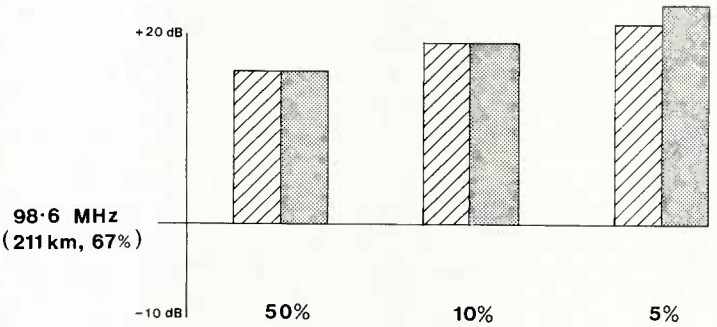

Figure 5: Difference (M–P) between Measured (M) and Predicted (P) Field Strength (dB),
without corrections ▨, with corrections ▩

DISCUSSION

J.Arnbak, Ne

I am wondering whether it would be possible to interpret your results for Southminster and Wennington, which are closer to the sea, not so much in terms of their clearance angles or Δh as in terms of higher probability of anomalous (ducting) conditions over sea.

It is popular knowledge in the city of The Hague that the reciprocal experiment – that of receiving UK FM transmissions – has a much higher chance of success within a few kilometres of the sea (in the most urban area) than further inland where local obstructions are fewer. Terrain is flat in both cases, true to the nature of the Netherlands.

Author's Reply

Certainly, it might be expected that field strengths received near the coast would tend to exceed those inland due to anomalous propagation conditions occurring more frequently over the sea. However, in comparing the results from different monitoring sites relating to the *same* percentage of the time, e.g. median time values, the concept of location variability must be involved in order to reconcile any differences.

---

* As a point of clarification, Southminster and Wennington are not on the coast but of the order of 10 km inland.

IMPLICATIONS OF PROPAGATION UNCERTAINTIES IN FREQUENCY SHARING ANALYSES

Thomas M. Sullivan

ORI, Inc.
1400 Spring Street
Silver Spring, MD 20910
USA

SUMMARY

Frequency sharing analyses are used for a variety of spectrum management purposes. These applications include procedures for identifying frequency assignment coordiantion requirements, the planning of telecommunication services, the derivation of frequency sharing criteria, and detailed Electromagnetic Compatibility (EMC) analyses. An examination of interfering signal power levels that are exceeded for no more than some specified percentage(s) of time is generally required in frequency sharing analyses. Also, depending on the application, an analysis of the desired signal power levels exceeded for at least some specified time percentage(s) is needed. These evaluations of the desired or interfering signal power levels are based on service quality objectives, equipment parameter values, and propagation predictions. The latter two factors embody uncertainties that affect not only service quality, but also spectrum utilization efficiency.

The objectives of various frequency sharing analysis applications and the potential consequences of analytical uncertainties were considered. Analytical techniques used in frequency sharing analyses and the associated sources of analytical uncertainties were reviewed. Finally, the implications of propagation uncertainties in frequency sharing analyses were examined in light of other analytical uncertainties. The implications of propagation prediction uncertainties depend on the frequency sharing analysis application and can range from unacceptable interference to inefficient use of the spectrum.

1. INTRODUCTION

Congestion of the radio frequency spectrum has never been of greater concern than it is today, except perhaps in the early days of radio when the usable spectrum was thought to be limited to some tens of megahertz in bandwidth. This concern is evident in the regulatory and radio-technical forums of the International Telecommunication Union (ITU): World and Regional Administrative Radio Conferences (WARCs and RARCs) and the International Radio Consultative Committee (CCIR). Many participants in these forums believe that spectrum requirements can, for the most part, continue to be fulfilled through efficient spectrum utilization and the availability of less desirable but satisfactory frequencies. However, a new dimension in the spectrum congestion problem has evolved in the ITU, where guarantees are now sought for the future availability of spectrum resources that must be shared on an international basis.

The 1985 WARC will consider means for ensuring the future availability of spectrum resources for geostationary satellite systems, including detailed a priori frequency/orbit position allotment plans. Detailed a priori plans can guarantee the fulfillment of a specified demand for the quasi-limited orbit/spectrum resource, thereby serving as one example of a means for alleviating some spectrum congestion concerns. More traditional methods for treating the congestion problem are embodied in the Final Acts of WARC-79, wherein a variety of technical standards and sharing criteria have been enacted to prevent excessive consumption of the spectrum resource and promote compatibility. Frequency sharing analyses are fundamental to the derivation of these regulatory provisions as well as to the implementation of particular systems.

There are a variety of types of frequency sharing analyses that require an evaluation of signal propagation. Propagation predictions that are used in these analyses can be made with only a limited degree of confidence, even over paths that are well defined in terms of topography and radiometeorology. At the same time, values for other parameters used in sharing analyses are not always characteristic of actual operational equipment or performance requirements. The net effect of sharing analysis inaccuracies, whether deliberate for the purpose of conservativeness or incidental, can be inefficient spectrum utilization. We can thus concede that propagation prediction uncertainties contribute to the limitation of the spectrum resource, but perhaps with relative insignificance. The implications of propagation prediction uncertainties in particular sharing analysis applications is of greater practical concern.

This paper addresses the implications of propagation uncertainties in the context of four general types of frequency sharing analysis applications. Typical analytical techniques are presented first. The sharing analysis applications and associated implications of propagation prediction uncertainties are then presented. Finally, these implications are summarized and conclusions are made with respect to the impact of propagation prediction errors in frequency sharing analyses.

2. ANALYTICAL TECHNIQUES

There are two fundamental analytical techniques that are typically used in assessing interference between stations: 1) the carrier-to-interference power ratio (C/I) technique and 2) the interference-to-noise power ratio (I/N) technique. These techniques are matched to interference criteria: 1) a protection ratio (PR) to be exceeded for a specified percentage of time and 2) an interference-to-thermal noise power ratio (INR) to be exceeded for no more than a specified percentage of time. The exceedance time percentages associated with the interference criteria are typically "average-year" values or "worst-month" values, the latter being a more rigorous specification for system performance in the presence of interference. Generalized expressions used in the two analytical techniques are presented below. The techniques are compared and error domains are considered.

2.1 PROTECTION RATIO TECHNIQUE

A protection ratio (PR) is a carrier (or signal)-to-interference power ratio that is to be exceeded for a certain percentage of time. When no percentage of time is specified, the PR is usually interpreted as being the mean required C/I. Commonly used approximate equations are given below.

$$\frac{C}{I}(p) = C(p) - I(p) \quad (1)$$

$$\frac{C}{I}(p) = \begin{cases} C(50) - I(q), \text{ for } I(q) - I(50) >> C(50) - C(p) & (2a) \\ C(50) - I(q/2), \text{ for } I(q) - I(50) \simeq C(50) - C(p) & (2b) \\ C(p) - I(50), \text{ for } I(q) - I(50) << C(50) - C(p) & (2c) \end{cases}$$

$$C = P_W + G_{TW} + G_{RW} - L_W \quad (3)$$

$$I = P_I + G_{TI}(\phi) + G_{RW}(\theta) - L_I \quad (4)$$

where:

$\frac{C}{I}(p)$ = C/I exceeded for p percent of the time;

$C(p), I(p)$ = carrier and interfering signal power levels, in dBW exceeded for p percent of the time, respectively;

$I(q)$ = interfering signal power level, in dBW, exceeded for q percent of the time, where q is the complement of p (i.e., q = 100 - p);

P_W, P_I = wanted and interfering signal power levels respectively, in dBW, at the antenna input;

G_{TW}, G_{RW} = antenna gains, in dBi, of the desired transmitter and the receiver, respectively;

$G_{TI}(\phi)$ = antenna gain of the interfering transmitter, in dBi, in the direction ϕ toward the receiver;

$G_{RW}(\theta)$ = antenna gain of the receiver, in dBi, in the direction θ toward the interfering transmitter;

L_W, L_I = basic transmission loss over the desired and interfering signal paths, in dB, respectively.

Equations 1, 2a, 2b and 2c represent extremes in correlation between C and I. Equation 1 is used when C and I are expected to be highly correlated; equation 2a, 2b or 2c is used when C and I are not expected to be correlated and the C/I is dominated by the variability of the interfering or desired signal or both. The choice between high and low correlation cases is not always clear. For example, if some earth stations in two satellite networks are close together (i.e., separated by less then the correlation distance), the associated Cs and Is will be correlated. On the other hand, interference between satellite networks whose respective earth stations are well separated in distance might not be correlated with desired signal levels. In this uncorrelated case, the magnitude of interference enhancements would be typically less than that of desired signal fading and equation 2c would be used. However, if earth station power control is used to overcome fading, then the variability of both the interference and the carrier might dominate the C/I and equation 2b would be used.

Once the form of the C/I equation has been determined, equations 3 and 4 can be solved for the dependent variable (e.g., EIRP). The PR interference criteria is typically applicable for particular combinations of desired and interfering signal modulations (e.g., CCIR, 1978a), separations in desired and undesired signal carrier frequencies, and performance objectives such as carrier-to-noise power ratio and link availability (CCIR, 1978b).

2.2 INTERFERENCE-TO-NOISE POWER TECHNIQUE

An INR is an interference-to-thermal noise power ratio that is to be exceeded for no more than a certain percentage of time. A commonly used equation for determining I/Ns is given below (CCIR, 1978c).

$$\frac{I}{N}(q) = P_I + G_{TI}(\phi) + G_{RW}(\theta) - L_I(p) - FDR(\Delta f) - 10 \log kT_eB \quad (5)$$

where:

$\frac{I}{N}(q)$ = interference-to-thermal noise power ratio, in dB, exceeded for no more than q percent of the time;

$L_I(p)$ = basic transmission loss over the interfering signal path, in dB, exceeded for p percent of time (p = 100 - q);

$FDR(\Delta f)$ = frequency dependent rejection of the receiver to the interfering signal, in dB, as a function of the separation in the interfering signal and receiver tuned frequencies (Δf);

k = Boltzmann/s constant, in J/K;

T_e = effective thermal noise temperature of the receiver, in ^oK, at the receiving antenna output;

B = receiver noise bandwidth, in Hz.

Equation 5 is suitable for use with single channel receivers where the interference component of the INR pertains to particular interfering signal modulations. In other cases, the interference component of the INR is assumed to be noise-like, a receiver transfer function is substituted for FDR, and a reference bandwidth is used for B to embody the effects of particular desired and undesired signal modulations. It is important to note that the wanted signal is not directly addressed in the INR technique.

2.3 ERROR DOMAINS IN THE ANALYTICAL TECHNIQUES

The PR technique appears to present more opportunities for analytical error than the INR technique. This is not necessarily true in practice. The main difference between techniques is the consideration of the desired signal, as in equation 3. The wanted system characteristics (P_W, G_{TW}, and G_{RW} in equation 3) that are used to evaluate the desired signal level are often precisely known. This would then leave only the basic transmission loss over the wanted signal path as the element that differs between techniques where significant error might occur. At the same time however, the INR technique assumes that the system operates satisfactorily in the absence of interference, as determined through independent analysis or demonstrated in operation, but has no excess margin of tolerance for interference above that allowed in the INR. Thus, both techniques present opportunities for error with regard to the desired signal.

The potential error domains in the two analytical techniques can be categorized as follows:

1) Interference criteria;
2) Desired link factors;
3) Interfering transmitter power;
4) Interference path antenna gains;
5) Interference path propagation losses.

Errors in predicting propagation losses over the interfering signal path can have a variety of consequences. When required propagation loss is the dependent variable, errors resulting from propagation prediction uncertainties would typically be embodied in the propagation parameters that are subsequently expected to provide the required losses (e.g., site shielding needs, required separation distance). On the other hand, errors resulting from propagation prediction uncertainties could be manifested in any other parameter that is utilized as the dependent variable. The net effect of all errors can be viewed in terms of the interference criteria: the interference criteria will be either over-satisfied or unfulfilled by some margin. The implications of these margins which arise in part from propagation prediction uncertainties depend on the particular frequency sharing analysis application.

3. IMPLICATIONS OF PROPAGATION UNCERTAINTIES

A primary objective of spectrum management is the prevention of interference. This is accomplished in part through the enactment and implementation of a number of regulatory provisions, including sharing criteria, frequency assignment coordination procedures and telecommunication service implementation plans. Detailed electromagnetic compatibility (EMC) analyses are used in cases where complete sharing criteria have not been established, there is an interference potential, and the situation is not in conformance with a service implementation plan. The implications of propagation prediction uncertainties in these four frequency sharing analysis applications are considered below.

3.1 DERIVATION OF SHARING CRITERIA

The general objective of frequency sharing criteria is to promote compatibility between systems or services through limitations on pertinent system characteristics. Sharing criteria typically take the form of restrictions on antenna input power, equivalent isotropically radiated power (EIRP), or frequency or distance separation. For example, satellite spectral power flux density (PFD) and terrestrial station EIRP limits have been enacted in the ITU Radio Regulations to promote compatibility between space and terrestrial services. These generic inter-service criteria establish upper bounds on interference for assumed deployments of stations and equipment characteristics.

Sharing criteria must be stringent enough to promote compatibility and prevent excessive consumption of the spectrum resource by any one system. On the other hand, sharing criteria must not be overly restrictive so that service or system performance requirements can be fulfilled in a practical manner. These requirements relate directly to the potential consequences of propagation prediction errors in the derivation of frequency sharing criteria:

- If the predicted propagation losses over the interfering signal paths are higher than the actual losses, unacceptable interference will occur if all assumptions made in the sharing criteria derivation are valid.

- If the predicted propagation losses over the interfering signal paths are lower than the actual losses, the interfering system design specifications have been overly restricted.

A number of assumptions must be made in the derivation of sharing criteria. While it is desired to make realistic assumptions, allowance must be made for the worst-case. This generally leads to conservative assumptions. There is consequently some tolerance for predicting propagation losses that are higher than those encountered in actuality. For example, erroneously high propagation loss predictions can be tolerated to a certain extent in the derivation of PFD limits for geostationary satellites since the following conservative sharing analysis assumptions could preclude interference:

- The geostationary orbit is densely occupied (e.g., satellites spaced at 3^{o} intervals).
- All satellites produce the maximum PFD that is to be determined in the analysis.
- The emissions of all satellites are within a common bandwidth (co-channel).
- The terrestrial station antenna is characterized by a reference radiation pattern (e.g., power gain envelope of 90% of the sidelobe peaks).
- The terrestrial systems have "typical" desired signal levels and receiver noise figures.

There is also some tolerance for predicting propagation losses that are lower than those encountered in actuality. This adds a degree of conservativeness to the sharing criteria which, in some cases, could be detrimental. Considering the PFD example again, the resultant overly conservative PFD limits would unnecessarily restrict the achievable space-to-earth link availability or minimum usable earth station G/T for satellite networks requiring the highest permissible downlink EIRP.

3.2 DETERMINATION OF COORDINATION REQUIREMENTS

A new or revised frequency assignment should be coordinated with the authorities of all other frequency assignments that might cause or experience interference. The general objective of methods for determining when coordination is needed is to identify all potential cases of interference. These methods utilize concepts such as coordination area: the area around an earth station within which terrestrial stations may cause or experience more than a permissible level of interference (ITU Radio Regulations Appendix 28). Other examples include bilateral border area coordination criteria and, in sharing between satellite networks, the concept of the permissible increase in equivalent link noise temperature.

Methods for determining coordination requirements must identify all situations where there may be unacceptable interference. At the same time however, it is desired that unnecessary coordination resulting from overly conservative analyses be avoided. These requirements are related to propagation prediction errors in the following manner:

- If the predicted propagation losses over the interfering signal paths are higher than the actual losses, the analysis method may fail to identify a potential interference situation.
- If the predicted propagation losses over the interfering signal paths are lower than the actual losses, unnecessary coordination may be effected.

A number of assumptions must be made in the determination of coordination requirements, although the number of assumptions is minimized to the greatest possible extent. Where actual equipment characteristics are not known, worst-case assumptions must be made. For example, the worst-case characteristics are typically assumed for terrestrial radio-relay stations when earth station coordination areas are calculated. Thus, there is generally some tolerance for predicting propagation losses that are higher than those encountered in practice. The following types of conservative assumption are typically made:

- Frequency sharing is on a co-channel basis.
- Antennas are characterized by reference radiation patterns that are representative of easily achievable antenna performance.
- The modulations are relatively uncompatible and offer no reduction in the interference potential.
- Characteristics of other systems are the probable worst-case with regard to sharing.

There is an administrative burden associated with unnecessary coordination, but this burden is much more acceptable than that which results when a coordination requirement omission leads to unacceptable interference. There is consequently an appreciable tolerance for predicting propagation losses that are lower than actual losses. This enables the use of simplified propagation analyses, but only to the extent that prediction errors do not greatly over-sensitize the coordination process.

3.3 DETAILED EMC ANALYSES

Detailed EMC analyses are conducted to determine the actual potential for interference or the conditions under which there will be negligible interference between particular telecommunication systems. As such, they are used to examine conformance with sharing criteria or to resolve coordination requirements. Typical EMC analysis results are frequency-distance separation criteria, site shielding requirements, and equipment or operational requirements. For example, detailed EMC analysis techniques for assessing interference between satellite networks have been established (CCIR, 1978d).

EMC analyses must be accurate to ensure that interference will not occur while not being overly conservative. In most cases, conservative EMC analyses can result in inefficient spectrum utilization and a premature "saturation" of a frequency band. These requirements relate to propagation prediction error consequences:

- If the predicted propagation losses over the interfering signal paths are higher than the actual losses, unacceptable interference is likely to occur.
- If the predicted propagation losses over the interfering signal paths are lower than the actual losses, the spectrum resource is being wasted.
- The converse of the above consequences applies with regard to the desired signal in the C/I approach.

The latter consequences pertaining to the desired signal are included since detailed EMC analyses frequently use the C/I approach. This is not generally true for coordination requirement analyses or the derivation of sharing criteria. The consequences of propagation prediction errors in detailed EMC analyses imply that there is little tolerance for error. This is a result of the general use of system-specific and deployment-specific characteristics. The main assumptions that are typically made in detailed EMC analyses involve antenna off-axis gain characteristics (co-polar and cross-polar), thereby affording few circumstances for mitigating propagation prediction errors.

In many instances, the conservation of spectrum resources is almost as important as the avoidance of interference. For example, heavily used services such as land mobile, broadcasting, and the fixed-satellite services must make the most efficient use of the spectrum resource to maximize the number of telecommunication requirements that can be fulfilled. This is limited by the need for practical equipment (affordable) and any further limitation by analytical methods is extremely detrimental.

3.4 TELECOMMUNICATION SERVICE IMPLEMENTATION PLANS

The general objective of service planning is to provide means for the fulfillment of particular telecommunication requirements through the adoption of a service implementation agreement. Implementation agreements can include sharing criteria (intra- and inter-service) and coordination procedures for systems not specifically addressed in the plan. The details of the service implementation plan are based on EMC analyses, wherein the achievable density of spectrum utilization is typically maximized for the agreed system parameters. For example, the 1977 WARC for the Broadcasting-Satellite Service (BSS) established an orbit position/frequency channel allotment plan and methods for determining requirements for coordination of Fixed and BSS frequency assignments.

The terms of a service implementation agreement must be based on realistic analyses in order to meet its goals. The consequences of propagation prediction errors are greater than those of the detailed EMC analysis, in that the effect of an error may not be perceived until implementation under the plan has been substantially accomplished. The net effect of propagation prediction errors could then be a failure to fulfill requirements in terms of the number of systems or the performance of individual systems. Increasing demands on the spectrum resource have made planning desirable on an international level, where the consequences of errors can have more serious repercussions than in planning on a national level.

4. CONCLUSIONS

The tolerance for propagation prediction error varies between frequency sharing analysis applications. The implications of propagation prediction uncertainties are multifaceted. Unacceptable interference is the obvious implication, however an increasingly important consequence is poor utilization of the spectrum.

REFERENCES

CCIR, 1978a, Provisional Signal-to-Interference Protection Ratios Required for Spectrum Utilization Investigations, Report 525-1, Geneva, Switzerland.

CCIR, 1978b, Methods for Determining Interference in Terrestrial Radio-Relay Systems and Systems in the Fixed Satellite Service, Report 388-3, Geneva, Switzerland.

CCIR, 1978c, A Method for Calculating Adjacent Band Interference, Report 654, Geneva, Switzerland.

CCIR, 1978d, Frequency Sharing Between Networks of the Fixed Satellite Service, Report 455-2, Geneva, Switzerland.

DISCUSSION

D. Davidson, US

As the "voice from Tampa Bay", I'd like to comment on uplink power control by merely monitoring downlink signal at the much lower frequency. Our measurements at 19 and 29 GHz in Tampa and in the Boston area showed a wide variation of attenuation ratio from minute to minute in heavy rain, even though statistically, over the long term, the median value is quite stable. Furthermore, one doesn't know equipment levels that well (to within 1 dB) within a redundant system. Intelsat finds that uplink power control in this manner cannot be held to within ± 1dB so one has to go to much more complicated measurements, such as measuring the uplink signal at the satellite ("a smart satellite") and the like, or active over and back measurements, taking into account satellite transponder compression.

J. Arnbak, Ne

Now that Mr Davidson introduced the notion of a complex satellite for measurements of the uplink carrier power for control purposes, we could perhaps add that with a complex satellite such as DSCS-III having a multiple-beam antenna (MBA), one might avoid the interference problems described by Mr Sullivan in his representation. Instead of raising uplink transmit power (which inevitably increases interference in the geo-stationary orbit), real-time adaptive control of the satellite receive MBA can maintain up-link C/N selectively in the face of rain, *without* causing extra interference to adjacent satellites (see paper 54, International Communications Conference (ICC-81), 14–18 June, 1981).

B.G. Evans, UK

I would like to comment on the assumption of a frequency scaling model in up-path power control between 12/17 GHz. We have recently examined the attenuation ratio 17/12 GHz using results from the Rutherford and Appleton dual polarization radar. This enables detailed weather paths to be investigated and the distribution of particles in small gates along the path to be assessed. We have found that A17/A12 is very dependent on the type of weather and nature of precipitation along the path. Light widespread rainfall does not produce the same ratio as heavy intense rain. Thus a simple frequency scaling ratio for up-path power control in real rain might be difficult.

G.H. Hagn, US

The paper and the discussion have focussed heavily on satellite system examples. You did mention that in cellular and mobile systems 1 or 2 dB errors in the interference analysis can produce a big effect on the quality of service which is predicted. The propagation uncertainty at 800 MHz is probably larger than 3dB (Dr Hughes' results presented this morning seem to say the models are not as good as 3dB). Even the measurements accuracy for basic transmission loss is probably no better than ± 3dB. This minimum uncertainty translates to communication range uncertainties of at least 20 percent. This uncertainty seems to contribute to less efficient use of the spectrum for land mobile systems. Any comments?

Author's Reply

One area propagation model, the ITS area propagation model, shows significant location and temporal availability changes for small changes in loss when it is applied to cellular-type services. The propagation analysis errors inherent in the use of this or other models may be interpreted in terms of failure to meet availability requirements. The analytical problems associated with the optimization of cellular system parameters are formidable but this is still an experimental service and there are opportunities to further address these problems with better models.

PROPAGATION PREDICTION USAGE IN AUTOMATED FREQUENCY ASSIGNMENTS BASED ON COSITE AND REMOTE SYSTEM SPECTRUM SHARING

SAMUEL M. SEGNER

US ARMY COMMUNICATIONS-ELECTRONICS COMMAND
CENTER FOR SYSTEMS ENGINEERING AND INTEGRATION
C^3 SURVIVABILITY AND SPECTRUM MANAGEMENT DIVISION
FORT MONMOUTH, NEW JERSEY, UNITED STATES

ABSTRACT

This paper covers the use of propagation predictions in the US Army (automated) Battlefield Spectrum Management and Engineering (ABSM&E) capability development program. This program is divided into nine tasks. The major task is the US Army (automated) Tactical Frequency Engineering System (ATFES) Pilot Program. This task will set up the experimental and test structure by fielding a "vertical" slice of an integrated capability in US Army Europe. These ADP systems will initially spectrum manage LOS, TROPO, and HF systems. Eventually, all communications and electronic (radar, sensors and avionics) will be managed by new software now in development for these spectrum dependent assets of command control and weapons systems. A major function of ABSM&E is to provide coordination of friendly force use of spectrum with friendly force ECM systems. The basic common interest here is the propagation aspect of each spectrum dependent system in each community.

INTRODUCTION

My organization is concerned with managing the electromagnetic spectrum effectively while simultaneously surviving under the postulated electronic threat to the spectrum dependent telecommunications equipment required by the US Army command and control systems and weapons systems.

In general, the military community recognizes that mutual interference degrades performance of combat telecommunications equipment and are therefore willing to accept constraints for the sake of electromagnetic compatibility.

Based on groundwork carried out by the US Army, other DOD services and allied force organizations, it is apparent that Automated Data Processing (ADP) aids for battlefield spectrum managers is needed, even though the exact nature of the added capabilities is still being explored. The CCIR activities in this area are at Ref 1.

Many observers feel the capabilities should have been fielded a decade ago instead of still being in research and development. To some extent, the US Army has recognized this and is attempting to get spectrum management capabilities up to the high technology levels already being implemented in military telecommunications systems. However, the success of all frequency engineering, whether manual or ADP aided, is a function of the validity of the propagation models to predict system performance and interference, and environmental noise.

THE ABSM&E PROGRAM (Fig 1)

A comprehensive program has been in-being at USACECOM for several years with the stated goals. The program is driven by the needs of the current fielded forces and the forecasted needs as a result of review of the telecommunications systems currently being planned and/or procured by the US Army and joint service programs.

Incidentally, the word "telecommunications" in this paper is being used in the broad sense to include all communications and non-communications (usually called electronic) services which are in the international frequency allotment plans.

ENGINEERING JUDGEMENT FACTORS

Figure 2 lists some of the factors which should be taken into account when determining how much is essential for battlefield spectrum management. The equipment receiving frequency assignments are normally mobile and/or transportable. The deployment will change several times a day in forward combat zone and several times a week in rear areas. Expecting to find extensive data on each site for each equipment and that the environment can accurately be developed does not appear practical. It can be assumed that the spectrum management ADP hardware would be some form of minicomputer supporting an organization which has to produce answers (frequency assignments) for planned deployments within time limitations.

The terrain features have limited accuracy due to quantization error when digitized terrain maps are provided and as a result of structures and/or foliage.

The enemy also would use the spectrum for his command control communications and combat surveillance and target acquisition/engagement electronics systems, (aside from conducting radio electronic warfare against friendly force telecommunications systems) which creates uncontrollable EMC problems.

Thus, the approach being used in the ABSM&E program has to temper the software complexity with the practical limitations of the combat formations and their missions. Where extensive computation is necessary to provide electromagnetically compatible frequency assignments, e.g. for peacetime training and

tactical exercises, in-nation supporting ADP facilities can be made available.

A final point to be noted in this section is identifying the cosite or co-location cases. In some cases where the equipment and antennas are on a common land vehicle or aircraft, the relative geometry is fixed and the computations, as shown in Fig 3, for 1 to 5 meter antenna spacing are "good".

Where the antennas are on different vehicles, the spacing is based on engineering judgement that the two vehicles will be in the same vicinity and the antenna spacing is then estimated based on field experience. The experienced field officer knows that the soldiers making the actual setup are "smart" enough to follow "good engineering practice" in many cases to avoid interference.

ABSM&E TASKS (Fig 4)

For convenience, the ABSM&E program has been broken into nine tasks. Except for tasks three and five, all other tasks are greatly influenced by propagation factors and will be discussed as such.

Before dismissing tasks three and five from further discussion, it should be noted that the US Army concept is to make the signal planning and engineering staff of multichannel communications systems at each echelon responsible for spectrum management and coordination of all spectrum dependent communications and electronic systems organic to that echelon as well as non-spectrum dependent capabilities required for engineering and maintaining the multichannel systems.

ATFES PROGRAM (Fig 5)

Reference 2 discussed this program in some detail as an alternative to the standard development cycle. It gives the user a "now" capability by installing ADP equipment in his current communications system control and engineering facilities. The user is provided with an initial set of software capabilities based on mutual engineering judgement of the user and the developer. By using the capabilities provided in day to day training activities, as well as in tactical exercises, the user is able to refine the judgement of what is needed and, when the initial capabilities have been upgraded, evaluate them in the field.

A basic feature introduced in this ADP equipment is the ability to predict propagation based on digitized terrain maps produced by the US Defense Mapping Agency.

Several software capabilities used in ATFES ADP are worth noting (Fig 6). The first is the Terrain Resources Analysis Program (TRAP) for determining the propagation mode and losses between two radio sets using the terrain profile between the two sites. The primary propagation model is the DOD/ECAC Terrain Integrated Rough Earth Model (TIREM) described in Ref 3. Since more than one mode may be present, TIREM computes path loss as a weighted combination of losses. The US Army line of sight radio relay systems involved are listed in Fig 6. Propagation computations are being upgraded to account for polarization differences.

One of the issues worthy of study is the effect of foliage when in the direct path and at a multipath reflection point. Most military communications will show less concern for clearing trees below 500 MHz than for radio systems above 500 MHz.

Two capabilities in ATFES are candidates for growth to include propagation effects. One of these is the line of sight area coverage which can be used to study siting of land and airborne communications, intelligence/EW radar systems. Currently, it only uses terrain obstructions as a criteria but is being augmented to allow overlay of signal levels.

Another is the Frequency Assignment Capability for Tactical Systems (FACTS). It currently has rules of thumb to avoid image frequencies and third and fifth order intermodulation products based on judgement of common vehicle/cosite affiliation. This may result in significantly overconservative frequency assignments, which could be overcome by adding propagation factors for cosited radio systems.

GMFSATCOM SYSTEMS (Fig 7)

References 4, 5 and the paper preceeding this one discuss the complexity of coordinating satellite communications systems with terrestrial systems as a result of Appendix 28 of the ITU radio regulations. Appendix 28 covers all possible forms of propagation related to interference mechanisms. The computations required have been programmed as a result of the late Mr. Fansler's activities and is currently resident in a VAX computer system at DOD/ECAC called the Operational System Support Cell. Studies are underway to determine how much of this capability should be organic to the field.

EFFECTIVE USE OF THE HF SPECTRUM (Fig 8)

The US Army activities in HF imply substantial use of this part of the band in the future. Since this band is quite limited due to sun activity impact in the ionosphere, several approaches are being studied.

The ability of ATFES to forecast HF propagation is being upgraded from an ECAC MINIMUF to a US Navy PROPHET MINIMUF along with groundwave propagation capability. However, the validity of skywave propagation predictions is dependent on the national and international organizations to predict sunspot activity.

One form of ionospheric probe is the HF Chirpsounder, AN/TRQ-35. The US Army is developing operational concepts for using this equipment. It is anticipated that the use of sounders will enable development of local, short time accurate prediction. The engineering unknowns seem to be how to apply point to point data (of limited accuracy in itself) to an area, and whether North-South soundings in an area are good for East-West communications links. Also, how much sounding is enough for a given area. Equally important as propagation is noise prediction in this band as shown in Fig 4 or Ref 5.

COMMONALITY WITH ALLIED FORMATIONS SPECTRUM MANAGEMENT (Fig 9)

In order to be consistent with spectrum management planning and activities of allied armies, several activities have been initiated.

A Land Warfare Battlefield Spectrum Management Symposium, sponsored by USACECOM, was hosted by DOD/ECAC at the US Naval Academy. NATO and ABCA Frequency Managers were invited.

A Special Working Party for Frequency Allotment and Assignments (SWP/FAA) was established in 1978 within the ABCA Quadripartite Working Group for Combat Communications (QWG/COMMS). NATO ARFA was briefed on SWP/FAA in December 1979 by the Canadian Representative. The ABCA Concept Paper on Frequency Management was furnished to an ATCA Air Working Group during the Summer of 1981.

Figure 10 shows the major products of SWP/FAA to date. The QSTAG's are currently more qualitative than quantitative, but the format allows growth without impacting on the basic agreement. It is anticipated that all QSTAG's will be in final draft by Fall of 1983.

VHF SPECTRUM MANAGEMENT (Fig 11)

By using a variety of propagation models, such as those discussed in Ref 6, rules of thumb have been developed which rate combat net radios in terms of range (distance) with some variation sometimes for traffic mode. Using these range ratings and other rules of thumb, frequencies are being reused, usually where the distances between nets are in the order of 30 KM.

The ATFES actual assignment procedure is dependent of cositing rules of thumb derived from frequency vs distance (F/D) measurements. The identification of cosited equipment is a matter of field judgement. The ATFES capability to analyze for cosite interference can call for actual path loss computation. It should be noted that the effect of foliage and polarization is normally neglected below 100 MHz.

Of great current interest is the frequency management approach for frequency hopping spread spectrum systems. The studies underway are described in Ref 7 and 8. Based on review of Ref 9, the US Army is also studying the appropriate approach to alloting frequencies in the SINCGARS time frame.

SYSTEM INTEGRATION (Fig 12)

An obvious major user of the spectrum is the passive electronic surveillance and the active EW systems of friendly forces. These friendly force intelligence and EW systems are normally geographically closer to friendly force spectrum dependent equipment than to intended victim equipment. The approach being studied by USACECOM is to attain the benefits of the Intelligence/EW missions with minimum impact on friendly force combat operations. Obviously, propagation prediction at all frequency bands is basic to "optimizing" solutions. Again, stress has to be placed on short term arrangements with recognition that it is likely that the model being studied only approximates the actual deployment and excessive details may not be available and may not be warranted.

SPECTRUM OPTIMIZATION STUDIES

Figure 13 indicates ABSM&E oriented interests in developing and applying EMC/EMV models for each frequency band.

Part of the problem is establishing the data base for each equipment. A relevant problem is trying to get all analysis agencies to agree on propagation and noise models for each frequency band. It is difficult doing this within a nation and even more so internationally because the differences in models can result in median propagation loss calculation whichdiffers by 10 to 20 dB which translates to range rating difficulties in excess of 3:1.

FOLIAGE PROPAGATION

An interest of all ground forces is propagation through foliage in the tactical combat net radio bands, namely, the HF (2 to 30 MHz), VHF (30 to 100 MHz) and UHF (225 to 400 MHz) bands and the effect of foliage on line of sight radio relay bands starting at 225 MHz.

The scientific community has provided several models to compute foliage losses (L_{fol} in dB). Most take the form of:

$$L_{fol} = \text{Constant} \times f^a d^b \qquad (1)$$

where f is the frequency, usually MHz

d is the distance, usually meters of foliage to be penetrated.

An example, good for d up to 400 meters, is in Ref 9.

$$L_{fol} = 1.33 \times \left(\frac{f}{1000}\right)^{0.284} \times d^{0.588} \qquad (2)$$

Other formulas can be found which have different exponential dependence on "f" and "d".

With all other factors assumed fixed for the sake of simplicity, the range of given radio is usually based on its transmission loss, L_{btl}:

$$L_{btl} = \text{Constant} = 10 \log f^c + 10 \log D^e \qquad (3)$$

With D normally in kilometers, for free space "c" and "e" are 2. Assuming that power cannot be used to compensate for foliage loss, the usual option is to decrease range (Distance) or:

$$L_{btl} + L_{fol} = \text{Constant} \quad (4)$$

Or, again using simplifying assumption and forumulas (2) and (3):

$$10 \log D^2 + \text{Constant} \times d^b = \text{Constant} \quad (5)$$

Different formulas found in the literature have been studied. The investigation was intended to show the relative effect of using different formula on radio range and was not intended to give credence to any one formula. The effect of using different formula had considerable impact on D.

In the case of investigating an interference path, especially above 100 MHz, foliage losses can help frequency sharing and re-use if parties concerned can agree on formula to be used. It is heartening to note that in the case of satellite communications, the telecommunications engineers and the propagation scientists seem to agree on a set of "standard" formula or curves (Ref 5).

CONCLUDING REMARKS

The goal of this paper is to help set priorities for propagation studies by providing the user point of view.

The "bottom line" user is a combat commander who wants his signal staff to get him frequency assignments so that single channel communications by voice and/or data can be established over a net of mobile users within a given combat area. Another "bottom line" user is the multichannel communications planner who wants to interconnect nodes with multichannel radio systems. Still another is a unit interested in electronic surveillance for particular targets and their engagement with electronic sensors.

These "bottom line" users really do not care about what frequency they are assigned as long as it does not impact on their "performance". This "performance" criteria can usually be simplified down to coverage or radio/radar range.

The frequency management group of the signal staff are the actual users of propagation studies, whether as formula or "rules of thumb" based on experience with applying formula for propagation range, interference and noise.

The ATFES program is trying to help and via automation, fine tune the "rules of thumb" by using formula wherever possible. The goal is to get the military and civil, usually host nation, community to agree to much more sharing (frequency reuse) in the spectrum. This involves getting agreement on how to calculate propagation, interference and noise.

It is recognized that many propagation studies are endeavoring to provide data which fits measurements. However, one should take the viewpoint of how does the "fine tuning" of formula affect the simplist criteria, radio or radar range, vs how much does it hold up standardization of methods of computing range in each frequency band. From the point of view of one who is trying to provide the battlefield frequency managers of the US Army with appropriately accurate ability to compute radio and radar range and interference levels, it would see m that a worthy goal of this group would be to provide agreed standard methods of computation rather than different formulas which, in the long run, may not affect coverage very significantly.

From the more general civil and government view, Interim Working Party 1/2 (Ref 1) has recognized the value of computer aided techniques and would seem to be an appropriate forum for applying each standardized formula outside of the military. This would be of great aid to military frequency managers planning peacetime tactical and training exercises.

REFERENCES

1. Draft Report of AF/1, Addendum 1 to Doc 1/122, 30 July 1980 (CCIR Study Group 1), "Spectrum Management and Computer Aided Techniques".

2. The ATFES Pilot System - A User/Developer Interactive Program, S. Segner, AFCEA, Ft Monmouth, NJ, 23/24 September 1981.

3. ECAC Propagation User's Manual, Weissberger and Baker, ECAC-UM-78-001, Electromagnetic Analysis Center, Annapolis, Maryland, April 1978.

4. The Interrelation of Propagation Effects and Design Factors for Fixed Service Communications Satellite Systems, Fansler and Segner, AGARD, Rome, Italy, 11 May 1973.

5. Techniques for the Management of Frequency Bands Shared Between Terrestrial Stations and Mobile or Transportable Earth Stations, Phillips and Sullivan, IEEE Transactions on EMC, Joint Special Issue on WARC 79, August 1981, Vol EMC-23, No 3.

6. Radio System Performance Model for Predicting Communications Operating Ranges in Irregular Terrain, Hagn, 29th IEEE Vehicular Technology Conference, Arlington, Illinois, 28 to 30 March 1979.

7. US Presentation on the SINCGARS-V EMC/EMV Analysis, AC-302 Subgroup 2, Week of 13 October 1980.

8. ECAC-CR-80-070-N: Interim Report on Frequency Assignment Techniques for SINCGARS-V, March 1981, TSGCEE Subgroup 2, Week of 6 April 1981.

9. SHAPE Technical Center TM-646, VHF-FM Central Region Frequency Planning Study, RPJ Endean, May 1981.

10. Modelling the Increase in Loss Caused by Propagation Through a Grove of Trees, Weissburger and Hauber, URSI, Quebec, 2 to 6 June 1980.

FIGURE 1

USACECOM/CENSEI PROGRAM

GOAL:

- PROVIDE THE US ARMY COMBAT FORMATIONS WITH:
  - AUTOMATED BATTLEFIELD SPECTRUM MANAGEMENT AND ENGINEERING (ABSM&E) CAPABILITIES.
- THE CAPABILITIES SHOULD BE HOSTED IN AND/OR INTEGRATED WITH THE INVENTORY AND IN-DEVELOPMENT TACTICAL COMMUNICATIONS SYSTEMS PLANNING AND CONTROL ELEMENTS AND/OR FACILITIES.

FIGURE 2

ENGINEERING JUDGEMENT FACTORS

- ACTUAL DEPLOYMENTS DIFFER FROM PLANNED DEPLOYMENTS.
- ACTUAL DEPLOYMENTS CONTINUALLY CHANGE BASED ON COMBAT OPPORTUNITIES.
- TIME LIMITED COMPUTATION MUST PROVIDE ANSWERS.
- DATA BASE ACCURACY, INCLUDING TERRAIN FEATURES.
- ENEMY USES SPECTRUM.
- PEACETIME TACTICAL AND TRAINING EXERCISES CAN BE SUPPORTED ELSEWHERE.

FIGURE 3

IMAGE AND INTERMODULATION ANALYSES

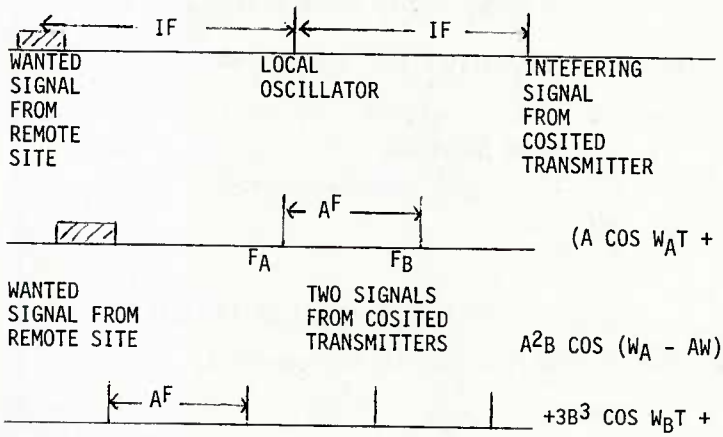

$(A \cos W_A T + B \cos W_B T)^3$

$A^2B \cos (W_A - AW)T + 3A^3 \cos W_A T$

$+3B^3 \cos W_B T + AB^2 \cos (W_B + AW)T + \ldots$

FIGURE 4

ABSM&E TASKS

TASK 1	ARMY TACTICAL FREQUENCY ENGINEERING SYSTEM (ATFES) PILOT PROGRAM.
TASK 2	SPECTRUM MANAGEMENT OF GROUND MOBILE FORCES SATELLITE COMMUNICATION (GMFSATCOM) SYSTEMS.
TASK 3	SYSTEM INTEGRATION WITH TRI-TAC JOINT SERVICE PROGRAM.
TASK 4	EFFECTIVE USE OF HF SPECTRUM.
TASK 5	CONFORMANCE WITH US ARMY CONCEPTUAL AND OPERATIONAL GUIDANCE FOR BATTLEFIELD SPECTRUM MANAGEMENT: - CORPS AND BELOW - ECHELONS ABOVE CORPS
TASK 6	COMMONALITY WITH ALLIED FORMATIONS SPECTRUM MANAGEMENT.
TASK 7	MANAGEMENT OF VHF (30 TO 90 MHZ) BAND.
TASK 8	SYSTEM INTEGRATION STUDIES.
TASK 9	SPECTRUM OPTIMIZATION STUDIES.

FIGURE 5

ARMY TACTICAL FREQUENCY ENGINEERING SYSTEM (ATFES) PILOT PROGRAM

- SINGLE UNIT OR MULTI-SHELTER INSTALLATION IN US ARMY EUROPE:
  - 5TH SIGNAL COMMAND @ WORMS (THEATER HQ COMPONENT)
  - 7TH SIGNAL BRIGADE @ MANNHEIM (ECHELON ABOVE CORPS)
  - 7TH CORPS @ STUTTGART
  - 3D INFANTRY DIVISION @ WURZBURG
- CONUS SYSTEMS
  - S-W DEVELOPMENT FACILITY @ DOD ECAC
  - US ARMY SIGNAL CENTER TRAINING FACILITY
- BASIC HARDWARE AN/GYQ-21(V) (BUNKER-RAMO)
  - CPU DEC 11/70, INTERNAL 512 KBYTES
  - DISK 67 TO 300 MBYTES
  - CRT VIDEO & COLER GRAPHICS TERMINAL
  - PRINTER
  - PLOTTER

FIGURE 6

PROPAGATION RELATED CAPABILITIES IN ATFES

- TERRAIN RESOURCES ANALYSIS PROGRAM (TRAP)

- AN/GRC-50	LO		600 TO 1000 MHZ
	HI		1350 TO 1850 MHZ
- AN/GRC-103 BAND		I	220 TO 400 MHZ
		II	395 TO 705 MHZ
		III	695 TO 1000 MHZ
		IV	1350 TO 1850 MHZ
- AN/GRC-144			4400 TO 5000 MHZ

- LINE OF SIGHT AREA COVERAGE CAPABILITY

FIGURE 7

TASK 2 SPECTRUM MANAGEMENT OF GMFSATCOM SYSTEMS

- SATELLITE CAPABILITY STUDY FOR HIGH LEVEL ATFES-ECAC
- JCS OPERATIONAL SYSTEM SUPPORT CELL (OSSC)
- INTERFACES WITH SATELLITE AUTOMATIC MEASURING SYSTEM AN/MSQ-114

FIGURE 8

TASK 4 EFFECTIVE USE OF HF SPECTRUM

- APPLICATION OF ARMY PROPHET EVALUATION STUDY
- INTEGRATION WITH HF CHIRPSOUNDERS
- STUDY DEMAND ACCESS AND/OR HF POOLING

FIGURE 9

TASK 6 COMMONALITY WITH ALLIED FORMATIONS SPECTRUM MANAGEMENT

- DEVELOP STANDARDIZED CONCEPTS, OPERATIONAL PROCEDURES AND INTERFACES FOR COMBINED FORCES TACTICAL SPECTRUM MANAGEMENT.
- CHAIR ABCA SPECIAL WORKING PARTY FOR FREQUENCY ASSIGNMENTS AND ALLOCATIONS:
  - ABCA FREQUENCY MANAGEMENT CONCEPT
  - QSTAGS
  - LONDON MEETING: MAY 1982
- CROSS FERTILIZE SWP/FAA WITH NATO ARFA AND ATCA.

FIGURE 10

SWP/FAA ACTIVITIES

CATEGORY IV CONCEPT PAPER, FREQUENCY MANAGEMENT, CORPS AND BELOW

DRAFT QUADRIPARTITE STANDARDIZATION AGREEMENTS

#715	(AS)	- BATTLEFIELD SPECTRUM MANAGEMENT:	HF (1.5-30 MHZ)
#716	(UK)	- " " "	VHF (30-100 MHZ)
#717	(UK)	- " " "	VHF (100-225 MHZ)
#718	(CA)	- " " "	UHF (225-400 MHZ)
#719	(US)	- " " "	MULTICHANNEL LOS & TROPO
#720	(US)	- " " "	GMFSATCOM
#721	(US)	- " " "	RADAR, POS/NAV & SENSORS
#679	(CA)	- " " "	MM WAVE & LASERS
#723	(US)	- " " "	C^3I/EW INTEROP

FIGURE 11

TASK 7 MANAGEMENT OF VHF (30 TO 88 MHZ) BAND

- DEVELOP ATFES CAPABILITY TO GENERATE COMMUNICATIONS-ELECTRONICS OPERATING INSTRUCTIONS (CEOI) AT CORPS AND DIVISION (FREQUENCY ASSIGNMENT & CALL SIGNS).
- DEVELOP CAPABILITY TO ELECTRONICALLY DISSEMINATE AND LOAD STORAGE DEVICES WITH FREQUENCY ASSIGNMENTS.
- DEVELOP CAPABILITY TO PERFORM VHF COSITE ANALYSIS.

FIGURE 12

TASK 8 SYSTEM INTEGRATION STUDIES

- o INTERFACES/INTEROPERABILITY
  - EW/INTEL CONTROL AND ANALYSIS FACILITIES
  - COMMAND CONTROL FACILITIES
- o APPLICABILITY OF ATFES CAPABILITIES
- o DATA BASE PROTECTION

FIGURE 13

TASK 9 SPECTRUM OPTIMIZATION STUDIES

- o DEVELOP EMC/EMV MODEL OF NATO ELECTRONIC BLUE/RED BATTLEFIELD
  - 1980'S
  - 1990'S
  - BEYOND 2000
- o DEVELOP RAPID ASSESSMENT TOOLS FOR ASSIGNMENT ALGORITHMS
  - SYSTEM PERFORMANCE: SELF INTERFERENCE/JAMMING
  - SYSTEM SURVIVABILITY: INTERCEPT AND LOCATE

DISCUSSION

G.H.Hagn, US

Considerable data were taken on jungle propagation about 15 years ago in Thailand. I am pleased to hear that new data will be obtained on propagation through vegetation in Europe (Germany and UK). It is important to describe vegetation adequately when such measurements are made in order to permit extrapolation to other locations and situations.

Author's Reply

The program has an advisory group of US propagation experts who recognize that the results of the measurements program must lead to propagation models applicable to other locations, at minimum other temperate zone foliage situations.

ON COMBATING MULTIPATH EFFECTS USING SPREAD-SPECTRUM SYSTEMS

C. P. Tou
Department of Electrical Engineering
Technical University of Nova Scotia
Halifax, Nova Scotia, Canada B3J 2X4

ABSTRACT

This paper discusses briefly the origins of multipath propagation, their effects on radio communication systems, and schemes for suppressing these effects. Major attention is given to spread-spectrum schemes to demonstrate their capacity to combat multipath effects, to examine conditions under which the schemes would be effective, and to assess the merits of the schemes.

Multipath propagation can occur under various atmospheric and geographical conditions as illustrated by simple examples. The adverse effects of multipath propagation on communication systems can be described in terms of selective fading and intersymbol interference. Simple measures can be found if the multipath propagation is predictable, but sophisticated techniques are required to combat unpredictable multipath interference.

It has been shown that spread-spectrum systems are superior to other approaches in terms of effectiveness in combating multipath interference and other valuable features. However, the ability of spread-spectrum systems to suppress interference depends on the process gain of the system and the system performance depends on the degree of synchronization which can be established by the system.

1. INTRODUCTION

Multipath propagation is a phenomenon in which a signal proceeds to the receiver along more than one path. Every component signal at the receiver will have different amplitude and phase because of the different nature and length of each path. The received signal is a vector sum of the component signals. As a result, the received signal may fluctuate and suffer severe fading causing degradation of radio communication systems.

Multipath interference is different from other types of interference in that the interference signals originate from the same signal source. It may be considered as a type of cochannel interference.

In some cases when multipath propagation can be predictable, certain simple measures may be found to tackle the multipath effects, but multipath problems are in general quite difficult to overcome. This is mainly because, in most cases, multipath cannot be accurately predicted and varies with time and space due to changing atmospheric and geographical conditions. It is therefore essential to have a technique which can combat multipath effects without the need of prior knowledge of multipath characteristics. The Rake system represents a sophisticated adaptive receiver technique which estimates and compensates for the channel characteristics by combining knowledge of the transmitted waveform together with the receiver decision, but its implementation is very complex and expensive, thus precluding its use in many applications.

Spread-spectrum technique is a passive suppression scheme which requires no prior knowledge of multipath characteristics. It can reject multipath interference once a synchronization between the transmitter and the receiver is established. Such systems can operate at the same frequency and at the same time by using different codes. Irrespective of the direction of arrival, the technique can distinguish the desired signal from the interferring signal.

This paper will discuss briefly the origins of multipath propagation, its effect on radio communication, and the schemes for suppressing the effect in order to justify the application of spread-spectrum systems. The basic principles of direct-sequence systems are reviewed to demonstrate their capabilities of suppressing interference/noise and, especially, multipath interference; to show other significant advantages of using such systems, to examine the factors which affect the ability of the system to reject interference/noise and the performance of the systems.

2. ORIGINS OF MULTIPATH

Multipath propagation can happen under various atmospheric and/or geographic conditions. The multipath may be due to stratified layers and inhomogeneties of the atmosphere, such as reflection from an inversion layer, partial reflection from an atmospheric sheet, refraction in an inhomogeneous layer, and scattering by a turbulence as shown in Fig. 1 (a) - (d), respectively. It has been known that multipath propagation of atmospheric origin is more frequent when the atmosphere is not turbulent (a stable atmosphere can easily form stratified layers) and they appear more often at night and in summer (Beckmann, P., and A. M. Spizzichino, 1963).

Multipath propagation caused by geographical (terrain) conditions may be due to reflections from the ground or water, from buildings or objects, from mountains or hills, and from

aircraft as shown in Fig. 2(a) - (d), respectively.

In addition to ground-to-ground links, multipath can exist between air-to-ground or ground-to-air links, aircraft-to-aircraft links, aircraft-to-satellite or satellite-to-aircraft links, and satellite-to-satellite links due to reflections from the surface of the earth as shown in Fig. 3 (a) - (d), respectively.

The above cited cases represent only a few simple and separate examples in order to get some feeling about the many possibilities of multipath propagation due to various atmospheric and geographical conditions. In fact, multipath propagation of both atmospheric and geographical origins can occur simultaneously. Meterological conditions are changing with atmospheric conditions which vary with time and with geographical locations. Thus, multipath may appear or disappear with time under certain meterological conditions. Terrain conditions also change with time for mobile communications. Again, multipath may appear or disappear with time under certain geographical conditions.

In some simple cases, multipath may be predictable based on known atmospheric and/or terrain conditions, but in most cases they are not easily and accurately predictable due to changing meterological and geographical conditions. This is especially true in the case of mobile communications.

3. MULTIPATH EFFECTS ON COMMUNICATION SYSTEMS

The adverse effects of multipath propagation on communication systems can be described in terms of selective fading and intersymbol interference, which degrade the performance of analog and digital radio communication systems in the form of distortion and bit error, respectively.

Selective fading can take place when a transmitted signal arrives at the receiver through more than one path. The received signal consists of a direct-path signal and one or more indirect-path signals. The amplitude and phase of these component signals depend on the frequency and the natures and lengths of the individual paths. The received signal is a vector sum of the direct and indirect signals, and, therefore, its strength depends on the relative amplitudes and phases among the direct and indirect signals. If the resultant of the indirect signals are in phase with the direct signal, the received signal will become stronger. It will become weaker if they are out of phase. As a result, the received signal will fluctuate and may suffer severe fading due to changing atmospheric and geographical conditions. We may therefore observe large variations in the received signal either as a function of time at a single frequency or as a function of frequency at a given time (i.e. selective fading).

Intersymbol interference of digital radio systems is associated with the different time delays through the multipath which can cause bit error due to overlapping of digital signals. The error probability will increase as the bit rate of digital transmission is increased.

Multipath propagation can cause both amplitude and frequency distortion of the received signal and affects various communication systems in different manners. Amplitude distortion may be serious in AM radio systems, but it may not be as detrimental as frequency distortion to FM radio systems (Corrington, M. S., 1945). Multipath effects on PSK systems were investigated both theoretically and experimentally (Morgan, D. R., 1972; Nesenbergs, M., 1967; Ott, R. H., et al, 1978). The effects of multipath on FSK systems were analyzed in detail (Kwon, S. Y., et al, 1978; Chadwick, H. D., 1971). In addition, multipath propagation can cause serious error to low-angle tracking radar (Skalink, M. I., 1980).

4. MULTIPATH SUPPRESSION TECHNIQUES

For some cases when the multipath can be accurately predicted, simple and effective measures may be found to combat the multipath effects on radio systems. For example, we can avoid or reduce multipath interference by selecting suitable receiving sites, by using narrow-beam antennas, by providing adequate link margins, by building metal fence to block multipath signals, etc. These techniques may work quite well for fixed point-to-point communications. Special system designs are also used for combating multipath effects such as the use of synchronous detection for AM radio systems and the use of various forms of diversity systems to minimize selective fading, and multiple subcarrier each having long symbol waveforms have been used to overcome intersymbol interference.

However, for most cases, multipath cannot be easily predicted due to changing meterological and terrain conditions, especially in the case of mobile communications. Simple measures and those as cited above will not be effective. Diversity reception systems can be effective in combating multipath effects for fixed point-to-point communications, but the systems may not be easily implemented for mobile communications and the scheme of using multiple subcarriers may not be very effective.

Multipath suppression techniques may be divided into passive and active suppressions. The passive suppression technique is to minimize the multipath effects without the actual knowledge of the multipath characteristics. Diversity reception and spread-spectrum systems are typical examples. For active suppression techniques, the receiver performs continuous measurements of multipath characteristics and the knowledge is then used to combat the multipath effects such as Rake system (Price, R., et al, 1958) and adaptive spectral equalization systems (Morgan, D. R., 1978).

The Rake system was designed to combat random multipath and additive noise. The essence of this system is that the multipath signals are detected individually by a correlation technique and add them algebraically rather than vectorically to fight selective fading. Intersymbol interference is eliminated by reinserting different delays into the various detected signals so that they fall into step again. It represents a sophisticated approach to the multipath problems by reducing selective fading and intersymbol interference. However, the system is rather complicated for implementation.

Great interest has been directed toward the schemes of suppressing all but one dominant path signal, and this approach may be implemented by means of spread-spectrum techniques using pseudo-random codes. The following sections are devoted to the spread-spectrum schemes to introduce the basic principle of operation, to demonstrate their capabilities to combat multipath effects, and to examine conditions for high performance.

5. BASIC PRINCIPLES OF SPREAD-SPECTRUM SYSTEMS

A spread-spectrum system transmits a signal by spreading it over a much wider bandwidth than the minimum bandwidth required for transmitting the signal and the desired signal is recovered by despreading the received signal with a locally generated reference code at the receiver.

A basic spread-spectrum scheme is illustrated in Fig. 4 (a) and (b). In the transmitter a spread-spectrum code $p_i(t)$ is used to spread the modulated signal $s_i(t)$, where $s_i(t) = m_i(t) \cos(\omega_0 t + \theta_i)$, over a much wider bandwidth than that of the original modulated signal. The transmitted signal may be expressed by equation (1).

$$p_i(t)\, s_i(t) = p_i(t)\, m_i(t) \cos(\omega_0 t + \theta_i) \tag{1}$$

where $p_i(t)$ is the spreading code; $m_i(t)$ is the message signal; ω_0 is the carrier frequency and θ_i is the phase angle of the carrier.

Assume that undesired signals and interference/noise are also received along with the desired signal $r_i(t)$. The composite signal and noise at the receiver input may be expressed by equation (2).

$$r(t) = \sum_{j=1}^{N} r_j(t) + n(t) \tag{2}$$

where $r_j(t) = p_j(t-\tau_j)\, A_j s_j(t-\tau_j)$; j^{th} received signal

$p_j(t-\tau_j)$; j^{th} spread spectrum code received

$s_j(t-\tau_j) = m_j(t-\tau_j) \cos[(\omega_0 + \omega_j)t + \theta_j]$; j^{th} modulated signal received

$n(t)$ = interference/noise

and A_j, τ_j, ω_j, and θ_j represent the amplitude, the delay time, the Doppler shift frequency, and the phase angle of the j^{th} signal, respectively.

It is intended to show the extraction of the desired signal $s_i(t)$ and rejections of all others by the receiver of the spread-spectrum system. As shown in Fig. 4 (b), following the RF filtering (for simplicity negligible distortion is assumed) the composite signal is multiplied by the locally generated oscillator frequency ω_1 (here $\omega_1 = \omega_0$ is assumed for simplicity of analysis, but a heterodyne correlation is preferred, i.e. $\omega_1 \neq \omega_0$) and the reference code $p_i(t-\hat{\tau}_i)$ (the delayed replica of transmitted code) in order to achieve correlation between the desired signal and the local reference code. The output of the multiplier is given by equation (3)

$$u(t) = \sum_{j=1}^{N} u_j(t) + n_0(t) \tag{3}$$

where $u_j(t) = p_i(t-\hat{\tau}_i) \cos[(\omega_0 + \hat{\omega}_i)t + \hat{\theta}_i] \cdot r_j(t)$

$n_0(t) = p_i(t-\hat{\tau}_i) \cos[(\omega_0 + \hat{\omega}_i)t + \hat{\theta}_i] \cdot n(t)$

The values of the delay time $\hat{\tau}_i$, the Doppler shift frequency $\hat{\omega}_i$, the phase angle $\hat{\theta}_i$ are provided by the synchronization tracking loops (which are not shown in Fig. 4 (b) for simplicity of the diagram) at the receiver in an attempt to align the receiver oscillator and the reference code generator with the corresponding desired signal parameters. If the receiver is perfectly synchronized with the i^{th} transmitter, then $\hat{\tau}_i = \tau_i$, $\hat{\omega}_i = \omega_i$, and $\hat{\theta}_i = \theta_i$. That is, the reference code of the receiver is synchronized with that of the transmitter and their frequency and phase are perfectly locked to each other. The desired and undesired signals and noise terms at the output of the multiplier are given as follows:

The desired signal (j = i) is:

$$u_i(t) = p_i^2(t-\tau_i)\ A_i m_i(t-\tau_i)\ \cos^2\ [(\omega_0+\omega_i)t + \theta_i] \tag{4}$$

The undesired signals ($j \neq i$) are:

$$\sum_{\substack{j=1 \\ (j\neq i)}}^{N} u_j(t) = \sum_{\substack{j=1 \\ (j\neq i)}}^{N} p_i(t-\tau_i)\ p_j(t-\tau_j)\ A_j m_j(t-\tau_j) \quad .$$

$$\cos\ [(\omega_0+\omega_i)t + \theta_i]\ \cos\ [(\omega_0+\omega_j)t + \theta_j] \tag{5}$$

The interference/noise is:

$$n_0(t) = n(t)\ p_i(t-\tau_i)\ \cos\ [(\omega_0+\omega_i)t + \theta_i] \tag{6}$$

If the spread-spectrum codes $p_i(t)$'s have the property of orthogonality such that $p_i^2(t) = 1$ and $p_i(t)\ p_j(t) = 0$ for $j \neq i$, then equation (4) becomes

$$u_i(t) = \frac{1}{2} A_i m_i(t-\tau_i) \tag{7}$$

after the second harmonics is filtered out and equation (5) becomes

$$\sum_{\substack{j=1 \\ (j\neq i)}}^{N} u_j(t) = 0 \tag{8}$$

Thus, the i^{th} receiver code is correlated with the i^{th} transmitter code and, as a result, each receiver will be able to extract its own signal and reject other undesired signals spread by different codes even through they are of the same nominal carrier frequency, same bandwidth, and same code rate. In other words, the correlation process with the spread-spectrum code compresses the desired signal into the bandwidth of the baseband filter and simultaneously spreads the interference power. The baseband filter has a bandwidth comparable to the bandwidth of the modulated signal. Assuming that the RF filter and the multiplier have caused little distortion, the output of the baseband filter is given by

$$v_i(t) = \int_{-\infty}^{\infty} \frac{1}{2} A_i\ h(t-\alpha)\ m_i(\alpha-\tau_i)\ d\alpha \tag{9}$$

where $h(t)$ is the impulse response function of a baseband filter.

The autocorrelation and cross-correlation properties are very important in determing the performance of the spread-spectrum system. In practice it is, however, difficult to achieve the complete orthogonality implied by $p_i(t)\ p_j(t) = 0$ condition. Pseudo-random noise (PN) codes can provide the required correlation properties and can be generated easily and therefore suitable for applications to spread-spectrum systems. The auto-correlation function and its power spectrum of PN codes are shown in Fig. 5 (a) and (b), respectively.

To further demonstrate the capability of suppressing noise and interference by spread-spectrum systems, let us analyze the system based on the power spectra of the received signal before and after correlation. Assuming that both desired and undesired signals have the same carrier frequency and the same code rate, but spread by different PN codes. It is also assumed that the PN code of the desired signal is completely syn-chronized with the reference code at the receiver. The desired and undesired signals are each spread by its own code of rate R as shown in Fig. 6 (a) and each have a power spectrum of the form:

$$S(\omega) = A^2 T \left[\frac{\sin\ (\omega-\omega_0)\ T/2}{(\omega-\omega_0)\ T/2} \right]^2 \tag{10}$$

where A is the amplitude of the PN codes, T is the bit period, and ω_0 is the carrier frequency. The thermal noise of the receiver is also taken into account across the band of interest.

The composite signals and noise is applied to the input of the correlator. Then the spreading code on the desired signal is removed by multiplying the replica of the trans-mitted code. The desired signal will occupy a bandwidth approximately equal to the original baseband with an IF center frequency. As the codes of undesired signals are uncorrelated with the reference code, the power spectra of the undesired signals will remain spread before and after the correlation process and the spectrum of the thermal noise will be essentially unchanged as shown in Fig. 6 (b). Consequently, the desired signal can appear at the output of the baseband filter while only a small portion of the power spectrum of the undesired signals and noise pass through the baseband filter

and only that portion falling into the IF bandwidth of the receiver will cause interference to the desired signal. Similarly, any unspread or CW type interfering signals at the input to a spread-spectrum receiver will be spread by the reference code and be rejected in a similar manner. The effects of white Gaussian noise, sinusoidal interference, and undesired PN signals on system performance have been given (Davies, N. G., 1973).

It is of interest to observe that the larger the ratio of the spreading bandwidth of the baseband of the signal (called process gain) the lesser interference will be produced by the undesired signals. However, as the code rate is increased such that the interference levels produced by undesired signals become lower than thermal noise, any further increase of code rate will not improve the signal-to-noise ratio of the desired signal. Therefore, the code rate under this condition is the optimum code rate for the system.

The interference rejection property can provide a multiple access capability to enable many spread-spectrum signals (with their codes uncorrelated) to occupy a common RF spectrum if they have distinct PN codes. Actually each signal treats the other coded signals as additive interference.

6. REJECTION OF MULTIPATH INTERFERENCE

A simple multipath propagation model to be analyzed is shown in Fig. 7. At some frequencies, the relative time delay between these paths may cause the signal components to cancel one another at the receiver, while the components may reinforce one another at other frequencies. These will give rise to selective fading and intersymbol interference. Error probability for specular multipath and that with diffusive multipath have been treated in some detail (Cahn, C. R., 1973). Here, however, a simple analysis will be made to show that spread-spectrum communication systems can reject multipath interference.

The received multipath signals may be expressed by

$$r(t) = s_d(t)\ p_1(t) + \sum_{i=1}^{N} \beta_j\ s_d(t-\tau_j)\ p_1(t-\tau_j) + n(t) \tag{11}$$

where $s_d(t) = m_1(t) \cos(\omega_0+\theta)$; the direct-path signal

$p_1(t)$ = PN code of the desired signal

β_j = coefficient of an indirect-path signal

τ_j = time delay of an indirect-path signal

$n(t)$ = interference/noise

In equation (11) the first term represents the direct-path signal, the second term represents the indirect-path signals, and the third term represents other forms of interference/noise.

The received signal $r(t)$ is multiplied by a locally generated signal, $p(t) = p_1(t) \cos \omega_1 t$, and the resultant signal at the output of the correlator is given by

$$\begin{aligned} r_0(t) &= r(t) \cdot p(t) \\ &= [s_d(t)\ p_1(t) + \sum_{j=1}^{N} \beta_j s_d(t-\tau_j)\ p_1(t-\tau_j) + n(t)] \cdot p_1(t) \cos \omega_1 t \\ &= s_d(t)\ p_1^2(t) \cos \omega_1 t + \sum_{j=1}^{N} \beta_j s_d(t-\tau_j)\ p_1(t)\ p_1(t-\tau_j) \cos \omega_1 t \\ &\quad + n(t)\ p_1(t) \cos \omega_1 t \end{aligned} \tag{12}$$

After passing through the IF bandpass filter with center frequency $\omega_2 = \omega_0-\omega_1$, the desired signal is recovered as the first term of equation (12) becomes

$$s_d'(t) = \frac{1}{2}\ m_1(t) \cos(\omega_2 t + \theta_2) \tag{13}$$

since $p_1^2(t) = 1$ for the PN code. It is of interest to examine the second term (multipath interference) of equation (12) as follows:

(i) When the delay time $\tau_j \approx 0$, then $p_1(t)\ p_1(t-\tau_j) \approx p_1^2(t) = 1$. This means that there is no obvious j^{th} multipath in existence.

(ii) When the delay time $\tau_j \geq T$, where T is the bit period, then $p_1(t)\ p_1(t-\tau_j) \approx 0$ according to the correlation property of the PN code as shown in Fig. 5 (a). In this

case, the j^{th} multipath interference is rejected.

(iii) When the delay time is that $0 < \tau_j < T$, then the value of $p_1(t)\ p_1(t-\tau_j)$ will become large enough to make the j^{th} multipath signal either reinforcing or cancelling the direct path signal depending on the nature of $\beta_j s_d(t-\tau_j)$.

If we increase the bit rate of the PN code so as to make $\tau_j \geq T$, then, the value of $p_1(t)\ p_1(t-\tau_j)$ would be negligibly small because of the autocorrelation property of the PN code. Therefore, the interference due to multipath propagation can be rejected. When the indirect-path signal is delayed more than one bit period of the PN code, the signal can be treated exactly the same as any other uncorrelated input signals. The higher the code bit rate for a particular system the greater multipath protection will be provided by the system. The third term of equation (12) is spread and rejected.

7. FACTORS AFFECTING SYSTEM PERFORMANCE

As indicated in Section 5 the abilities of rejecting interference and noise and other applications depend on the magnitude of the process gain of the system, that is the ratio of the spread bandwidth to the baseband of the signal and on the correlation properties of the codes used.

So far we have assumed that a perfect synchronization exists between the desired signal and the local reference code signal. The autocorrelation function for a PN code sequence is a peak pulse as shown in Fig. 5 (a). For signals encoded by such a sequence, the maximum signal output from the correlator occurs only when the incoming code and the local code are in synchronization. The optimum signal-to-noise ratio occurs when the local and received codes are exactly aligned because this is the point of maximum signal output. Therefore, the system performance depends on whether the synchronization is established or not. When the desired signal is not exactly matched with the local reference code, a part of the desired signal will become noise due to imperfect synchronization. The amount of noise depends on the degree of synchronization. When there is no synchronization, the output produced is all noise.

8. ADVANTAGES AND APPLICATIONS

In addition to the capability of rejecting various interference and noise, the low power density of spread signal will not cause interference to other systems and is not to be intercepted easily. Message security is inherent in spread signals because of their coded transmission format. These features warrant the spread-spectrum systems to have significant applications for the times of emergencies and other security measures in adverse electromagnetic environments. The ability to recognize a particular signal and rejecting code-related undesired signals make it possible to achieve selective addressing. Assignment of a particular code to a given receiver will allow it to be contacted only by a transmitter which is using that same code to modulate its signal. With different codes assigned to all the receivers in a network, a transmitter can select any one receiver for communication by simply transmitting the assigned code of that receiver. Similarly, code-division multiple access is possible because that a number of transmitters and receivers can operate on the same frequency at the same time by employing different modulating codes. Consequently, it becomes possible to accommodate more channels in the same frequency band. So, the spread-spectrum systems can save frequency spectrum under certain circumstances.

9. CONCLUSIONS

In this paper the origins of multipath propagation, their effects on radio communication systems, and schemes of suppressing these effects have been briefly reviewed.

Multipath propagation can happen under various atmospheric and/or geographical conditions. In most cases multipath are not easily predictable due to changing meterological and terrain conditions.

The effects of multipath propagation on radio communication systems may be in various forms, but they can be described in terms of selective fading and intersymbol interference.

Simple measures may be found to combat the multipath effects on radio systems when the multipath can be accurately predicted. However, for most cases sophisticated schemes are required, especially in the case of mobile communications.

It has been shown, based on analysis, that spread-spectrum schemes are superior to other approaches in combating multipath interference. In addition, the spread-spectrum schemes can provide other valuable features such as interference/noise rejection, message security, selective addressing, and multiple access. The ability of spread-spectrum systems to suppress interference depends on the process gain of the system and on the degree of synchronization which can be established by the system.

REFERENCES

1. Beckmann, P. and A. M. Spizzichino, 1963, "The scattering of electromagnetic waves from rough surfaces", Pergamon and Macmillan.

2. Cahn, C. R., 1973, "Spread-spectrum applications and state-of-the-art equipments", AGARD Lecture Series, No. 58, pp. 5-82 to 5-92.

3. Chadwick, H. D., 1971, "The error probability of a wide-band FSK receiver in the presence of multipath fading", IEEE Trans. Comm. Tech., Vol. COM-19, pp. 699-707.

4. Corrington, M. S., 1945, "Frequency modulation distortion, caused by multipath transmission", Proc. IRE, Vol. 33, pp. 878-891.

5. Davies, N. G., 1973, "Performance and synchronization considerations", AGARD Lecture Series, No. 58, pp. 4-6 to 4-11.

6. Kwon, S. Y., et al, 1978, "Noncoherent detection of FSK signals in the presence of multipath fading", IEEE Trans. Comm., Vol. COM-26, No. 1, pp. 164-168.

7. Morgan, D. R., 1972, "Error rate of phase-shift keying in the presence of discrete multipath interference", IEEE Trans. Inform. Theory, Vol. IT-18, No. 7, pp. 525-528.

8. Morgan, D. R., 1978, "Adaptive multipath cancellation for digital data communications", IEEE Trans. Comm., Vol. COM-26, No. 9, pp. 1380-1390.

9. Nesenbergs, M., 1967, "Error probability for multipath fading - The "slow and flat idealization", IEEE Trans. Comm., Vol. COM-15, No. 12, pp. 797-805.

10. Ott, R. H., et al, 1978, "Experimental and theoretical assessment of multipath effects on QPSK", IEEE Trans. Comm., Vol. 26, No. 10, pp. 1475-1477.

11. Price, R. and P. E. Green, Jr., 1958, "A communication technique for multipath channel", Proc. of the IRE, pp. 555-570.

12. Skolnik, M. I., 1980, "Introduction to radar systems", 2nd edition, McGraw-Hill Book Company.

ACKNOWLEDGEMENT

The author wishes to acknowledge the support of this work given by The National Sciences and Engineering Research Council of Canada.

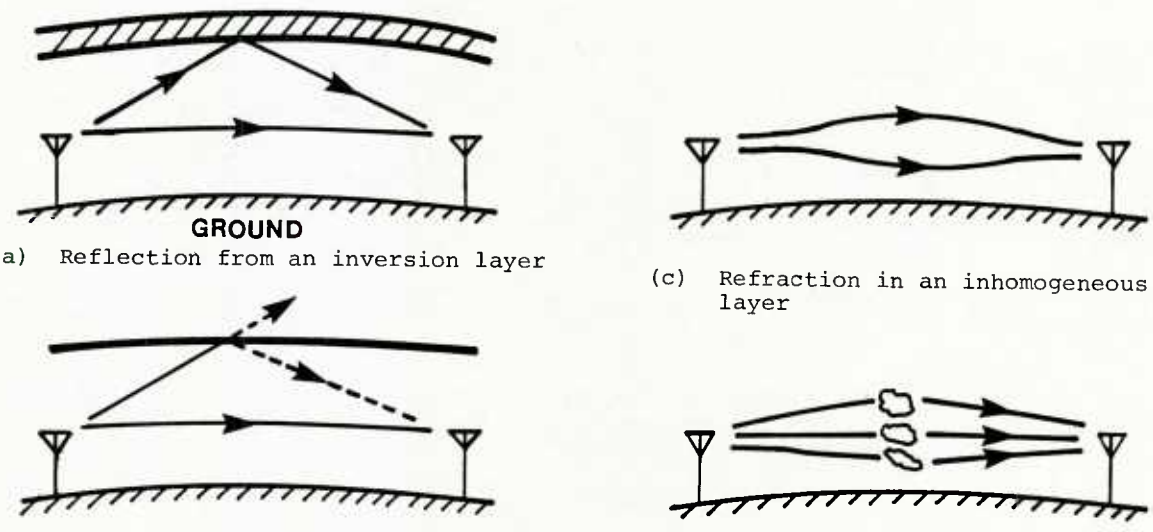

(a) Reflection from an inversion layer

(b) Partial reflection from an atmospheric sheet

(c) Refraction in an inhomogeneous layer

(d) Scattering by a turbulence

FIG. 1 (a) - (d) TYPICAL CAUSES OF MULTIPATH PROPAGATION DUE TO ATMOSPHERIC CONDITIONS

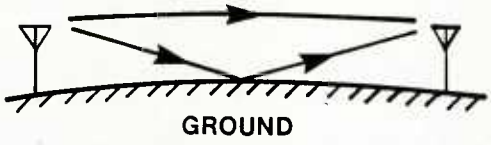

(a) Reflection from ground (or water)

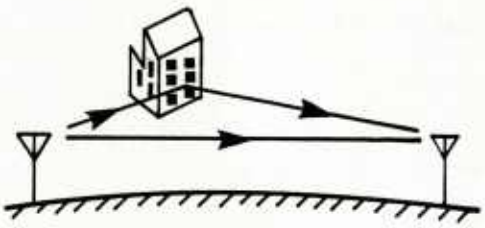

(b) Reflection from a building (or obstacle)

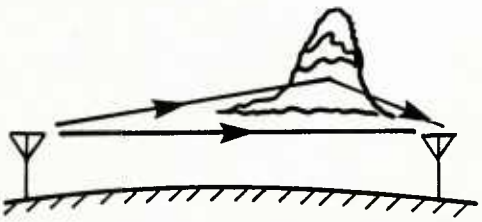

(c) Reflection from a mountain (or hill)

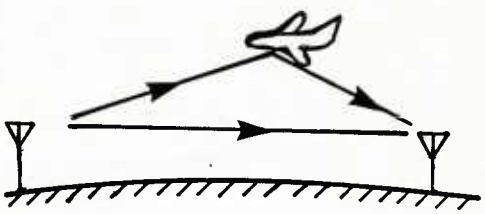

(d) Reflection from an aircraft (or object)

FIG. 2 (a) - (d) TYPICAL CAUSES OF MULTIPATH PROPAGATION DUE TO GEOGRAPHICAL CONDITIONS

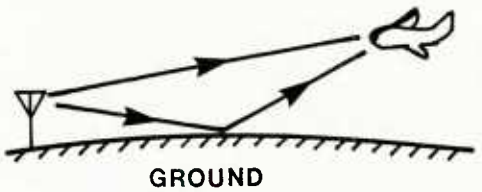

(a) Ground-to-air (or air-to-ground) link

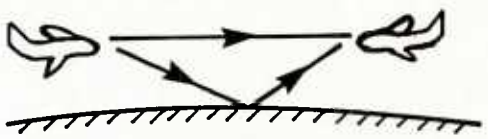

(b) Aircraft-to-aircraft link

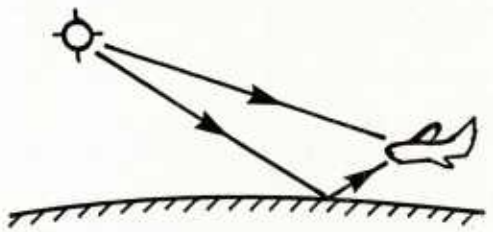

(c) Aircraft-to-satellite (or satellite-to-aircraft) link

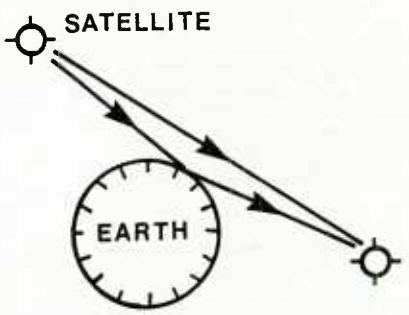

(d) Satellite-to-satellite link

FIG. 3 (a) - (d) EXAMPLES OF MULTIPATH PROPAGATION OF COMMUNICATION LINKS

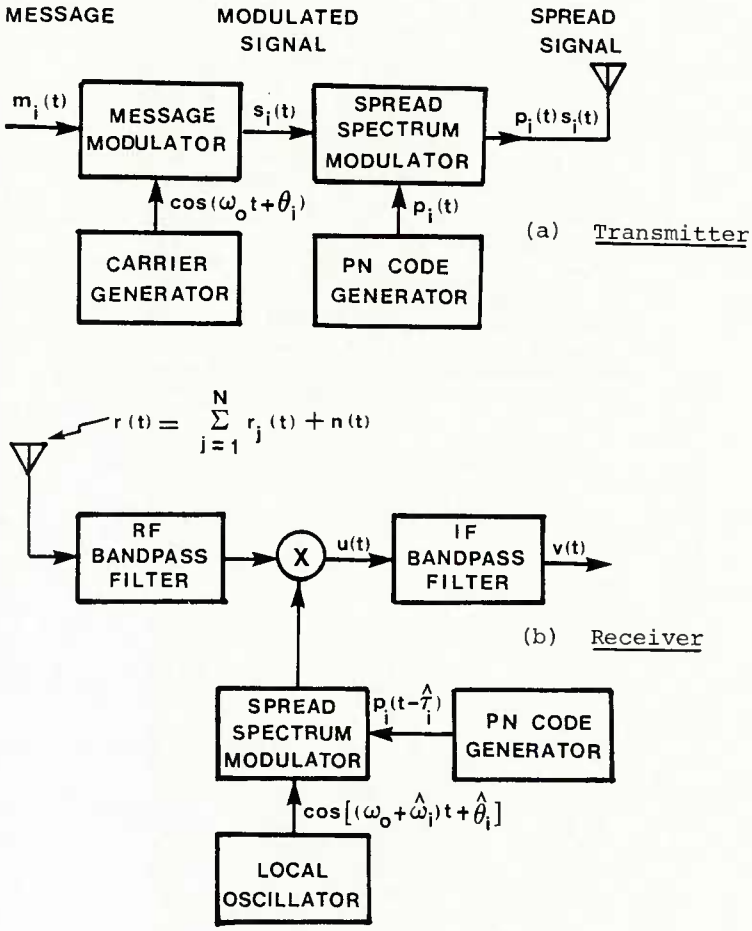

FIG. 4 BASIC DIRECT-SEQUENCE SPREAD-SPECTRUM SYSTEM

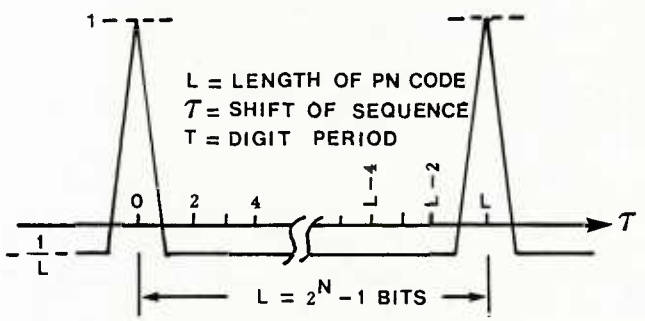

FIG. 5 (a) NORMALIZED AUTOCORRELATION FUNCTION OF A PN CODE

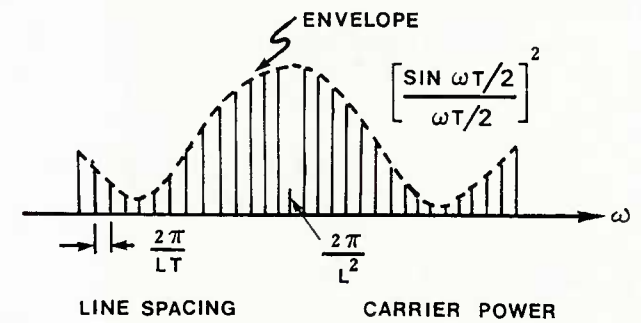

FIG. 5 (b) POWER SPECTRUM OF THE PN CODE SHOWN IN FIG. 2 (a)

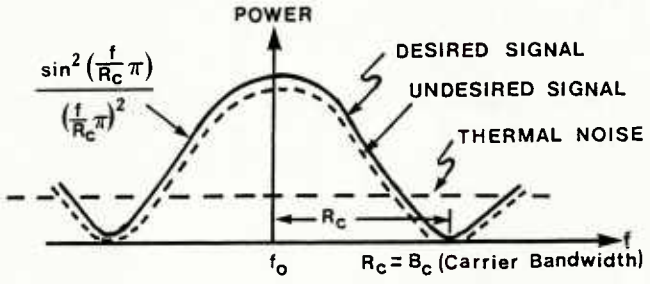

(a) Spectrum before correlation

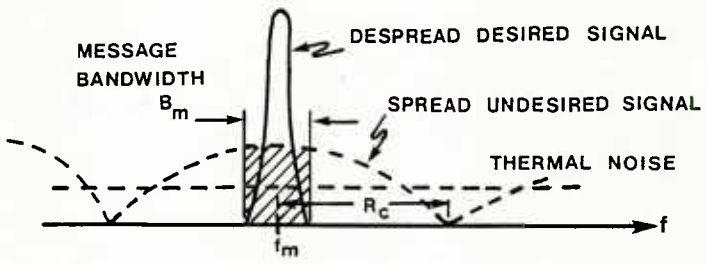

(b) Spectrum after correlation

FIG. 6. POWER SPECTRA OF THE RECEIVED SIGNALS BEFORE AND AFTER CORRELATION

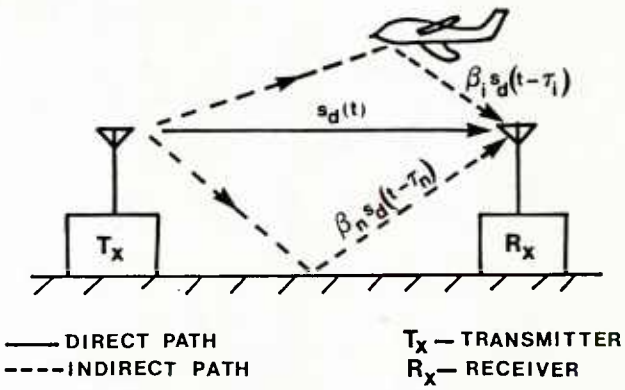

FIG. 7. A MULTIPATH PROPAGATION MODEL

DISCUSSION

D. Davidson, US

The FCC in its current Notice of Inquiry Docket 81-413 is looking into the cohabitation of spread-spectrum and ordinary systems. The IEEE Communications Society submitted an excellent set of comments in this Docket that is worth reading; Prof. Cooper was a contributor. As to frequency-hopping (FH) advantages, I believe Cooper's former colleague, Henry, at Bell Labs showed that the apparent FH advantages are not as great as originally projected.

T.Sullivan, US

Is there any advantage with regard to multiple performance associated with frequency hopping systems as opposed to PN systems?

Author's Reply

My discussion of the rejection of multipath effects in this paper is based on the study of direct-sequence systems and I do not have exact information regarding the multipath performance associated with frequency hopping systems. However, in my opinion, the DS system is superior to FH system as far as combatting multipath effects is concerned.

S. Segner, US

The paper claims that spread spectrum systems can share better. In CCIR SG 4 papers on FDMA vs. TDMA vs. Code Division Multiple Access (CDMA) it appears that CDMA will get less frequency sharing than orthogonal FDMA or TDMA. Can the statement in the paper be rationalized against the CCIR SG 4 statement?

Author's Reply

Besides suppressing multipath effects and other advantages as cited in the paper, the system can still have the possibility of frequency sharing. However, the total channel which can be accommodated within a given bandwidth may be comparable but not necessarily better than those of FDMA and TDMA. So, I am not in a position to speak against the CCIR SG 4 statement. It can share better only under certain circumstances when other factors are taken into consideration.

M. Niemeyer, Ge

(1) If you have a flat fading condition, that means that you have a broadband weak signal. Is the spread spectrum system able to combat this sort of multipath effect?

(2) If you consider a broad system bandwidth (in the case of a communications system with very high bit rates), the probability of having selective fadings is much greater than if you consider a system with a small bandwidth. So, if you broaden the communications bandwidth with a spread spectrum system, a channel might become a selective fading channel, which was originally not a fading channel. Does this make the fading statistics worse?

Author's Reply

(1) The signal transmitted by a spread spectrum system is indeed a broadband weak signal and the system can still serve useful purpose to combat multipath effects.

(2) A spread spectrum can prevent selective fading from happening due to the fact that the system can reject indirect-path signals.

C. Goutelard, Fr

L'auteur utilise la propriété des fonctions de corrélation périodiques des séquences PN égale à 1/L en dehors du pic central. En ce qui concerne la protection vis à vis des trajets multiples cette propriété ne peut pas être utilisée si le traitement du signal se fait par corrélation, car, en effet, c'est alors la fonction de corrélation apériodique qui intervient dans les calculs. Ce point se vérifie très simplement dans le cas d'une transmission numérique du type PSK. Il s'ensuit que les résultats sont très différents de ceux annoncés car l'autocorrélation apériodique prend des valeurs très supérieures à 1/L. Il faut alors utiliser pour le signal d'étalement des signaux dont la fonction d'autocorrélation en dehors du pic central soit minimalisée. Ces codes existent et donnent des résultats meilleurs que ceux obtenus aves les codes PN.

Author's Reply

I agree that PN code may not be the best code for combatting multipath effects, but it is the easiest code to generate. The ability of suppressing multipath effects depends on the correlation properties of the code used. Therefore great effort is required to find the best possible code for the system.

A Spectral Emission Mask for Digital Tropospheric Scatter Transmission

R. K. P. Galpin
SHAPE Technical Centre
The Hague
The Netherlands

SUMMARY

A spectral emission mask definition for high power digital radio transmission is proposed. Developed for use in the specification of digitalized ACE High troposcatter links, it is offered for consideration by industry and frequency planning authorities. Similar in form to the FCC mask definition for digital LOS radio, the proposed definition is believed to be a reasonable compromise between minimizing interference into adjacent radio channel allocations and avoiding the imposition of costly constraints upon the manufacturers and operators. Computer simulations supported by spectral measurements at 10 kW have shown that well-designed filtering (with negligible intersymbol interference) before the high power amplifier is very effective in reducing out-of-band emission, and that the proposed mask can be satisfied with a signal having a bandwidth utilization efficiency of 1.6 bit/s/Hz when operating at 2 dB below saturation of the klystron amplifier.

1. INTRODUCTION

The definition of the emitted spectrum of an analogue microwave transmisson is, traditionally, rather vague. With one or two exceptions, most present-day point-to-point microwave radio communication falls under the ubiquitous classification of F9, (Ref.1) which is associated with a number which should represent the 'necessary bandwidth', but which more commonly is used to represent the 'occupied bandwidth' (Ref.2). Manufacturers and operators are asked by CCIR to keep emission levels outside these bandwidths "as low as possible". The successful operation of both line-of-sight (LOS) links and over-the-horizon or troposcatter (OTH) links with these rather vague constraints is due to the benign spectral distribution of the analogue frequency-division-multiplex/frequency modulation (FDM/FM) signal (Ref.3). Of particular importance is the fact that this spectral distribution, which is illustrated in Fig. 1, relates to a constant envelope form of modulation and remains substantially unchanged when passed through the non-linear characteristics of, for example, a high-power klystron amplifier.

2. THE PROBLEM

The advent of the digitalization of radio communications has changed this situation. The digitalization of voice and other analogue signals, especially by pulse code modulation, is profligate in the use of bandwidth, and extraordinary measures are being developed to convert multichannel analogue LOS radio links to digital operation within the same overall bandwidth (Ref.4). A variety of digital modulation schemes have been proposed to provide high bandwidth utilisation efficiency (BUE), but it is unfortunate that such schemes cannot avoid envelope variations in the modulation signal. Perhaps the highest efficiency obtainable with a constant envelope is the 1.25 bit/s/Hz of the Philips 'Tamed f.m.' (Ref.5).

For various reasons four-phase modulation is favoured for high power digital radio, and most of the schemes referred to above are derivations of this form of modulation. However, simple quadrature phase shift keying (QPSK) has a spectrum which decays very slowly (Fig. 2) compared with the FDM/FM spectrum in Fig. 1, and requires filtering to remove the higher-order sidebands and to reduce the width of the main lobe. The problem is that, before such filtering can be imposed, a spectral definition is required which will on one hand provide the manufacturer with a specification to be satisfied by his design, and on the other will provide frequency planning authorities with a basis for realistic coordination between transmissions in adjacent channel positions. Such a definition has been adopted for digital LOS radio in the USA by the FCC (Ref. 6) by which the spectral decay outside an "authorised bandwidth" is clearly specified. This constraint can be met for low power transmissions with reasonable BUE by careful modulation and filtering at baseband and IF, followed by linear mixing, linearized power amplification and post-amplifier filtering. Unfortunately it is very difficult to achieve such a constraint at the high power levels required for digital troposcatter transmission: even the analogue FDM/FM spectrum shown in Fig. 1 would not satisfy the FCC mask corresponding to its occupied bandwidth; so, although the concept of an unambiguous spectral definition is desirable for high power digital radio, the FCC mask appears to be too stringent.

3. RATIONALE

As digital troposcatter transmissions will have to be coordinated with existing analogue FDM/FM transmissions during the transition to digitalization, it seems reasonable to attempt to constrain the digital spectrum to that of an FDM/FM emission having the same occupied or authorized bandwidth. To this end a spectral emission mask definition was proposed by SHAPE Technical Centre (STC), (Ref.7), which was derived from the FDM/FM spectral curves published by CCIR (Ref.3), by curve fitting, and relating the spectral roll-off to the calculated occupied bandwidth, that is the bandwidth containing 99% of the emitted power.

This proposed constraint was defined as follows:

$$A = \left[10 \log_{10} B + 0.5\ (P-50) + 3\right] \text{dBc}$$

where:- A is the attentuation of the spectral density outside the authorized bandwidth measured as the power falling in a 4 kHz band, below the total mean emitted power;

B is the authorized bandwidth in kHz, that is to say the bandwidth given in the emission designation;

P is the displacement from the centre frequency of the emission expressed as a percentage of B;

A has a minimum value of 40 dBc, but a maximum defined value of 80 dBc.

It was similar to the FCC 19311 constraint (Ref.6), except for relaxing decay outside the authorized band to 0.5(P-50) instead of 0.8(P-50) and the minimum value to 40dBc instead of 50 dBc.

Two masks according to the definition are shown in Fig. 3, for 3.8 MHz and 8.7 MHz, together with the FDM/FM curves from which they were derived, and with the corresponding FCC masks. It seemed unnecessarily restrictive to define the constraint beyond 80 dBc for several reasons: the interference potential is already low at 80 dBc, the means employed to satisfy the mask will probably continue to attenuate the spectrum as the frequency displacement from carrier increases, and other constraints such as transmitter-receiver frequency spacing will require further suppression of the out-of-band spectrum.

4. FEASIBILITY

4.1 Computer simulations

The feasibility of achieving this spectral constraint was investigated in the context of digital troposcatter transmission in the ACE High network. The requirement is to transmit at rates of up to 6.4 Mbit/s in bandwidths of 4 MHz at UHF or about 6 MHz at C-band. Extensive computer simulations were carried out using the Plessey TSIM (Ref.8) programme, incorporating the measured characteristics of high power klystron amplifiers (HPA), with and without pre-distortion linearization, for data rates of 4.3 and 6.4 Mbit/s. Using low-intersymbol-interference pre-HPA filtering (shared equally between the transmitter and receiver) and 4-phase modulation, the enhancement of out-of-band emission caused by the HPA non-linearity was simulated for various levels of HPA back-off. A typical set of curves in Fig. 4 shows the computed spectra of 6.4 Mbit/s transmission at various levels of input back-off using pre-distortion linearization of the HPA, together with the input spectrum and the proposed masks for 4 MHz and 6.3 MHz. The smaller envelope variation obtained with full cosine filtering at 4.3 Mbit/s did not lead to a noticeable improvement (Fig. 5), but it is seen that the use of off-set QPSK with this filtering led to much less out-of-band enhancement and more or less satisfied the proposed mask with zero back-off. (In fact only 0.5 dB output back-off was required to satisfy the mask). It should be noted that the advantage of the off-set technique diminishes rapidly as the BUE is increased above 1 bit/s/Hz (Ref.9): with 6.4 Mbit/s in 4 MHz the out-of-band enhancement is almost as severe as that shown in Fig. 4.

The preliminary conclusions drawn from these simulations were:

a. well-designed pre-HPA filtering with rapid spectral roll-off is effective in reducing out-of-band spectral emission;

b. using this filtering at 4.3 Mbit/s, the proposed mask can be satisfied with an output power back-off of about 2 dB;

c. using this filtering at 6.4 Mbit/s, pre-distortion linearization (with back-off) and post-HPA filtering would be needed to satisfy the mask.

4.2 Practical measurements

To verify these computer simulations, an experiment was arranged with the cooperation of the English Electric Valve Company and the Marconi Company to measure the spectral spreading actually obtained when amplifying a tightly-filtered digital signal to an output power of the order of 10 kW, and to observe the effects of backing-off. A digital transmitter was built at STC having 7-pole Butterworth digital filtering at baseband. This was normalized to the selected data rate by the data clock generator, and produced very little intersymbol interference when convolved with the associated matched filtering in the receiver, as shown in the eye diagrams for 4.3 Mbit/s and 6.4 Mbit/s (Figs. 6a and 6b). The corresponding output spectra at the intermediate frequency of 70 MHz are shown in Figs. 7a and b, including wider-bandwidth anti-aliassing analogue filtering. This signal was up-converted to 810 MHz in a radio sub-system provided by Marconi and fed to the driver amplifier, the 4.3 Mbit/s and 6.4 Mbit/s output spectra at 810 MHz (at full power) being shown in Fig. 8. It should be noted that the smooth spectra shown in these photographs is due to the use of a pseudo-random test pattern of length $(2^{23}-1)$ bits for these measurements.

This output signal drove an English Electric K386 UHF klystron amplifier operating with a gain of about 30 dB and a saturated output power of about 10kW. The spectra of this output of the klystron at saturation and at 1,2 and 3 dB output back-off are shown in Fig. 9 (a-d) for 4.3 Mbit/s and Fig. 10 (a-d) for 6.4 Mbit/s. The term 'saturation' in the context of this paper means the operating point at which the output power of the digitally modulated signal was at a maximum, which was 10.9 kW for this set of measurements.

The effects of more gentle filtering were also studied. With full-cosine roll-off filtering at baseband, the output spectra of a 4.2 Mbit/s signal at saturation and with 1 dB and 2 dB output back-off were measured using QPSK modulation (Fig. 11 a-c) and off-set QPSK (Fig. 12 a-c).

5. DISCUSSION

Several points can be noted from the feasibility studies.

(a) Although differing in detail, due to the limited random pattern length used in the computer simulations, the general correspondence between the simulated and measured spectra at saturation and at various levels of back-off was very close.

(b) Comparison of the measured spectra with the unfiltered QPSK spectrum drawn in Fig. 2 clearly shows that well-designed pre-HPA filtering is very effective in reducing the out-of-band spectral density of the HPA output.

(c) Comparison of the output spectra of the tightly-filtered 4.3 Mbit/s signal in Fig. 9 with the full-cosine roll-off filtered 4.2 Mbit/s signal in Fig. 11 confirms that, despite the substantially increased envelope variation of the tightly-filtered signal, the spectral spreading is less. It should be noted that the tighter filtering was designed to minimise intersymbol interference as seen in Fig. 6.

(d) The spectral spreading of the 4.2 Mbit/s off-set QPSK signal shown in Fig. 12 was much less than that of the normal QPSK, and almost satisfied the initially proposed mask at saturation, confirming the computer simulation (Fig.5).

(e) In the region of the lower-level spectral components, where the accuracy of the computer simulations deteriorated, the measured spectra showed almost monotonic decay down to the noise level of the measuring equipment.

With the computer simulations supported by measurements, the feasibility of achieving the initially-proposed mask can be assessed more confidently. Careful study of the spectra confirms that the initial mask could be met with a tightly-filtered 4.3 Mbit/s signal with 1-2 dB of output back off, but that post-HPA filtering would be needed to meet the mask with a 6.4 Mbit signal, even with up to 3 dB output back-off. Thus the initial mask is seen to be a reasonable first attempt at a spectral specification, certainly for signals with a BUE of about 1 bit/s/Hz. Even for signals with a BUE of 1.5 bit/s/Hz or more, the infringements are relatively minor. A closer look at measures to reduce out-of-band emission and at the details of the spectral definition is needed to determine a cost-effective compromise in reaching realistic specifications.

The measures that can be used for reducing the out-of-band spectral components include back-off, with or without predistortion linearization, and post-HPA filtering. Considering the effects of back-off first, it is seen from a study of the spectra in Figs. 9 and 10 that a considerable reduction in third order distortion components is obtained for 1 dB of output back-off, but that increasingly less reduction is obtained for further amounts of back-off. The computer simulations showed that rather more back-off was needed to realise the potential benefit of predistortion linearization, but that the advantage over back-off without predistortion linearization appeared to be marginal. Post-HPA filtering, although feasible (Ref. 10) at UHF frequencies, represents a significant cost increase. Thus it seems that operating with an output power of say 1-2 dB below saturation, without predistortion linearization, is a reasonable measure to be considered for conforming with a specified mask.

The initial spectral definition comprised two factors, the first relating the nominal or "authorized " bandwidth to the 4 kHz bandwidth used to define the spectral density, and expressed as a function of the total transmitted power:

$$A_1 = 10\log_{10}B \text{ dBc}$$

where B, in kHz, is the number associated with the F9 nomenclature currently used in CCIR. Thus a 4 MHz channel allocation for a troposcatter transmission would be 4000F9. The second term defines the spectral decay out-of-band as a function of displacement from the centre frequency:

$$A_2 = 0.5\ (P-50) \text{ dBc}$$

There is a minimum value of 40 dBc, a maximum defined value of 80 dBc and, as always, a constant, 3 dB in this case.

From the frequency coordination viewpoint it is reasonable to assume that a given band may be assigned to a number of allocations or channel slots of the same width. On this assumption, it would be convenient if the maximum value of 80 dBc were to be achieved within one channel slot, so that the next-but-one channel slot would be relatively free from interferece. Thus the intermediate channel slot can be considered to accommodate the spectral decay of the transmission together with the roll-off of the receiver filtering in the next-but-one channel, but would be allocated for transmission to a geographically remote link. In dividing this transitional region between the requirements of the transmitter and the receiver, the latter can be considered to have a monotonic roll-off, similar to the spectra shown in Fig. 7. Taking a normal shape factor (ratio of bandwidth at 60 dB to bandwidth at 3 dB) of 2:1 for the receiver filtering leaves 3/4 of the transition band to the transmitter; so a more relaxed shape factor of 3:1, leaving half the transition band to the transmitter, provides a comfortable margin for the receiver. The complement of a 3:1 shape factor corresponds to a coefficient of 0.6 in the expression for A2:

$$A_2 = 0.6(P-50) \text{ dBc}$$

The minimum value of 40 dBc at the edge of the pass band is practicable and provides a clear definition for the pass band of the transmission with reference to the total power rather than to a relative spectral point, such as the mid-band spectral density. This avoids the definition being dependent upon the form of modulation.

The remaining component of the definition is the constant. A value of -15 dBc is suggested. This would terminate the decay slope at 80 dBc close to one channel bandwidth from the band edge.

6. SPECTRAL MASK DEFINITION

The revised spectral definition now proposed is:

$$A = \left[10 \log_{10} B + 0.6(P-50) - 15\right] \text{dBc}$$

where:- A is the attenuation of the spectral density outside the authorized bandwidth measured as the power falling in a 4 kHz band, below the total mean emitted power;

B is the authorized bandwidth in kHz, that is to say the bandwidth given in the emission designation;

P is the displacement from the centre frequency of the emission expressed as a percentage of B;

A has a minimum value of 40 dBc, but a maximum defined value of 80 dBc.

Examples of this mask are shown in Fig. 13 for authorized bandwidths of 2, 4 and 8 MHz. It is seen that immediately beyond the 40 dBc minimum limit the mask has a shoulder which will allow a modest amount of third-order intermodulation products which would otherwise have to be removed by exeessive back-off or post-HPA filtering, but that the decay beyond the shoulder is better matched than in the initial definition to the complementary receiver filtering in the next-but-one channel position.

Comparing this new definition for a 4 MHz channel mask with the measured spectra in Figs 9, 10, 11 and 12 leads to the following observations:

(a) QPSK at 4.2 Mbit/s with full cosine roll-off filtering satisfies the mask with 2 dB back-off (Fig.11c).

(b) Off-set QPSK at 4.2 Mbit/s with full cosine filtering almost meets the mask at saturation and meets it comfortably with 1 dB back-off (Fig 12a, and b).

(c) QPSK at 4.3 Mbit/s with 7-pole Butterworth filtering satisfies the mask with 1 dB back-off (Fig.9b).

(d) QPSK at 6.4 Mbit/s with 7-pole Butterworth filtering satisfies the mask with 2 dB back-off (Fig.10c).

7. CONCLUSIONS

A new spectral emission mask for high power digital radio transmission has been proposed for use in the specification of tropospheric scatter and other high power radio systems. Developed from an initial proposal which had been based on currently-used spectra of FDM/FM transmissions, the new definition is believed to be a reasonable compromise between, on one hand, minimising interference into near-by channels and, on the other, avoiding the imposition of costly constraints on the manufacturer and operator.

It has been shown by computer simulations and confirmed by practical measurements that highly selective filtering (with low intersymbol interference) used before the non-linear high power amplifier is effective in reducing out-of-band emission, and that, by using this filtering and backing-off the output power by 1 or 2 dB below the saturation level, the proposed mask can be satisfied, even for digital signals with bandwidth utiliziation efficiencies of up to 1.6 bits per second per Hertz of authorised bandwidth.

This definition is offered for detailed consideration by industry and spectrum management authorities concerned with the ACE High digitalization programme, and for consideration by CCIR under Question 7 -3/9 (Ref.11)

8. ACKNOWLEDGEMENTS

The author is grateful to the Marconi Company and the English Electric Valve Company for their assistance and cooperation during this study and for the facilities made available for the conduct of the experimental measurements.

REFERENCES

1. Recommendation 328-4; CCIR, Kyoto 1978, Vol. I, p.307

2. Radio Regulation 90, ITU, 1976.

3. Report 780; CCIR, Kyoto 1978, Vol.IX, p.37

4. Davies, M.C. and Chisholm, J.A., "Spectrum conserving digital transmission systems for the 4 and L-6 GHz bands". IEE Conference Publiciation No. 188, July 1980, p.84.

5. de Jager, F. and Dekkers, C.B., "Tamed frequency modulation - a novel method to achieve spectrum economy in digital transmission" IEEE Trans. Vol. COM-26, May 1978, p.534.

6. US Federal Communications Commission, Docket No. 19311, Sept. 1974.

7. Galpin, R.K.P., "A spectral emission mask for digital troposcatter transmission", I.E.E. Colloquium on Troposcatter Communications - Digital Developments, London, October 1981.

8. Hedderly, D.L. and Lindquist, L., "Computer simulation of a digital satellite communication link" IEEE Trans. Vol. COM-21., April 1973, p.321.

9. Moreno, L., "Sensitivity of PSK modulation techniques to non-linear distortions" IEEE Trans. Vol. COM-27, May 1979, p.806.

10. Hutchinson, R., "Rotamode filter networks" Communications and Broadcasting, Vol. 6, March 1981, p.15.

11. CCIR Question 7-7/9, "Transhorizon radio-relay systems", CCIR, Kyoto 1978, Vol. IX, p.238.

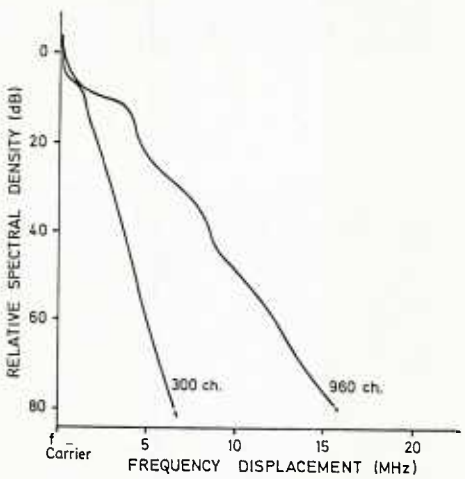

Fig. 1 FDM/FM spectra (CCIR Rep. 780)

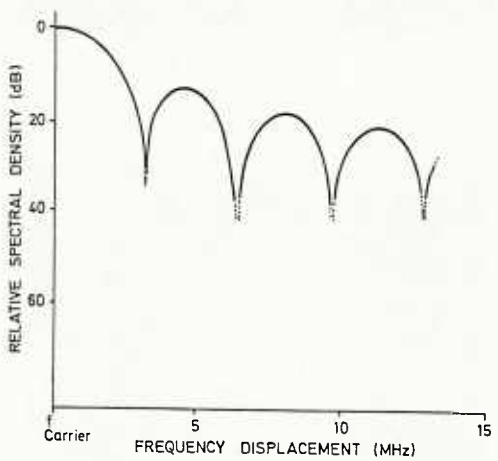

Fig. 2 6.4 Mbit/s QPSK spectrum

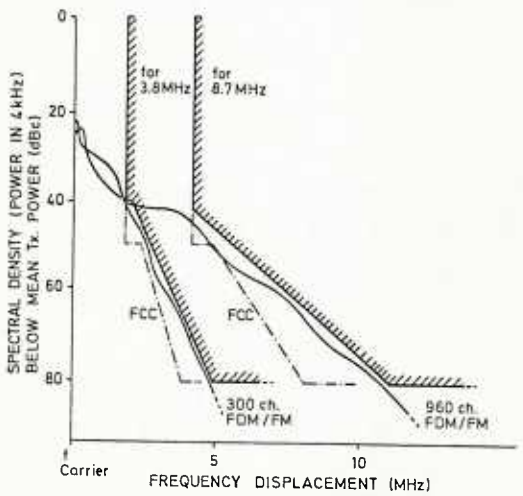

Fig. 3 Derivation of masks from FDM/FM spectra

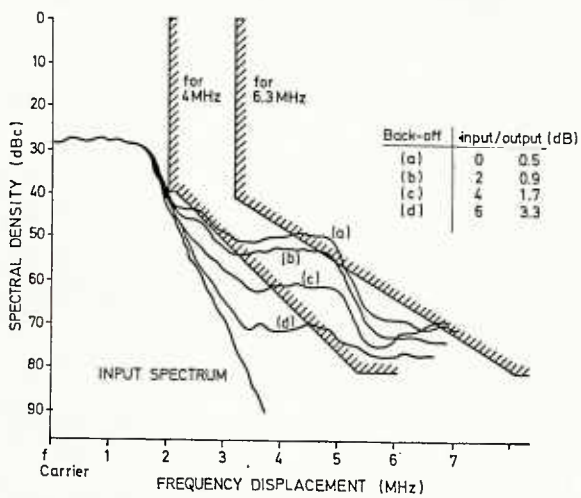

Fig. 4 6.4 Mbit/s spectra with HPA back-off using predistortion

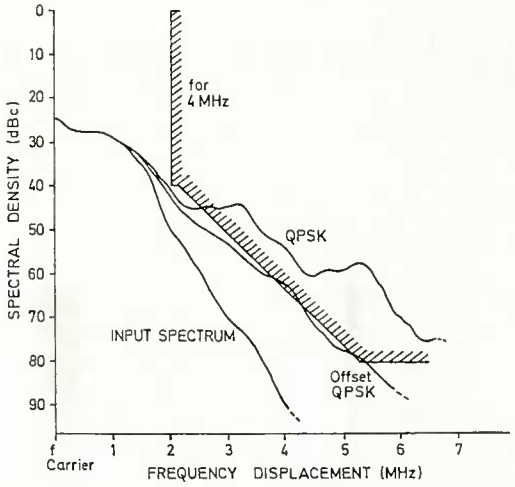

Fig. 5 4.3 Mbit/s output spectra (no back-off)

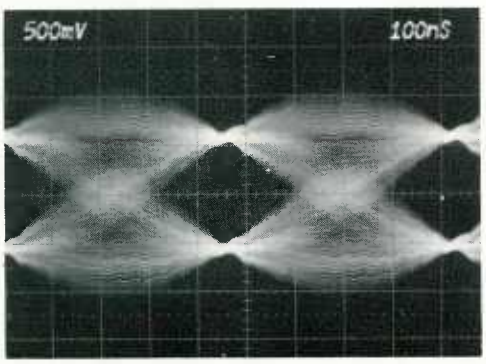

(a) 2.15 Mbauds (4.3 Mbit/s)

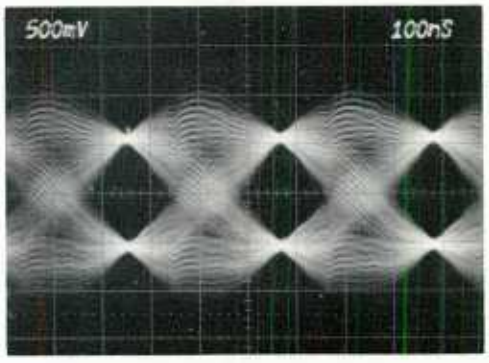

(b) 3.2 Mbauds (6.4 Mbit/s)

Fig. 6 Receiver eye diagrams

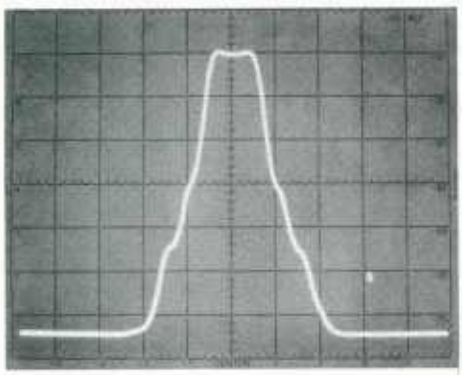

(a) 4.3 Mbit/s

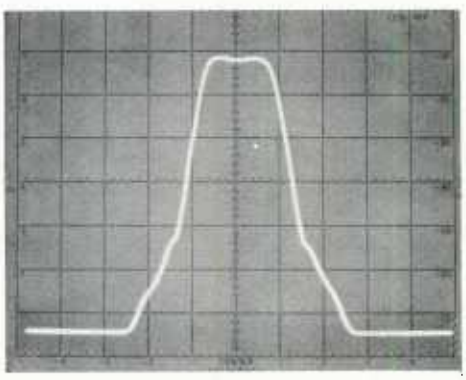

(b) 6.4 Mbit/s

Fig. 7 I.F. spectra (70 MHz)

Hor. 2 MHz/div
Ver. 10 dB/div

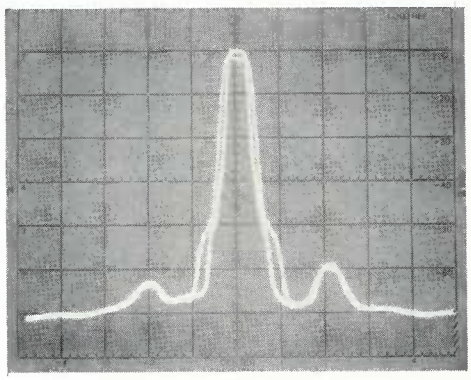

Inner - 4.3 Mbit/s
Outer - 6.4 Mbit/s

Fig. 8 Driver output spectra (810 MHz)

Hor. 5 MHz/div
Ver. 10 dB/div

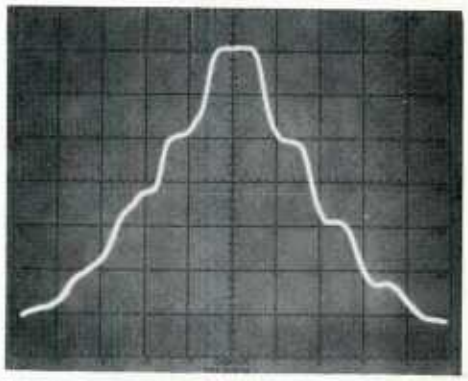

(a) Saturation

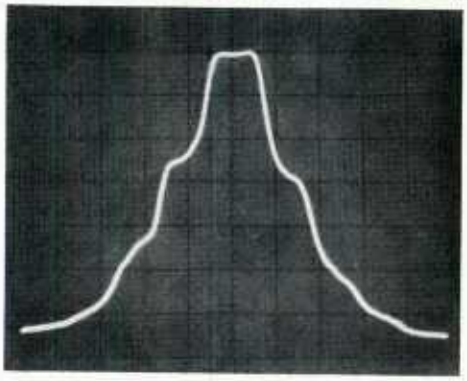

(b) 1 dB back off

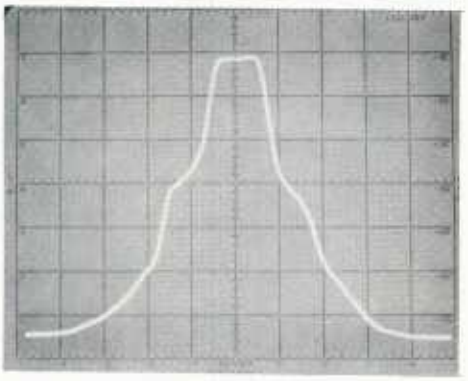

(c) 2 dB back off

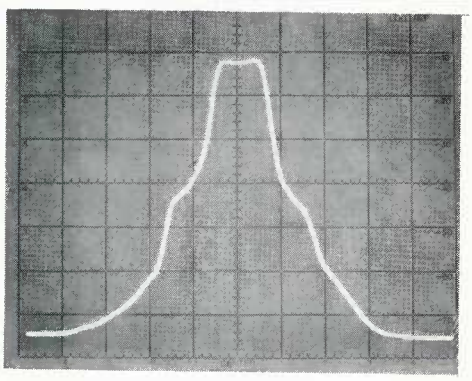

(d) 3 dB back off

Fig. 9 4.3 Mbit/s

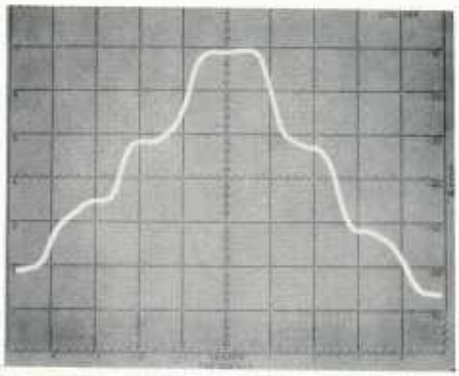

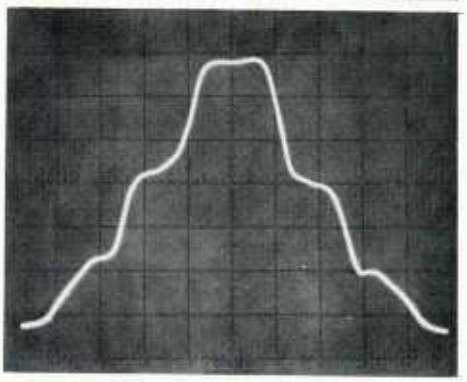

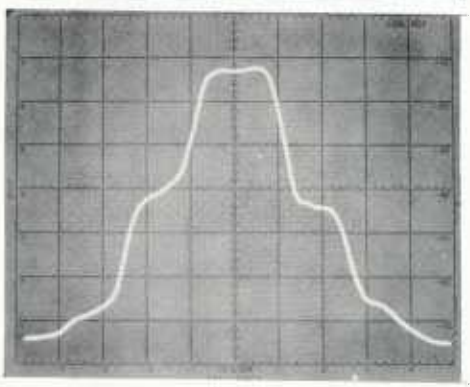

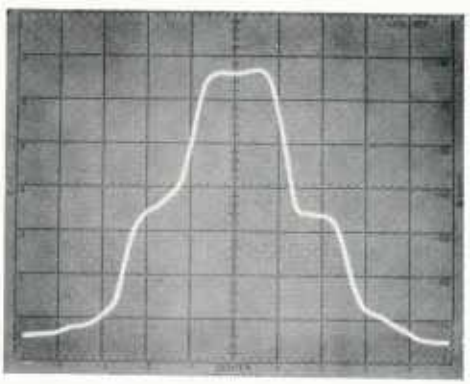

Fig. 10 6.4 Mbit/s

Klystron output spectra with 7-pole Butterworth baseband filtering

Hor. 2 MHz/div
Ver. 10 dB/div

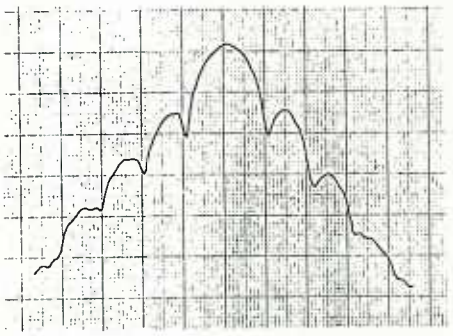

(a) saturation

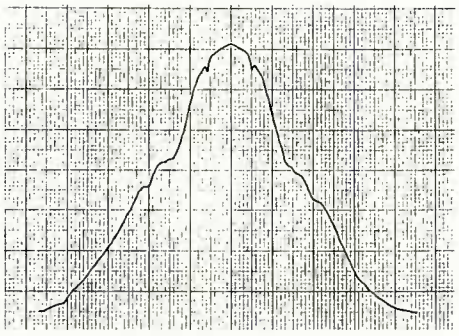

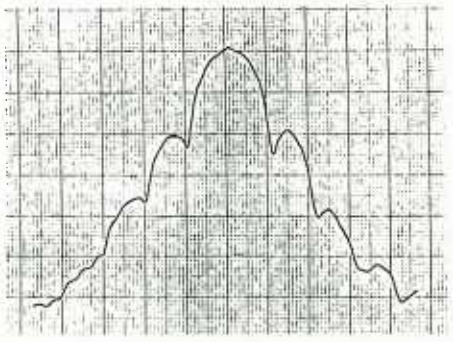

(b) 1 dB back-off

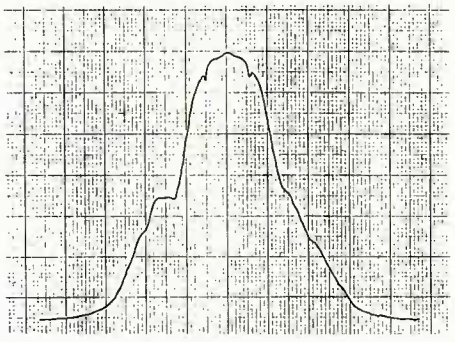

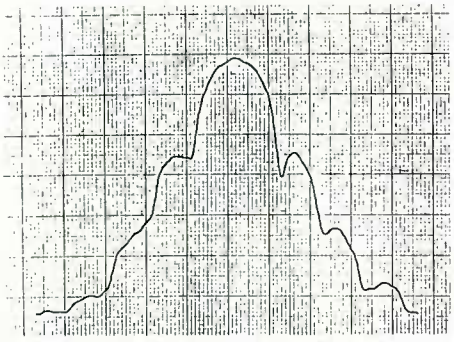

(c) 2 dB back-off

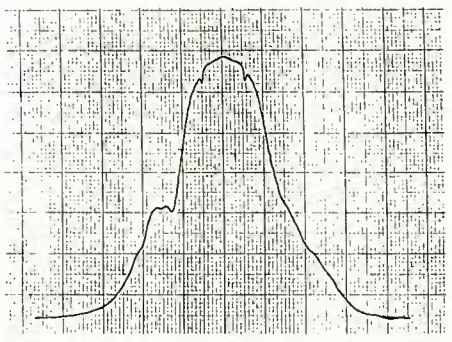

Fig. 11 4.2 Mbit/s QPSK

Fig. 12 4.2 Mbit/s off-set QPSK

Klystron output spectra with

full cosine roll-off baseband filtering

Hor. 2 MHz/div
Ver. 10 dB/div

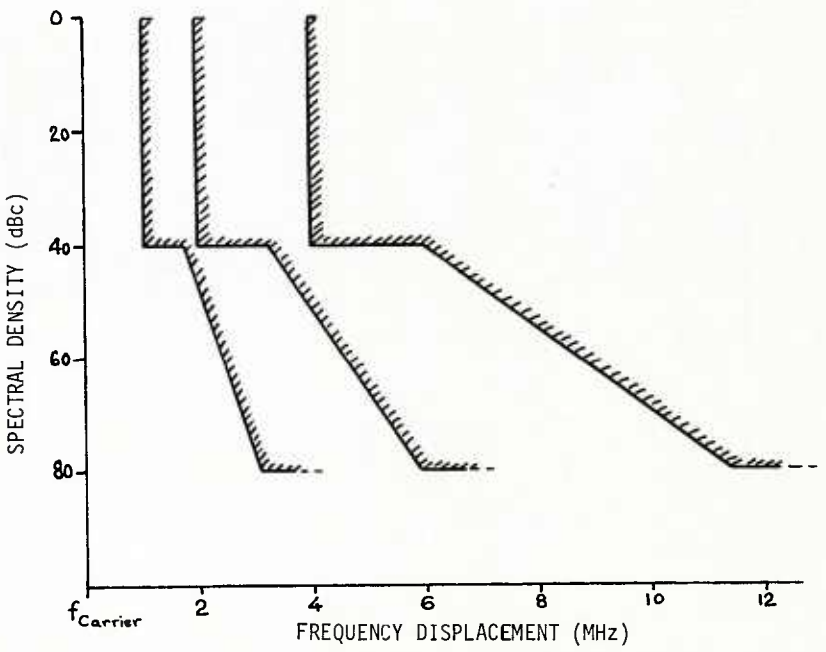

Fig. 13 Proposed spectral masks for 2, 4 and 8 MHz authorized bandwidths

DISCUSSION

J.Arnbak, Ne

You have stated your interesting results in term of HPA back-off, that is, in terms of transmit power sacrificed. Do you have any indications of the corresponding loss in link performance (say, BER)?

Author's Reply

Our computer simulations showed that the performance degradation due to the intersymbol interference caused by saturation in the high-power amplifier was a little over 1 dB. The reduction in distortion gained by backing-off the transmitter suggests that the degradation due to saturation would be recovered, as the sacrifice in transmitter power would be compensated for to some extent in the overall system performance.

INTERFERENCE REJECTION BY AUXILIARY FEEDS IN CASSEGRAIN EARTH TERMINALS

J. Arnbak, M.H.A.J. Herben and R.A.C.M. van Spaendonk*

Telecommunications Division
Department of Electrical Engineering
Eindhoven University of Technology
P.O. Box 513, NL-5600 MB Eindhoven, Netherlands
(* Now with Physics Laboratory TNO, The Hague, Netherlands)

Abstract

Presently, satellite crowding in the geostationary orbit is becoming a serious restriction on further development of operations in the communication bands. The enormous investments already made in existing earth terminals does not encourage complete antenna replacements to achieve lower sidelobe envelopes. However, at WARC-79 the E-W stationkeeping tolerance was tightened significantly (to $\pm$ 0.1^{o}). Consequently, it will become feasible to co-ordinate two potentially interfering satellite networks in accordance with Appendix 29 of the Radio Regulations, simply by reducing a few specific sidelobes in the respective earth terminals. This may be achieved by a much simpler retrofit of any earth terminals constraining orbit occupancy.
This paper reviews progress in an ongoing study of interferometric sidelobe suppression by auxiliary feeds in Cassegrain antennas. The isolation improvements are explored and related to the feed geometry, orbital spacing between satellites, and required excitation levels. The system value of this modernization option is very relevant as an interference mitigation scheme in the various satellite networks now in widespread use.

1. INTRODUCTION

Mutual interference among satellite networks serving the same or adjacent geographical areas is becoming a serious limitation in achieving sufficient utilization of the geo-stationary orbit and the frequency bands allocated to the fixed satellite service. Technical means of reducing satellite orbit spacings are under intensive study by the CCIR [2] and include improvements in the radiation characteristics of earth-station antennas. Up to the present, the method recommended by the CCIR and adopted by the ITU in the Radio Regulations has been to limit the radiated power-flux densities and the antenna sidelobe patterns [3] in order to control inter-system interference. This isolation method relies, inter alia, on the generic spatial filtering capability of all antenna systems outside their main beam. Hence, the method does not exploit any specific knowledge of the positions of those particular satellites which may be the sources or victims of excessive interference. Such apriori knowledge will, however, become available to network planners in the near future, following the tightening of the E-W satellite station-keeping accuracy to $\pm$ 0.1^{o} agreed at the 1979 World Administrative Radio Conference.

Given the orbital position of a satellite source (or victim) of interference, it would suffice -in an operational sense- to reduce the antenna sidelobe level in a small region centered on that orbital position. The size of this region would be dependant on the relative orbital movements of the two satellites, as seen from the earth terminal concerned. Reduction of specific wide-angle sidelobes has been realized in the past by placing a second antenna directed towards the (terrestrial) interference source and adding the signals properly [12]. Specific near-angle sidelobes directed towards an adjacent satellite can be suppressed by placing an auxiliary (defocused) feed in the focal region of the reflector system of the earth terminal [9]. In this way, unwanted sidelobes can be cancelled in an interferometric mode by the scanned main lobe set up by the auxiliary feed.

In the present paper, this concept will be examined further. The theoretical analysis is made for a general double-reflector antenna system, noting that major limitations on RF-spectrum and orbit utilization are imposed by the hundreds of earth stations already deployed. Following a description of the antenna geometry and scanning properties, the optimum location and excitation of the auxiliary feed are determined. Results of side-lobe suppression are presented for different orbital separations, orbital tolerances and excitation strengths. The paper concludes with a discussion and suggestions for further investigations of this approach to improved communications capacity of the increasingly interference-limited fixed satellite service.

2. GEOMETRY AND SCANNING PROPERTIES OF AN EXISTING FACILITY

2.1. Description of method

The earth terminal under study is assumed to be equipped with an existing double-reflector antenna, with the geometry shown in Fig. 1. This Figure also defines the coordinates adopted. The boresight direction coincides with the z-axis, and the points in the aperture plane ($z = 0$) are described by the polar coordinates (r,ξ). The far-field point P is given by the usual spherical coordinates (R,θ,ϕ). With perfect tracking, the desired satellite is kept on boresight ($\theta = 0$). The auxiliary feed is assumed to be offset in the plane $y = 0$, resulting in scanning of the main-beam to a direction $\theta_o \neq 0$.

The feed pattern is modelled as a power of a cosine, chosen such that the gain factor of the given antenna is maximum in the focused situation. The same feed pattern is maintained during scanning, but is inclined to minimize the sub- and main-reflector spillover

when the feed is moved away from the focus. The polarization of the feed is chosen to be that of a Huygens source, resulting in linear polarization in the antenna aperture in the focused condition. Other field conditions (e.g. circular polarization) can be obtained by vectorial superposition of more feed patterns of this nature.

The far-field patterns, both in the focused and defocused condition, are determined numerically from the corresponding geometrical-optical aperture field vector $\bar{E}_A$. Its amplitude E_A is found first in a suitable triangular grid of aperture points, using power conservation within suitable ray tubes. Subsequently, the amplitude can be approximated in any arbitrary aperture point (r,ξ) by linear interpolation using the three grid points which form the corners of the smallest triangle enclosing the point (r,ξ). The phase distribution Φ_A is derived from the geometrical distance along optical rays from the feed phase centre to the aperture plane and is approximated by

$$\Phi_A(r,\xi) = \alpha_o + \alpha_1 r\cos\xi + \alpha_2 r^2 + \alpha_3 r^2\cos^2\xi + \alpha_4 r^3\cos\xi + \alpha_5 r^4 \qquad (1)$$

for an offset of the feed in the plane y = 0.

Changing to the rectangular coordinates x and y, Eq. 1 may be written for the symmetry plane as

$$\Phi_A(x,0) = \alpha_o + \alpha_1 x + (\alpha_2 + \alpha_3)x^2 + \alpha_4 x^3 + \alpha_5 x^4 \qquad (2)$$

From this equation one can determine the constant coefficients α_o, α_1, $\alpha_2 + \alpha_3$, α_4 and α_5 by means of an one-dimensional least-squares fitting procedure. The individual coefficients α_2 and α_3 can be obtained from $\Phi_A(r,\xi)$ in a single point outside the symmetry plane. To determine the vector field distribution in the aperture, the vector properties of the feed and the polarization properties upon reflection at both reflector surfaces have been taken into account.

Now the far-field is available from a two-dimensional integral over the aperture plane. For numerical computation of this integral, a double integration procedure is used to obtain the main beam, while the sidelobes can be computed more economically by the stationary phase method [5]. The latter approach is fruitful because of the oscillating nature of the integrand in this region.

The coefficients α_i with $i \geq 2$ are unwanted phase aberrations causing degradations of the scanned pattern, whereas α_1 is the term corresponding to the desired beam squint [10] in the direction of the sidelobe(s) to be cancelled. The unwanted aberrations can be minimized by locating the auxiliary feed on a particular surface. This optimum scanning locus is known to be parabolic, if merely quadratic aberrations (corresponding to α_2 and α_3) are minimized along the aperture rim (r = D/2) of a Cassegrain system [4]. For greater precision, and in order not to preclude study of more general double-reflector systems [11], it is desirable to extent the minimization to the variance of a sum of unwanted aberrations over the entire aperture plane, in the manner recently demonstrated for the front-fed paraboloid [8]. This extension has been included here, using the amplitude aperture distribution $E_A(r,\xi)$ as a weight function in the minimization of the unwanted aberrations in Eq. 2, and thus determining the optimum feed locus of any double-reflector system.

2.2. Scanning properties of an existing Cassegrain system

Table 1 shows the key parameters of the existing Cassegrain antenna studied numerically in this paper. The two feed loci for scanning, as determined from Ref. 4 (L_A) and from the above more general procedure (L_B), are shown in Fig. 2.

Diameter-to-wavelength ratio	$D/\lambda = 200$
Focal length-to-diameter ratio	$F/D = 0.32$
Main-reflector-to-subreflector diameter ratio	$D/D_s = 11.1$
Relative reflector depth	$\alpha = 0.623$

Table 1: Key parameters for the Cassegrain antenna system studied

Although the two surfaces are almost coincident for small scan angles θ_o, the interior aperture field points required for accurate determination of the scanned far-field pattern from the defocused system also allow ready calculation of the more accurate surface L_B in all events.

Examples of the radiation pattern of the defocused system in the plane of scan (y = 0) are given in Fig. 3, which also includes the pattern of the focused system. To give an impression of the two-dimensional patterns, the copolar and cross-polar patterns in three different planar cuts ($\phi' = 0^o$, 45^o and 90^o) through the scanned main beam are shown in Fig. 4a and 4b, respectively. For $\phi' = 0^o$, the cross-polar field vanishes.

In all events, the cross-polar field caused by a defocused feed of the type considered is seen to be very small. Additional calculations have shown that the scanned co- and cross-polar patterns are almost independent of the polarization vector of the feed used. The consequence of these observations is that the sidelobe suppression realised with the interferometric method described in this paper will be virtually independent of the direction of the feed polarization vector. This is important for the success of the method, since the various earth-station locations will correspond to different orientations of the feed polarization vector relative to the scan plane. The local polarization vector(s) must obviously match the satellite to be accessed, whereas the scan plane will also be

decided by the local direction to the nominal position of the adjacent satellite θ_c off boresight.

3. EXCITATION AND LOCATION OF THE AUXILIARY FEED

The objective is now to minimize the co-polar sidelobe power summed over N equidistant sampling points of the complex radiation pattern E_r within a suitable region $\Delta\theta_c$ around the nominal position θ_c of the adjacent satellite. A first step to realize this is by minimizing the objective function

$$|E_r|^2 = \sum_{i=1}^{N} E_{ri} \cdot E_{ri}^* = \sum_{i=1}^{N} (E_{pi} + C\,E_{ai})(E_{pi} + C\,E_{ai})^* \tag{3}$$

with
E_p: the complex radiation pattern of the antenna system due to the primary (focused) feed
E_a: the complex radiation pattern of the antenna system due to the auxiliary (defocused) feed
C : the complex relative excitation of the auxiliary feed
E_r: the complex radiation pattern of the antenna system due to both the primary and auxiliary feed
* : the complex conjugate.

Assuming unit excitation of the primary feed, the complex excitation C of a single auxiliary feed is given by [9]

$$|C| = \frac{\left| \sum_{i=1}^{N} |E_{pi}|\,|E_{ai}| \cos(\arg C + \arg E_{ai} - \arg E_{pi}) \right|}{\sum_{i=1}^{N} |E_{ai}|^2} \tag{4}$$

$$\arg C = \tan^{-1} \left\{ \frac{-\sum_{i=1}^{N} |E_{pi}|\,|E_{ai}| \sin(\arg E_{ai} - \arg E_{pi})}{\sum_{i=1}^{N} |E_{pi}|\,|E_{ai}| \cos(\arg E_{ai} - \arg E_{pi})} \right\} \tag{5}$$

With these equations, it is theoretically possible to realize complete suppression at one point (N = 1, "nulling") as well as reduction of the power sum (3) in a wider angular region $\Delta\theta_c$. The latter approach may be considered to reduce the (time-)averaged interference power entering when the satellite spacing varies within a given tolerance $\Delta\theta_c$ corresponding to known (temporal) movements around the nominal spacing θ_c.

However, the least-squares solution of Eq. 3 can be extended to yield an approximate minimax solution, i.e., the solution which seeks to minimize the maximum sidelobe power throughout the region $\Delta\theta_c$. This may be operationally more relevant, since the adjacent satellite does not only produce a time sum of interference samples, but also a certain interference level at any one time. To minimize the worst-case interference throughout the considered interval, we introduce a (real) weight vector $\bar{w}$ multiplying E_p and E_a. Then Eq. 3 becomes

$$|E_r|^2 = \sum_{i=1}^{N} w_i^2\, E_{ri}\, E_{ri}^* = \sum_{i=1}^{N} w_i^2\, (E_{pi} + C\,E_{ai})(E_{pi} + C\,E_{ai})^* \tag{6}$$

The complex excitation coefficient now becomes

$$|C| = \frac{\left| \sum_{i=1}^{N} w_i^2\, |E_{pi}||E_{ai}| \cos(\arg C + \arg E_{ai} - \arg E_{pi}) \right|}{\sum_{i=1}^{N} w_i^2\, |E_{ai}|^2} \tag{7}$$

$$\arg C = \tan^{-1} \left\{ \frac{-\sum_{i=1}^{N} w_i^2\, |E_{pi}|\,|E_{ai}| \sin(\arg E_{ai} - \arg E_{pi})}{\sum_{i=1}^{N} w_i^2\, |E_{pi}|\,|E_{ai}| \cos(\arg E_{ai} - \arg E_{pi})} \right\} \tag{8}$$

The iteration process starts with $\bar{w} = \bar{1}$ (Eqs. 4-5). After each iteration by the computer the coefficient w_i belonging to the largest $|E_{ri}|^2$ sample is increased by Δw. The process

stops when the difference between the largest of the increasing $|E_{ri}|^2$ samples and the largest of the decreasing $|E_{ri}|^2$ samples is below a prescribed value. Then the difference between this weighted least-squares solution and the minimax solution is also smaller than this prescribed value.

Fig. 5 shows examples of the speed of convergence to this value. Fig. 5 shows that the necessary number of iterations can be reduced by scaling down Δw during the process. The computer procedure also includes determination of the best scan angle θ_o of the squinting main beam generated by the auxiliary feed.

4. SIDELOBE SUPPRESSION RESULTS

Fig. 6 shows some examples of the maximum residual $|E_{ri}|^2$ inside the suppression region $\Delta\theta_c$, as a function of the scan angle θ_o, for several orbital tolerances $\Delta\theta_c$. It is seen that for increasing tolerance $\Delta\theta_c$, the realized suppression decreases. For $\Delta\theta_c = 0.4^o$, the maximum residual $|E_{ri}|^2$ is 11, 17 and 18.5 dB for nominal spacings $\theta_c = -1.2$, -1.1 and -1.0 degrees respectively. Compared with the unmodified Cassegrain system this is an improvement of 14, 8 and 6.5 dB, respectively.

The corresponding radiation patterns are shown in Fig. 7. This figure shows that immediately outside the suppression interval the sidelobes may increase. In spite of this, the envelope of the resulting radiation pattern remains below the CCIR reference curve [3].

Finally, Fig. 8 shows the complex excitation coefficient C as a function of $\Delta\theta_c$ with the nominal position θ_c of the adjacent satellite as a parameter. For $\Delta\theta_c = 0.4$ the relative value of C is seen to be -29.2, -33.2 and -26.8 dB for $\theta_c = -1.2$, -1.1 and -1.0 degrees, respectively. Because of such exceedingly weak excitations it is evident that the cross-polarization introduced by the defocused auxiliary feed as shown in Fig. 4 may be neglected. For example, with $|C| = -30$ dB the peak of this crosspolar pattern would be 61 dB below boresight gain.

5. DISCUSSION AND CONCLUSIONS

From the above results, it appears theoretically feasible to improve intersystem isolation between two satellite networks significantly, provided that the two satellites are both kept at their nominal stations within the tolerance of $\pm 0.1^o$ laid down in the ITU Radio Regulations in force from Jan. 1, 1982. The orbital spacing can be reduced by a factor of 3 to 6, relative to what is obtained using the recommended CCIR sidelobe envelope [3]. The use of weakly excited defocused feeds, corresponding to the local direction(s) in which excessive interference must be eliminated, avoids major perturbations of the antenna co- and cross-polar radiation in other directions. Hence the method may be repeated for each adjacent satellite which is a potential source (or victim) of intersystem interference, without upsetting any intrasystem link budgets or intersystem isolations already obtained. Accordingly, this approach may be attractive for low-cost upgrading of existing earth terminals to the more exigent interference environments expected in the future.

Fig. 9 shows that amplitude and phase tolerances of the required weak excitations of the extra feeds must be tight and could present a problem. However, reliable interference compensation networks with similar accuracy requirements will also be required to maintain sufficient cross-polarization discrimination in the face of precipitation conditions in satellite networks with polarization frequency reuse. It will be necessary, however, to take due account of amplitude and phase scintillations on the propagation paths involved [6].

Another problem still requiring study is the viability of introducing adequate defocused feeds in existing reflector systems. The dielectric-rod antenna [1] is being investigated as a candidate solution [7], due to its small transverse dimensions and the low mutual coupling with adjacent feed elements. Finally the frequency sensitivity and the two-dimensional characteristics of the created suppression need further investigation in relation to typical bandwidth requirements and relative N-S movements of the satellite concerned.

6. REFERENCES

[1] Bach Andersen, J., 1971, "Metallic and dielectric antennas", (Dr. tech. thesis, Technical University Denmark, Lyngby, Denmark), Polyteknisk Forlag.

[2] CCIR Rep. 453-2, 1982.

[3] CCIR Rec. 465-1 and CCIR Rec. 580, 1982.

[4] Gniss, H., and Ries, G., 1970, "Bemerkungen zum Konzept des äquivalenten Parabols bei Cassegrain-Antennen", Electronics Letters, Vol. 6, pp. 737-739.

[5] Herben, M.H.A.J., Middelkoop, R., and Gielkens, F.J.J., 1980, "Stationary phase method for far-field computation of defocused reflector antennas", Electronics Letters, Vol. 16, pp. 519-521; Errata, ibid, Vol. 16, p. 644.

[6] Herben, M.H.A.J., 1982, "Amplitude and phase scintillation measurements on 8.2 km line-of-sight path at 30 GHz", Electronics Letters, Vol. 18, pp. 287-289.

[7] Lynggaard, S., 1982, "The dielectric rod as an auxiliary feed for sidelobe reduction in reflector antennas", Unpublished Report, Eindhoven University of Technology, Eindhoven, Netherlands.

[8] Mrstik, A.V., 1979, "Scan limits of off-axis fed parabolic reflectors", IEEE Trans., Vol. AP-27, pp. 647-651.

[9] van Ommeren, M.J.S., Herben, M.H.A.J., and Arnbak, J.C., 1980, "Improved orbit utilization by interferometric sidelobe suppression", Electronics Letters, Vol. 16, pp. 937-938.

[10] Ruze, J., 1965, "Lateral feed displacement in a paraboloid", IEEE Trans., Vol. AP-13, pp. 660-665.
[11] Scheeren, P.M.J., Herben, M.H.A.J., and Maanders, E.J., 1981, "Scan properties of the Schwarzschild antenna", Proc. 11th European Microwave Conference, Amsterdam, 7-10 September 1981, pp. 561-566.
[12] White, N., Brandwood, D., and Raymond, G., 1975, "The application of interference cancellation to an earth station", Proc. Conf. Satellite Communications System Technology, London, 7-10 April 1975, (IEE Conf. Publ. 126, pp. 233-238).

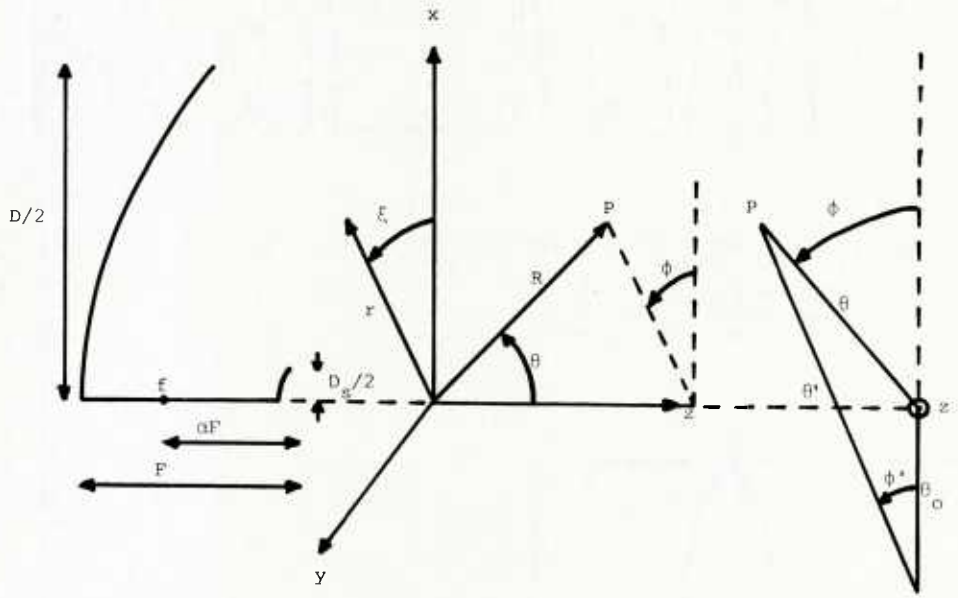

Fig. 1: Geometry, coordinates and symbols of the double reflector antenna system (only half of the reflector system is shown). f: focal point.

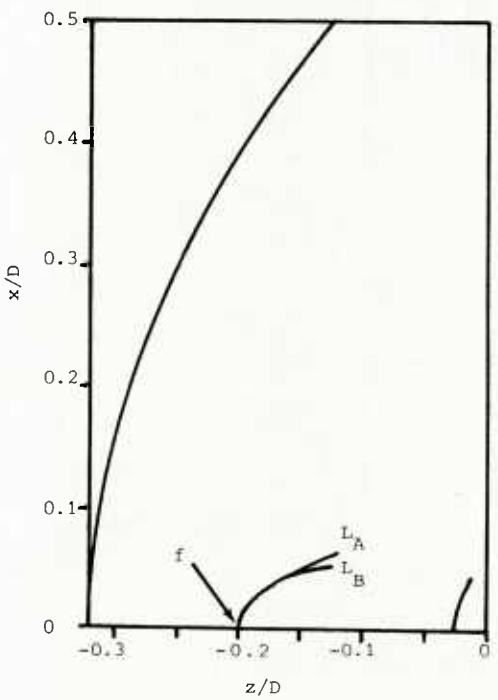

Fig. 2: Cassegrain antenna system with two feed loci for scanning.
L_A: feed locus determined from Ref. 4.
L_B: feed locus minimizing unwanted aberrations in Eq. 1.

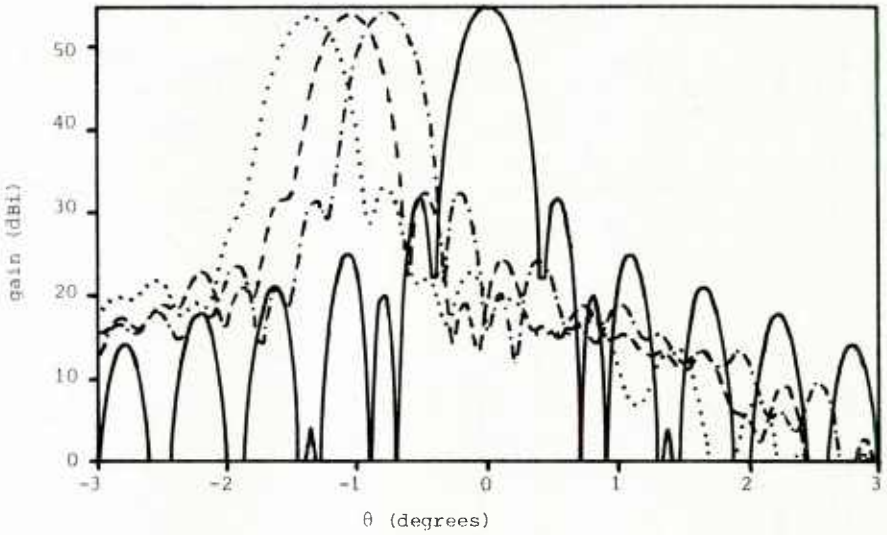

Fig. 3: Radiation pattern of focused and defocused system in plane of scan.
——— focused system
-.-. scan angle θ_o = 0.77°
---- scan angle θ_o = 1.05°
.... scan angle θ_o = 1.40°

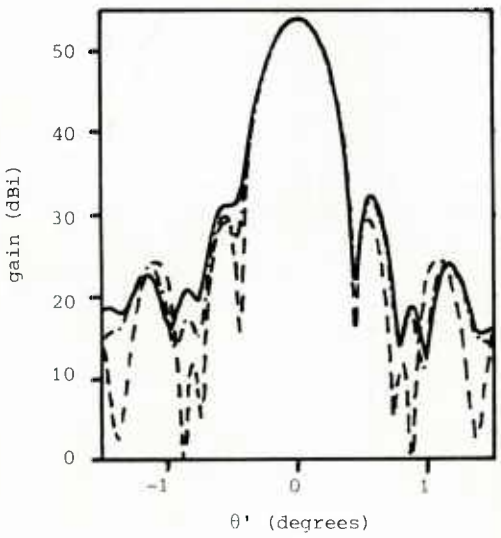

Fig. 4a: Co-polar pattern cuts of defocused system scanned to θ_o = 1.05°
——— ϕ' = 0°
-.-. ϕ' = 45°
---- ϕ' = 90°

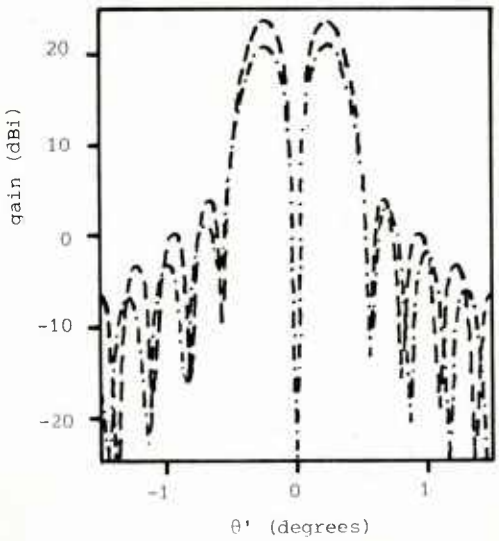

Fig. 4b: Cross-polar pattern cuts of defocused system scanned to θ_o = 1.05°
-.-. ϕ' = 45°
---- ϕ' = 90°

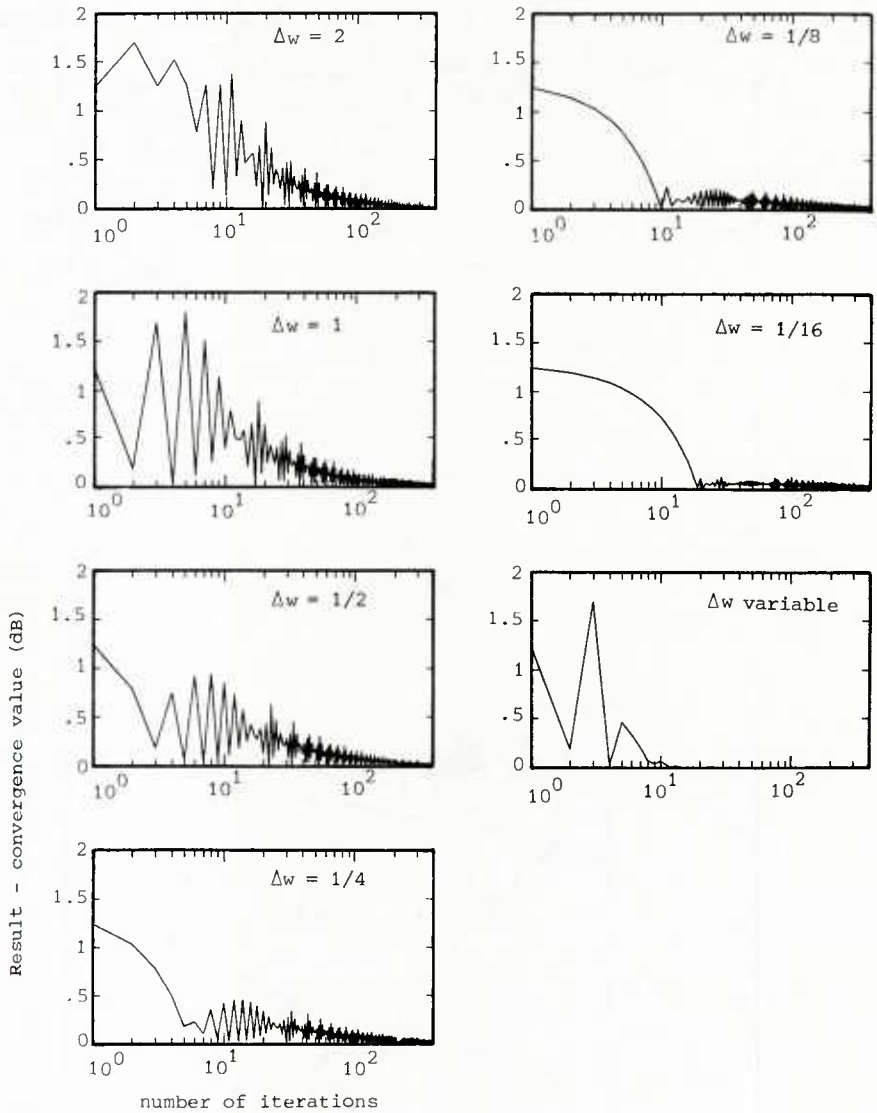

Fig. 5: Speed of convergence of minimax iteration for various scaling terms Δw. Difference (in dB) from final value, as a function of the number of iterations. The number of equidistant sampling points N = 13 (Eq. 3). $\theta_c = -1.1^o$ and $\Delta\theta_c = 0.4^o$.

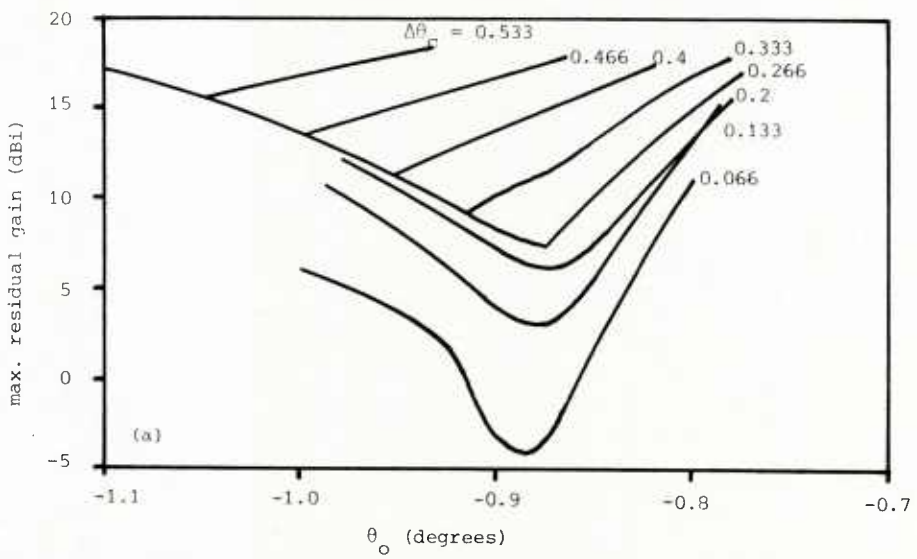

Fig. 6: Minimum residual gain for various orbital tolerances ($\Delta\theta_c$ in degrees), as a function of a scan angle θ_o.
(a) Nominal satellite spacing $\theta_c^o = -1.2^o$.

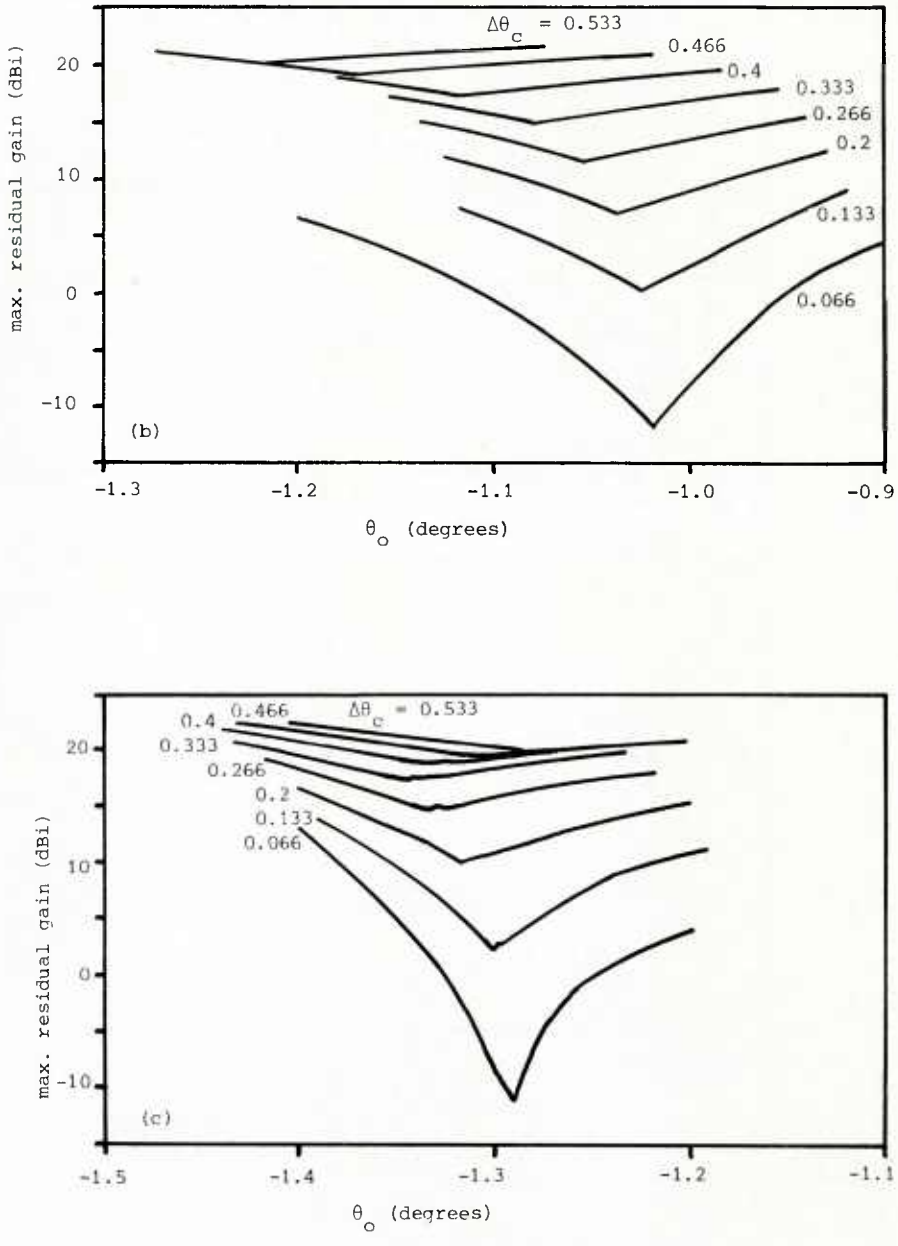

Fig. 6: Maximum residual gain for various orbital tolerances ($\Delta\theta_c$ in degrees), as a function of scan angle θ_o.
(b) Nominal satellite spacing $\theta_c = -1.1^o$.
(c) Nominal satellite spacing $\theta_c = -1.0^o$.

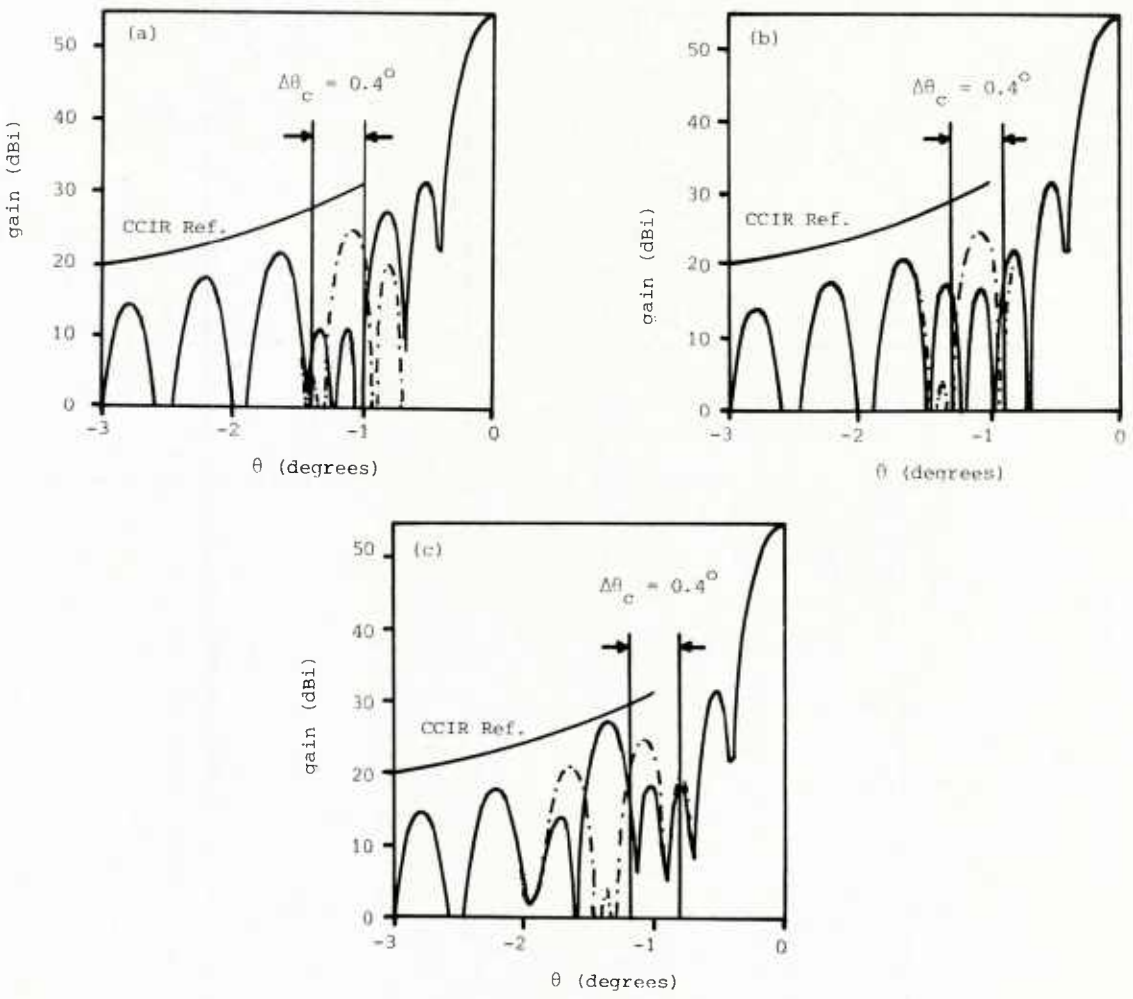

Fig. 7: Examples of sidelobe suppression for $\Delta\theta_c = 0.4^\circ$.
——— Radiation pattern of modified system
-.-. Radiation pattern of unmodified system
(a) Nominal satellite spacing $\theta_c = -1.2^\circ$
(b) Nominal satellite spacing $\theta_c = -1.1^\circ$
(c) Nominal satellite spacing $\theta_c = -1.0^\circ$

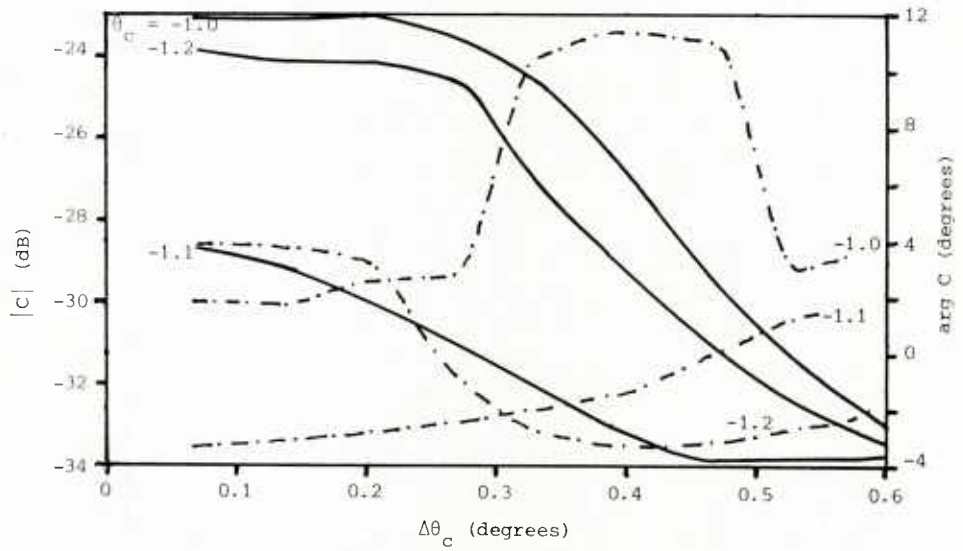

Fig. 8: The complex excitation coefficient C as a function of orbital tolerance $\Delta\theta_c$, with the nominal position θ_c of the adjacent satellite as a parameter (θ_c in degrees).
——— |C|
-.-. arg C

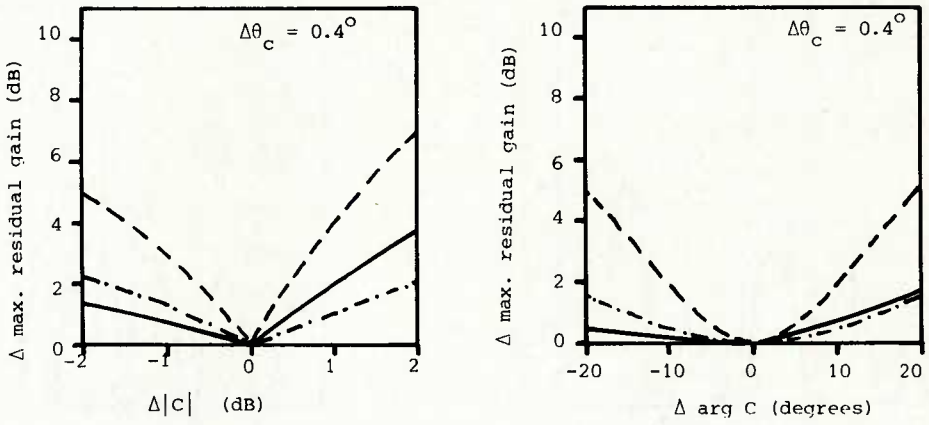

Fig. 9: The increase of the maximum residual gain as a function of excitation amplitude and phase tolerances.
——— $\theta_c = -1.0^\circ$
-.-. $\theta_c = -1.1^\circ$
---- $\theta_c = -1.2^\circ$

DISCUSSION

K.D. Becker, Ge

Can you say something on the dependence of your results on the transient character of a signal?

Author's Reply

Not yet. This aspect is related to the bandwidth of the obtained suppression which will be looked into in the coming year. Obviously, your question is extremely relevant to the use of TDMA in the Fixed Satellite Service. I have an intuitive feeling that – owing to the use of main-beam properties of a quasi-optical reflector system – bandwidth problems or transient problems may not be as serious as in "tuned" systems, say, Yagi's or phased arrays.

I. Anderson, UK

The minimum spacing between the angles of the desired and undesired satellites for the author's rejection scheme will be limited by feed-feed coupling and this will degrade the antenna gain. What is the minimum angle?

Author's Reply

The optimum locus (L_B) depends on the particular feed and reflector design considered, so we cannot offer a general answer. Some modern systems with near-field excitation will be more difficult to upgrade, but are normally already better in respect of sidelobes than the majority of existing earth terminals, in which the main feed horn is at some distance form the sub-reflector apex. However, let us not forget that in principle, mutual coupling is a linear problem, so that it may be possible to determine a modified excitation coefficient (C′) of the auxiliary feed if it is coupled to the main feed horn by near fields. Admittedly, this could give rise to bandwidth problems of the nature queried just now by Professor Becker!

Our goal is to develop a computer programme that give answers to these kinds of questions, given any particular geometry of an existing earth-terminal antenna. Note that the real need is to improve existing systems, since these present the worst constraints on utilization of the geostationary orbit and, at the same time, represent a very substantial invested capital.

S. Segner, US

Will the auxiliary feeds cause a problem with the coordination contours of your receiver?

Author's Reply

If you look at Fig.7(a)–(c) in our paper, you will note that the radiation diagram is hardly modified more than two beamwidths away from the "null" region. Hence, the diagram related to App.28 and the (terrestrial) coordination contours is not affected by our more lofty effort to improve the pattern towards the geostationary orbits (as required for application of App.29 of the ITU Radio Regulations). This, in fact, is the virtue of using the scanned main beam to suppress the critical sidelobes, but leaving the remaining pattern largely unaffected.

GAIN PATTERNS OF MICROWAVE COMMON CARRIER ANTENNAS

A.G. Hanson and P.M. McManamon
Institute for Telecommunication Sciences
National Telecommunications and Information Administration
U.S. Department of Commerce
325 Broadway
Boulder, Colorado 80303, USA

SUMMARY

The proliferation within the microwave radio bands has resulted in increasing interference problems caused by the installation of more microwave transmitters sharing within the terrestrial microwave service and with communications satellite services. This frequency sharing has been the subject of study within the past decade by several Working Groups of the International Radio Consultative Committee (CCIR). This CCIR work has resulted in a widely employed, statistically derived analytical expression (for all 2 to 11 GHz common carrier antennas) based on gain data compiled on 100 common carrier antennas, published by the CCIR in 1972. This paper presents a comprehensive update to the CCIR report.

This paper summarizes analytical expressions which describe the off-axis radiation characteristics of 924 transmit antenna models in use within the continental United States in the 2, 4, 6, and 11 GHz common carrier microwave terrestrial radio service. Data are presented in a uniform format which permits the user to determine power gain for any antenna identified, at any off-axis azimuthal angle. The primary application of these data is for interference prediction among microwave links and between microwave links and communication-satellite earth terminals sharing a common frequency band.

1. INTRODUCTION

Interference sharing criteria depend upon simplified antenna models to represent the antenna gain in off-axis directions. Earlier studies reviewed about 15,600 microwave relay sites in the United States and found that the antennas could be represented by nominally 100 different antenna patterns (CCIR, 1972 and 1974). These 100 patterns were reduced to only 22 patterns to represent 95% of the data statistically. This analysis yielded the now well-known, two-straight-line-segment curve expressed as:

$$G = 38 - 25 \log_{10}\theta \; ; \quad 1° < \theta < 33.1°$$

$$G = 0 \; ; \quad 33.1° < \theta < 180°$$

where G is the gain, in dBi, at an angle, θ, in degrees off the axis of the main lobe. This function is illustrated in Figure 1. This equation is presented in Section 3 of "Results of measurements on the antennae of existing radio relay links," CCIR Report 614, Reference Radiation Patterns for Radio-Relay System Antennae Study Programme 17A/9 (CCIR, 1974).

This paper is limited to active transmit antennas used for the U.S. Federal Communications Commission (FCC)-allocated common carrier frequency bands of 1.990-2.200 GHz, 3.700-4.200 GHz, 5.925-6.425 GHz and 10.700-11.700 GHz (FCC, 1976). These bands are commonly referred to as the 2, 4, 6, and 11 GHz bands, respectively.

The primary objective of the study summarized in this paper has been to provide a more up-to-date model for off-axis antenna patterns in the frequency bands listed above. The avoidance of interference in terrestrial path coordination usually involves assuring that no antenna main lobe is pointed within a small angle ($0°<\theta<10°$) of another antenna location. In this paper, emphasis has been placed on reasonably accurate sidelobe data for all angles off boresight, including those less than 10 degrees. This attention has been prompted, to a large degree, by the growing concerns over potential interference among microwave links and between microwave links and satellite earth stations.

Data were obtained for 924 antenna models. This includes parabolic reflectors, horns, periscope systems, etc. This information was derived from contact with all major U.S. common carrier microwave antenna manufacturers. The data were augmented by interrogation of the FCC common carrier data base (FCC, 1980). This data base contains tabulations of transmit antennas deployed at individual microwave transmitter sites. Because adequate, measured data in the vertical plane are scarce (as was also noted by CCIR), all data apply only to horizontal patterns.

Because of unavailability of measured data, passive ("billboard reflector") repeater antennas are not included. The billboard reflector is a planar antenna, typically employed in a link to change path direction, to avoid obstructions such as mountains or tall buildings. The reader who is concerned with calculating interference for specific links employing passive repeaters is directed to an exhaustive manual on the subject (Microflect, 1976).

2. GAIN PATTERN DATA SUMMARY

Figures 2, 3, 4, and 5 show curves representing composite worst-case deviations between upper and lower bounds of gain for all antennas evaluated in, respectively, the 2, 4, 6, and 11 GHz bands. The CCIR curve given in Section 1 is displayed as a reference. These figures illustrate the deviations possible at any specific angle, relative to the CCIR reference model. The most significant deviations are below the reference, particularly beyond 20 degrees off-axis.

Figure 6 shows radiation envelope patterns, in the 4 GHz band, for two geometrically similar 2.4-meter diameter parabolic antennas having a difference in main lobe gain of only 0.3 dBi. Again, the CCIR curve is superimposed. These illustrations, derived from manufacturers' data, show the need for a nonstatistical approach if quantitative information on individual antennas is to be made available. As indicated in Figure 6, antennas of similar geometry and size cannot be treated as having similar off-axis gain characteristics in detailed interference analysis. Another method of combining antennas with like gain characteristics has been devised.

In an effort to eliminate redundancy and to reduce the size of the quantitative data base, antennas displaying similar radiation patterns were grouped into sets and "general set patterns" were developed for each of these sets. "Similar radiation patterns" have been concisely defined as those antenna gain patterns which do not exceed a maximum excursion of 5 dBi ($\pm$2.5 dBi) among the patterns of all antennas within any set, for any angle over the range of 1°-180° (see Fig. 7). In addition, the set pattern gain limits developed should be at most 4 dBi above the gain for any antenna at any angle off-axis and should be at most 2 dBi below the gain at any angle for any antenna. This tolerance provides acceptable accuracy in the tradeoff against a data bank of rather massive size. A maximum of ten straight-line segments is used to describe each general set pattern.

3. UNIFORM DATA FORMAT

The very large volume of manufacturers' information which has been analyzed mandated that these data be organized into a uniform format, while preserving their integrity. One assumption was made in this data organization process: the user of this interference-prediction data bank will not know the transmit polarization or the feed orientation used by the operator of a given site. It thus became necessary to derive the "worst-case" gain values for all possible combinations of feed and polarization (using manufacturers' data), as discussed below. Four issues were found to require considerable attention, and have been treated as follows:

(a) Format: All data were converted to semi-logarithmic plots, the ordinate being relative gain in dBi, the abscissa being given in degrees off the main lobe, from 1°-180°. This follows the CCIR approach, permitting comparability with the CCIR statistically derived curve, and is readily adaptable to computer automation.

(b) Antenna feed: For antennas with asymmetrical left field/right field pattern envelopes, the worst-case value (highest gain) has been taken for equivalent angles off axis (e.g., 1°/359°, 10°/350°, etc.), and these worst-case values have been plotted over the 1°-180° range. This follows the CCIR methodology and assures use of the highest gain measured by the manufacturer, independent of feed orientation.

(c) Polarization: For any pair of dual-polarization antennas, the four operational modes are transmit horizontal-receive horizontal, transmit horizontal-receive vertical, transmit vertical-receive vertical, and transmit vertical-receive horizontal. With the exception of very few such antennas, the highest off-axis gain for any given antenna fluctuates, as a function of angle, among two or more of these four modes. As in the case of asymmetric antennas, it has been necessary to ascertain the worst-case value for each angle, from manufacturers' data. In the case of asymmetric antennas with dual polarization, the worst case has been derived taking all six variables into account (left field/right field, four polarization modes).

(d) Specification of Gain Values: In the interest of uniformity, all manufacturers' data have been converted from discrimination values to relative gain. For some high performance models, manufacturers' graphic plots of discrimination go off scale at some angle less than 180° (or 360° for left-field plots) -- presumably exceeding measurement capabilities. In these instances, the last measured value (highest discrimination) is used from the associated angle through 180°.

In accordance with these guidelines, the smoothed radiation pattern envelope for each of the 924 antennas was graphically plotted as illustrated in Figure 8.

4. GENERAL PATTERNS FOR SETS OF ANTENNAS

Figure 8 is an illustration, derived from manufacturers' data, of one antenna in Set 1 of the 2 GHz band, superimposed on the plot of the Set 1 general set pattern. Figure 9 gives the composite upper- and lower-bound gains for the nine antennas grouped within Set 1, and illustrates the +2 dBi, -4 dBi tolerances shown in Figure 7. This type of plot

was not used in preparation of the data base, but is shown here to illustrate the maximum 5 dBi employed in set grouping.

Table 1 lists antennas within Set 1 and presents computer-generated equations derived from the ten continuous straight-line segments of the general set pattern for Set 1 (see Fig. 8). These equations permit the user to calculate rapidly and simply the gain for any off-axis angle between 0.1° and 180°. For example, suppose the user requires the gain for an antenna of Set 1 for 5°. Since 5° is within the range of line 4 of Table 1 ($3.00° \leq \theta < 10.00°$), we can calculate the gain as:

$$G = 40.14 - 27.54 \log 5° \text{ dBi} \cong 21 \text{ dBi}.$$

Table 1. Gain Pattern for Set 1 of Common Carrier Microwave Transmit Antennas 2 GHz Band

Angle Off-Axis θ (Degrees)	Gain G(dBi)	
$0.00 \leq \theta < 0.10$	$G = G_{max}$	(1)
$0.10 \leq \theta < 1.00$	$G = 29.50 + (29.50G_{max})\log \theta$	(2)
$1.00 \leq \theta < 3.00$	$G = 29.50 - 5.24 \log \theta$	(3)
$3.00 \leq \theta < 10.00$	$G = 40.14 - 27.54 \log \theta$	(4)
$10.00 \leq \theta < 20.00$	$G = 24.56 - 11.96 \log \theta$	(5)
$20.00 \leq \theta < 30.00$	$G = 45.94 - 28.39 \log \theta$	(6)
$30.00 \leq \theta < 60.00$	$G = 17.25 - 8.97 \log \theta$	(7)
$60.00 \leq \theta < 100.00$	$G = 7.71 - 3.61 \log \theta$	(8)
$100.00 \leq \theta < 110.00$	$G = 63.31 - 31.41 \log \theta$	(9)
$110.00 \leq \theta < 120.00$	$G = 118.05 - 58.22 \log \theta$	(10)
$120.00 \leq \theta < 130.00$	$G = 224.28 - 109.31 \log \theta$	(11)
$130.00 \leq \theta \leq 180.00$	$G = -6.80$	(12)

The reader will note that the illustrations show no entries for angles less than 1°. This is because adequate measured data within this angular range are unavailable. It is seen from equation (1) of Table 1 that G_{max}, the on-axis gain for each individual antenna, is assumed for the narrow range between 0° and 0.1°, and that the measured values for G_{max} and the gain at 1.0° are used as end points for calculating approximate gain between 0.1° and 1.0°. This is used as the best approximation in the absence of adequate measured data within these regions.

Computer-generated equations have been derived for the other 502 sets of general set patterns. These are available in the format shown here but were not presented in this paper because of page limitations. Antenna model numbers and other identifying data have been retained in the computer-coded and stored data base.

5. REFERENCES

CCIR, 1972, Radiation diagram of line-of-sight radio-relay antennae for use in interference studies with communications satellite earth stations, CCIR Doc. 9/38-E, March 21.

CCIR, 1974, Reference radiation patterns for radio-relay system antennae, CCIR Report 614 (Study Programme 17A/9).

FCC, 1976, Federal Communications Commission, Rules and regulations, §2.106, Table of frequency allocations, August.

FCC, 1980, Common carrier microwave antenna, licensee, and transmitter file, NTIS Accession No. PB80-116940, Springfield, VA.

Microflect, 1976, Passive repeater engineering, Manual No. 161A, Second Edition, Microflect Co. Inc., Salem, Oregon.

6. ACKNOWLEDGEMENTS

The authors would like to acknowledge the significant contributions of D.P. Anderson.

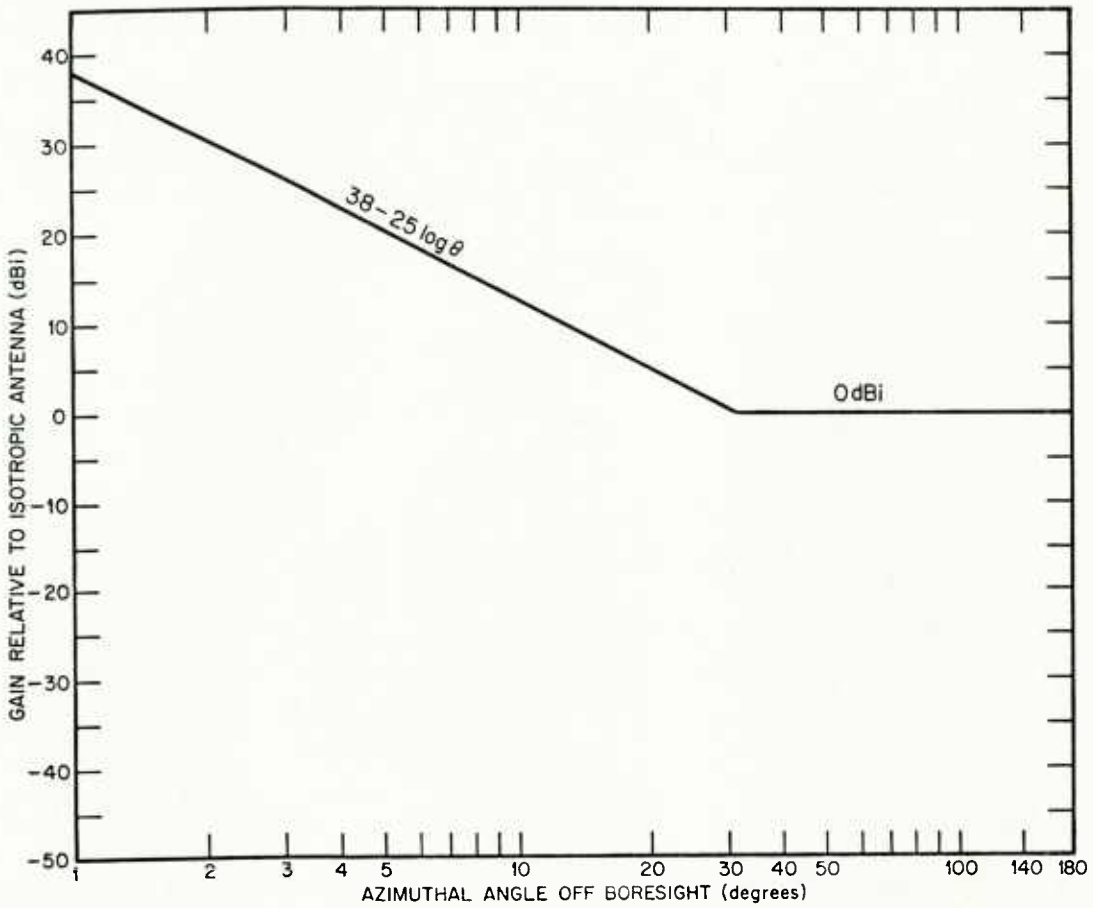

Figure 1. Distribution of gain for line-of-sight radio relay antennas (After CCIR Study Programme 17A/9, 1974).

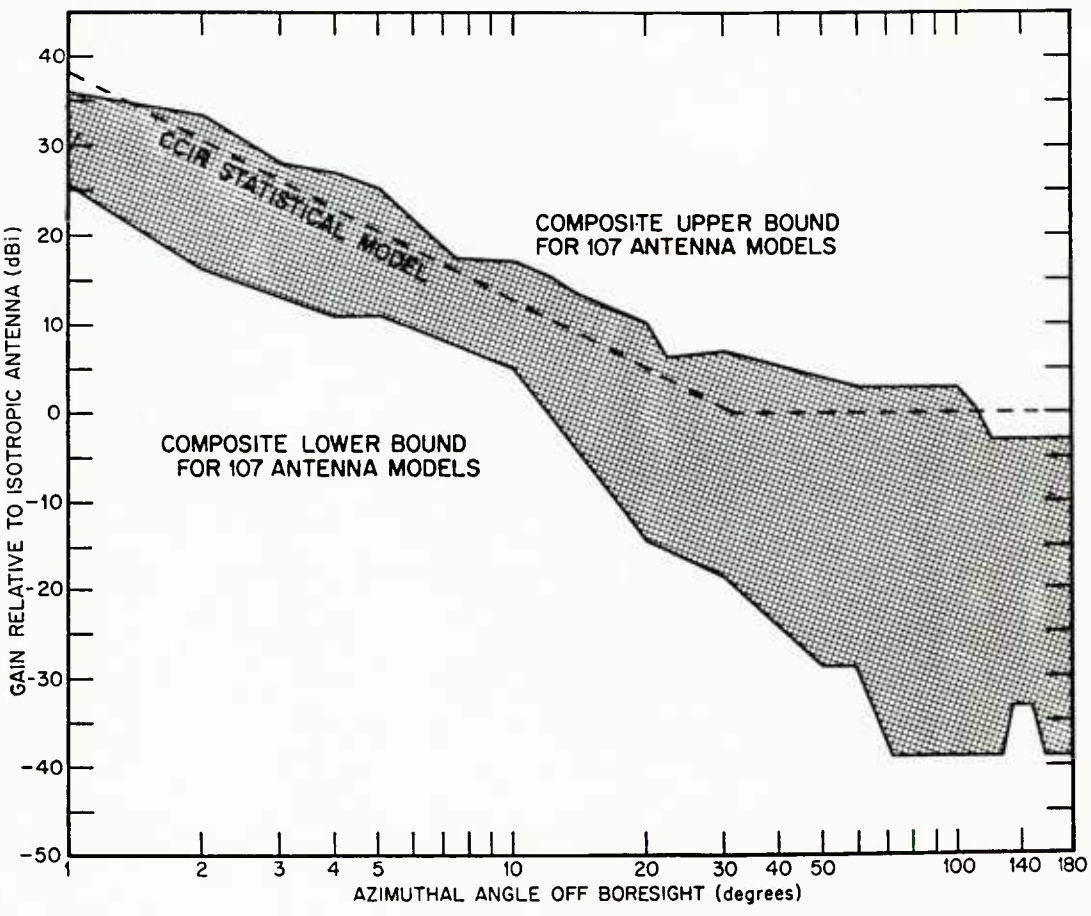

Figure 2. Upper and lower gain bounds for a composite of 107 antenna models in the 2 GHz band.

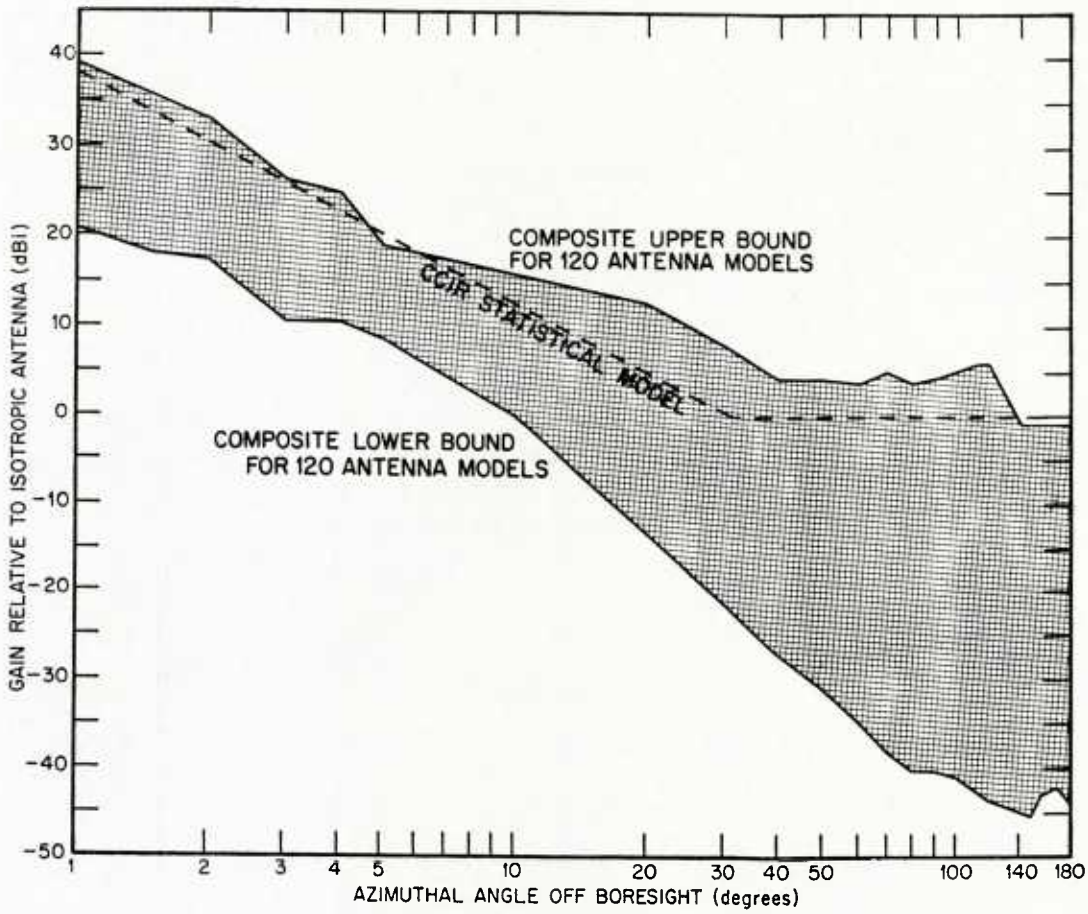

Figure 3. Upper and lower gain bounds for a composite of 120 antenna models in the 4 GHz band.

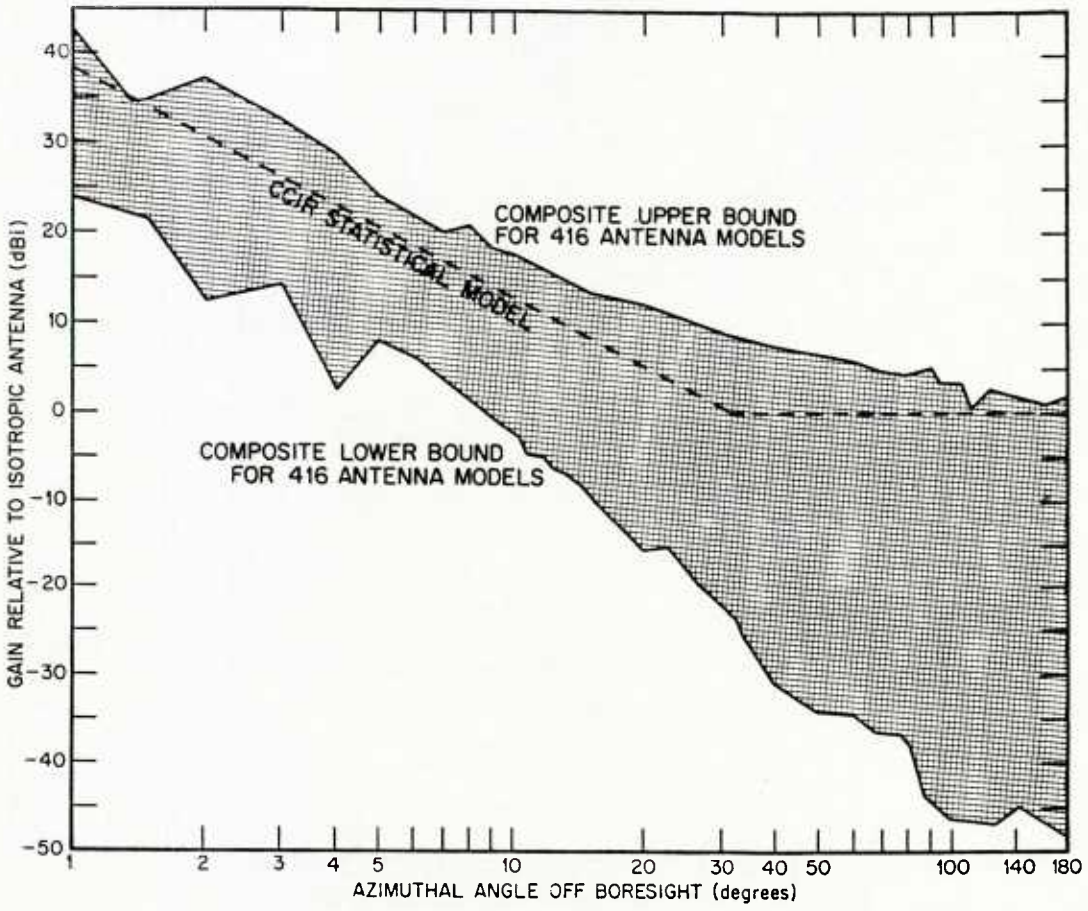

Figure 4. Upper and lower gain bounds for a composite of 416 antenna models in the 6 GHz band.

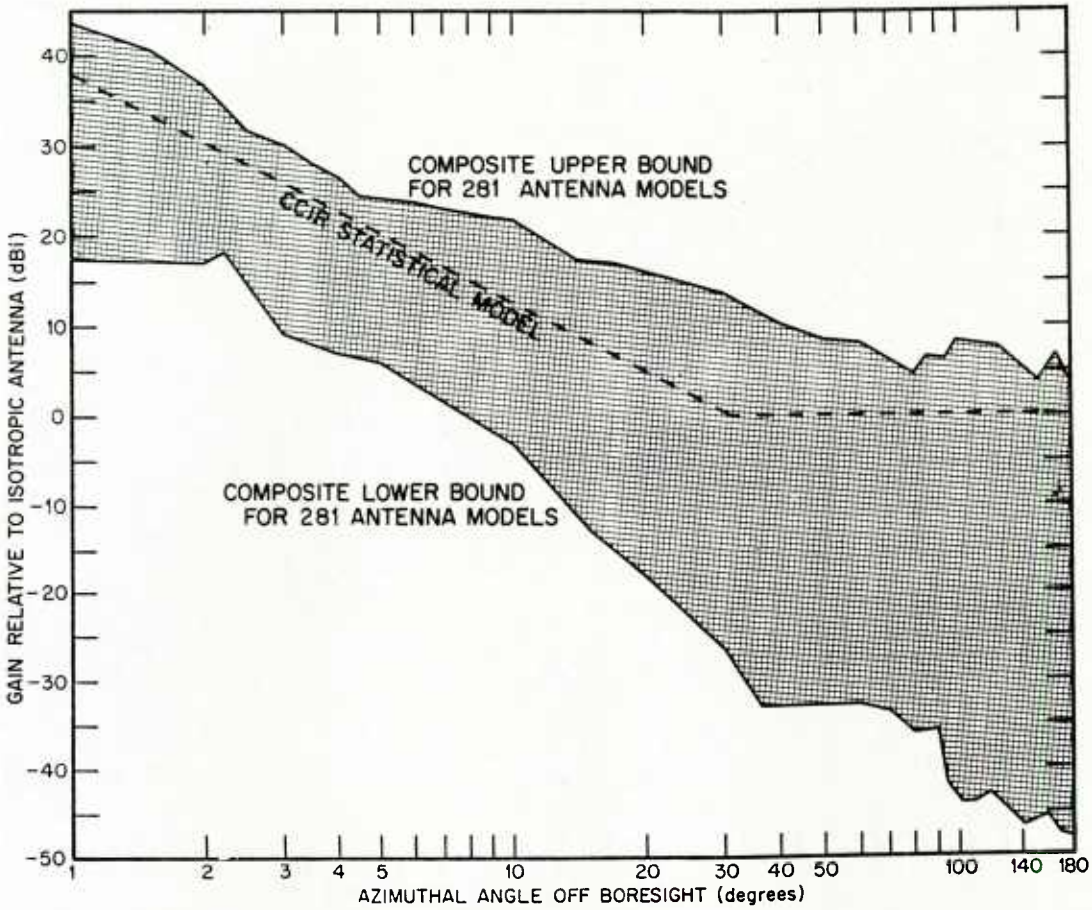

Figure 5. Upper and lower gain bounds for a composite of 281 antenna models in the 11 GHz band.

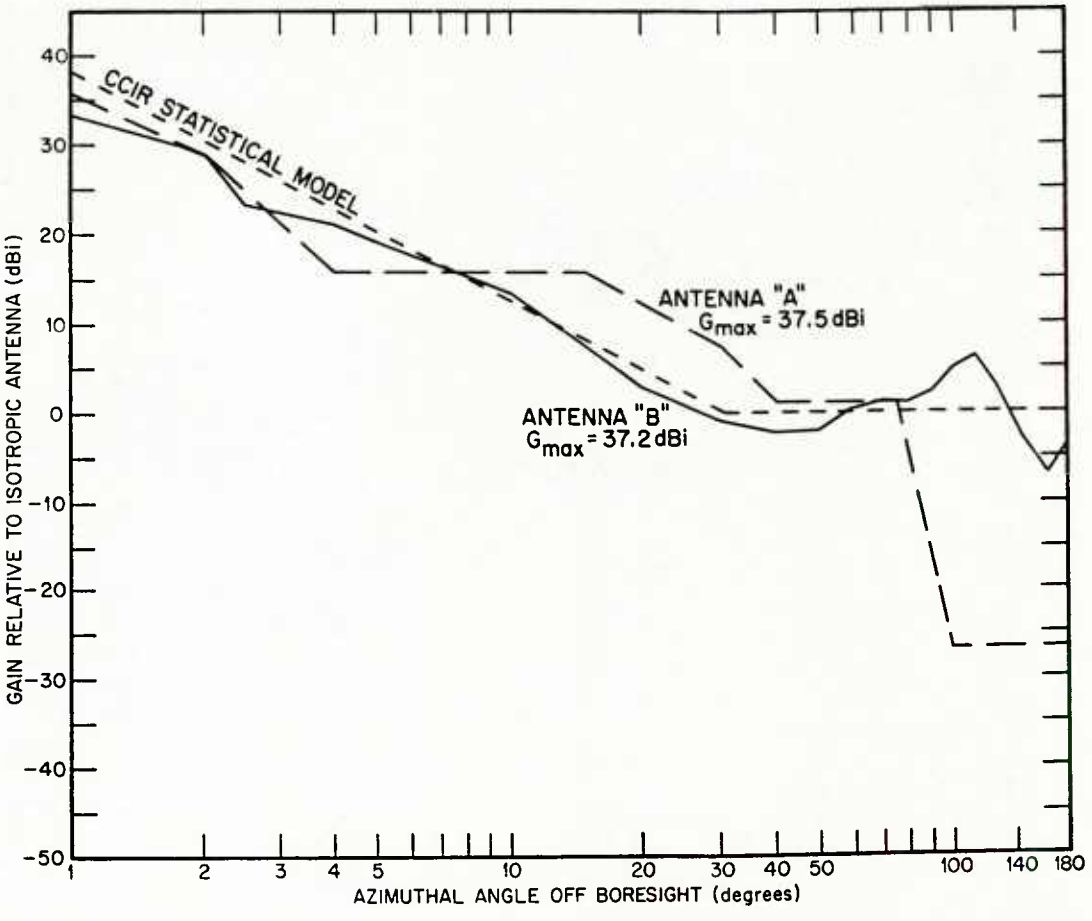

Figure 6. Dissimilar radiation pattern envelopes for two 2.4-meter parabolic antennas (4 GHz band).

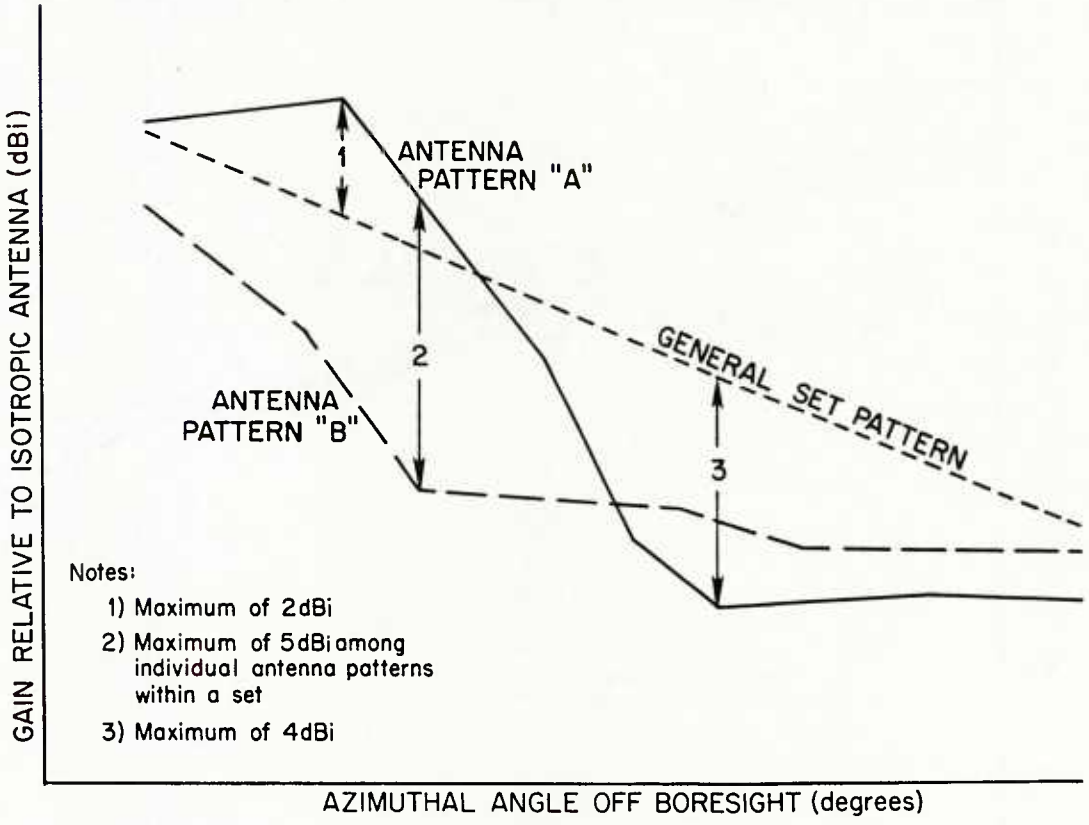

Figure 7. Gain tolerance for set grouping of antenna models.

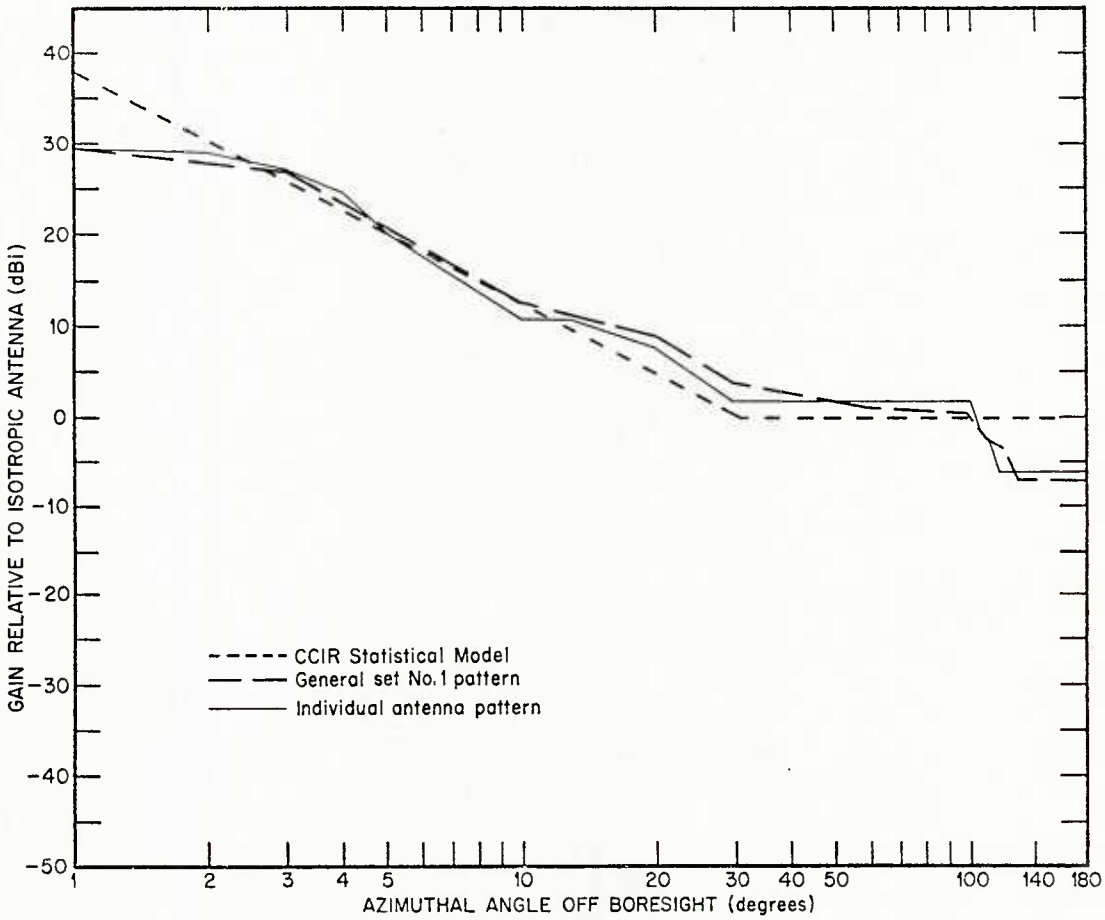

Figure 8. General set pattern 1 and pattern of one antenna from this set.

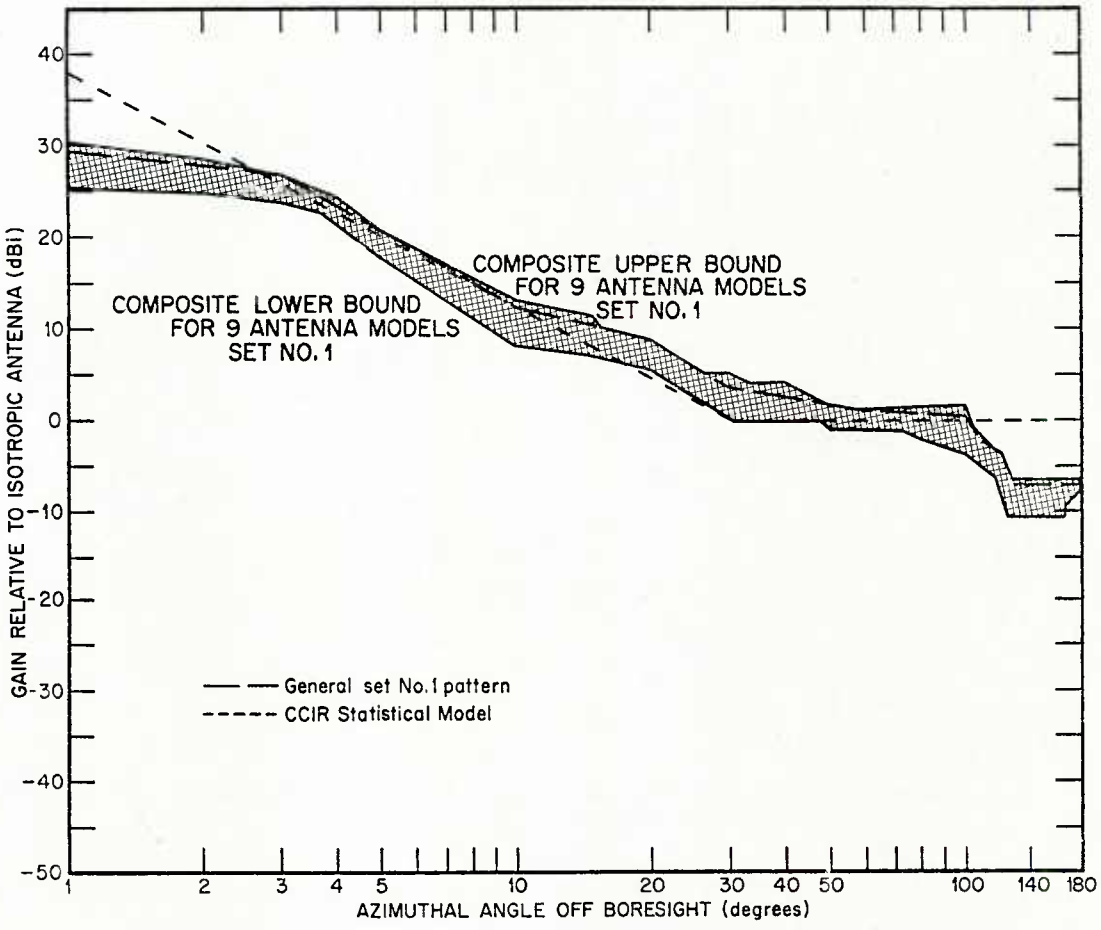

Figure 9. Upper and lower gain bounds for the nine antenna models of general set 1.

DISCUSSION

E.J.Holliman, US

What would be the impact if antenna designers/manufacturers were forced to improve the supression of transmitted energy beyond about 140°?

Author's Reply

We did not see any consistent patterns among the manufacturers' models and data on antenna patterns. The potential seems to exist to improve the suppression beyond 140 degrees.

S.Segner, US

Was there a relation between efficiency and sidelobe suppression?

Author's Reply

No.

L.Boithias, Fr

Vous avez groupé ensemble toutes les antennes sans tenir compte de leurs dimensions par rapport à la longueur d'onde. Vous avez donc obtenu une dispersion très grande mais qui n'est pas significative. Le CCIR donne une formule qui contient un terme en 10 log D/λ dont on doit tenir compte pour comparer les antennes.

Author's Reply

We did not organize the antenna patterns in accordance with D/λ, which is an analysis which should be done. There are questions about the relevance of the D/λ parameter outside the main beam.

SUMMARY OF THE FINAL ROUND TABLE DISCUSSION

Panel Members: R.K.Craine, Chairman
L.W.Barclay
L.Boithias
E.Lampert
J.Neessen

A round table discussion was held at the final session of the AGARD Conference on Propagation Aspects of Frequency Sharing, Interference and System Diversity. Short presentations were given by each of the panel members followed by comments from the floor. The summary presented herein is abstracted from the recordings of the proceedings. The presentations and comments have been severely edited by the chairman to provide only a substantive record of the panel discussion. Any omission of an important point is the fault of the Chairman.

Opening Remarks: R.K.Crane: The chairman noted that the presentations made during the past few days were by members of two communities: the propagation community and the user community. He hoped that the round table discussion would begin a dialogue between the two groups. The propagation specialist tries to respond to the questions asked by the user. In the absence of specific questions, he responds to the questions he thinks should be asked. At times, the answers do not address the actual problems of the user.

The propagation specialist provides statistical models of the phenomena of importance to the system designer or the frequency allocator. These models attempt to predict the occurrence probabilities of service or interference level fields. The relative importance of the different propagation modes depends upon the occurrence probabilities of interest. For example, attenuation or interference due to rain can affect systems for only time percentages less than a few percent of the year because it does not rain more often than that. On a path susceptible to ducting or multipath fading, such conditions may occur for more than 20 percent of the worst month and more than 10 percent of the year. When interference due to ducting occurs, most operators are aware of the problem. When the much less probable occurrence of interference by rain scatter occurs, many operators will not be able to recognize its existence. Rain scatter has been modelled well and experience is as expected but our models for ducting are less than adequate and interference by ducting still occurs using current design practices.

The propagation specialist attempts to provide statistical models for both phenomena. It is up to the user to determine the required occurrence probabilities for his system and then decide which phenomenon affects his design. A two-way discussion is needed between the user and the propagation specialist to set the priorities for the continued improvement of the models.

A number of propagation questions still remain. In the area of millimetre wave system design, the prediction of transmission loss (interference) for coupling by scattering by snow, the prediction of diversity improvement when using space diversity to combat rain attenuation, and the prediction of the occurrence probabilities for attenuation by clouds are not addressed adequately by existing models. Similar problems remain in propagation areas such as HF propagation, ionospheric scintillation, etc. This afternoon's discussions should focus on the important propagation uncertainties and the identification of work still to be done.

L.Boithias: I would like to add that there are frequent misunderstandings between the users or the engineers in charge of a service based on the use of radio waves on the one hand and, on the other, the scientists who study these phenomena. Scientists are very often satisfied when they have fully explained a particular phenomenon which they have observed on a given day, under given conditions, etc.; without wondering, most often, whether this phenomenon occurs 30 or 40% of the time or only 1/10,000th of the time. Now, for the system engineer, the phenomenon is important in the first case and obviously a little less important in the second case. There are often disagreements, from this standpoint, on the importance of a phenomenon.

To come back to the question of time percentage, passing on from ionospheric to tropospheric studies, I'd like to say that there is a rather considerable change in time percentages. Ionospheric communications are concerned with time percentages of the order of 10%, 5%. 1% seems to be the extreme time percentage (when I say 1%, I mean 99% of satisfactory operation). In communications based on the use of the troposphere, Hertzian waves or satellites, there are two orders of magnitude more, and we are led to considering time percentages of 10^{-2} or 10^{-3}%. This modifies completely the perspective of the studies, although we are not always aware of it. I do not wish to expand further on this subject. These were just two ideas which I wanted to emphasize to account for some misunderstandings between physicists and engineers.

J.Neessen: You mentioned interference. It is not a hypothetical problem, as our experience in the Netherlands has shown. When it happens it can be quite costly because either you have to rearrange your frequency plans or your neighbours have to rearrange theirs.

A second point is the question of rain scatter. In my country ducting establishes the coordination distances towards the sea but rain scatter defines the inland coordination area. This occurs at 11 GHz and it is a question what happens at 20 and 30 GHz. As a practical matter, rain scatter is important for coordination.

Finally, atmospheric phenomena which reduce service fields may also cause interference. For example, interference by ducting and multipath fading are caused by the same phenomenon and may occur simultaneously. Likewise, attenuation can be produced by the same rain cell that causes scattered interference. The question of the joint occurrence of fading and interference must be studied. Existing models treat service and interference level fields as independent but this assumption must be questioned when the same meteorological phenomenon gives rise to both.

L.W.Barclay: Mr Chairman, you started by saying that the propagation models are statistical. I think it would be a brave man who would say that the data base is large enough to have a reliable statistical model, particularly when we talk about the sort of time percentages that Mr Boithias was mentioning. Indeed, a small fraction of the time, perhaps in the worst month, may require data gathering over a very long period of time.

Suppose you have a statistical model. How do you know you have the right parameters in the model? In Dr Hughes' paper he discussed a variability parameter which he suggests considering in a very different way. How can you expect the users to know what question to ask if no one knows what the important parameters are? I don't know how to solve this one but dialogue will be important.

Finally, what are the confidence intervals for a statistical model? These are not often stated by a model but are required for the application of the model. One paper addressed the advantages of underprediction or overprediction. The desire to use an unprediction or an overprediction may be a way to compensate for the lack of an error model and a specification of the year-to-year and location-to-location variability associated with a model and underlying data.

E.Lampert: From this morning's session it seems we still have a considerable gap between those who plan systems and those who have to operate the systems. As system engineers we often proceed to develop a system without a knowledge of how the new system will affect existing systems and services. It is not only the engineer who is to blame but also the customer who has under his authority the people who issue contracts for the new systems and the people who issue frequency assignments for those and other systems. The two groups, the designers and frequency managers do not talk with each other because each believes the other party does not know anything about their problems. For instance, the designers feel the frequency authorities assign frequencies on too restrictive a basis. They do not take into account the varying distributions of spectral occupancy.

Comment from the Floor: Dr Soicher: Modelling needs to be considered from two points of view: one the long range models required by system designers and two the short range models for use by operators or frequency managers. In the area of long range modelling for the ionosphere we have a good handle on the way the ionosphere behaves as a function of solar cycle, etc. But, for the operator who needs to know the conditions 5 hours from now, we do not have models that can be used with confidence. The short range models cannot be statistical in nature, at least not in the same way as our long range models, but must be based on the physics of the situation and perhaps the real time measurement of parameters that can be used for short range prediction.

Mr Segner: Are we looking for parameters we can monitor that will alert the operator to impending troubles? As the propagation specialist studies the problem, he should look for parameters that can be used to alert an operator or control a system rather than build models. For instance, if a system is operating with a 40 dB fade margin but only needs 10 dB for the foreseeable future, a reduction in transmitter power could save energy and perhaps reduce the potential for interference.

Dr Crane: In the early days of X-band satellite communication system design the question was raised of the possibility of a short range – perhaps 10 or 20 minutes – warning of loss of margin due to attenuation by rain. A warning system might be possible based on the use of data from a weather radar. It would require the installation of such a radar at each earth station. The major question was the cost effectiveness of such a system.

Dr Belrose: First, in Canada we have a very variable ionosphere because of the auroral zone. We have taken the approach that short term HF predictions are not particularly useful. We use the hand shaking type of system where you sound the link by a burst of transmission on your assigned frequencies and when communication is possible send all your information in short bursts.

In Canada we have been devising a computer based spectrum management system which, when a customer wants a frequency assignment in the VHF/UHF land mobile band, will consider all the relevant information for a particular area and the desired communication system, make a complete electromagnetic compatibility analysis considering all other existing users, and assign a frequency on the basis of the computer model analysis. To obtain information for this system we have been monitoring channel occupancy in all the major cities.

Finally, more attention must be given to the problem of intermodulation in electromagnetic compatibility analysis. With the increased number of land mobile users some of whom will use digital transmission with the base station on all the time, the possibility of producing intermodulate products between 3 transmitters must be considered.

Dr Dougherty: The systems engineer is only concerned with the severest effects of rainfall and couldn't care less for the problems of interest to the propagation specialist. The most striking characteristic of rainfall is its variability, the tremendous year-to-year variations in the magnitude and deviation of attenuation or scattering events. A prediction model must take this variability into account so the system engineer can build an adequate margin into his system.

Mr Boithias: There is a problem of economy of means raised by Mr Segner. I would like to point out that, as far as economy is concerned, we used a troposcatter link between France and Portugal over a period of ten years. This was one of the longest commercial links since it extended over 500 km. To develop it, extensive propagation studies had been concluded by CNET. It had been concluded that 10 Kw were sufficient in the wintertime, and only 1 Kw in the summertime. This economic concept leads us to the following problem: we try to determine the necessary margin for the worst month or the worst year, or the worst month in the worst year, and we dimension the equipment on the basis of this factor. This implies that the equipment is over-dimensioned during the rest of the time. Or else we select a more or less adaptive system, but it is costly, likely to have failures or even to amplify defects.

This problem can be considered from a logical standpoint: just the necessary power available would suffice. It can also be considered from an economic standpoint: then, if we take into account all the expenses, including those resulting from reliability considerations, the advisability of an adaptive system is not obvious. Other aspects can also be taken into account, e.g. jamming problems, chances of being detected by the enemy, in a military context. This will lead to different conclusions.

I believe that this is a truly complex problem, and that propagation is finally one of many components, but not always the most important.

Mr Galpin: We will need the troposcatter systems for military applications even though line-of-sight systems may present a significantly lower interference potential. Some of our long haul links cannot be replaced because there are no convenient islands for repeaters. The troposcatter system with fewer transmitter and receivers is also more survivable in times of stress than a string of line-of-sight links.

For a system having many links in tandem, the reliability per link must be very high to obtain an acceptable reliability for the entire system.

Mr Holliman: The radio propagation community should keep the following in mind:

(1) The purpose of this work is to support the effective use of the entire radio spectrum. Their investigation should be driven by operational problems.

(2) Spectrum congestion is a real problem. Congestion will increase as new requirements and systems emerge.

Dr Ong: I am in favour of more information on variability of rain rate, rain attenuation, signal level predictions, etc.

In tropospheric scatter system design, the variability is included in the concept of a service probability, a safety margin related to the standard deviation of the signal levels. In mobile radio prediction, two types of standard deviations are used: one to describe the time variability and the other the space variability (location-to-location). The variability does not mean very much unless we know the corresponding median signal level.

Dr E.Vilar: On the subject of the relationship between user and propagation experimenter, this is a plea that the user allows access to data from operational systems to obtain propagation statistics. Traditionally, administration have been reluctant to allow access even when the propagation experiment involves the absolute minimum or no interference with the operation of the system. If the user would allow access to his system for propagation experiments, the propagation specialist would understand better the needs of the user and the user may acquire a far more reliable set of data for future planning efforts.

Dr Arnbak: The suggestion of real-time adaptive control as an important remedy has cropped up repeatedly at this symposium. I whole-heartedly support the significance of this which is already proving itself in satellite communications, on HF links, and in the land-mobile service, i.e. in the Nordic Mobile Telephone System. However, it means that propagation workers should dedicate much more work to short-time variability and can no longer be satisfied with cumulative statistics. Event studies are going to be more important in the future to reveal the typical time constants of fading or interference.

Mr M.P.M.Hall: Mr Barclay commented on the limited data available for evaluating interference. One problem is that organizations proposing earth-space or terrestrial systems are obliged to have confidence in the models used to predict availability. To gain that confidence they conduct specific studies to obtain the data to assist in producing the models.

By contrast, interference may arrive over one or more of a multiplicity of paths and studies have focused only on the paths that have produced operational problems. CCIR Study Group 5 has data banks for earth-space and terrestrial link availability but lacks data for interference assessment. A program has been proposed for Europe that would remedy the situation. It would be helpful if Mr Neessen could tell us something about it.

Mr Neessen: In addressing the data collection problems for propagation analysis, a unified method of measurement and a unified method of analysis is required. It is quite difficult to compare data taken on different measurement systems under a different range of observing conditions when the data have been analyzed in several places in different ways. The COST projects have attempted to remedy the situation. We have completed a study of terrestrial links in Europe and have a study of attenuation on slant paths in progress. In the future we will have a study of interference. We plan to have transmitters at four frequencies, 1.3, 11.7, 20 and 30 GHz at several locations in Europe and collect data on as many links as possible. The data will be analyzed by a single organization. Hopefully the interference program will start in 1984.

Dr Fang: I would like to comment about the dialogue between propagation specialists and users. There are a number of different types of users. For many system planners, the propagation models available in the CCIR documents are satisfactory. Operators do not believe the propagation models. MF system operators just want to change frequency or change the circuit by turning a switch. They do not want to look at MUF curves and make predictions. It is not up to the user to tell the propagation specialist what to do next. The propagation specialist must take the time to understand the user's problems and then provide the information that the user needs.

Professor Hunsucker: Precursor events that could warn of propagation problems usually occur at HF before affecting higher frequency satellite communication links. Dr Akasufu of the University of Alaska has developed a parameter ϵ derived from satellite observations of the interplanetary magnetic field and solar wind that has shown promise for the forecasting of propagation disturbances.

High latitude propagation phenomena still need more investigation. The Alaskan panhandle may be a region with severe rain attenuation problems. Ionospheric scintillation at 4 and 6 GHz may be more of a problem at polar latitudes than at the equator.

Finally, new diagnostic tools are available which may be of use in measuring atmospheric parameters of interest. The MST radars can detect the Cn^2 values of turbulence and the atmospheric winds along a microwave or millimetre wave propagation path.

Mr Segner: Is there any attempt to start standardizing propagation models? With the work of the CCIR of providing computerized propagation models, it seems to me that they will soon be asking for standardized models.

Dr Crane: The CCIR Study Group 5 is in the process of recommending attenuation prediction models for use at frequencies above 10 GHz. These models are internationally agreed to and in effect are standardized models.

G.Hagn: At VHF the models are largely empirical. There is a need for a data base that was not used for model development but is to be used to validate candidate models.

J.Belrose: Models for use in urban areas at VHF or UHF have to be statistical in nature and have to be readily adapted for computer use.

G.Hagn: In addition to propagation being described as a statistical process, spectrum occupancy must also be described statistically. The definition of occupancy as a random variable provided by CCIR Study Group 1 is recommended to anyone making occupancy measurements.

APPENDIX A

LIST OF PARTICIPANTS

AARONS, J. Dr	46 Kingswood Road, Auburnale, MA 02166, US
ALBRECHT, H.J. Dr Ing.	FGAN, Konigstrasse 2, D-5307 Wbg.-Werthhoven, Ge
ANDERSON, I. Dr	Room 10/6S15, Govt. Communications Hqs., Benhall, Cheltenham, Glos., GL51 5RJ, UK
ARNBAK, J. Prof.	Eindhoven University of Technology, Dept. of Electrical Engineering, P.O. Box 513, Telecommunications Div., 5600 MB Eindhoven, Ne
BARCLAY, L.W.	Home Office, Dir. Radio Technology, Waterloo Bridge House, Waterloo Road, London SE1 8UA, UK
BATTESTI, J. Mr	C.N.E.T., 38–40, rue du Général Leclerc, 92131 Issy-les-Moulineaux, Fr
BECKER, K.D. Prof. Dr	Theoretische Elektrotechnik, Universität des Saarlandes, 6600 Saarbrucken, Ge
BELROSE, J.S. Dr	C.R.C., P.O. Box 11490, Station H, Ottawa K2H 8S2, Ca
BLYTHE, J.H. Dr	Communications Research Lab., Marconi Research Centre, West Hanningfield Road, Great Baddow, Chelmsford, CM2 8HN, UK
BOITHIAS, Mr	C.N.E.T., 38–40, rue du Général Leclerc, 92131 Issy-les-Moulineaux, Fr
BOSSY, L. Prof.	174 Avenue W. Churchill, UCCLE, 1180 Brussels, Be
BRADLEY, P. Mr	Bldg. R25, Rutherford Appleton Laboratory, Chilton, Didcot, Oxfordshire OX 110 QX, UK
BRUNT, A.A.K. Mr	Thorn EMI Electronics Ltd., Penleigh Works, Wookey Hole Road, Wells, Somerset BA5 1AA, UK
BRUNT, G. Mr	Thorn EMI Electronics Ltd., Wookey Hole Road, Wells, Somerset BA5 1AA, UK
BULAT, T. Assoc. Prof. Dr	Faculty of Engineering, Geophysics Department, Vezneciler, Istanbul, Tu
BURGESS, B. Dr	Radio Navigation Dept., Royal Aircraft Est., Farnborough, Hants., GU14 6TD, UK
CARUSO, L. Mr	Comando del Corpo Technico, Dell'Esercito – Via Antonio SCARPA No.18 – Roma, Italy
CHARLTON, D.G. Mr	Dept. of Mathematics, University of Essex, Wivenhoe Park, Colchester, CO4 3SQ, Essex, UK
COYNE, V.J. Mr	Asst. Chief Strategic Surveillance Branch, Surveillance Division, Rome Air Development Center/OCS, Griffiss AFB, N.Y. 13441, US
CRANE, R.K. Prof.	Thayer School of Engineering, Dartmouth College, Hanover, NH 03753, US
DAVIDSON, D. Dr	GTE Laboratories Incorporated, 40 Sylvan Road, Waltham, MA 02254, US
DIJK, J. Mr	University of Technology, P.O. Box 513, 5600MB Eindhoven, Ne
DOBLE, J.E. Mr	R.6.2.1. British Telecommunications, Research Laboratories, Martlesham Heath, Ipswich, IP5 7RE, UK
DOMVILLE, A.R. Mr	SHAPE Technical Center, P.O. Box 174, 2501 CD Den Haag, Ne
DOUGHERTY, H.T. Dr	c/o U.S. Dept. of Commerce, NTIA/ITS, 325 Broadway, ITS 3.4, Boulder, CO 80303, US
DUBOIN, M.L. Mrs	RPE/EMI, CNET, 38–40, rue du Général Leclerc, 92131 Issy-les-Moulineaux, Fr
ENGEN, P.G. Mr	NODECA, P.O. Box 7020, Homansbyen, N-Oslo 3, No
EVANS, B.G. Dr	Dept. Elec. Eng. Science, University of Essex, Wivenhoe Park, Colchester CO4 3SQ, UK
FANG, D.J. Dr	Propagation Studies Dept., COMSAT Laboratories, Clarksburg, MD 20871, US
FER, A. Prof.	Middle East Technical Univ., Ankara, Tu
FOREST, A. Mr	S.A.T., 32 rue Cantagrel, 75624 Paris, CEDEX 13, Fr

GALPIN, R.K.P. Mr	SHAPE Technical Centre, P.O. Box 174, 2501 CD Den Haag, Ne
GIOVENALI, L. Mr	Comando Corpo Technico Esercito, Via SCARPA 18, Roma, It
GOODMAN, J.M. Dr	Code 4180, Space Science Division, Naval Research Laboratory, 4555 Overlook Ave. S.W., Washington, D.C. 20375, US
GOTT, G.F. Dr	Dept. Electrical Eng. & Electronics, UMIST, P.O. Box 88, Manchester M60 1QD, UK
GOUTELARD, C.G. Prof.	Laboratoire d'Etude des Transmission, Université Paris Sud, 9, Ave de la Division Leclerc, 94230 Cachan, Fr
GRANTHAM, R. Mr	Maritime Telegraph & Telephone Ltd., 1505 Barrington St.,— 3 North, Halifax, B3J 2W3 Nova Scotia, Ca
HAGN, G.H. Mr	SRI International, 1611 North Kent Street, Arlington, VA 22209, US
HALL, M.P.M. Mr	Rutherford Appleton Laboratories, Chilton, Didcot, Oxon, OX11 OQX, UK
HALLEY, P.M. Mr	4, Avenue des Vignettes, 8300 Toulon, Fr
HANBABA, R. Dr	LAB/MER/SPI, CNET, BP 40, 22301 Lannion Cedex, Fr
HOLLIMAN, E.J. Mr	US Army Spectrum Manager, Office of Dep. Chf. of Staff Ops/Plan, Attn: DAMO – C4Z – S, Washington, D.C. 20310, US
HOPPONEN, J.D. Dr	0/62-41, B/562, Lockheed Missiles & Space Company, P.O. Box 504, Sunnyvale, CA 94086, US
HORTENBACH, K.J. Dr	Deutsche Welle Abt. HF, Postfach 100 444, D-5000 Köln 1, Ge
HOUMINER, Z. Dr	Director, Radio Observatory, National Committee for Space Research, P.O. Box 911, Haifa, Israel, (US Invited)
HOWELL, R.G.	British Telecom, Research Laboratories, Martlesham Heath, Ipswich IP5 7RE, UK
HUGHES, K.A. Dr	Home Office, Dir. Radio Technology, Waterloo Bridge House, Waterloo Road, London SE1 8UA, UK
HUNSUCKER, R.D. Prof.	Geophysical Institute, University of Alaska, 903 Koyukuk Avenue North, Fairbanks, Alaska 99701, US
ISENSEE, U. Mr	Fernmeldetechnisches Zentralamt, Postfach 5000, D 6100 Darmstadt, Ge
JONES, T.B.	Physics Dept., The University, Leicester LE1 7RH, UK
JOY, Monique	CNET, 38–40 rue du Général Leclerc, 92131 Issy-les-Moulineaux, Fr
KERN, J. Mr	BWB-ML, Dachauerstrasse 128, D 8000 München 19, Ge
LAMPERT, E. Dr	Siemens AG, Fr Fu E F 27, Hofmannstr. 27, 8000 München, Ge
LANGE-HESSE, G. Dr	Max-Planck-Institut für Aeronomie, D-3411 Katlenburg-Lindau 3, Ge
LANGER, G. Mr	CNET, 38–40, rue du Général Leclerc, 92131 Issy-les-Moulineaux, Fr
LARSEN, R. Mr	Marconi Research Centre, Great Baddow, Chelmsford, Essex CM2 8HN, UK
LAVERGNAT, J. Dr	CNET/RPE, 38–40, rue du Général Leclerc, 92131 Issy-les-Moulineaux, Fr
MARTIN, L. Mr	CNET/LAB., Route de Tregastel, 22301 Lannion, Fr
McMANAMON, P. Dr	Associate Director, NTIA/ITS4-1, U.S. Dept. of Commerce, 325 Broadway, Boulder, CO 80303, US
MON, J.P. Prof. Dr	CNET/ETP, 38–40, rue du Général Leclerc, 92131 Issy-les-Moulineaux, Fr
NEESSEN, J. Ir.	Dr Neher Laboratories, St. Paulusstraat 4, 2260 AK Liedschendam, Ne
NIEMEYER, M. Dr	Siemens AG, Hofmann Str 51, 8000 München 70, Ge
OCHS, A. Mr	Forschungsinstitut der DBP, Postfach 5000, D-6100 Darmstadt, Ge
OLIVERA, J. Major Eng.	Direccao Serviso Electricidade e Telecomunicoes, Rua Escola Exercito 13, 1100 Lisboa, Po
ONG, J.T. Dr	Cable and Wireless PLC, Technology and Engineering Div., Mercury House, Theobalds Road, London WCLX 8RX, UK
PILLET, G. Dr	CNET/DICET, 38–40, rue du Général Leclerc, 92131 Issy-les-Moulineaux, Fr
PRESTON, R.J. Mr	RACAL-SES Ltd., Duke Street, Windsor, Berks., SL4 1FB, UK
REMBOLD, B. Dr	AEG-Telefunken, Sedanstr. 10, D-7900 Ulm, Ge
REVAH, I. Dr	CNET/PAB/RPE, 38–40, rue du Général Leclerc, 92131 Issy-les-Moulineaux, Fr

ROORYCK, M. Mr	CNET, 38–40, rue du Général Leclerc, 92131 Issy-les-Moulineaux, Fr
SANDELL, R. Mr	BBC Research Department, Kingswood Warren, Tadworth, Surrey, UK
SCHEUR, M. Van Der Mr	Physics Laboratory TNO, P.O. Box 96864, 2509 JG Den Haag, Ne
SCHOLZ, D. Mr	Streitkrafteamt, Deutschherrenstrasse, 5300 Bonn 2, Ge
SCHWAB, L.M. Dr	M.I.T. Lincoln Laboratory, P.O. Box 73, Rm. D-422, Lexington, Massachusetts 02173, US
SEGNER, S.M.	US Army Comm-Electronics Cmd., Ctr. for Sys. Eng. & Int., Attn. DRSEL-SEI-A, Ft. Monmouth, N.J. 07703, US
SIMMONS, A.J. Dr	M.I.T. Lincoln Laboratory, P.O. Box 73, Rm. D-422, Lexington, Massachusetts 02173, US
SOICHER, H. Dr	US Army Comm-Electronics Command, CENCOMS/DRSEL – COM-RN-1, Fort Monmouth, N.J. 07703, US
SOLIZ, P. L/Col.	Director, Aer. Sc., 223/231 Old Marylebone Road, London NW1 5TH, UK
SORAIS, D. Mr	16, rue du Fosse Blanc, 92231 Gennevilliers, Fr
SPAENDONK, R. Van Mr	Klatteweg 1, 2597 KA Den Haag, Ne
SPANJAARD, N. Mr	C.N.E.T., 38–40, rue du Général Leclerc, 92131 Issy-les-Moulineaux, Fr
SPRENKELS, C. Mr	Commandant 22em Wing Logistique, Quartier Roi Albert 1, 70 Rue de la Fusée, B-1130 Bruxelles, Be
STARK, A. Dipl. Ing.	Rhode & Schwarz Abtlg. 4 PN, Muhldorfstr. 15, D-8000 München 80, Ge
STRAUSS, B. Mr	Service Meteorologique Metropolitain, 2 Avenue Rapp, 75340 Paris, CEDEX 07, Fr
SULLIVAN, T. Mr	ORI, Inc., 1400 Spring St., Silver Spring, MD 20910, US
THIRLWELL, J. Dr	British Telecom, Research Laboratories, Martlesham Heath, Ipswich IP5 7RE, UK
VAN TIGGELEN, J.A.C.M. Mr	Dr Neher Labs., St. Paulusstraat 4, Leidschendam, Ne
TOU, Ching Po, Dr	Dept. of Electrical Engineering, Technical University of Nova Scotia, Halifax, Nova Scotia B3J 2X4, Ca
UTLAUT, W.F. Dr	US Dept. of Commerce, NTIA/ITSD 1, 325 Broadway, Boulder, CO 80303, US
VILAR, E. Dr	Dept. of Electrical and Electronic Engineering, Portsmouth Polytechnic, Anglesea Rd., Portsmouth, PO1 3DJ, Hants., UK
WANG, J. Mr	Office of Science & Technology, Federal Communications Commission, Washington, D.C. 20554, US

AGARD Conference Proceedings No.332
Advisory Group for Aerospace Research and Development, NATO
PROPAGATION ASPECTS OF FREQUENCY SHARING, INTERFERENCE SYSTEM DIVERSITY
by H.Soicher
Published March 1983
432 pages

These Proceedings include the papers and discussions presented at the AGARD Electromagnetic Wave Propagation Panel Symposium on "Propagation Aspects of Frequency Sharing, Interference and System Diversity" held in Issy-les-Moulineaux, France, in October 1982.

Increasing demands for radio service will necessitate more frequency sharing. An assessment of the

P.T.O

AGARD-CP-332

Frequency Spectrum Management
Frequency Sharing
Frequency Interference
Electromagnetic Wave Propagation
Propagation Phenomena
Radio Communication
Propagation Models

AGARD Conference Proceedings No.332
Advisory Group for Aerospace Research and Development, NATO
PROPAGATION ASPECTS OF FREQUENCY SHARING, INTERFERENCE SYSTEM DIVERSITY
by H.Soicher
Published March 1983
432 pages

These Proceedings include the papers and discussions presented at the AGARD Electromagnetic Wave Propagation Panel Symposium on "Propagation Aspects of Frequency Sharing, Interference and System Diversity" held in Issy-les-Moulineaux, France, in October 1982.

Increasing demands for radio service will necessitate more frequency sharing. An assessment of the

P.T.O

AGARD-CP-332

Frequency Spectrum Management
Frequency Sharing
Frequency Interference
Electromagnetic Wave Propagation
Propagation Phenomena
Radio Communication
Propagation Models

AGARD Conference Proceedings No.332
Advisory Group for Aerospace Research and Development, NATO
PROPAGATION ASPECTS OF FREQUENCY SHARING, INTERFERENCE SYSTEM DIVERSITY
by H.Soicher
Published March 1983
432 pages

These Proceedings include the papers and discussions presented at the AGARD Electromagnetic Wave Propagation Panel Symposium on "Propagation Aspects of Frequency Sharing, Interference and System Diversity" held in Issy-les-Moulineaux, France, in October 1982.

Increasing demands for radio service will necessitate more frequency sharing. An assessment of the

P.T.O

AGARD-CP-332

Frequency Spectrum Management
Frequency Sharing
Frequency Interference
Electromagnetic Wave Propagation
Propagation Phenomena
Radio Communication
Propagation Models

AGARD Conference Proceedings No.332
Advisory Group for Aerospace Research and Development, NATO
PROPAGATION ASPECTS OF FREQUENCY SHARING, INTERFERENCE SYSTEM DIVERSITY
by H.Soicher
Published March 1983
432 pages

These Proceedings include the papers and discussions presented at the AGARD Electromagnetic Wave Propagation Panel Symposium on "Propagation Aspects of Frequency Sharing, Interference and System Diversity" held in Issy-les-Moulineaux, France, in October 1982.

Increasing demands for radio service will necessitate more frequency sharing. An assessment of the

P.T.O

AGARD-CP-332

Frequency Spectrum Management
Frequency Sharing
Frequency Interference
Electromagnetic Wave Propagation
Propagation Phenomena
Radio Communication
Propagation Models

possibility of additional frequency sharing included the following points: propagation effects on the practicability of frequency sharing, mechanisms responsible for and limits posed by interference from strong signals, and techniques available for the control of such interference and for the increase in channel capability.

The overview session examined frequency sharing with reference to RF propagation limitations, principles and international procedures. Other session dealt specifically with the subject with regard to terrestrial propagation (ionospheric modifications and ionospheric modes), terrestrial propagation (ground and tropospheric modes), EHF propagation, propagation along earth-space paths, and interference control and increase in channel capacity.

Included with the 36 papers presented are the discussions that followed the presentation of each paper.

Papers presented at the 31st Symposium of the Electromagnetic Wave Propagation Panel held in Issy-les-Moulineaux, France, 18–22 October, 1982.

ISBN 92-835-0329-5

possibility of additional frequency sharing included the following points: propagation effects on the practicability of frequency sharing, mechanisms responsible for and limits posed by interference from strong signals, and techniques available for the control of such interference and for the increase in channel capability.

The overview session examined frequency sharing with reference to RF propagation limitations, principles and international procedures. Other session dealt specifically with the subject with regard to terrestrial propagation (ionospheric modifications and ionospheric modes), terrestrial propagation (ground and tropospheric modes), EHF propagation, propagation along earth-space paths, and interference control and increase in channel capacity.

Included with the 36 papers presented are the discussions that followed the presentation of each paper.

Papers presented at the 31st Symposium of the Electromagnetic Wave Propagation Panel held in Issy-les-Moulineaux, France, 18–22 October, 1982.

ISBN 92-835-0329-5

possibility of additional frequency sharing included the following points: propagation effects on the practicability of frequency sharing, mechanisms responsible for and limits posed by interference from strong signals, and techniques available for the control of such interference and for the increase in channel capability.

The overview session examined frequency sharing with reference to RF propagation limitations, principles and international procedures. Other session dealt specifically with the subject with regard to terrestrial propagation (ionospheric modifications and ionospheric modes), terrestrial propagation (ground and tropospheric modes), EHF propagation, propagation along earth-space paths, and interference control and increase in channel capacity.

Included with the 36 papers presented are the discussions that followed the presentation of each paper.

Papers presented at the 31st Symposium of the Electromagnetic Wave Propagation Panel held in Issy-les-Moulineaux, France, 18–22 October, 1982.

ISBN 92-835-0329-5

possibility of additional frequency sharing included the following points: propagation effects on the practicability of frequency sharing, mechanisms responsible for and limits posed by interference from strong signals, and techniques available for the control of such interference and for the increase in channel capability.

The overview session examined frequency sharing with reference to RF propagation limitations, principles and international procedures. Other session dealt specifically with the subject with regard to terrestrial propagation (ionospheric modifications and ionospheric modes), terrestrial propagation (ground and tropospheric modes), EHF propagation, propagation along earth-space paths, and interference control and increase in channel capacity.

Included with the 36 papers presented are the discussions that followed the presentation of each paper.

Papers presented at the 31st Symposium of the Electromagnetic Wave Propagation Panel held in Issy-les-Moulineaux, France, 18–22 October, 1982.

ISBN 92-835-0329-5

U21382

AGARD
NATO OTAN
7 RUE ANCELLE · 92200 NEUILLY-SUR-SEINE
FRANCE
Telephone 745.08.10 · Telex 610176

DISTRIBUTION OF UNCLASSIFIED AGARD PUBLICATIONS

AGARD does NOT hold stocks of AGARD publications at the above address for general distribution. Initial distribution of AGARD publications is made to AGARD Member Nations through the following National Distribution Centres. Further copies are sometimes available from these Centres, but if not may be purchased in Microfiche or Photocopy form from the Purchase Agencies listed below.

NATIONAL DISTRIBUTION CENTRES

BELGIUM
Coordonnateur AGARD – VSL
Etat-Major de la Force Aérienne
Quartier Reine Elisabeth
Rue d'Evere, 11

CANADA
Defence Science
Department of
Ottawa, Ontari

DENMARK
Danish Defenc
Østerbrogades
Copenhagen Ø

FRANCE
O.N.E.R.A. (I
29 Avenue de
92320 Châtill

GERMANY
Fachinforma
Physik, Math
Kernforschu
D-7514 Egge

GREECE
Hellenic Air
Research an
Holargos, Athens

ICELAND
Director of Aviation
c/o Flugrad
Reykjavik

ITALY
Aeronautica Militare
Ufficio del Delegato Nazionale all'AGARD
3, Piazzale Adenauer
Roma/EUR

(ARGE)

Defence Research Information
Station Square House
St. Mary Cray
Orpington, Kent BR5 3RE

UNITED STATES
National Aeronautics and Space Administration (NASA)
Langley Field, Virginia 23365
Attn: Report Distribution and Storage Unit

THE UNITED STATES NATIONAL DISTRIBUTION CENTRE (NASA) DOES NOT HOLD STOCKS OF AGARD PUBLICATIONS, AND APPLICATIONS FOR COPIES SHOULD BE MADE DIRECT TO THE NATIONAL TECHNICAL INFORMATION SERVICE (NTIS) AT THE ADDRESS BELOW.

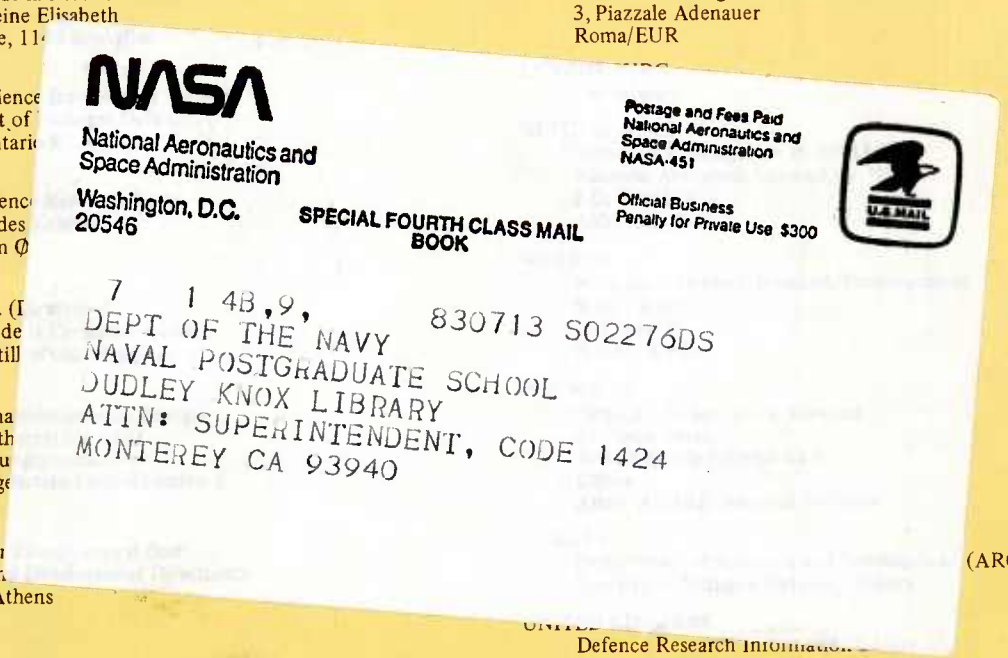

PURCHASE AGENCIES

Microfiche or Photocopy
National Technical
Information Service (NTIS)
5285 Port Royal Road
Springfield
Virginia 22161, USA

Microfiche
Space Documentation Service
European Space Agency
10, rue Mario Nikis
75015 Paris, France

Microfiche or Photocopy
British Library Lending
Division
Boston Spa, Wetherby
West Yorkshire LS23 7BQ
England

Requests for microfiche or photocopies of AGARD documents should include the AGARD serial number, title, author or editor, and publication date. Requests to NTIS should include the NASA accession report number. Full bibliographical references and abstracts of AGARD publications are given in the following journals:

Scientific and Technical Aerospace Reports (STAR)
published by NASA Scientific and Technical
Information Facility
Post Office Box 8757
Baltimore/Washington International Airport
Maryland 21240, USA

Government Reports Announcements (GRA)
published by the National Technical
Information Services, Springfield
Virginia 22161, USA

Printed by Specialised Printing Services Limited
40 Chigwell Lane, Loughton, Essex IG10 3TZ

ISBN 92-835-0329-5